NASA CR-121128

INVESTIGATION OF NOISE SUPPRESSION BY SONIC INLETS FOR TURBOFAN ENGINES

Volume III: An Experimental Investigation of the Internal Noise Field of Two Axisymmetric Sonic Inlet Models

D6-40818

July 1973

by F. Klujber and J. Louisse

BOEING COMMERCIAL AIRPLANE COMPANY

prepared for

NATIONAL AERONAUTICS AND SPACE ADMINISTRATION

NASA Lewis Research Center
Contract NAS3-15574

1. Report No.	2. Government Accession No.	3. Recipient's Catalog No.
NASA CR-121128		

4. Title and Subtitle	5. Report Date
INVESTIGATION OF NOISE SUPPRESSION BY SONIC INLETS FOR TURBOFAN ENGINES–Volume III: An Experimental Investigation of the Internal Noise Field of Two Axisymmetric Sonic Inlet Models	July 1973
	6. Performing Organization Code
7. Author(s)	8. Performing Organization Report No.
F. Klujber and J. Louisse	D6-40818
	10. Work Unit No.
9. Performing Organization Name and Address	11. Contract or Grant No.
Boeing Commercial Airplane Company P.O. Box 3707 Seattle, Washington 98124	NAS3-15574
	13. Type of Report and Period Covered
12. Sponsoring Agency Name and Address	Contractor report
National Aeronautics and Space Administration Washington, D.C. 20546	14. Sponsoring Agency Code

15. Supplementary Notes

NASA Project Manager, J. P. Lewis

16. Abstract

This document presents near-field acoustic data taken inside two sonic inlet models. The experiment was carried out with a high-frequency-response transducer on a stinger probe which surveyed the inlet at three different planes and three different radii. The range of inlet throat Mach numbers was from 0.5 to 1.0.

17. Key Words (Suggested by Author(s))	18. Distribution Statement
Near-field noise Sonic inlets Noise attenuation	Unclassified–unlimited

19. Security Classif. (of this report)	20. Security Classif. (of this page)	21. No. of Pages	22. Price*
Unclassified	Unclassified	260	$3.00

*For sale by the National Technical Information Service, Springfield, Virginia 22151

INVESTIGATION OF NOISE SUPPRESSION BY SONIC INLETS FOR TURBOFAN ENGINES

BY: F. KLUJBER,
J. C. BOSCH, R. W. DEMETRICK, AND W. L. ROBB

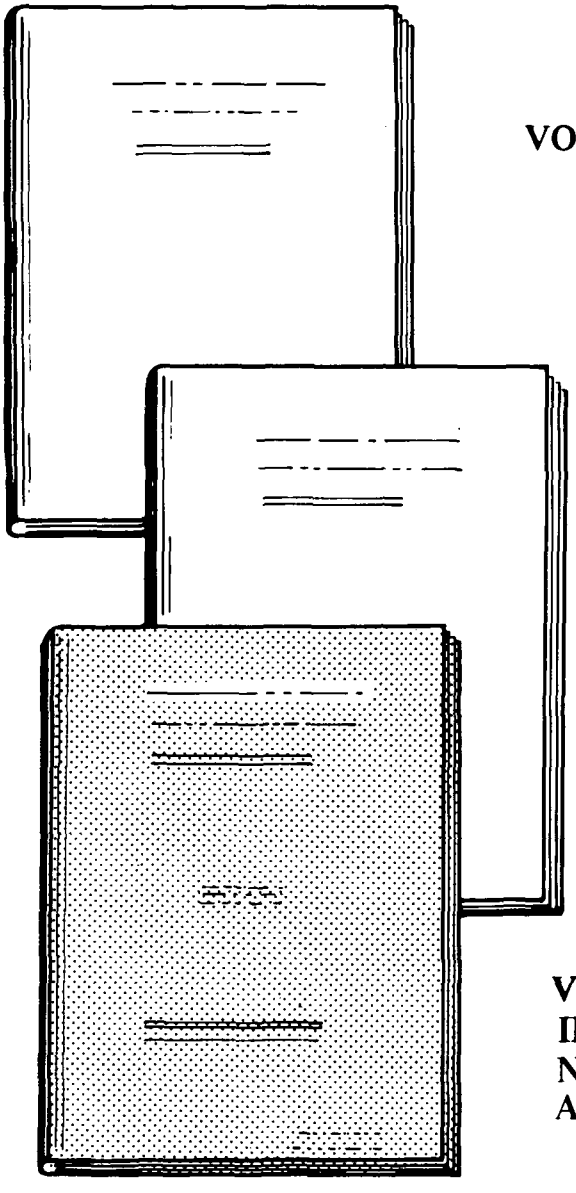

VOLUME I: PROGRAM SUMMARY

CR-121126 D6-40855

VOLUME II: APPENDIXES

CR-121127 D6-40855-1

A. MECHANICAL DESIGN STUDY AND TEST CONFIGURATION SELECTION

B. DETAIL DESIGN OF MODELS

C. INSTRUMENTATION DETAILS

D. DATA ANALYSIS PROCEDURE

E. CONCEPT SCREENING.

VOLUME III: AN EXPERIMENTAL INVESTIGATION OF THE INTERNAL NOISE FIELD OF TWO MODEL AXISYMMETRIC SONIC INLETS

CR-121128 D6-40818

CONTENTS

SUMMARY

This report covers part of a study made by The Boeing Company Commercial Airplane Group, under NASA Lewis Research Center, contract NAS3-15574, titled: "Investigation of Noise Suppression by Sonic Inlets for Turbofan Engines." This part of the Sonic Inlet Noise Suppression program was aimed at investigating noise attenuation trends at different inlet throat Mach numbers, ranging from 0.5 to 1.0. In particular, attention was focused on the attenuation of blade passing tone and multiple pure tone noise by sonic inlets and on noise generation by the sonic plane itself.

Two 305-mm (12-in.) diameter, single-passage, converging-diverging cowl wall inlets, one sized for approach and another for takeoff conditions, were investigated. The length-over-diameter ratios of the approach and takeoff inlets were 2.0 and 1.0, respectively. Each inlet was surveyed with a high-frequency-response transducer mounted at the tip of a stinger probe and a static tap 26 mm (1 in.) behind the tip (fig. 1). The airflow rates of the fan were chosen to cover the range of throat Mach numbers in the inlets. The survey locations and test instrumentation are shown in figure 1a. The following conclusions were drawn from the test with the two sonic inlets:

1. Increasing the inlet throat Mach number from about 0.5 to 1.0 resulted in an increasing noise attenuation at blade passing frequency (figs. 2 and 3).

2. The rate of decay of the blade passing tone was found to be less on the centerline than near the outer wall. This was attributed to the radial Mach number gradient in the throat area (figs. 4 and 5).

3. No significant noise generation by the sonic plane was observed (fig. 6).

4. The multiple pure tone ("buzz-saw") noise, which was only observed at fan blade speeds above the sonic velocity, did not propagate through the inlet throat plane (fig. 7).

5. No evidence was found of noise leakage at blade passing frequency through the inlet throat boundary layer (fig. 8).

The results of this experiment are of importance in the design and selection of sonic inlet concepts. Further, it will serve in the understanding of noise propagation in sonic inlets with Mach number gradient in view of the lack of analytical tools.

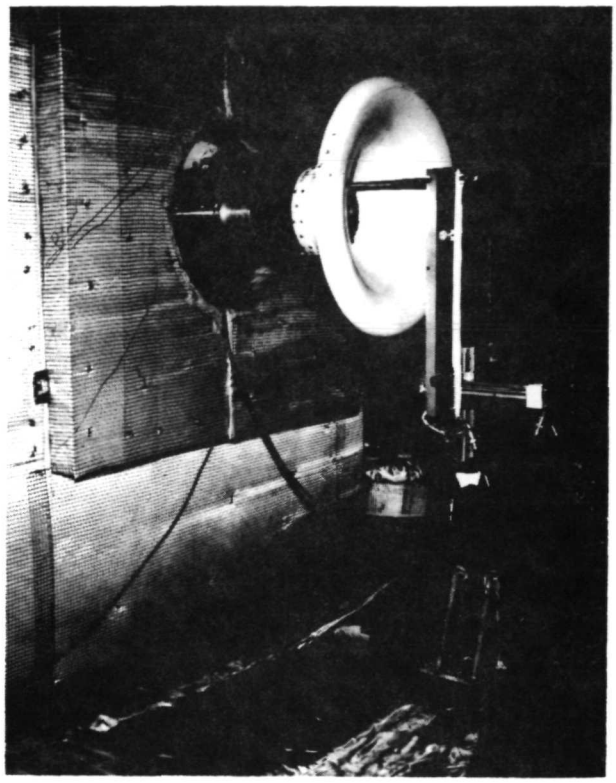

Test Setup

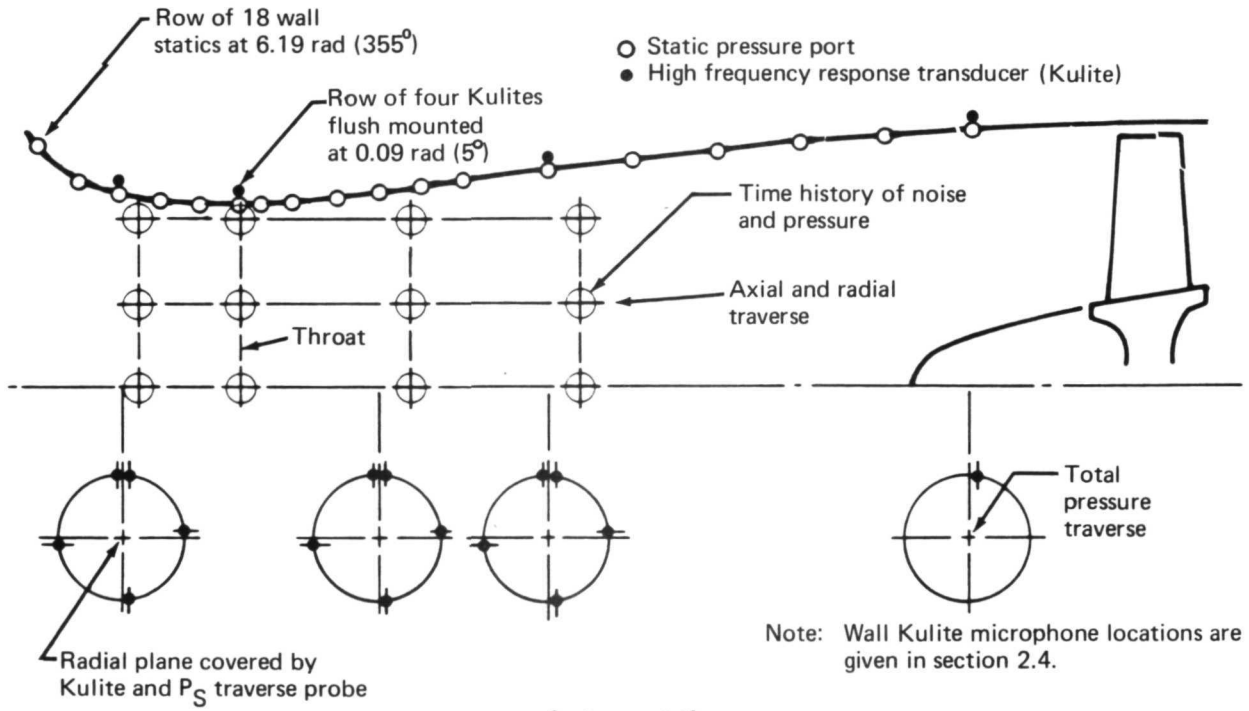

Instrumentation

FIGURE 1.–TEST SETUP AND INSTRUMENTATION

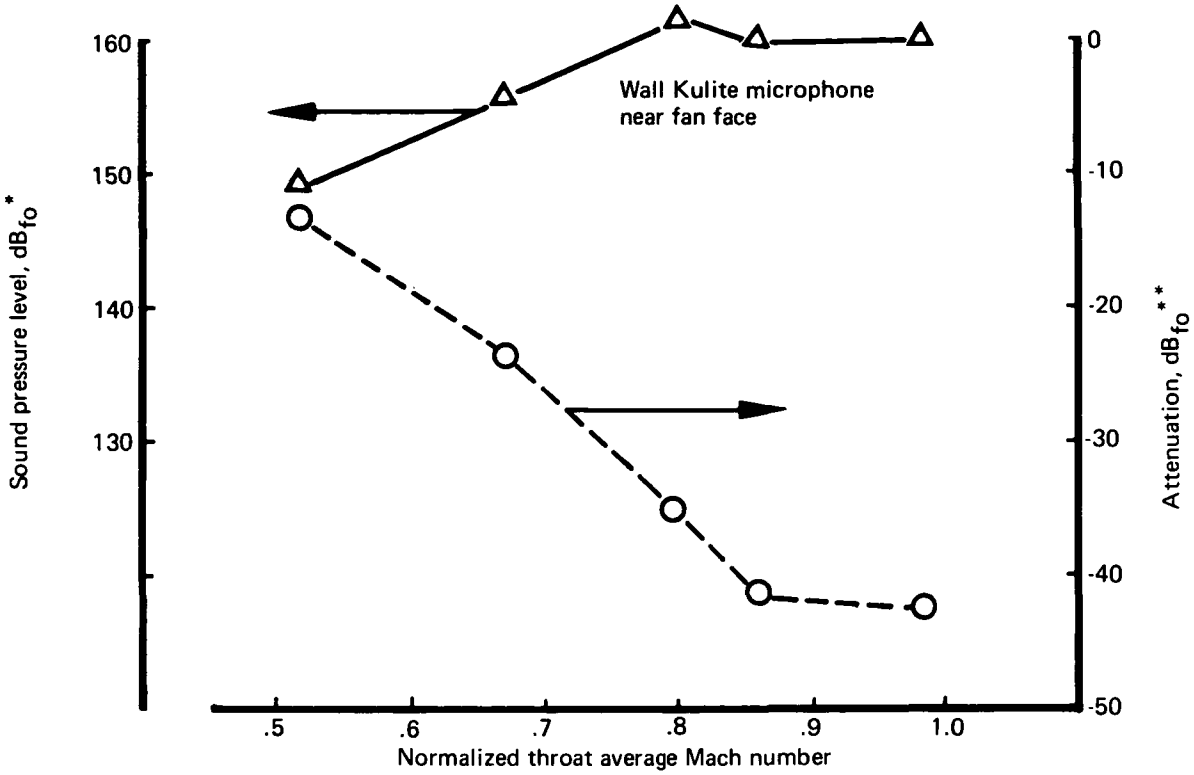

FIGURE 2.–ATTENUATION AT BLADE PASSING FREQUENCY VERSUS THROAT MACH NUMBER–APPROACH INLET

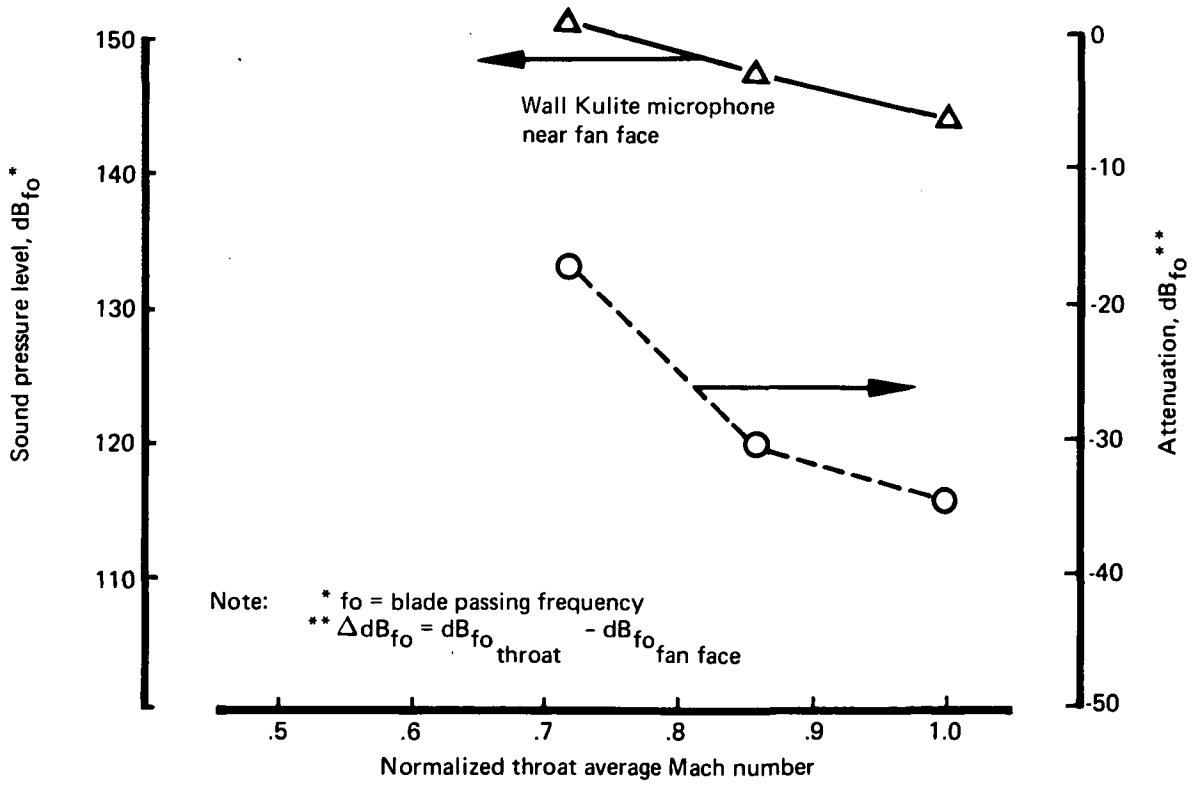

FIGURE 3.–ATTENUATION AT BLADE PASSING FREQUENCY VERSUS THROAT MACH NUMBER–TAKEOFF INLET

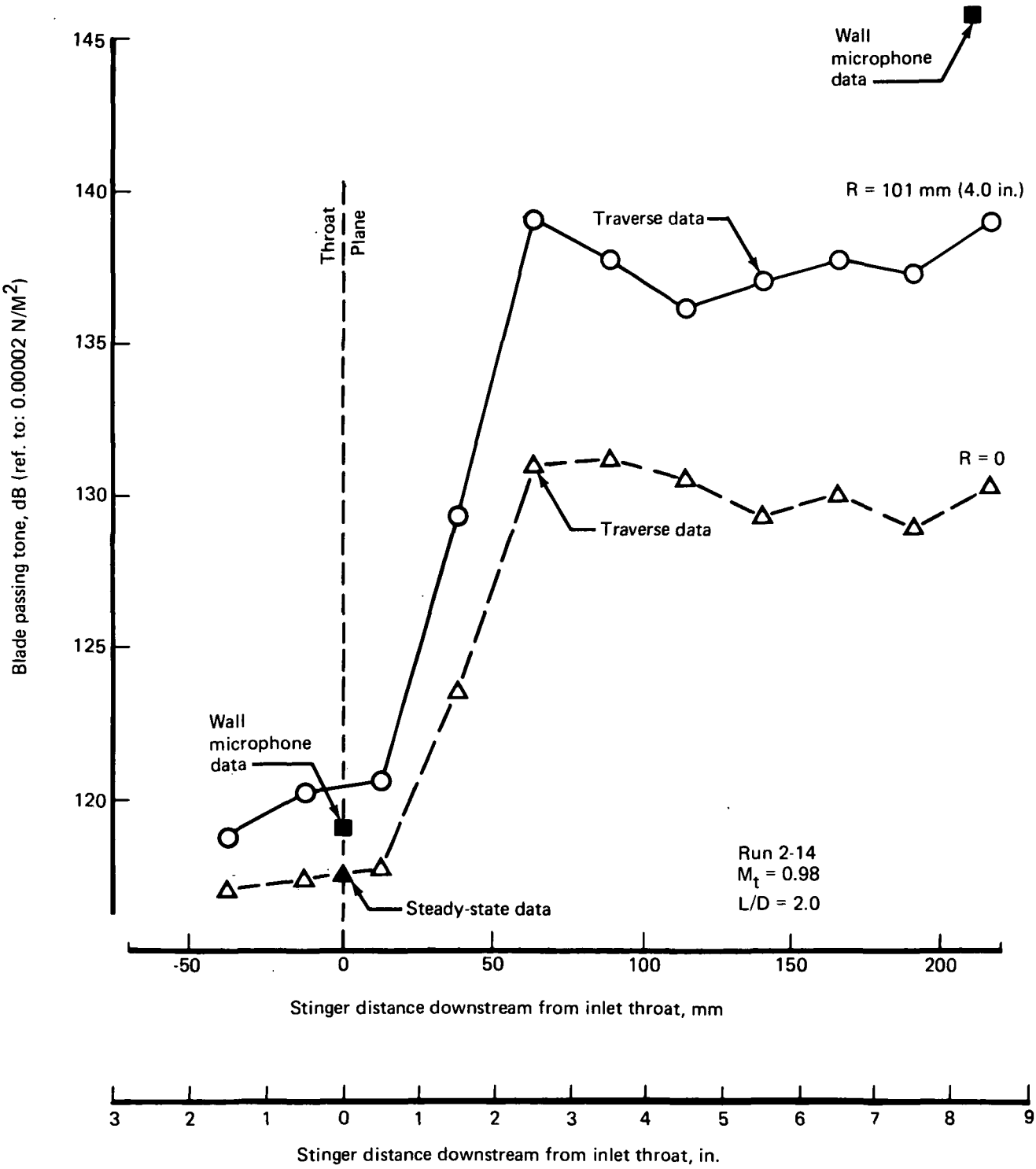

FIGURE 4.—AXIAL DISTRIBUTION OF BLADE PASSING TONE IN APPROACH INLET

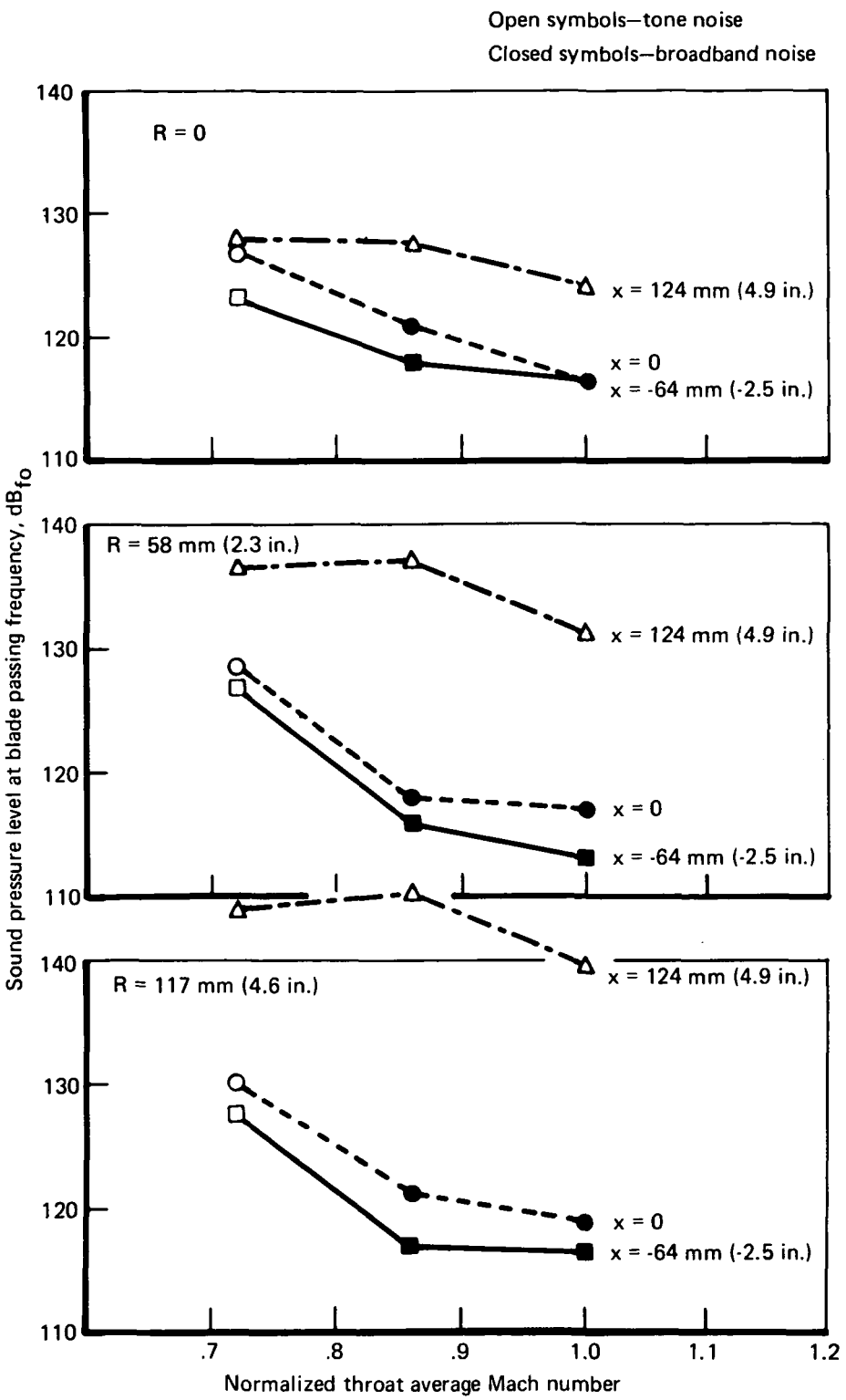

FIGURE 5.—BLADE PASSING TONE VERSUS THROAT MACH NUMBER IN TAKEOFF INLET

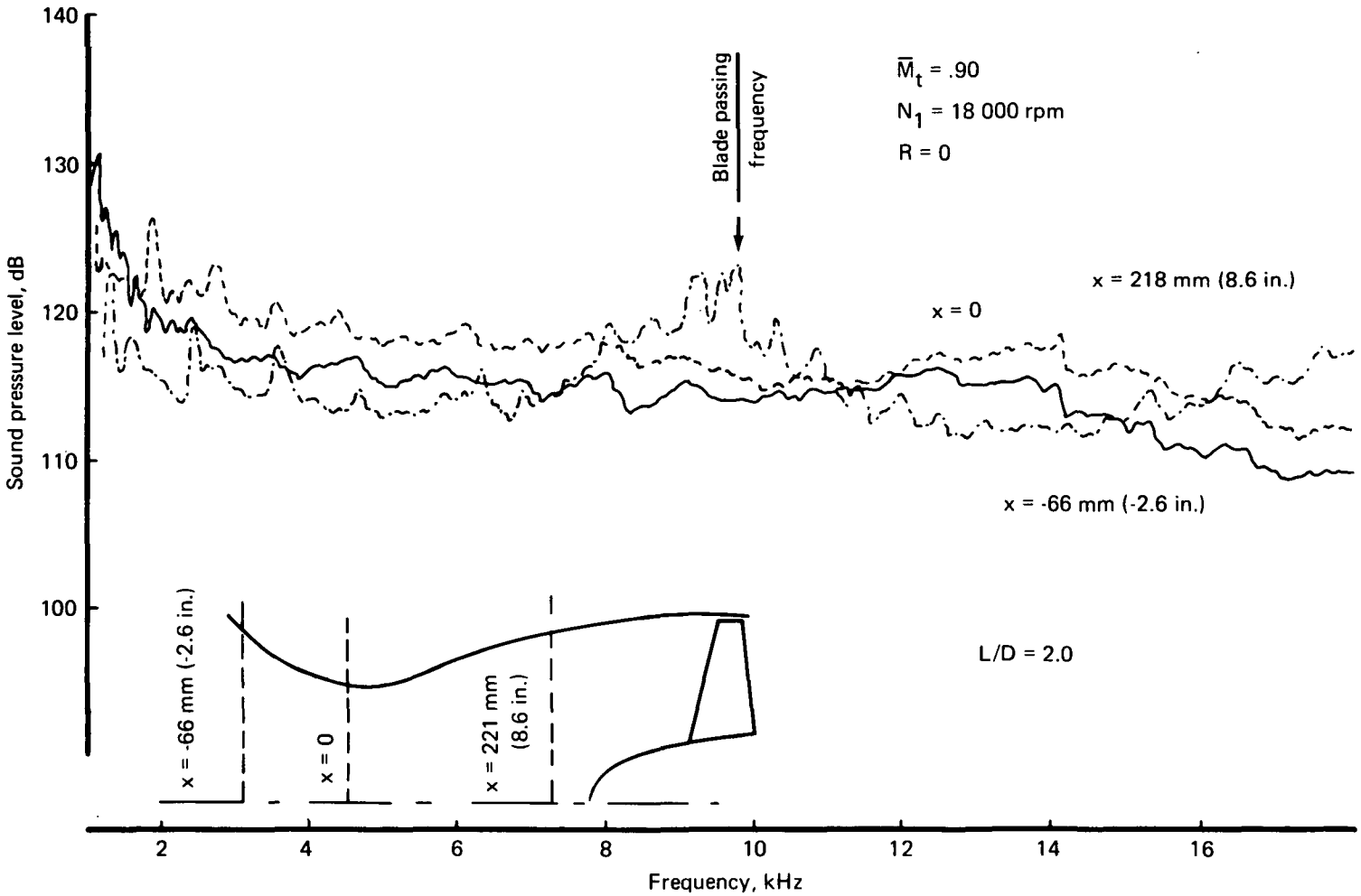

FIGURE 6.—NEAR FIELD NOISE SPECTRA INSIDE FUNDAMENTAL APPROACH INLET

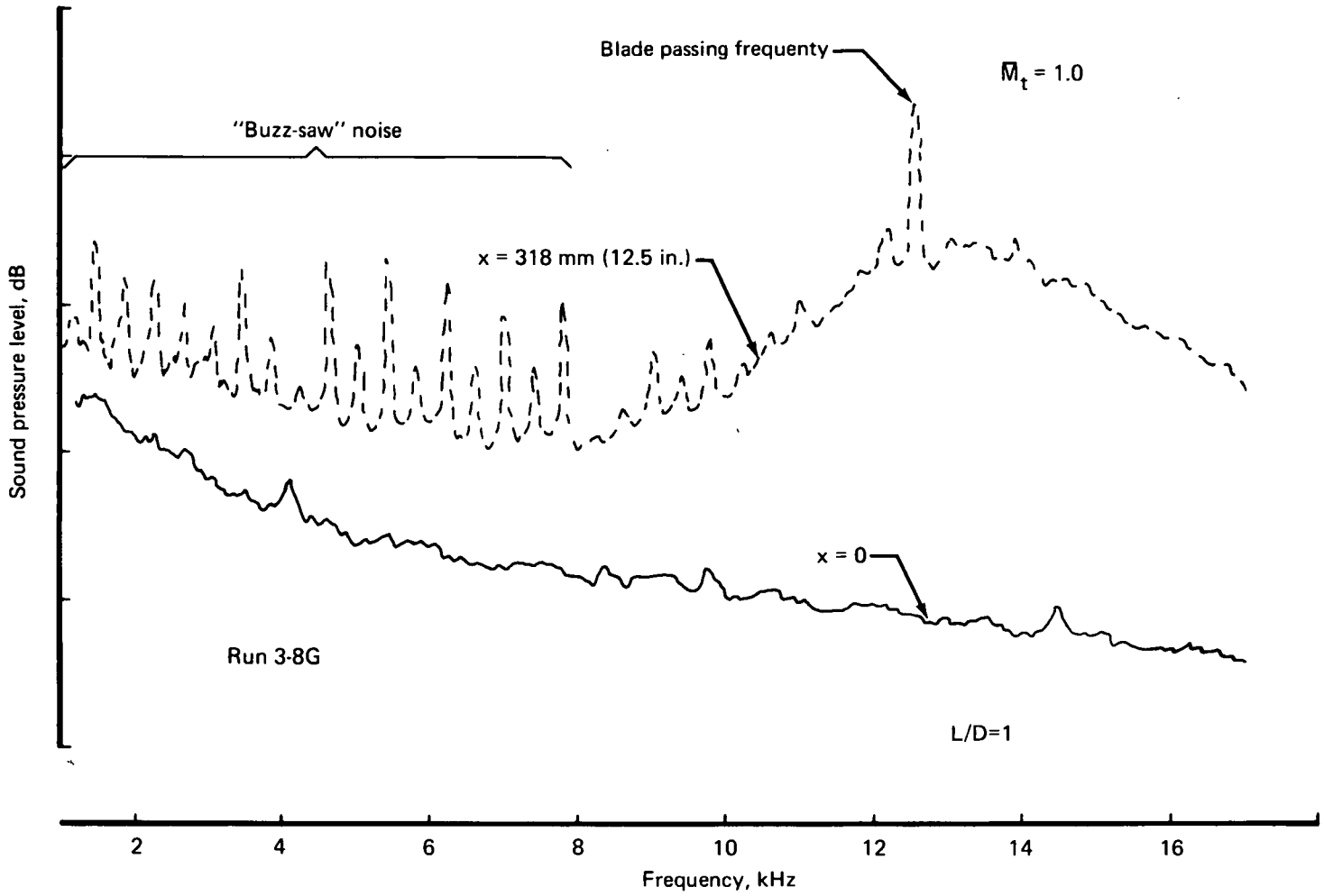

FIGURE 7.—NEAR FIELD, WALL KULITE, NOISE SPECTRA IN TAKEOFF INLET

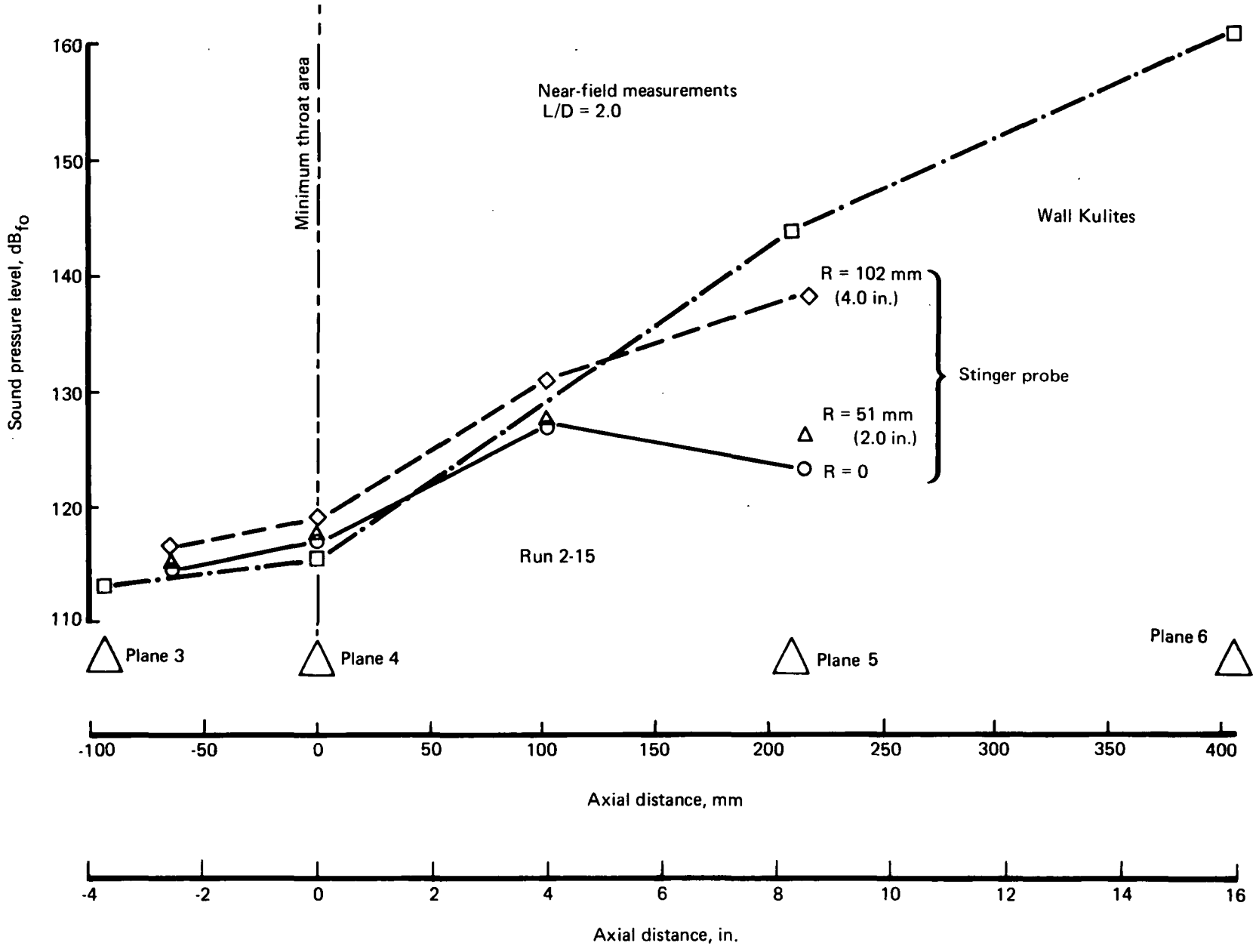

FIGURE 8.—BLADE PASSING TONE VERSUS AXIAL DISTANCE IN APPROACH INLET

1.0 INTRODUCTION

The very low noise objectives that are planned for Q-STOL aircraft result in propulsion systems designed in great part by noise requirements. High bypass engines, which are the most likely candidates for this group of airplanes, have significantly lower jet noise levels than inlet (compressor) noise levels. To obtain substantial noise reductions (25 PNdB), the sonic inlet might be an attractive concept (ref 1).

The acoustic principle of sonic inlets is straightforward. Sound waves, generated by the compressor fan, are attenuated while traveling upstream in high Mach number flow. The limiting case is when a sonic plane is generated in the inlet. In this case, theoretically, no pressure perturbations (sound waves) can travel through the sonic plane.

The aerodynamic principle of sonic inlets is also relatively simple. The flow entering the inlet is accelerated to produce a high velocity in the throat and then diffused to provide acceptable flow velocities at the fan face.

Sound attenuation which results from increasing the throat Mach number is very difficult to predict analytically. The state of the art has not progressed sufficiently that sound attenuation can be computed with the required accuracy in the immediate future. Therefore, it was decided to experimentally investigate the sonic inlet inside with a high-frequency-response microphone. This approach involves the following problems:

1. Placing a high-frequency-response probe in the flow field of the inlet causes a wake which generates pressure fluctuations (vortices) at the diaphragm of the probe.

2. The probe wake travels downstream and changes the flow field at the compressor rotor. This leads to some degree of change in noise generation by the rotor.

3. The pressure fluctuations measured by the probe cannot be readily identified as to whether they are acoustic or aerodynamic in origin.

4. Placing the probe in a high-subsonic-flow field results in shock wave patterns all around the stem.

Although these problems cannot be eliminated, they can be minimized by the measuring techniques applied.

This report describes a test and its results that was specifically designed for measuring noise and static pressure distribution in a near-sonic-flow environment.

2.0 DESCRIPTION OF TEST SETUP AND INSTRUMENTATION

2.1 TWELVE-INCH FAN RIG

The 305-mm (12-in.) fan rig consisted of a 32-bladed rotor mounted in a housing which contained a translating cone used for controlling the back pressure of the fan. Two rows of exit stators consisted of 27 blades per row. The leading edge of the first row of exit stators was located downstream at a distance equal to two true rotor chords. Fan face hub-to-tip ratio of the rotor was 0.35.

Drive power for the fan was provided by a turbodrive directly coupled to the fan shaft. Energy for the drive turbine was derived from plant air put through a combustion chamber prior to its introduction into the turbine nozzle.

2.2 INLETS

Two fundamental inlets, i.e., single-passage, with converging-diverging cowl wall, were built for this experiment:

1. One sized for approach, L/D = 2.0 (figs. 9 and 10)

2. One sized for takeoff, L/D = 1.0 (figs. 11 and 12)

The designations "approach" and "takeoff" refer to the area ratios between the throat and diffuser exit of each inlet. The area ratios for approach and takeoff were designed to be 0.59 and 0.76, respectively.

To make these inlets adaptable to static test conditions, the inlet lip near the highlight was modified to accommodate a standard 305-mm (12-in.) diameter bellmouth.

2.3 STINGER PROBE

The stinger probe was specifically designed to survey the near-field acoustics and static pressure distribution within the flowstream of the inlets (figs. 13 and 14). A high-frequency-response transducer, Kulite, 344 700 N/m^2 (50 psi), was mounted at the stinger. The wiring of the high-frequency transducer was led through a 622-mm (24.5-in.) long tapered tubing, having a diameter of 3 mm (1/8 in.) near the tip and 15 mm (5/8 in.) near the streamlined support strut. The static pressure was measured 26.75 mm (1.053 in.) upstream from the tip end of the stinger probe, by transmitting the

pneumatic signal to a 103 400-N/m^2 (15-psi) Statham transducer mounted externally to the streamlined support strut. The streamlined support strut was attached to an X-Y traversing mechanism (fig. 15), which was anchored to the floor. The maximum travel of the traversing mechanism in either X or Y direction was 305 mm (12 in.).

2.4 WALL MICROPHONES

In both inlets, four Kulite wall microphones were flush mounted on the inside of the inlet cowl. A schematic of a typical inlet with instrumentation planes is shown in figure 16.

The exact locations of the wall microphones, referenced from the throat plane (plane 4), are summarized below:

Plane number	Approach inlet (Run 2)	Takeoff inlet (Run 3)
3	-3.75 in. (-95.3 mm)	-2.50 in. (-63.5 mm)
4	0.0 in. (0.0 mm)	0.0 in. (0.0 mm)
5	8.25 in. (209.6 mm)	3.83 in. (97.3 mm)
6	19.71 in. (500.7 mm)	12.49 in. (317.2 mm)

The maximum rating of each high-frequency-response transducer wall microphone was 344 700 N/m^2 (50 psi).

2.5 ACOUSTIC INSTRUMENTATION

A schematic of the acoustic instrumentation is shown in figure 17. Two different routes of data recording, online and offline, are shown here.

Following is a list of electronic items used in the data reduction:

- Online
  - Bridge supply balance unit (Sigma-SC-610-S4)
  - Amplifier (Dana 3400)
  - Constant band frequency analyses (SD 101)

Tracking filter
AC-DC converter (Vidar model 326)
DC amplifier (EX-MOD 704)
Sweep oscillator (SD 104)
X-Y plotter (Autograf 2FR-A)

- Offline

  Bridge balance unit (Sigma-SC-610-S4)
  Amplifier (Dana 3400)
  Dynamic amplfier
  Preamplifier (Dynamic systems 7704)
  FM magnetic tape recorder (Ampex-FR-1800)

3.0 EXPERIMENTAL TECHNIQUE

Prior to the experiment, the high-frequency-response transducer was calibrated; the result is shown in appendix D. Test instrumentation is shown in figure 18. In addition to the transducer calibration, the noise floor was experimentally investigated (fig. 19) and was found to be about 80 dB. The pure sine waves, which are protruding through the noise floor, were artificially created with the aid of a tone generator. Each pure tone had an 82-dB level as compared with a standard B&K probe.

3.1 TESTING OF THE FUNDAMENTAL APPROACH INLET

The noise attenuation characteristic of the sonic inlet was measured at different throat Mach numbers (see sec. 4.1). The table below lists the six throat Mach numbers at which the inlet was surveyed.

Run	Fan rpm, N_1	Normalized throat average Mach number, $\bar{M}_t$
2-10	14 250	0.52
2-11	16 770	0.67
2-12	18 040	0.80
2-13	17 950	0.86
2-14	17 990	0.98
2-15	18 000	0.90

Run logs are shown in tables 1 through 6. At each power setting, the stinger probe was used to survey the inlet as follows:

1. The stinger probe was traversed radially from the inlet centerline to a radius of 102 mm (4.0 in.) at three axial locations, -66, 0, and 216 mm (-2.6, 0, and 8.5 in.) measured downstream from the inlet throat.

2. The stinger probe was traversed axially from -64 to 216 mm (-2.5 to 8.5 in.) downstream of the inlet throat at three radial positions, 0, 51, and 102 mm (0, 2.0, and 4.0 in.) from the inlet centerline.

Note: The travel time of the probe per inch in the axial and radial directions was 7.33 and 11.85 seconds, respectively.

The stinger probe microphone and the wall Kulite microphones were recorded simultaneously on magnetic FM tape.

During run 2-15 ($\bar{M}_t$ = 0.90) steady-state data were taken with the stinger probe positioned at -66, 0, 102, and 216 mm (-2.6, 0, 4.0 and 8.5 in.) downstream of the inlet throat at three radial positions and 0, 51, and 102 mm (0, 2.0, and 4.0 in.) from inlet centerline.

3.2 TESTING OF THE FUNDAMENTAL TAKEOFF INLET

The fundamental takeoff inlet was surveyed with the stinger probe at three power settings. Run logs are given in tables 7 through 9).

Run	Fan rpm, N_1	Normalized throat average Mach number, $\bar{M}_t$
3-6	22 010	0.72
3-7	23 050	0.86
3-8	23 650	1.00

For each test condition, near-field acoustic steady-state data were taken with the stinger probe at three axial locations, -64, 0, and 124 mm (-2.5, 0, and 4.9 in.) downstream from the throat for each of three radial positions, 0, 58, and 117 mm (0, 2.3, and 4.6 in.)from the inlet centerline.

The next step in the investigation was to traverse the stinger probe radially from 0 to 102 mm (0 to 4.0 in.) from the inlet centerline at the same axial locations as in the steady-state operation.

To complete the survey, axial traverses were made at three radii, 0, 58, and 117 mm (0, 2.3, and 4.6 in.).

TABLE 1.—RUN LOG, FUNDAMENTAL APPROACH INLET, L/D = 2.0, RUN 2-10

Power Setting

Corrected weight flow: 6.75 kg_m/sec (14.884 lb_m/sec)
Fan pressure ratio: 1.099
RPM: 14 250 (mechanical)

Run condition	Stinger, position		Refer to appendix
	X-direction mm (in.)	R-direction mm (in.)	
2-10A	66 (-2.6)	0	A and C
2-10B	0	0	A and C
2-10C	218 (8.6)	0	A and C
2-10D	0	Traverse	B
2-10E	102 (4.0)	Traverse	B
2-10F	218 (8.6)	Traverse	B
2-10G	Traverse	0	B
2-10H	Traverse	51 (2.0)	B
2-10I	Traverse	102 (4.0)	B

TABLE 2.—RUN LOG, FUNDAMENTAL APPROACH INLET, L/D = 2.0, RUN 2-11

Power Setting

Corrected weight flow: 7.97 kg_m/sec (17.560 lb_m/sec)
Fan pressure ratio: 1.147
RPM: 16 770 (mechanical)

Run condition	Stinger, position		Refer to appendix
	X-direction mm (in.)	R-direction mm (in.)	
2-11A	0	0	A and C
2-11B	0	Traverse	B
2-11C	102 (4.0)	Traverse	B
2-11D	216 (8.5)	Traverse	B
2-11E	Traverse	0	B
2-11F	Traverse	51 (2.0)	B
2-11G	Traverse	102 (4.0)	B

TABLE 3.–RUN LOG, FUNDAMENTAL APPROACH INLET, L/D = 2.0, RUN 2-12

Power Setting

Corrected weight flow: 8.60 kg_m/sec (18.966 lb_m/sec)
Fan pressure ratio: 1.170
RPM: 18 040 (mechanical)

Run condition	Stinger, position		Refer to appendix
	X-direction mm (in.)	R-direction mm (in.)	
2-12A	0	0	A and C
2-12B	0	Traverse	B
2-12C	102 (4.0)	Traverse	B
2-12D	216 (8.5)	Traverse	B
2-12E	Traverse	0	B
2-12F	Traverse	51 (2.0)	B
2-12G	Traverse	102 (4.0)	B

TABLE 4.—RUN LOG, FUNDAMENTAL APPROACH INLET, L/D = 2.0, RUN 2-13

Power Setting

Corrected weight flow: 8.80 kg_m/sec (19.395 lb_m/sec)
Fan pressure ratio: 1.157
RPM: 17 950 (mechanical)

Run condition	Stinger, position		Refer to appendix
	X-direction mm (in.)	R-direction mm (in.)	
2-13A	0	0	A and C
2-13B	0	Traverse	B
2-13C	102 (4.0)	Traverse	B
2-13D	216 (8.5)	Traverse	B
2-13E	Traverse	0	B
2-13F	Traverse	51 (2.0)	B
2-13G	Traverse	102 (4.0)	B

TABLE 5.–RUN LOG, FUNDAMENTAL APPROACH INLET, L/D = 2.0, RUN 2-14

Power Setting

Corrected weight flow: 8.95 kg_m/sec (19.721 lb_m/sec)
Fan pressure ratio: 1.145
RPM: 17 990 (mechanical)

Run condition	Stinger, position		Refer to appendix
	X-direction mm (in.)	R-direction mm (in.)	
2-14A	0	0	A and C
2-14B	0	Traverse	B
2-14C	102 (4.0)	Traverse	B
2-14D	216 (8.5)	Traverse	B
2-14E	Traverse	0	B
2-14F	Traverse	51 (2.0)	B
2-14G	Traverse	102 (4.0)	B

TABLE 6.—RUN LOG, FUNDAMENTAL APPROACH INLET, L/D = 2.0, RUN 2-15

Power Setting

Corrected weight flow: 8.80 kg_m/sec (19.404 lb_m/sec)
Fan pressure ratio: 1.152
RPM: 18 000 (mechanical)

Run condition	Stinger, position		Refer to appendix
	X-direction mm (in.)	R-direction mm (in.)	
2-15A	-66 (-2.6)	0	A and C
2-15B	-66 (-2.6)	51 (2.0)	
2-15C	-66 (-2.6)	102 (4.0)	
2-15D	0	102 (4.0)	
2-15E	0	51 (2.0)	
2-15F	0	0	
2-15G	102 (4.0)	0	
2-15H	102 (4.0)	51 (2.0)	
2-15I	102 (4.0)	102 (4.0)	
2-15J	216 (8.5)	102 (4.0)	
2-15K	216 (8.5)	51 (2.0)	
2-15L	216 (8.5)	0	A and C

TABLE 7.—RUN LOG, FUNDAMENTAL TAKEOFF INLET, L/D = 1.0, RUN 3-6

Power Setting

Corrected weight flow: 10.68 kg_m/sec (23.535 lb_m/sec)
Fan pressure ratio: 1.253
RPM: 22 010 (mechanical)

Run condition	Stinger, position		Refer to appendix
	X-direction mm (in.)	R-direction mm (in.)	
3-6B	Traverse	0	B
3-6C	Traverse	58 (2.3)	
3-6D	Traverse	117 (4.6)	
3-6E	124 (4.9)	Traverse	
3-6G	0	Traverse	
3-6H	-64 (-2.5)	Traverse	B
3-6I	-64 (-2.5)	0	A and C
3-6J	-64 (-2.5)	58 (2.3)	
3-6K	-64 (-2.5)	117 (4.6)	
3-6L	0	0	
3-6M	0	58 (2.3)	
3-6N	0	117 (4.6)	
3-6O	124 (4.9)	0	
3-6P	124 (4.9)	58 (2.3)	
3-6Q	124 (4.9)	117 (4.6)	A and C

TABLE 8.—RUN LOG, FUNDAMENTAL TAKEOFF INLET, L/D = 1.0, RUN 3-7

Power Setting

Corrected weight flow: 11.32 kg_m/sec (24.959 lb_m/sec)
Fan pressure ratio: 1.254
RPM: 23 050 (mechanical

Run condition	Stinger, position		Refer to appendix
	X-direction mm (in.)	R-direction mm (in.)	
3-7A	Traverse	0	B
3-7B	Traverse	58 (2.3)	
3-7C	Traverse	117 (4.6)	
3-7D	-64 (-2.5)	Traverse	
3-7E	153 (6.0)	Traverse	
3-7F	124 (4.9)	Traverse	B
3-7G	124 (4.9)	0	A and C
3-7H	124 (4.9)	58 (2.3)	
3-7I	124 (4.9)	117 (4.6)	
3-7J	0	117 (4.6)	
3-7K	0	58 (2.3)	
3-7L	0	0	
3-7M	-64 (-2.5)	0	
3-7N	-64 (-2.5)	58 (2.3)	
3-7O	-64 (-2.5)	117 (4.6)	A and C

TABLE 9.–RUN LOG, FUNDAMENTAL TAKEOFF INLET, L/D = 1.0, RUN 3-8

Power Setting

Corrected weight flow: 11.53 kg_m/sec (25.428 lb_m/sec)
Fan pressure ratio: 1.263
RPM: 23 640 (mechanical)

Run condition	Stinger, position		Refer to appendix
	X-direction mm (in.)	R-direction mm (in.)	
3-8A	Traverse	0	B
3-8B	Traverse	58 (2.3)	
3-8C	Traverse	117 (4.6)	
3-8D	-64 (-2.5)	Traverse	
3-8E	0	Traverse	
3-8F	124 (4.9)	Traverse	B
3-8G	124 (4.9)	0	A and C
3-8H	124 (4.9)	58 (2.3)	
3-8I	124 (4.9)	117 (4.6)	
3-8J	0	117 (4.6)	
3-8K	0	58 (2.3)	
3-8L	0	0	
3-8M	-64 (-2.5)	0	
3-8N	-64 (-2.5)	58 (2.3)	
3-8O	-64 (-2.5)	117 (4.6)	A and C

4.0 DATA REDUCTION

4.1 AERODYNAMIC DATA REDUCTION

An important aerodynamic parameter in this test was the normalized throat average Mach number. To obtain accurate measurements of the throat average Mach number, special attention was paid to the mass flow measurement through the inlet. Prior to the test with the stinger probe, the total pressure profiles in the straight section of the bellmouth inlet were determined and calibrated versus the static pressure at the same station. Then the highest obtainable weight flow was determined (inlet choked). The Mach number for the choked condition was defined as one. Based on the percentage flow, A/A* values were calculated for all lower weight flow settings. These A/A* values were finally used to determine the normalized throat average Mach number for all test conditions.

4.2 ACOUSTIC DATA REDUCTION

Online Data Reduction

Online data reduction was done while the stinger probe was traversing in the inlet. A schematic of the instrumentation for online data reduction is shown in figure 17. To display the blade passing tone as a function of radial or axial position, the output signal of the stinger probe transducer was fed together with the output of either the radial or axial traversing mechanism into an X-Y plotter.

The center frequency of the 50-cycle constant bandwidth filter was locked into the blade passing frequency of the fan rotor to ensure proper centering on the blade passing tone.

In addition to the blade passing tone, the static pressure was reduced on line. The output signal of the static pressure transducer and the output of the X-Y traversing mechanism were fed directly into the plotting machine.

Note: The damping factor selector on the X-Y plotter was 10 times higher during online data reduction of run 3 than of run 2. A low damping factor results in a more irregular trace than a high damping factor, but the mean line of the blade passing tone does not alter.

Offline Data Reduction

Each output signal of the transducers, such as rpm and X-Y traversing mechanism, was FM recorded on magnetic tape to provide a permanent record of each measurement for offline data reduction at a more convenient time.

Steady-state data were frequency analyzed with a 40-cycle, constant-bandwidth filter. The 40-cycle, narrow-band analyzer consisted of a bank of 500 filters covering a frequency range from 20 to 20 000 cycles per second. The sampling time was chosen as 32 seconds. To increase the dynamic range of the noise spectrum at the higher frequencies, a high-bypass filter of 1000 cycles was used.

5.0 PRESENTATION OF DATA

The near-field acoustic data are presented for the fundamental approach inlet in figures 20 through 39 and for the fundamental takeoff inlet in figures 40 through 53.

All steady-state data taken in the two inlets are presented in appendix A and traverse data in appendix B. The free-stream static pressure time histories for a select number of test conditions are presented in appendix C.

6.0 RESULTS AND DISCUSSION

6.1 FUNDAMENTAL APPROACH INLET

The blade passing tone versus axial distance is shown for three normalized throat Mach numbers, 0.67, 0.86, and 0.98 in figures 20 through 22.

The data were taken on line with the stinger probe traversing axially along a constant radius, while the acoustic signal was filtered through a 50-cycle bandwidth filter which was locked onto the blade passing frequency. The data points on each of these figures were sampled over a 26-mm (1-in.) travel time of the stinger probe. The main trend in each of these figures was the different rate of decay at the outer- and inner radii. The outer radius showed a steeper decay than the inner radius. This trend tends to be related to the local Mach number, especially in the throat area. By plotting the same data in a different way (figs. 23 through 25), the effect of Mach number on the blade passing tone can be better illustrated. Each of the three figures presents the blade passing tone level with respect to level at 102 mm (4.0 in.) downstream of the throat versus axial distance. The rate of decay of the blade passing showed a strong dependency on the throat Mach number at each radius tested.

The radial blade passing tone distribution was surveyed by traversing the stinger probe along a radial line at three axial stations in the inlet. The results of this survey are shown in figures 26 through 28 for three different throat Mach numbers, 0.67, 0.86, and 0.98. Here again the blade passing tone was filtered by a 50-cycle bandwidth filter; the sampling time was every half inch travel time of the stinger probe. Each of these figures showed a stronger radial variation of the blade passing tone near the fan face (X = 218 mm (8.5 in.)) than in the throat plane (X = 0).

Figure 29 shows the test results of steady-state measurements of the blade passing tone along the centerline versus the normalized throat Mach number. The data were filtered by a 40-cycle bandwidth filter and time average over 32 seconds. Again, increasing the throat Mach number resulted in decreasing levels of the blade passing tone. Of interest here was that the blade passing tone changed its character from tone noise into broadband noise while the throat Mach number increased from low subsonic to high subsonic velocity.

Another step in the data analysis of the approach inlet was to compare frequency spectra taken at steady-state conditions and different axial locations in the inlet. This was done at a fan speed of 18 000 rpm, which corresponded with a normalized throat Mach number of 0.90. The frequency spectra are shown in figures 30 through 32 for three radii, 0, 51, and 102 mm (0, 2.0, and 4.0 in.). Figure 30 shows the blade passing tone at 9600 Hz dominating over the broadband noise at an axial location 218 mm (8.6 in.) downstream from the inlet throat. In the throat (X = 0), the spectrum did

not show a pure tone at blade passing frequency, but a broadband type of noise. Further, no significant noise generation by the sonic plane was observed when comparing the sound pressure levels at 0 and -66 mm (0 and -2.6 in.) downstream from the inlet throat. The same trends were found at the other two radii tested (figs. 31 and 32).

The radial distribution of the blade passing tone in the inlet is shown in figure 33. The power setting was the same as above, namely 18 000 rpm. This figure shows two things very clearly: one, the strong radial variation of the blade passing tone near the fan face (X = 216 mm (8.5 in.) downstream from the throat plane) as compared to radial variation in the throat; and two, the change in character of the blade passing tone from tone noise to broadband noise (open and closed symbols, fig. 33) going from fan face to throat plane.

Until this time, no systematic data had been taken to analyze the behavior of sound along the cowl wall in a sonic inlet operating at different throat Mach numbers. This was because the stinger probe could not traverse or set near the cowl of the inlet due to construction of stinger probe itself. Therefore, Kulite microphones were placed flush with the cowl surface at four fixed locations in the inlet (for exact locations see sec. 2.4). The main problem was to make sure that the source (fan) did not change significantly in level for the different throat Mach numbers. It was found that by taking throat Mach numbers above 0.80 the levels at all frequencies did not vary near the source (fig. 34). Therefore, comparisons could be made. The noise spectra measured at 8.3 in. downstream from the inlet throat did not show much difference in sound pressure levels (fig 35). However, measurements both in the throat and at 97 mm (-3.8 in.) downstream from the throat clearly showed a Mach number dependency over the whole frequency range (figs. 36 and 37).

The blade passing tone as measured with the wall Kulite microphone near the fan face did change from the lower to the higher power setting, as shown in figure 38. It is interesting to note that the rate of attenuation changed remarkably at a throat Mach number of 0.86. The reason for this behavior was the change in character of the blade passing tone above and below a throat Mach number of 0.86 in the throat plane. Below a throat Mach number of 0.86 the blade passing tone was present as tone noise, but above 0.86 it was obscured by the broadband noise. Attenuation in the above figures is defined as the difference in blade passing tone at the fan face and the throat plane.

To investigate the noise leakage through the boundary layer, steady-state data with the stinger probe and the wall Kulite probes were taken. The results, presented in figure 39, indicated no noise leakage in the throat.

6.2 FUNDAMENTAL TAKEOFF INLET

Figures 40 through 42 show 40-Hz noise spectra taken at different power settings. Each figure represents a different axial plane in the inlet. When the stinger probe was located on the centerline of the inlet at 124 mm (4.9 in.) downstream of the inlet throat, the sound pressure level increased with increasing throat Mach number. This difference in level was caused by the increased fan speed (22 010 to 23 650 rpm) to obtain the desired throat Mach number. Increasing the throat Mach number showed a decreasing sound pressure level at the two other axial locations, 0 and 64 mm (0 and 2.5 in.) upstream from the throat plane (figs. 41 and 42).

Near-field noise spectra, taken with the stinger probe on the centerline, were compared at three axial locations, 124, 0, and -64 mm (4.9, 0, -2.5 in.) downstream from the inlet throat. The results are presented in figures 43 and 44 for normalized throat Mach numbers of 0.72 and 1.00, respectively. The sound pressure level above 8000 Hz was found to be the same at each of the three axial stations for the throat Mach number of 0.72 (fig. 43). However, below 8000 Hz the sound pressure level was higher at 102 mm (4.0 in.) downstream of the throat than at the throat. The same trend was found at a throat Mach number of 1.00, except that the frequency limit had shifted from 8000 Hz up to 16 000 Hz. It is believed that the probe reading was affected by vibrations of the fan spinner. Further, no significant noise generation by the sonic plane was observed when comparing the sound pressure levels at 0 and -66 mm (0 and -2.6 in.) downstream from the inlet throat (fig. 44).

The near-field noise spectra were also compared at different radii and axial stations. These results are shown in figures 44 through 46 for a normalized throat Mach number of 1.00. At each of the three radii investigated, the sound pressure level near the fan face, at 124 mm (4.9 in.) downstream from inlet throat, was higher than at the throat. It is interesting to note further that at the outer radius, the "buzz-saw" noise did not propagate to the other two stations (fig. 46).

The near-field spectra taken at 124 mm (4.9 in.) downstream from the inlet throat and at 0, 58, and 117 mm (0, 2.3, and 4.6 in.) radii were compared at a normalized throat Mach number of 1.00 in the inlet (fig. 47). The data showed that "buzz-saw" noise was present at a radius of 117 mm (4.6 in.). The next radius tested showed little "buzz-saw" noise, and the centerline none. This is to be expected, because "buzz-saw" noise can only be generated at fan blade speeds above the sonic velocity. The power setting at this data point was high enough so that the rotor blades at the outer radius were above sonic velocities while near the hub the velocities were subsonic.

The blade passing tone has been plotted versus radius at each of the axial stations, 124, 0, and -64 mm (4.9, 0, and -2.5 in.) downstream from the inlet throat. The results are shown for three normalized throat Mach numbers tested, namely 0.76, 0.86, and 1.00, in figures 48 and 49. A strong radial gradient of the blade passing tone was observed at a station 124 mm (4.9 in.) from the inlet

throat. This was attributed to the compressor rotor relative velocity gradient. The radial gradient of the blade passing tone in the throat plane was much less than near the fan face. The attenuation which took place between the stations near the fan face and the throat was found to be greater at the outer radius than on the inlet centerline. This was attributed to the strong radial Mach number gradient in the throat area. In addition to the change in gradient of the blade passing tone, the nature of the fan tone changed from pure tone (open symbols in the figures) to a tone obscured by broadband noise (closed symbols in the figures).

Near field, wall Kulite spectra taken at two power settings on the compressor fan are presented in figures 50 and 51. Each figure shows two spectra taken at two axial locations, 0 and 318 mm (0 and 12.5 in.) downstream from the inlet throat. The data taken at a normalized throat Mach number of 0.72 (fig. 50) showed strong attenuation of blade passing tone and "buzz-saw" noise but very little in broadband noise. The attenuation at a normalized throat Mach number ($\bar{M}_t = 1.0$) showed both a strong attenuation of blade passing tone and "buzz-saw" noise as well as broadband noise (fig. 51).

Figure 52 presents a summary of the blade passing tone measured near the fan face with the wall Kulite microphone at each throat Mach number tested. The data showed a decreasing blade passing tone with normalized throat Mach number. In addition to the blade passing tone, the attenuation was plotted versus throat Mach number. Here too, as was the case with the approach inlet, the rate of attenuation of the blade passing tone changed above a normalized throat Mach number of 0.86. The reason was that the blade passing tone character changed from a pure tone into a tone obscured by broadband noise.

The last step in the analysis of the near-field data was to plot all steady-state stinger probe data versus normalized throat Mach number. The results, presented in figure 53, show that increasing the throat Mach number resulted in lower blade passing tone levels. Maximum attenuation of the blade passing tone took place at the outer radius.

7.0 CONCLUSIONS

The conclusions derived from the internal noise field survey in the two sonic inlets are summarized below:

1. Increasing the inlet throat Mach number, from about 0.5 to 1.0, resulted in an increasing noise attenuation at blade passing frequency (figs. 38 and 52).

2. The rate of decay of the blade passing tone was found to be less on the centerline than near the outer wall. This was attributed to the radial Mach number gradient in the throat area. (figs. 20 through 22 and 53).

3. No significant noise generation by the sonic plane was observed (figs. 30 and 44).

4. "Buzz-saw" noise, which was only observed at a power setting above 22 000 rpm, did not propagate through the inlet throat plane. This power setting could only be reached with the fundamental inlet sized for takeoff (figs. 46, 50, and 51).

5. No evidence was found of noise leakage at blade passing frequency through the inlet throat boundary layer (fig. 39).

The test results of this experiment will serve in the understanding of sound propagation in sonic inlets and in the selection of sonic inlet concepts.

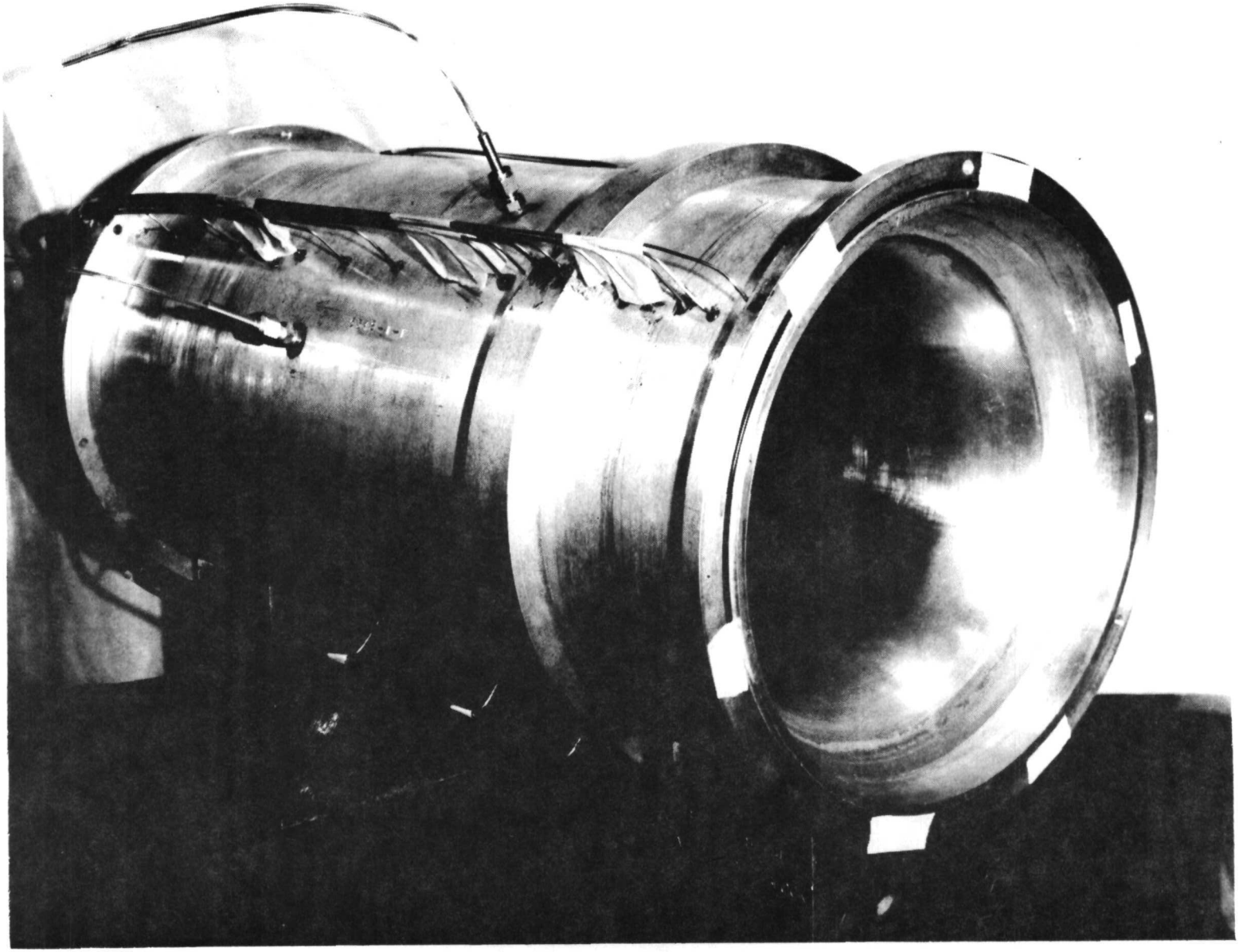

FIGURE 9.–FUNDAMENTAL INLET SIZED FOR APPROACH

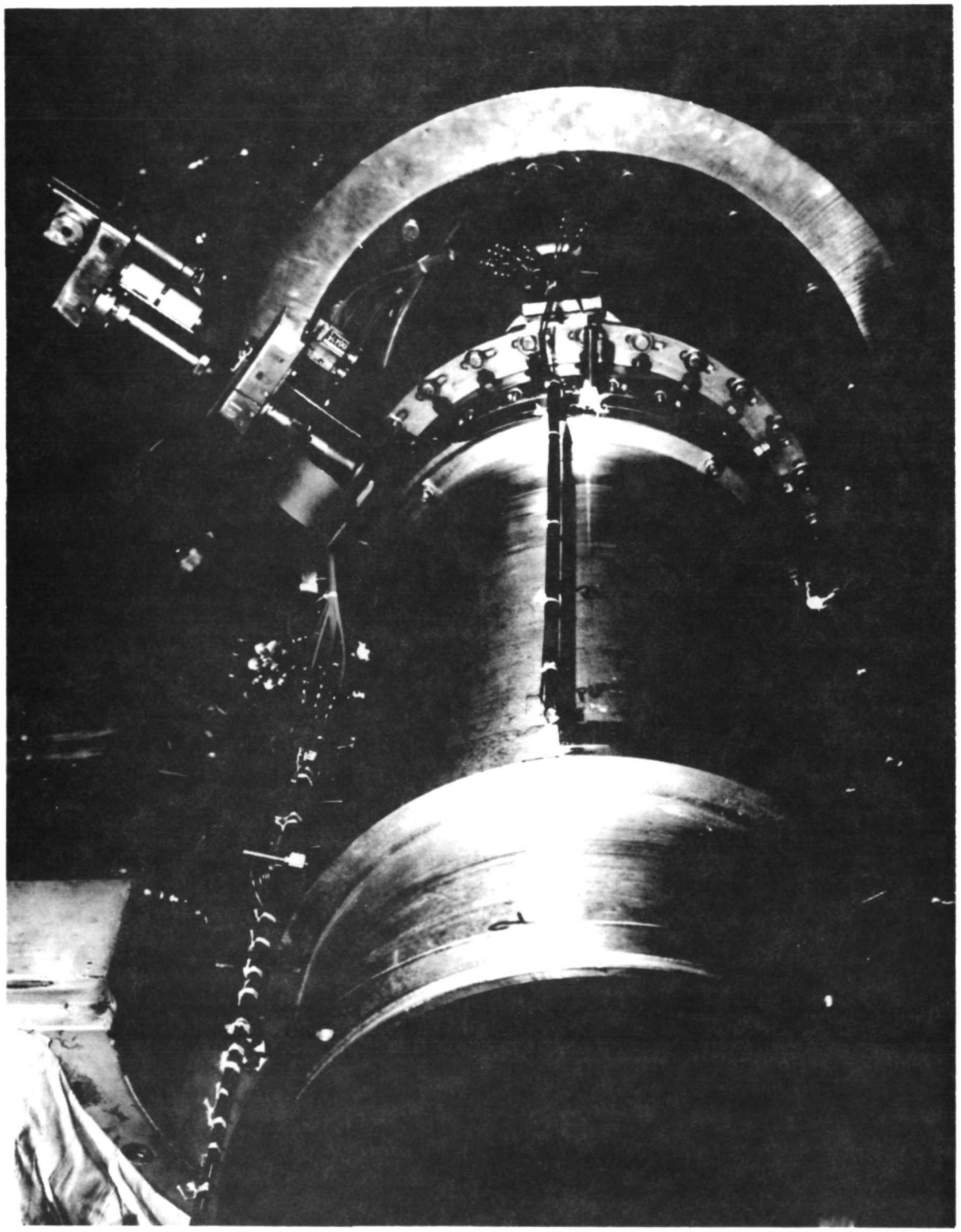

FIGURE 10.—FUNDAMENTAL INLET SIZED FOR APPROACH (INSTALLED)

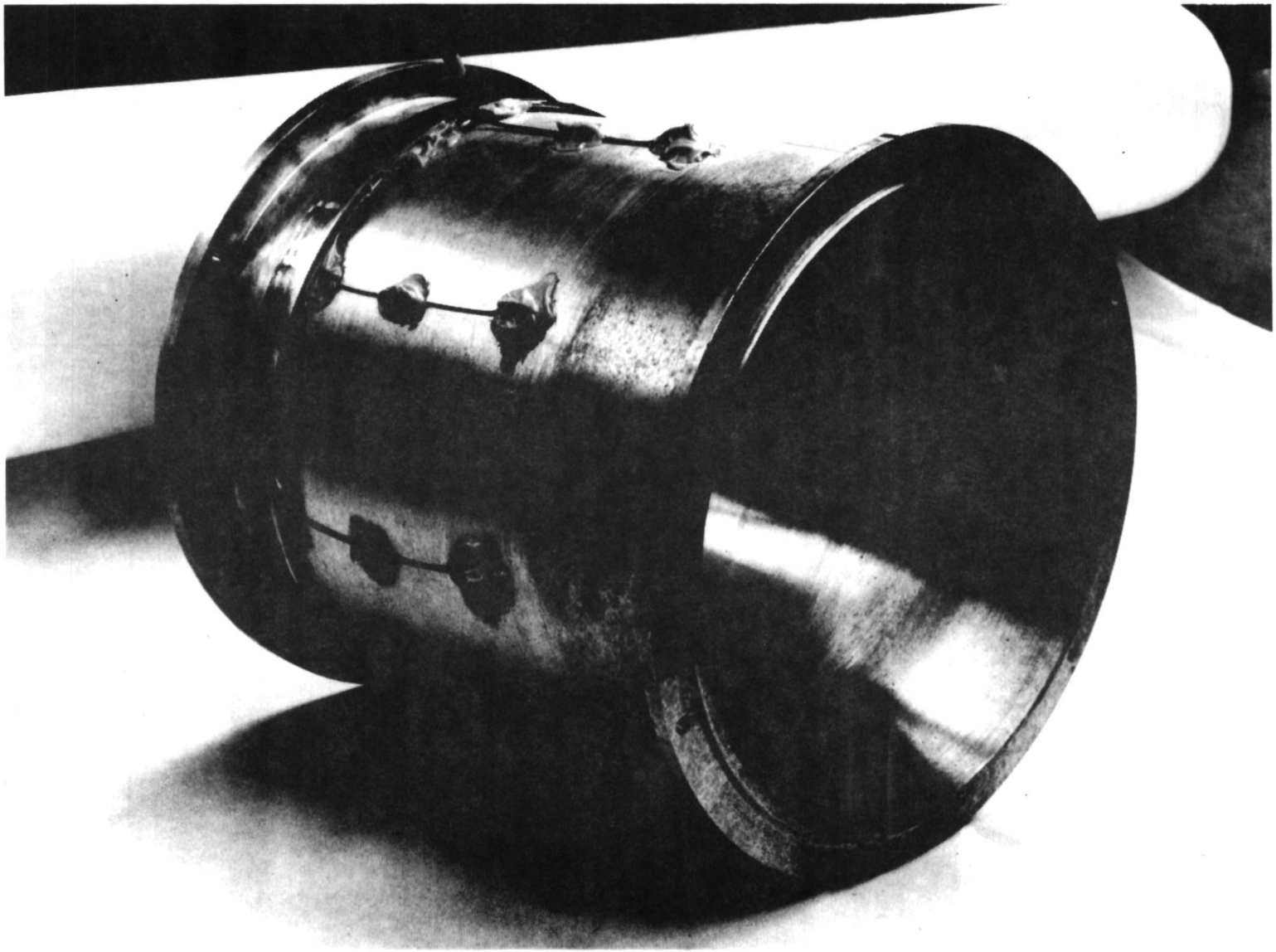

FIGURE 11.—INLET SIZED FOR TAKEOFF, SIDE VIEW

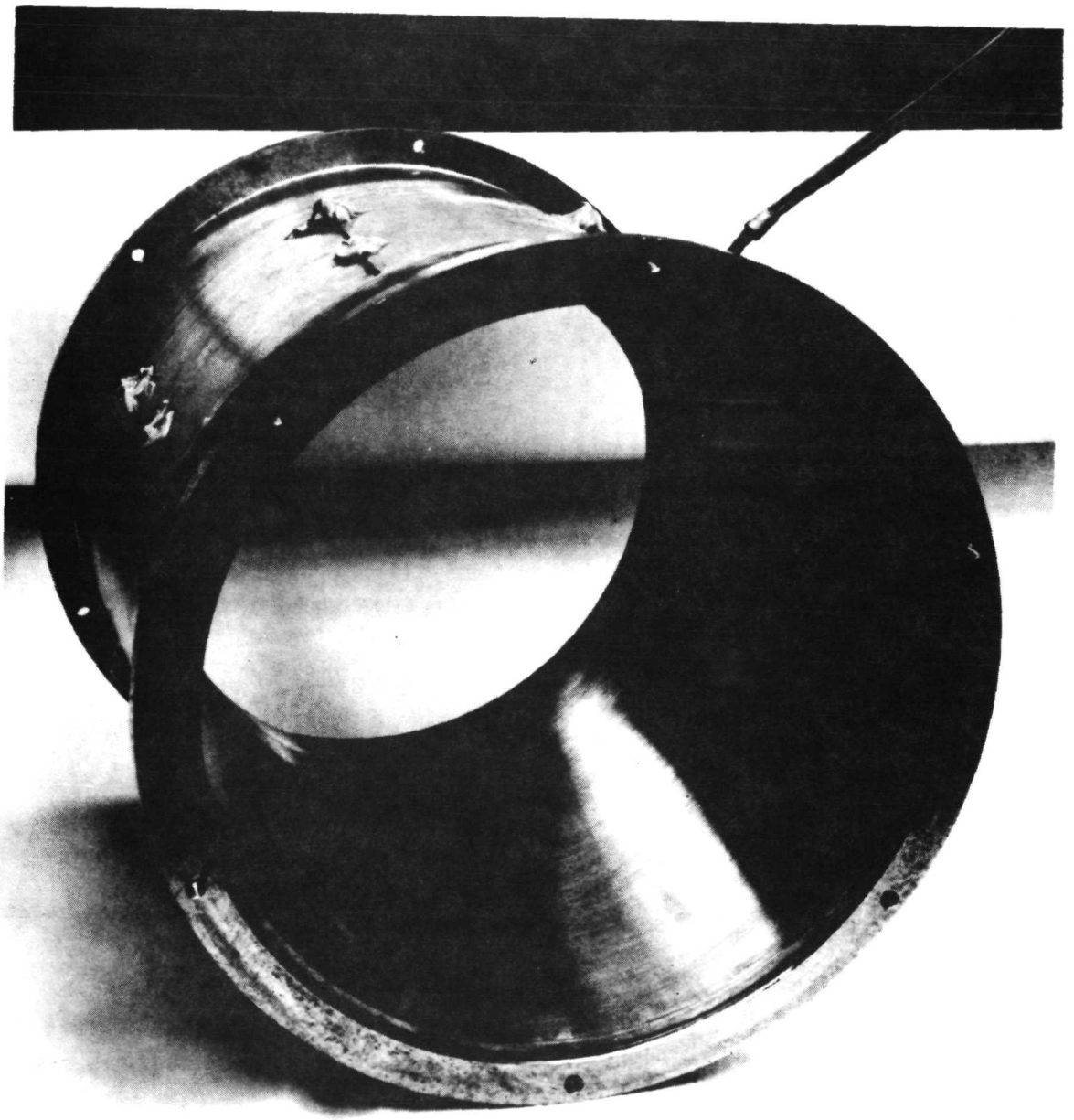

FIGURE 12.–INLET SIZED FOR TAKEOFF, FRONT VIEW

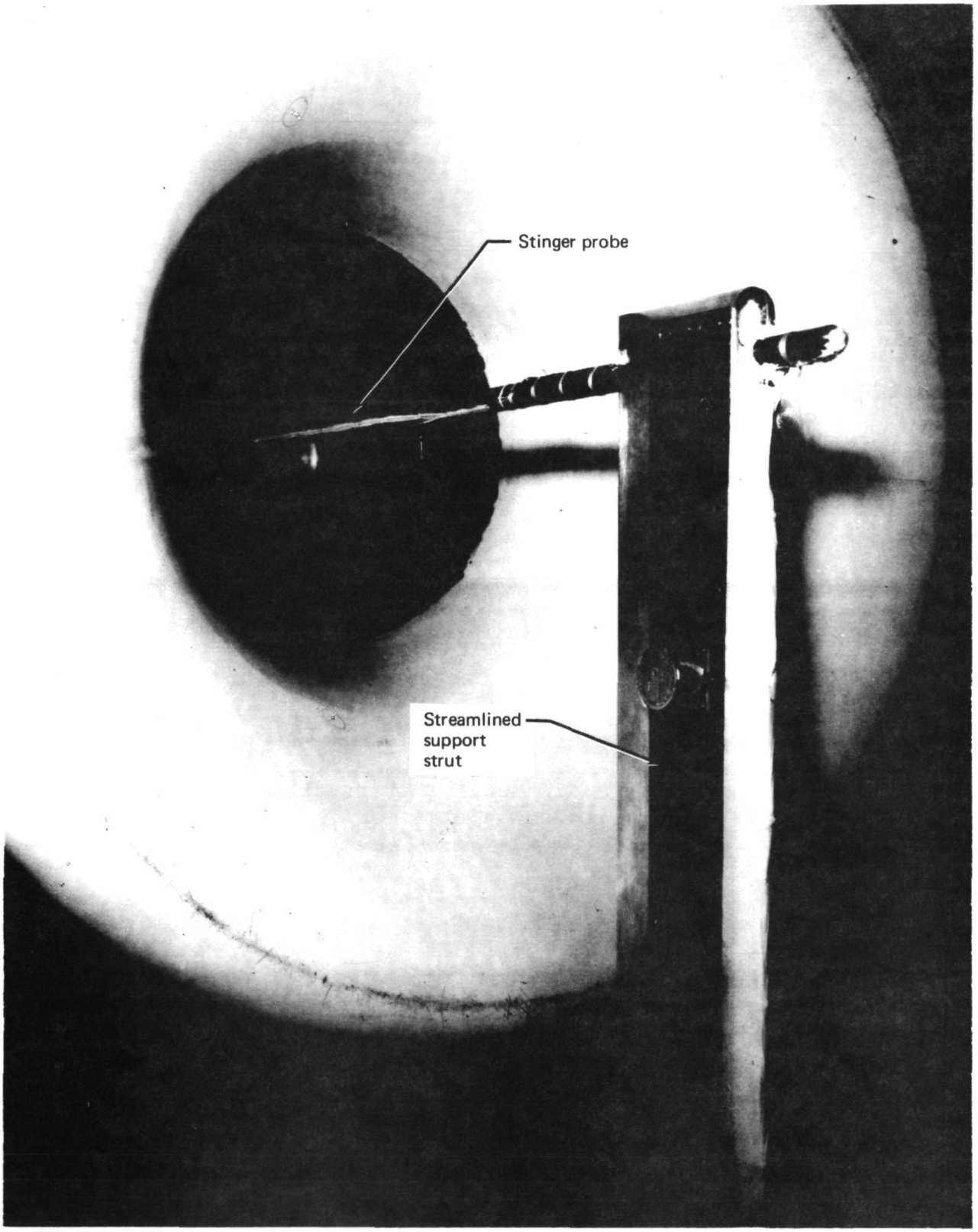

FIGURE 13.—STINGER PROBE

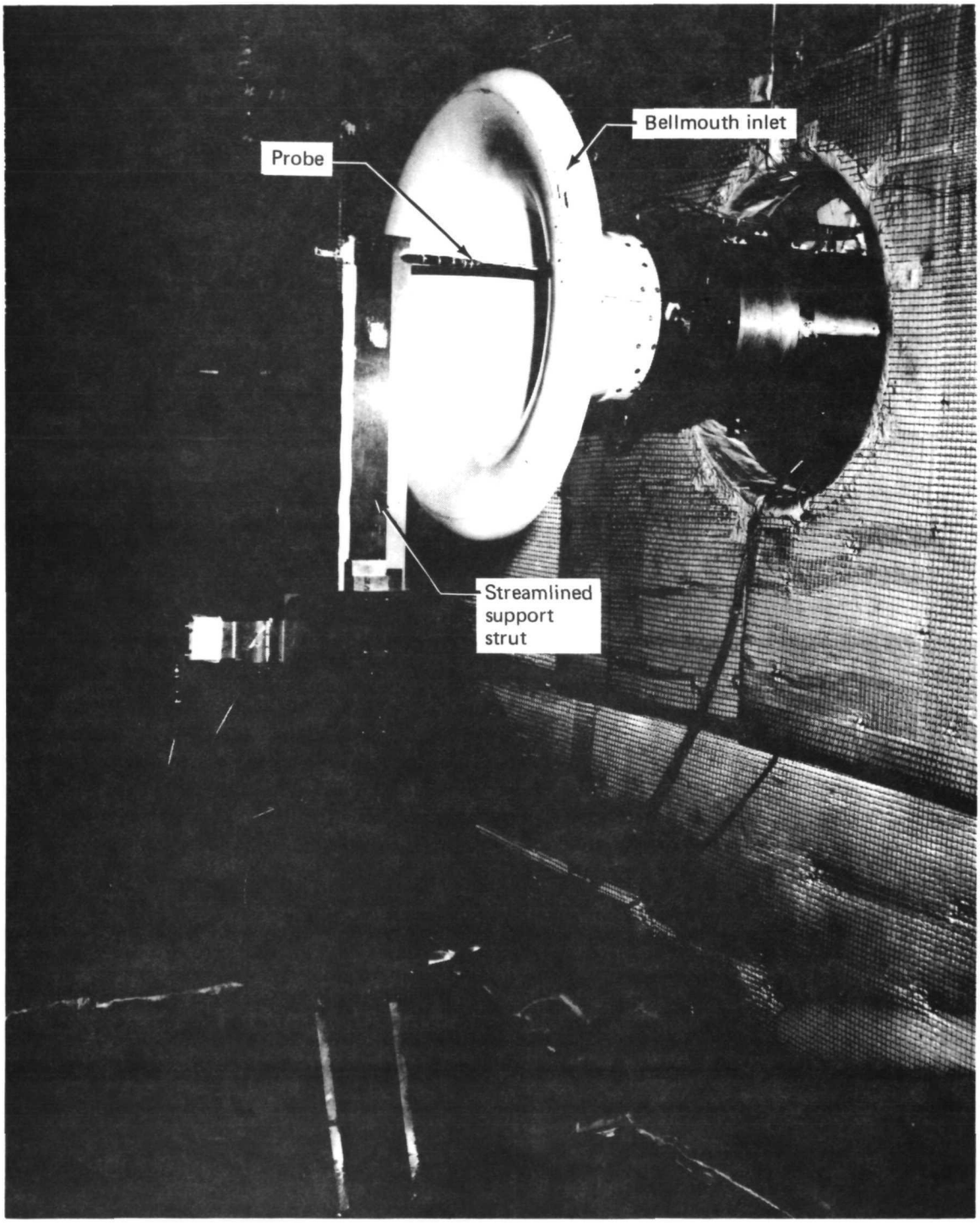

FIGURE 14.—STINGER PROBE INSTALLATION

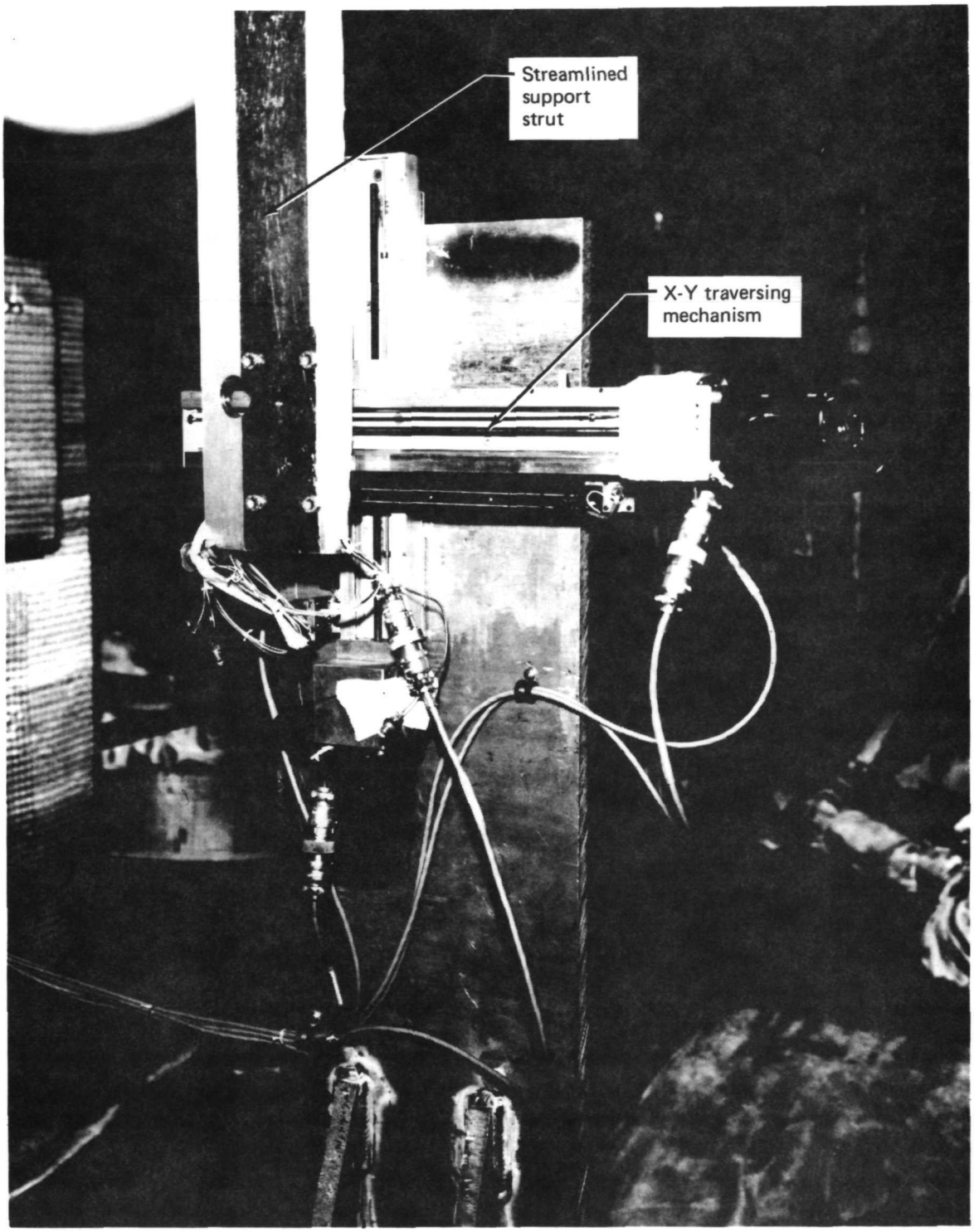

FIGURE 15.—STINGER PROBE, X-Y TRAVERSING MECHANISM

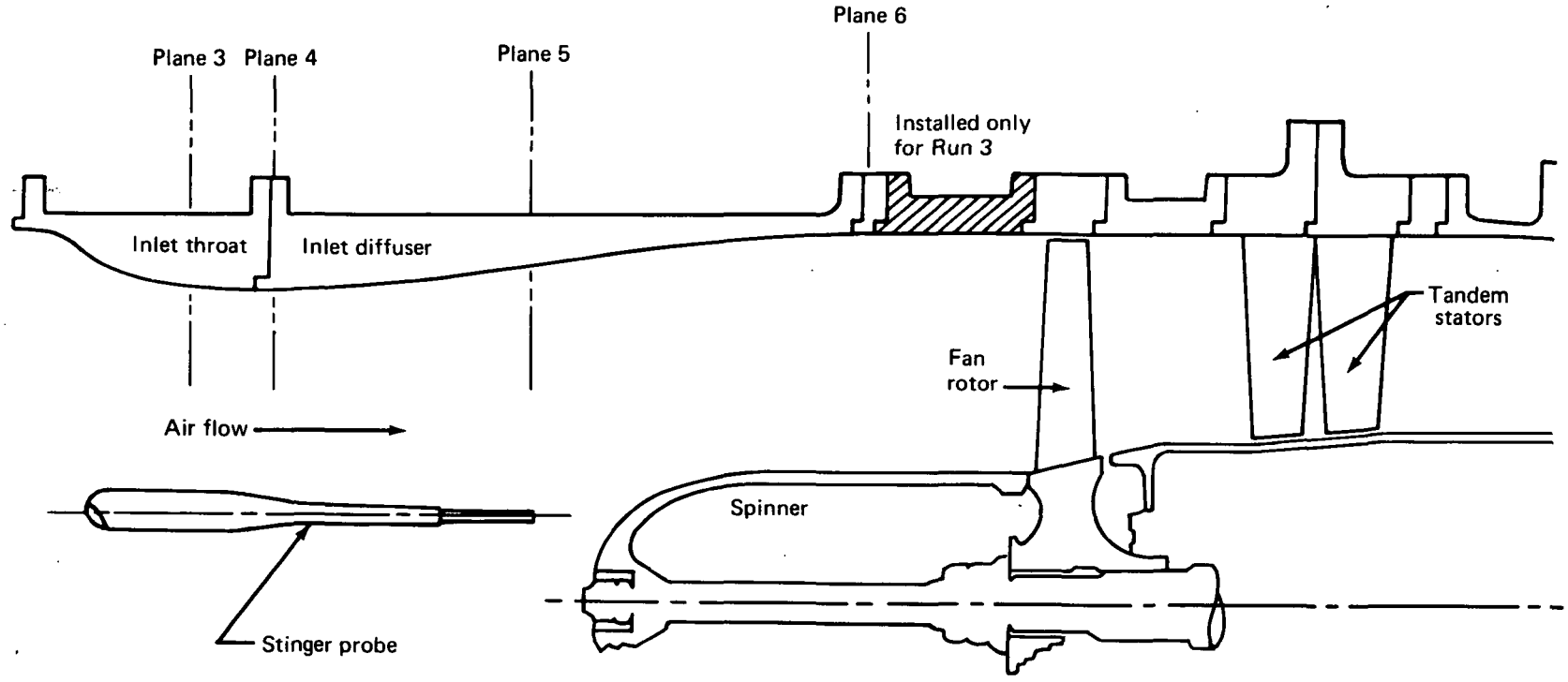

Note: Wall microphones are installed at planes 3, 4, 5, and 6. The exact plane locations are given in section 2.4.

FIGURE 16.—SCHEMATIC OF 305-MM (12-IN.) FAN WITH SONIC INLET

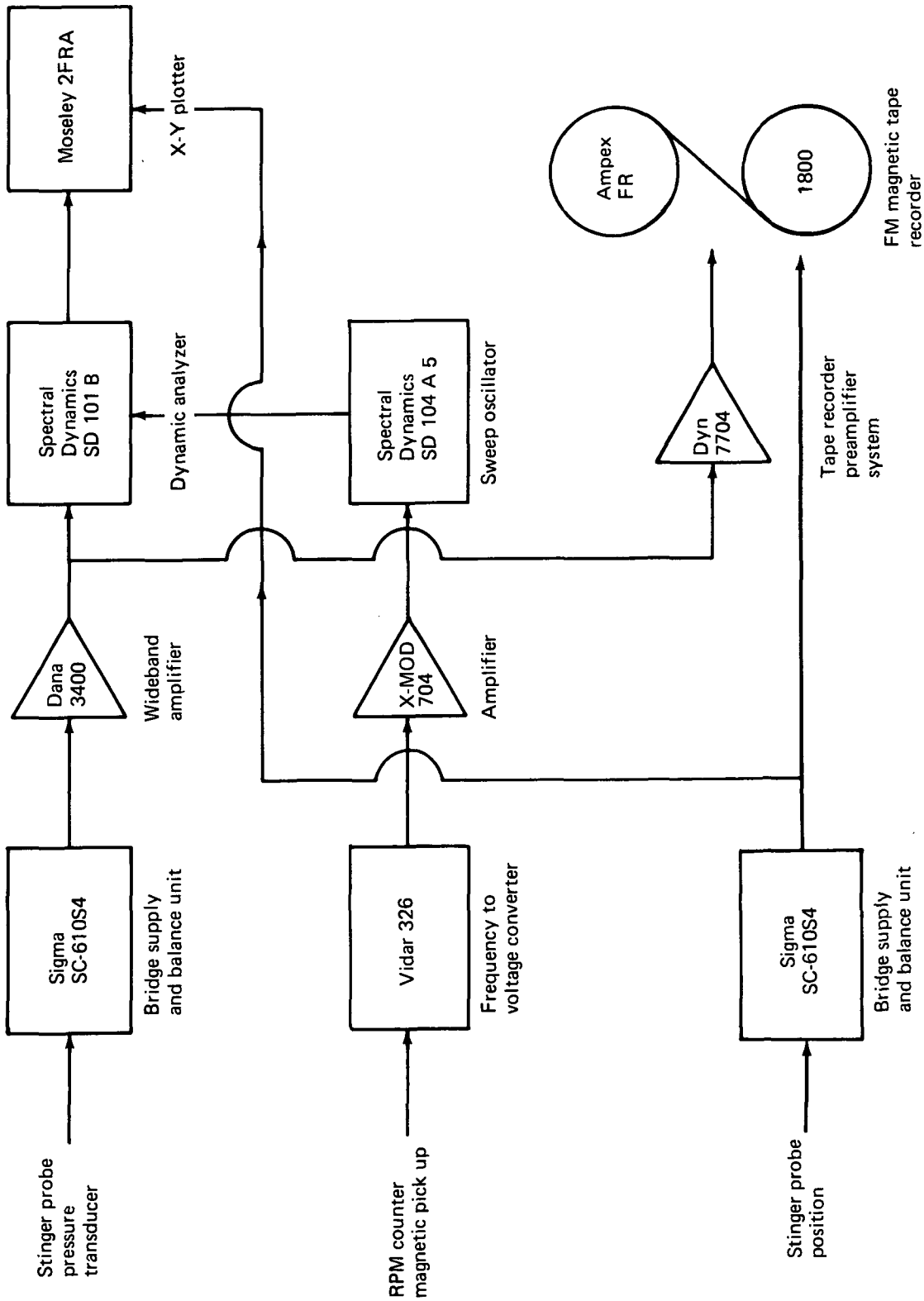

FIGURE 17.–BLOCK DIAGRAM, ACOUSTIC DATA RECORDING

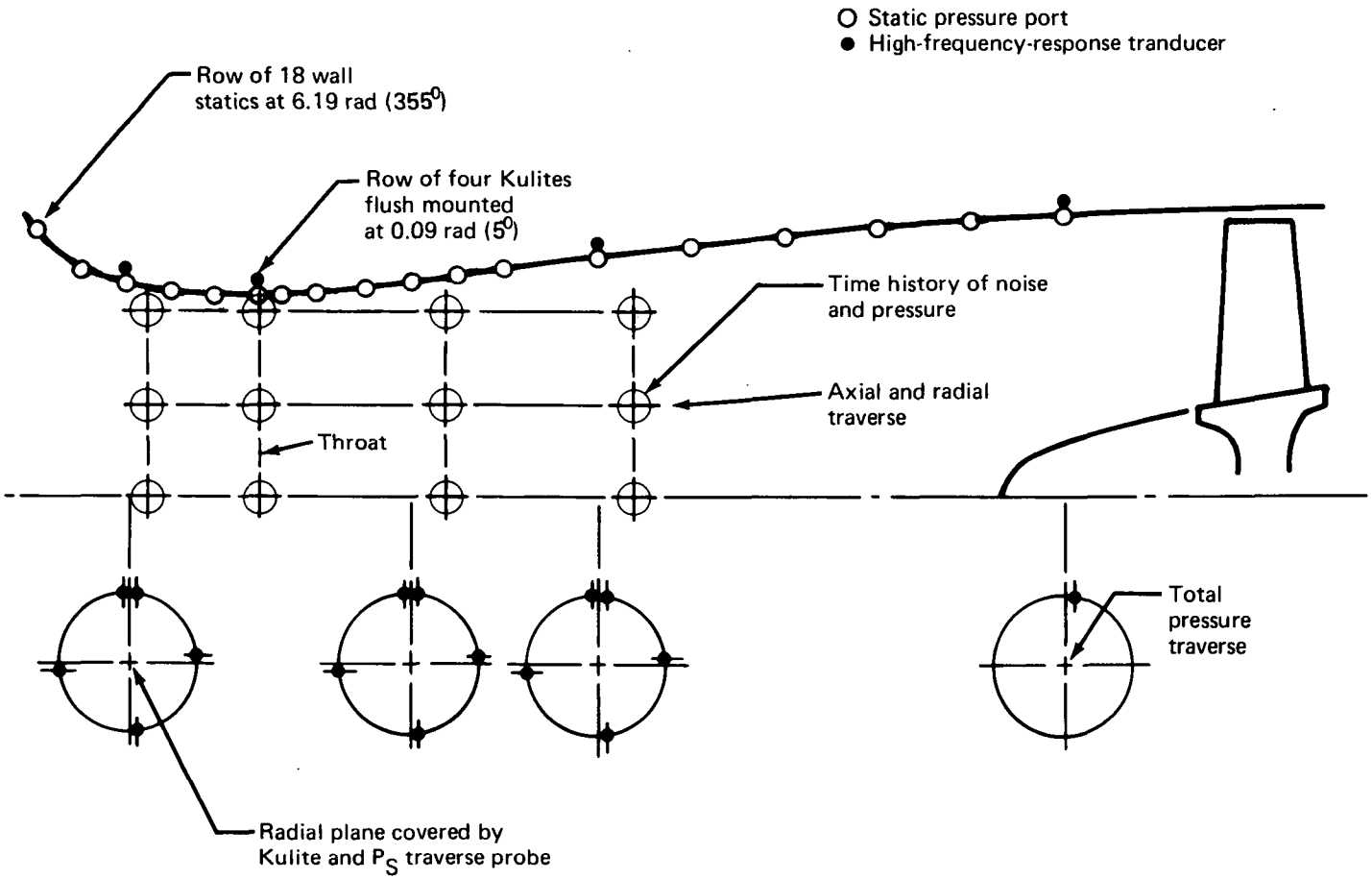

Note: Wall Kulite microphone locations are given in section 2.4

FIGURE 18.—TEST INSTRUMENTATION

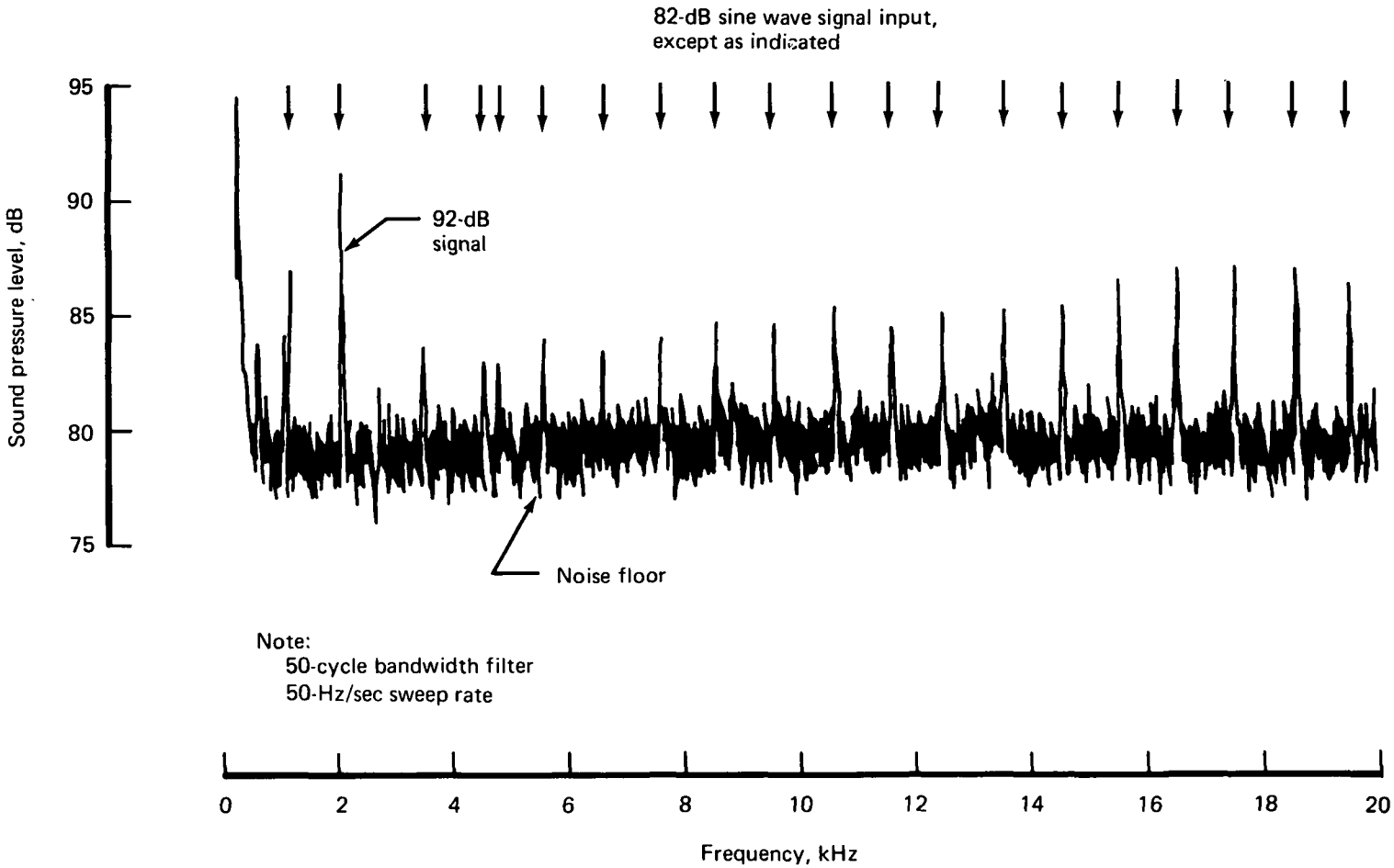

FIGURE 19.–NOISE FLOOR OF KULITE MICROPHONE AT ZERO FLOW VELOCITY

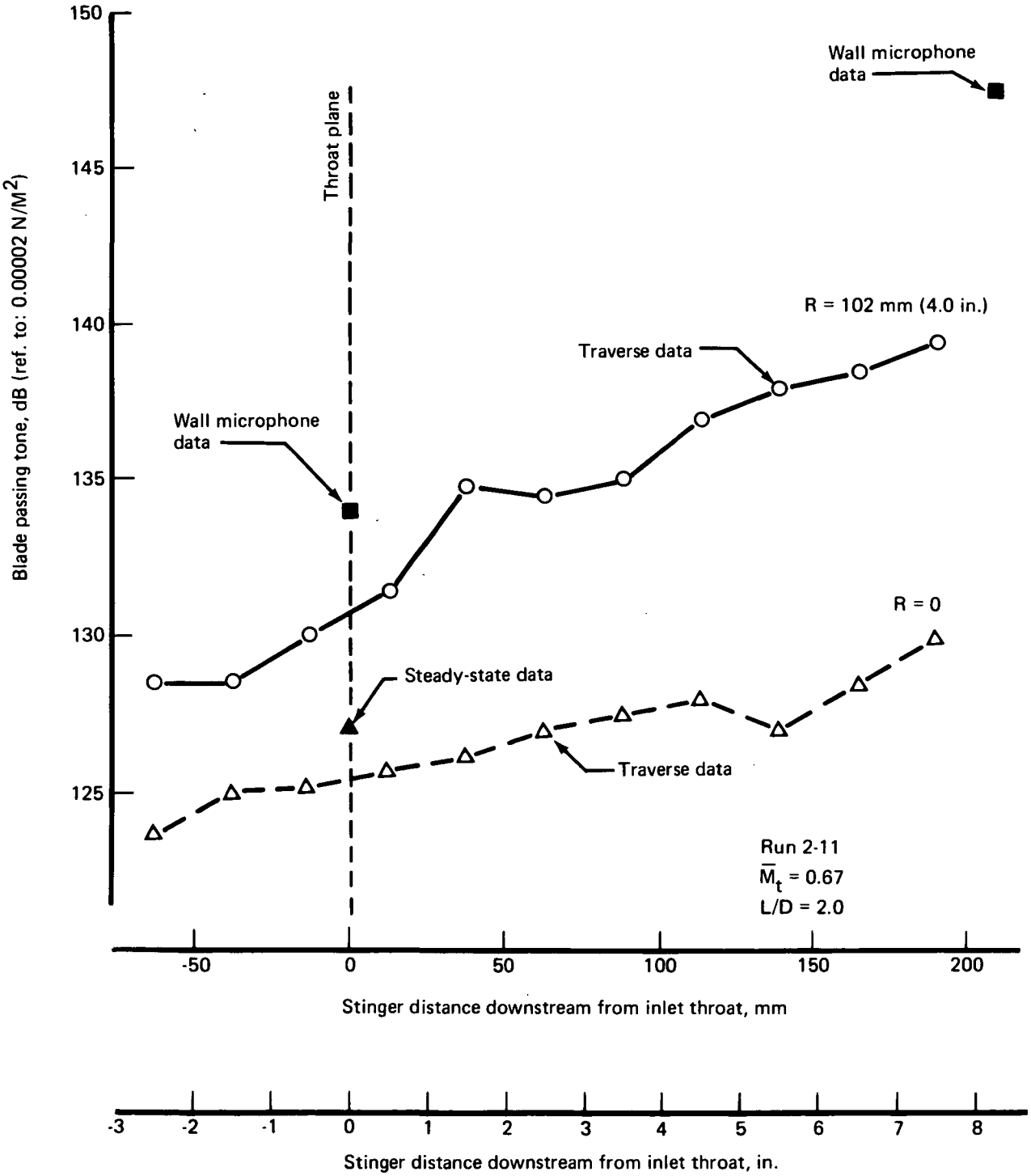

FIGURE 20.–AXIAL DISTRIBUTION OF BLADE PASSING TONE IN APPROACH INLET

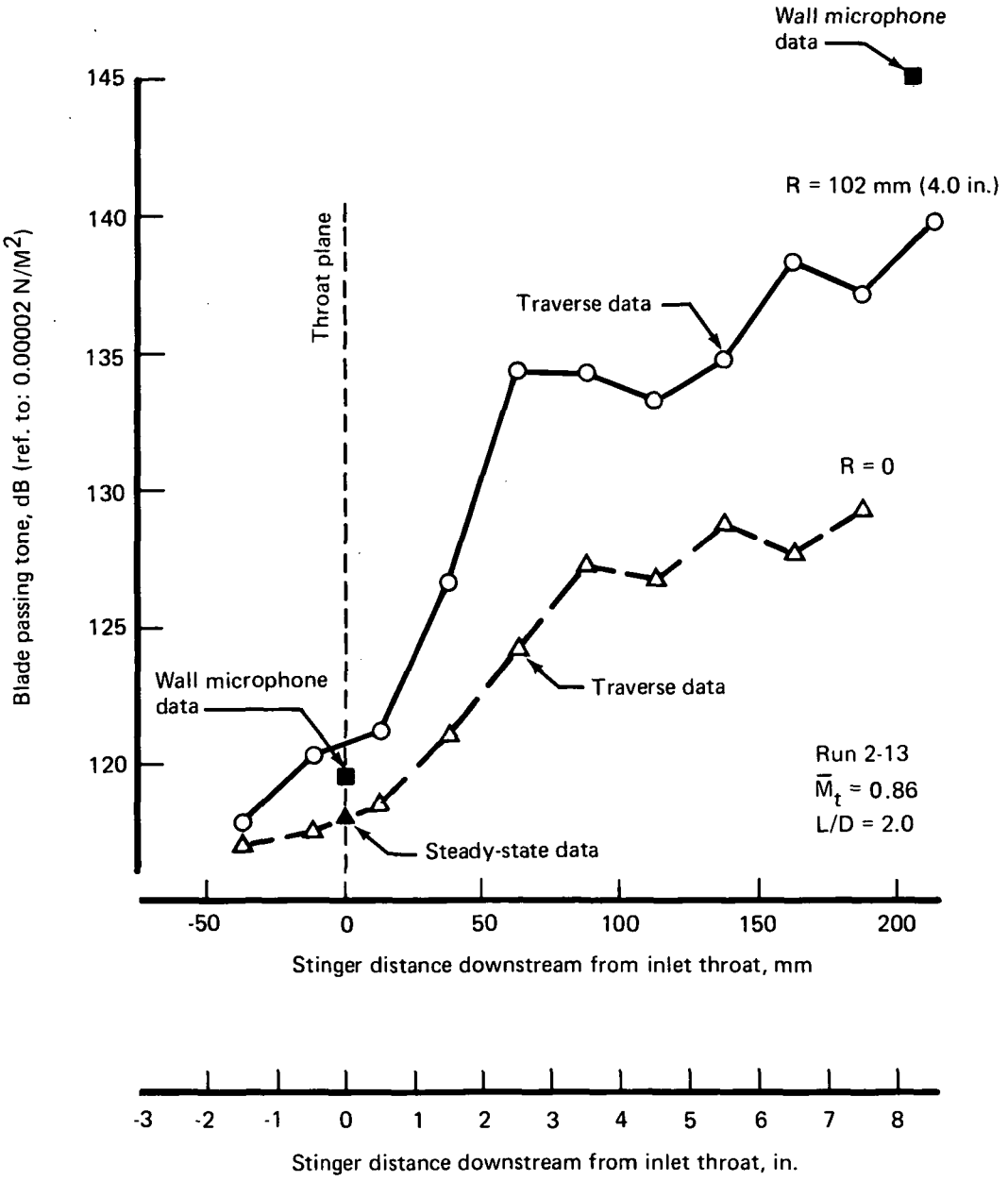

FIGURE 21.—AXIAL DISTRIBUTION OF BLADE PASSING TONE IN APPROACH INLET

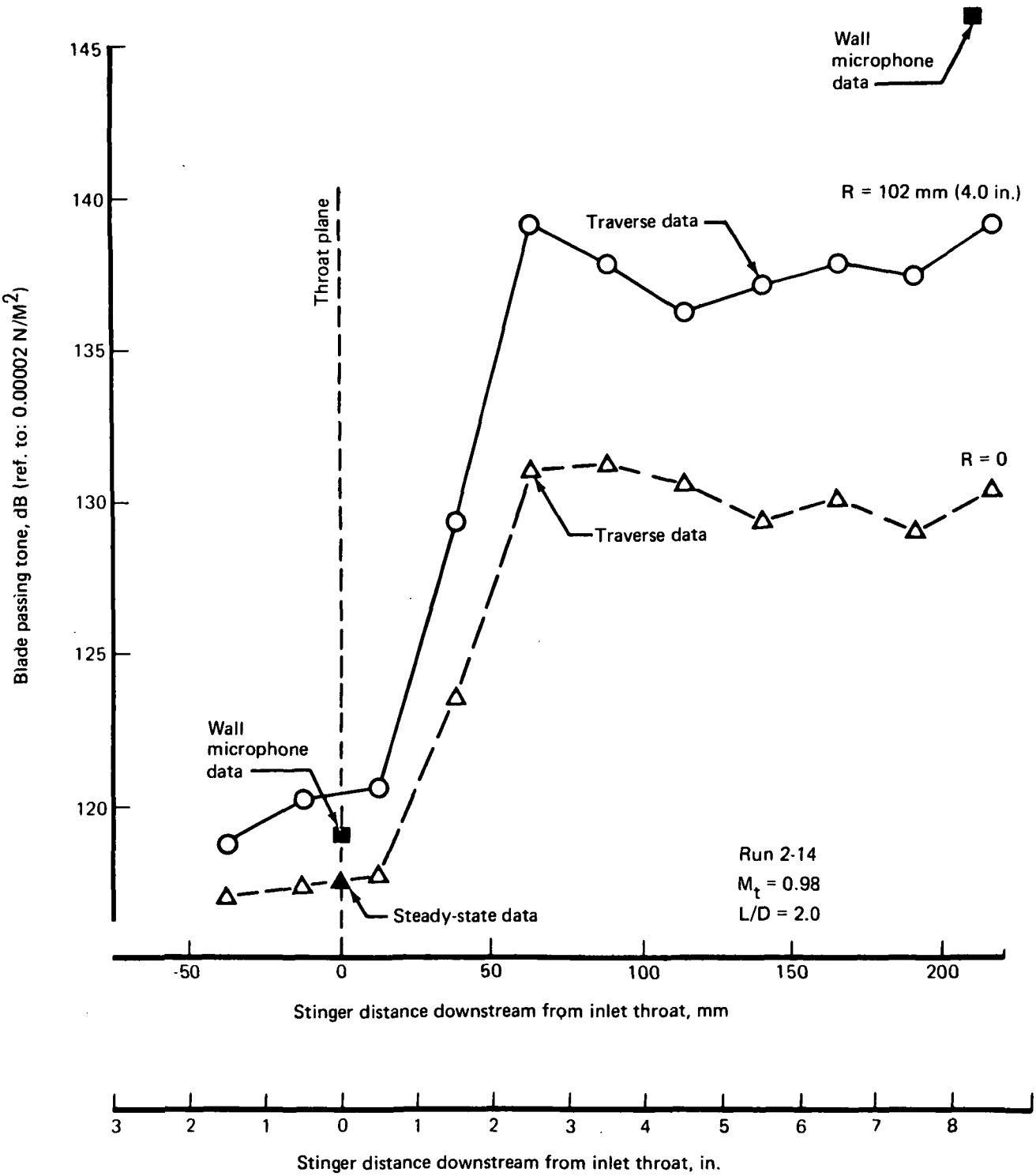

FIGURE 22.—AXIAL DISTRIBUTION OF BLADE PASSING TONE IN APPROACH INLET

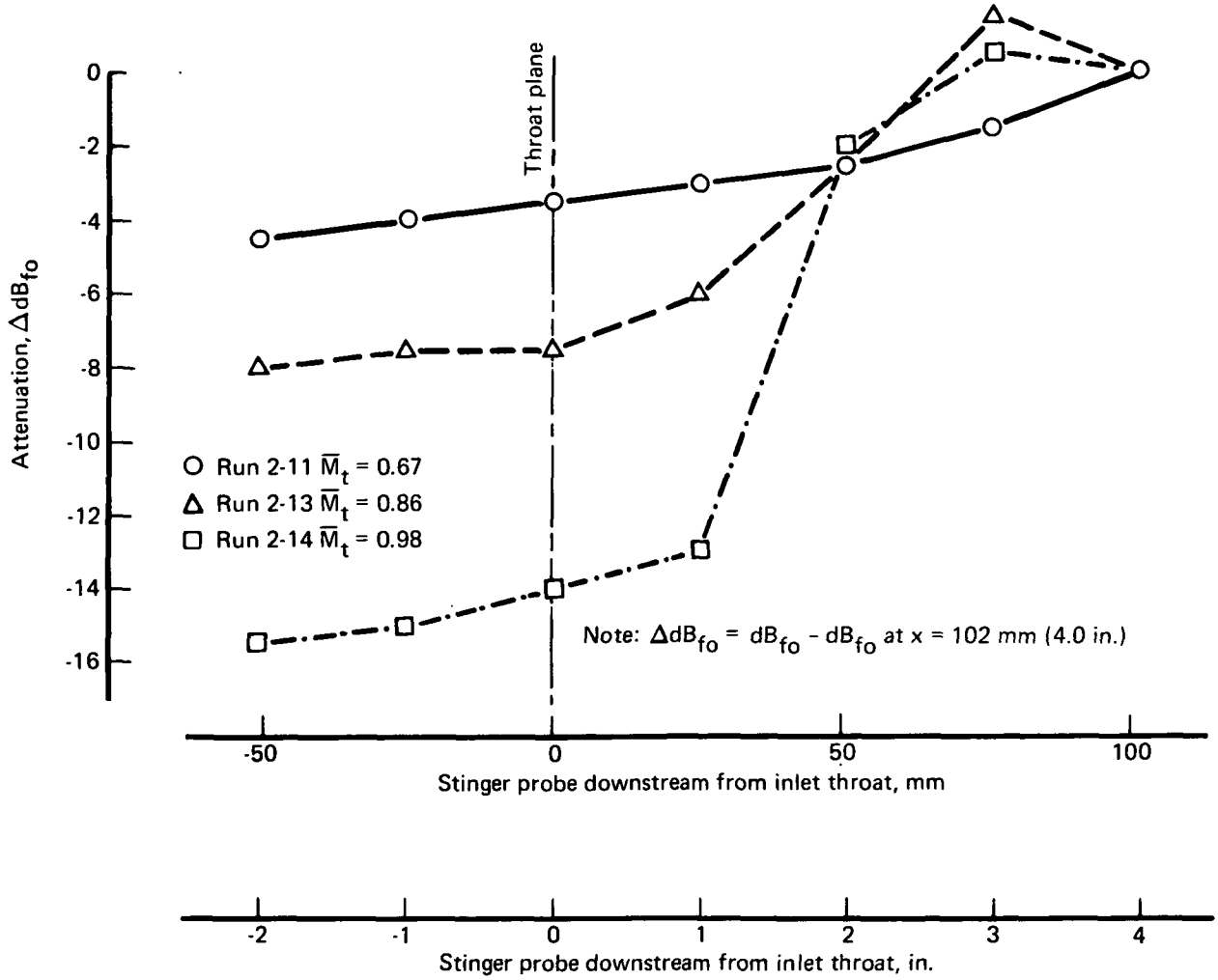

FIGURE 23.–ATTENUATION OF FAN TONE VERSUS AXIAL DISTANCE IN APPROACH INLET, R = 0

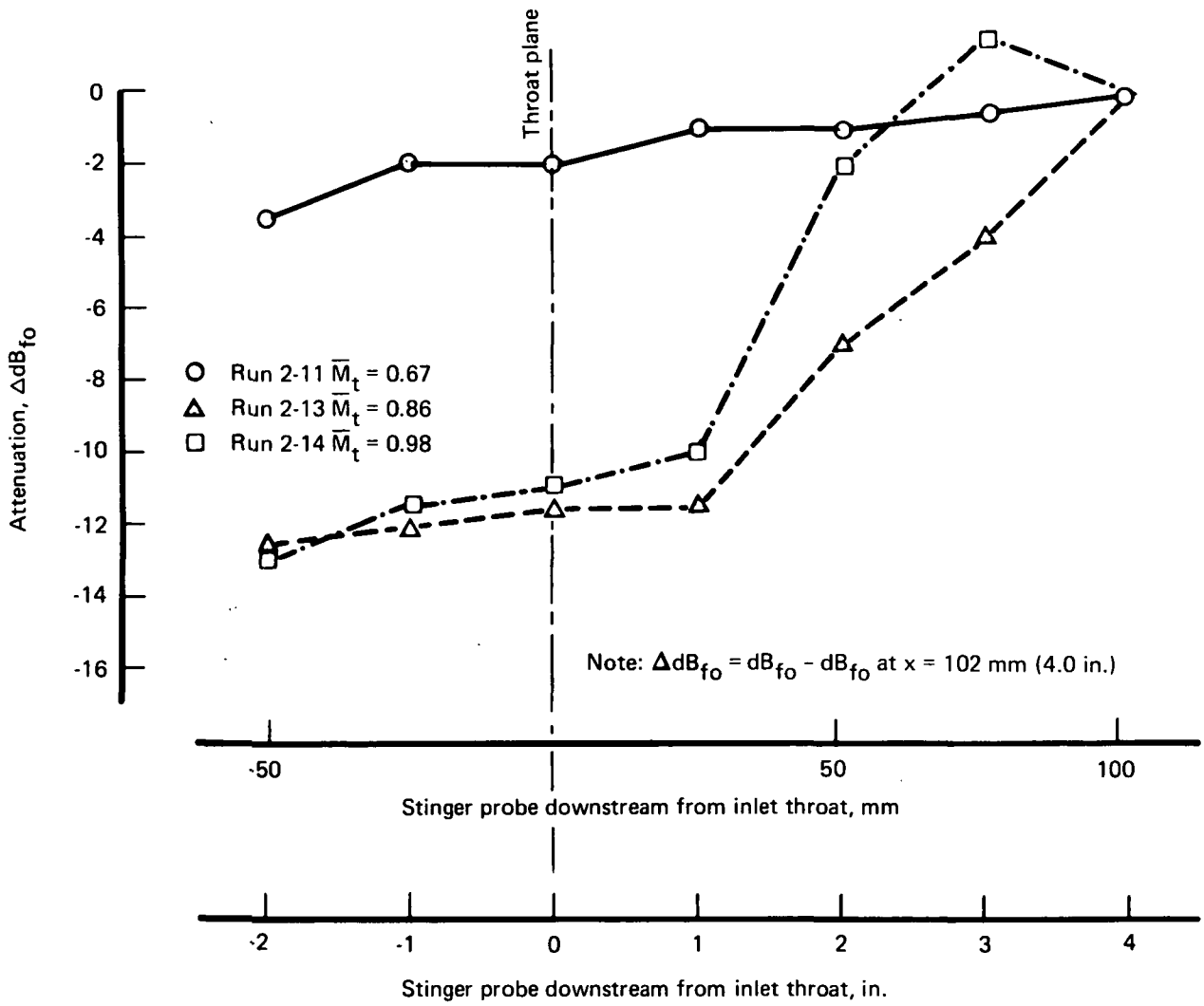

FIGURE 24.—ATTENUATION OF FAN TONE VERSUS AXIAL DISTANCE IN APPROACH INLET, R = 51 MM (2.0 IN.)

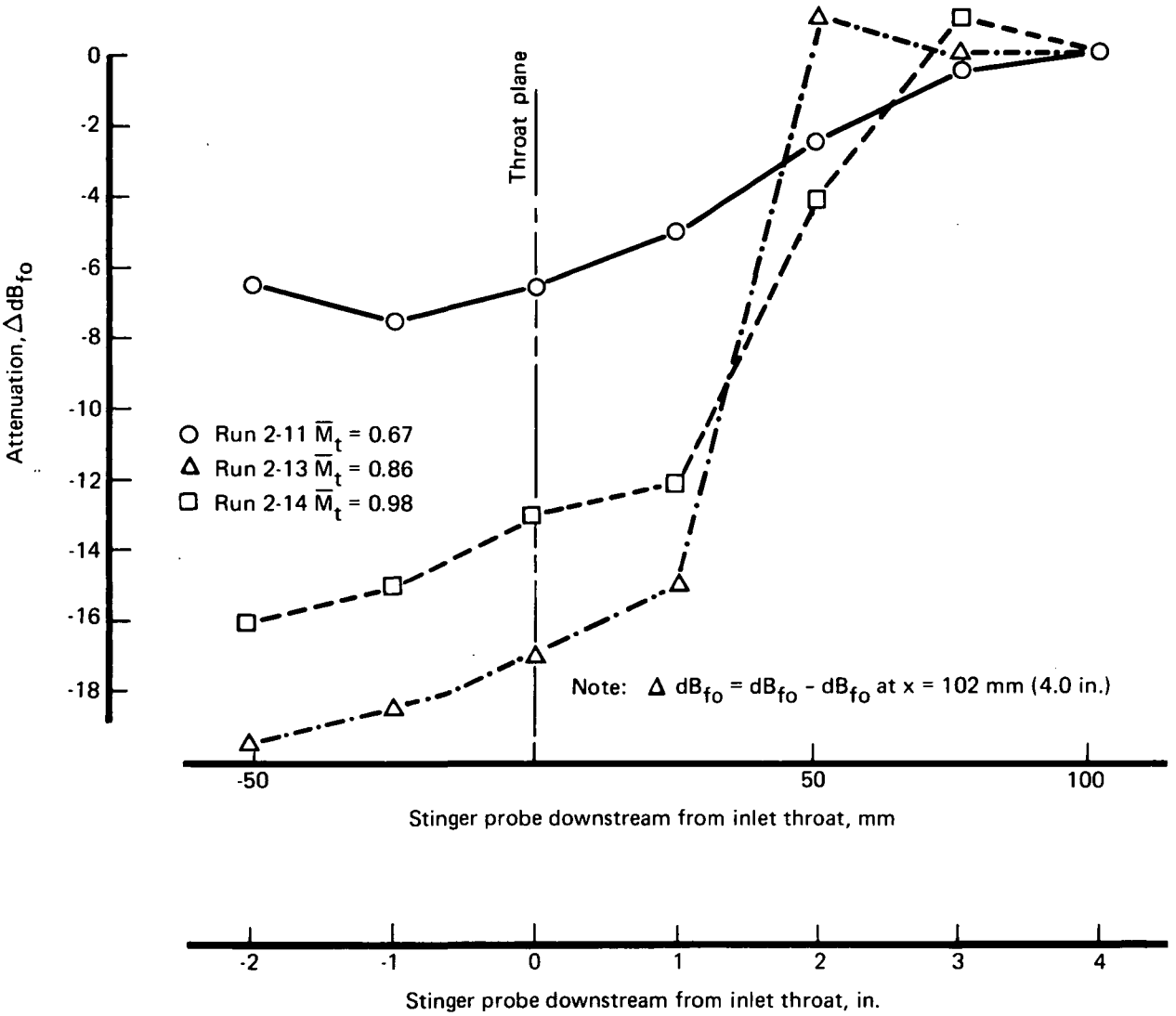

FIGURE 25.–ATTENUATION OF FAN TONE VERSUS AXIAL DISTANCE IN APPROACH INLET, R = 102 MM (4.0 IN.)

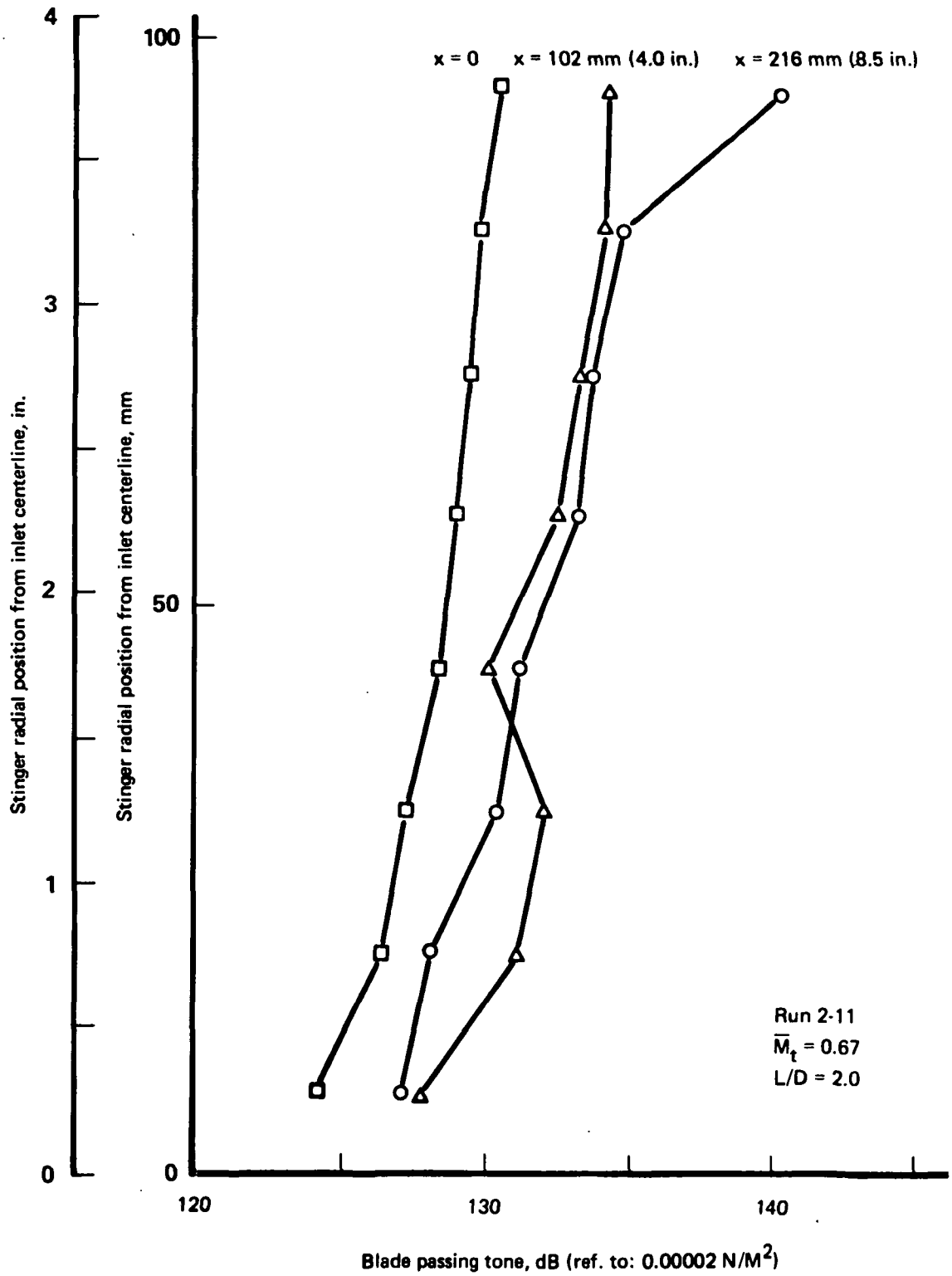

FIGURE 26.--RADIAL DISTRIBUTION OF BLADE PASSING TONE IN APPROACH INLET (TRAVERSE DATA)

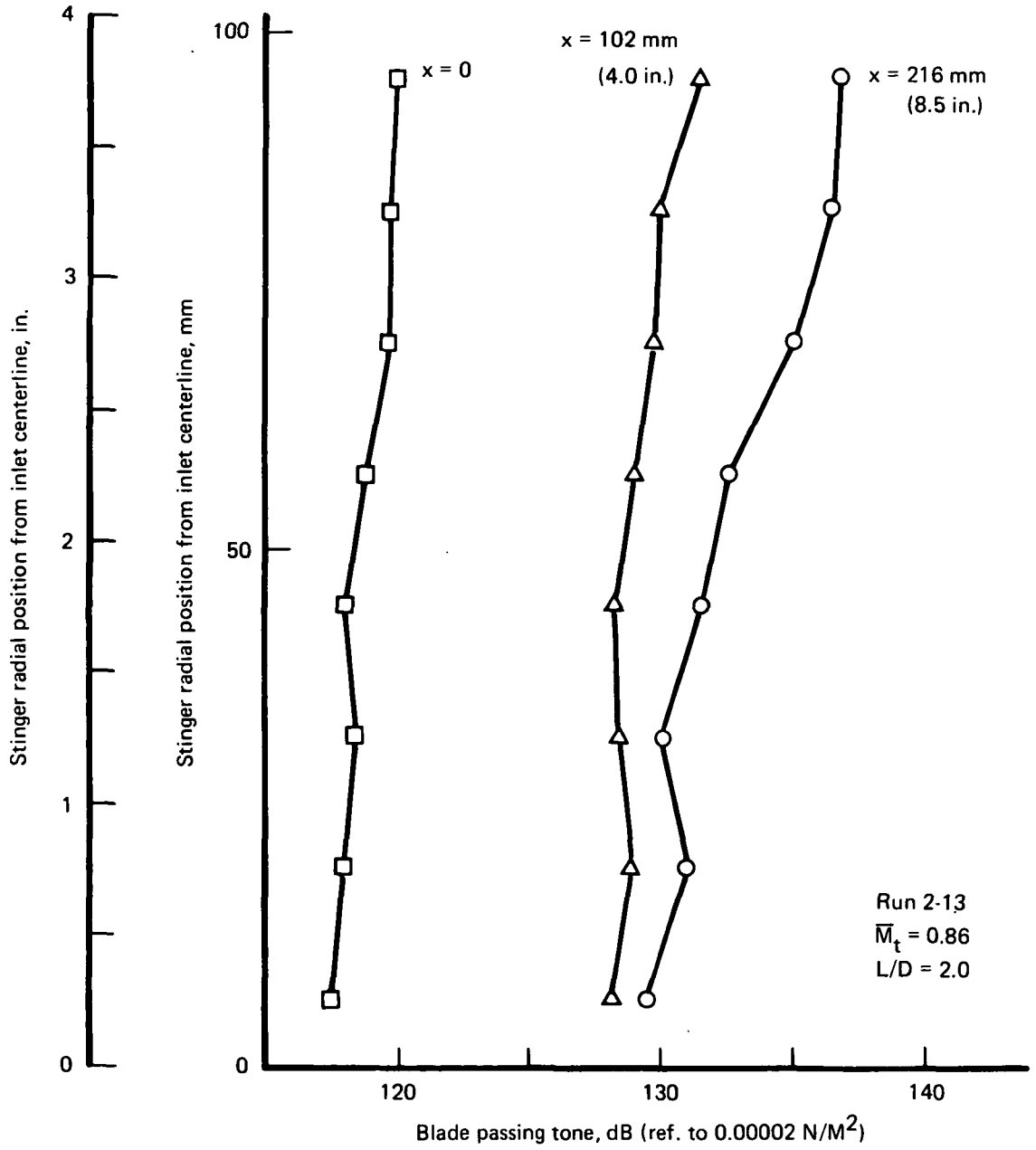

FIGURE 27.—RADIAL DISTRIBUTION OF BLADE PASSING TONE IN APPROACH INLET (TRAVERSE DATA)

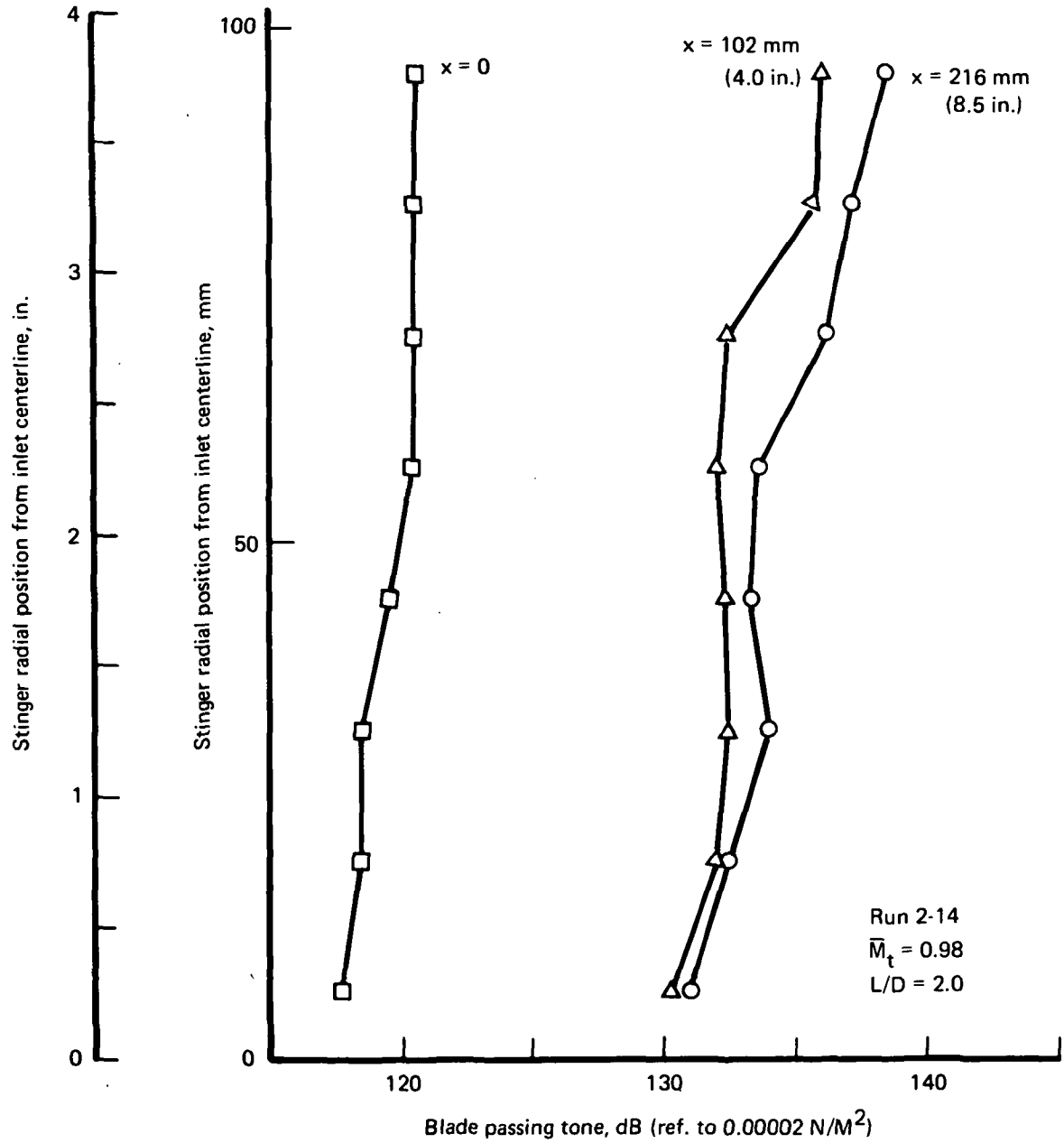

FIGURE 28.–RADIAL DISTRIBUTION OF BLADE PASSING TONE IN APPROACH INLET (TRAVERSE DATA)

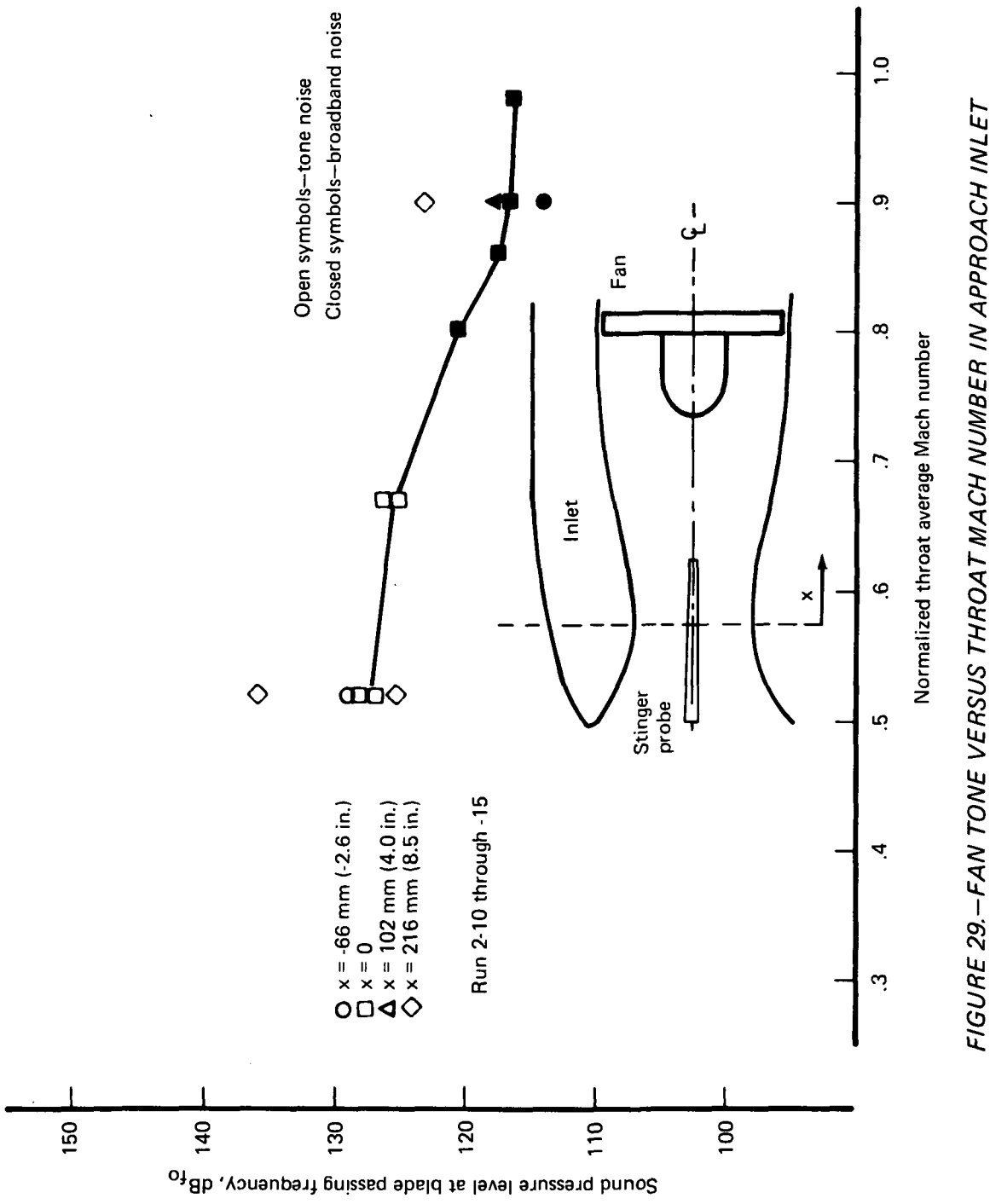

FIGURE 29.—FAN TONE VERSUS THROAT MACH NUMBER IN APPROACH INLET

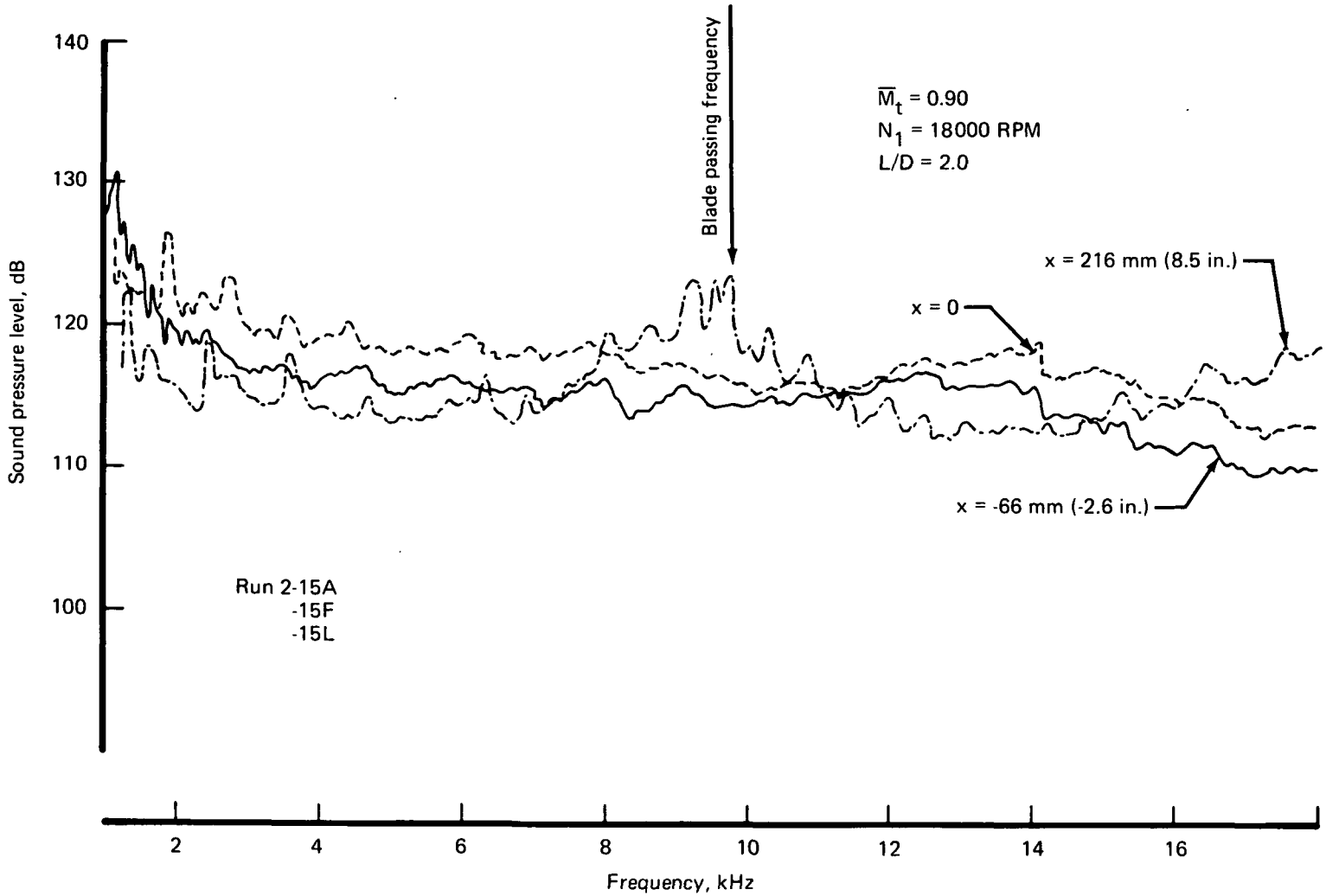

FIGURE 30.—NEAR FIELD NOISE SPECTRA INSIDE FUNDAMENTAL APPROACH INLET, R = 0

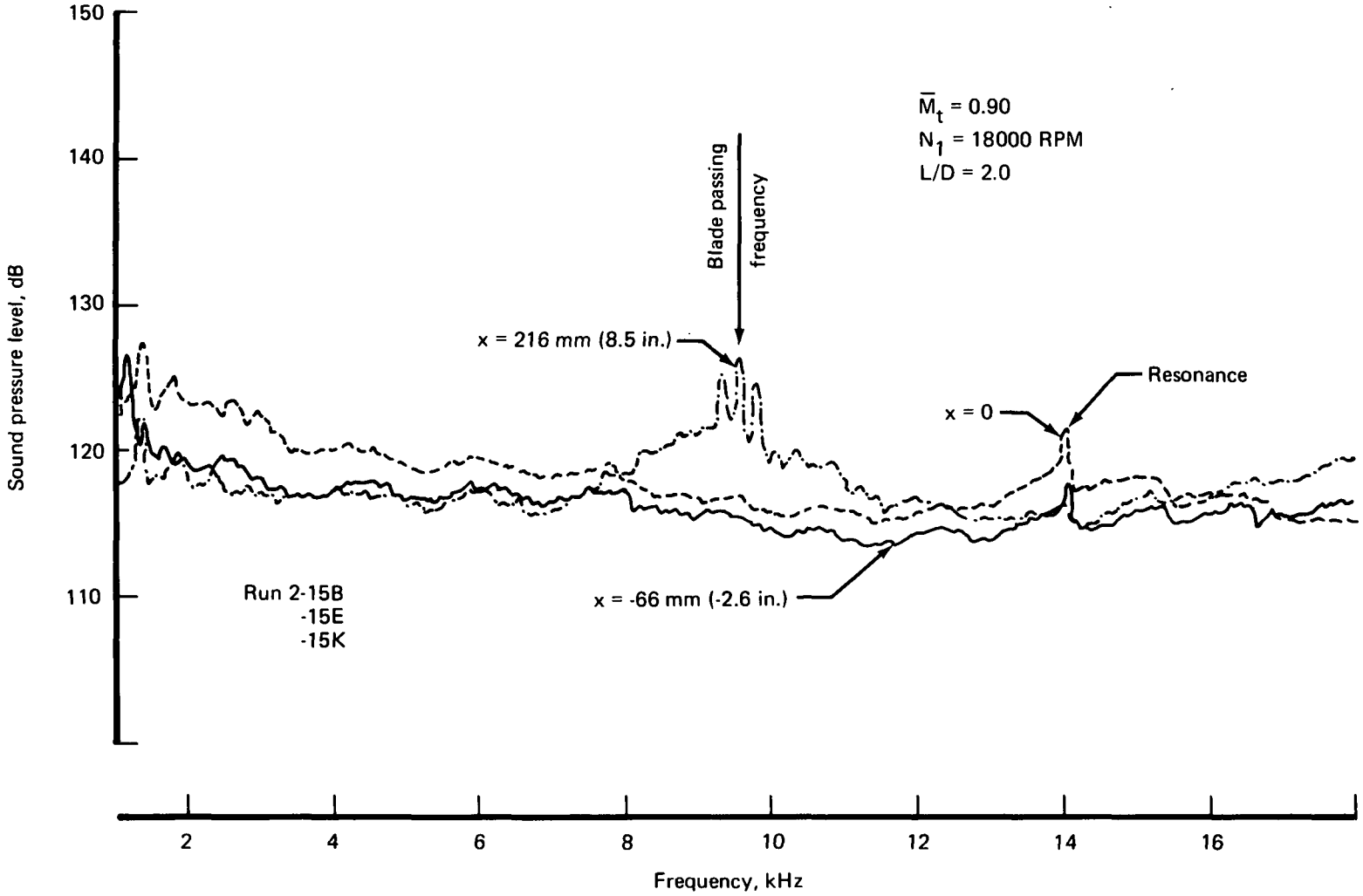

FIGURE 31.—NEAR-FIELD NOISE SPECTRA INSIDE FUNDAMENTAL APPROACH INLET, R = 51 MM (2.0 IN.)

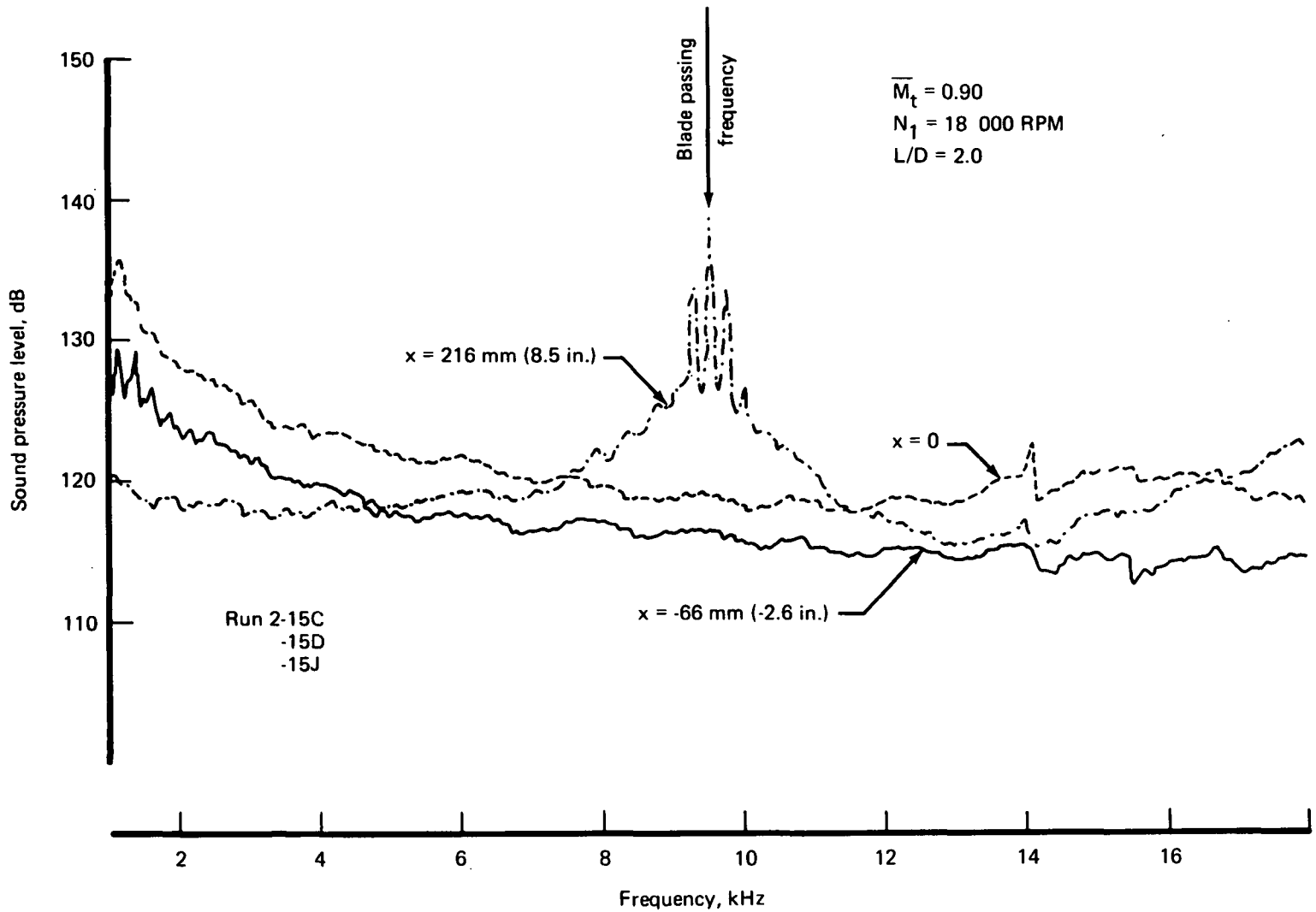

FIGURE 32.–NEAR FIELD NOISE SPECTRA INSIDE FUNDAMENTAL APPROACH INLET, R = 102 MM (4.0 IN.)

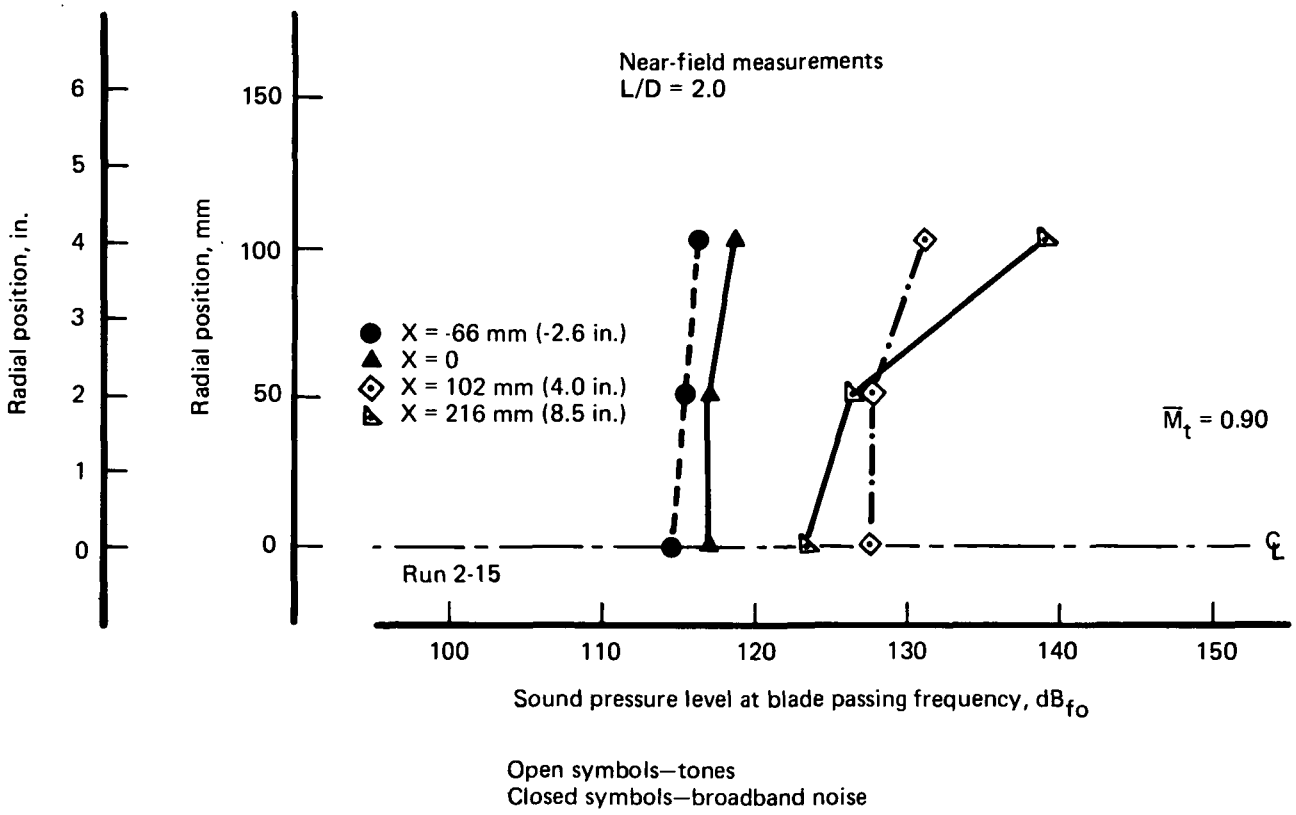

FIGURE 33.—RADIAL DISTRIBUTION OF BLADE PASSING TONE IN APPROACH INLET

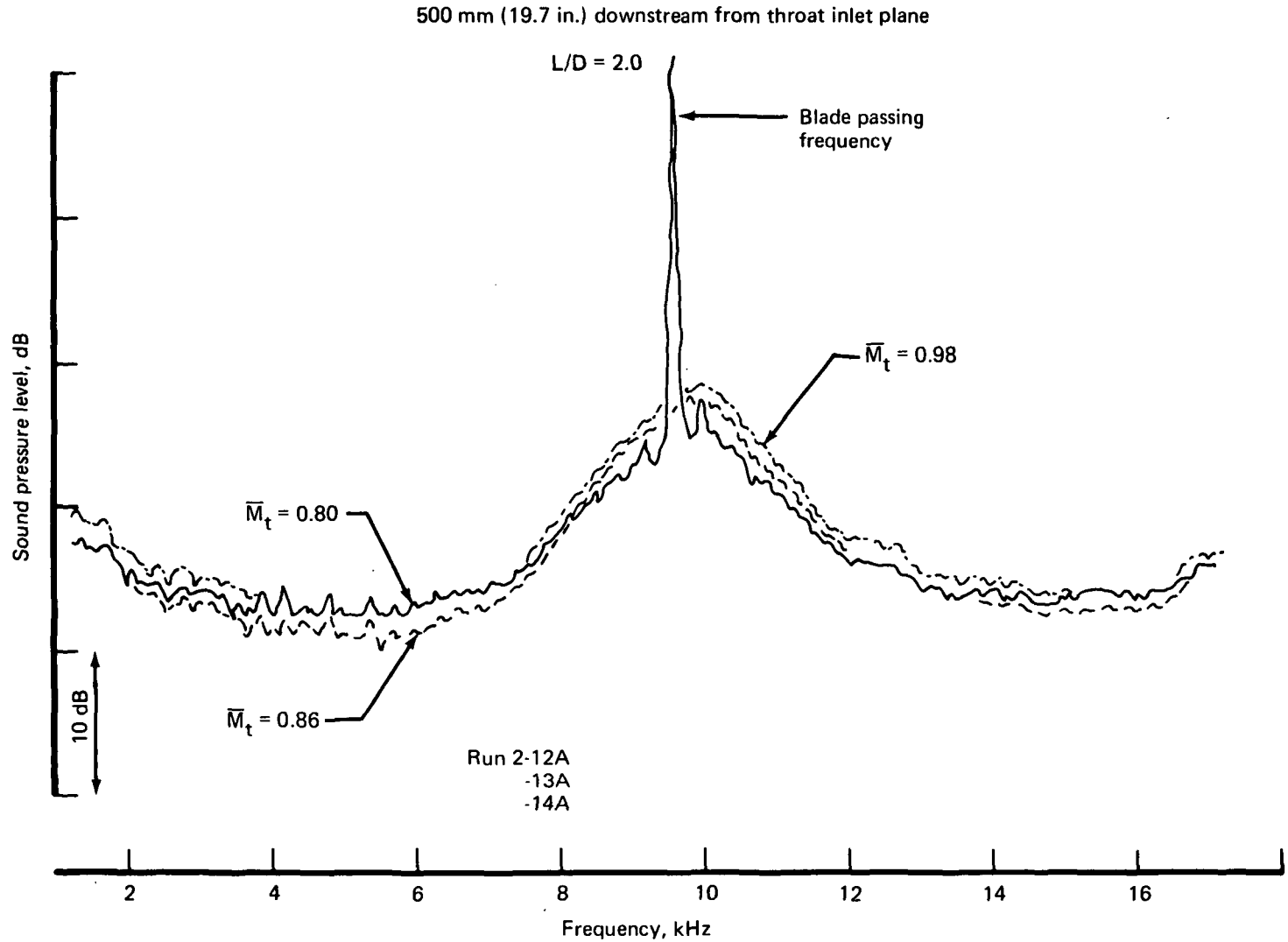

FIGURE 34.—NEAR FIELD, WALL KULITE, NOISE SPECTRA IN APPROACH INLET

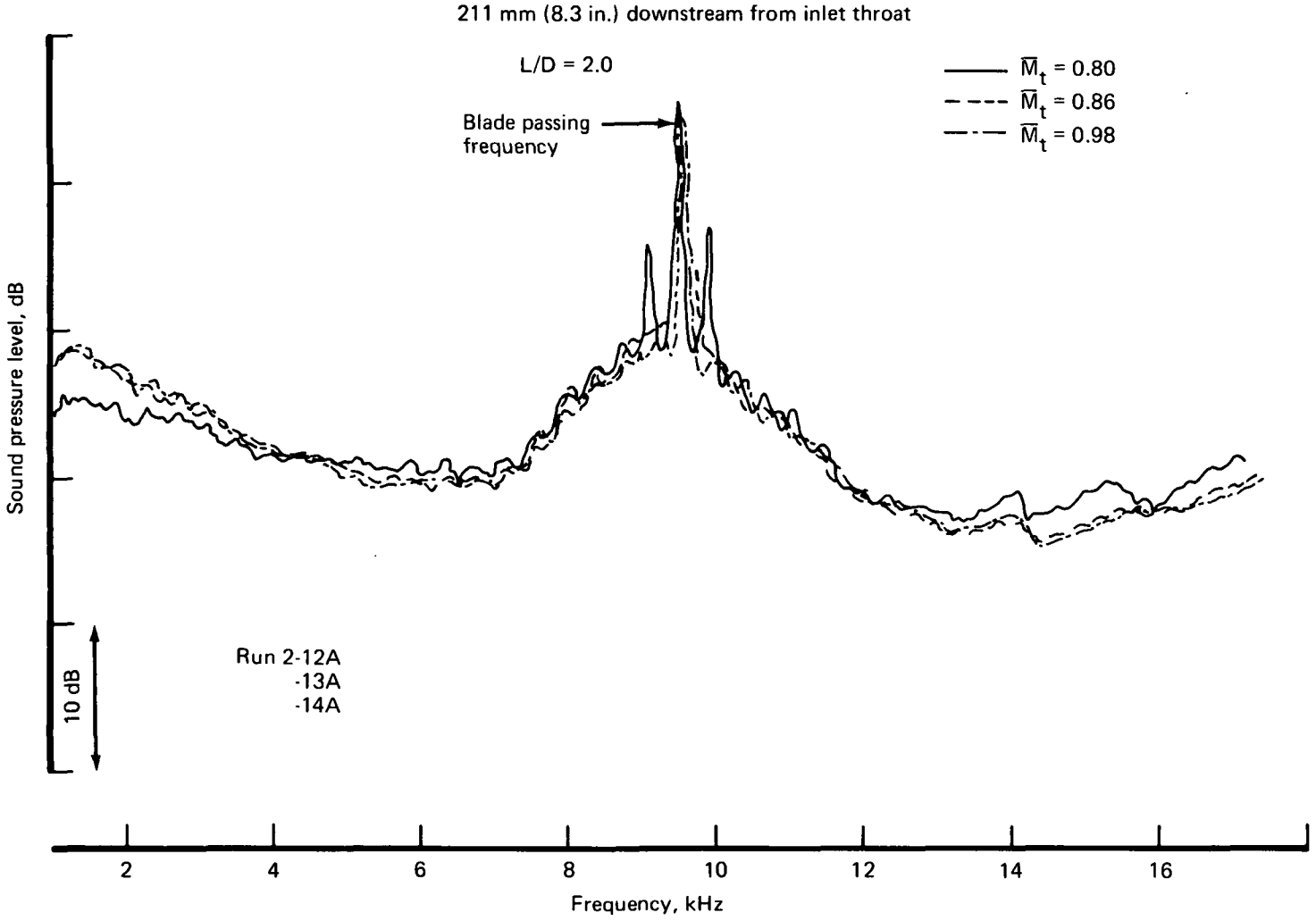

FIGURE 35.—NEAR FIELD, WALL KULITE, NOISE SPECTRA IN APPROACH INLET

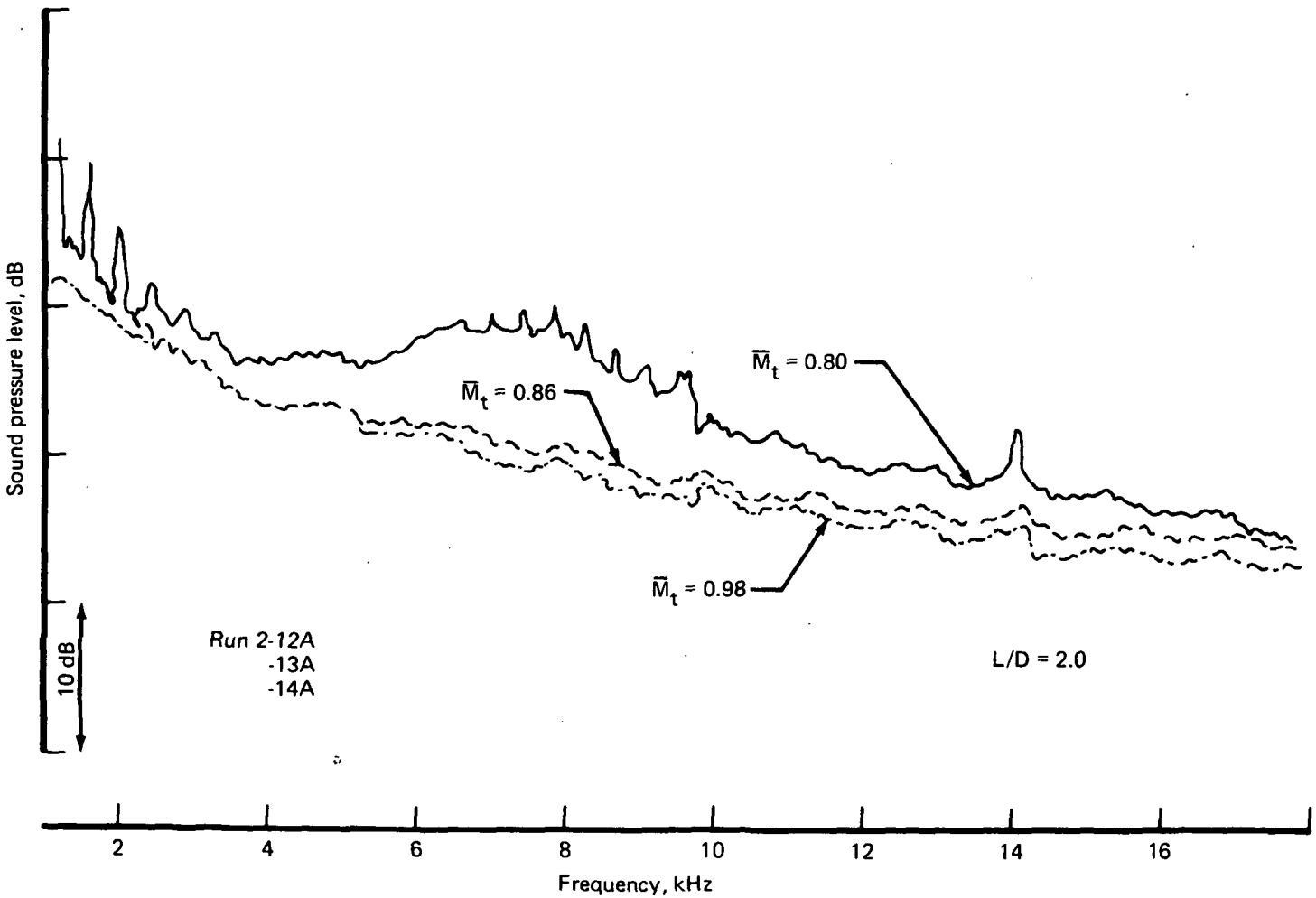

FIGURE 36.—NEAR FIELD, WALL KULITE, NOISE SPECTRA IN APPROACH INLET

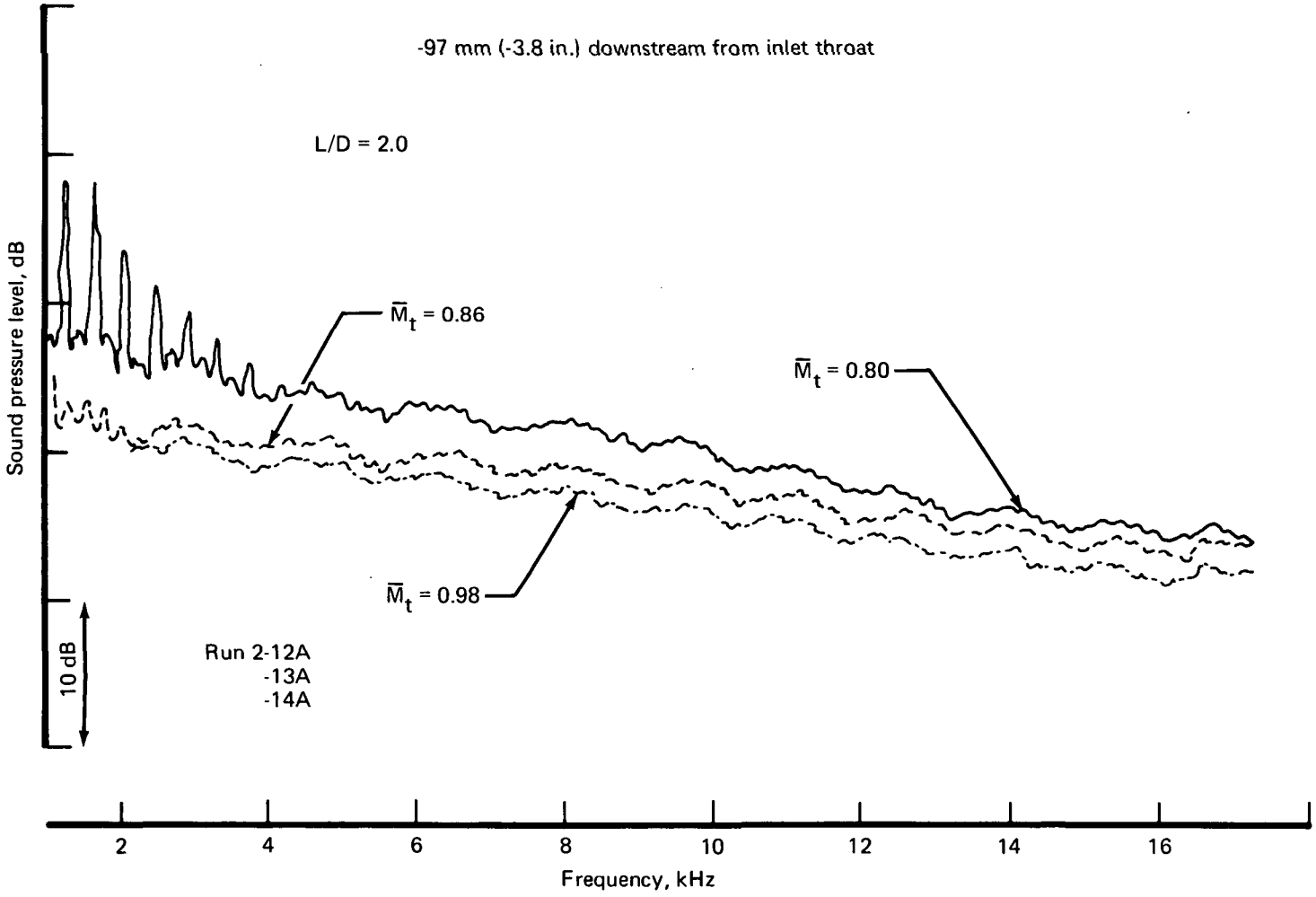

FIGURE 37.—NEAR FIELD, WALL KULITE, NOISE SPECTRA IN APPROACH INLET

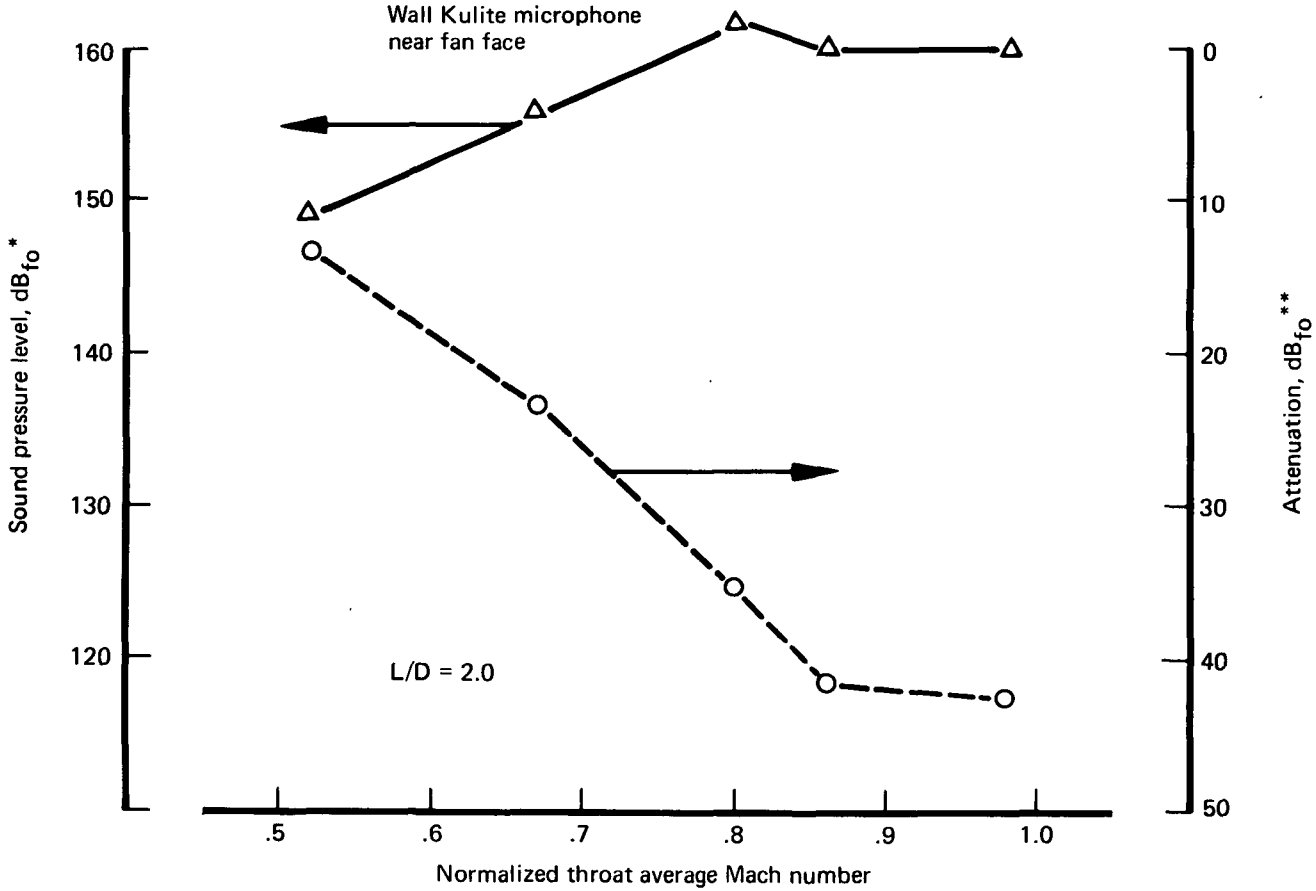

Note:
*fo = blade passing frequency
**$\Delta dB_{fo} = dB_{fo_{fan\ face}} - dB_{fo_{throat}}$

FIGURE 38.—ATTENUATION AT BLADE PASSING FREQUENCY VERSUS THROAT MACH NUMBER IN APPROACH INLET

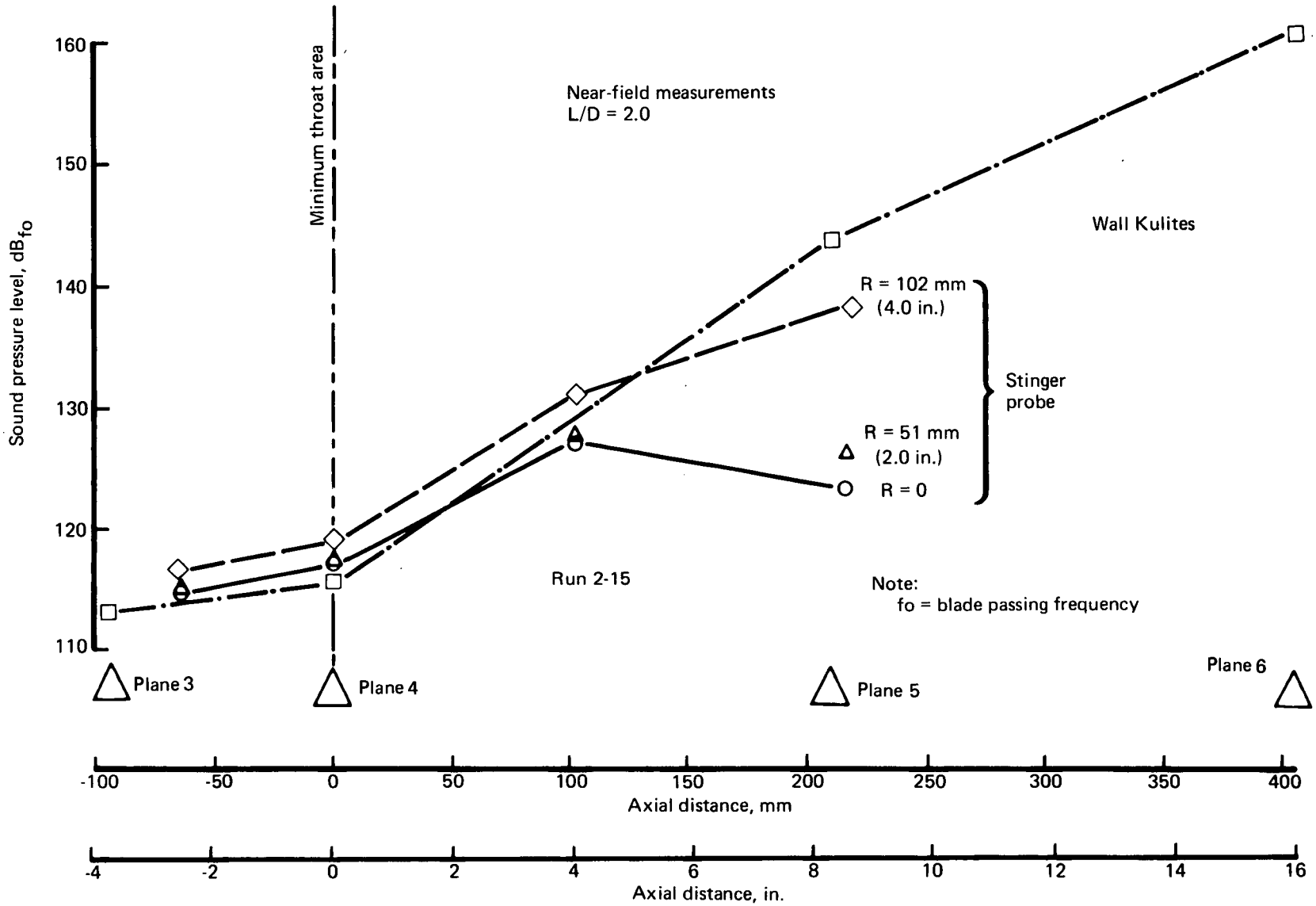

FIGURE 39.–BLADE PASSING TONE VERSUS AXIAL DISTANCE IN APPROACH INLET

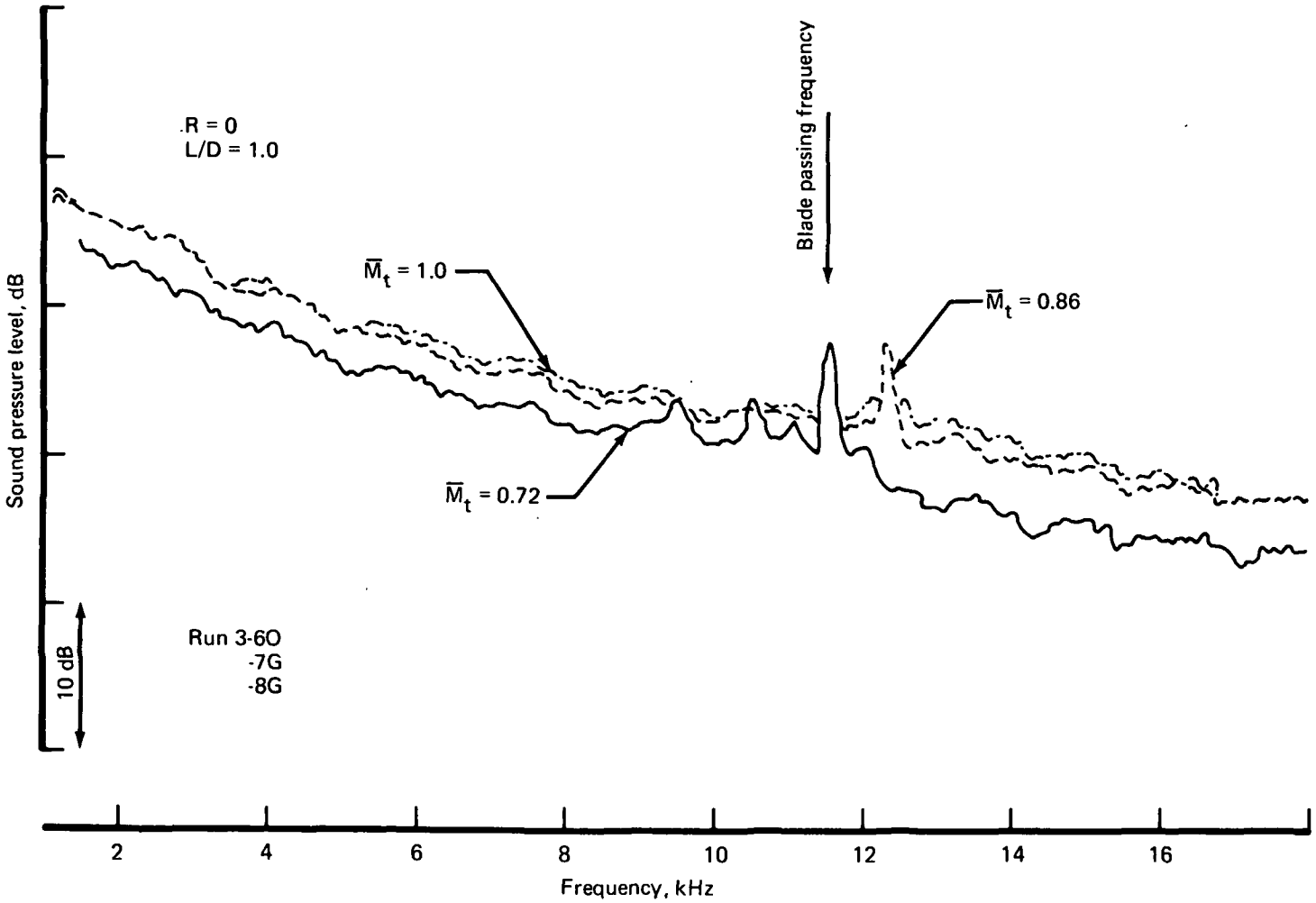

FIGURE 40.—NEAR FIELD NOISE SPECTRA IN TAKEOFF INLET, 124 MM (4.9 IN.) DOWNSTREAM OF INLET THROAT

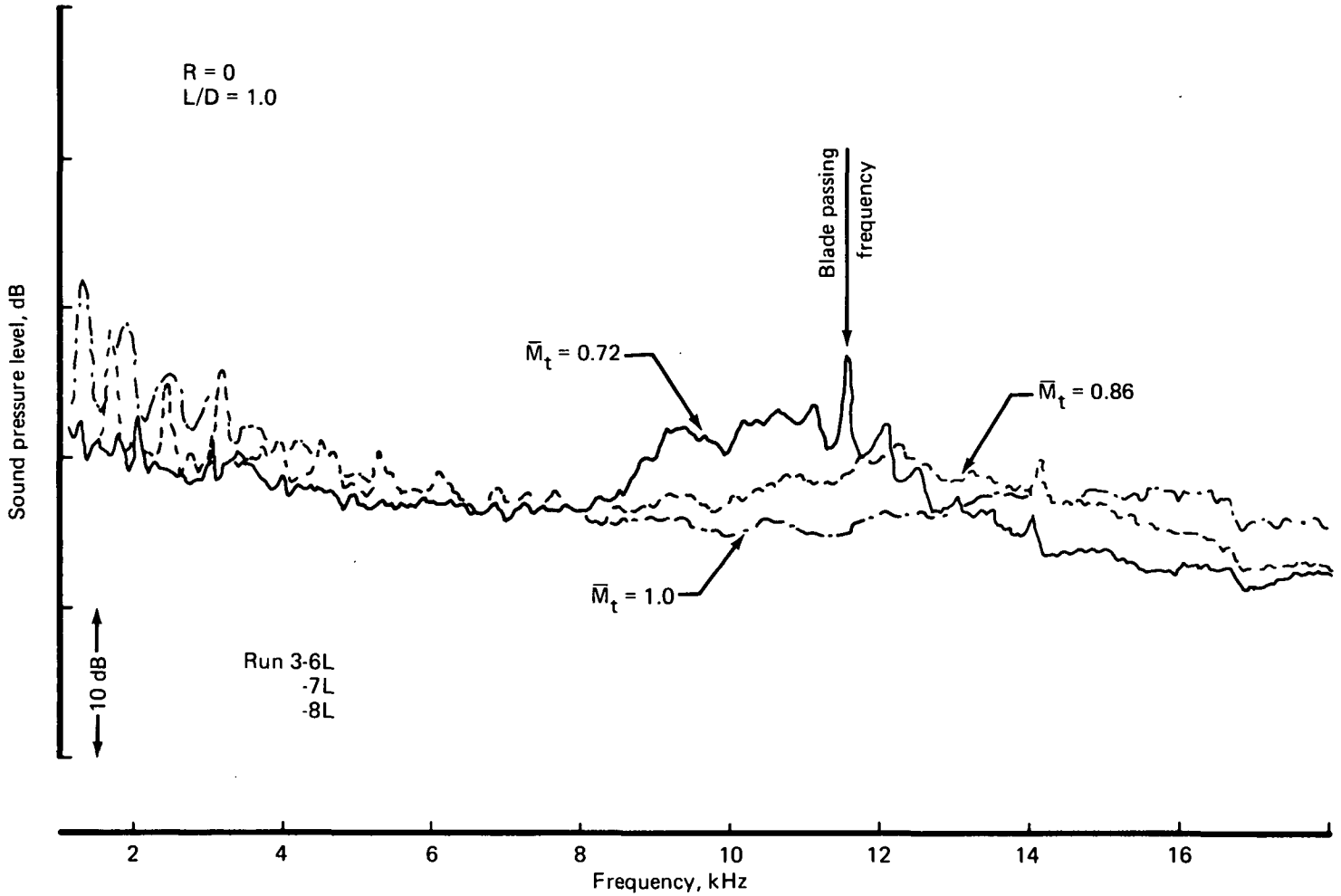

FIGURE 41.—NEAR FIELD NOISE SPECTRA IN TAKEOFF INLET IN PLANE OF THROAT

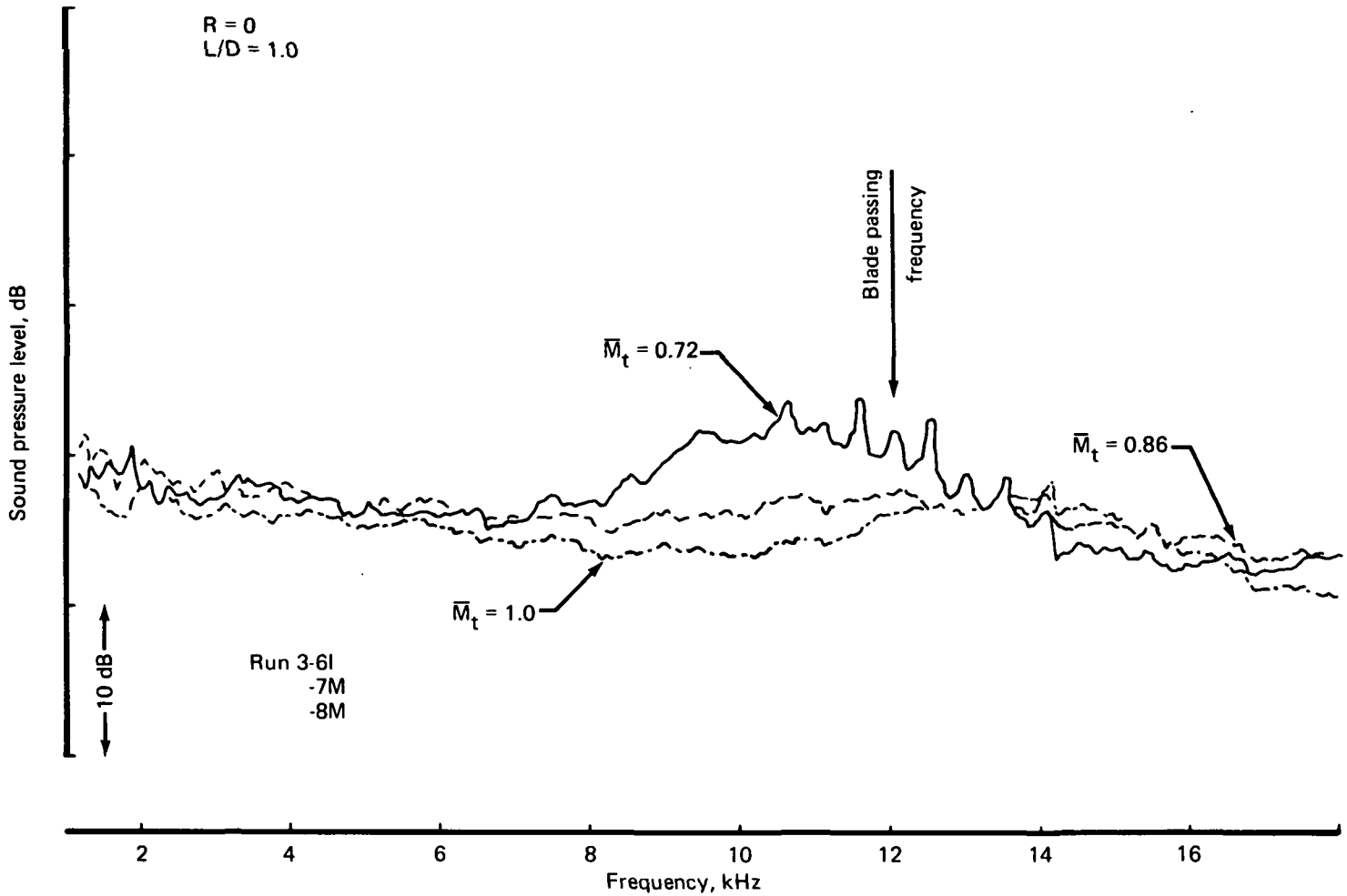

FIGURE 42.–NEAR FIELD NOISE SPECTRA IN TAKEOFF INLET, 63.5 MM (2.5 IN.) UPSTREAM OF INLET THROAT

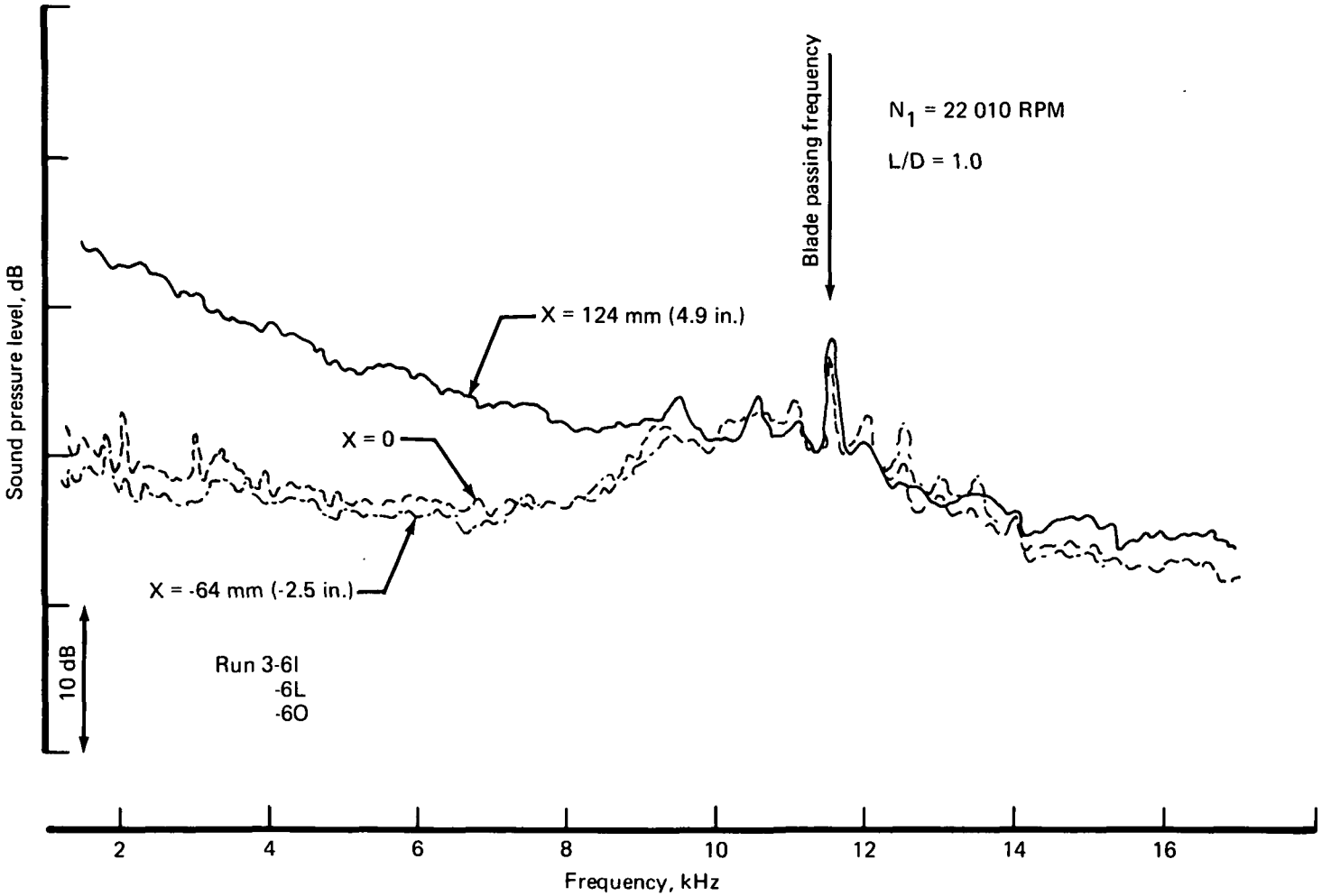

FIGURE 43.—NEAR FIELD NOISE SPECTRA IN TAKEOFF INLET $\bar{M}_t = 0.72$, R = 0

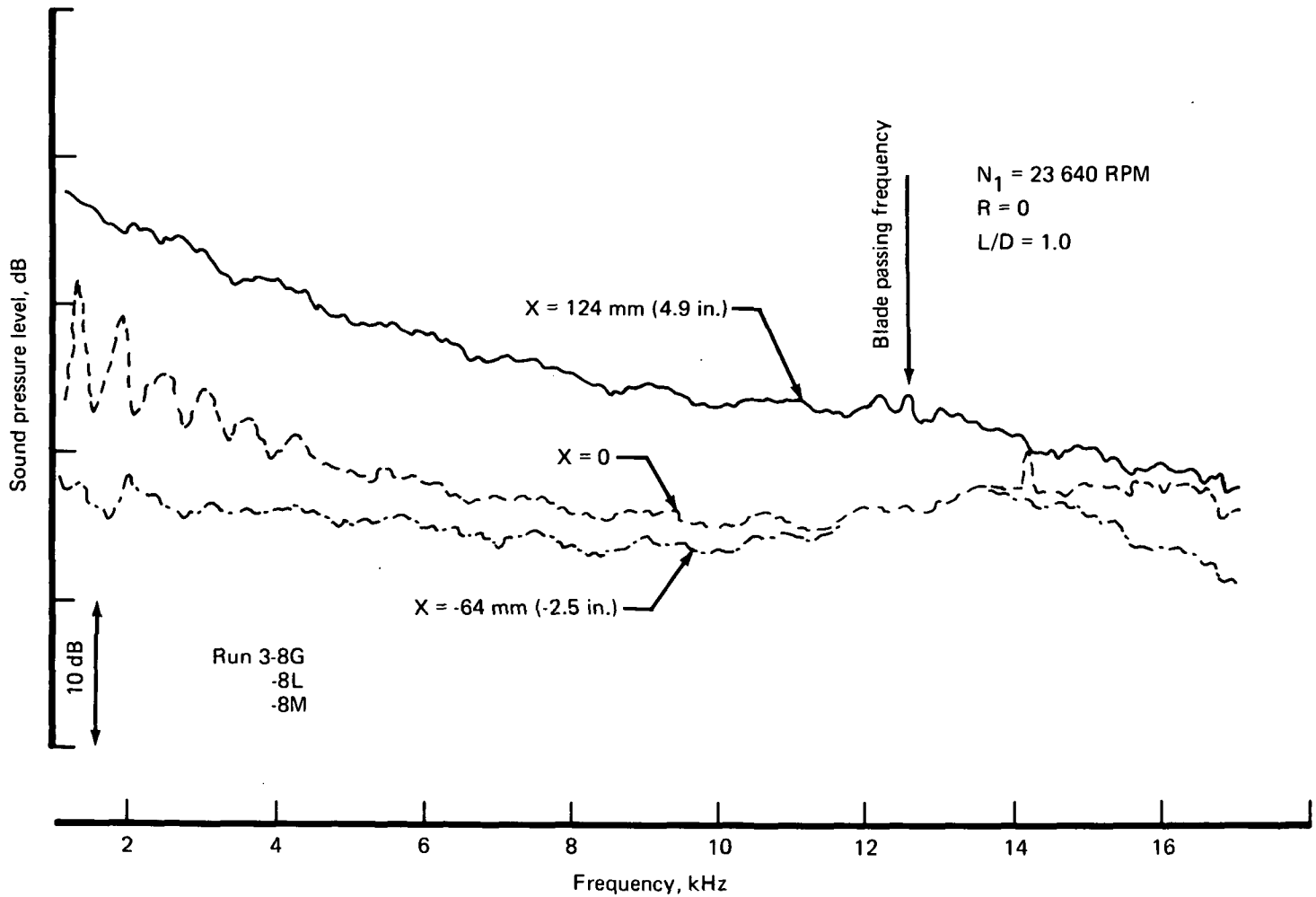

FIGURE 44.–NEAR FIELD NOISE SPECTRA IN TAKEOFF INLET $\bar{M}_t$ = 1.00, R = 0

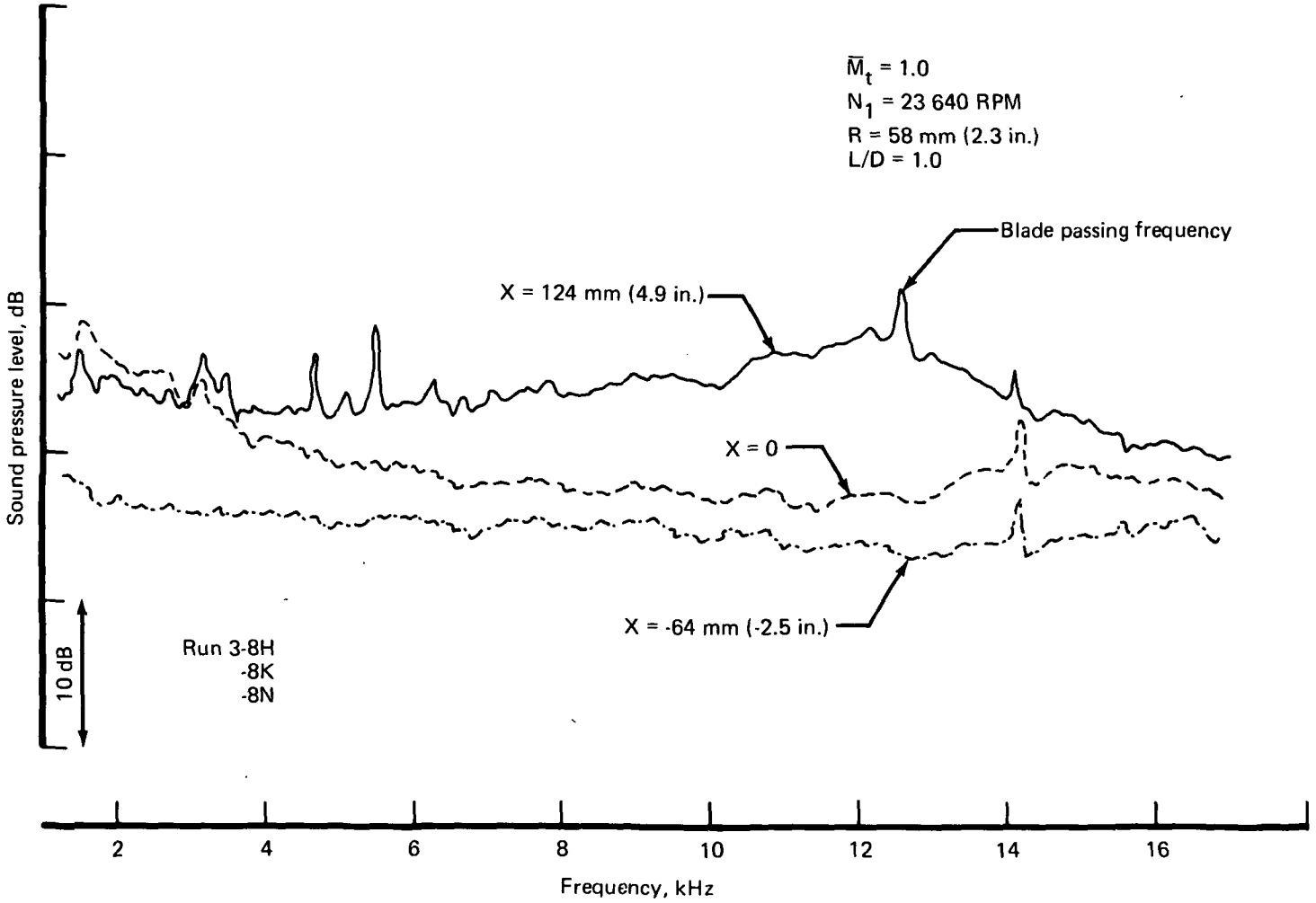

FIGURE 45.–NEAR FIELD NOISE SPECTRA IN TAKEOFF INLET, R = 58 MM (2.3 IN.)

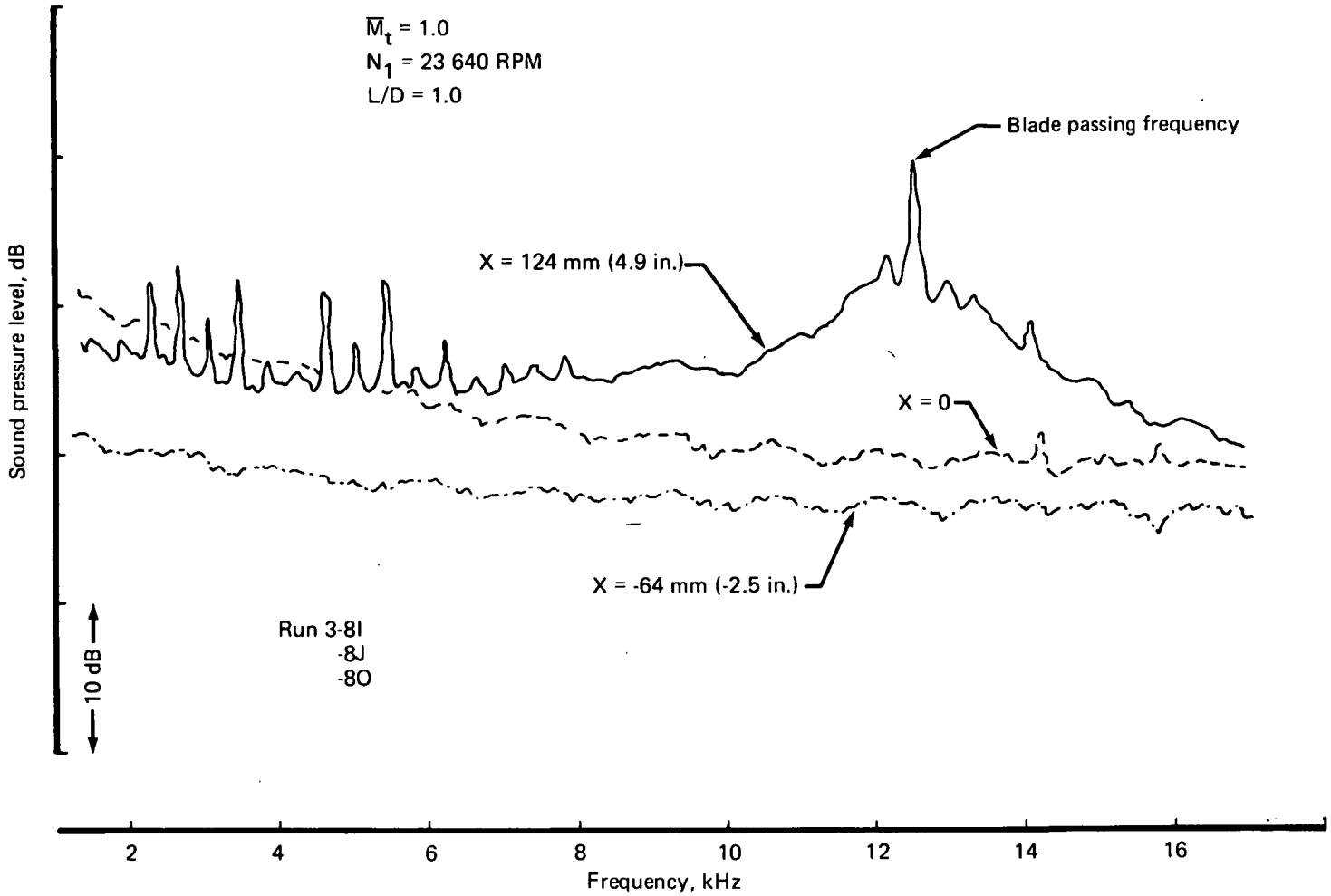

FIGURE 46.—NEAR FIELD NOISE SPECTRA IN TAKEOFF INLET, R = 117 MM (4.6 IN.)

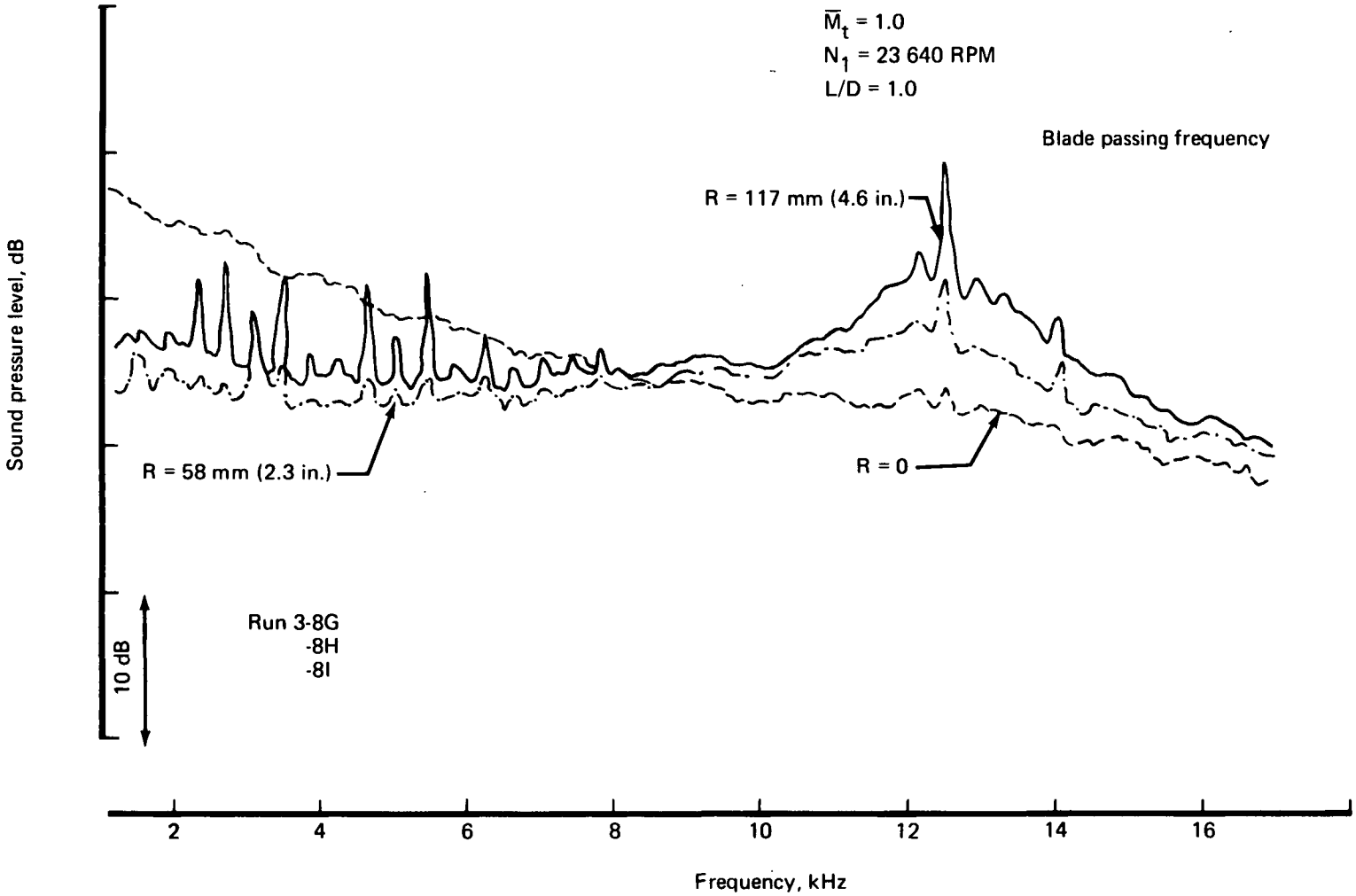

FIGURE 47.—NEAR FIELD NOISE SPECTRA IN TAKEOFF INLET, X = 124 MM (4.9 IN.)

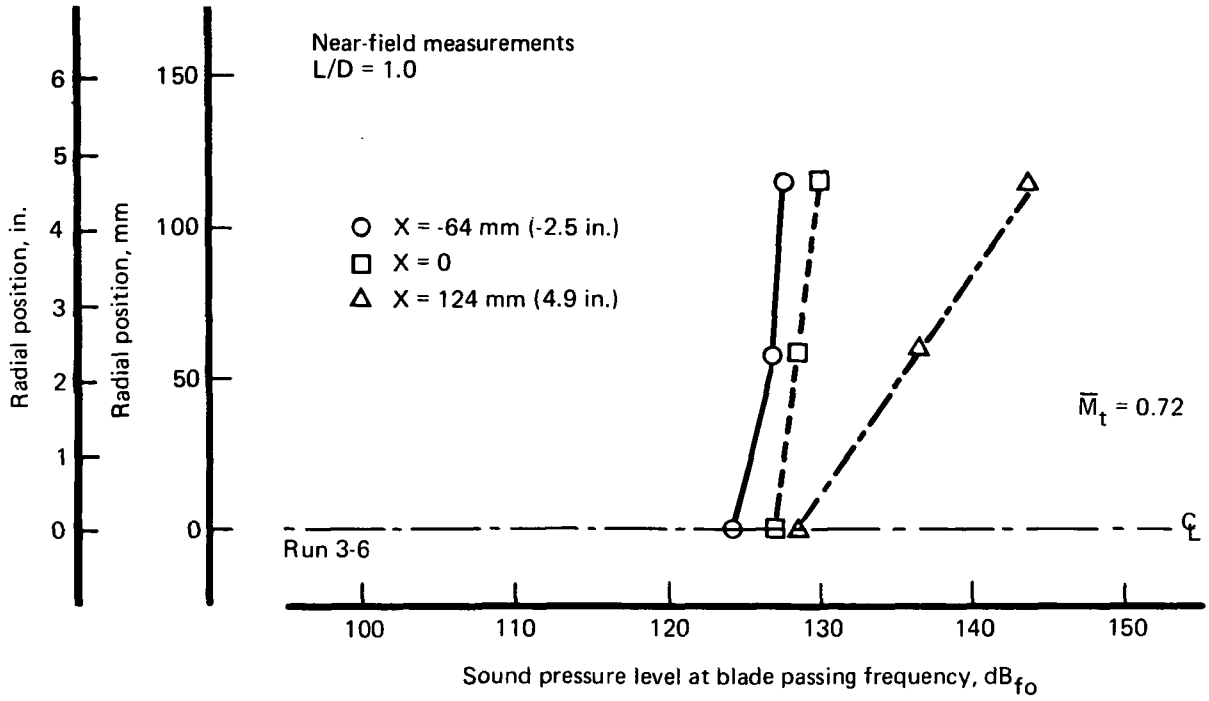

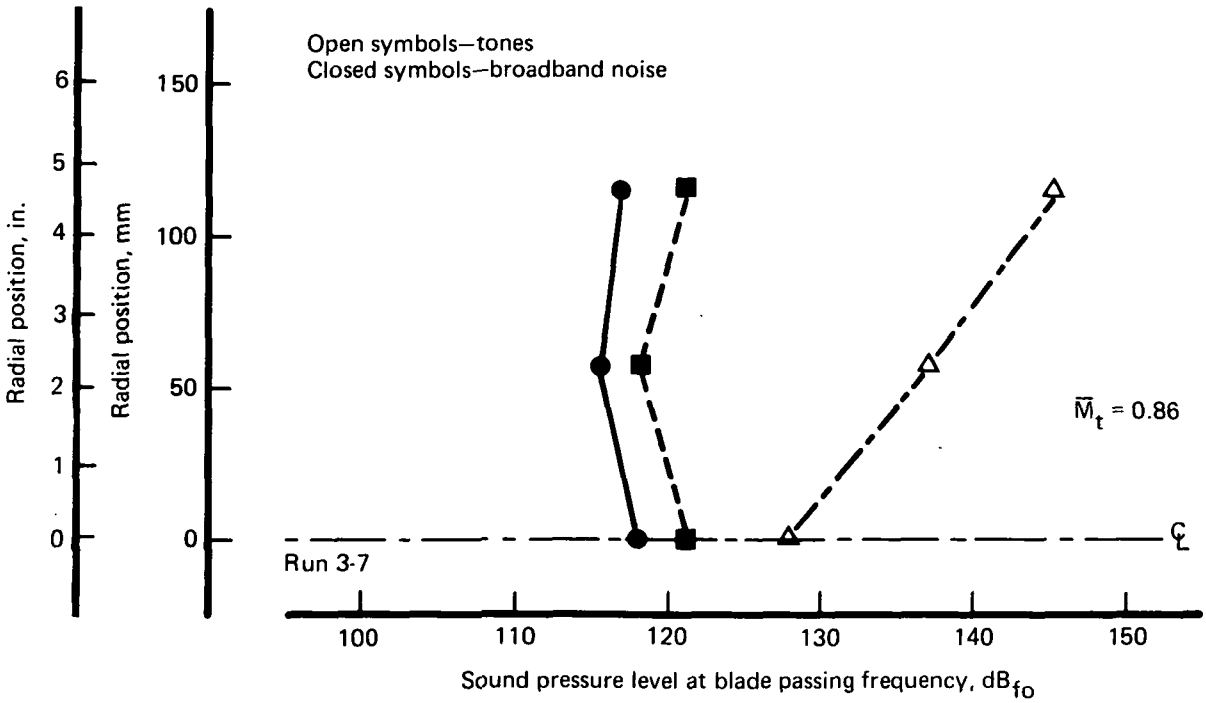

FIGURE 48.—RADIAL DISTRIBUTION OF BLADE PASSING TONE IN TAKEOFF INLET, $\bar{M}_t$ = 0.72 AND 0.86

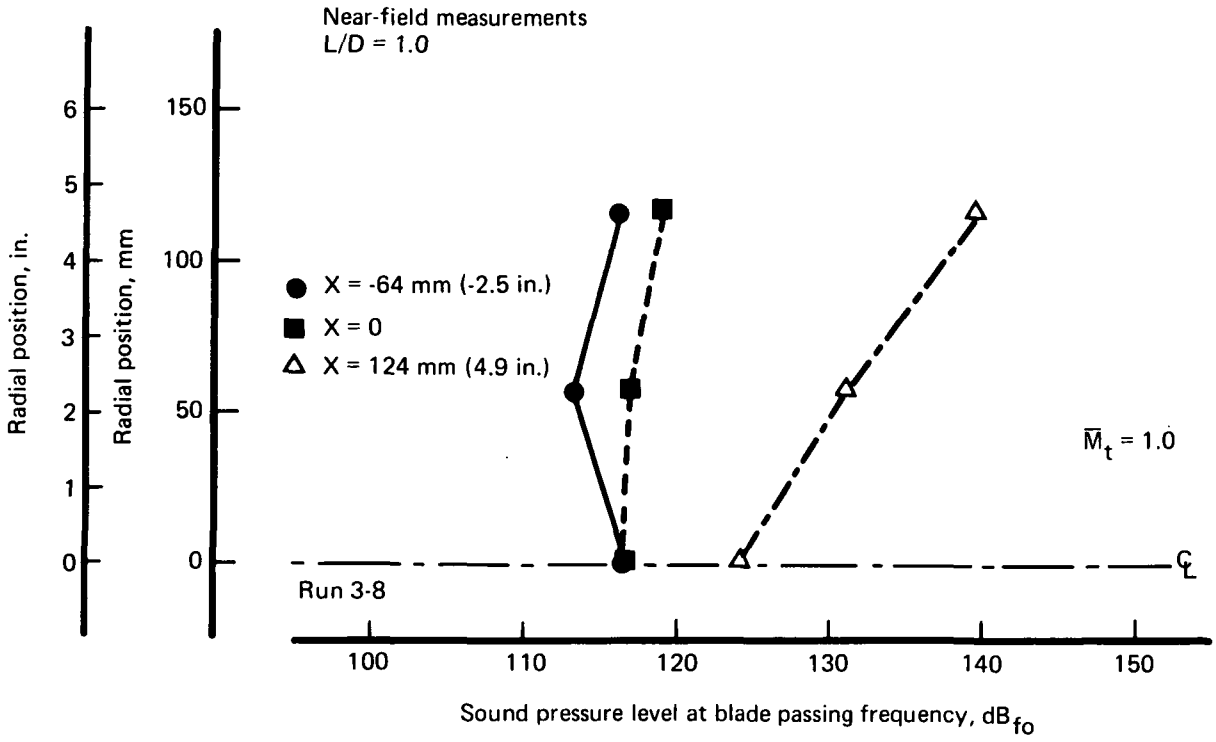

FIGURE 49.—RADIAL DISTRIBUTION OF BLADE PASSING TONE IN TAKEOFF INLET, $\bar{M}_t$ = 1.0

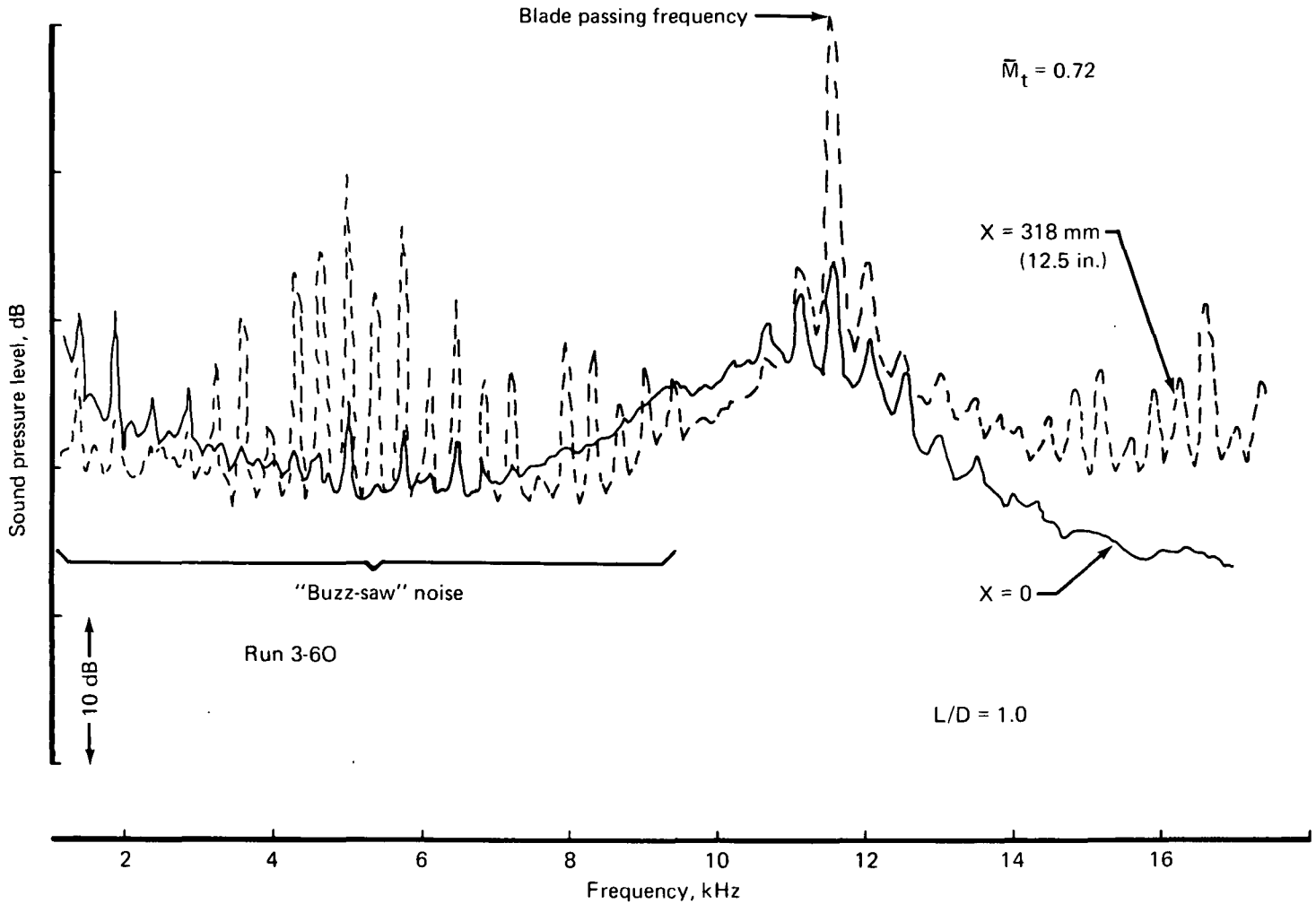

FIGURE 50.–NEAR FIELD, WALL KULITE, NOISE SPECTRA IN TAKEOFF INLET

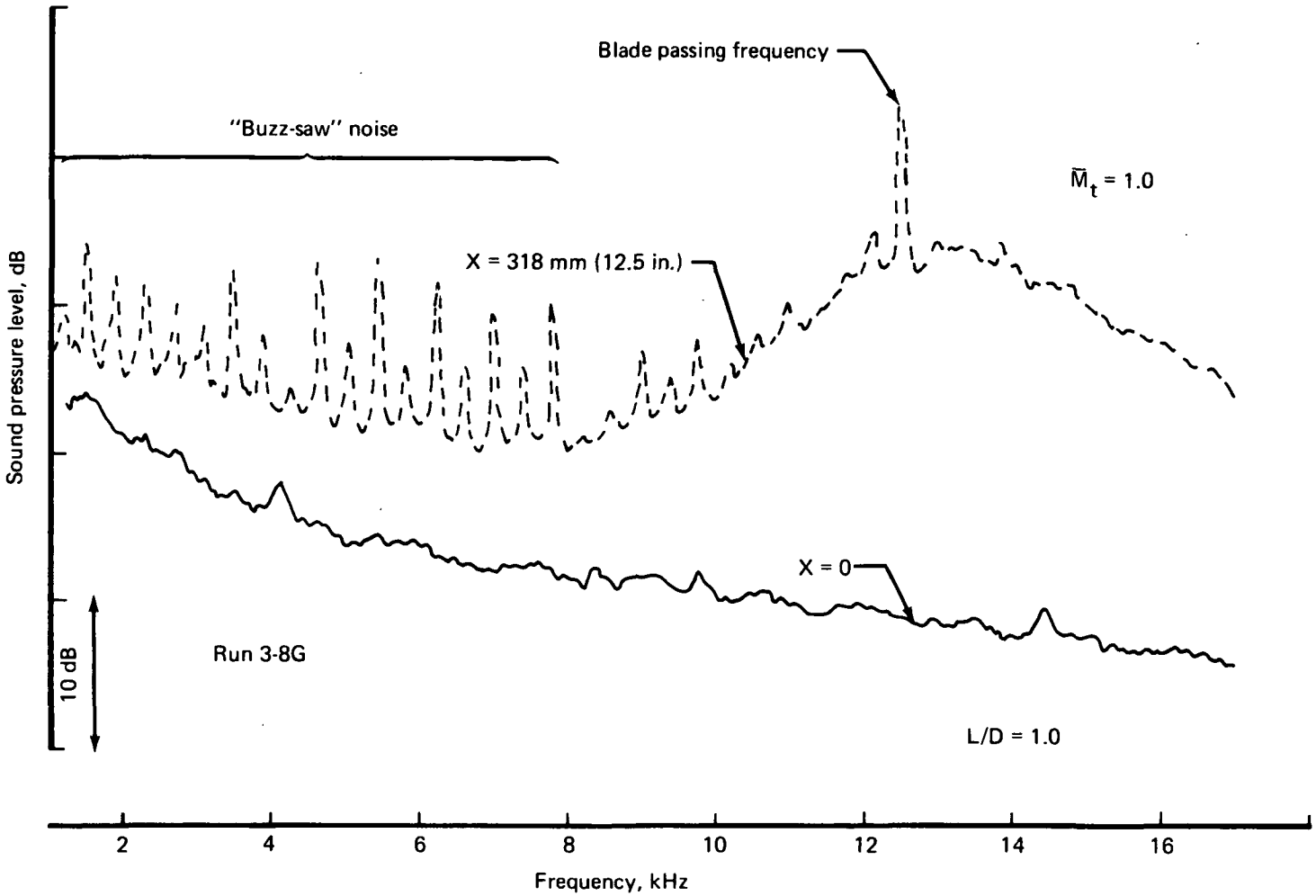

FIGURE 51.—NEAR FIELD, WALL KULITE, NOISE SPECTRA IN TAKEOFF INLET

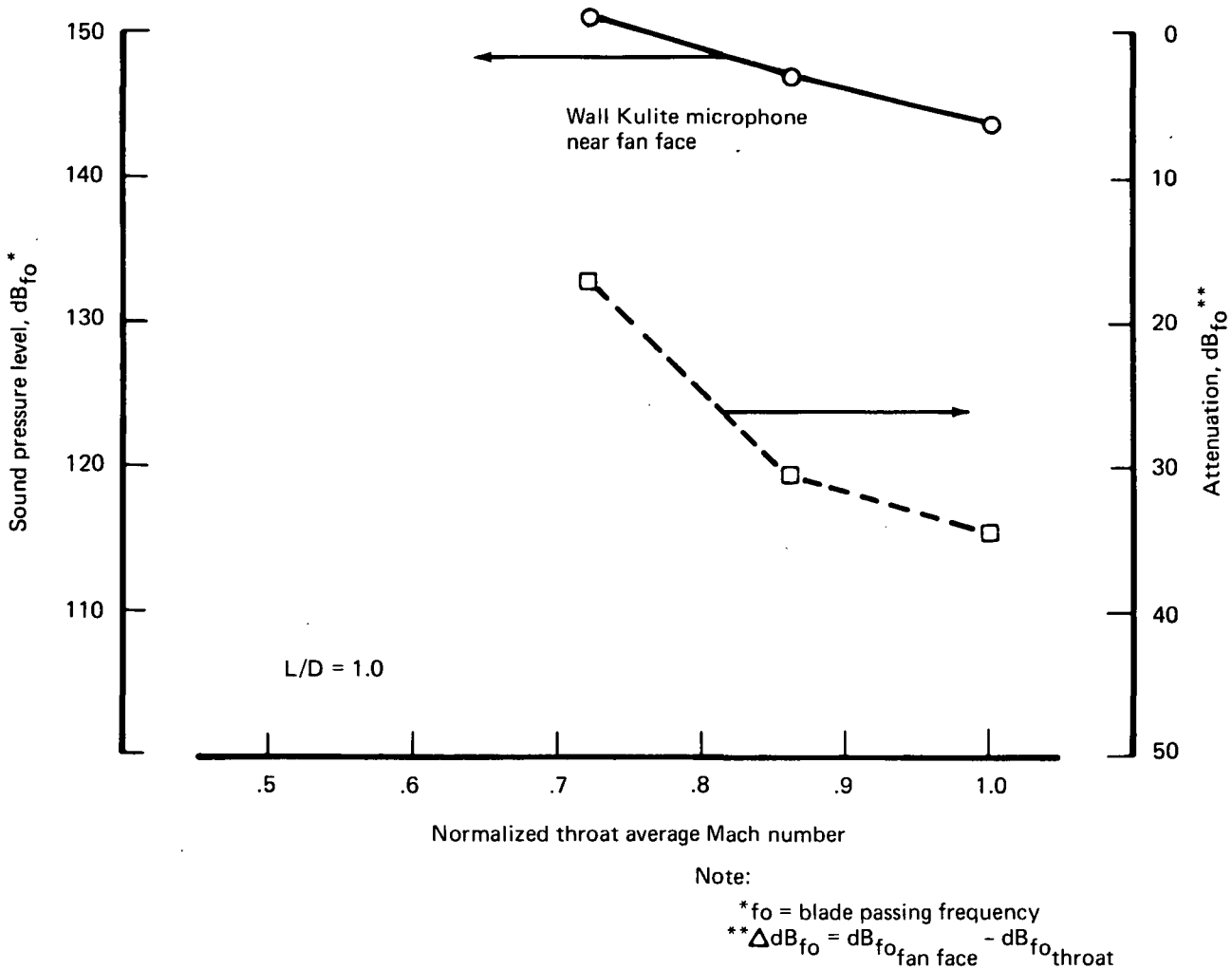

Note:

*fo = blade passing frequency

**$\Delta dB_{fo} = dB_{fo_{fan\ face}} - dB_{fo_{throat}}$

FIGURE 52.—ATTENUATION AT BLADE PASSING FREQUENCY VERSUS THROAT MACH NUMBER IN TAKEOFF INLET

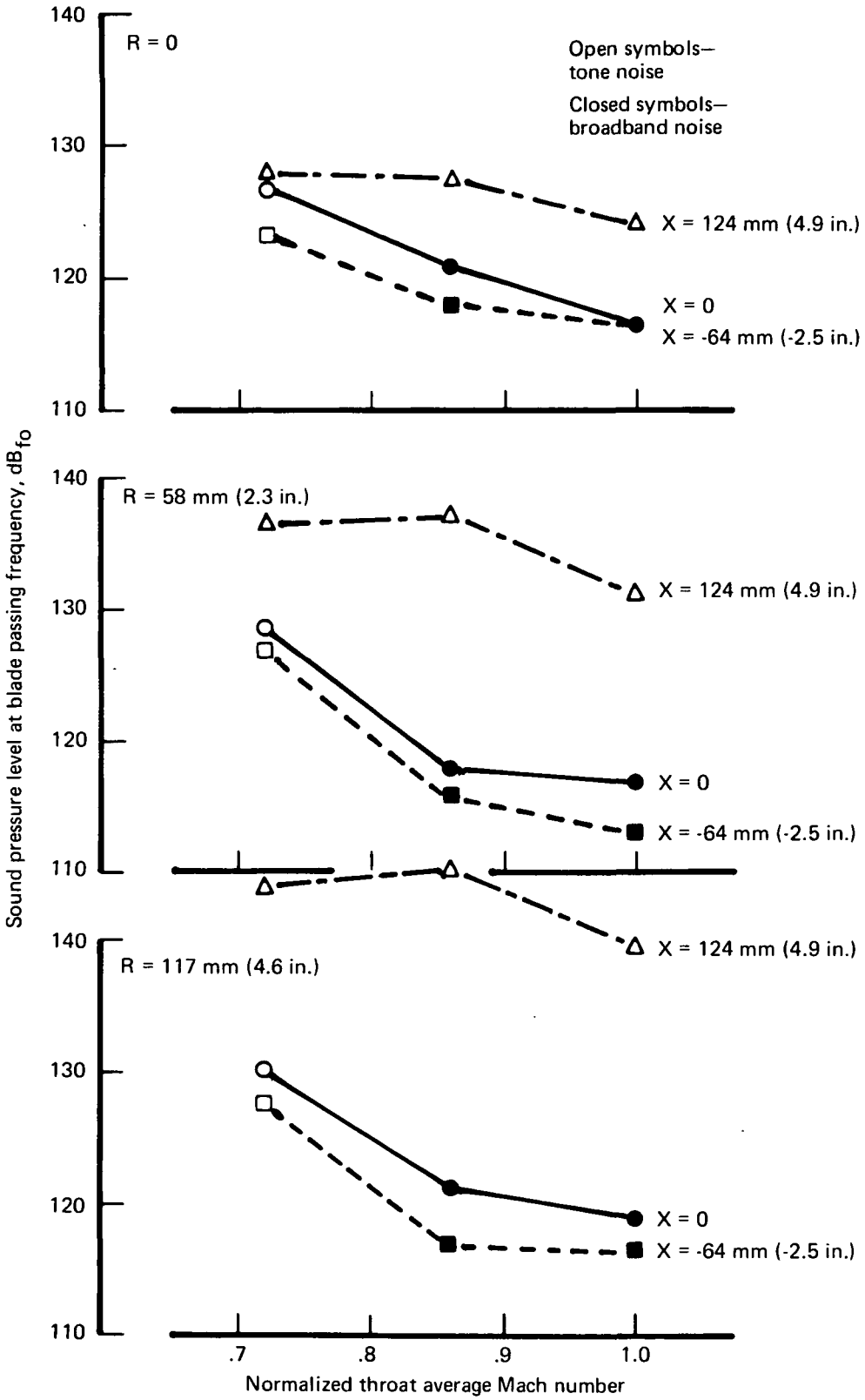

FIGURE 53.–BLADE PASSING TONE VERSUS THROAT MACH NUMBER IN TAKEOFF INLET

APPENDIX A

NARROWBAND FREQUENCY SPECTRA OF NEAR-FIELD NOISE MEASUREMENTS TAKEN INSIDE THE TWO SONIC INLETS

This appendix contains all the data taken during the steady-state operation of the stinger probe in the sonic inlets. The data are presented in constant (40-Hz) narrowband frequency spectra with a frequency range from 1000 to 20 000 Hz.

To facilitate access to the data, the spectra are arranged according to run number, as listed below.

Figure	Run	Title
A-1	2-10A	Wall Microphone Spectrum at -3.8 In. Downstream From Inlet Throat
A-2	2-10A	Wall Microphone Spectrum at 0.0 In. Downstream From Inlet Throat
A-3	2-10A	Wall Microphone Spectrum at 8.3 In. Downstream From Inlet Throat
A-4	2-10A	Wall Microphone Spectrum at 19.7 In. Downstream From Inlet Throat
A-5	2-10A	Stinger Probe Microphone Spectrum at (X; R)(-2.6 In.; 0.0 In.)
A-6	2-10B	Wall Microphone Spectrum at -3.8 In. Downstream From Inlet Throat
A-7	2-10B	Wall Microphone Spectrum at 0.0 In. Downstream From Inlet Throat
A-8	2-10B	Wall Microphone Spectrum at 8.3 In. Downstream From Inlet Throat
A-9	2-10B	Wall Microphone Spectrum at 19.7 In. Downstream From Inlet Throat
A-10	2-10B	Stinger Probe Microphone Spectrum at (X; R)(0.0 In.; 0.0 In.)
A-11	2-10C	Wall Microphone Spectrum at -3.8 In. Downstream From Inlet Throat
A-12	2-10C	Wall Microphone Spectrum at 0.0 In. Downstream From Inlet Throat
A-13	2-10C	Wall Microphone Spectrum at 8.3 In. Downstream From Inlet Throat
A-14	2-10C	Wall Microphone Spectrum at 19.7 In. Downstream From Inlet Throat
A-15	2-10C	Stinger Probe Microphone Spectrum at (X; R) (8.6 In.; 0.0 In.)
A-16	2-11A	Wall Microphone Spectrum at -3.8 In. Downstream From Inlet Throat
A-17	2-11A	Wall Microphone Spectrum at 0.0 In. Downstream From Inlet Throat

Figure	Run	Title
A-18	2-11A	Wall Microphone Spectrum at 8.3 In. Downstream From Inlet Throat
A-19	2-11A	Wall Microphone Spectrum at 19.7 In. Downstream From Inlet Throat
A-20	2-11A	Stinger Probe Microphone Spectrum at (X; R) (0.0 In.; 0.0 In.)
A-21	2-12A	Wall Microphone Spectrum at -3.8 In. Downstream From Inlet Throat
A-22	2-12A	Wall Microphone Spectrum at 0.0 In. Downstream From Inlet Throat
A-23	2-12A	Wall Microphone Spectrum at 8.3 In. Downstream From Inlet Throat
A-24	2-12A	Wall Microphone Spectrum at 19.7 In. Downstream From Inlet Throat
A-25	2-12A	Stinger Probe Microphone Spectrum at (X; R) (0.0 In.; 0.0 In.)
A-26	2-13A	Wall Microphone Spectrum at -3.8 In. Downstream From Inlet Throat
A-27	2-13A	Wall Microphone Spectrum at 0.0 In. Downstream From Inlet Throat
A-28	2-13A	Wall Microphone Spectrum at 8.3 In. Downstream From Inlet Throat
A-29	2-13A	Wall Microphone Spectrum at 19.7 In. Downstream From Inlet Throat
A-30	2-13A	Stinger Probe Spectrum Microphone at (X; R) (0.0 In.; 0.0 In.)
A-31	2-14A	Wall Microphone Spectrum at -3.8 In. Downstream From Inlet Throat
A-32	2-14A	Wall Microphone Spectrum at 0.0 In. Downstream From Inlet Throat
A-33	2-14A	Wall Microphone Spectrum at 8.3 In. Downstream From Inlet Throat
A-34	2-14A	Wall Microphone Spectrum at 19.7 In. Downstream From Inlet Throat
A-35	2-14A	Stinger Probe Microphone Spectrum at (X; R) (0.0 In.; 0.0 In.)
A-36	2-15A	Wall Microphone Spectrum at -3.8 In. Downstream From Inlet Throat
A-37	2-15A	Wall Microphone Spectrum at 0.0 In. Downstream From Inlet Throat
A-38	2-15A	Wall Microphone Spectrum at 8.3 In. Downstream From Inlet Throat
A-39	2-15A	Wall Microphone Spectrum at 19.7 In. Downstream From Inlet Throat
A-40	2-15A	Stinger Probe Microphone Spectrum at (X; R) (-2.6 In.; 0.0 In.)

Figure	Run	Title
A-41	2-15B	Stinger Probe Microphone Spectrum at (X; R) (-2.6 In.; 2.0 In.)
A-42	2-15C	Stinger Probe Microphone Spectrum at (X; R) (-2.6 In.; 4.0 In.)
A-43	2-15D	Stinger Probe Microphone Spectrum at (X; R) (0.0 In.; 4.0 In.)
A-44	2-15E	Stinger Probe Microphone Spectrum at (X; R) (0.0 In.; 2.0 In.)
A-45	2-15F	Stinger Probe Microphone Spectrum at (X; R) (0.0 In.; 0.0 In.)
A-46	2-15G	Stinger Probe Microphone Spectrum at (X; R) (4.0 In.; 0.0 In.)
A-47	2-15H	Stinger Probe Microphone Spectrum at (X; R) (4.0 In.; 2.0 In.)
A-48	2-15I	Stinger Probe Microphone Spectrum at (X; R) (4.0 In.; 4.0 In.)
A-49	2-15J	Stinger Probe Microphone Spectrum at (X; R) (8.5 In.; 4.0 In.)
A-50	2-15K	Stinger Probe Microphone Spectrum at (X; R) (8.5 In.; 2.0 In.)
A-51	2-15L	Stinger Probe Microphone Spectrum at (X; R) (8.5 In.; 0.0 In.)
A-52	3-6I	Stinger Probe Microphone Spectrum at (X; R) (-2.5 In.; 0.0 In.)
A-53	3-6J	Stinger Probe Microphone Spectrum at (X; R) (-2.5 In.; 2.3 In.)
A-54	3-6K	Stinger Probe Microphone Spectrum at (X; R) (-2.5 In.; 4.6 In.)
A-55	3-6L	Stinger Probe Microphone Spectrum at (X; R) (0.0 In.; 0.0 In.)
A-56	3-6M	Stinger Probe Microphone Spectrum at (X; R) (0.0 In.; 2.3 In.)
A-57	3-6N	Stinger Probe Microphone Spectrum at (X; R) (0.0 In.; 4.6 In.)
A-58	3-6O	Stinger Probe Microphone Spectrum at (X; R) (4.9 In.; 0.0 In.)
A-59	3-6P	Stinger Probe Microphone Spectrum at (X; R) (4.9 In.; 2.3 In.)
A-60	3-6Q	Stinger Probe Microphone Spectrum at (X; R) (4.9 In.; 4.6 In.)
A-61	3-60	Wall Microphone Spectrum at -2.5 In. Downstream From Inlet Throat
A-62	3-60	Wall Microphone Spectrum at 0.0 In. Downstream From Inlet Throat
A-63	3-60	Wall Microphone Spectrum at 3.8 In. Downstream From Inlet Throat

Figure	Run	Title
A-64	3-60	Wall Microphone Spectrum at 14.1 In. Downstream From Inlet Throat
A-65	3-7G	Stinger Probe Microphone Spectrum at (X; R) (4.9 In.; 0.0 In.)
A-66	3-7H	Stinger Probe Microphone Spectrum at (X; R) (4.9 In.; 2.3 In.)
A-67	3-7I	Stinger Probe Microphone Spectrum at (X; R) (4.9 In.; 4.6 In.)
A-68	3-7J	Stinger Probe Microphone Spectrum at (X; R) (0.0 In.; 4.6 In.)
A-69	3-7K	Stinger Probe Microphone Spectrum at (X; R) (0.0 In.; 2.3 In.)
A-70	3-7L	Stinger Probe Microphone Spectrum at (X; R) (0.0 In.; 0.0 In.)
A-71	3-7M	Stinger Probe Microphone Spectrum at (X; R) (-2.5 In.; 0.0 In.)
A-72	3-7N	Stinger Probe Microphone Spectrum at (X; R) (-2.5 In.; 2.3 In.)
A-73	3-7O	Stinger Probe Microphone Spectrum at (X; R) (-2.5 In.; 4.6 In.)
A-74	3-7G	Wall Microphone Spectrum at -2.5 In. Downstream From Inlet Throat
A-75	3-7G	Wall Microphone Spectrum at 0.0 In. Downstream From Inlet Throat
A-76	3-7G	Wall Microphone Spectrum at 3.8 In. Downstream From Inlet Throat
A-77	3-7G	Wall Microphone Spectrum at 14.1 In. Downstream From Inlet Throat
A-78	3-8G	Stinger Probe Microphone Spectrum at (X; R) (4.9 In.; 0.0 In.)
A-79	3-8H	Stinger Probe Microphone Spectrum at (X; R) (4.9 In.; 2.3 In.)
A-80	3-8I	Stinger Probe Microphone Spectrum at (X; R) (4.9 In.; 4.6 In.)
A-81	3-8J	Stinger Probe Microphone Spectrum at (X; R) (0.0 In.; 4.6 In.)
A-82	3-8K	Stinger Probe Microphone Spectrum at (X; R) (0.0 In.; 2.3 In.)
A-83	3-8L	Stinger Probe Microphone Spectrum at (X; R) (0.0 In.; 0.0 In.)
A-84	3-8M	Stinger Probe Microphone Spectrum at (X; R) (-2.5 In.; 0.0 In.)
A-85	3-8N	Stinger Probe Microphone Spectrum at (X; R) (-2.5 In.; 2.3 In.)
A-86	3-8Q	Stinger Probe Microphone Spectrum at (X; R) (-2.5 In.; 4.6 In.)

Figure	Run	Title
A-87	3-8G	Wall Microphone Spectrum at -2.5 In. Downstream From Inlet Throat
A-88	3-8G	Wall Microphone Spectrum at 0.0 In. Downstream From Inlet Throat
A-89	3-8G	Wall Microphone Spectrum at 3.8 In. Downstream From Inlet Throat
A-90	3-8G	Wall Microphone Spectrum at 14.1 In. Downstream From Inlet Throat

Page Intentionally Left Blank

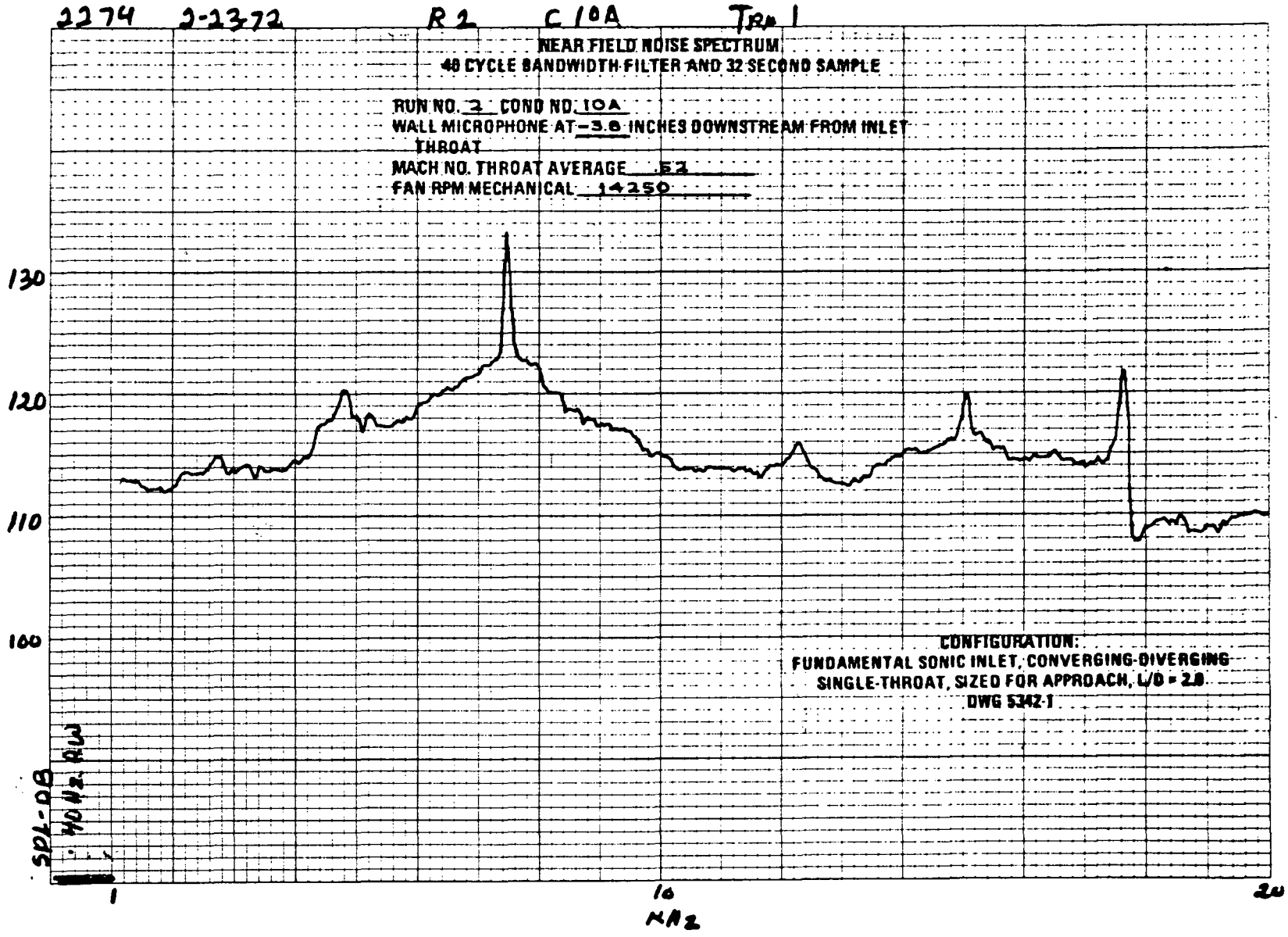

FIGURE A-1.—RUN 2-10A, WALL MICROPHONE SPECTRUM AT -3.8 IN. DOWNSTREAM FROM INLET THROAT

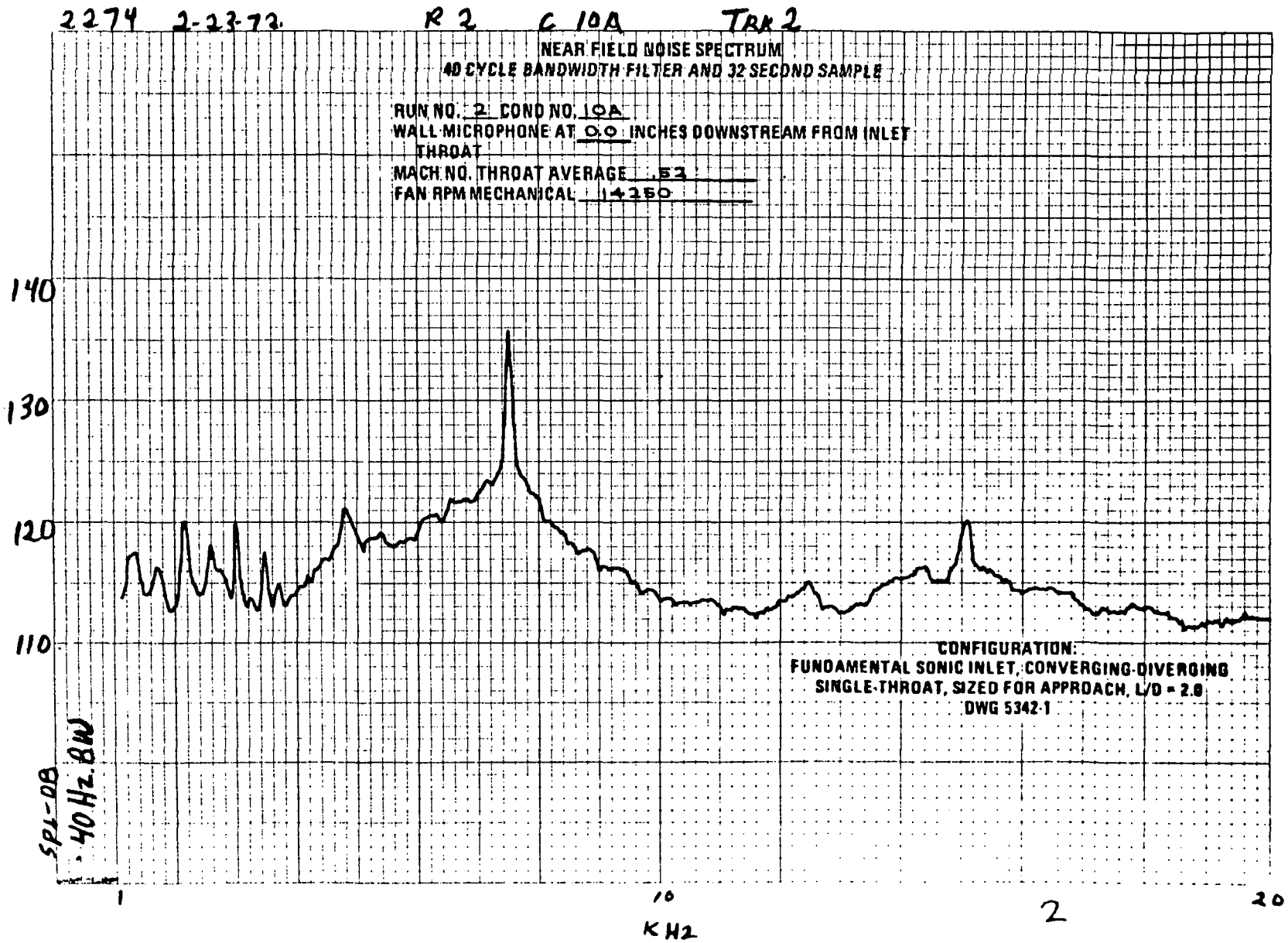

FIGURE A-2.—RUN 2-10A, WALL MICROPHONE SPECTRUM AT 0.0 IN. DOWNSTREAM FROM INLET THROAT

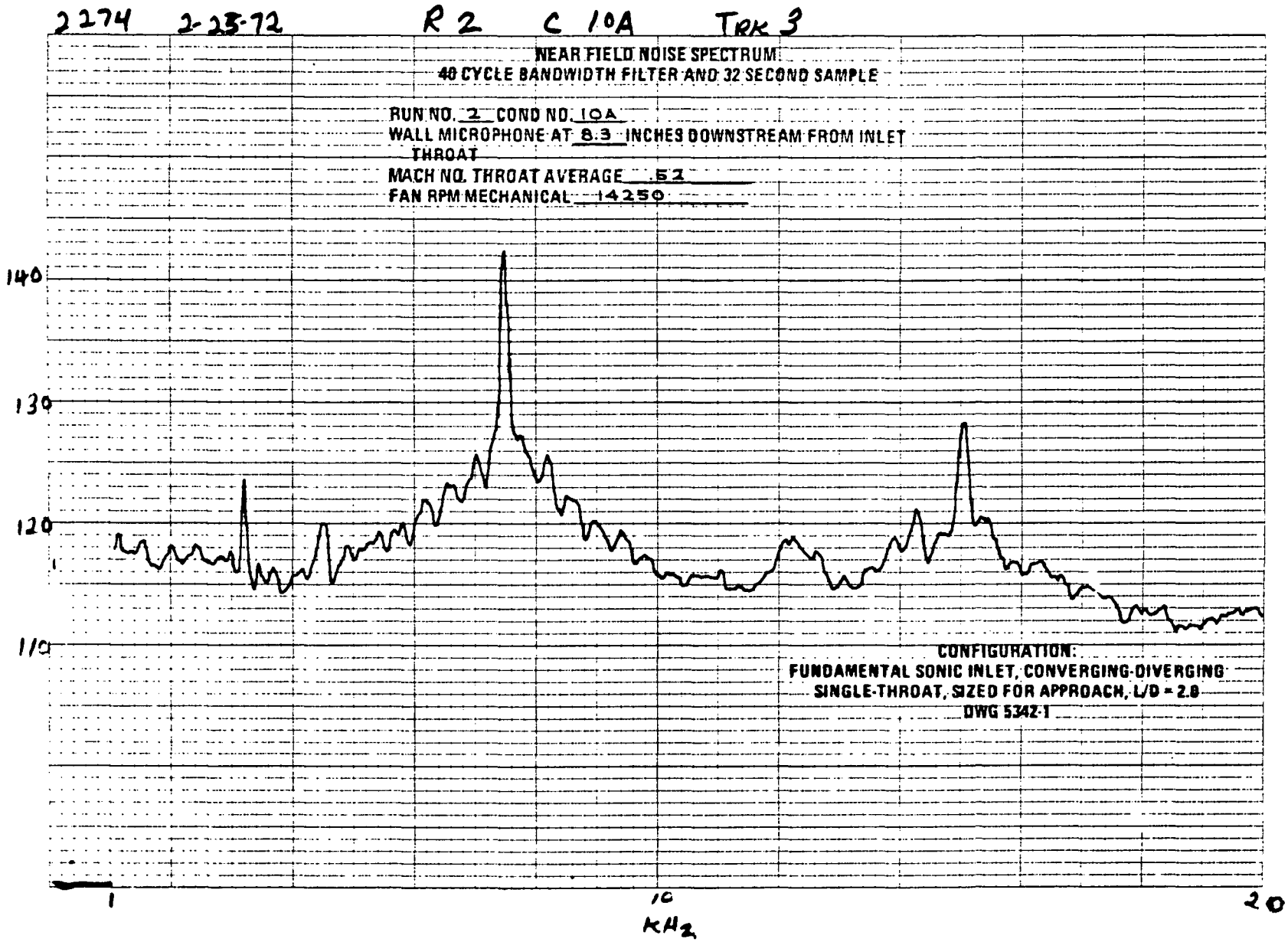

FIGURE A-3.—RUN 2-10A, WALL MICROPHONE SPECTRUM AT 8.3 IN. DOWNSTREAM FROM INLET THROAT.

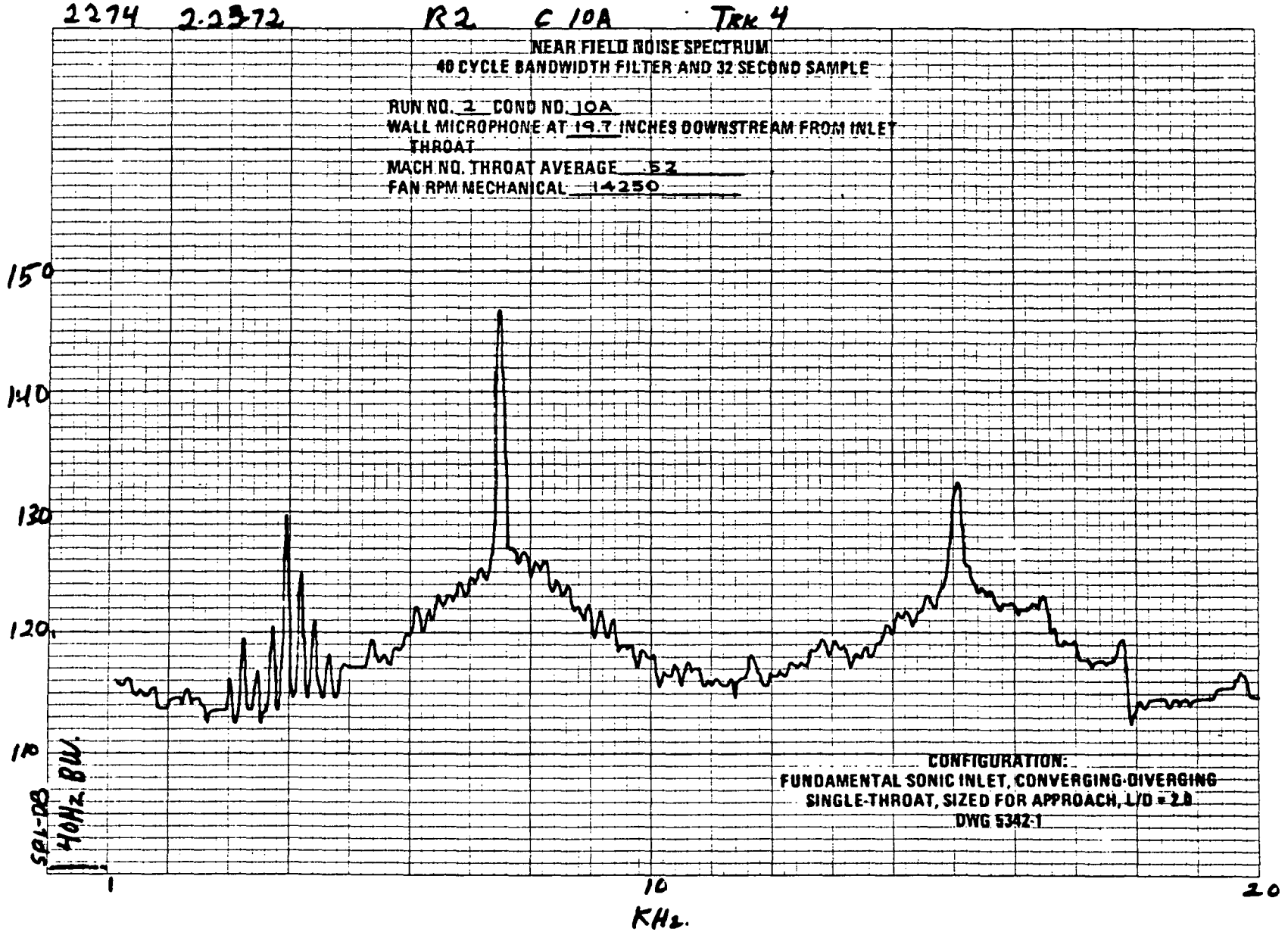

FIGURE A-4.—RUN 2-10A, WALL MICROPHONE SPECTRUM AT 19.7 IN. DOWNSTREAM FROM INLET THROAT

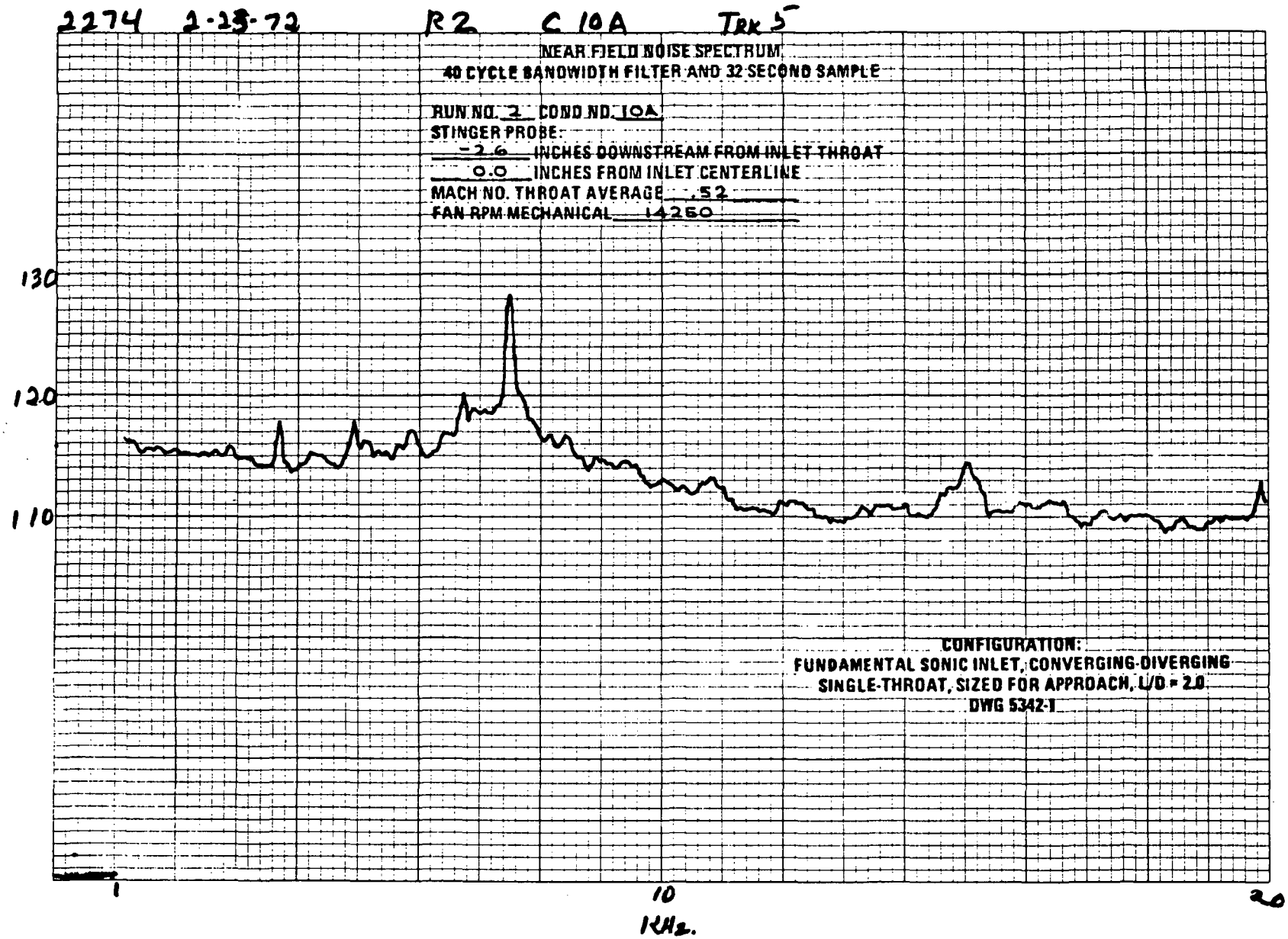

FIGURE A-5.—RUN 2-10A, STINGER PROBE MICROPHONE SPECTRUM AT (X; R) (-2.6 IN; 0.0 IN.)

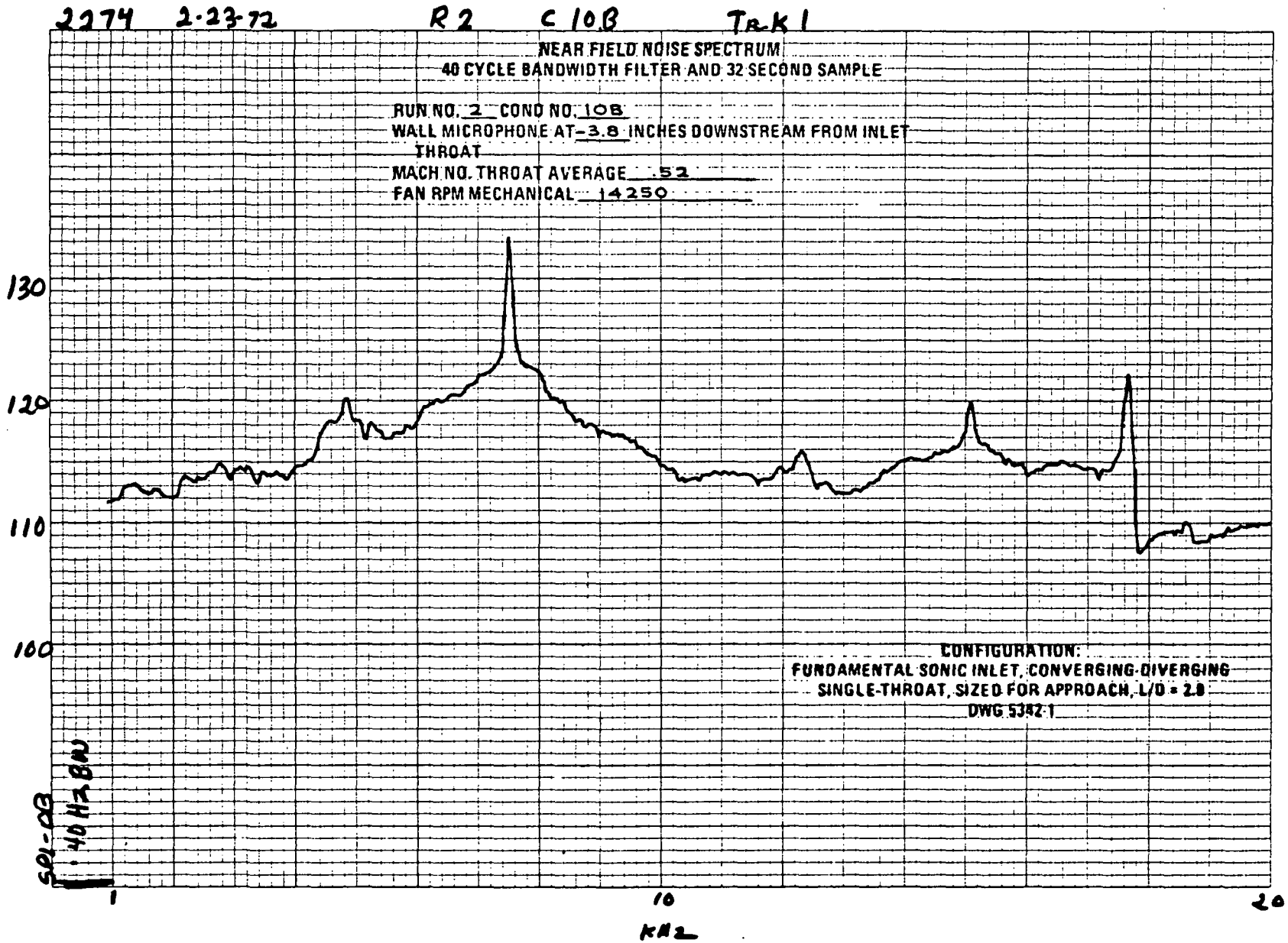

FIGURE A-6.—RUN 2-10B, WALL MICROPHONE SPECTRUM AT -3.8 IN. DOWNSTREAM FROM INLET THROAT

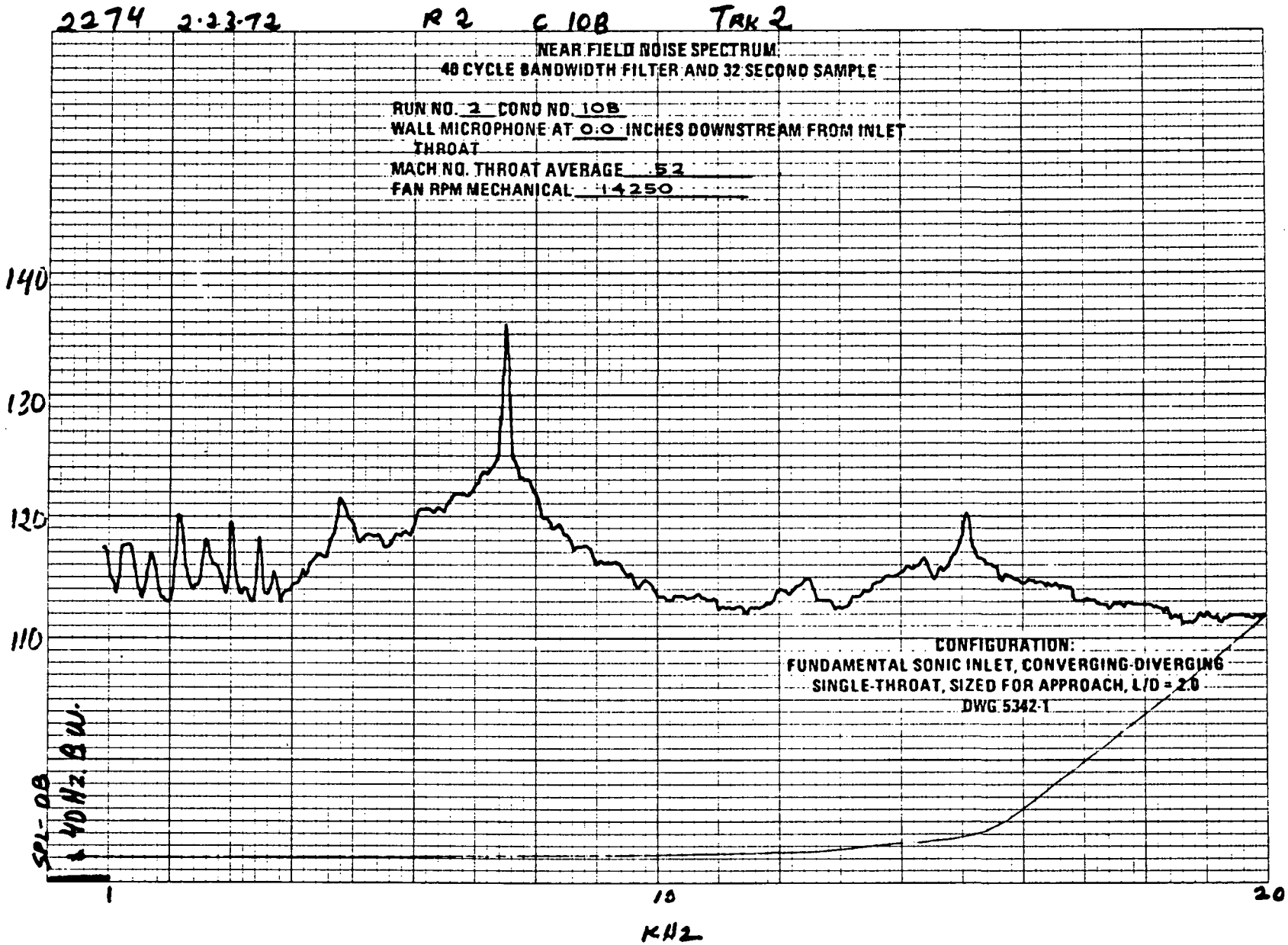

FIGURE A-7.—RUN 2-10B, WALL MICROPHONE SPECTRUM AT 0.0 IN. DOWNSTREAM FROM INLET THROAT

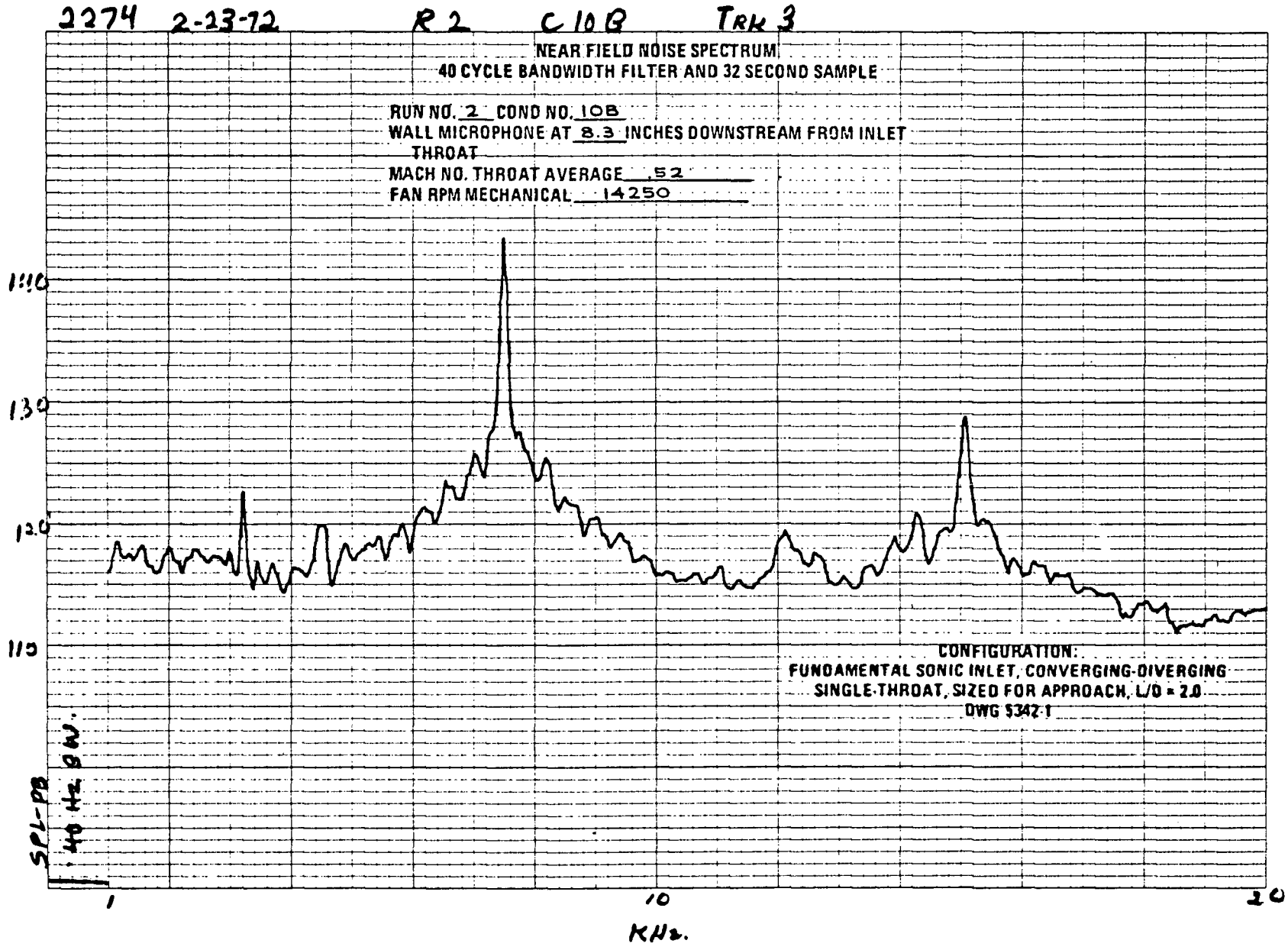

FIGURE A-8.—RUN 2-10B, WALL MICROPHONE SPECTRUM AT 8.3 IN. DOWNSTREAM FROM INLET THROAT

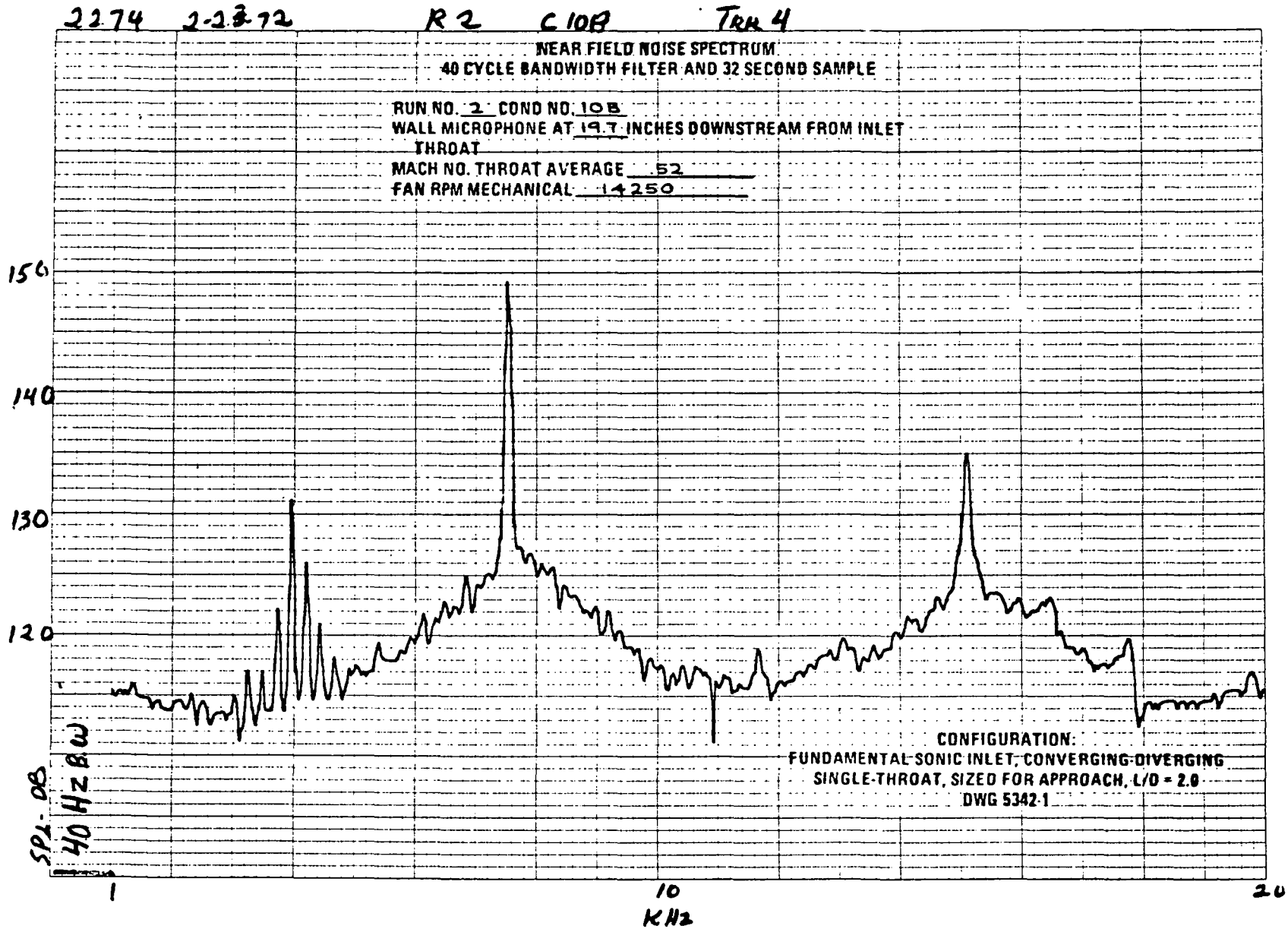

FIGURE A-9.—RUN 2-10B, WALL MICROPHONE SPECTRUM AT 19.7 IN. DOWNSTREAM FROM INLET THROAT

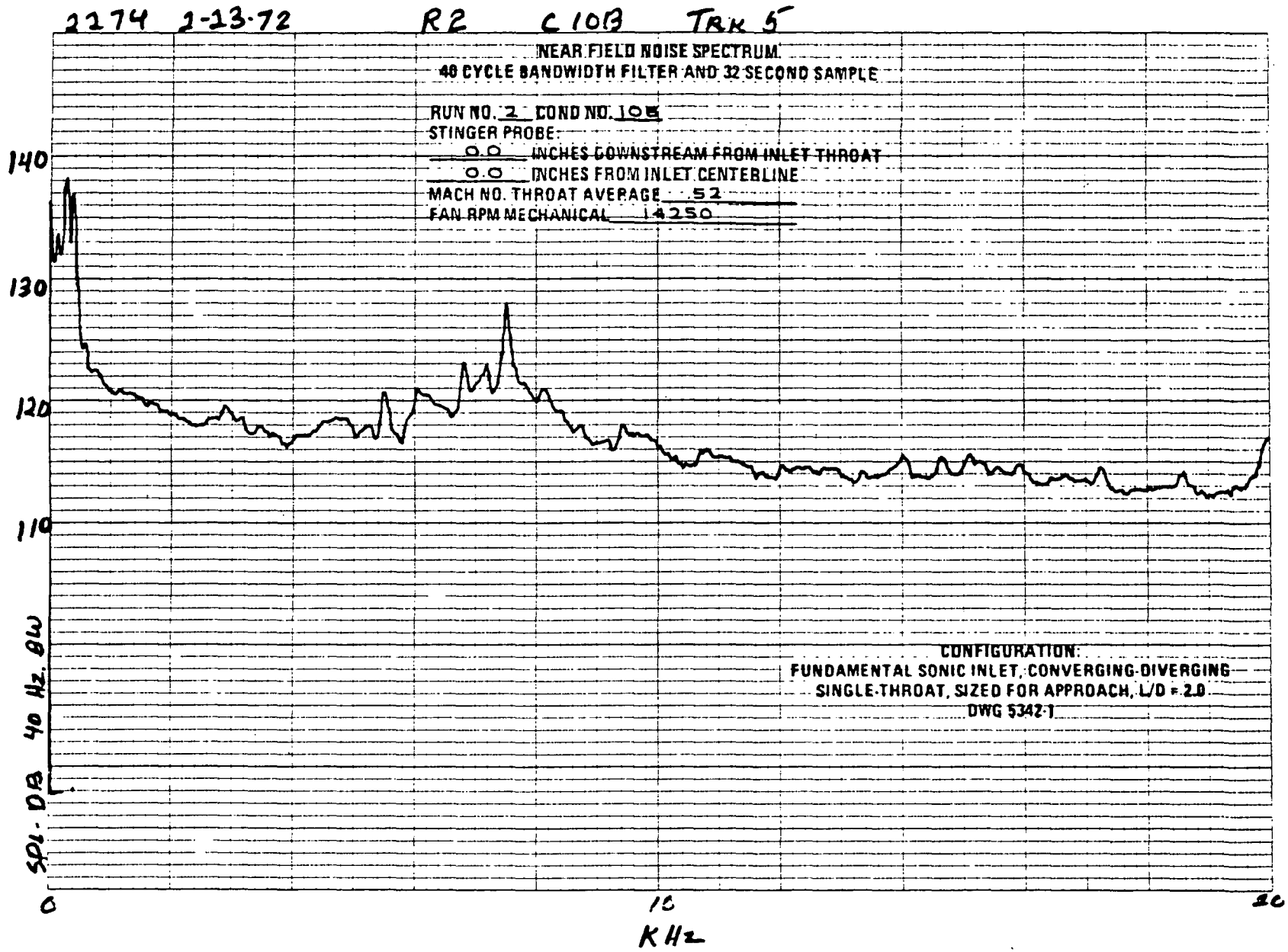

FIGURE A-10.—RUN 2-10B, STINGER PROBE MICROPHONE SPECTRUM AT (X; R) (0.0 IN.; 0.0 IN.)

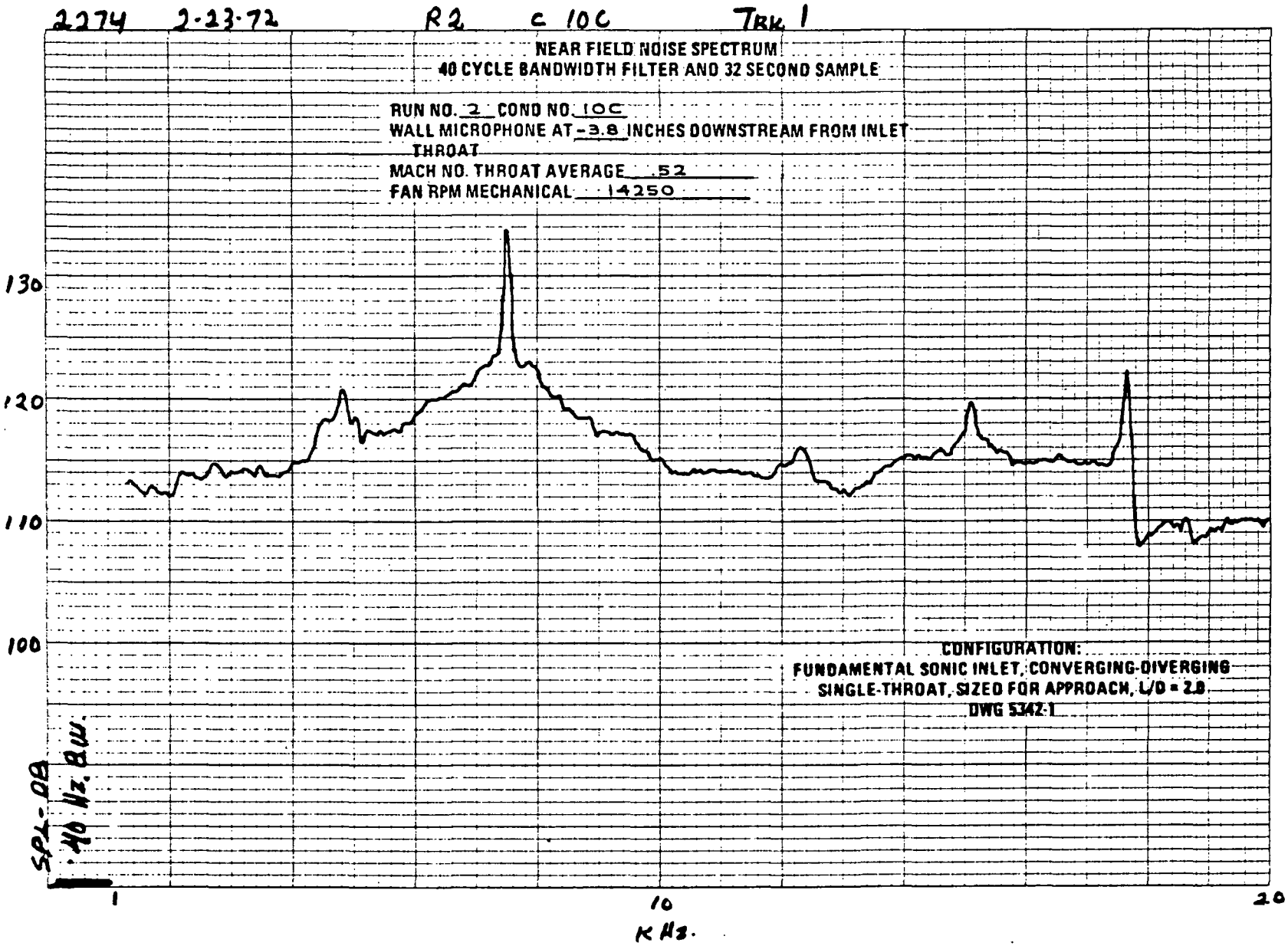

FIGURE A-11.—RUN 2-10C, WALL MICROPHONE SPECTRUM AT -3.8 IN. DOWNSTREAM FROM INLET THROAT

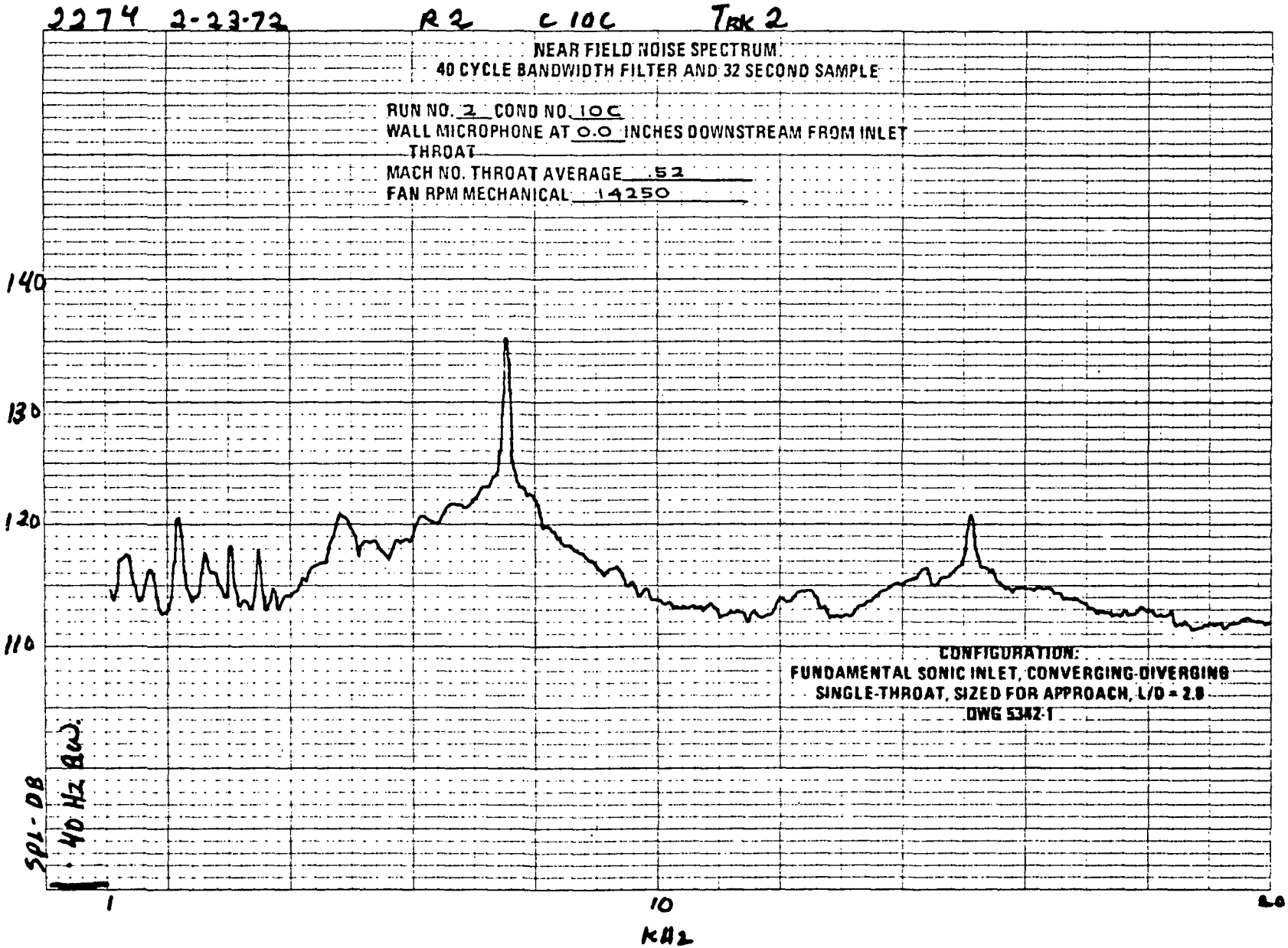

FIGURE A-12.—RUN 2-10C, WALL MICROPHONE SPECTRUM AT 0.0 IN. DOWNSTREAM FROM INLET THROAT

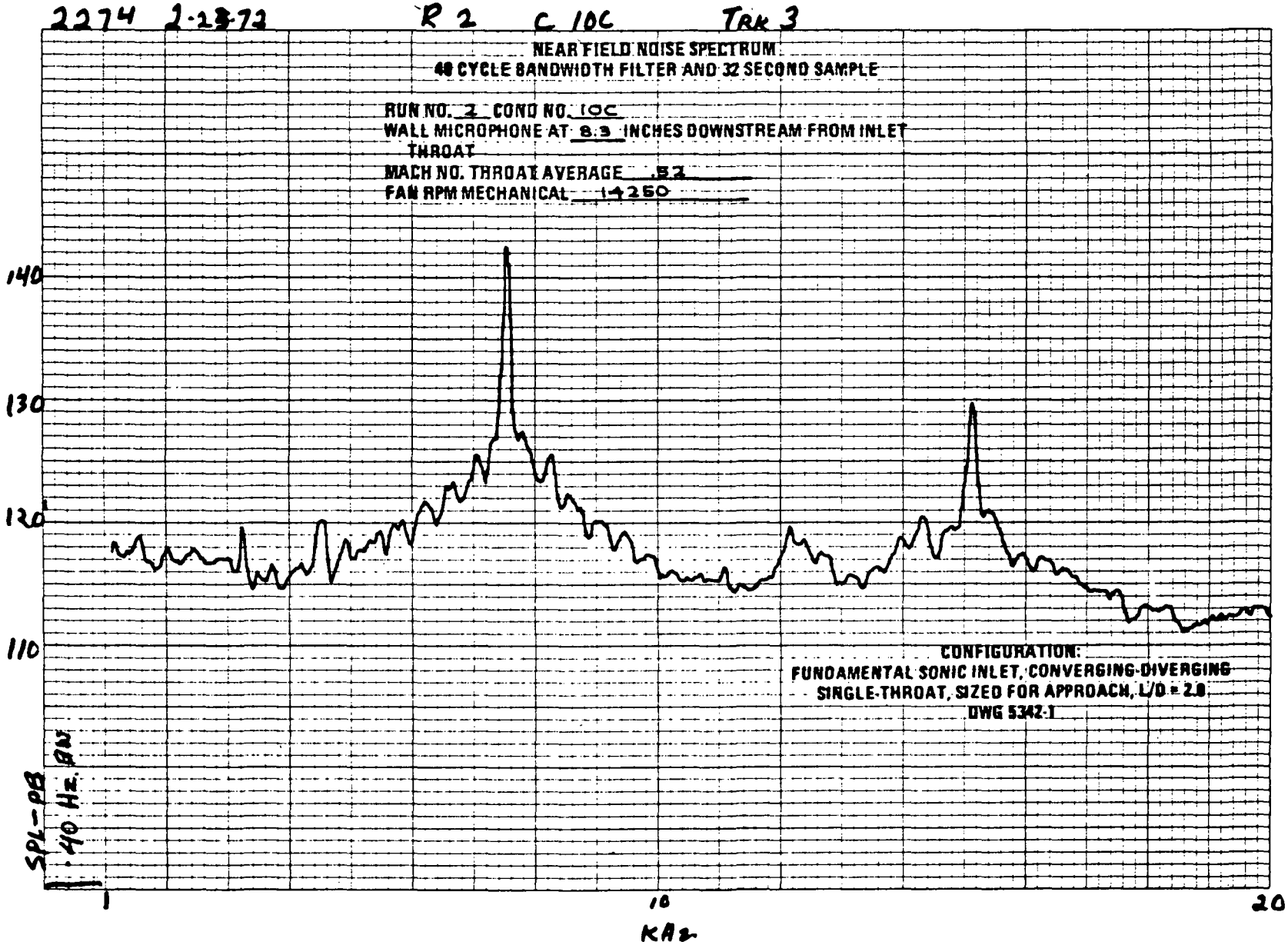

FIGURE A-13.–RUN 2-10C, WALL MICROPHONE SPECTRUM AT 8.3 IN. DOWNSTREAM FROM INLET THROAT

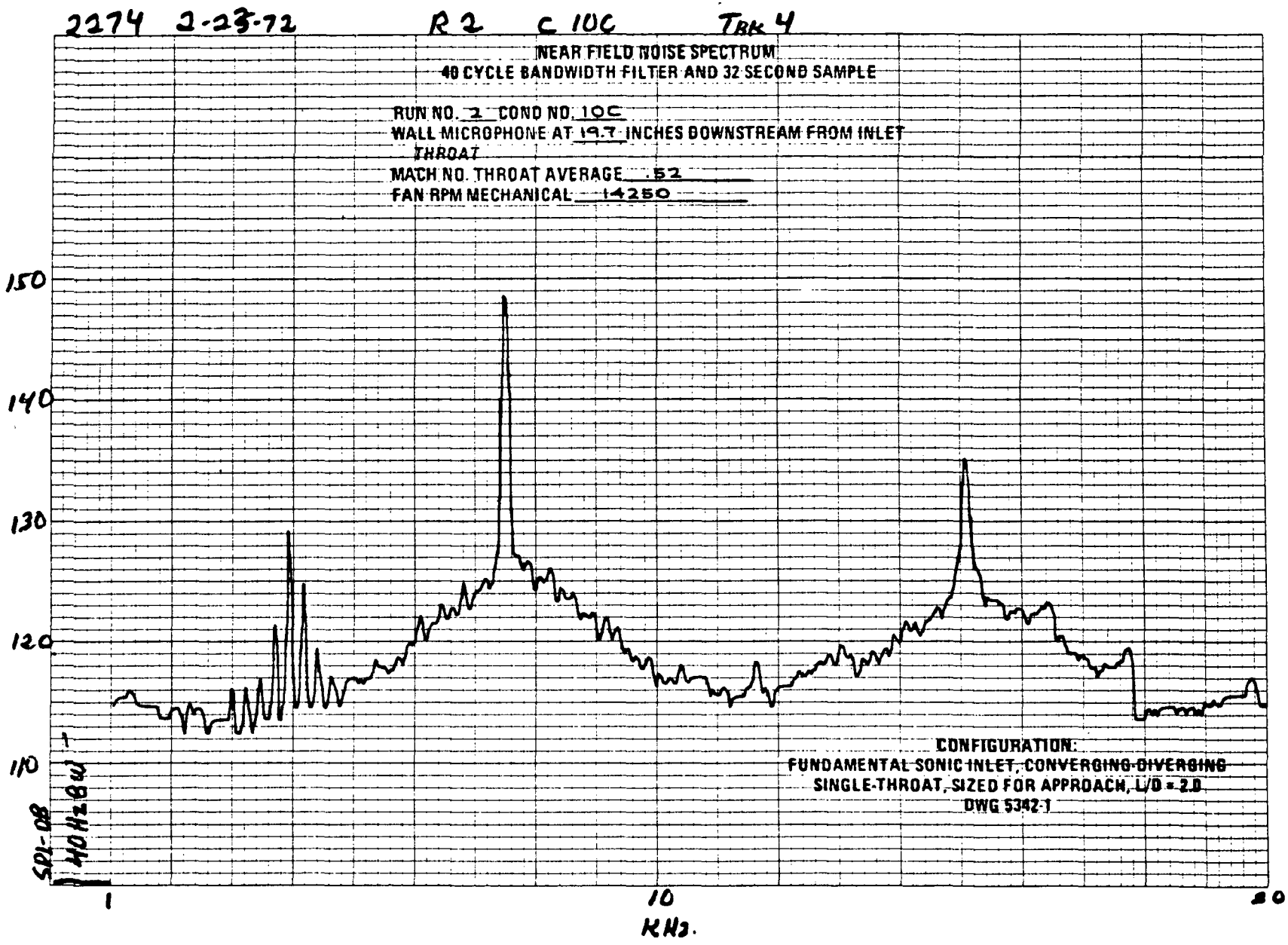

FIGURE A-14.—RUN 2-10C, WALL MICROPHONE SPECTRUM AT 19.7 IN. DOWNSTREAM FROM INLET THROAT

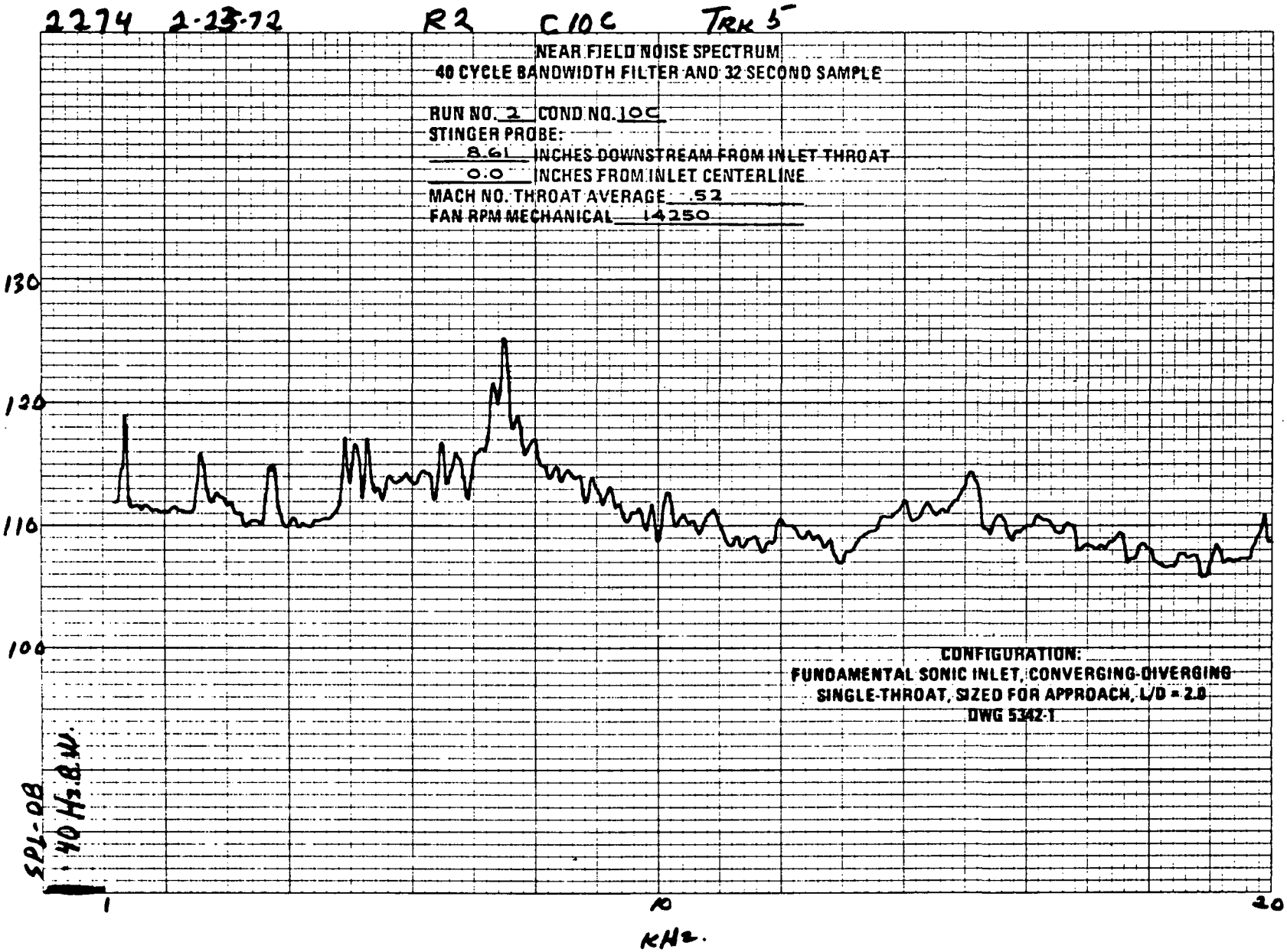

FIGURE A-15.—RUN 2-10C, STINGER PROBE MICROPHONE SPECTRUM AT (X; R) (8.6 IN.; 0.0 IN.)

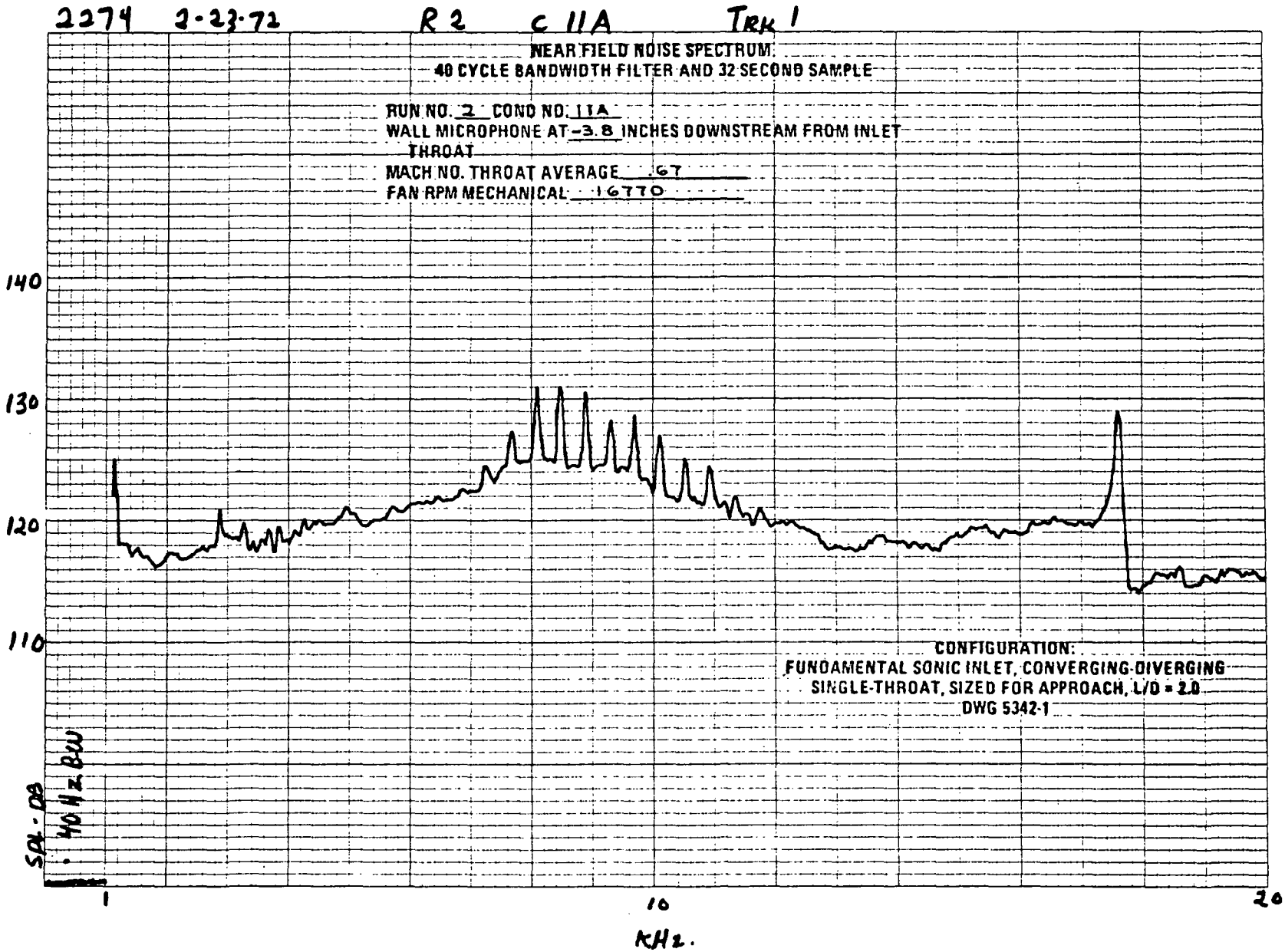

FIGURE A-16.—RUN 2-11A, WALL MICROPHONE SPECTRUM AT -3.8 IN. DOWNSTREAM FROM INLET THROAT

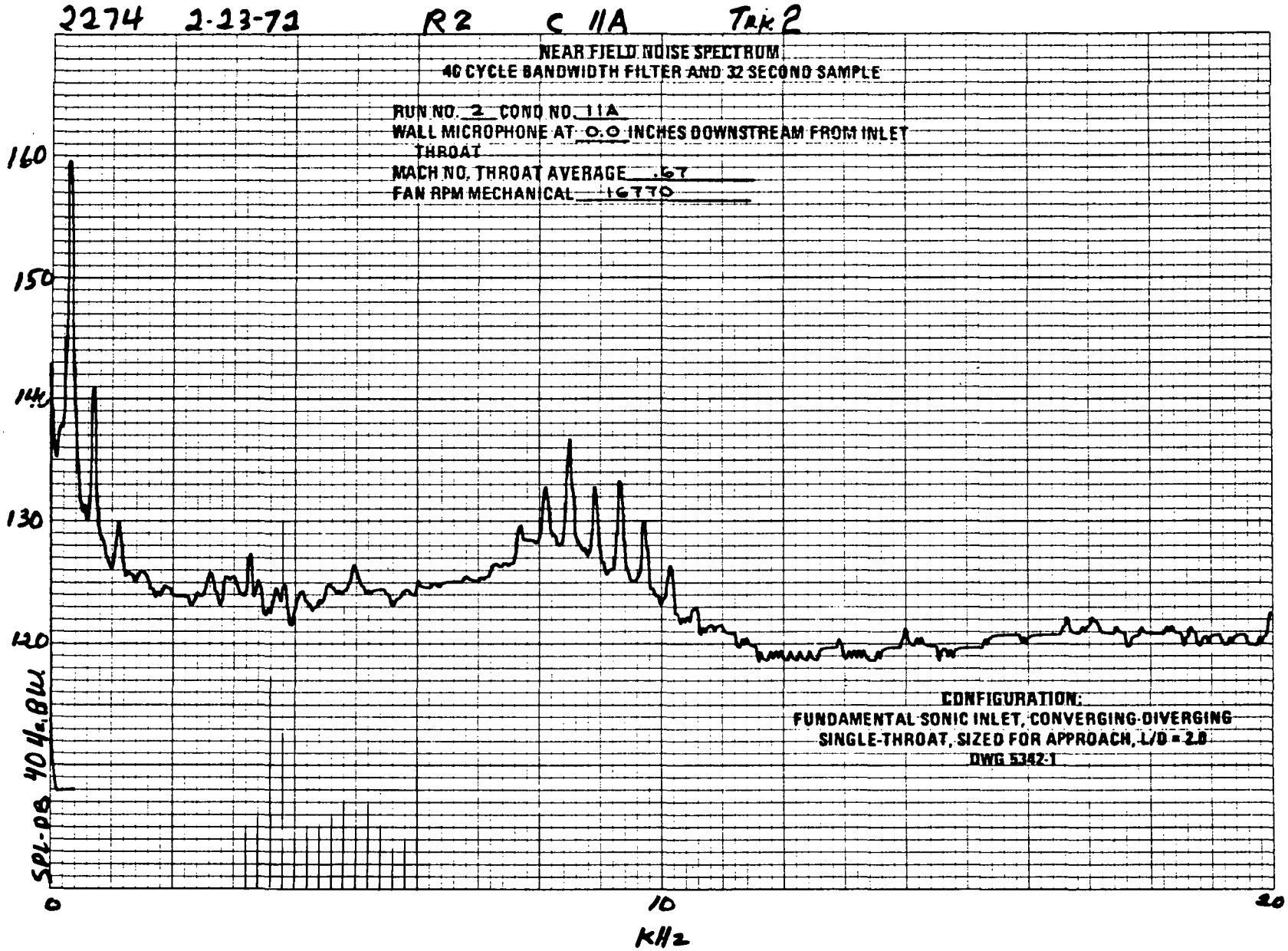

FIGURE A-17.—RUN 2-11A, WALL MICROPHONE SPECTRUM AT 0.0 IN. DOWNSTREAM FROM INLET THROAT

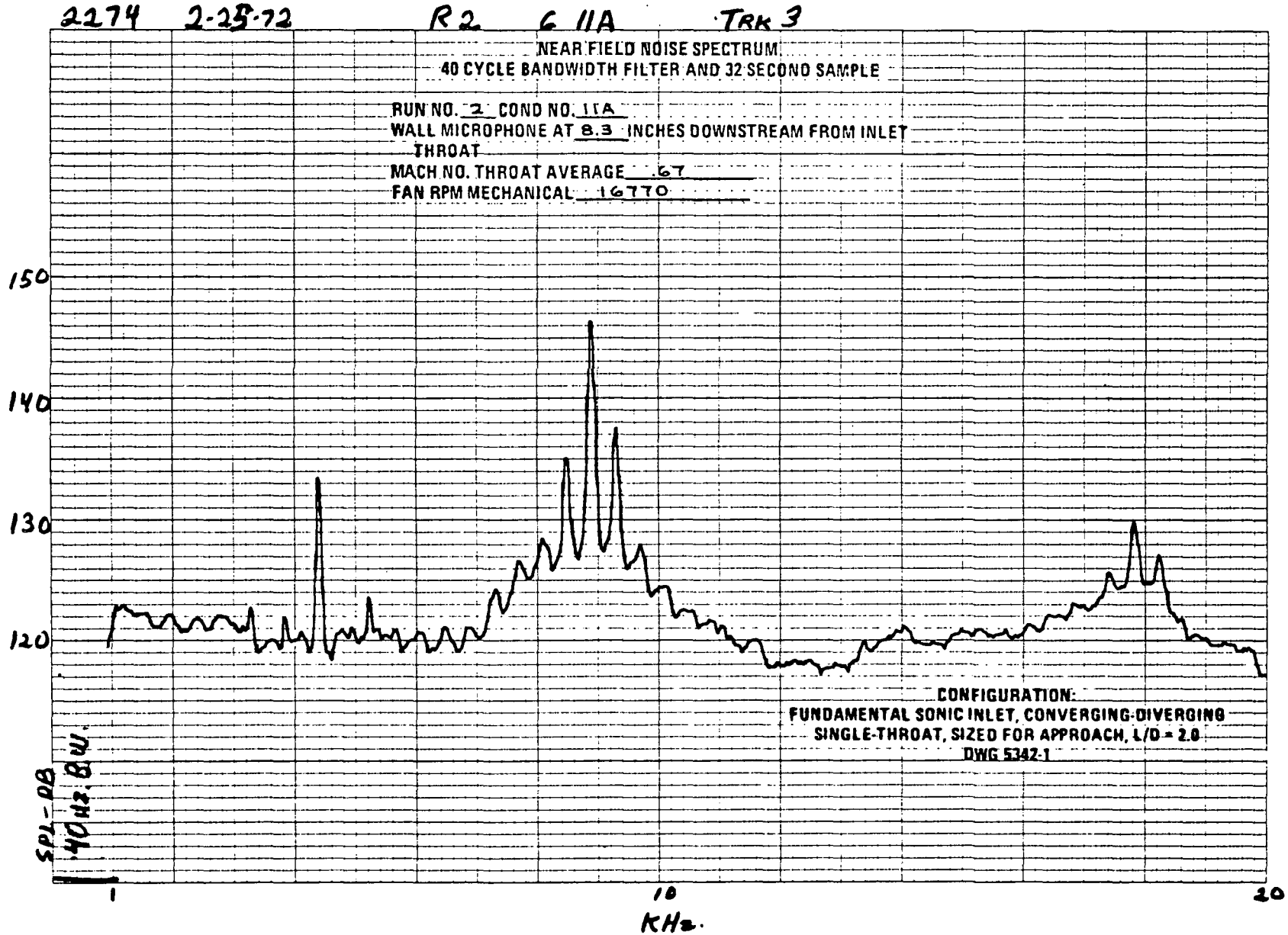

FIGURE A-18.—RUN 2-11A, WALL MICROPHONE SPECTRUM AT 8.3 IN. DOWNSTREAM FROM INLET THROAT

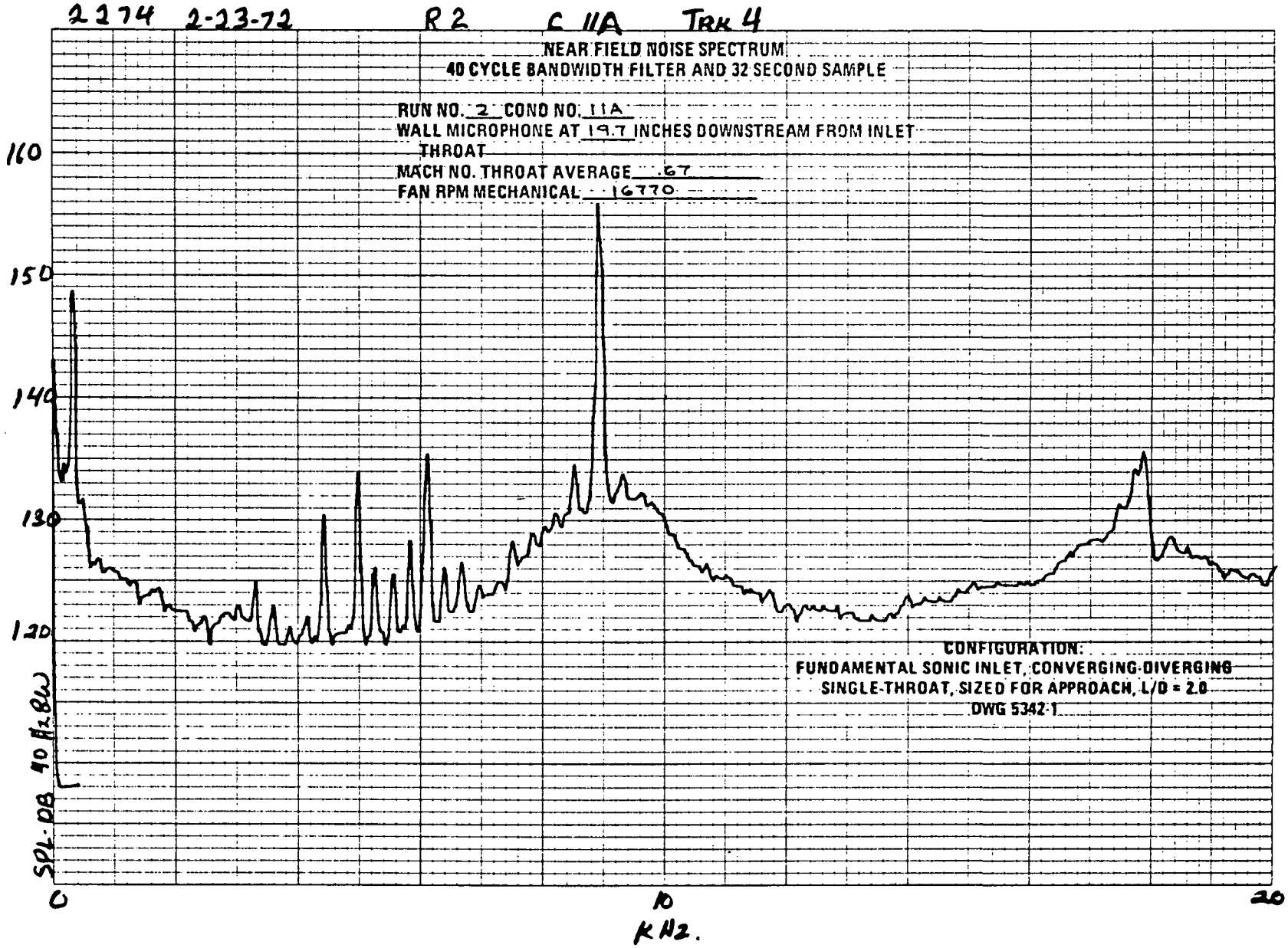

FIGURE A-19.—RUN 2-11A, WALL MICROPHONE SPECTRUM AT 19.7 IN. DOWNSTREAM FROM INLET THROAT

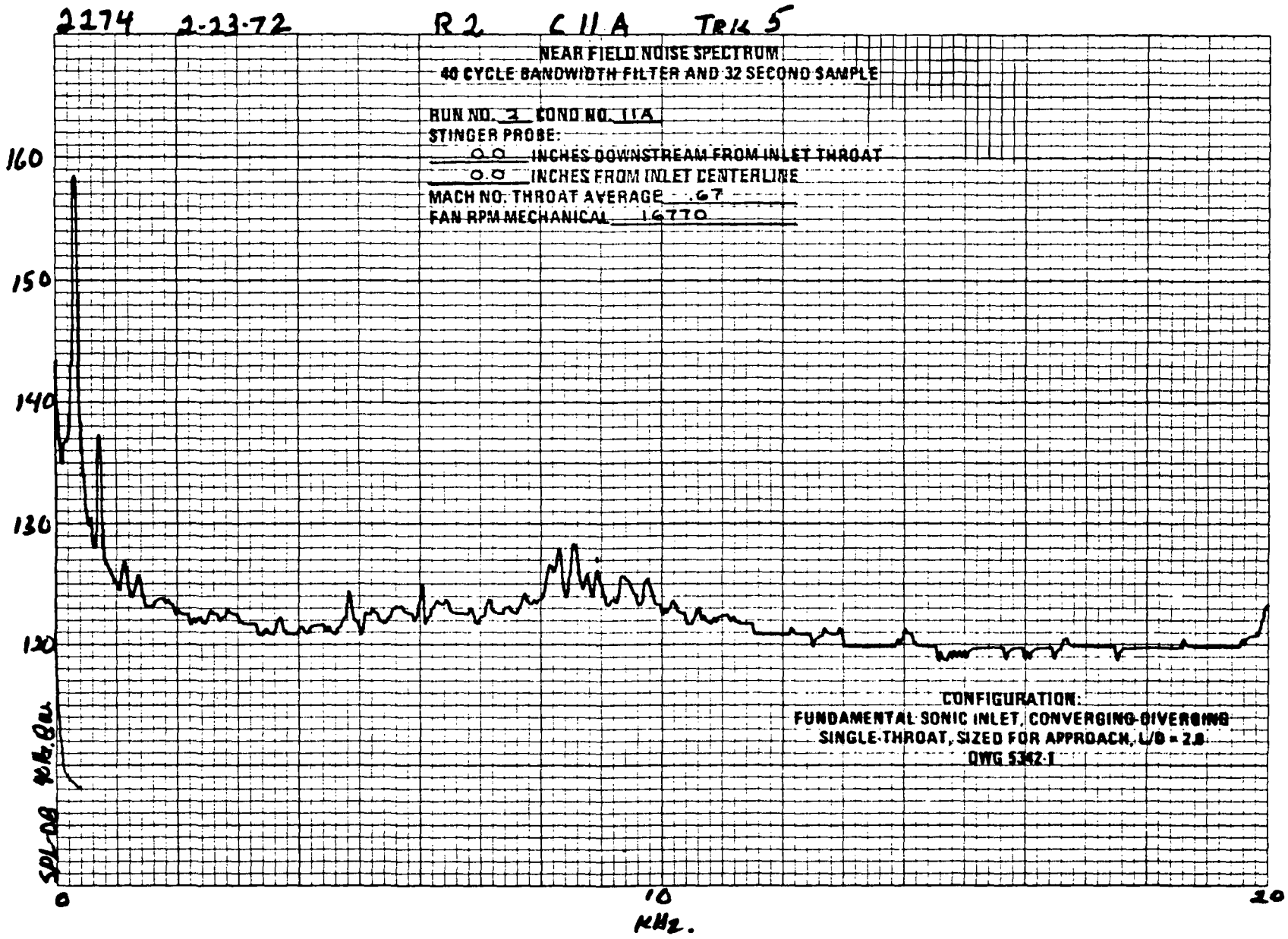

FIGURE A-20.—RUN 2-11A, STINGER PROBE MICROPHONE SPECTRUM AT (X; R) (0.0 IN.; 0.0 IN.)

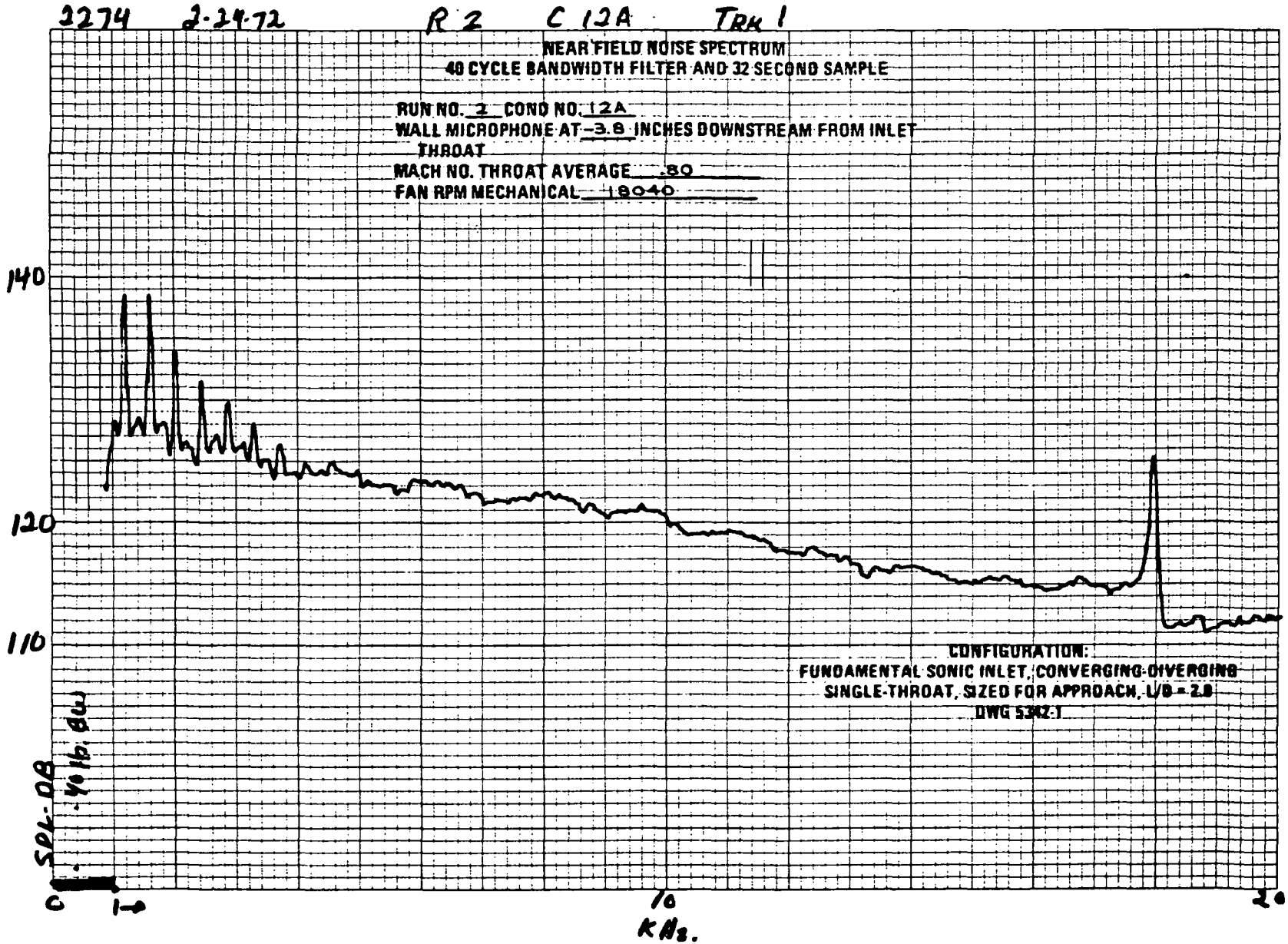

FIGURE A-21.—RUN 2-12A, WALL MICROPHONE SPECTRUM AT -3.8 IN. DOWNSTREAM FROM INLET THROAT

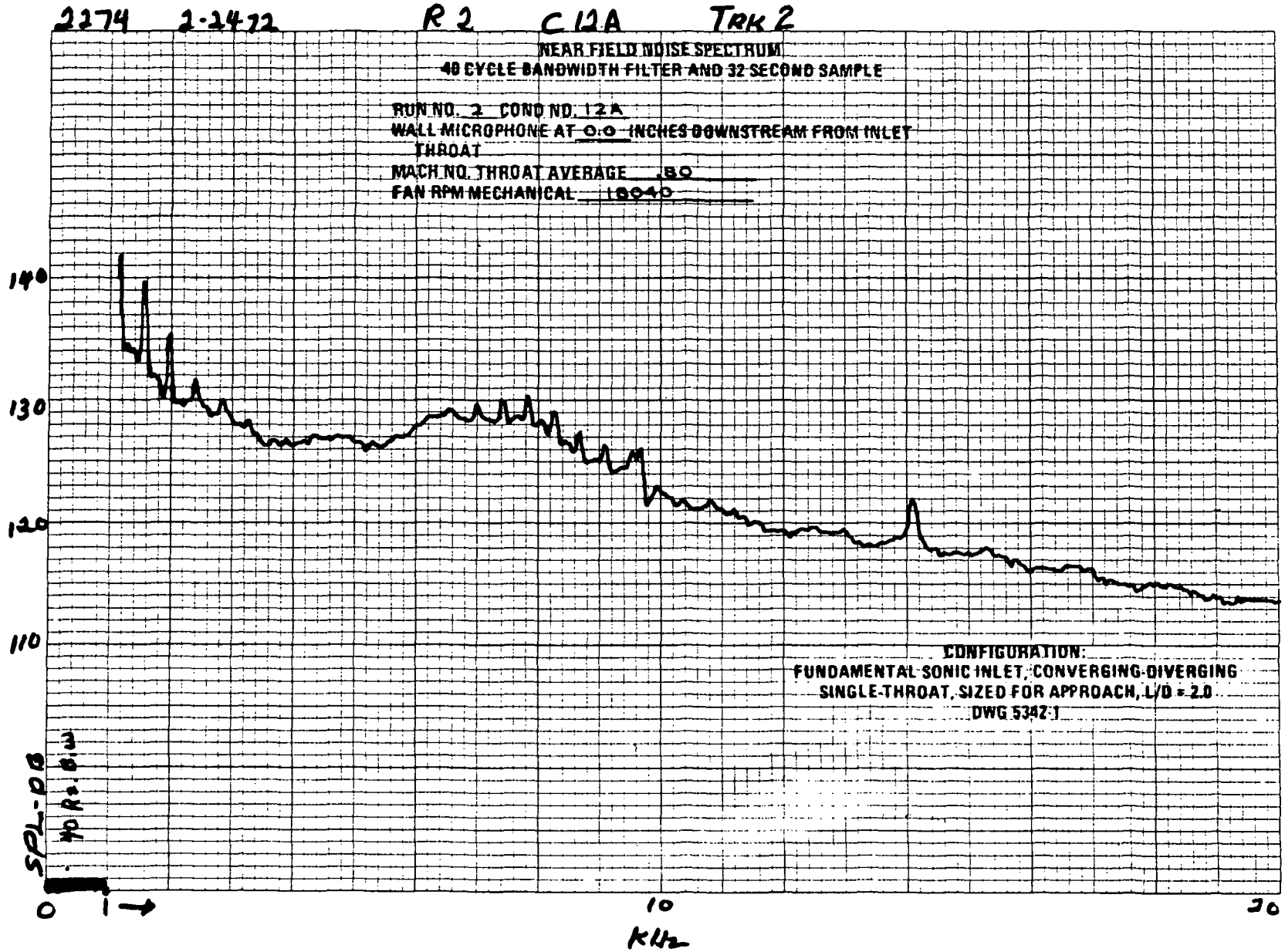

FIGURE A-22.—RUN 2-12A, WALL MICROPHONE SPECTRUM AT 0.0 IN. DOWNSTREAM FROM INLET THROAT

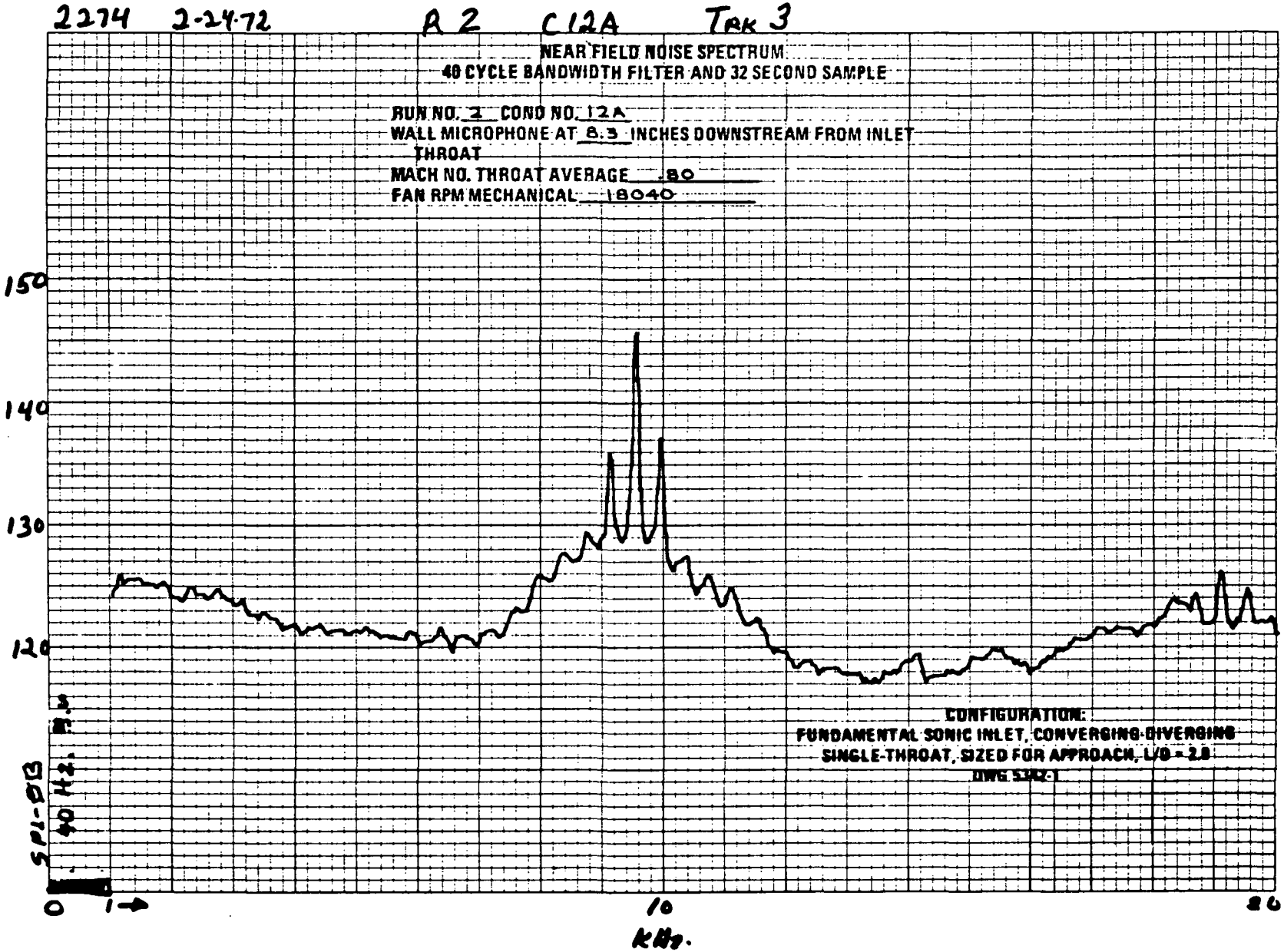

FIGURE A-23.—RUN 2-12A, WALL MICROPHONE SPECTRUM AT 8.3 IN. DOWNSTREAM FROM INLET THROAT

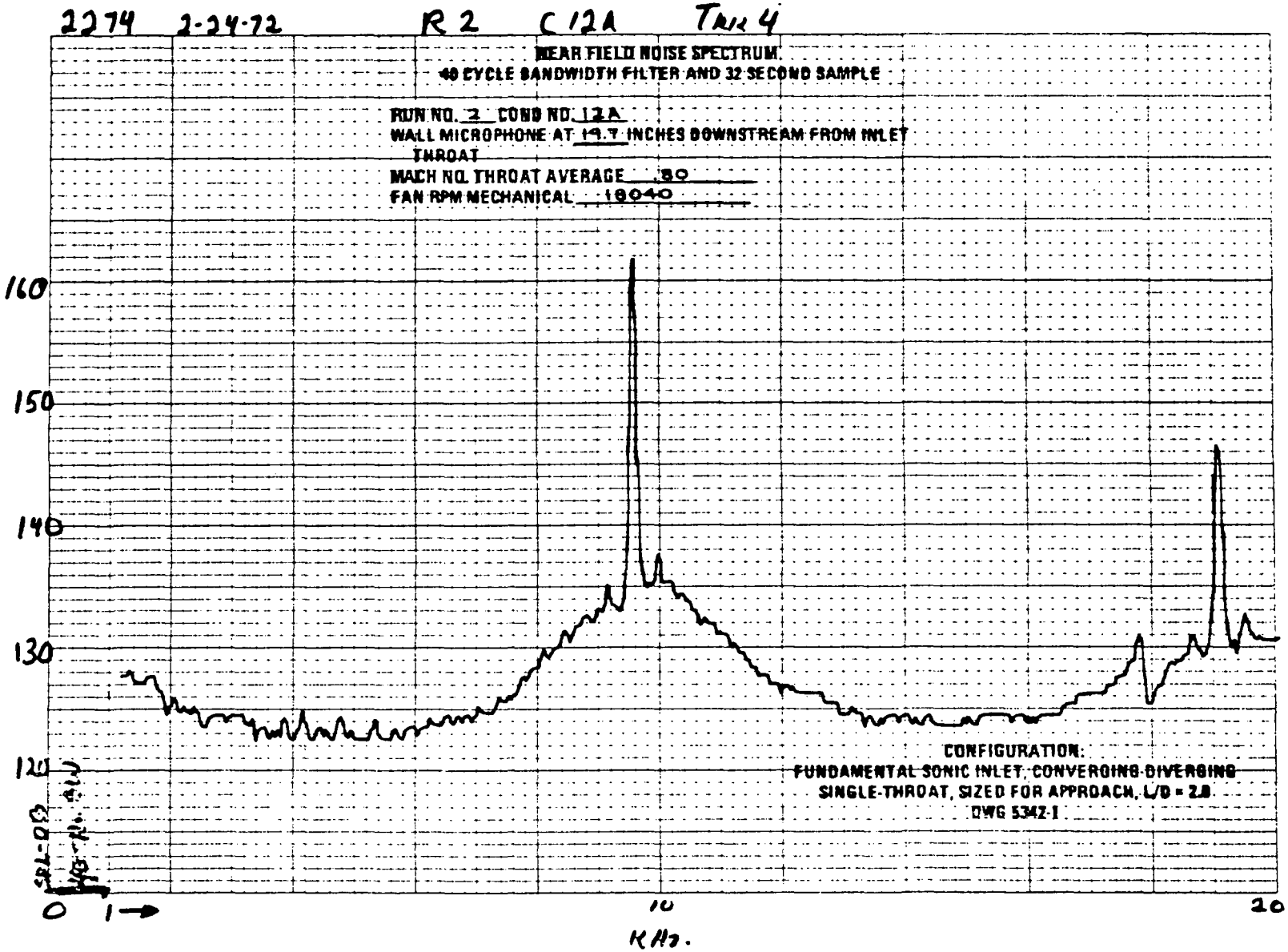

FIGURE A-24.—RUN 2-12A, WALL MICROPHONE SPECTRUM AT 19.7 IN. DOWNSTREAM FROM INLET THROAT

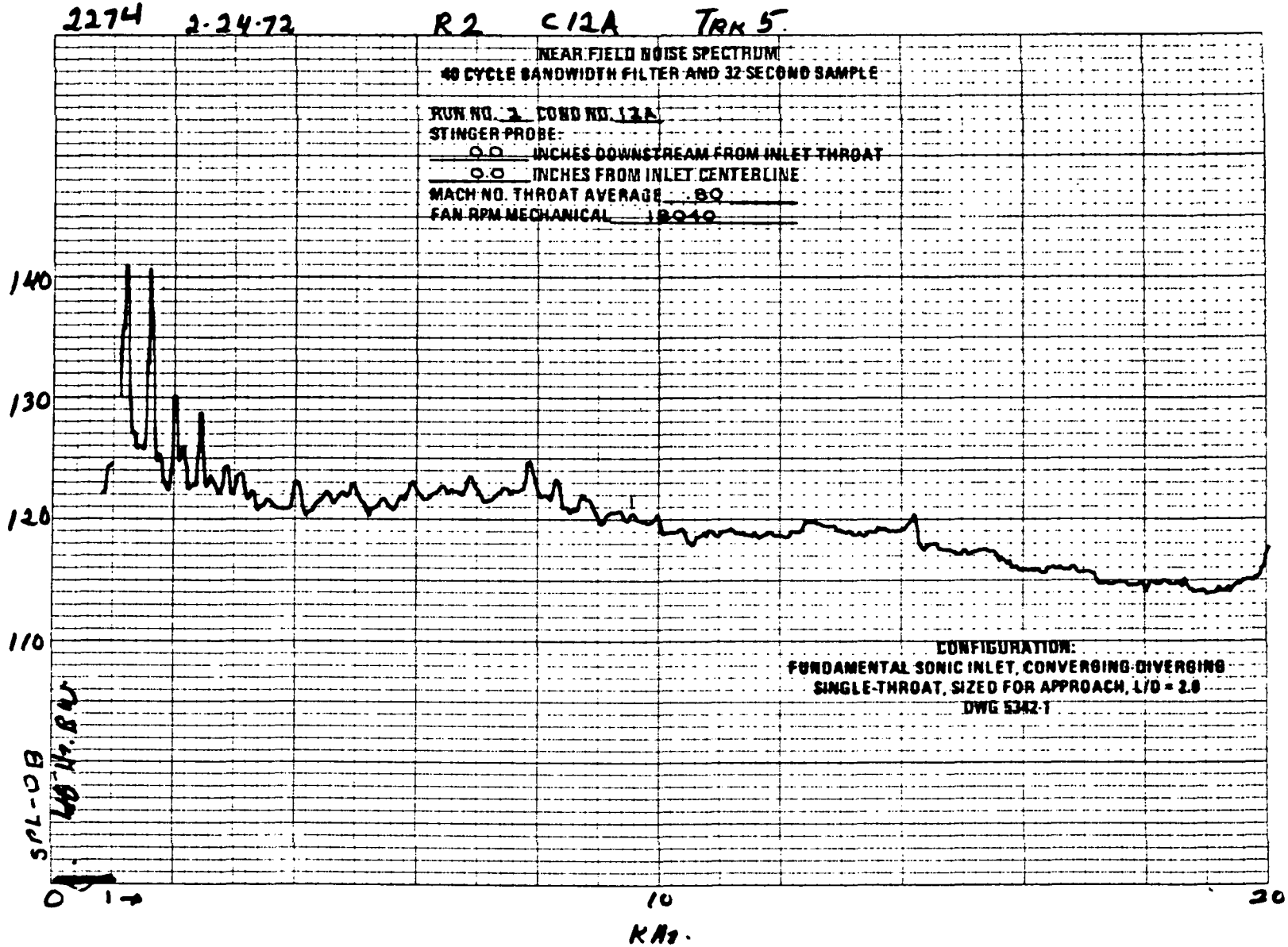

FIGURE A-25.—RUN 2-12A, STINGER PROBE MICROPHONE SPECTRUM AT (X; R) (0.0 IN.; 0.0 IN.)

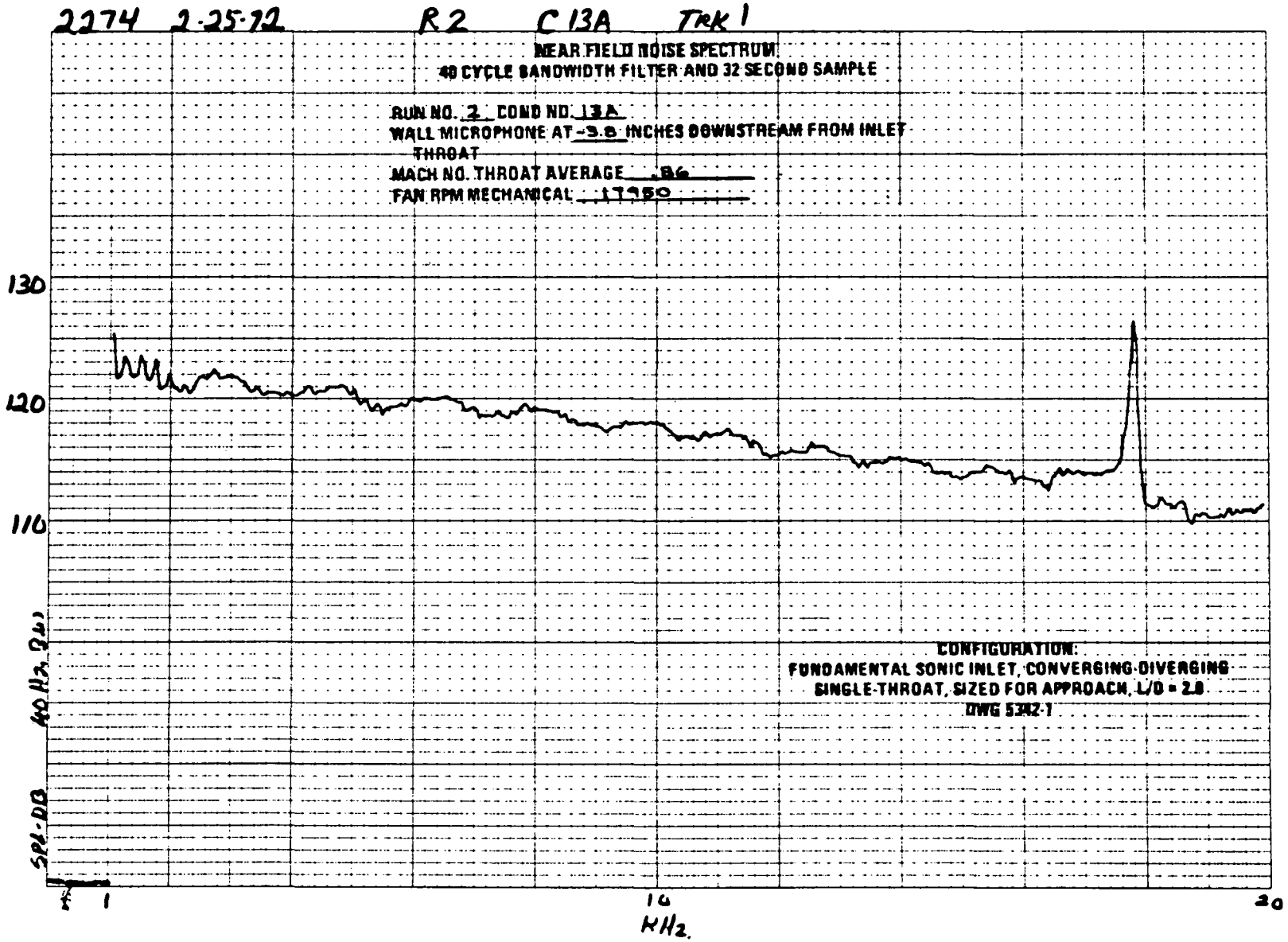

FIGURE A-26.—RUN 2-13A, WALL MICROPHONE SPECTRUM AT -3.8 IN. DOWNSTREAM FROM INLET THROAT

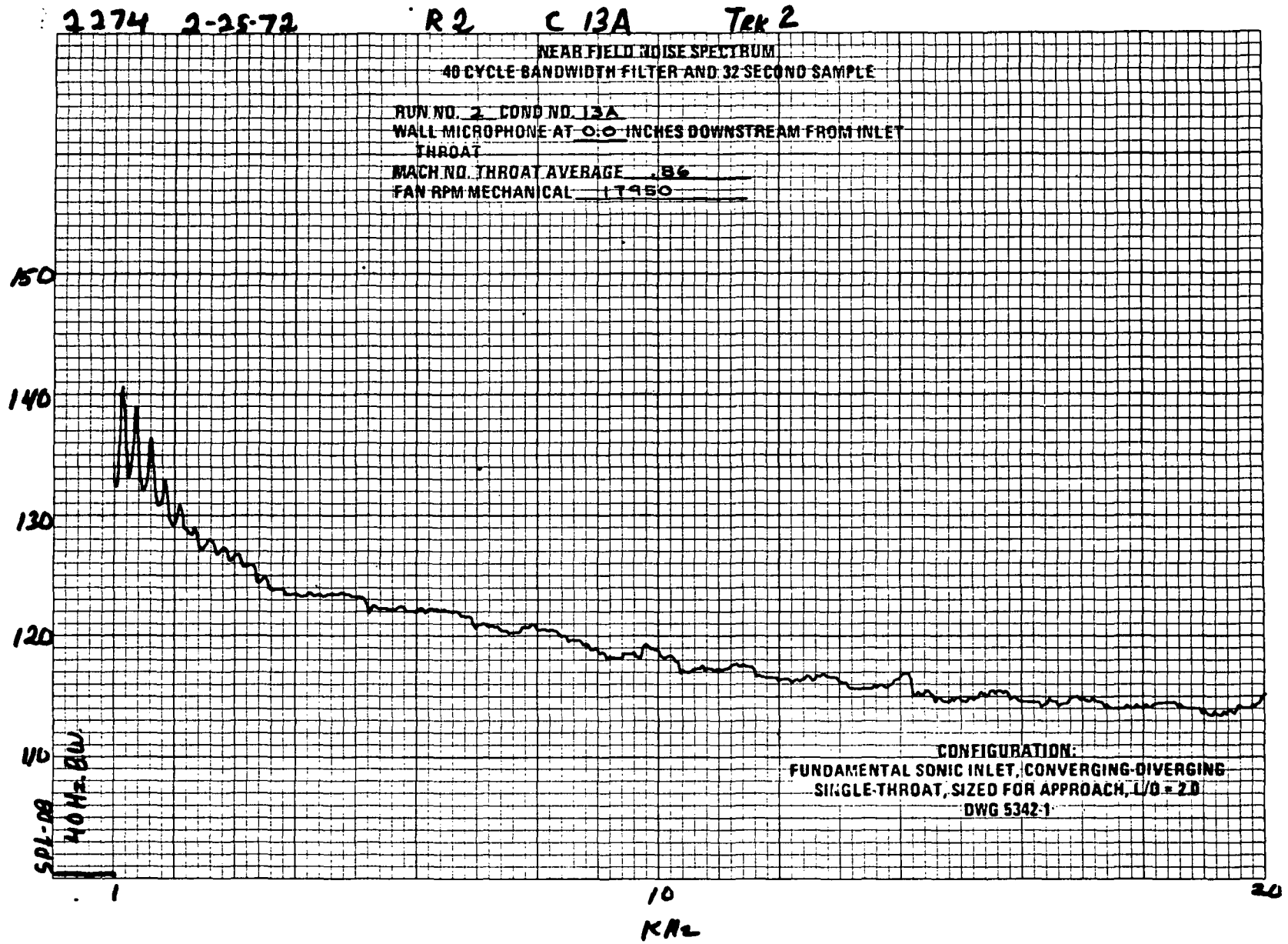

FIGURE A-27.—RUN 2-13A, WALL MICROPHONE SPECTRUM AT 0.0 IN. DOWNSTREAM FROM INLET THROAT

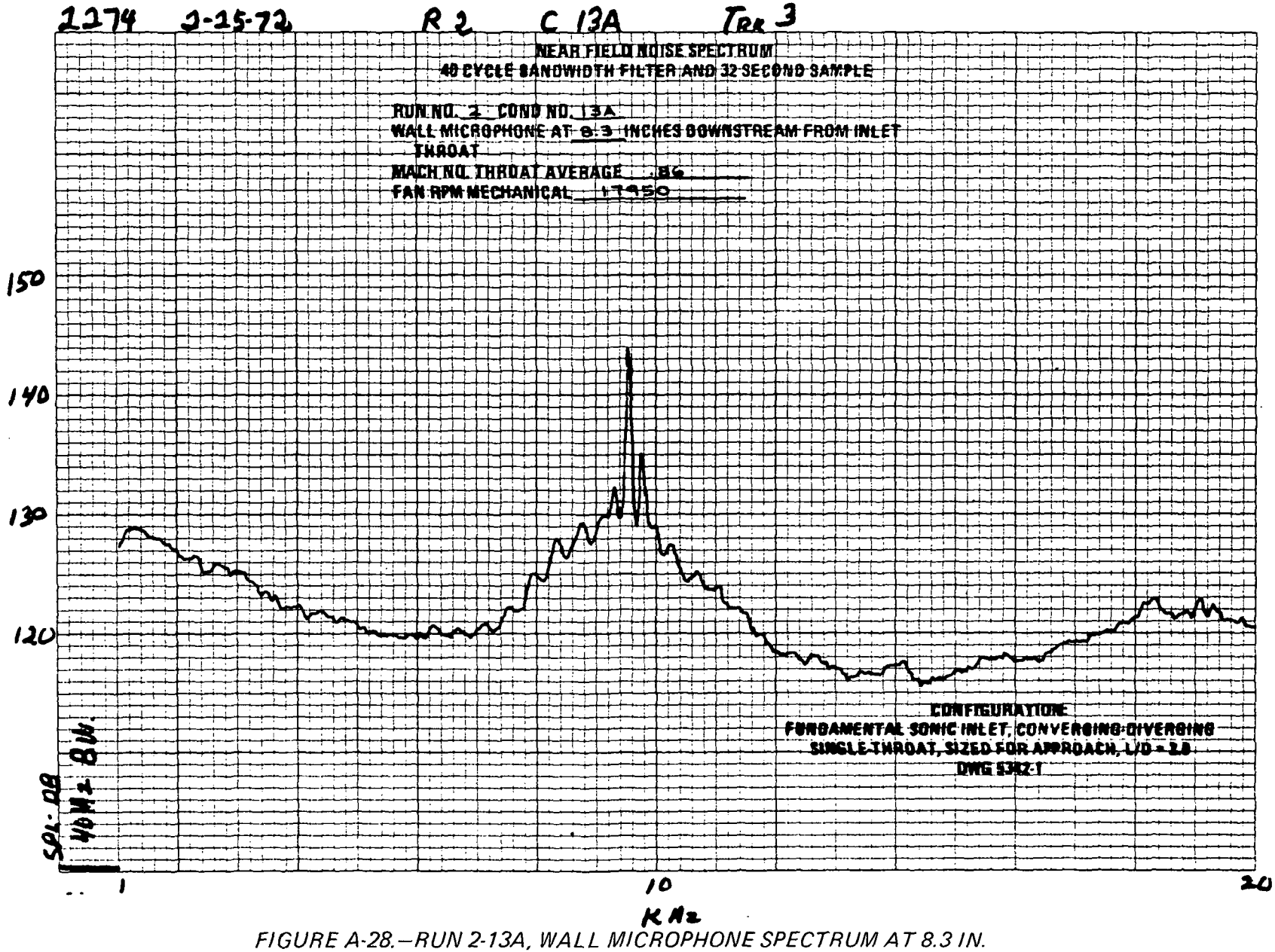

FIGURE A-28.—RUN 2-13A, WALL MICROPHONE SPECTRUM AT 8.3 IN. DOWNSTREAM FROM INLET THROAT

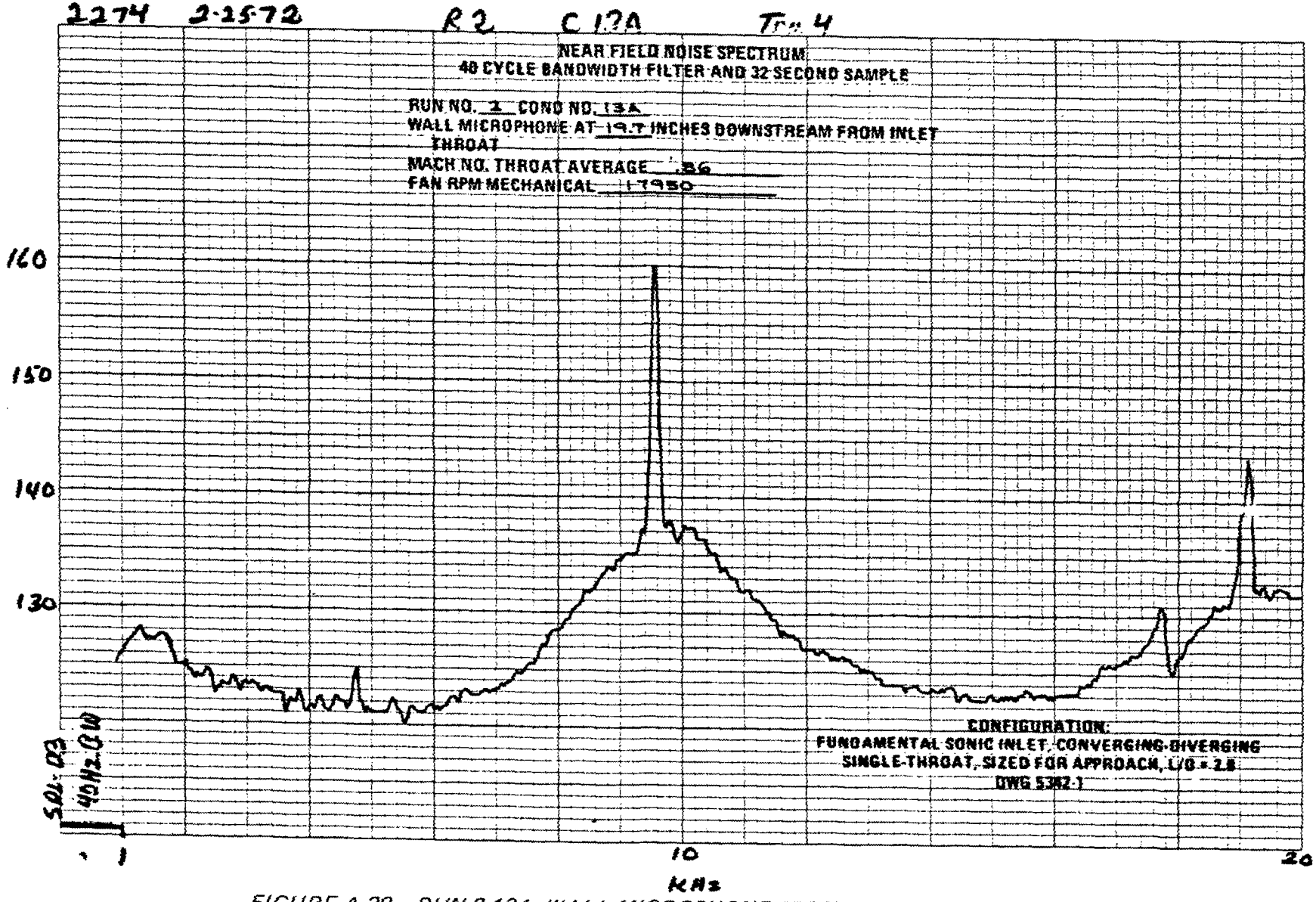

FIGURE A-29.—RUN 2-13A, WALL MICROPHONE SPECTRUM AT 19.7 IN. DOWNSTREAM FROM INLET THROAT

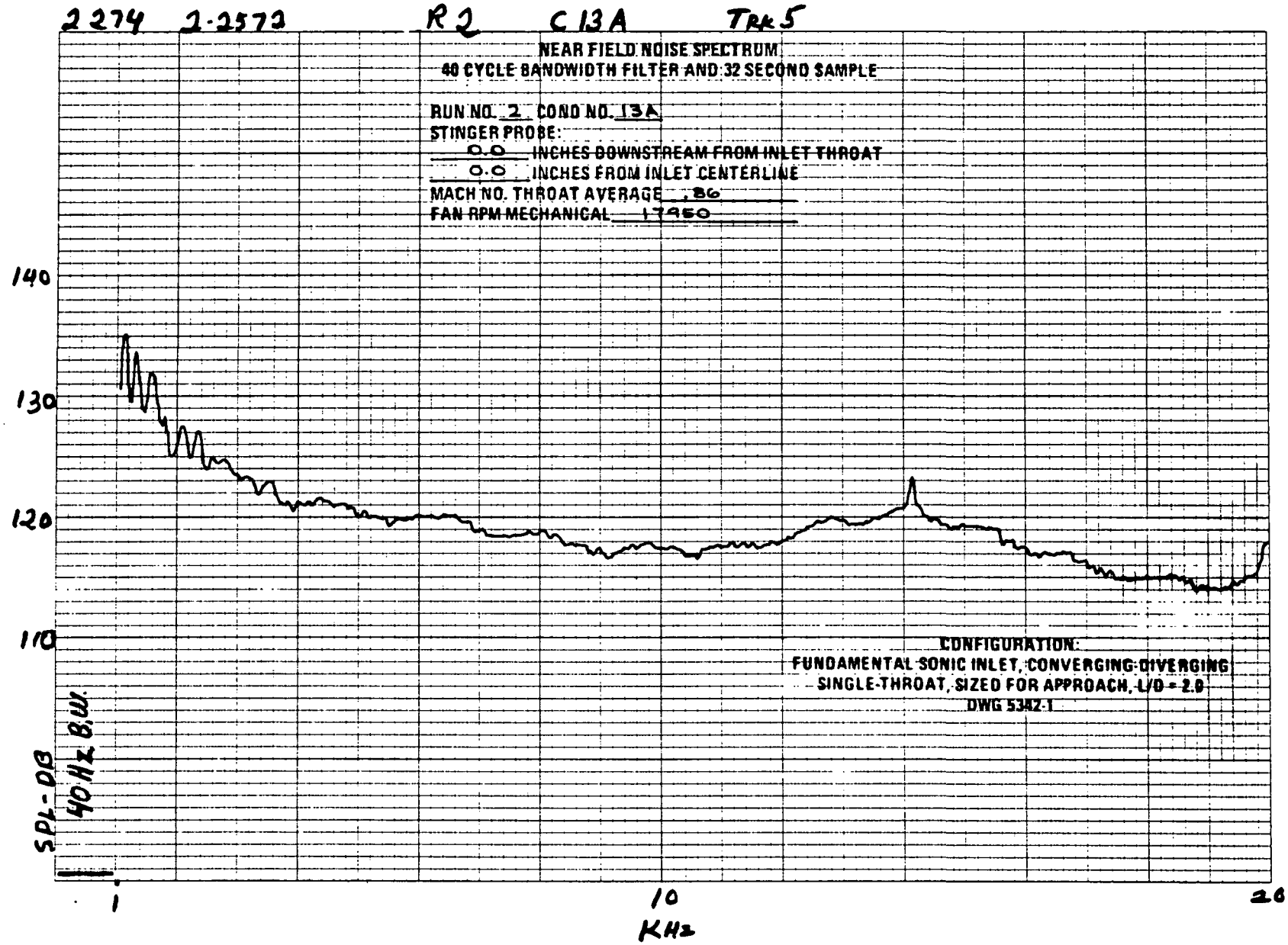

FIGURE A-30.—RUN 2-13A, STINGER PROBE MICROPHONE SPECTRUM AT (X; R) (0.0 IN.; 0.0 IN.)

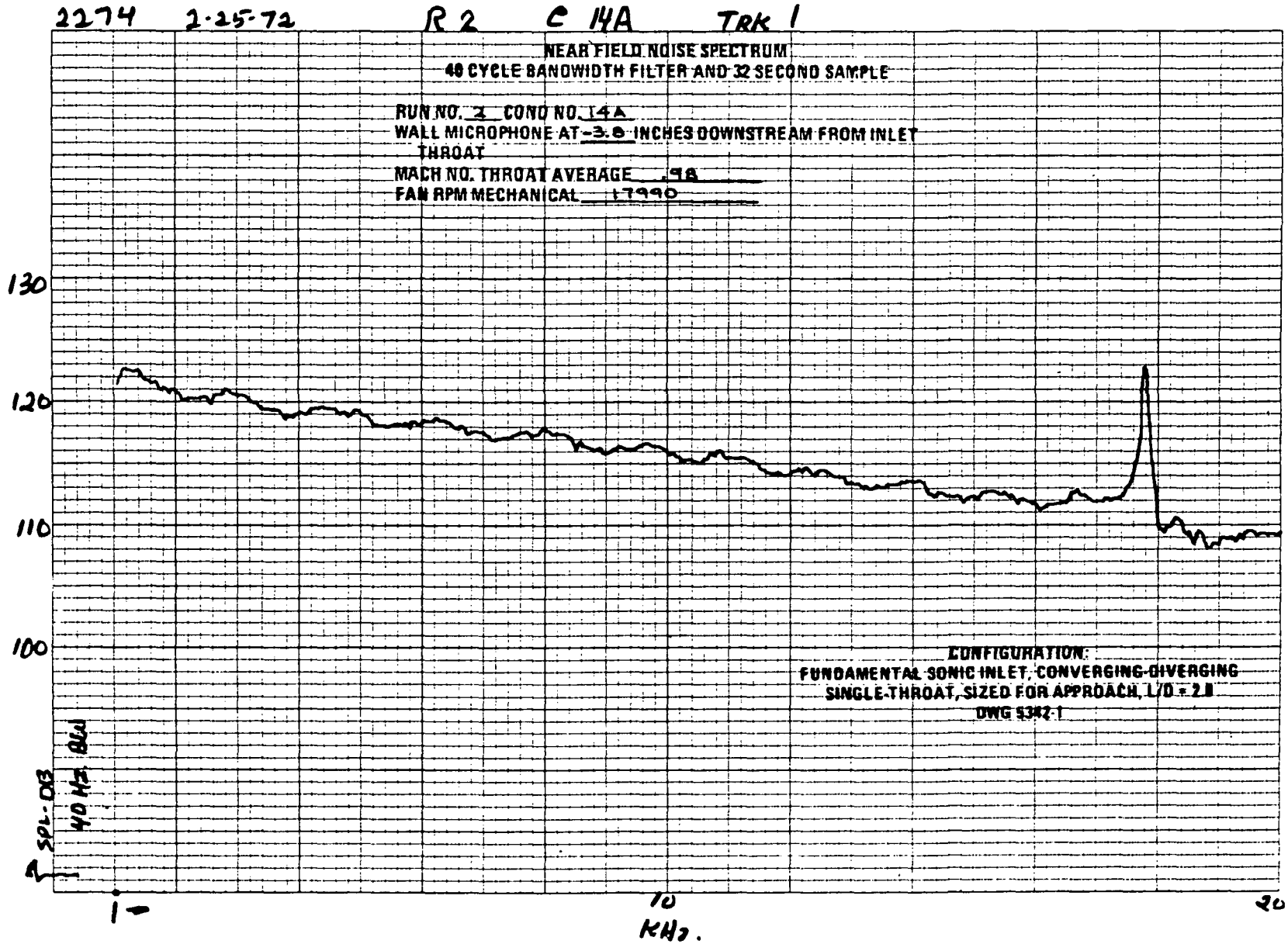

FIGURE A-31.—RUN 2-14A, WALL MICROPHONE SPECTRUM AT -3.8 IN. DOWNSTREAM FROM INLET THROAT

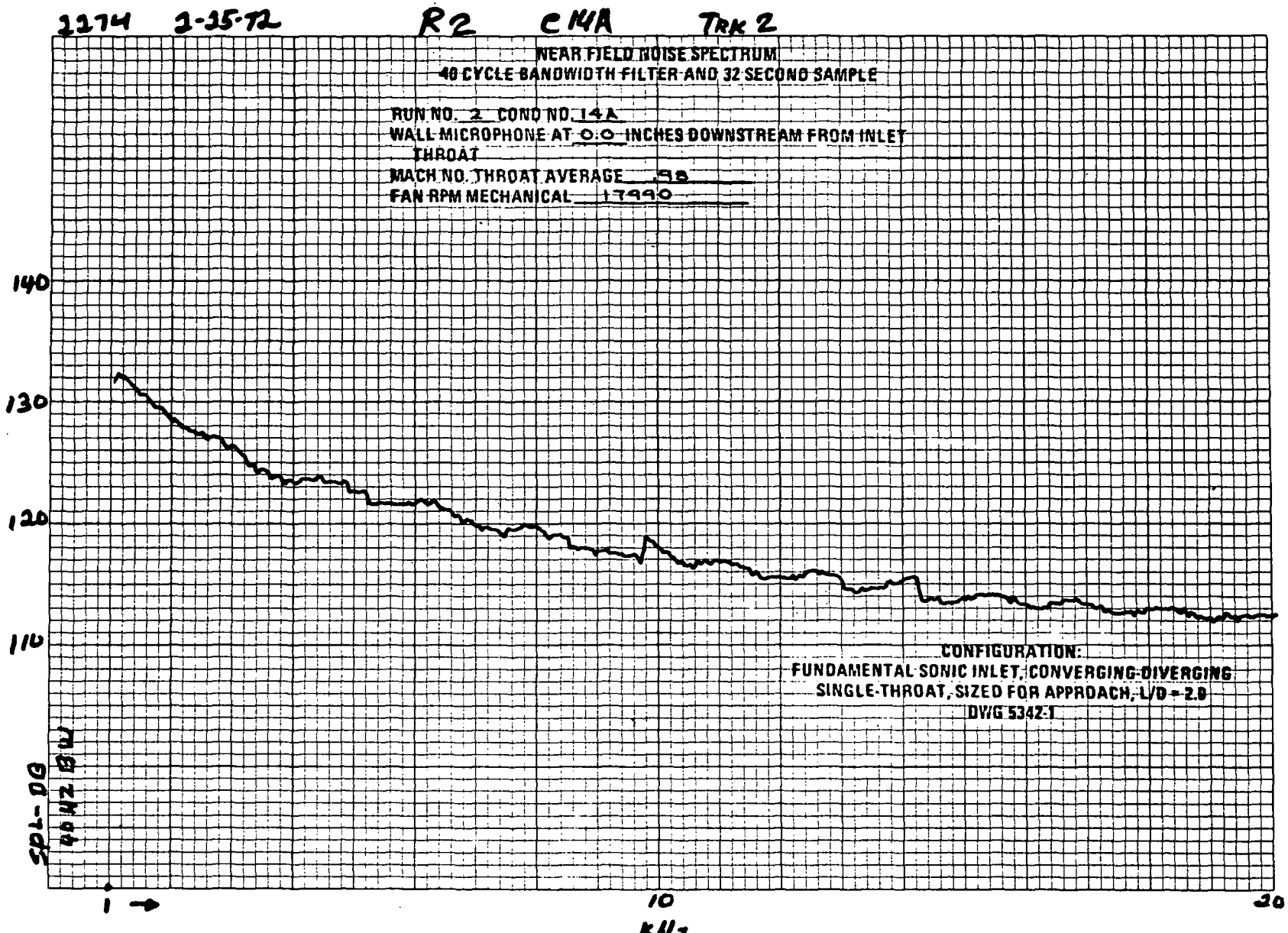

FIGURE A-32.—RUN 2-14A, WALL MICROPHONE SPECTRUM AT 0.0 IN. DOWNSTREAM FROM INLET THROAT

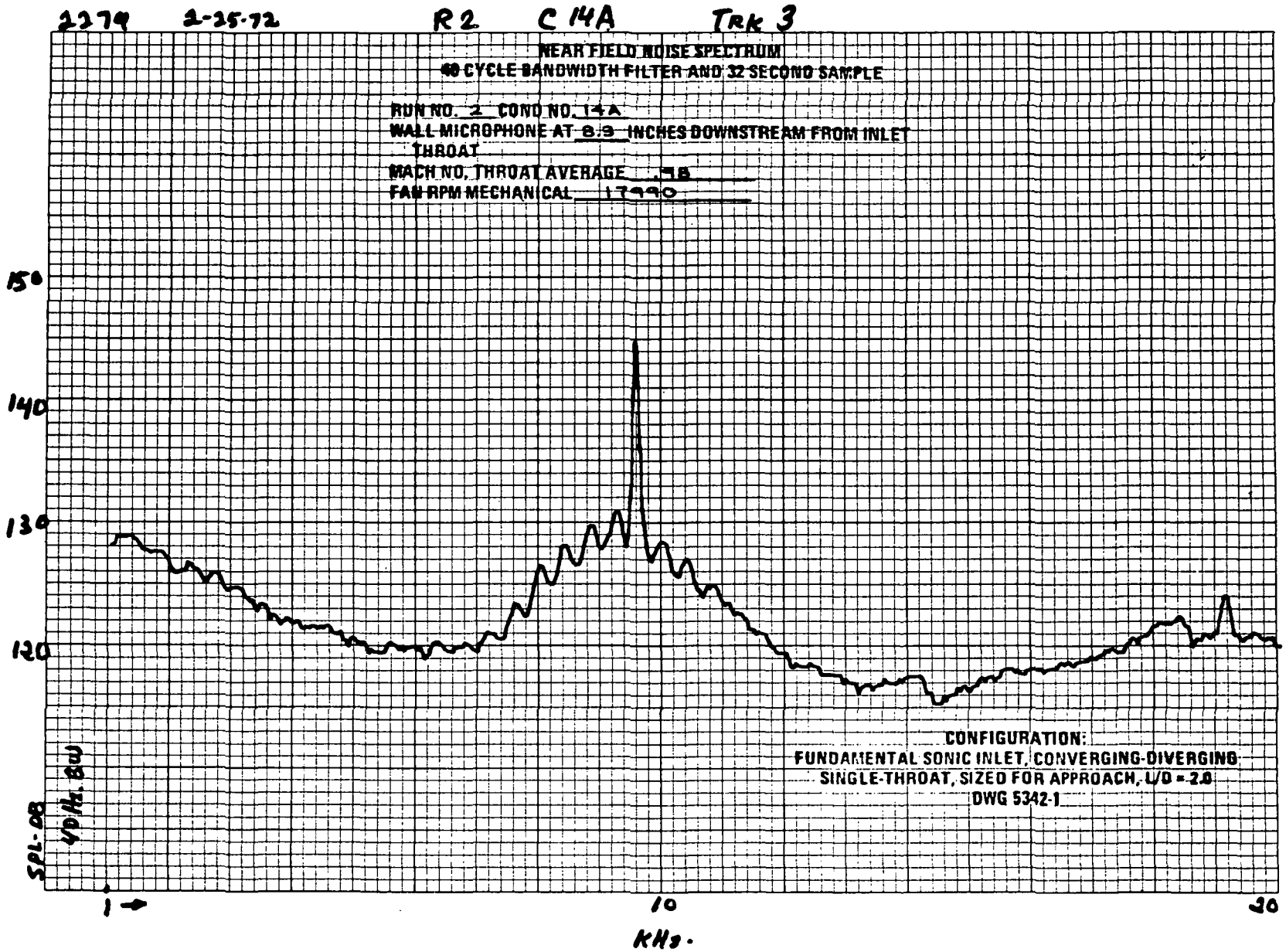

FIGURE A-33.—RUN 2-14A, WALL MICROPHONE SPECTRUM AT 8.3 IN. DOWNSTREAM FROM INLET THROAT

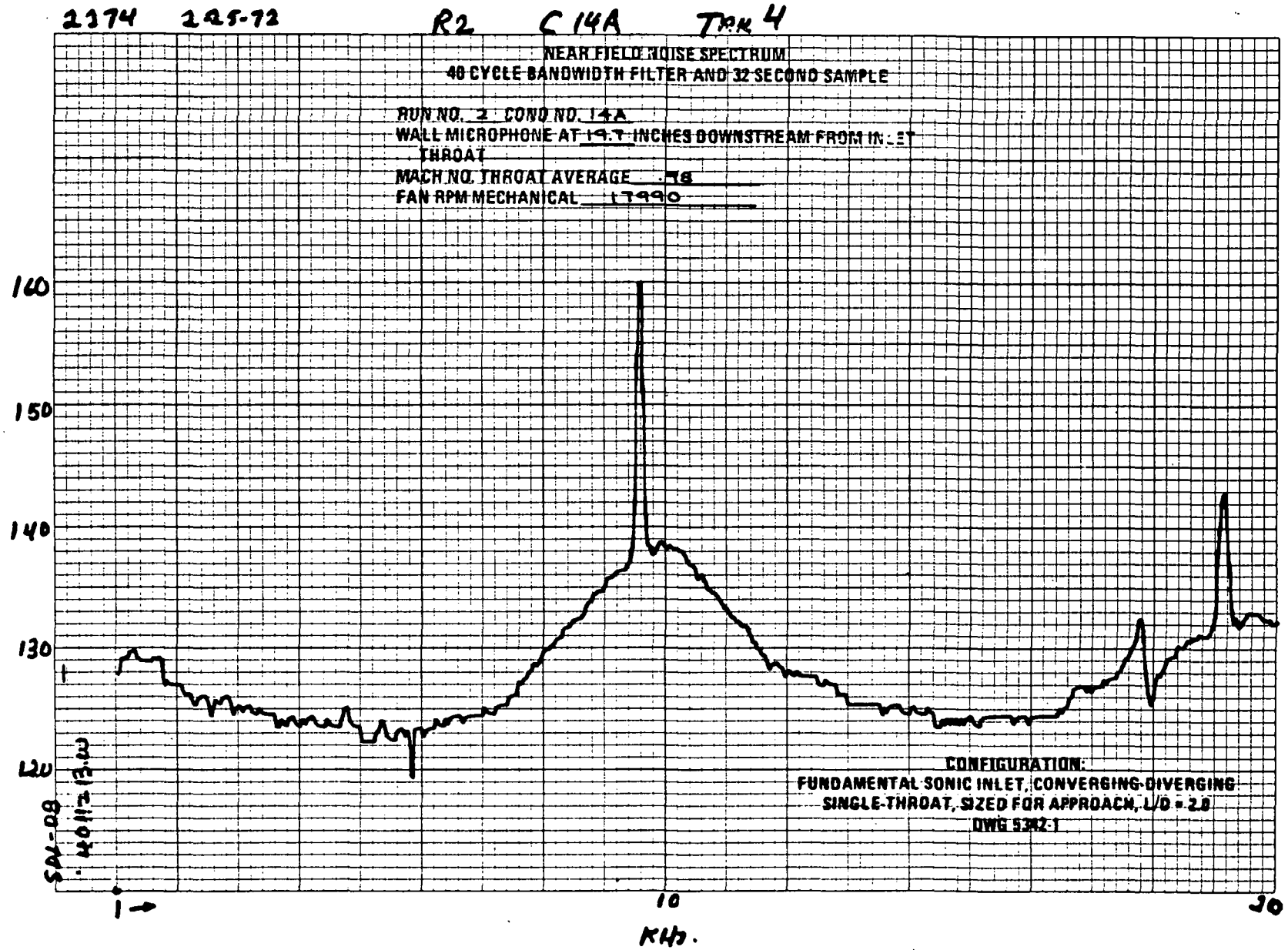

FIGURE A-34.—RUN 2-14A, WALL MICROPHONE SPECTRUM AT 19.7 IN. DOWNSTREAM FROM INLET THROAT

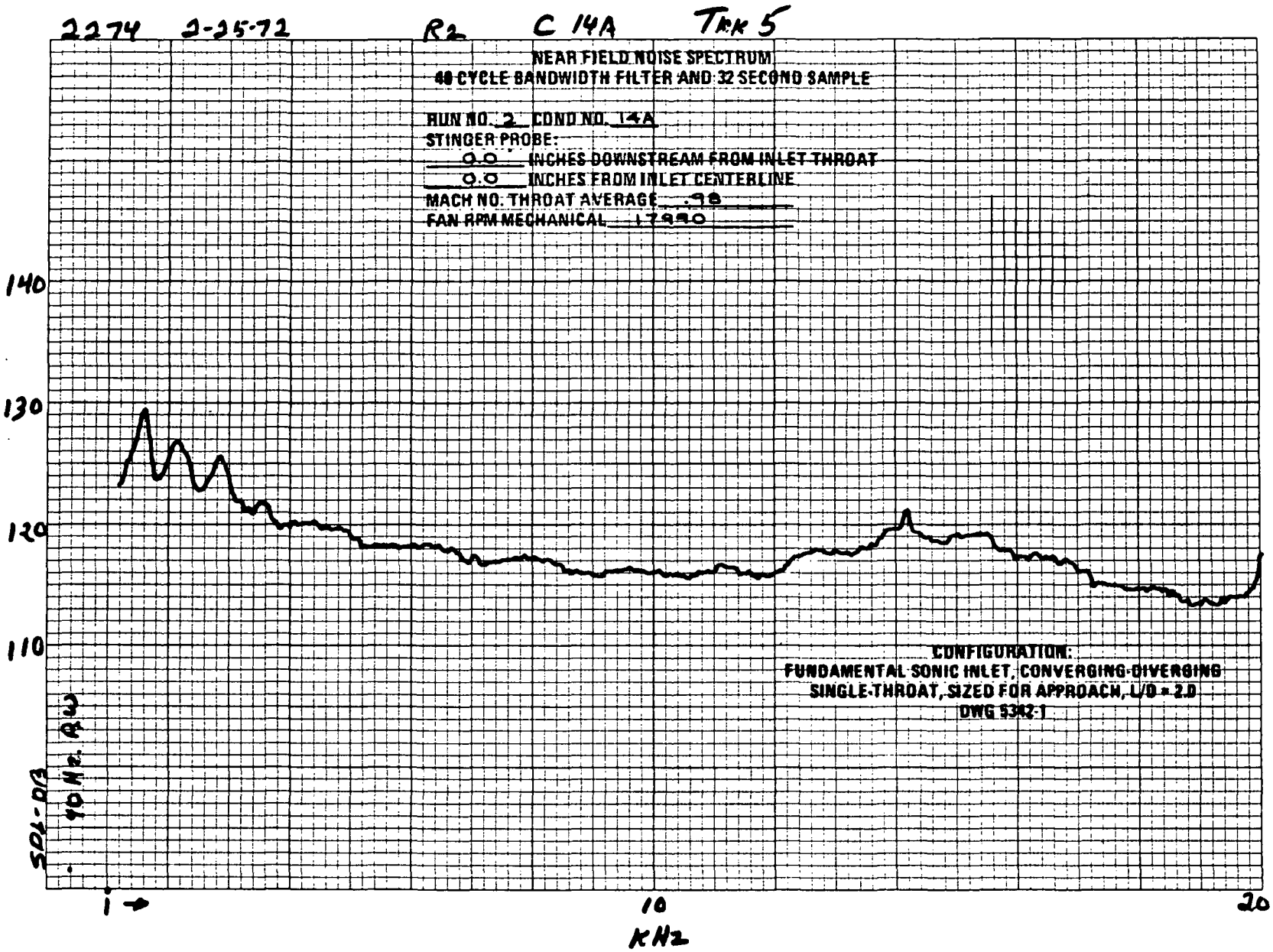

FIGURE A-35.—RUN 2-14A, STINGER PROBE MICROPHONE SPECTRUM AT (X; R) (0.0 IN.; 0.0 IN.)

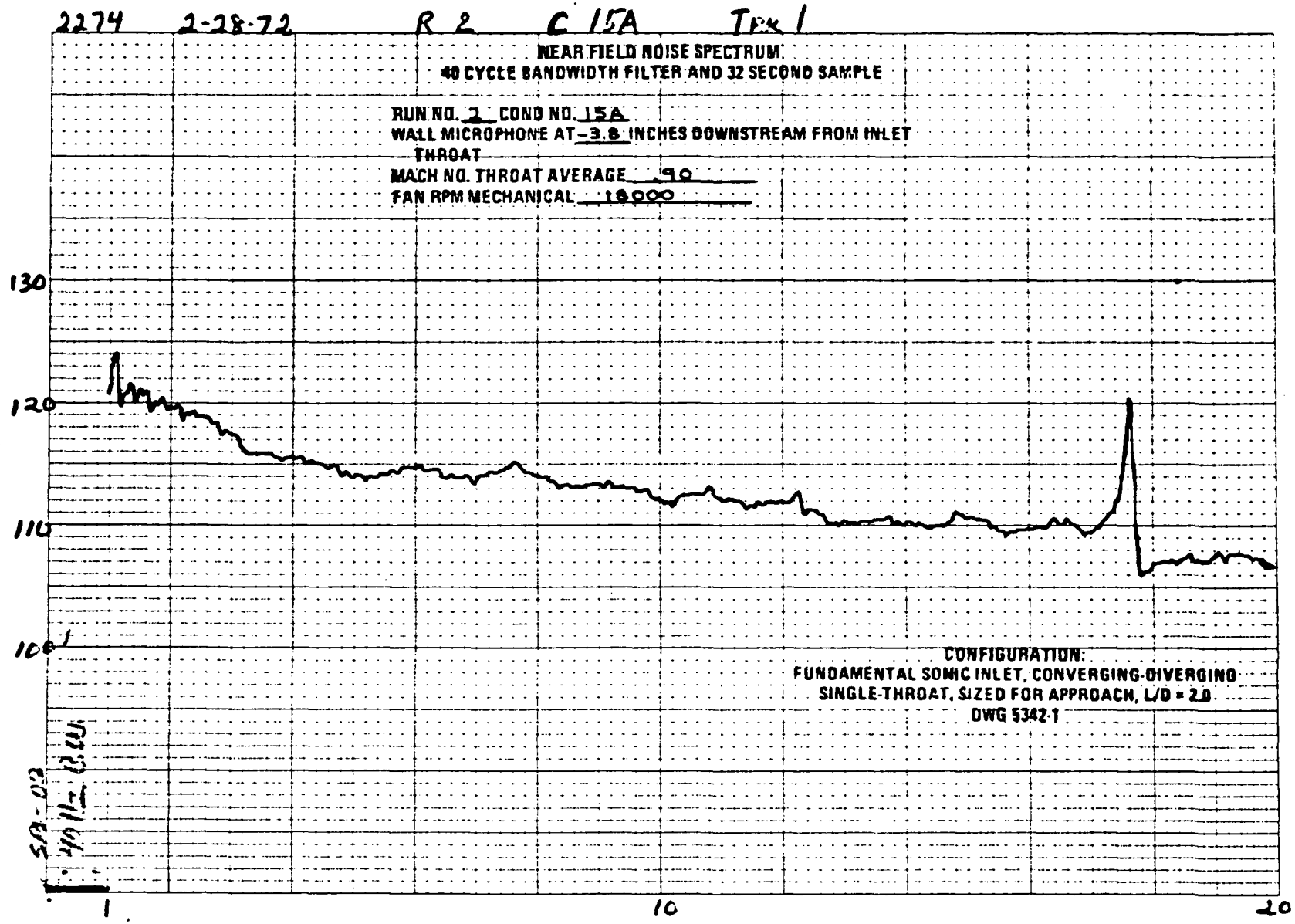

FIGURE A-36.—RUN 2-15A, WALL MICROPHONE SPECTRUM AT -3.8 IN. DOWNSTREAM FROM INLET THROAT

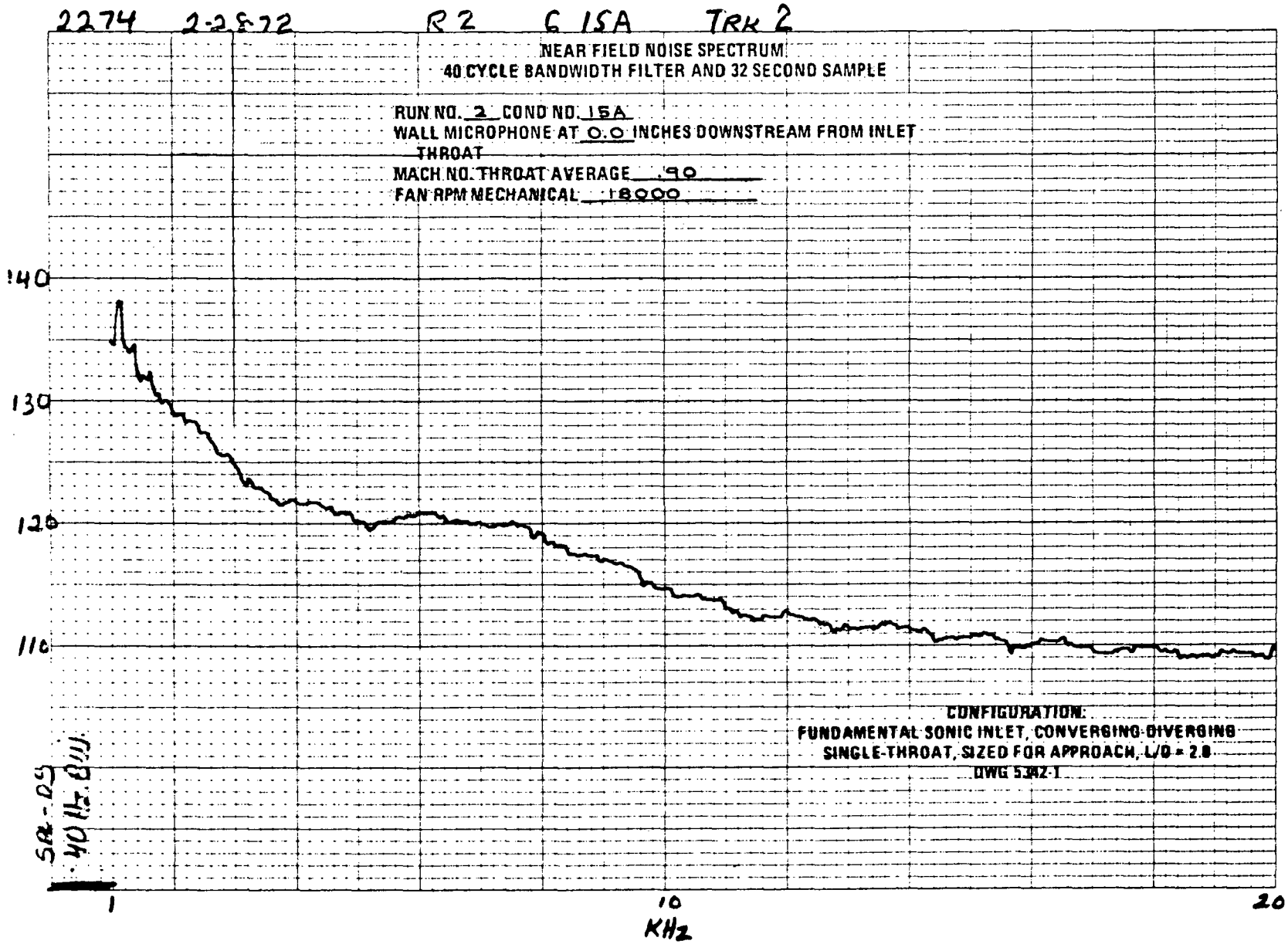

FIGURE A-37.—RUN 2-15A, WALL MICROPHONE SPECTRUM AT 0.0 IN. DOWNSTREAM FROM INLET THROAT

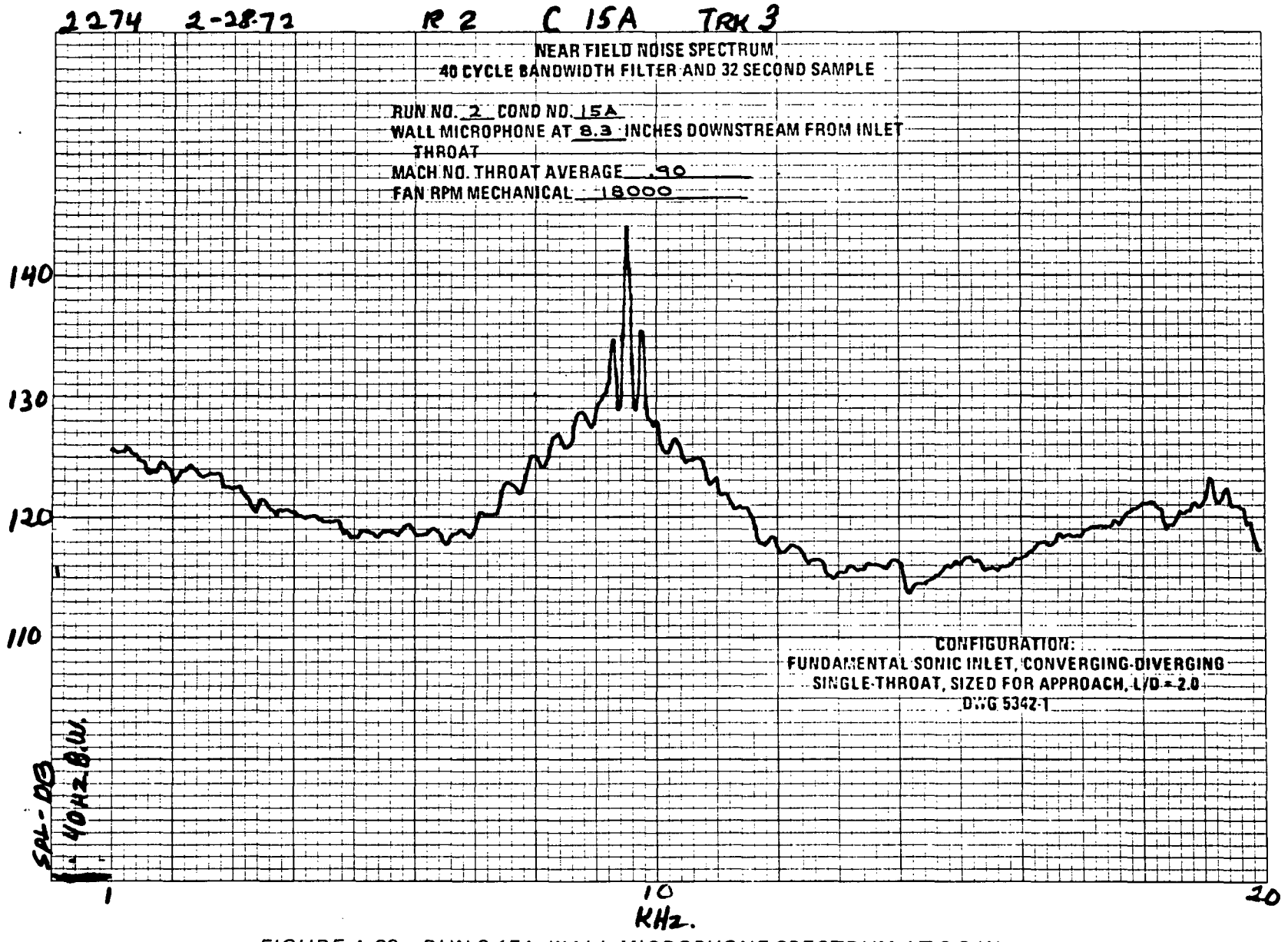

FIGURE A-38.—RUN 2-15A, WALL MICROPHONE SPECTRUM AT 8.3 IN. DOWNSTREAM FROM INLET THROAT

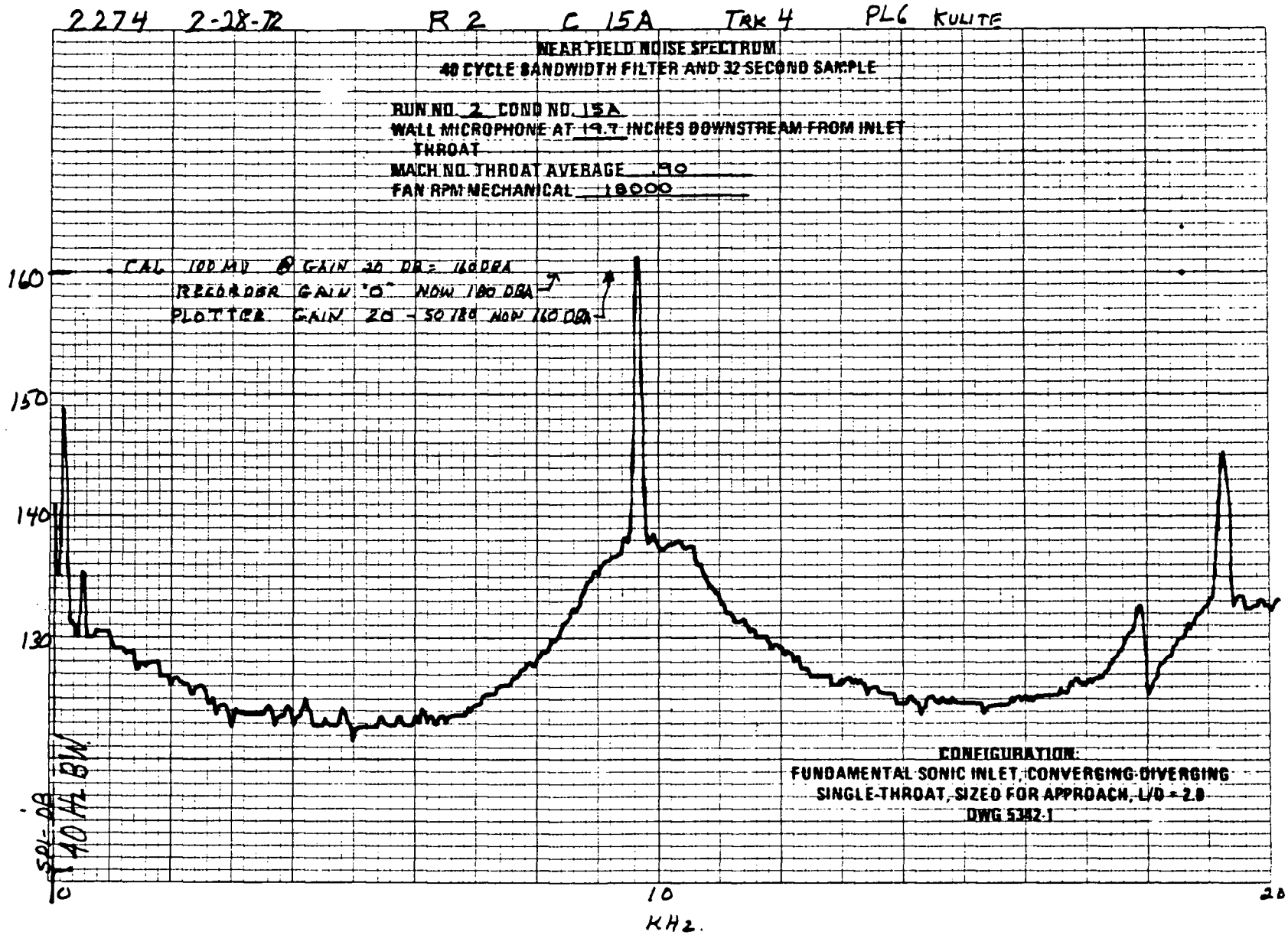

FIGURE A-39.—RUN 2-15A, WALL MICROPHONE SPECTRUM AT 19.7 IN. DOWNSTREAM FROM INLET THROAT

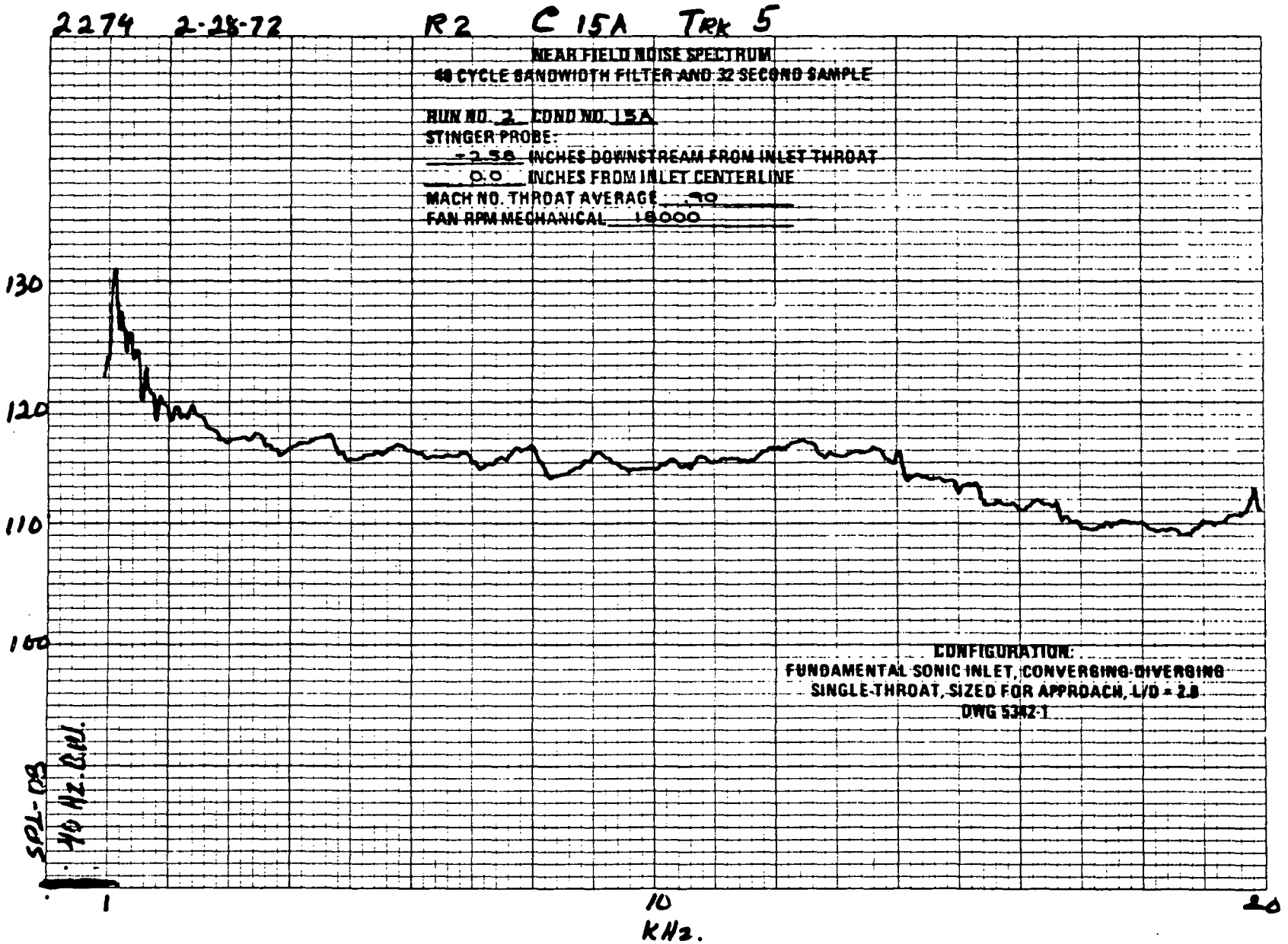

FIGURE A-40.—RUN 2-15A, STINGER PROBE MICROPHONE SPECTRUM AT (X; R) (-2.6 IN.; 0.0 IN.)

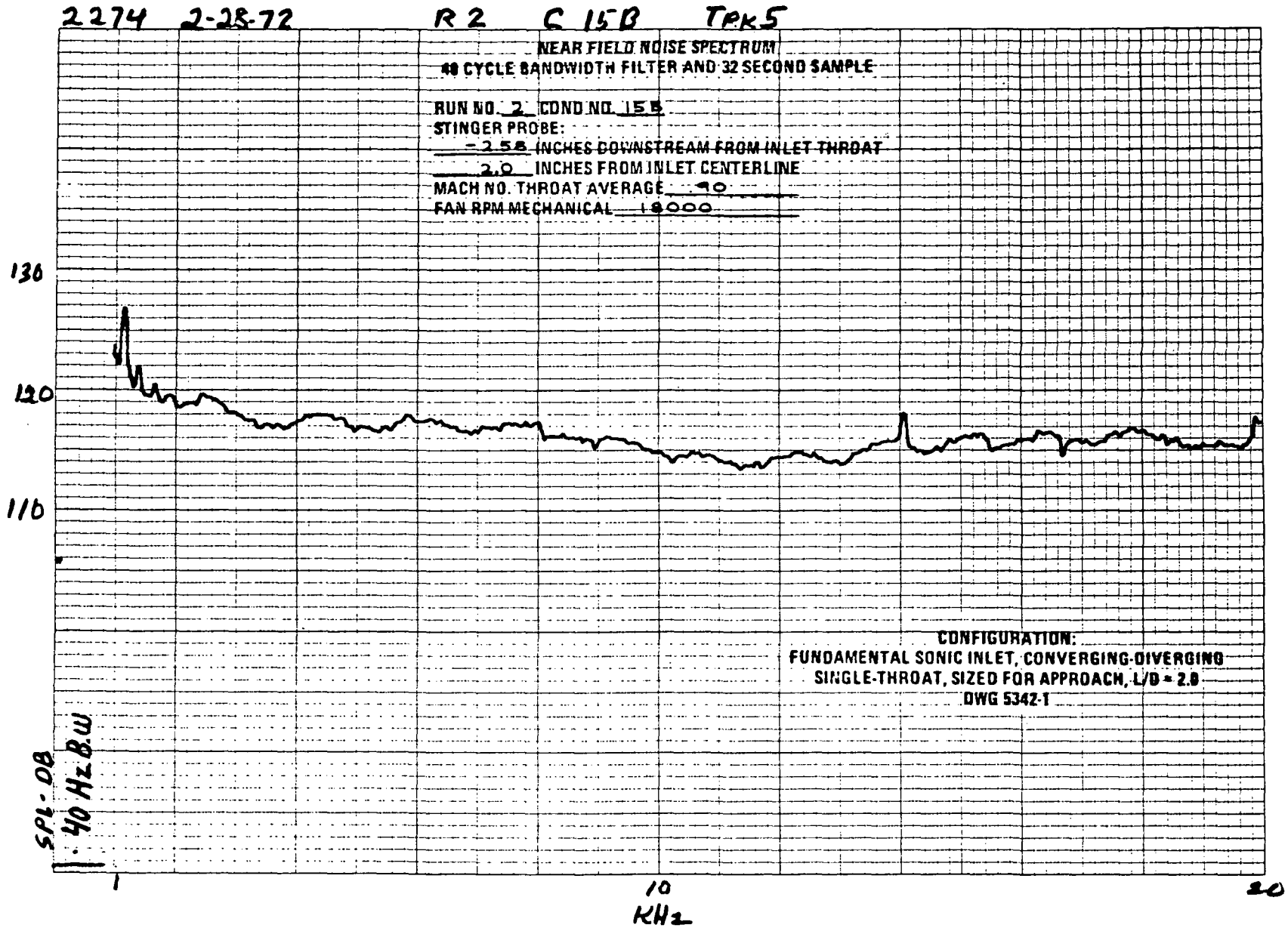

FIGURE A-41.—RUN 2-15B, STINGER PROBE MICROPHONE SPECTRUM AT (X; R) (-2.6 IN.; 2.0 IN.)

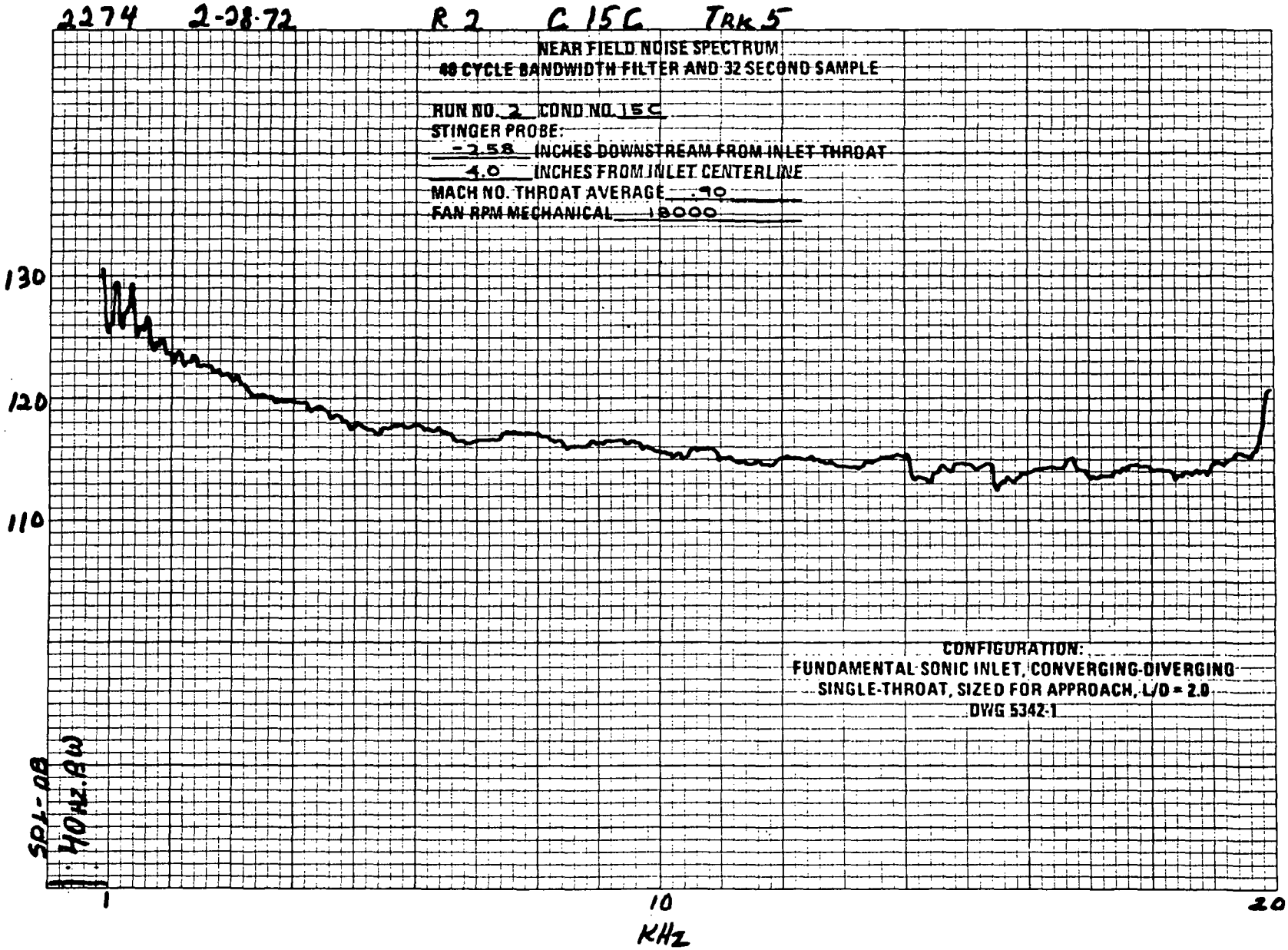

FIGURE A-42.—RUN 2-15C, STINGER PROBE MICROPHONE SPECTRUM AT (X; R) (-2.6 IN.; 4.0 IN.)

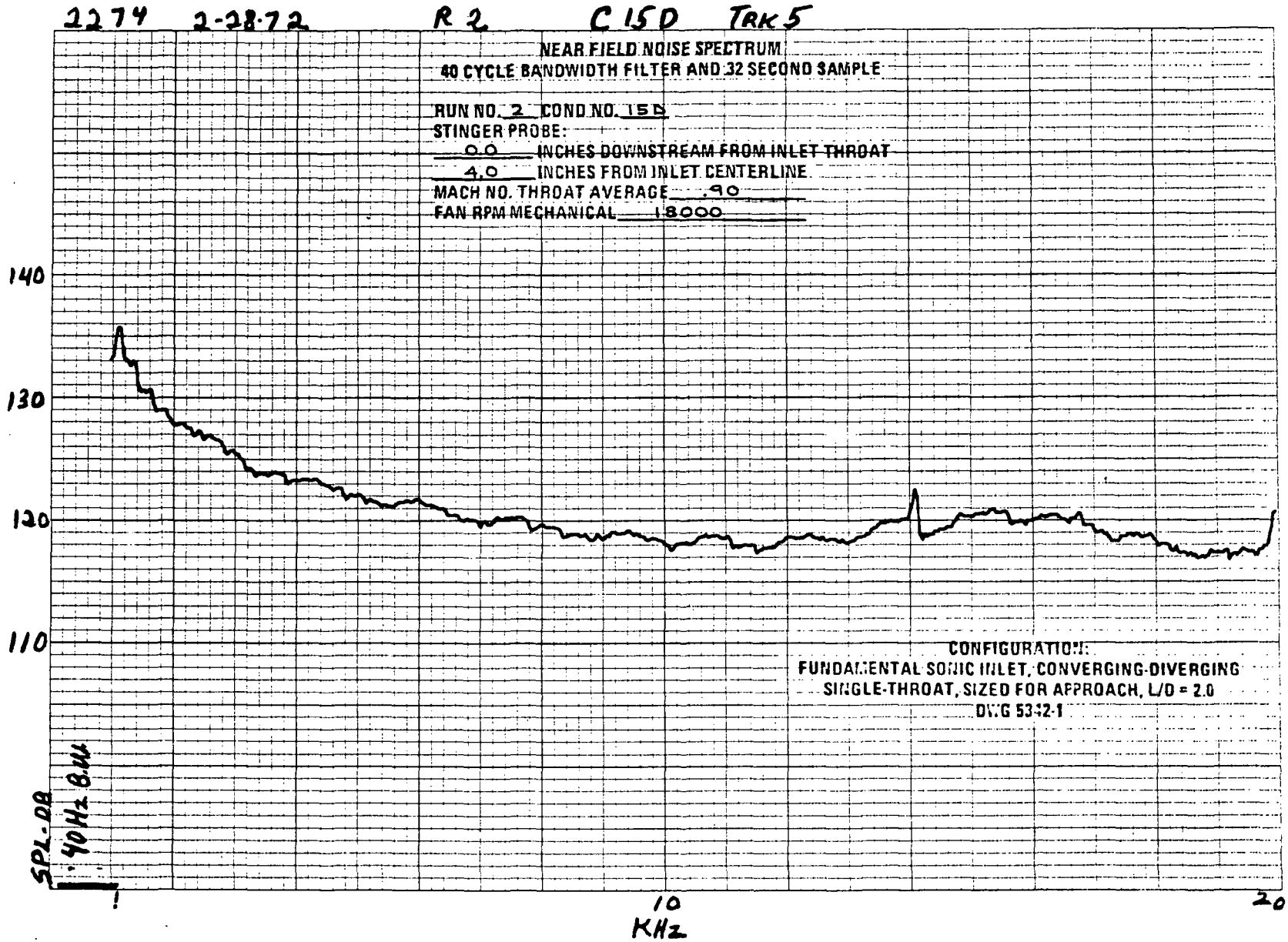

FIGURE A-43.—RUN 2-15D, STINGER PROBE MICROPHONE SPECTRUM AT (X; R) (0.0 IN.; 4.0 IN.)

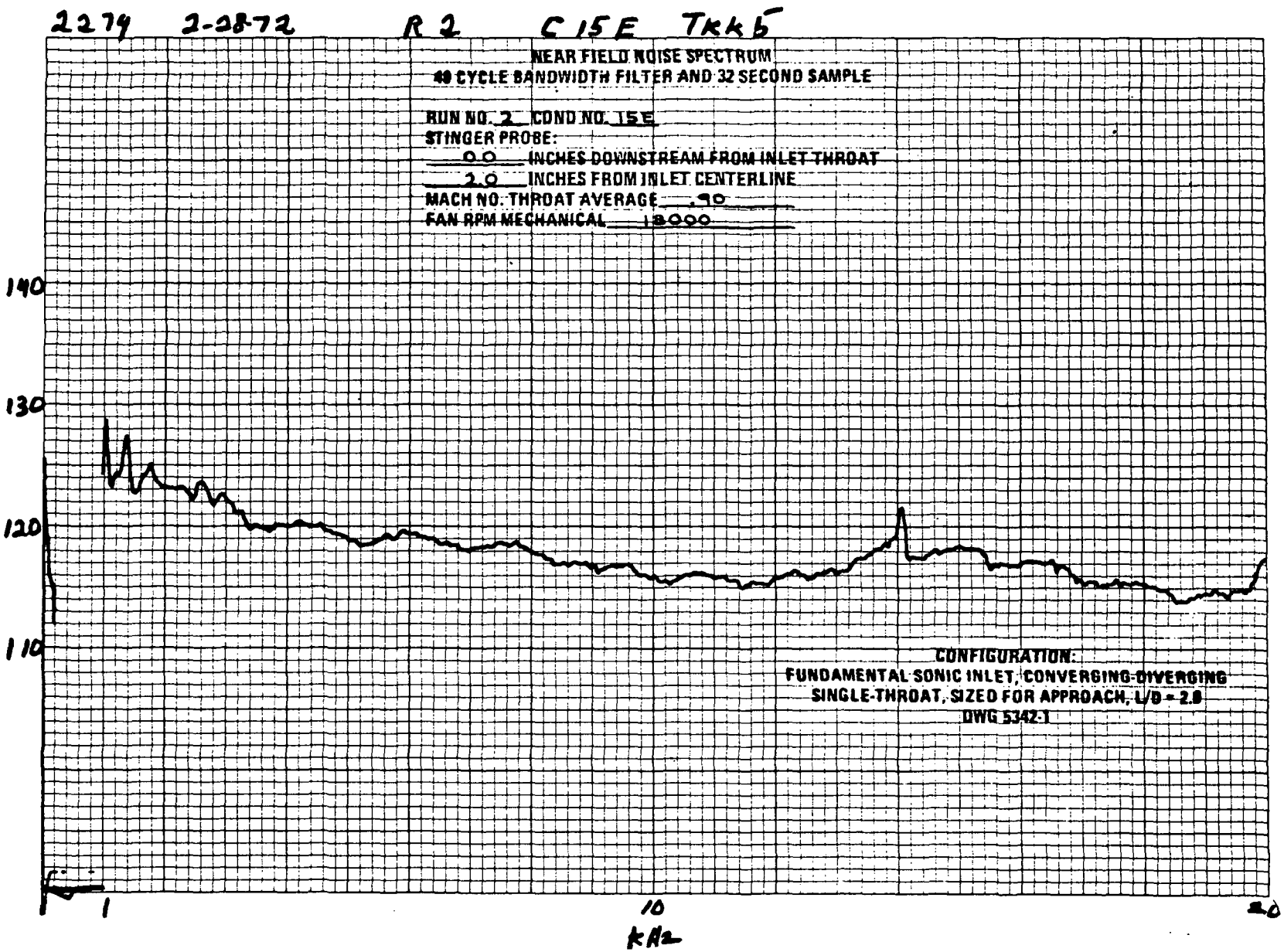

FIGURE A-44.—RUN 2-15E, STINGER PROBE MICROPHONE SPECTRUM AT (X; R) (0.0 IN.; 2.0 IN.)

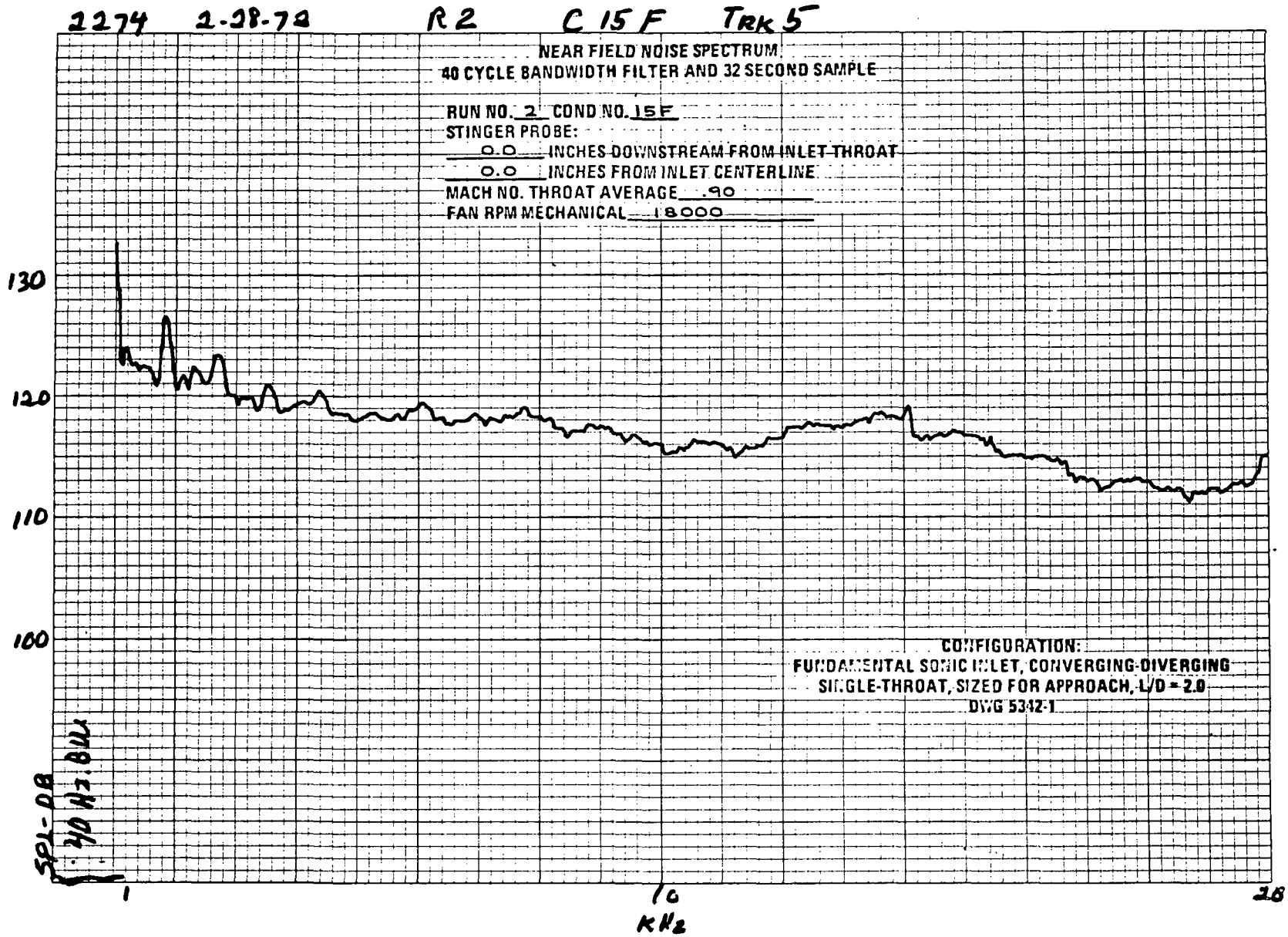

FIGURE A-45.—RUN 2-15F, STINGER PROBE MICROPHONE SPECTRUM AT (X; R) (0.0 IN.; 0.0 IN.)

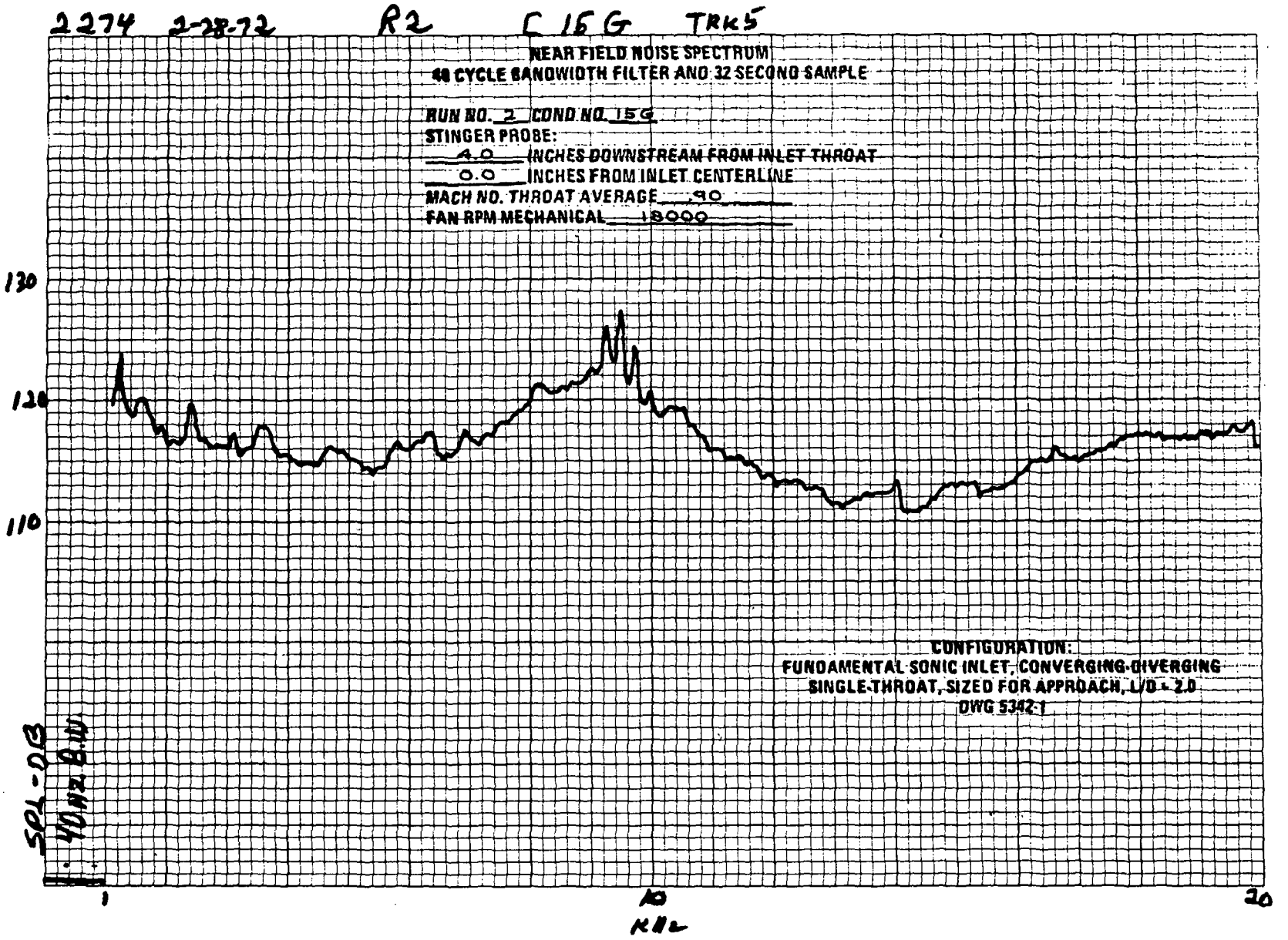

FIGURE A-46.—RUN 2-15G, STINGER PROBE MICROPHONE SPECTRUM AT (X; R) (4.0 IN.; 0.0 IN.)

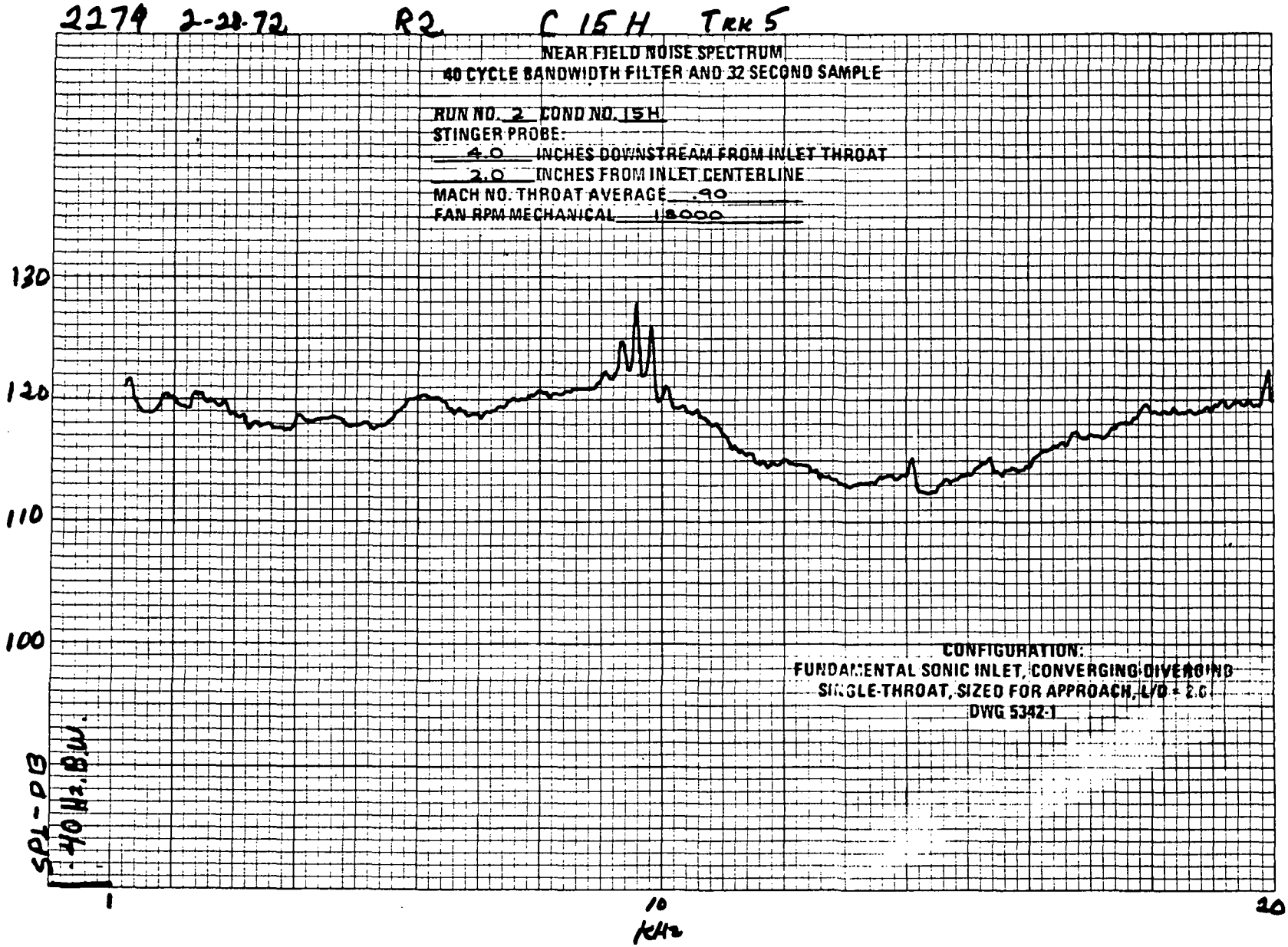

FIGURE A-47.—RUN 2-15H, STINGER PROBE MICROPHONE SPECTRUM AT (X; R) (4.0 IN.; 2.0 IN.)

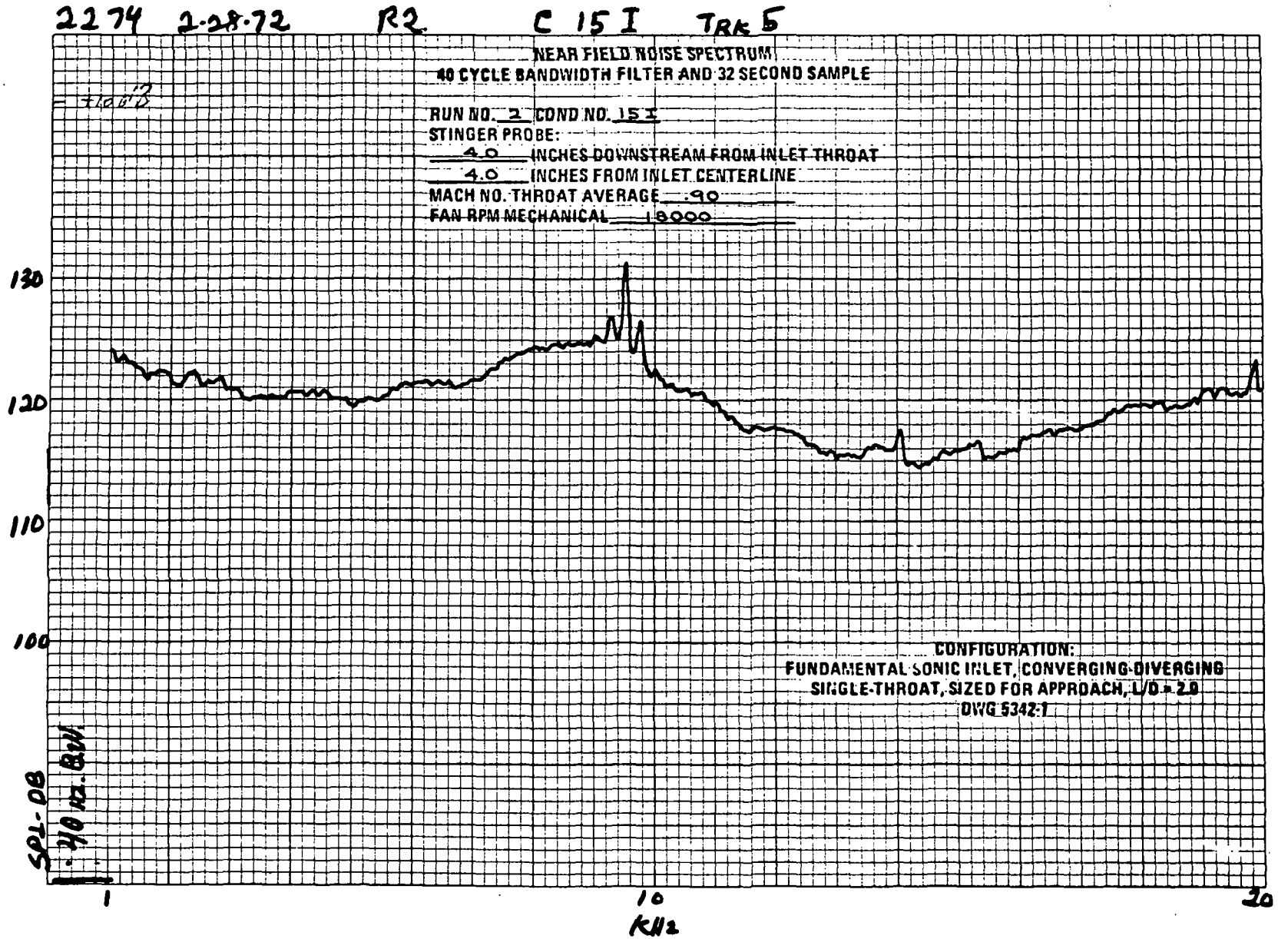

FIGURE A-48.—RUN 2-15I, STINGER PROBE MICROPHONE SPECTRUM AT (X; R) (4.0 IN.; 4.0 IN.)

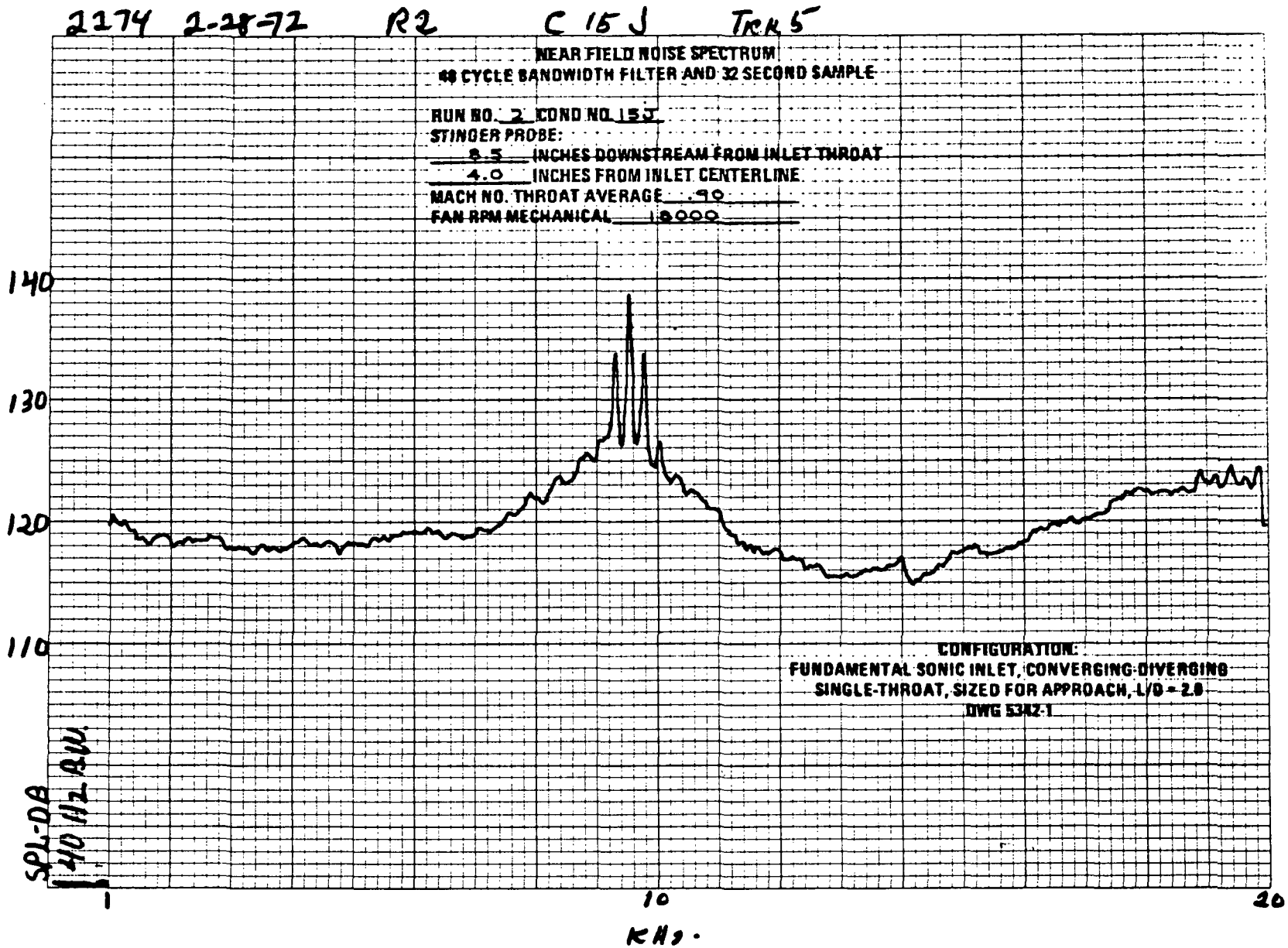

FIGURE A-49.—RUN 2-15J, STINGER PROBE MICROPHONE SPECTRUM AT (X; R) (8.5 IN.; 4.0 IN.)

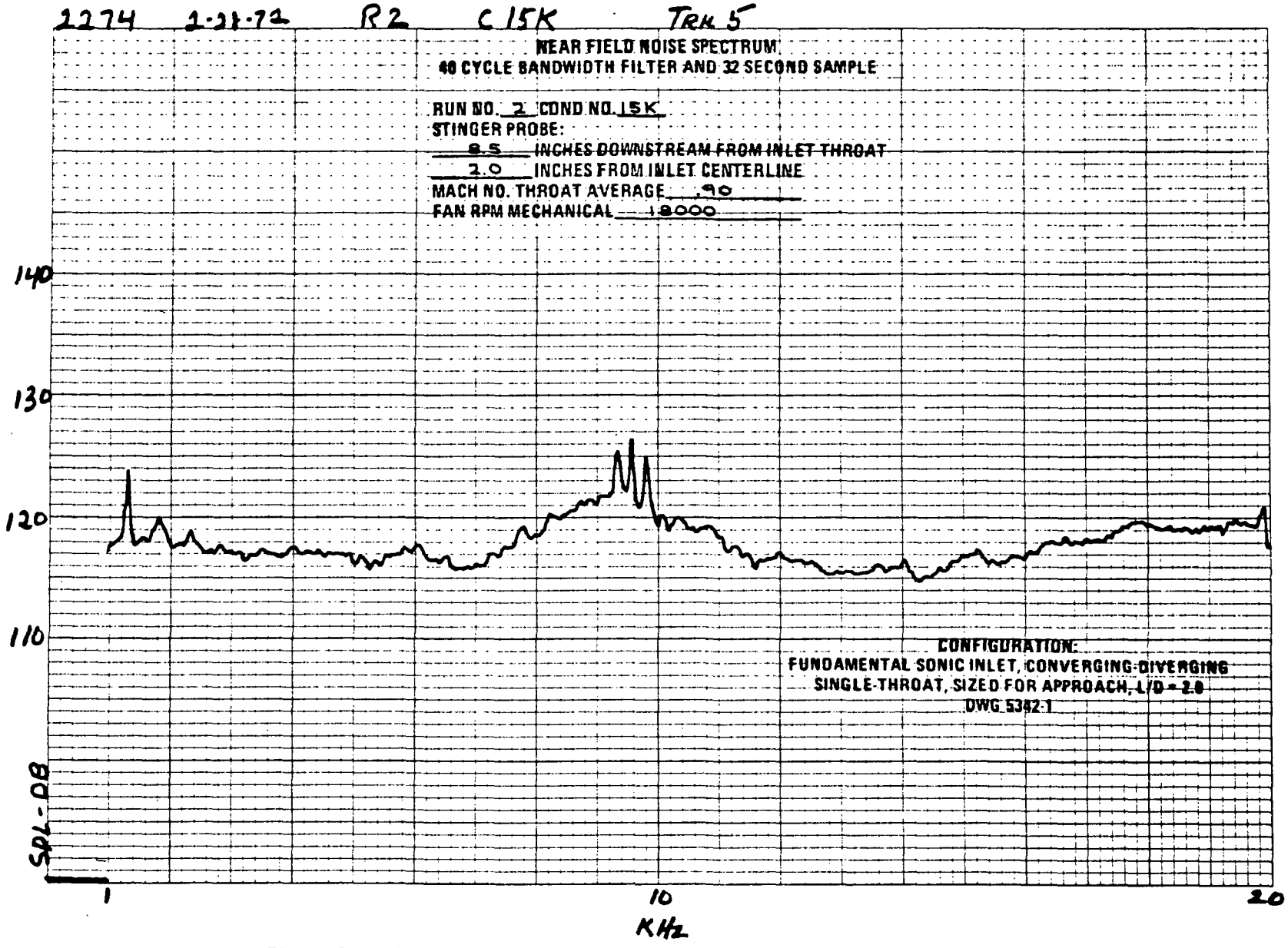

FIGURE A-50.—RUN 2-15K, STINGER PROBE MICROPHONE SPECTRUM AT (X; R) (8.5 IN.; 2.0 IN.)

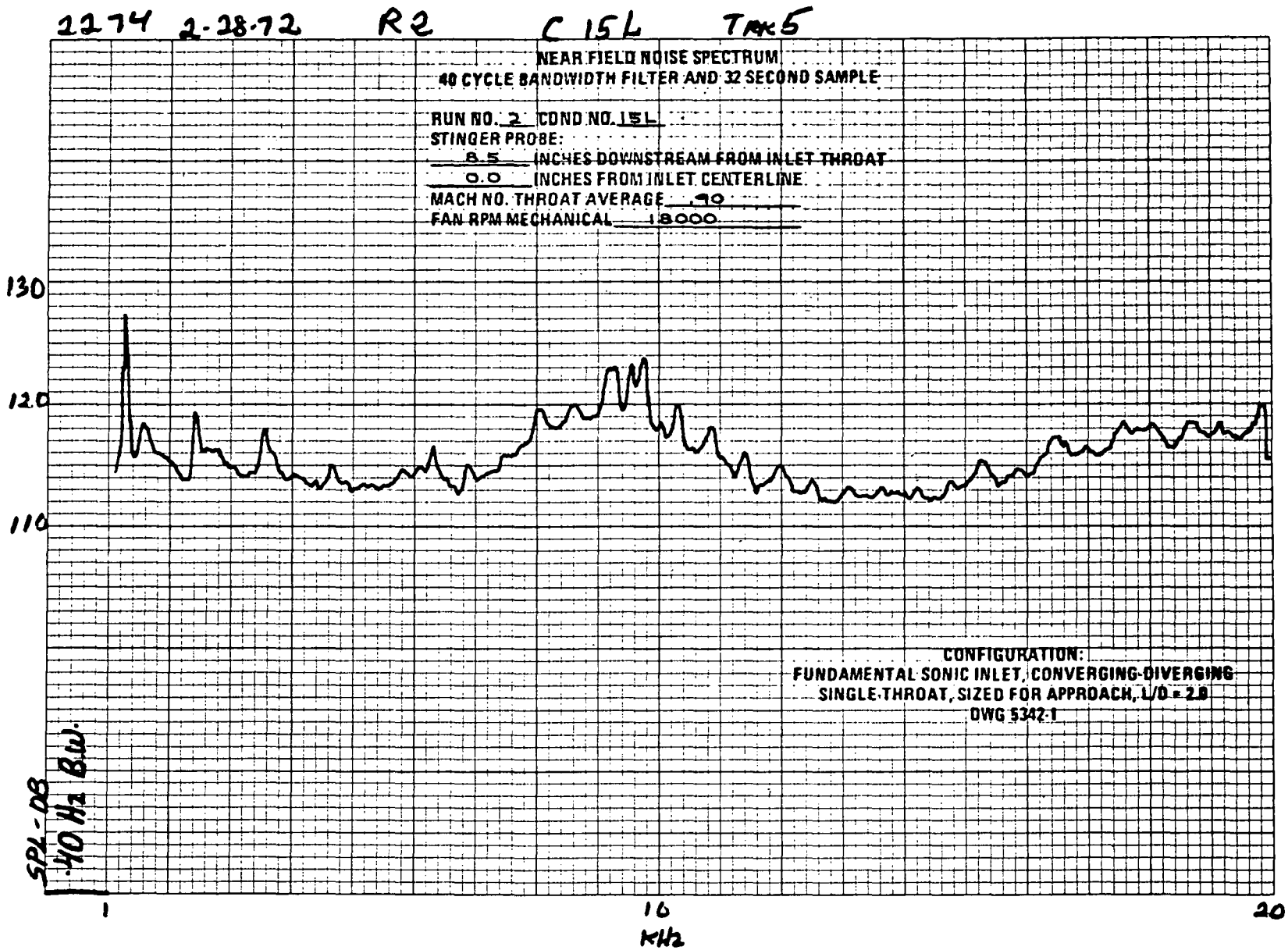

FIGURE A-51.—RUN 2-15L, STINGER PROBE MICROPHONE SPECTRUM AT (X; R) (8.5 IN.; 0.0 IN.)

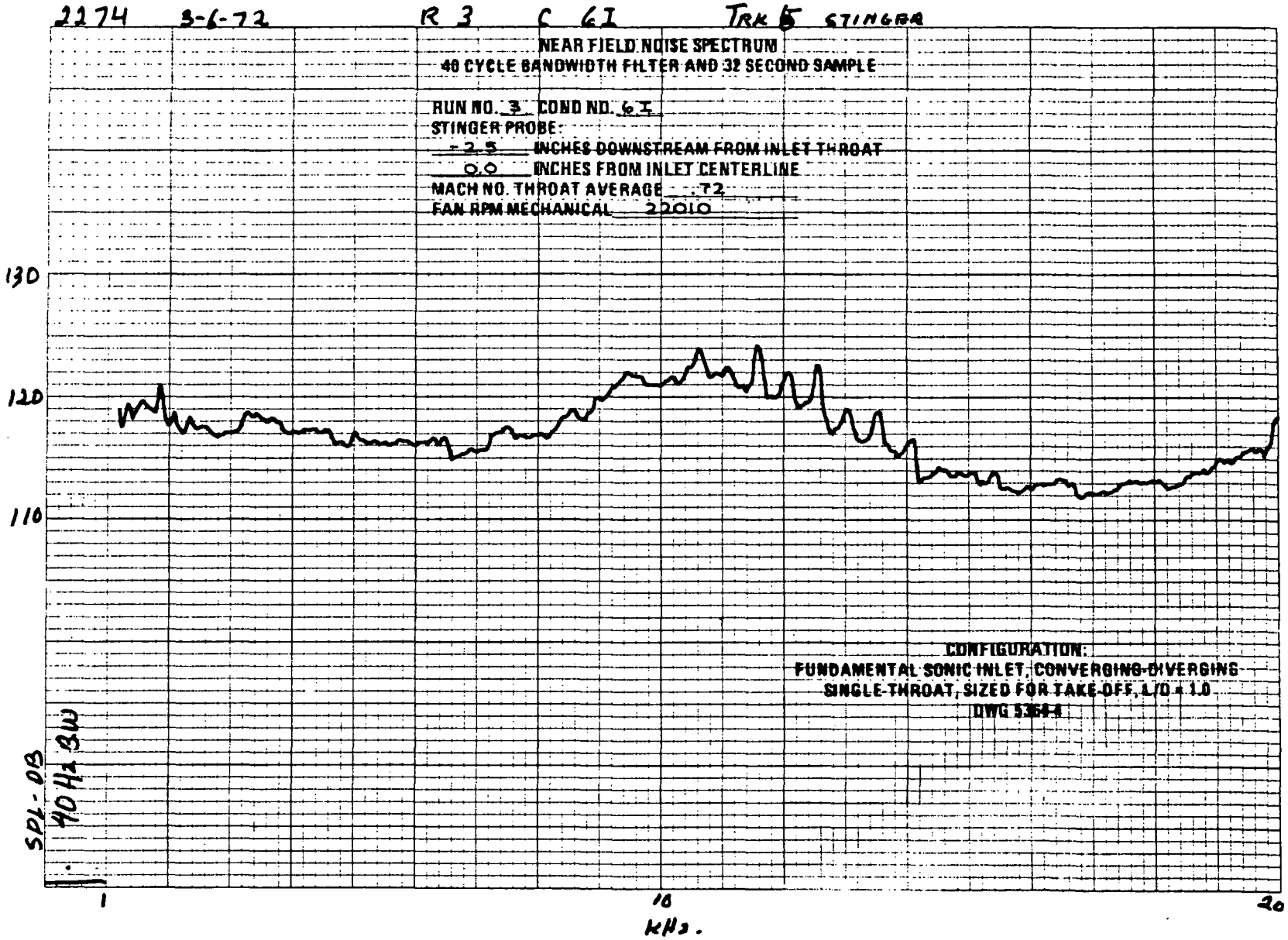

FIGURE A-52.—RUN 3-6I, STINGER PROBE MICROPHONE SPECTRUM AT (X; R) (-2.5 IN.; 0.0 IN.)

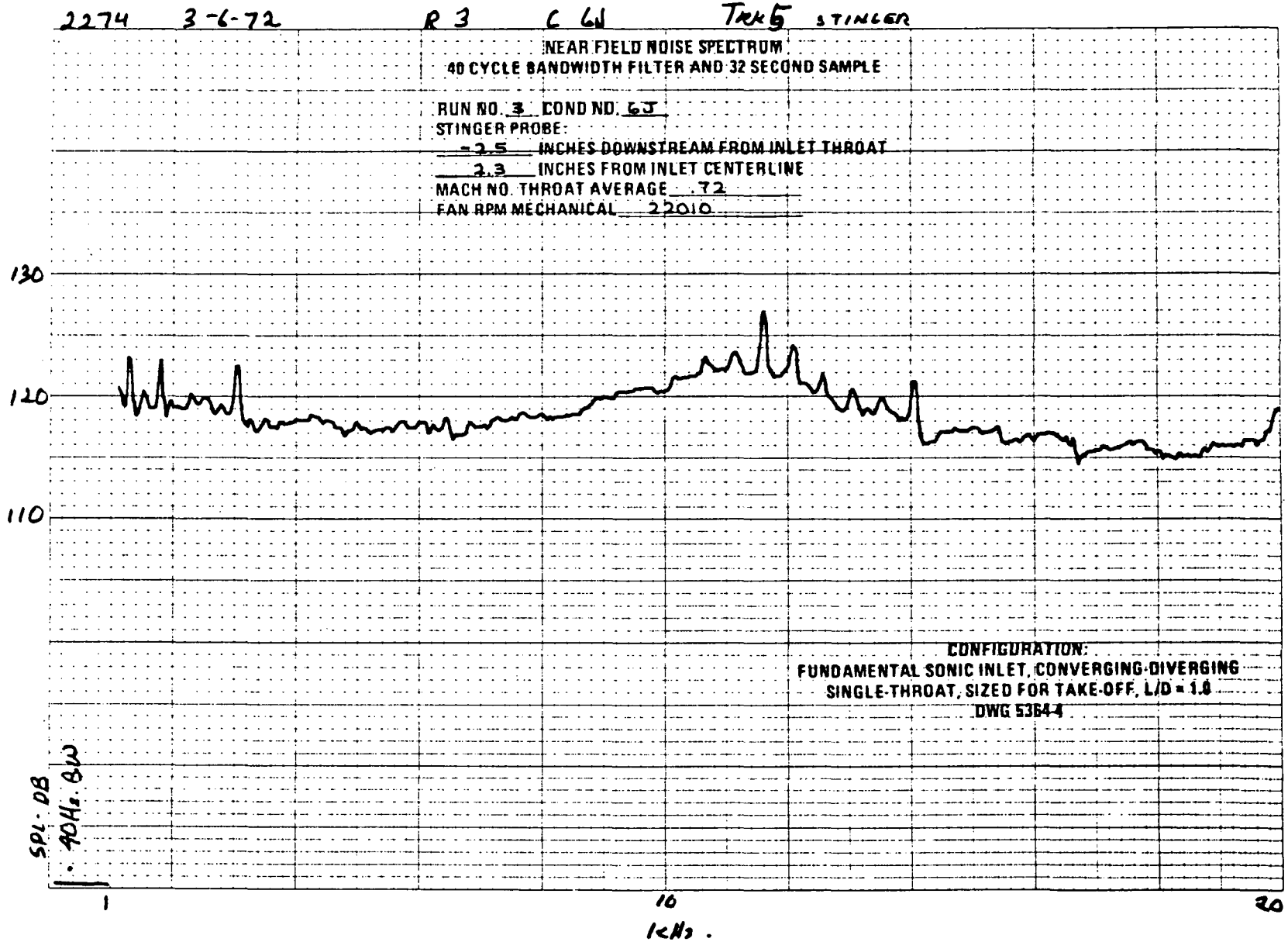

FIGURE A-53.—RUN 3-6J, STINGER PROBE MICROPHONE SPECTRUM AT (X; R) (-2.5 IN.; 2.3 IN.)

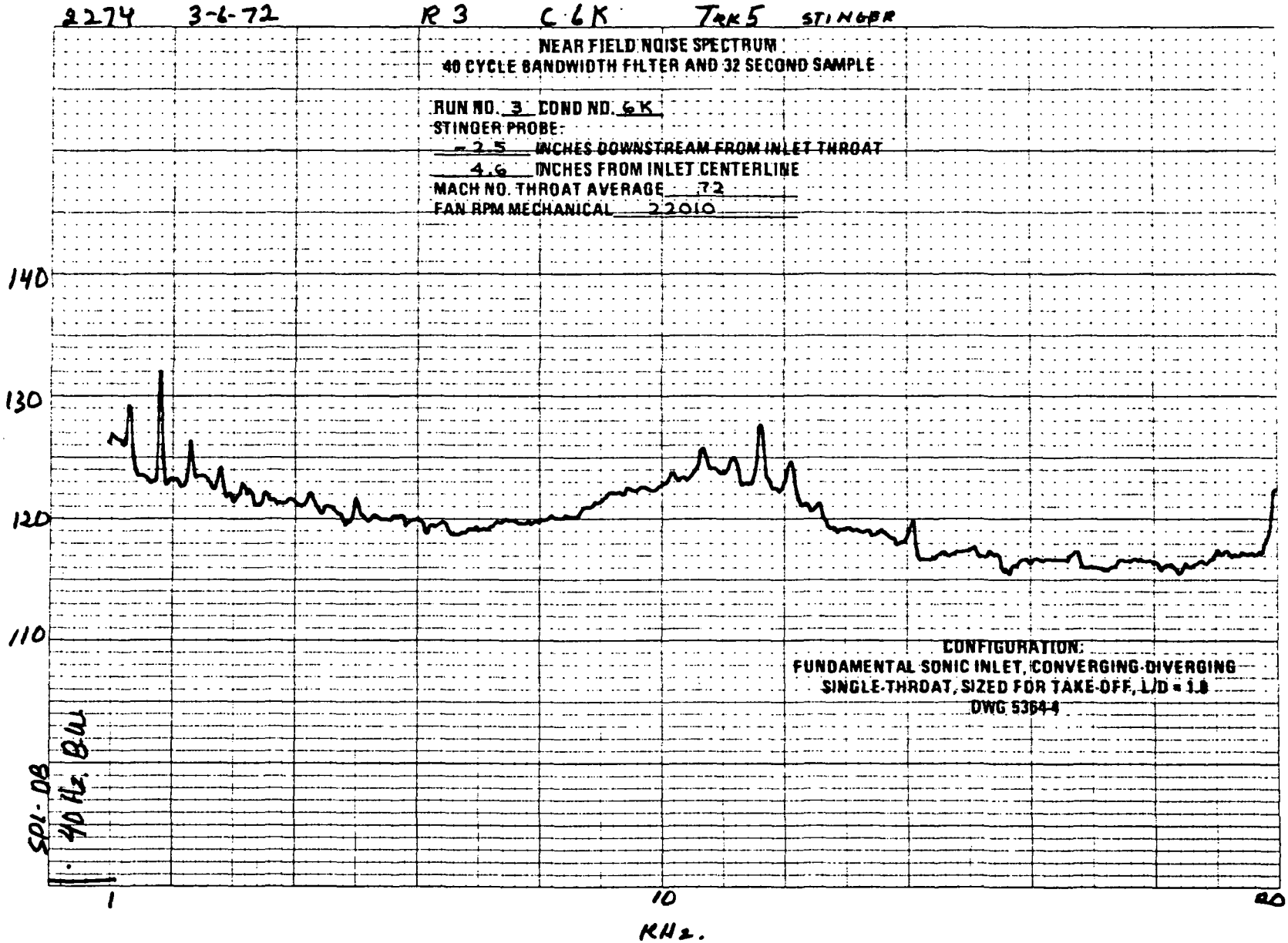

FIGURE A-54.—RUN 3-6K, STINGER PROBE MICROPHONE SPECTRUM AT (X; R) (-2.5 IN.; 4.6 IN.)

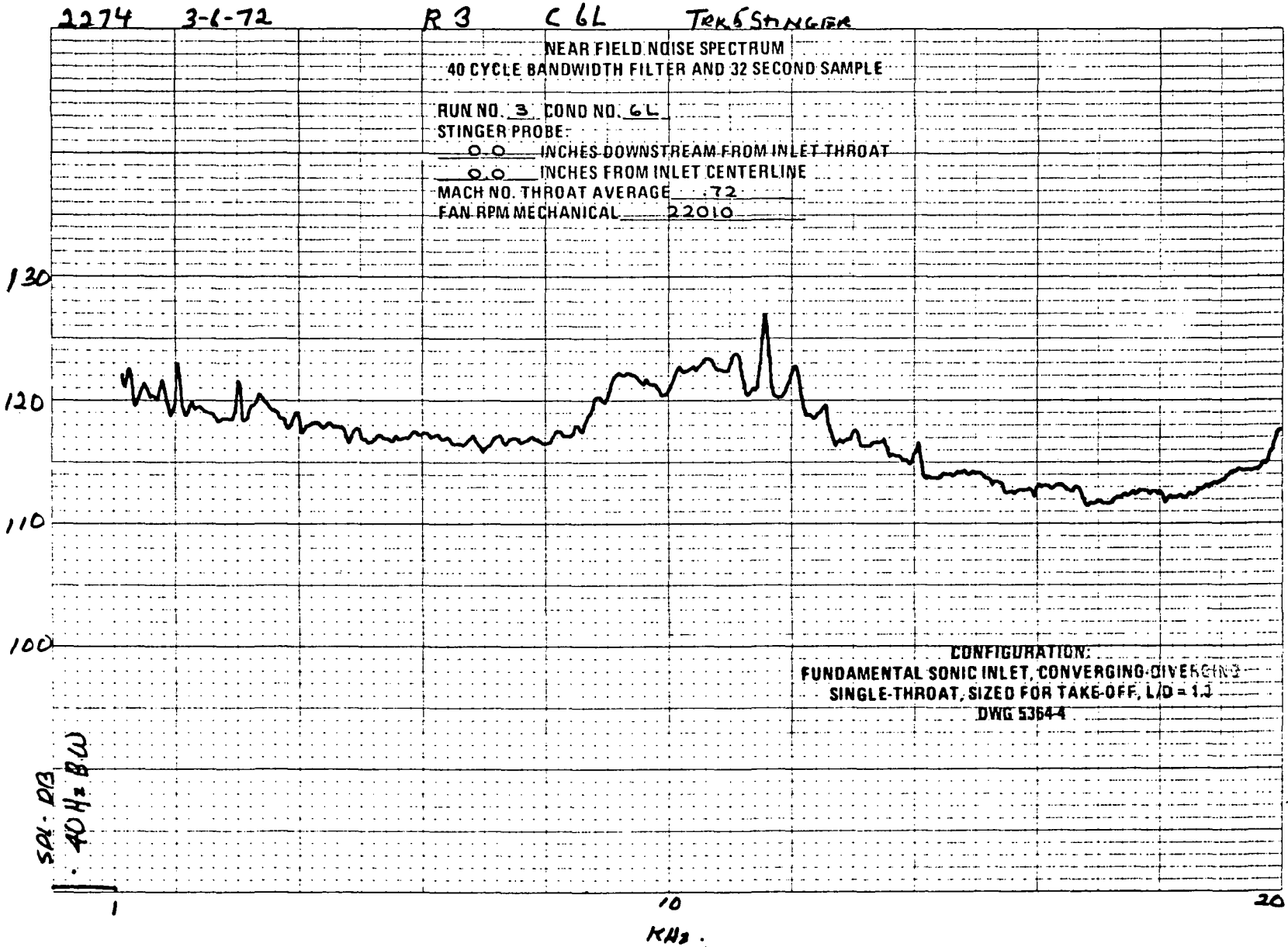

FIGURE A-55.—RUN 3-6L, STINGER PROBE MICROPHONE SPECTRUM AT (X; R) (0.0 IN.; 0.0 IN.)

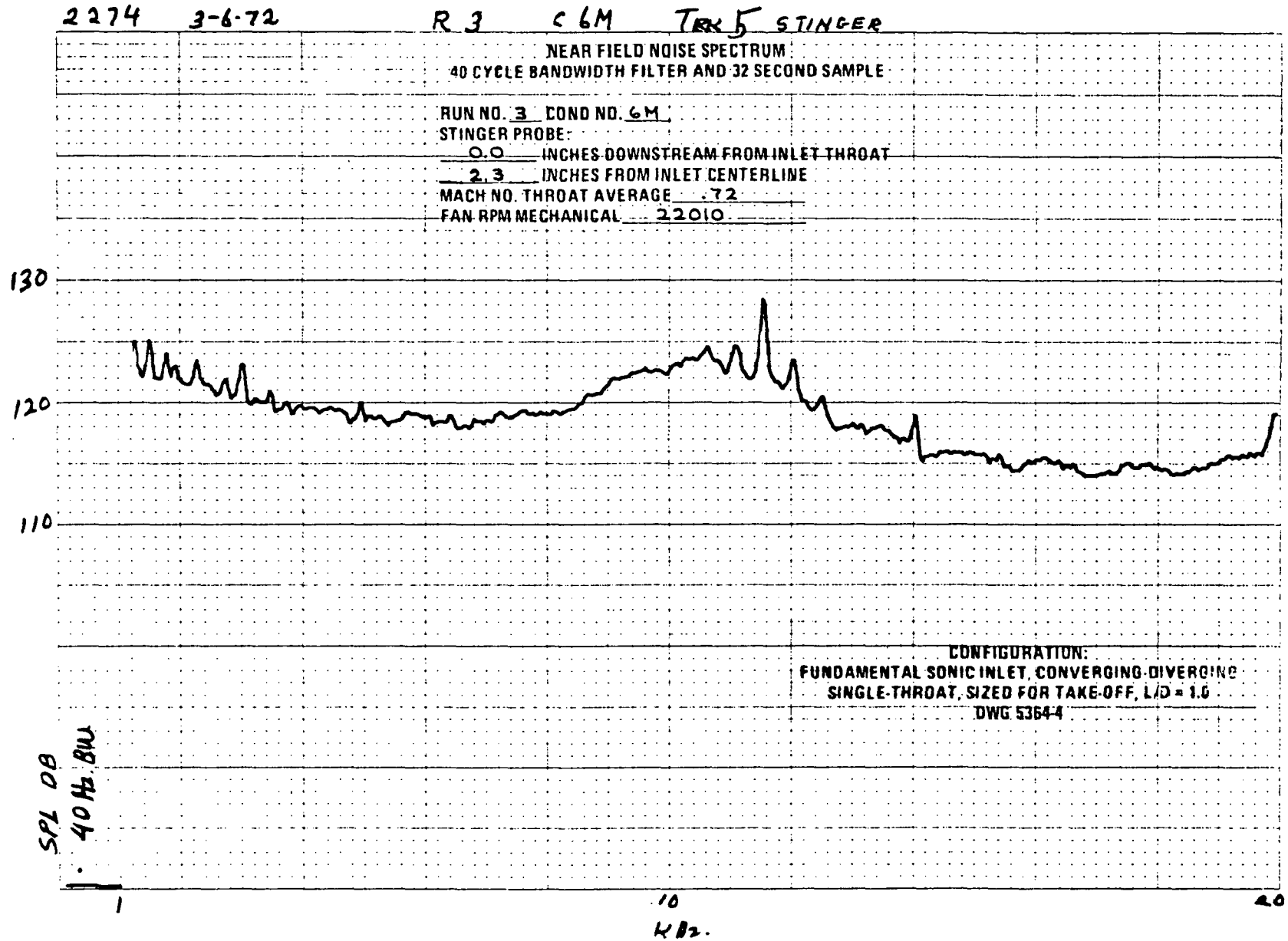

FIGURE A-56.—RUN 3-6M, STINGER PROBE MICROPHONE SPECTRUM AT (X; R) (0.0 IN.; 2.3 IN.)

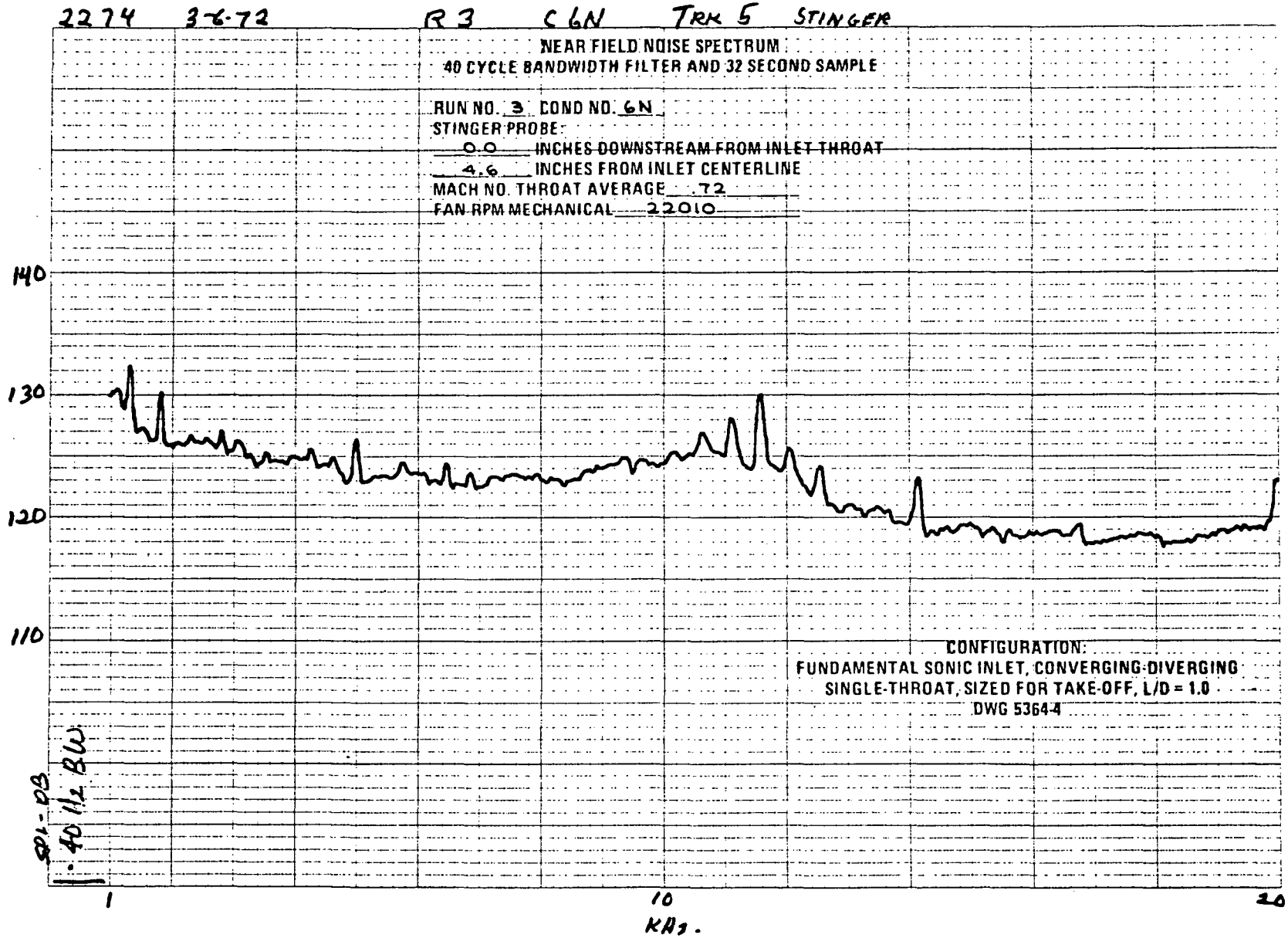

FIGURE A-57.—RUN 3-6N, STINGER PROBE MICROPHONE SPECTRUM AT (X; R) (0.0 IN.; 4.6 IN.)

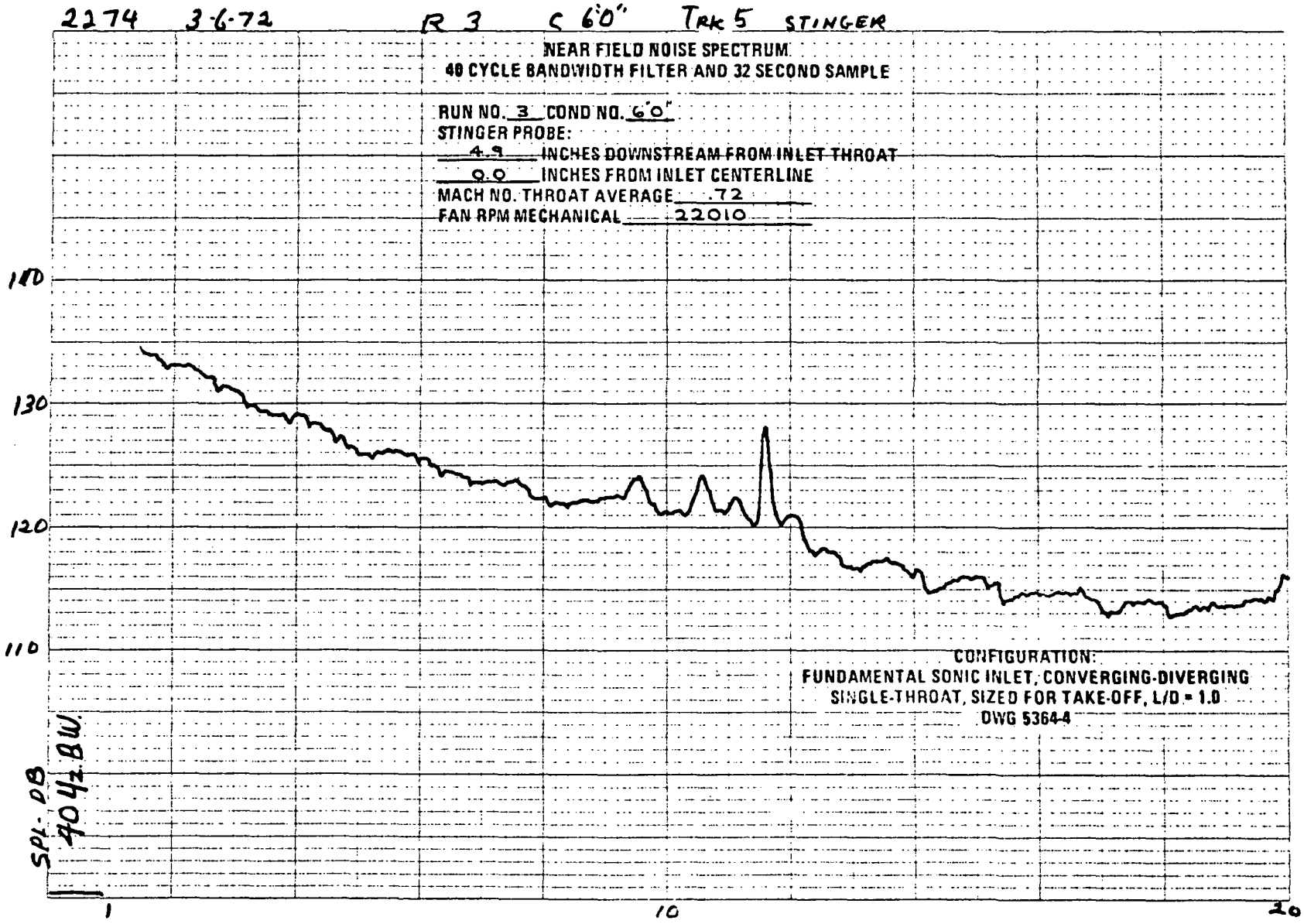

FIGURE A-58.—RUN 3-60, STINGER PROBE MICROPHONE SPECTRUM AT (X; R) (4.9 IN.; 0.0 IN.)

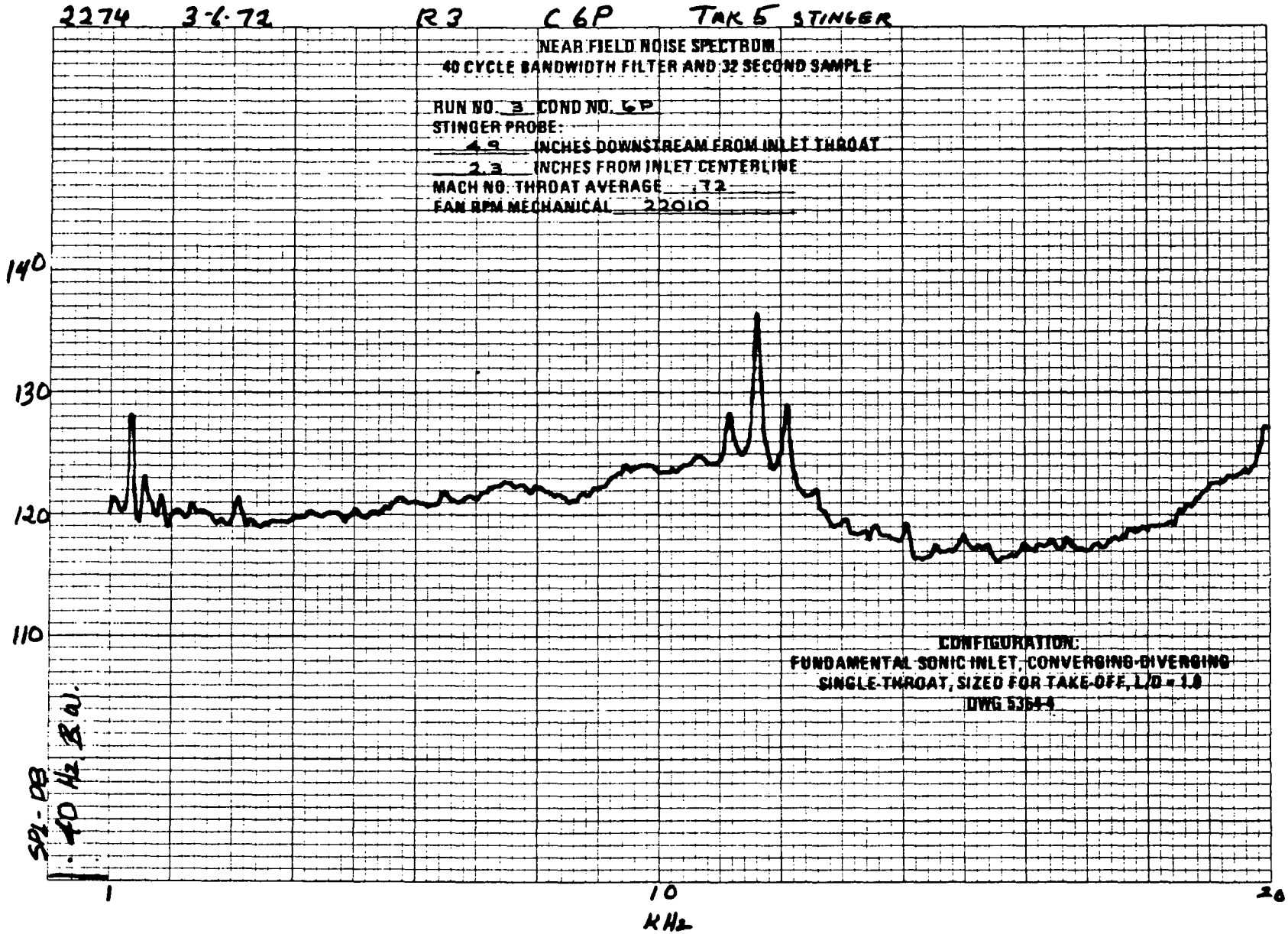

FIGURE A-59.—RUN 3-6P, STINGER PROBE MICROPHONE SPECTRUM AT (X; R) (4.9 IN.; 2.3 IN.)

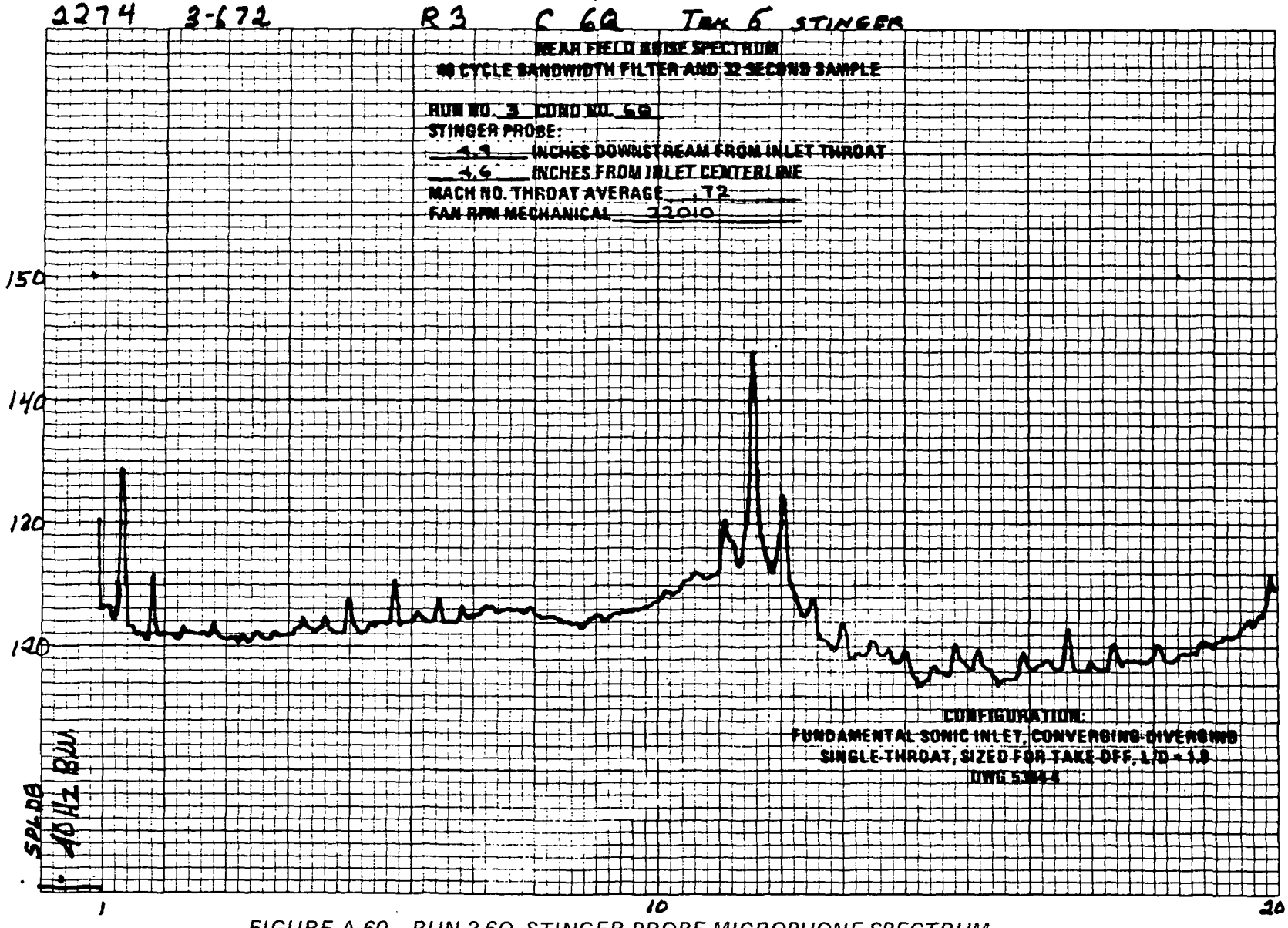

FIGURE A-60.—RUN 3-6Q, STINGER PROBE MICROPHONE SPECTRUM AT (X; R) (4.9 IN.; 4.6 IN.)

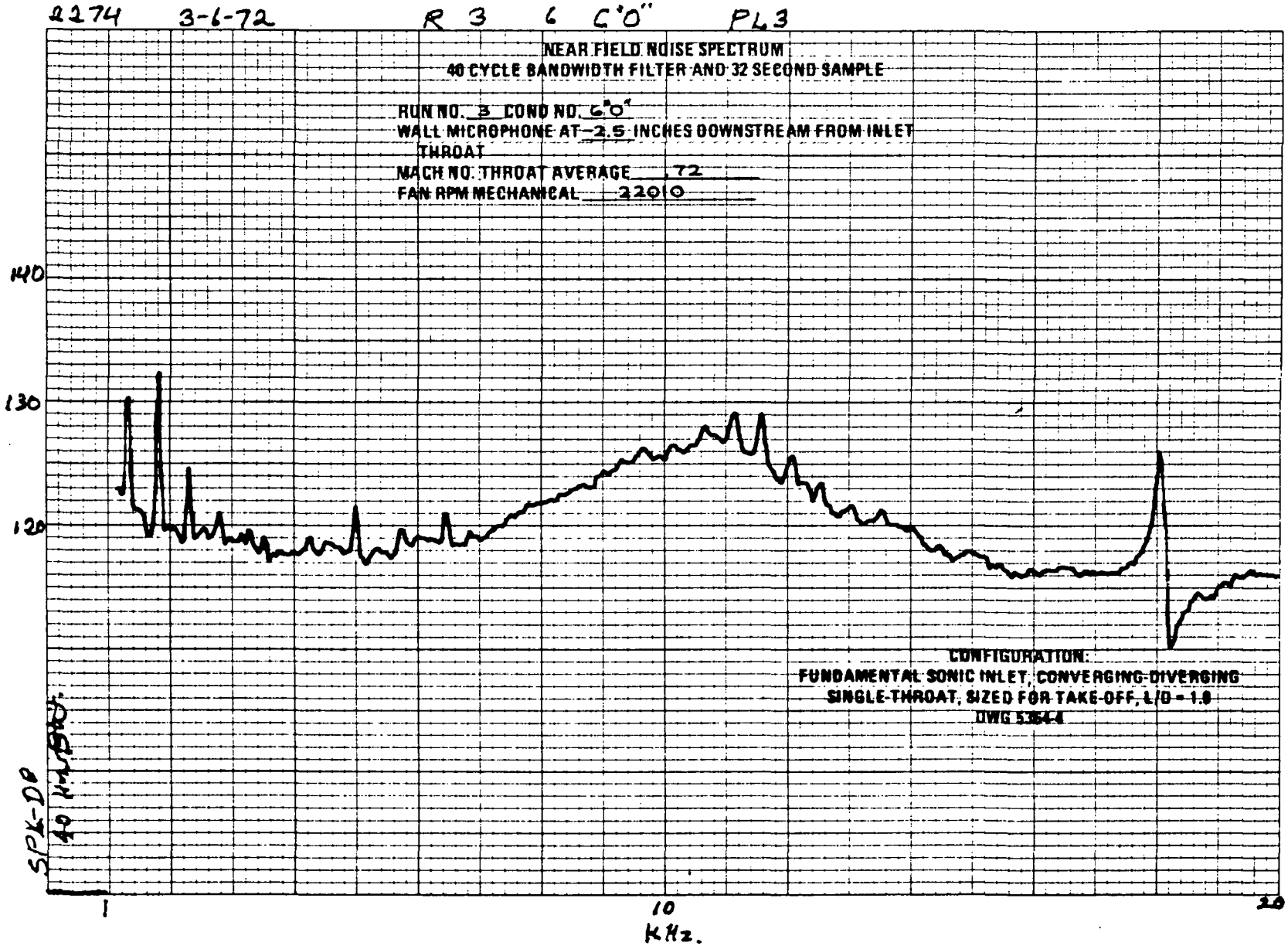

FIGURE A-61.—RUN 3-6O, WALL MICROPHONE SPECTRUM AT -2.5 IN. DOWNSTREAM FROM INLET THROAT

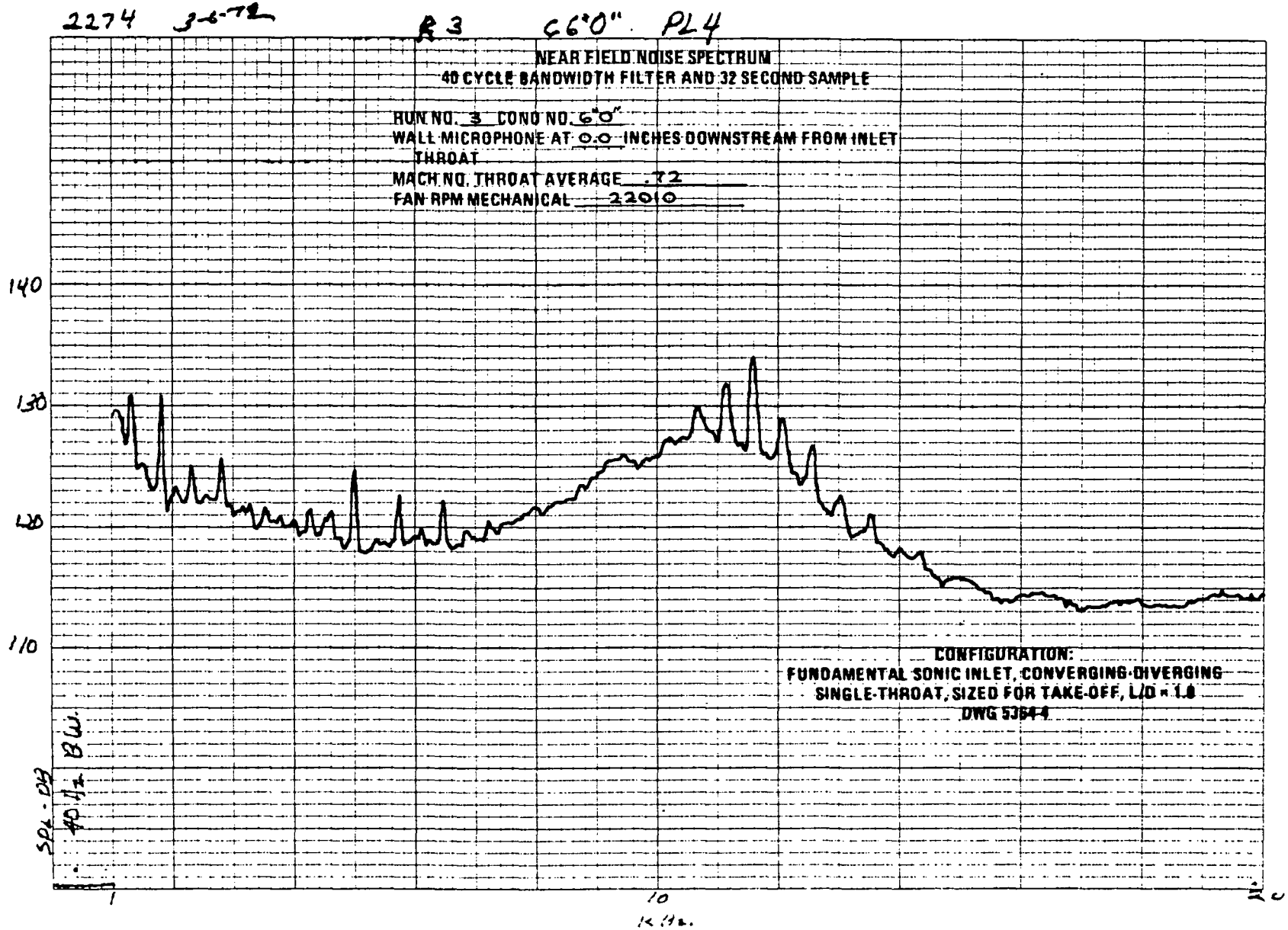

FIGURE A-62.—RUN 3-60, WALL MICROPHONE SPECTRUM AT 0.0 IN. DOWNSTREAM FROM INLET THROAT

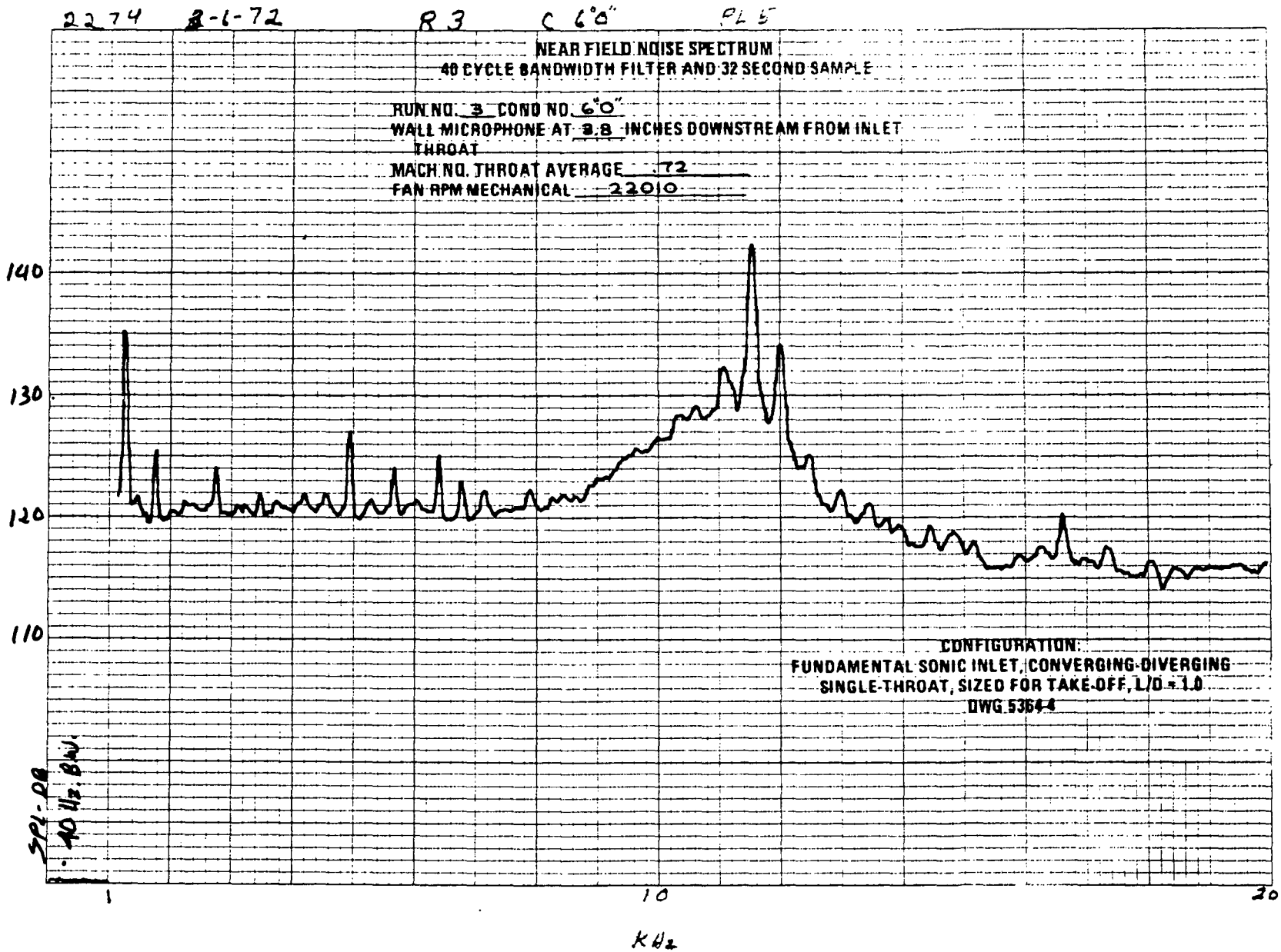

FIGURE A-63.—RUN 3-60, WALL MICROPHONE SPECTRUM AT 3.8 IN. DOWNSTREAM FROM INLET THROAT

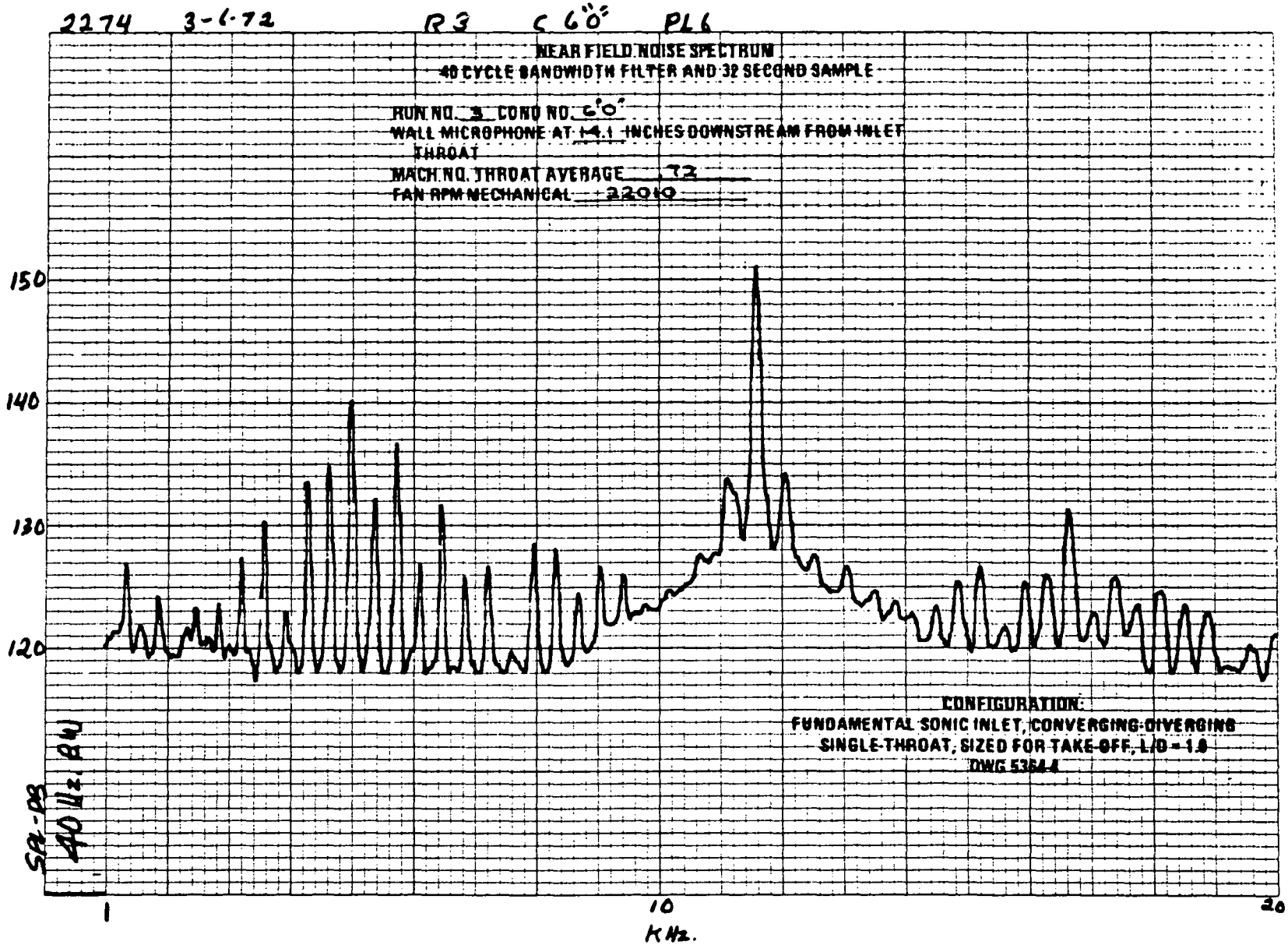

FIGURE A-64.—RUN 3-60, WALL MICROPHONE SPECTRUM AT 14.1 IN. DOWNSTREAM FROM INLET THROAT

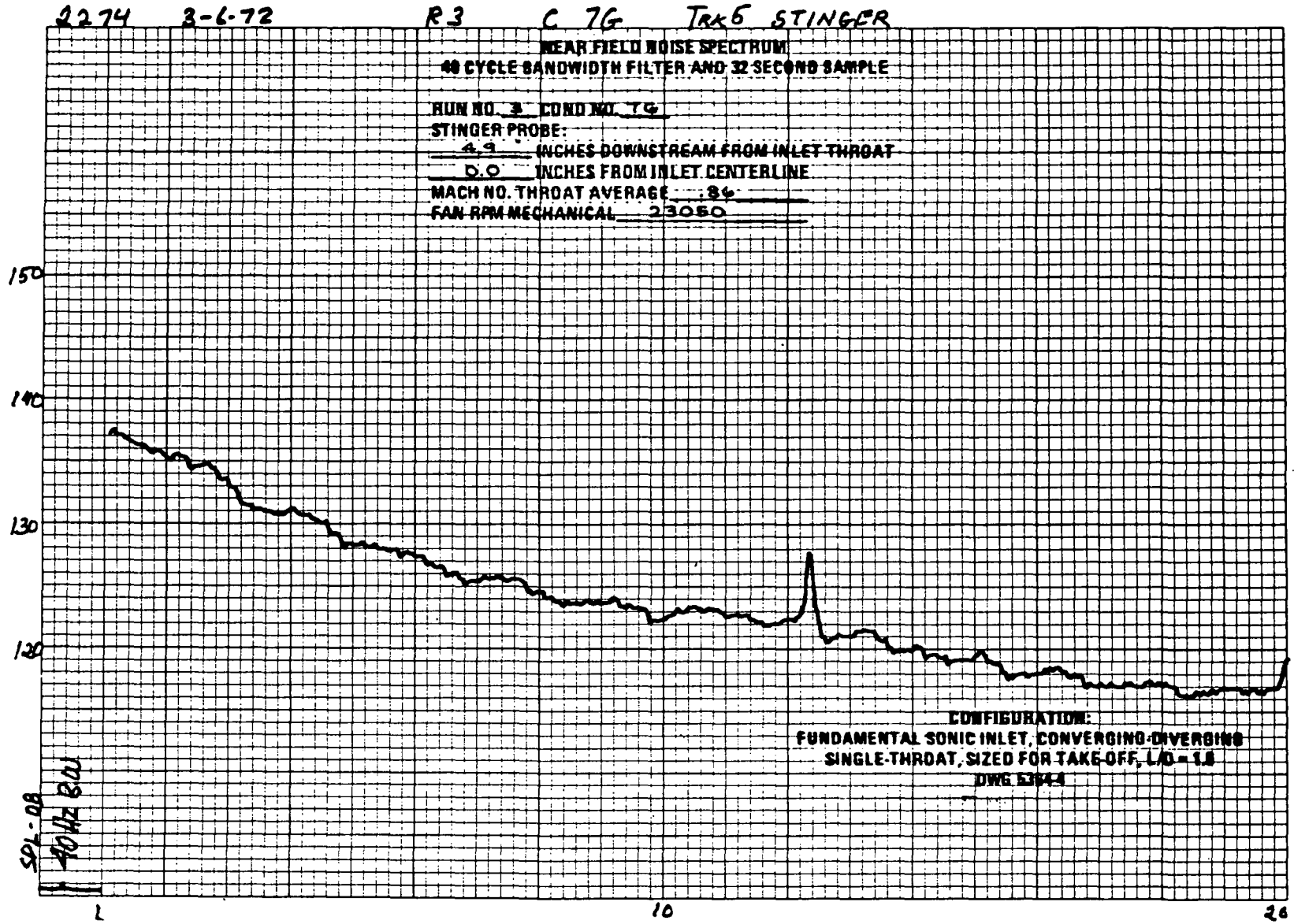

FIGURE A-65.—RUN 3-7G, STINGER PROBE MICROPHONE SPECTRUM AT (X; R) (4.9 IN.; 0.0 IN.)

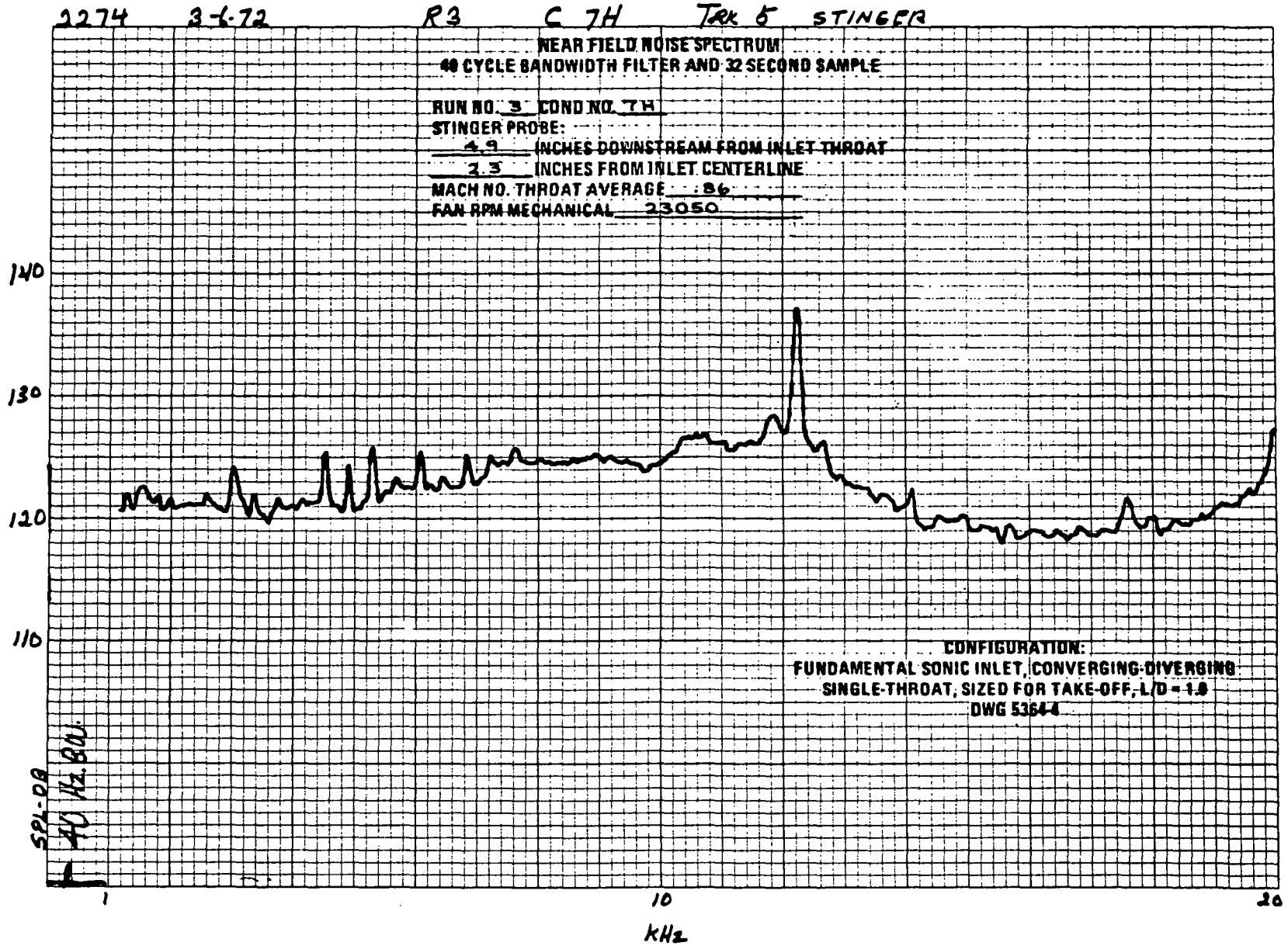

FIGURE A-66.—RUN 3-7H, STINGER PROBE MICROPHONE SPECTRUM AT (X; R) (4.9 IN.; 2.3 IN.)

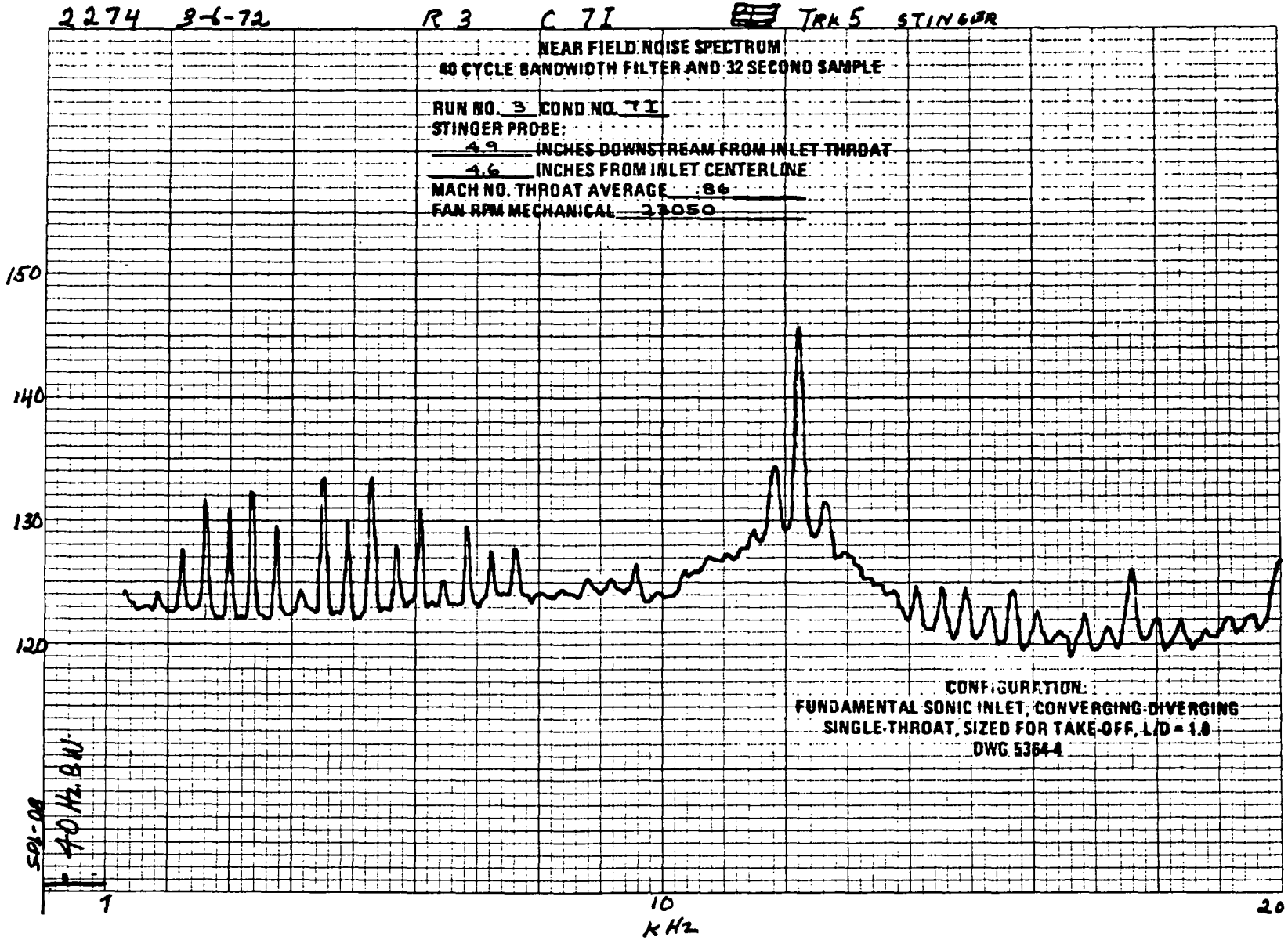

FIGURE A-67.—RUN 3-7I, STINGER PROBE MICROPHONE SPECTRUM AT (X; R) (4.9 IN.; 4.6 IN.)

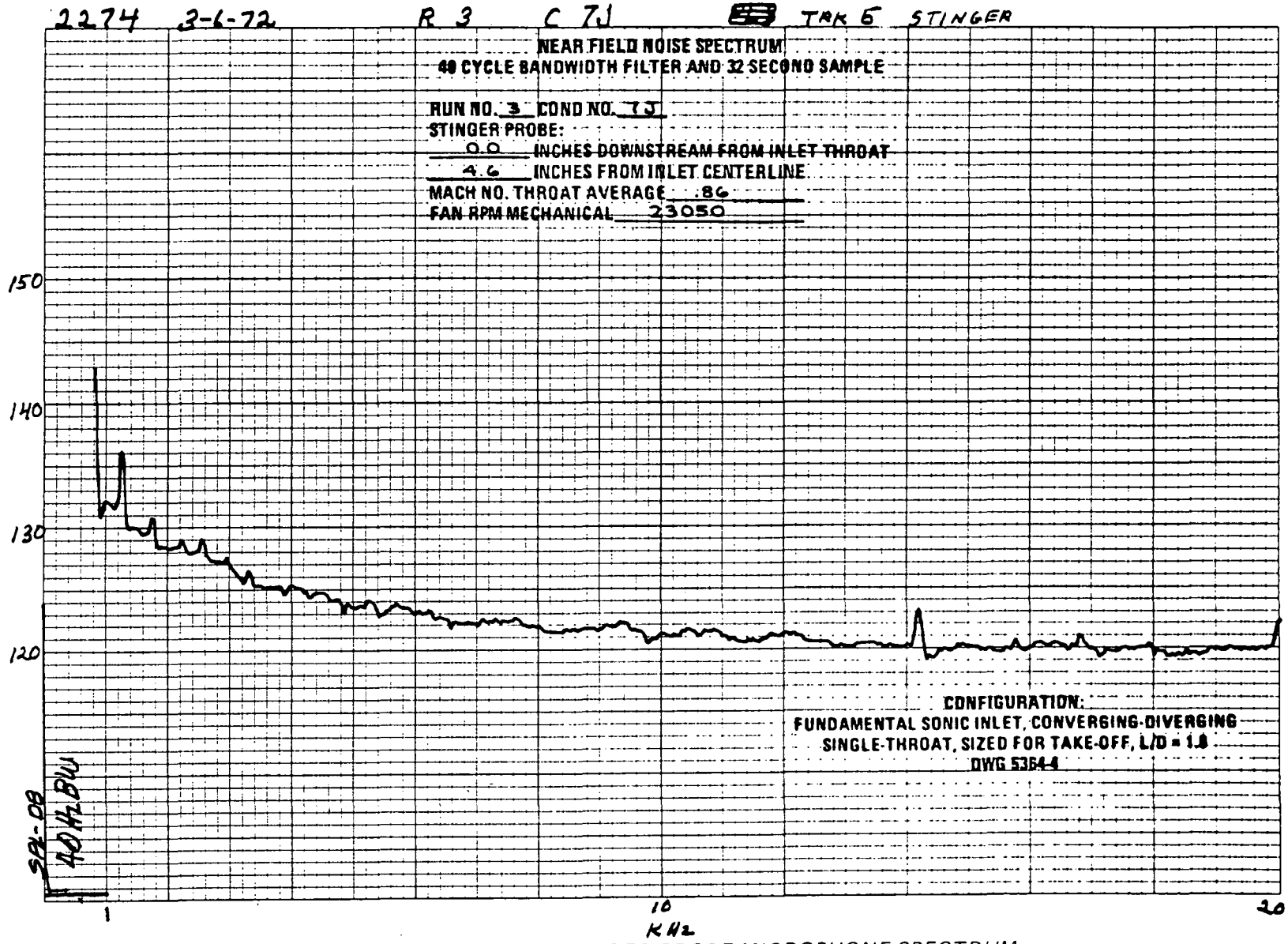

FIGURE A-68.—RUN 3-7J, STINGER PROBE MICROPHONE SPECTRUM AT (X; R) (0.0 IN.; 4.6 IN.)

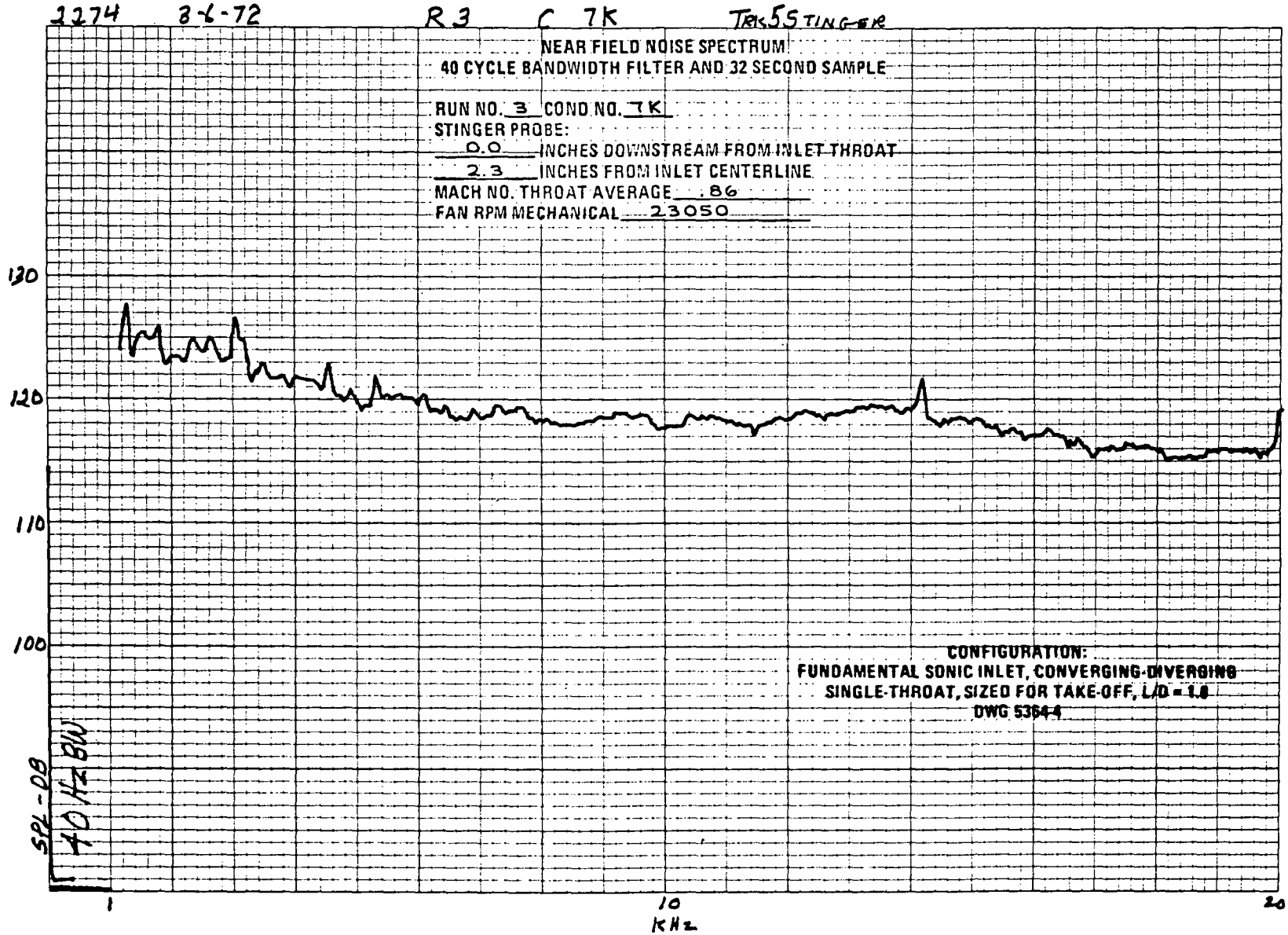

FIGURE A-69.—RUN 3-7K, STINGER PROBE MICROPHONE SPECTRUM AT (X; R) (0.0 IN.; 2.3 IN.)

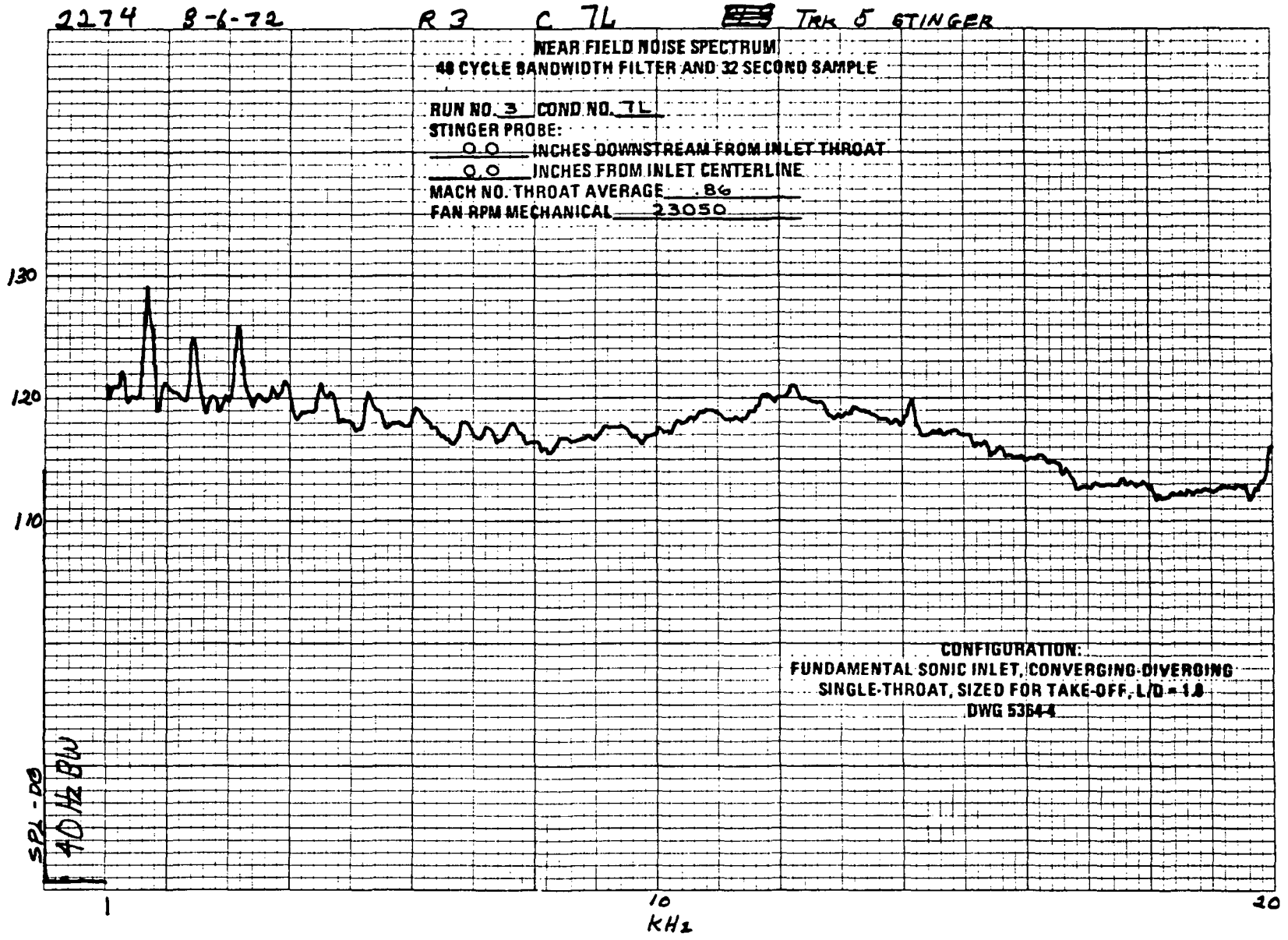

FIGURE A-70.—RUN 3-7L, STINGER PROBE MICROPHONE SPECTRUM AT (X; R) (0.0 IN.; 0.0 IN.)

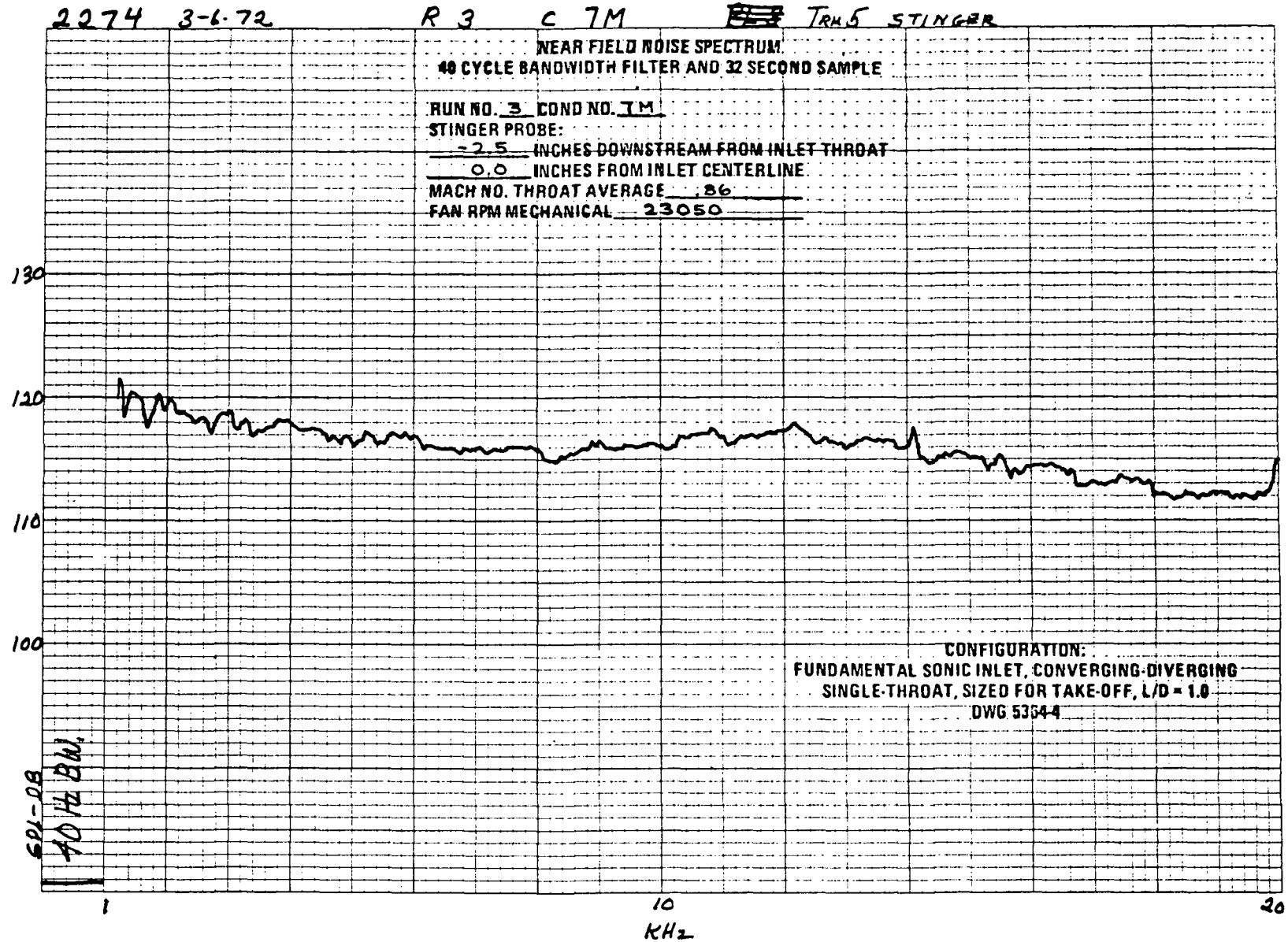

FIGURE A-71.—RUN 3-7M, STINGER PROBE MICROPHONE SPECTRUM AT (X; R) (-2.5 IN.; 0.0 IN.)

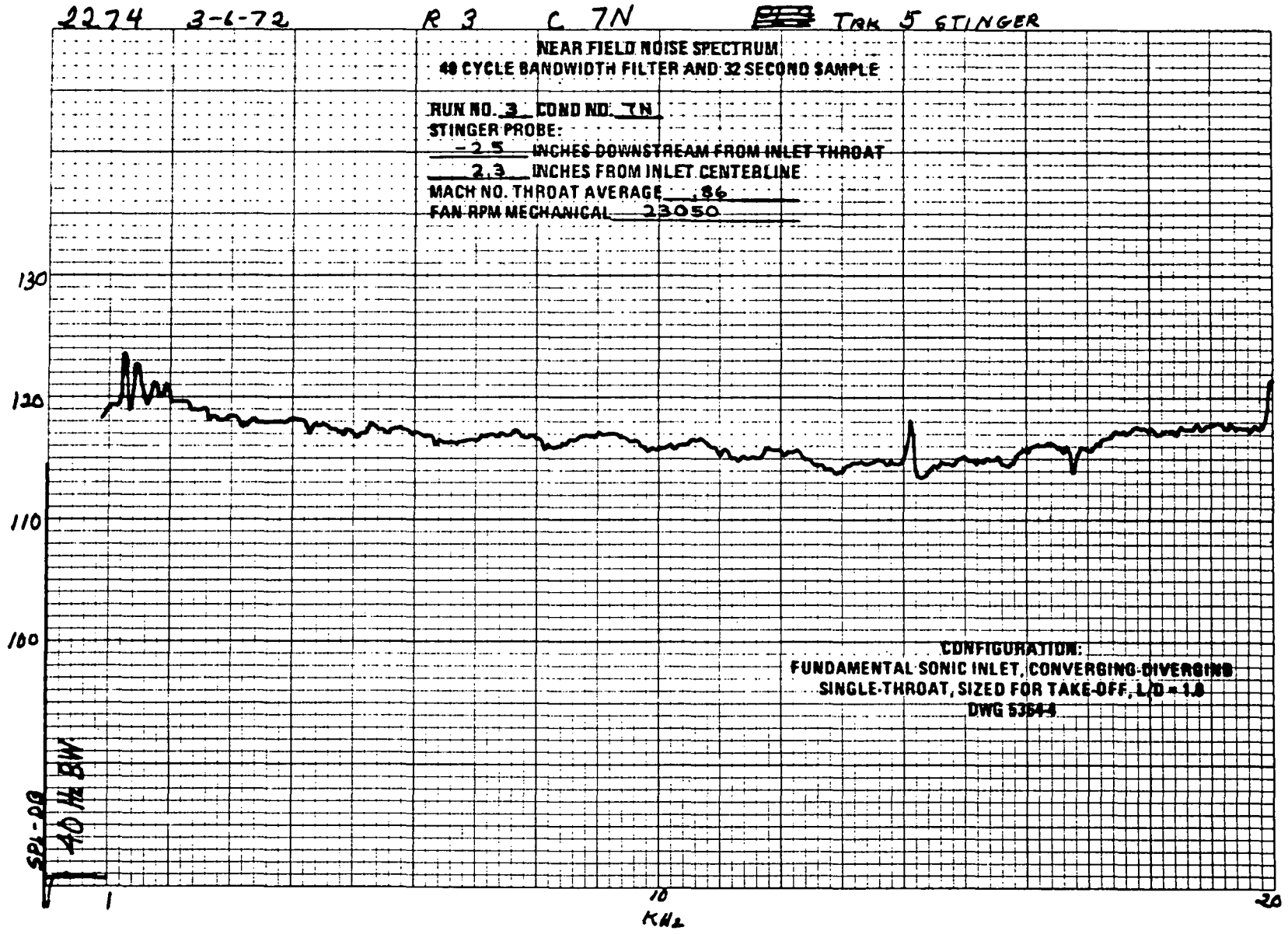

FIGURE A-72.—RUN 3-7N, STINGER PROBE MICROPHONE SPECTRUM AT (X; R) (-2.5 IN.; 2.3 IN.)

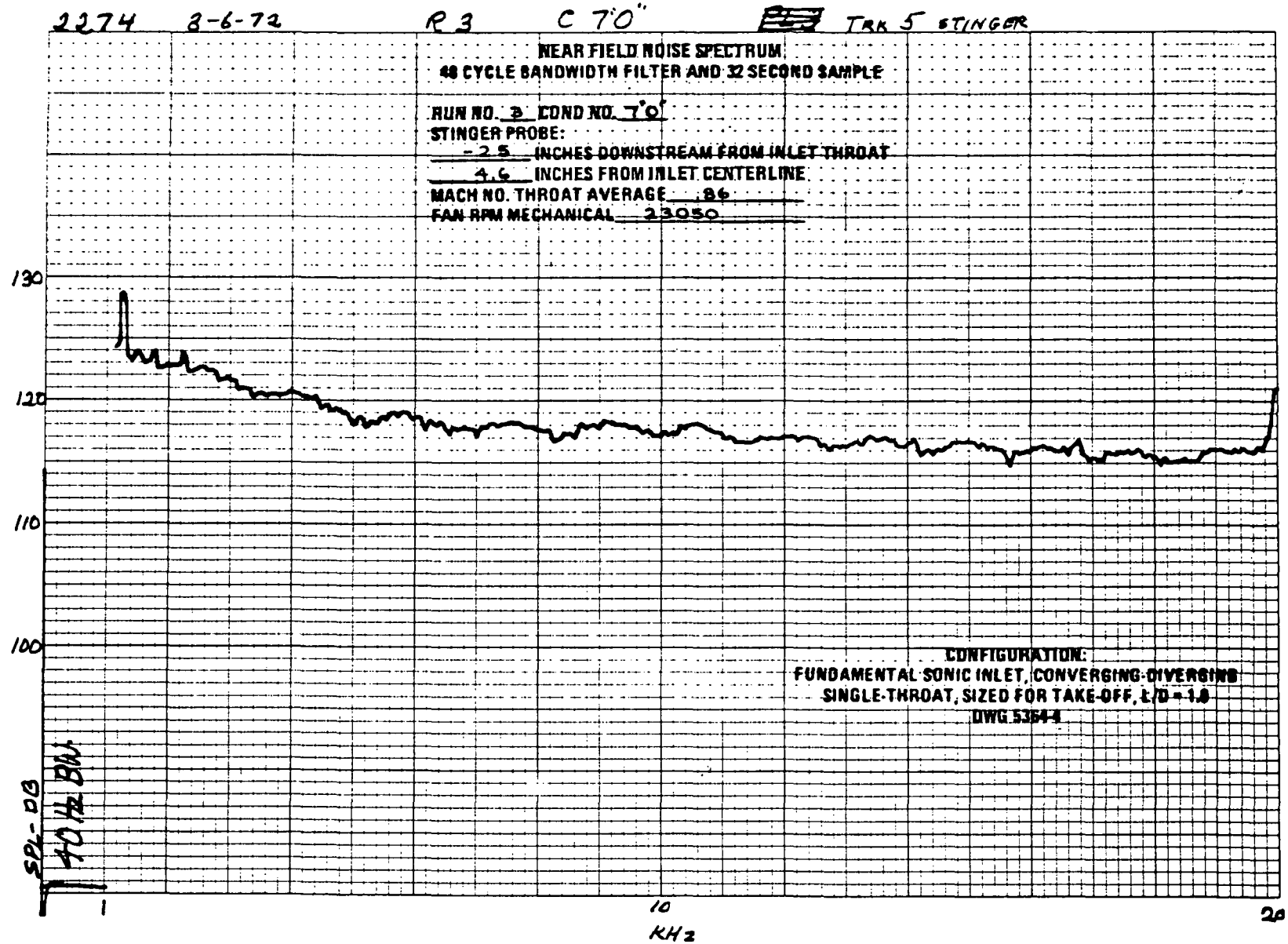

FIGURE A-73.—RUN 3-70, STINGER PROBE MICROPHONE SPECTRUM AT (X; R) (-2.5 IN.; 4.6 IN.)

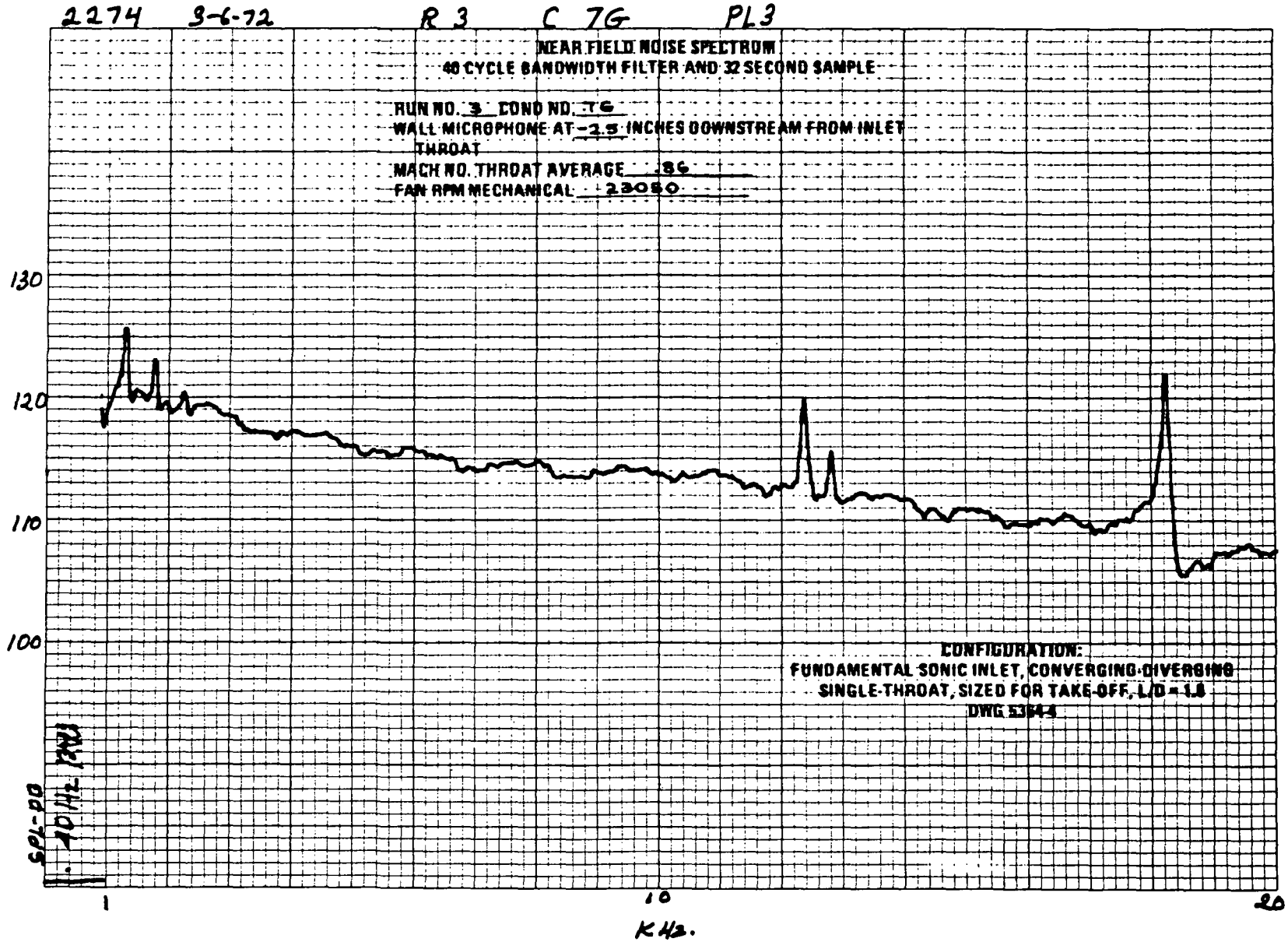

FIGURE A-74.—RUN 3-7G, WALL MICROPHONE SPECTRUM AT -2.5 IN. DOWNSTREAM FROM INLET THROAT

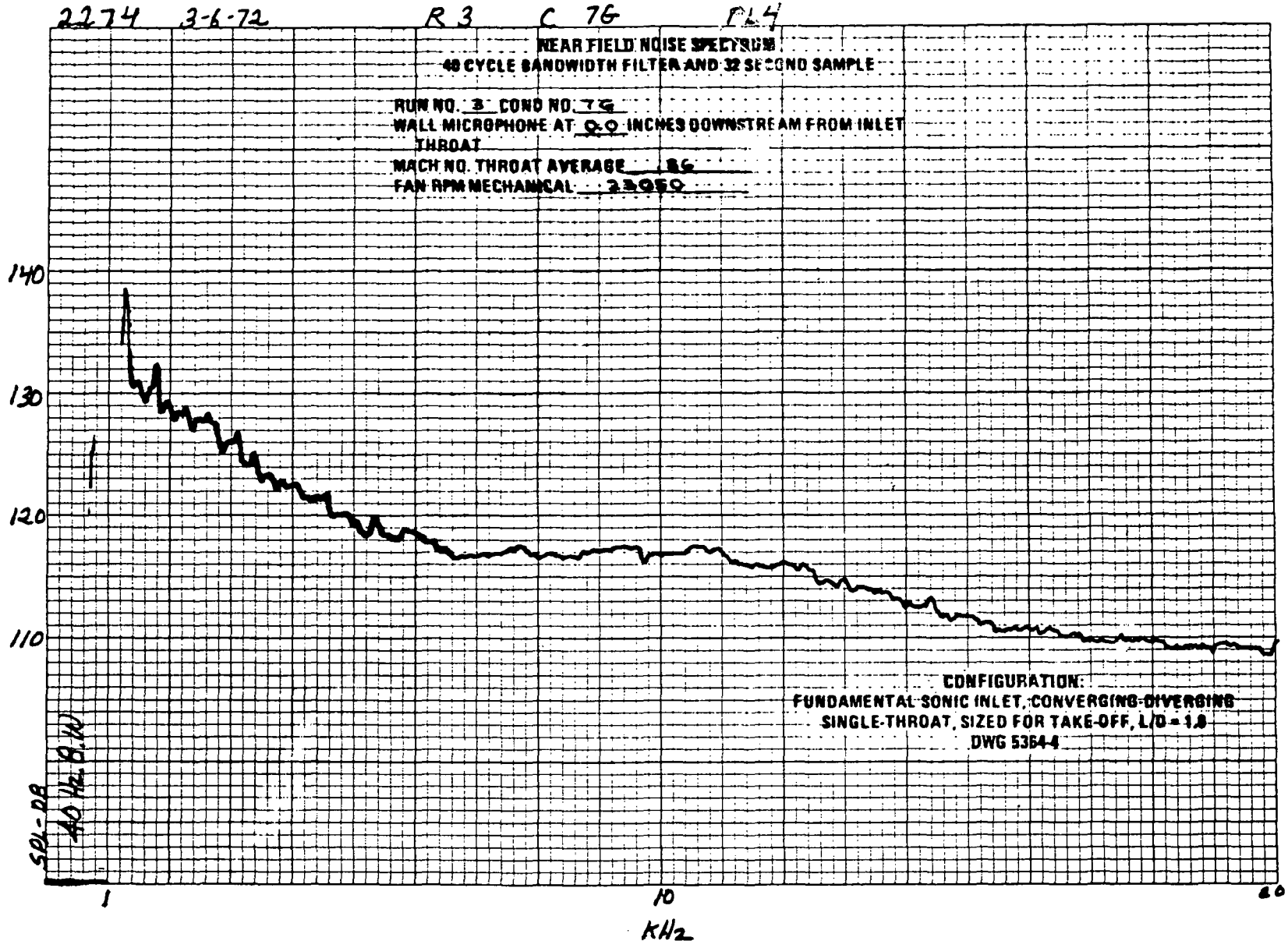

FIGURE A-75.—RUN 3-7G, WALL MICROPHONE SPECTRUM AT 0.0 IN. DOWNSTREAM FROM INLET THROAT

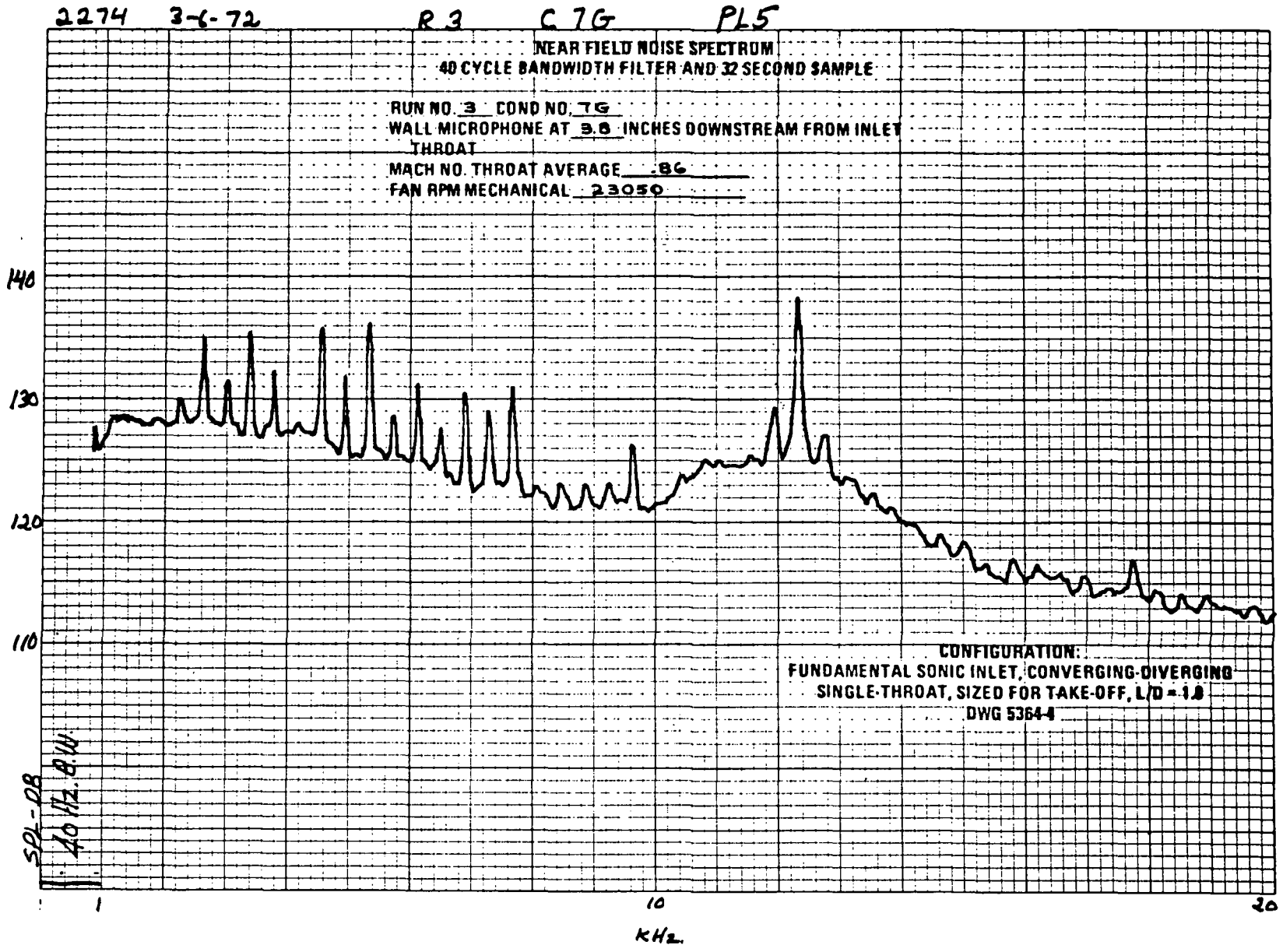

FIGURE A-76.—RUN 3-7G, WALL MICROPHONE SPECTRUM AT 3.8 IN. DOWNSTREAM FROM INLET THROAT

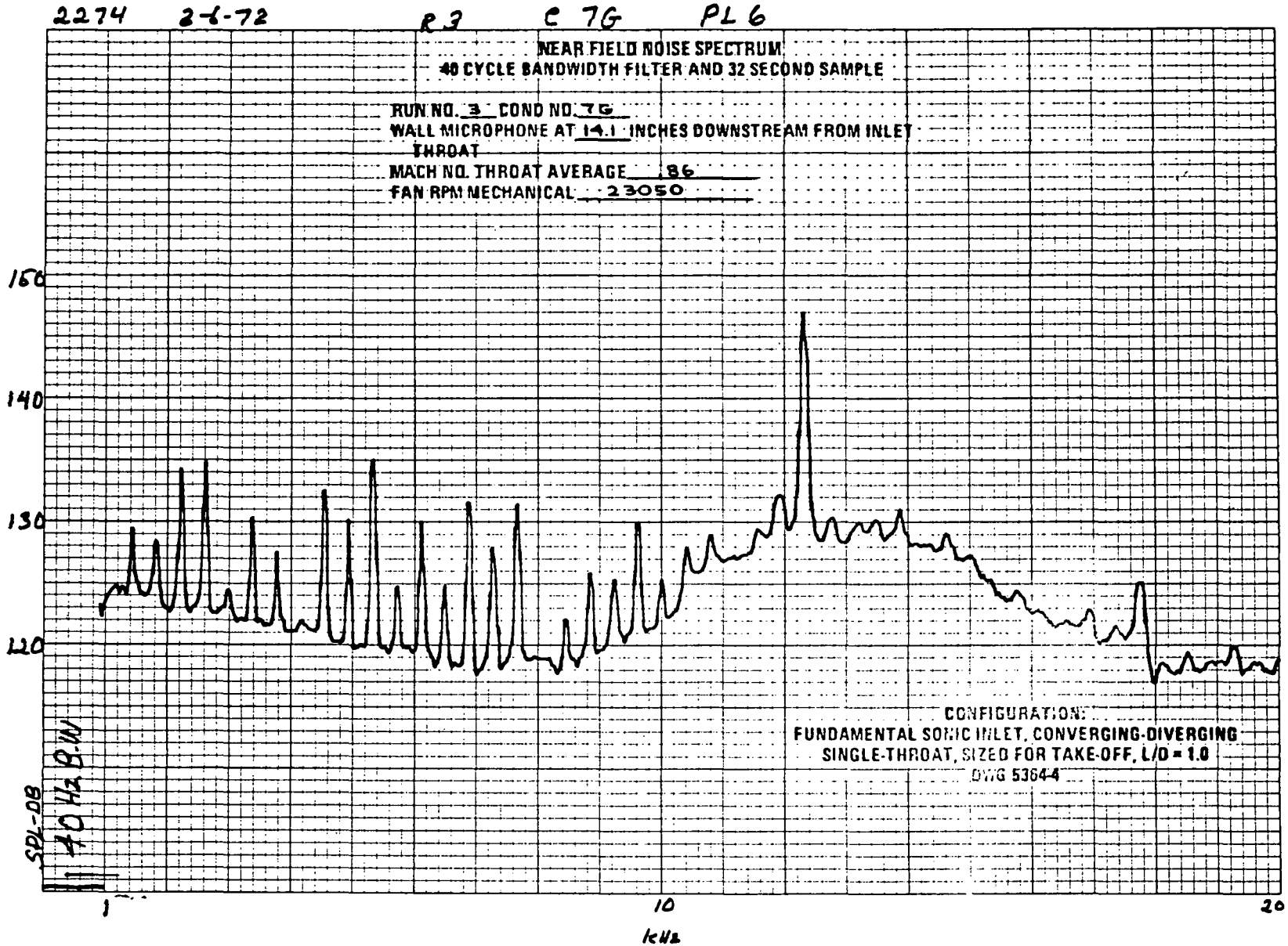

FIGURE A-77.—RUN 3-7G, WALL MICROPHONE SPECTRUM AT 14.1 IN. DOWNSTREAM FROM INLET THROAT

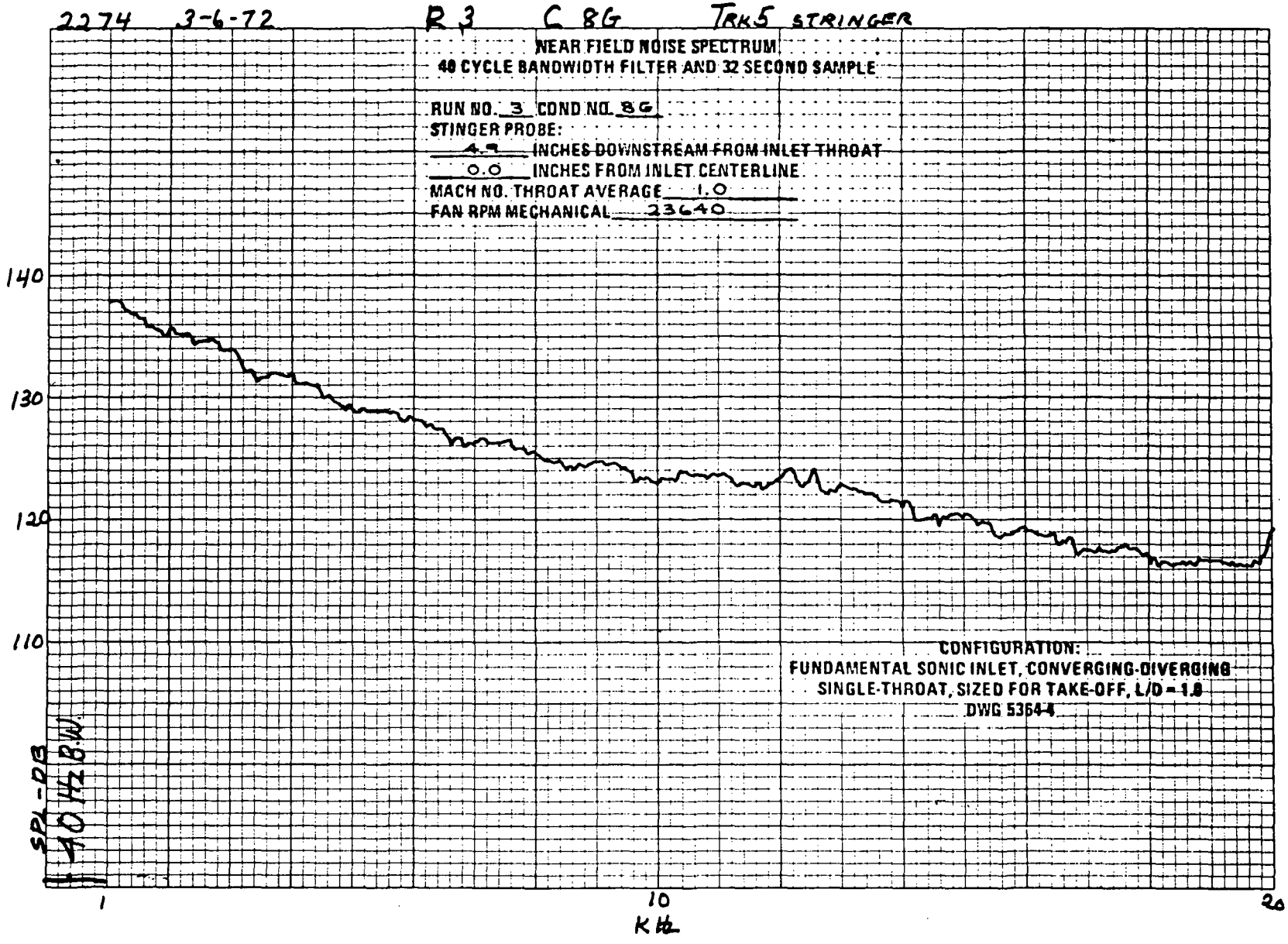

FIGURE A-78.—RUN 3-8G, STINGER PROBE MICROPHONE SPECTRUM AT (X; R) (4.9 IN.; 0.0 IN.)

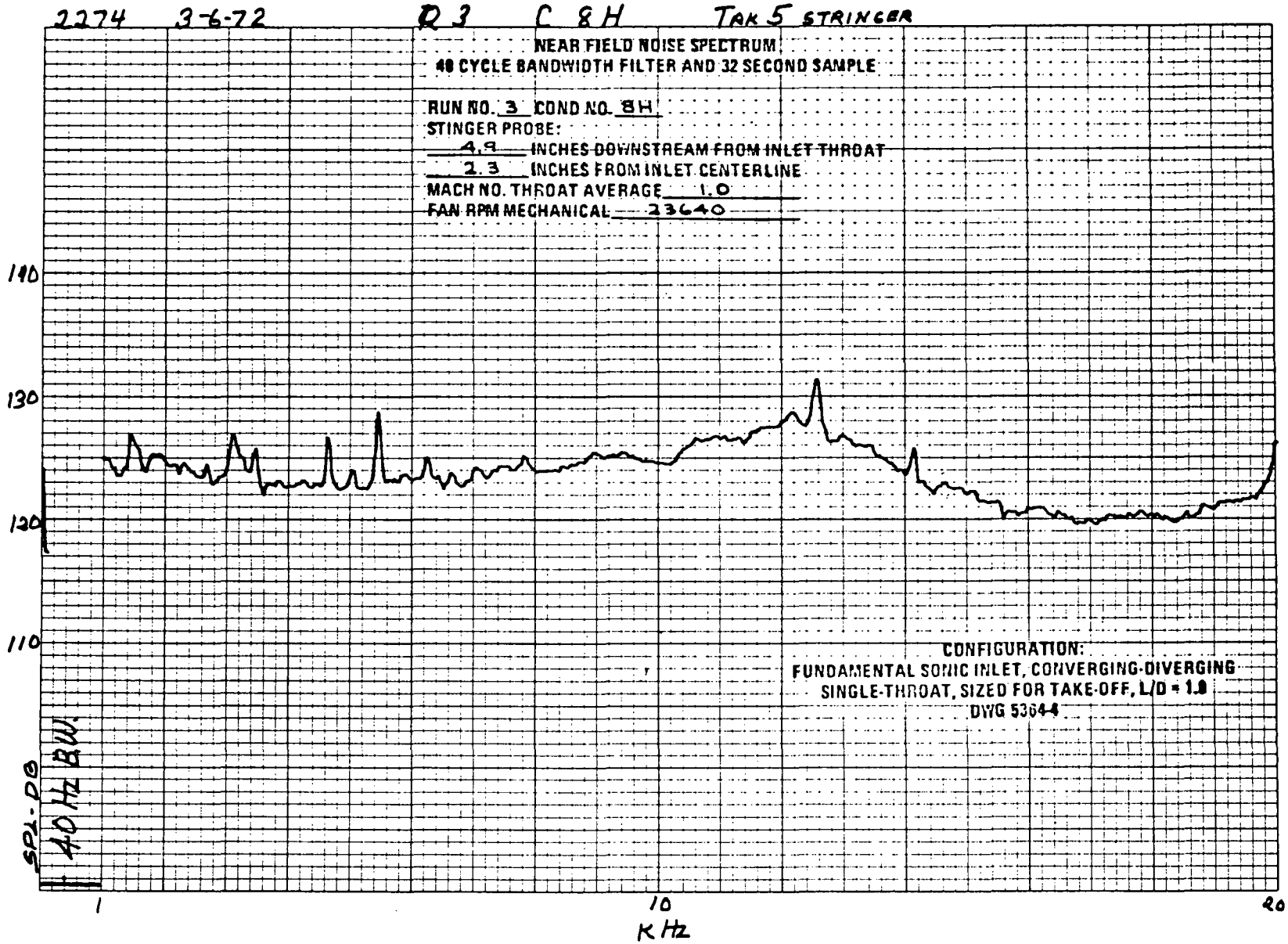

FIGURE A-79.—RUN 3-8H, STINGER PROBE MICROPHONE SPECTRUM AT (X; R) (4.9 IN.; 2.3 IN.)

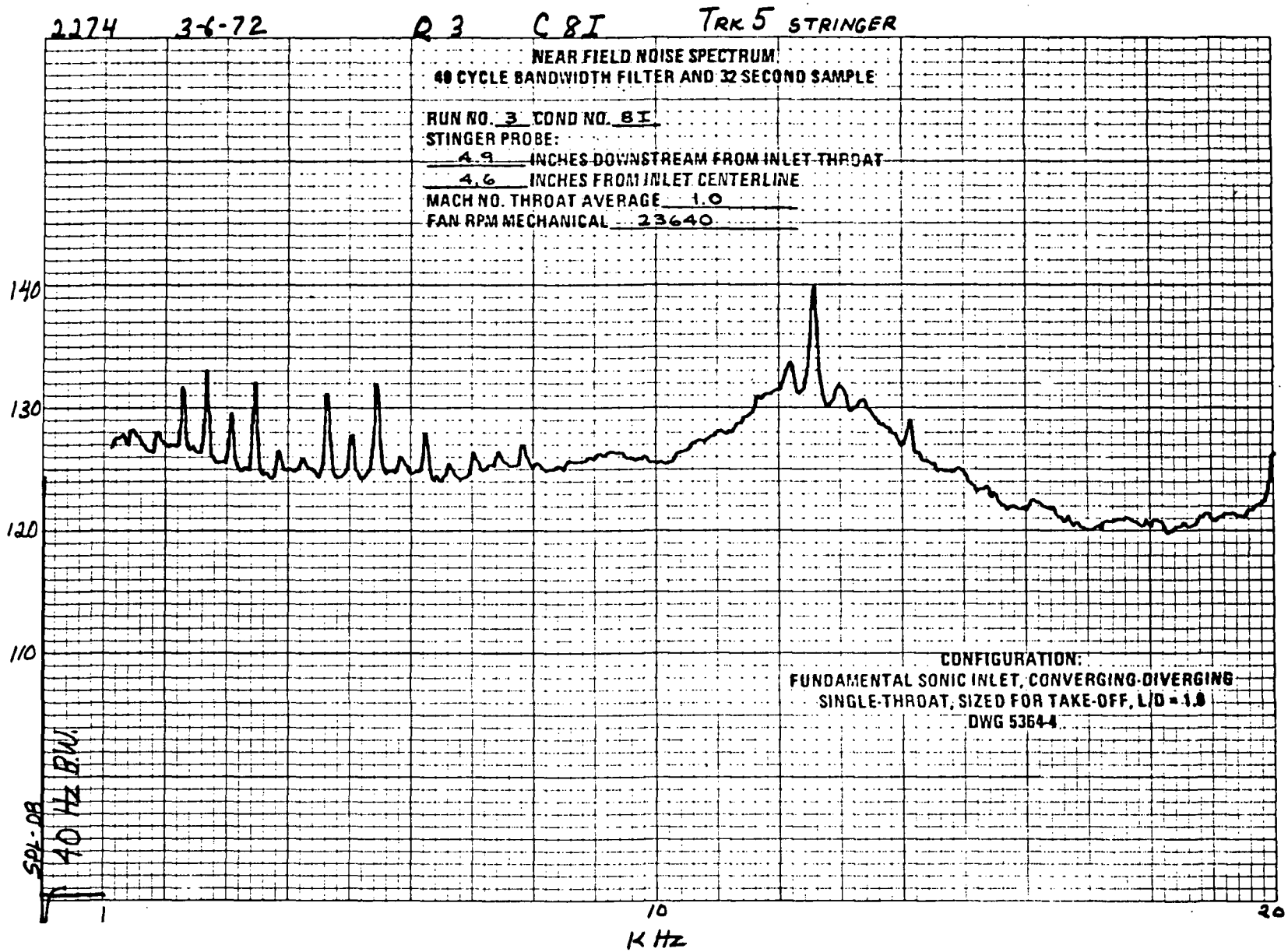

FIGURE A-80.—RUN 3-8I, STINGER PROBE MICROPHONE SPECTRUM AT (X; R) (4.9 IN.; 4.6 IN.)

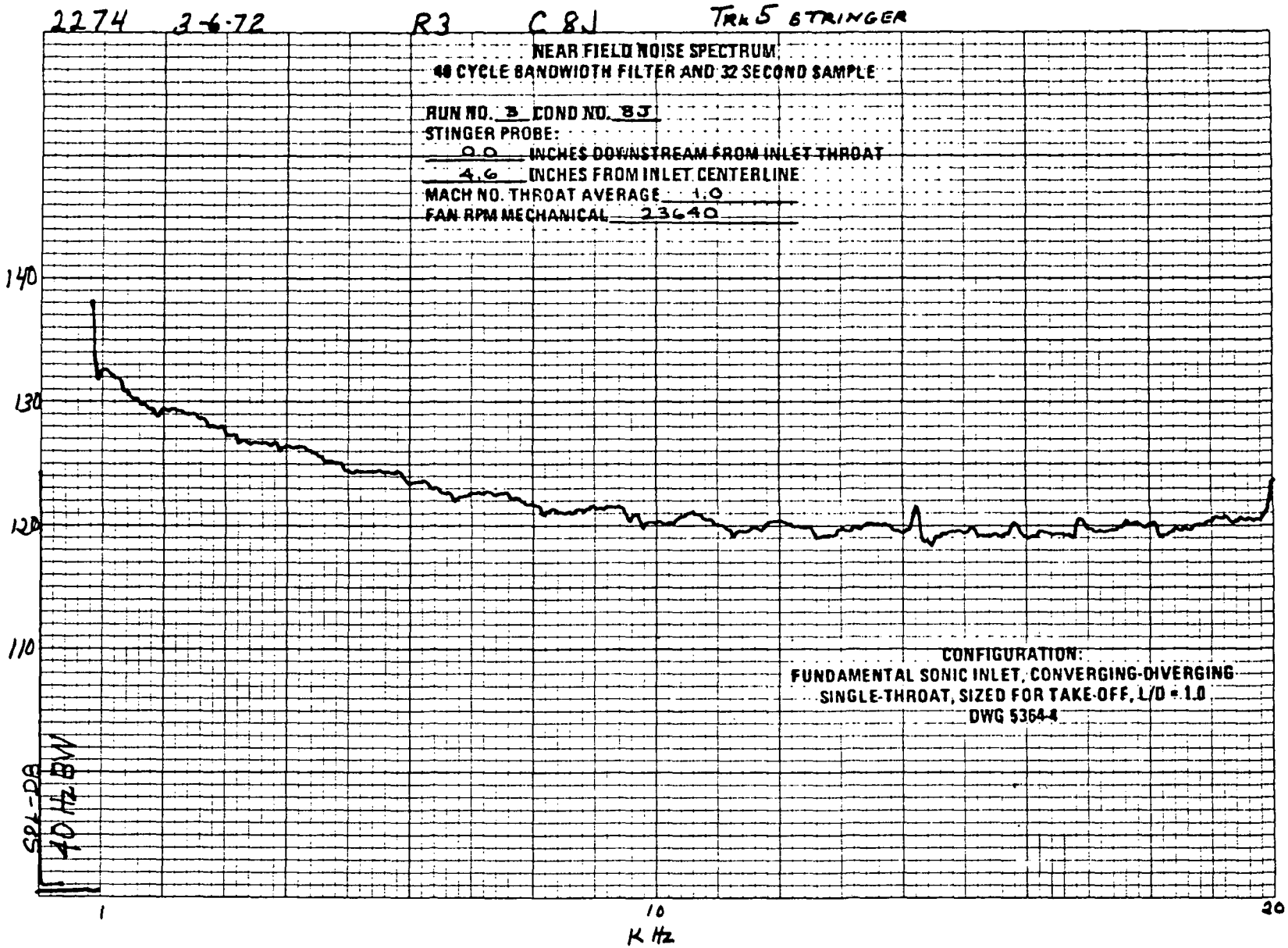

FIGURE A-81.—RUN 3-8J, STINGER PROBE MICROPHONE SPECTRUM AT (X; R) (0.0 IN.; 4.6 IN.)

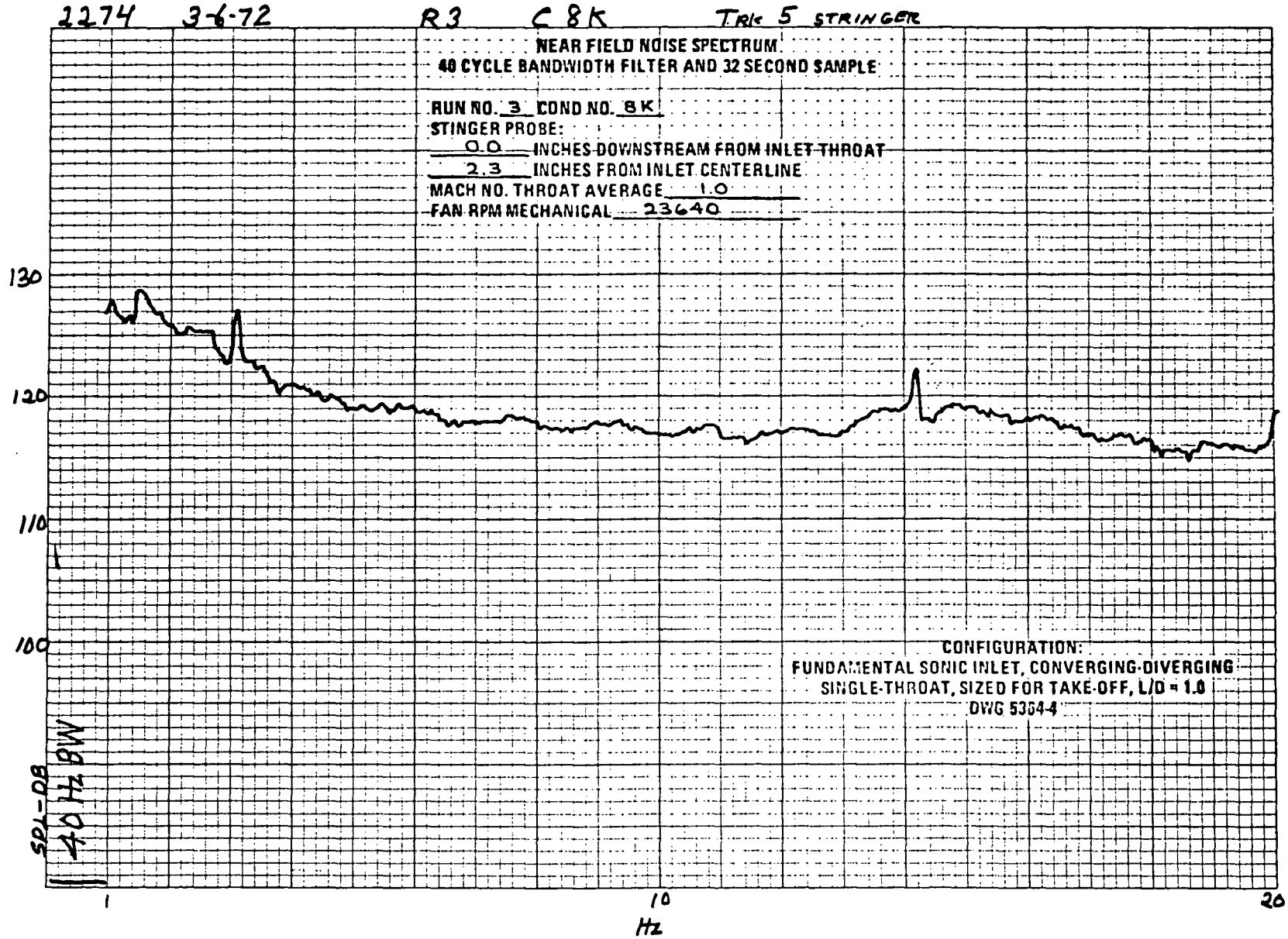

FIGURE A-82.—RUN 3-8K, STINGER PROBE MICROPHONE SPECTRUM AT (X; R) (0.0 IN.; 2.3 IN.)

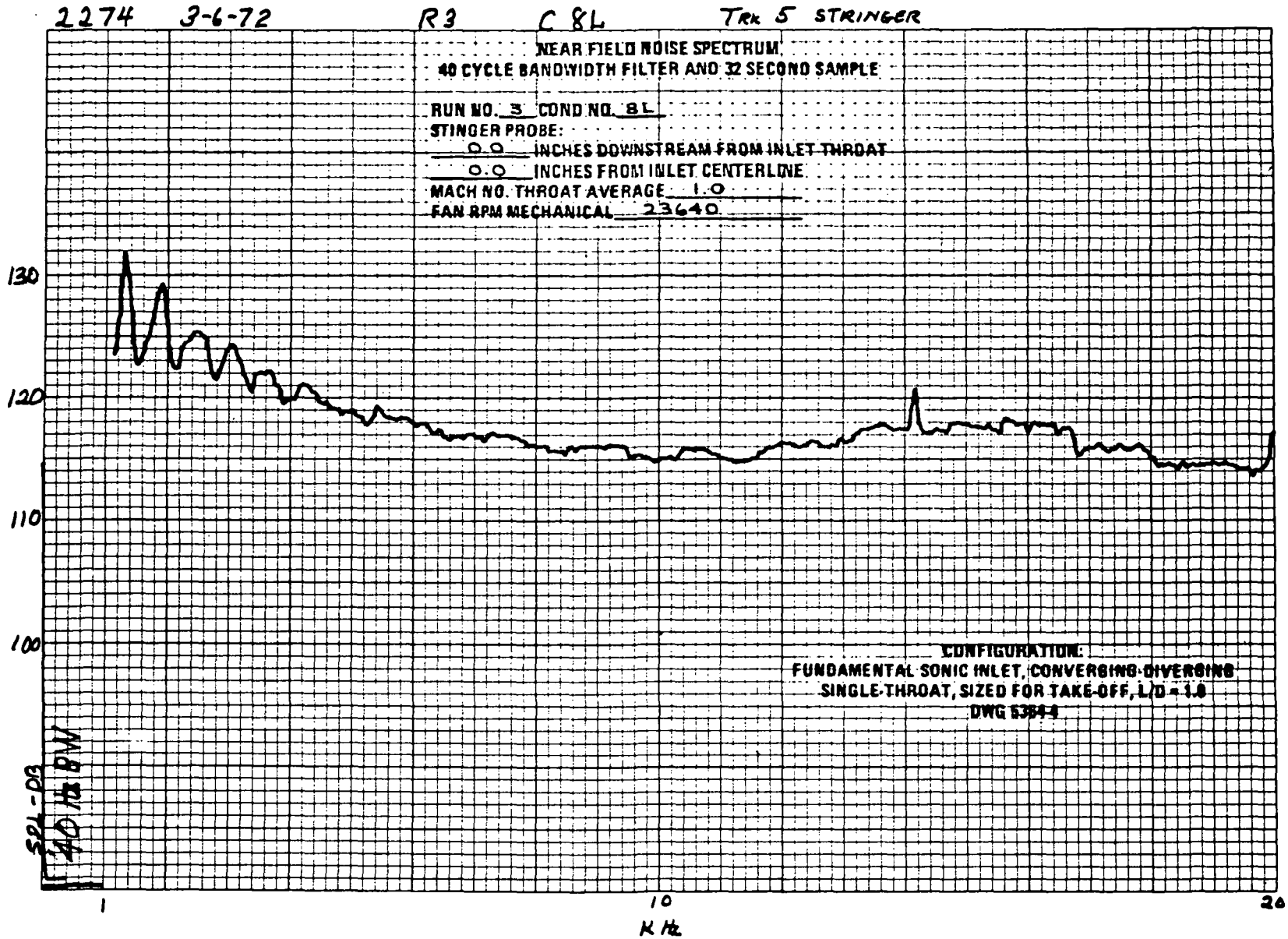

FIGURE A-83.—RUN 3-8L, STINGER PROBE MICROPHONE SPECTRUM AT (X; R) (0.0 IN.; 0.0 IN.)

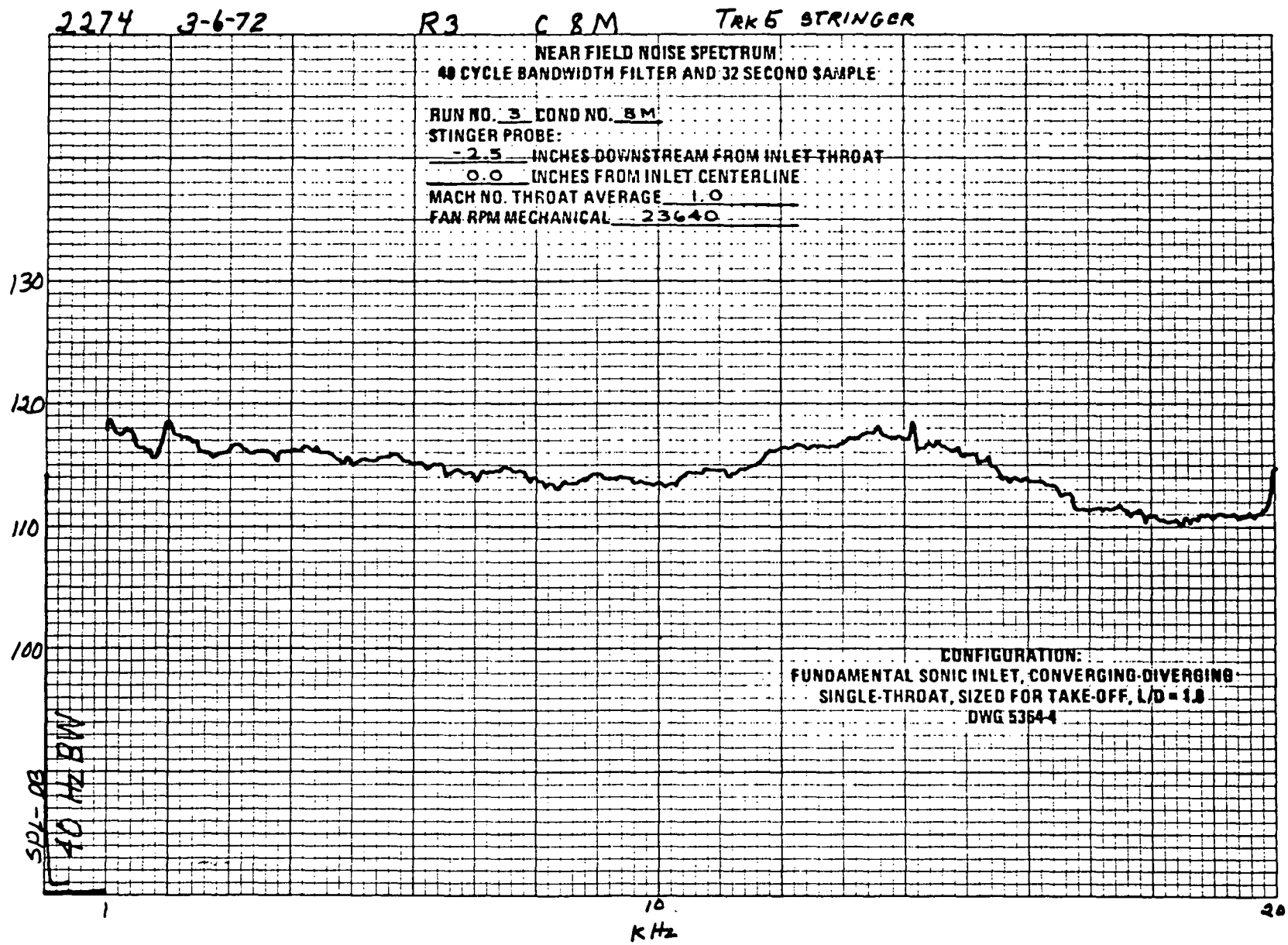

FIGURE A-84.—RUN 3-8M, STINGER PROBE MICROPHONE SPECTRUM AT (X; R) (-2.5 IN.; 0.0 IN.)

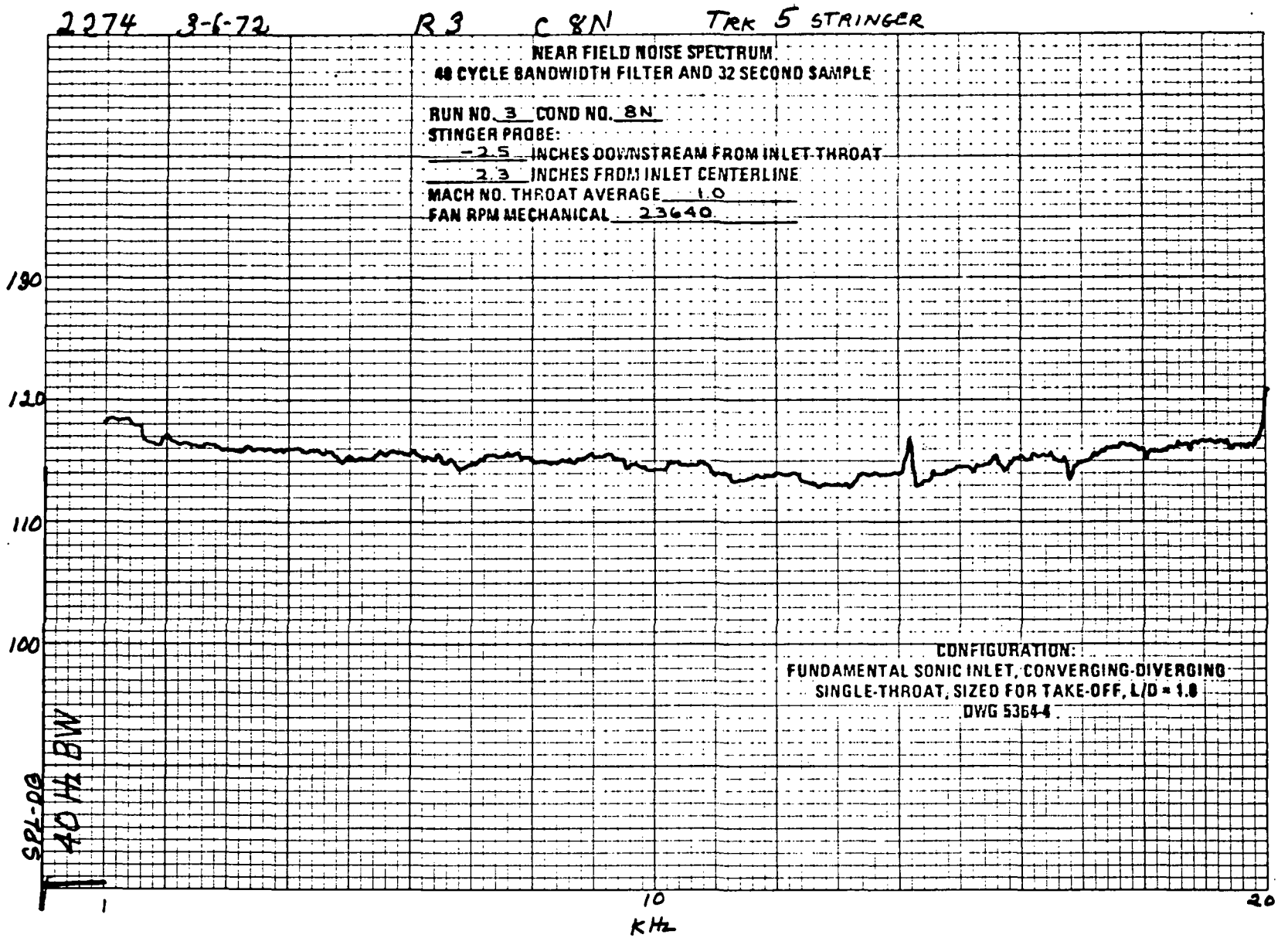

FIGURE A-85.—RUN 3-8N, STINGER PROBE MICROPHONE SPECTRUM AT (X; R) (-2.5 IN.; 2.3 IN.)

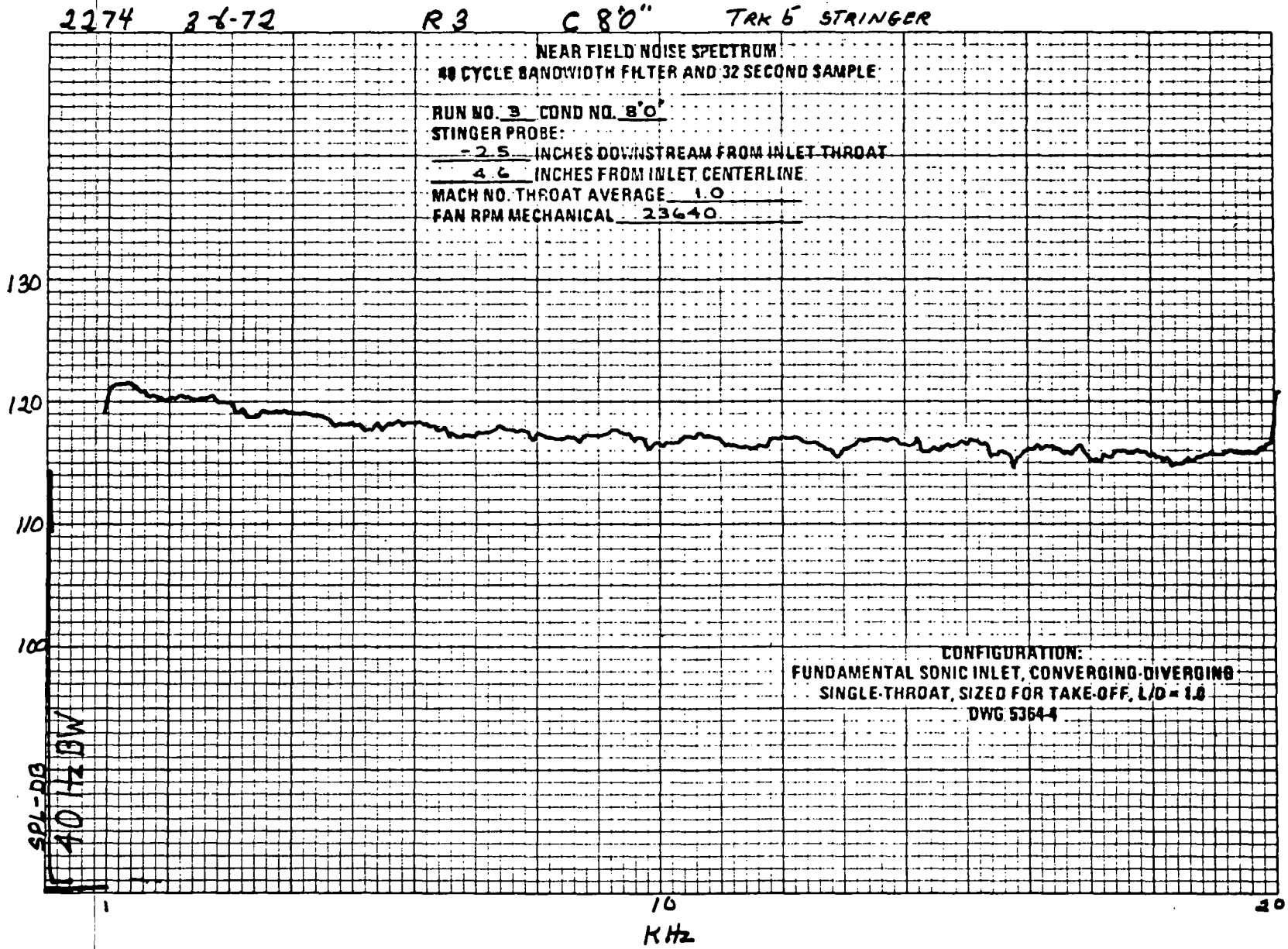

FIGURE A-86.—RUN 3-80, STINGER PROBE MICROPHONE SPECTRUM AT (X; R) (-2.5 IN.; 4.6 IN.)

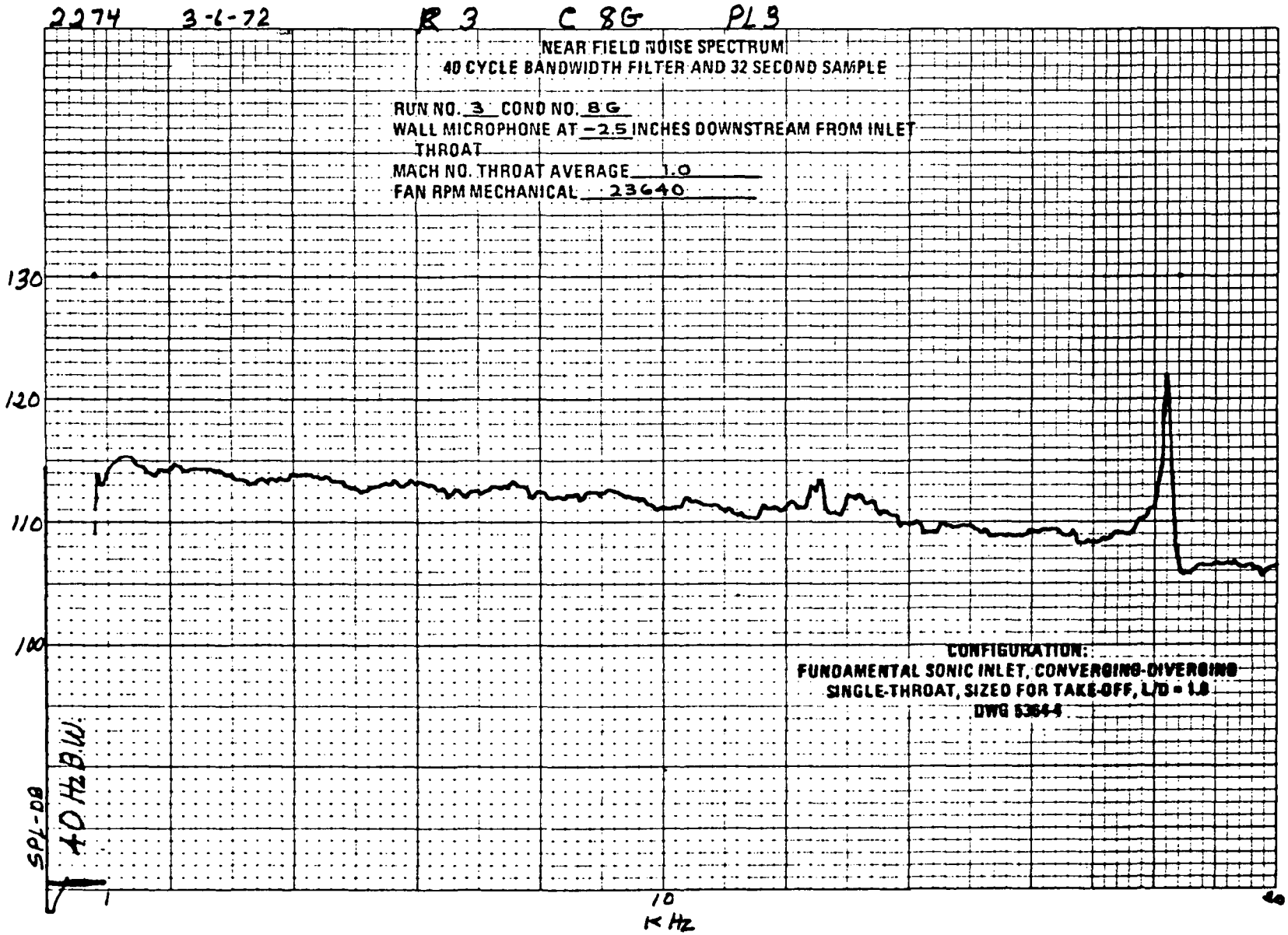

FIGURE A-87.—RUN 3-8G, WALL MICROPHONE SPECTRUM AT -2.5 IN. DOWNSTREAM FROM INLET THROAT

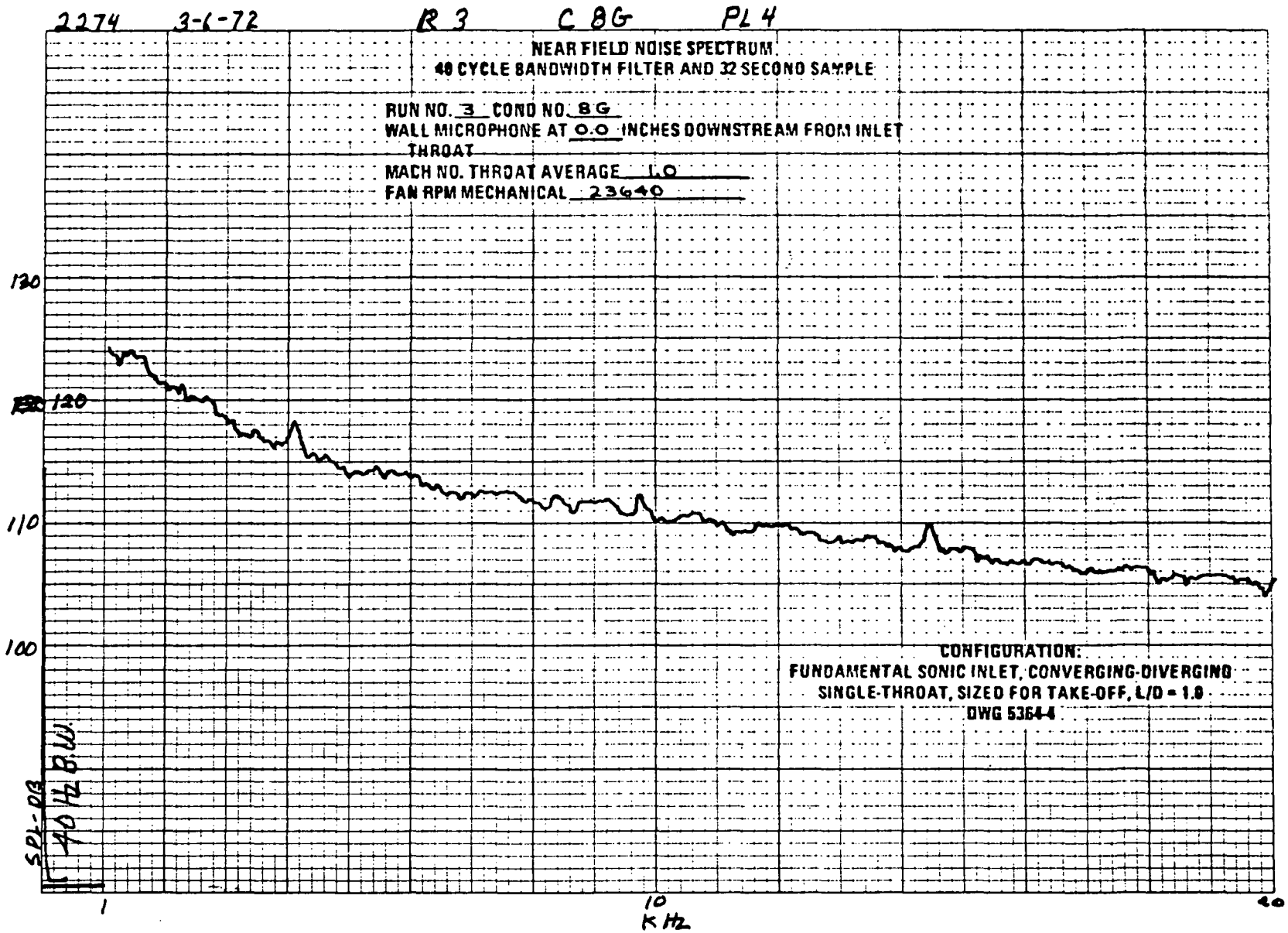

FIGURE A-88.—RUN 3-8G, WALL MICROPHONE SPECTRUM AT 0.0 IN. DOWNSTREAM FROM INLET THROAT

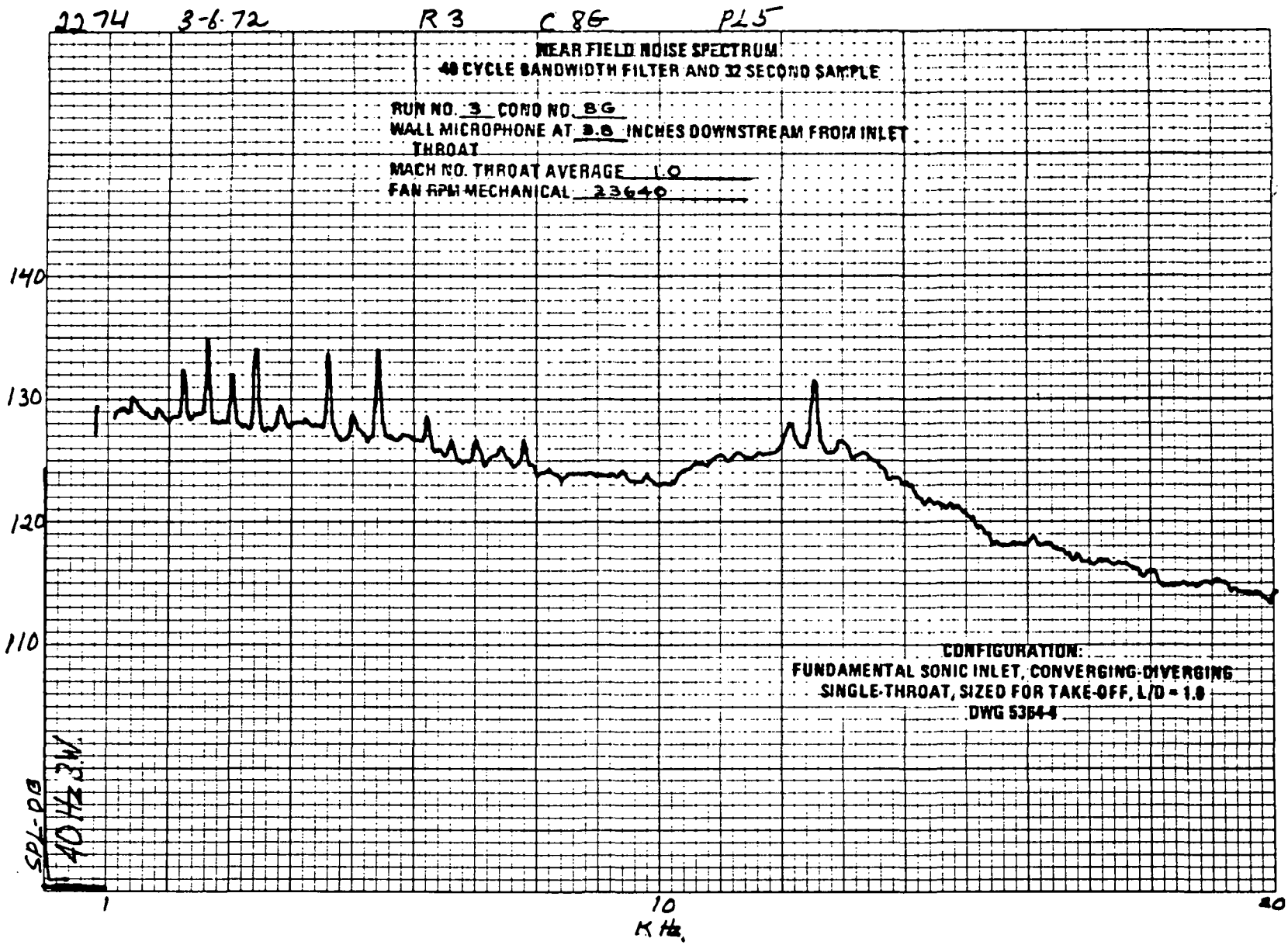

FIGURE A-89.—RUN 3-8G, WALL MICROPHONE SPECTRUM AT 3.8 IN. DOWNSTREAM FROM INLET THROAT

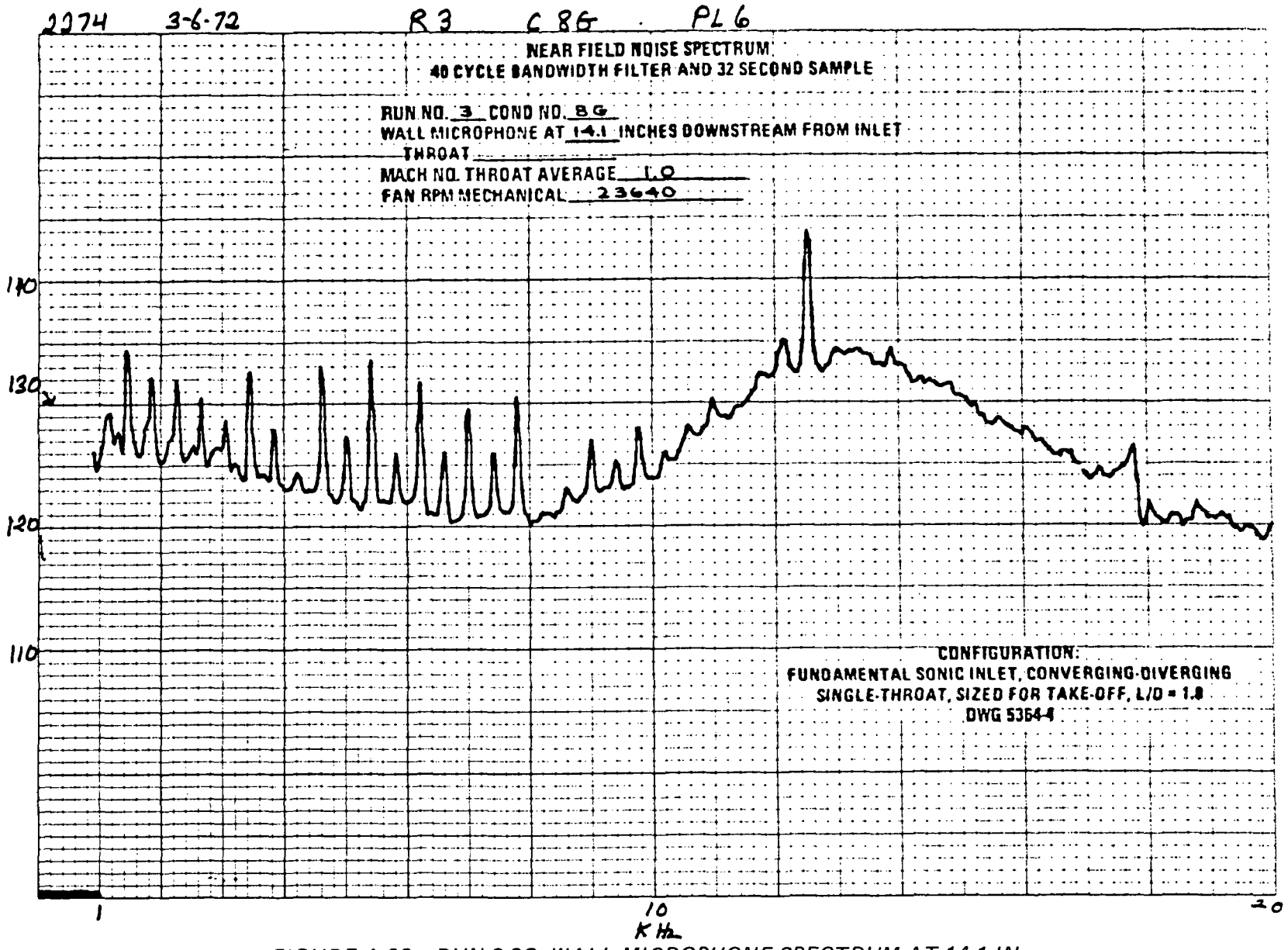

FIGURE A-90.—RUN 3-8G, WALL MICROPHONE SPECTRUM AT 14.1 IN. DOWNSTREAM FROM INLET THROAT

APPENDIX B

AXIAL AND RADIAL TRAVERSE BLADE PASSING TONE DISTRIBUTIONS INSIDE THE TWO SONIC INLETS

This appendix contains all the traverse data taken with the stringer probe inside the two sonic inlets. The data consist of both blade passing tone and static pressure measurements.

For easy access, the data are presented according to run number, as listed below.

Figure	Run	Title
B-1	2-10D	Blade Passing Tone vs Radial Position in a Plane 0.0 In. Downstream From Inlet Throat
B-2	2-10E	Blade Passing Tone vs Radial Position in a Plane 4.0 In. Downstream From Inlet Throat
B-3	2-10F	Blade Passing Tone vs Radial Position in a Plane 8.6 In. Downstream From Inlet Throat
B-4	2-10 D, E, F	Static Pressure vs Radial Position at X = -1.05, 2.95, and 7.55 In. Downstream From Inlet Throat
B-5	2-10G	Blade Passing Tone vs Axial Position at 0.0 In. From Inlet Centerline
B-6	2-10H	Blade Passing Tone vs Axial Position at 2.0 In. From Inlet Centerline
B-7	2-10I	Blade Passing Tone vs Axial Position at 4.0 In. From Inlet Centerline
B-8	2-10 G, H, I	Static Pressure vs Axial Position at R = 0.0, 2.0 and 4.0 In. From Inlet Centerline
B-9	2-11B	Blade Passing Tone vs Radial Position in a Plane 0.0 In. Downstream From Inlet Throat
B-10	2-11C	Blade Passing Tone vs Radial Position in a Plane 4.0 In. Downstream From Inlet Throat
B-11	2-11D	Blade Passing Tone vs Radial Position in a Plane 8.5 In. Downstream From Inlet Throat
B-12	2-11 B, C, D	Static Pressure vs Radial Position in Planes at -1.05, 2.95, and 7.45 In. Downstream From Inlet Throat
B-13	2-11E	Blade Passing Tone vs Axial Position at 0.0 In. From Inlet Centerline

Figure	Run	Title
B-14	2-11F	Blade Passing Tone vs Axial Position at 2.0 In. From Inlet Centerline
B-15	2-11G	Blade Passing Tone vs Axial Position at 4.0 In. From Inlet Centerline
B-16	2-11 E, F, G	Static Pressure vs Axial Position at 0.0, 2.0, and 4.0 In. From Inlet Centerline
B-17	2-12B	Blade Passing Tone vs Radial Position in a Plane 0.0 In. Downstream From Inlet Throat
B-18	2-12C	Blade Passing Tone vs Radial Position in a Plane 4.0 In. Downstream From Inlet Throat
B-19	2-12D	Blade Passing Tone vs Radial Position in a Plane 8.5 In. Downstream From Inlet Throat
B-20	2-12 B, C, D	Static Pressure vs Radial Position in Planes at -1.05, 2.95, and 7.45 In. Downstream From Inlet Throat
B-21	2-12E	Blade Passing Tone vs Axial Position at 0.0 In. From Inlet Centerline
B-22	2-12F	Blade Passing Tone vs Axial Position at 2.0 In. From Inlet Centerline
B-23	2-12G	Blade Passing Tone vs Axial Position at 4.0 In. From Inlet Centerline
B-24	2-12 E, F, G	Static Pressure vs Axial Position at 0.0, 2.0, and 4.0 In. From Inlet Centerline
B-25	2-13B	Blade Passing Tone vs Radial Position in a Plane 0.0 In. Downstream From Inlet Throat
B-26	2-13C	Blade Passing Tone vs Radial Position in a Plane 4.0 In. Downstream From Inlet Throat
B-27	2-13D	Blade Passing Tone vs Radial Position in a Plane 8.5 In. Downstream From Inlet Throat
B-28	2-13 B, C, D	Static Pressure vs Radial Position in Planes at -1.05, 2.95, and 7.45 In. Downstream From Inlet Throat
B-29	2-13E	Blade Passing Tone vs Axial Position at 0.0 In. From Inlet Centerline
B-30	2-13F	Blade Passing Tone vs Axial Position at 2.0 In. From Inlet Centerline
B-31	2-13G	Blade Passing Tone vs Axial Position at 4.0 In. From Inlet Centerline

Figure	Run	Title
B-32	2-13 E, F, G	Static Pressure vs Axial Position at 0.0, 2.0, and 4.0 In. From Inlet Centerline
B-33	2-14B	Blade Passing Tone vs Radial Position in a Plane 0.0 In. Downstream From Inlet Throat
B-34	2-14C	Blade Passing Tone vs Radial Position in a Plane 4.0 In. Downstream From Inlet Throat
B-35	2-14D	Blade Passing Tone vs Radial Position in a Plane 8.5 In. Downstream From Inlet Throat
B-36	2-14 B, C, D	Static Pressure vs Radial Position in Planes at -1.05, 2.95, and 7.45 In. Downstream From Inlet Throat
B-37	2-14E	Blade Passing Tone vs Axial Position at 0.0 In. From Inlet Centerline
B-38	2-14F	Blade Passing Tone vs Axial Position at 2.0 In. From Inlet Centerline
B-39	2-14G	Blade Passing Tone vs Axial Position at 4.0 In. From Inlet Centerline
B-40	2-14 E, F, G	Static Pressure vs Axial Position at 0.0, 2.0, and 4.0 In. From Inlet Centerline
B-41	3-6B	Blade Passing Tone and Static Pressure vs Axial Distance at 0.0 In. From Inlet Centerline
B-42	3-6C	Blade Passing Tone and Static Pressure vs Axial Distance at 2.3 In. From Inlet Centerline
B-43	3-6D	Blade Passing Tone and Static Pressure vs Axial Distance at 4.6 In. From Inlet Centerline
B-44	3-6E	Blade Passing Tone and Static Pressure vs Radial Position at 4.9 In. Downstream From Inlet Throat
B-45	3-6G	Blade Passing Tone and Static Pressure vs Radial Position at 0.0 In. Downstream From Inlet Throat
B-46	3-6H	Blade Passing Tone and Static Pressure vs Radial Position at -2.5 In. Downstream From Inlet Throat
B-47	3-7A	Blade Passing Tone and Static Pressure vs Axial Position at 0.0 In. From Inlet Centerline

Figure	Run	Title
B-48	3-7B	Blade Passing Tone and Static Pressure vs Axial Position at 2.3 In. From Inlet Centerline
B-49	3-7C	Blade Passing Tone and Static Pressure vs Axial Position at 4.6 In. From Inlet Centerline
B-50	3-7D	Blade Passing Tone and Static Pressure vs Radial Position at -2.5 In. Downstream From Inlet Throat
B-51	3-7E	Blade Passing Tone and Static Pressure vs Radial Position at 0.0 In. Downstream From Inlet Throat
B-52	3-7F	Blade Passing Tone and Static Pressure vs Radial Position at 4.9 In. Downstream From Inlet Throat
B-53	3-8A	Blade Passing Tone and Static Pressure vs Axial Distance at 0.0 In. From Inlet Centerline
B-54	3-8B	Blade Passing Tone and Static Pressure vs Axial Distance at 2.3 In. From Inlet Centerline
B-55	3-8C	Blade Passing Tone and Static Pressure vs Axial Distance at 4.6 In. From Inlet Centerline
B-56	3-8D	Blade Passing Tone and Static Pressure vs Radial Position at -2.5 In. Downstream From Inlet Centerline
B-57	3-8E	Blade Passing Tone and Static Pressure vs Radial Position at 0.0 In. Downstream From Inlet Throat
B-58	3-8F	Blade Passing Tone and Static Pressure vs Radial Position at 4.9 In. Downstream From Inlet Throat

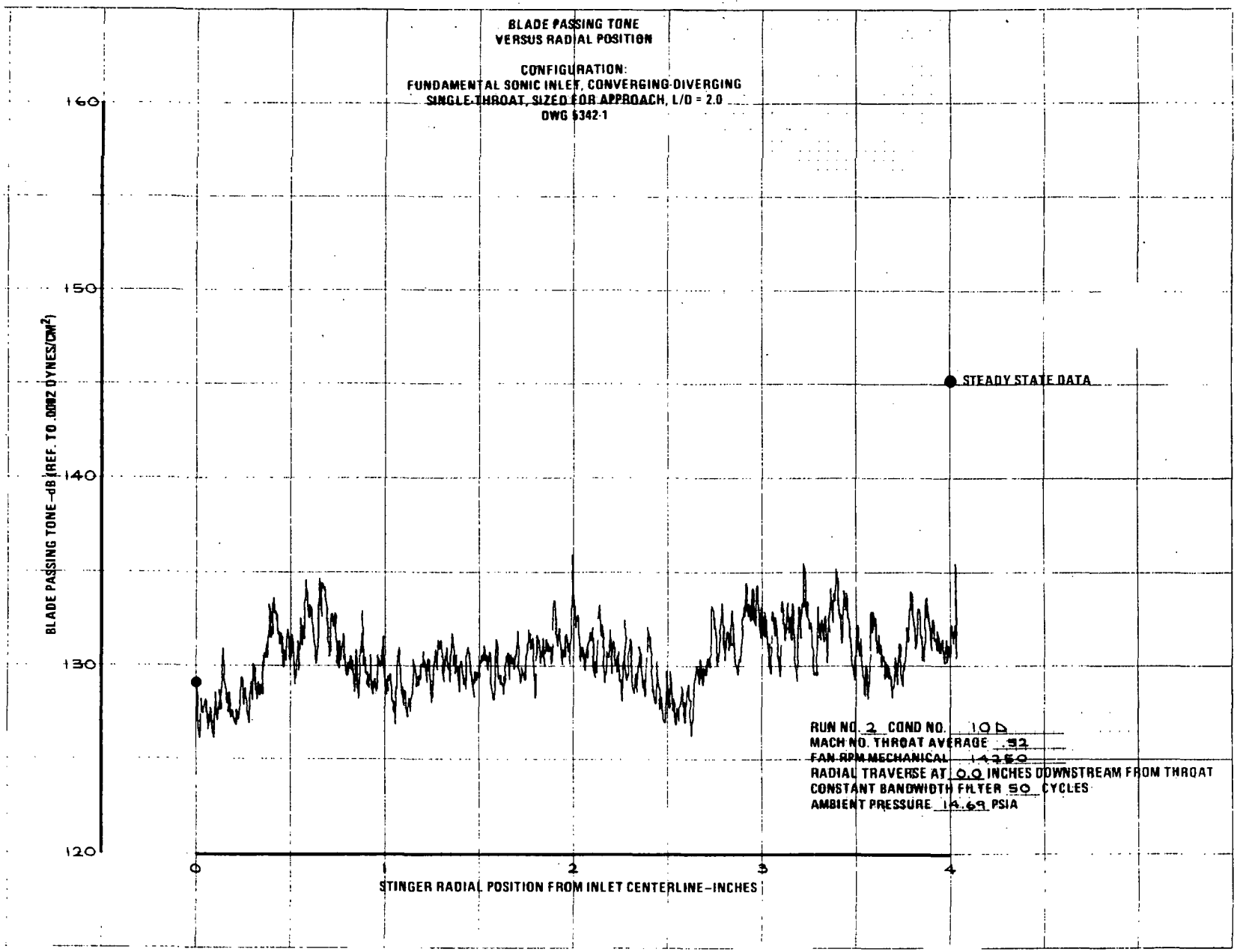

FIGURE B-1.—RUN 2-10D, BLADE PASSING TONE VS RADIAL POSITION IN A PLANE 0.0 IN. DOWNSTREAM FROM INLET THROAT

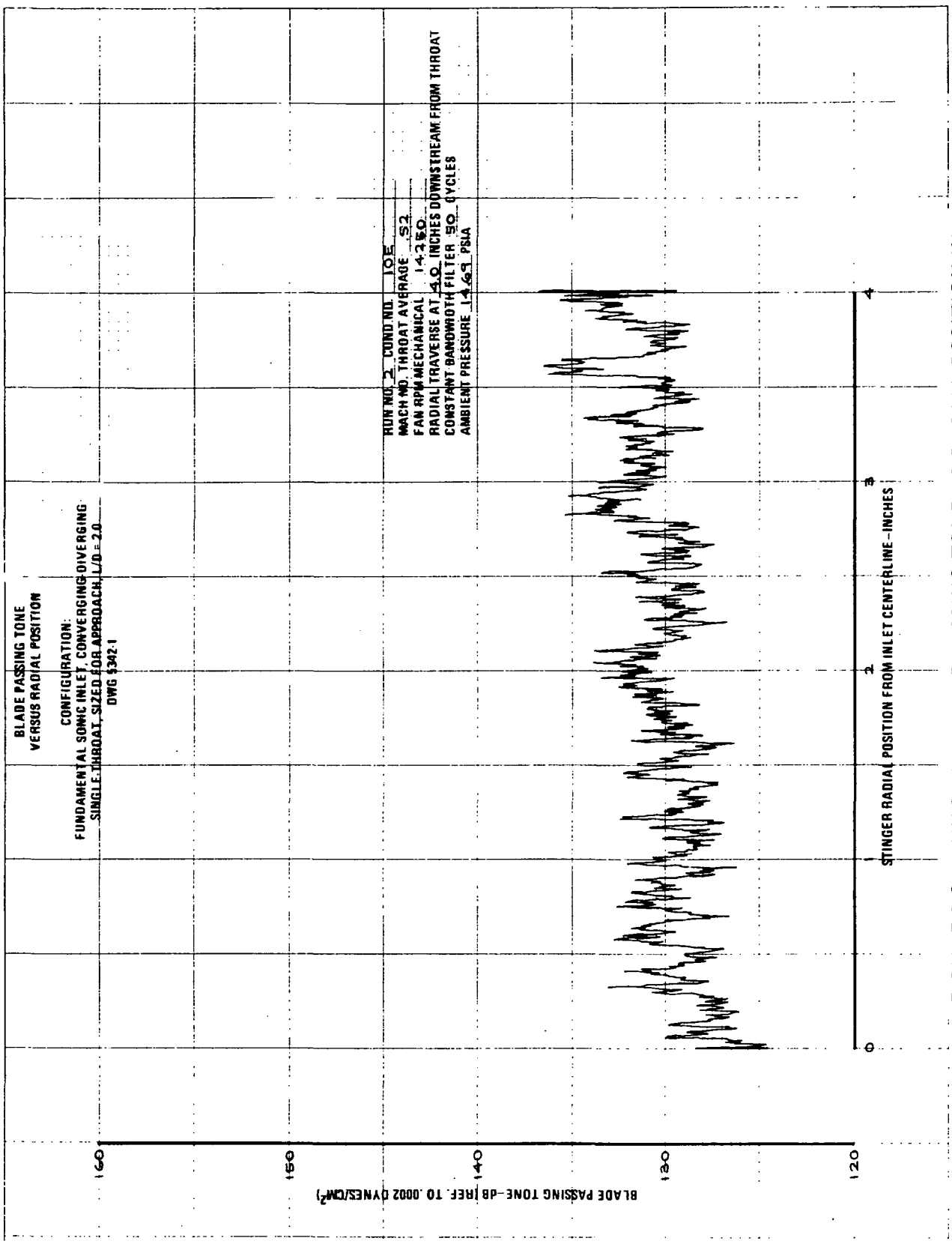

FIGURE B-2.—RUN 2-10E, BLADE PASSING TONE VS RADIAL POSITION IN A PLANE 4.0 IN. DOWNSTREAM FROM INLET THROAT

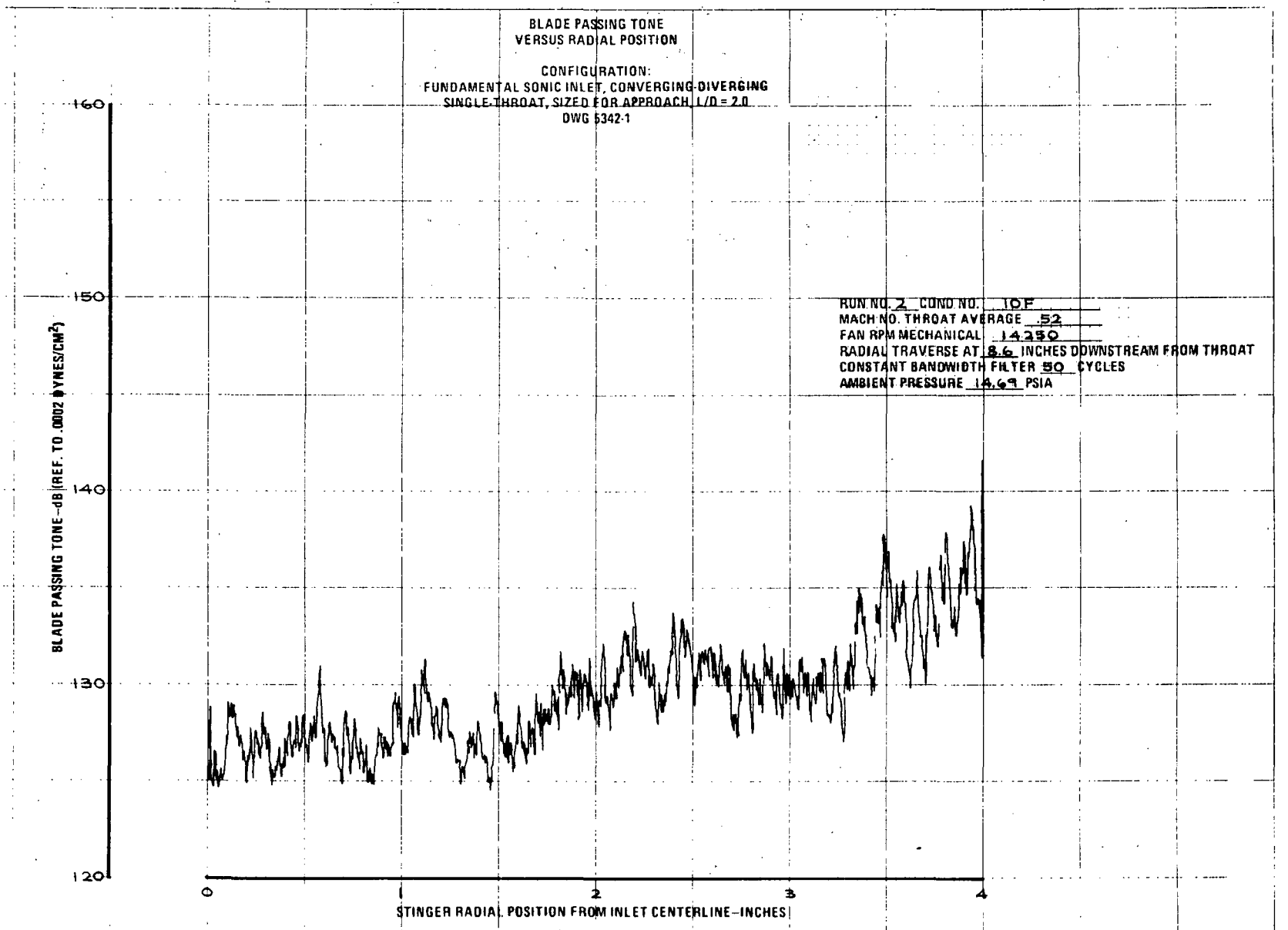

FIGURE B-3.—RUN 2-10F, BLADE PASSING TONE VS RADIAL POSITION IN A PLANE 8.6 IN. DOWNSTREAM FROM INLET THROAT

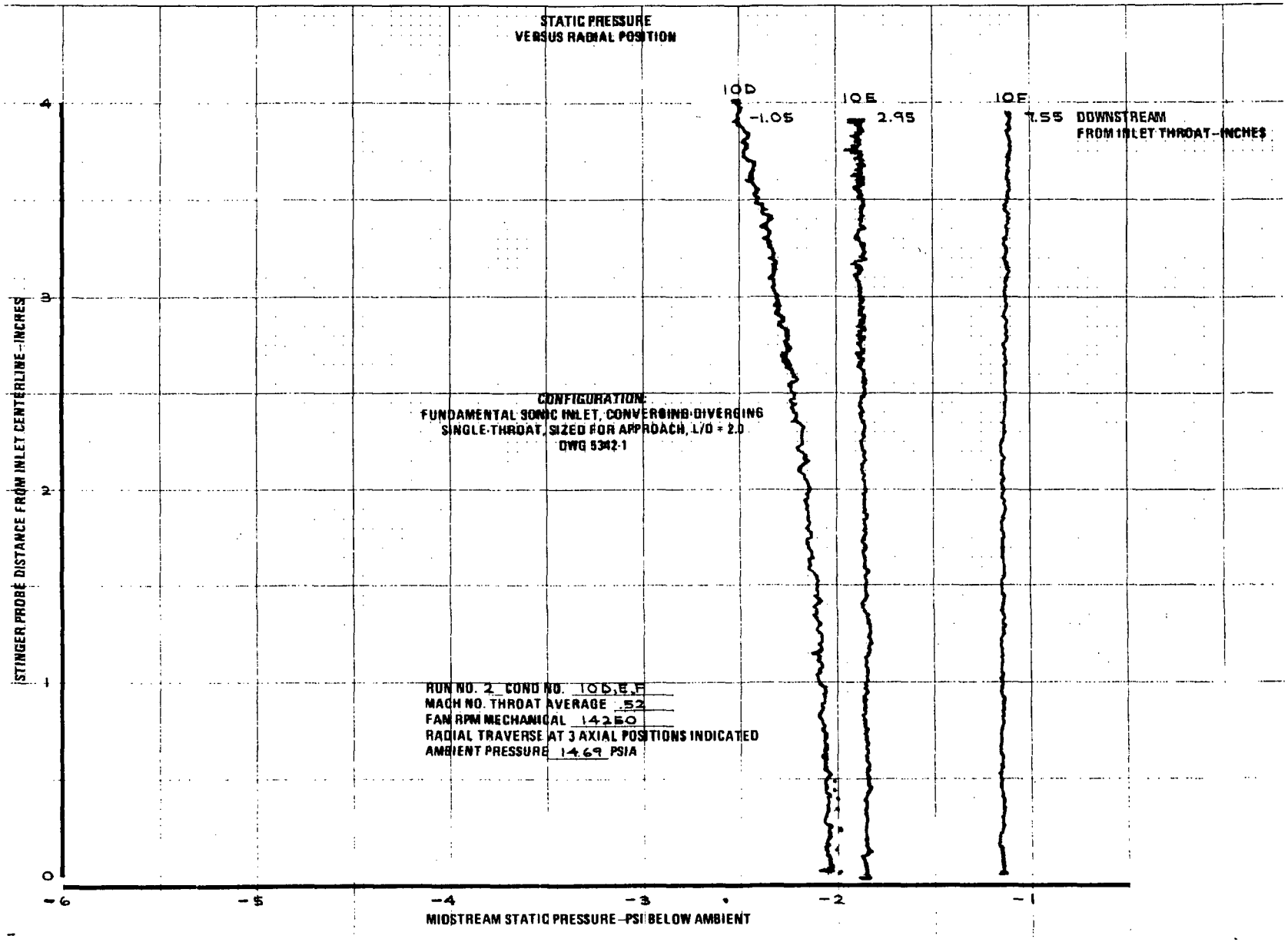

FIGURE B-4.—RUN 2-10 D,E,F, STATIC PRESSURE VS RADIAL POSITION AT X = -1.05, 2.95, AND 7.55 IN. DOWNSTREAM FROM INLET THROAT

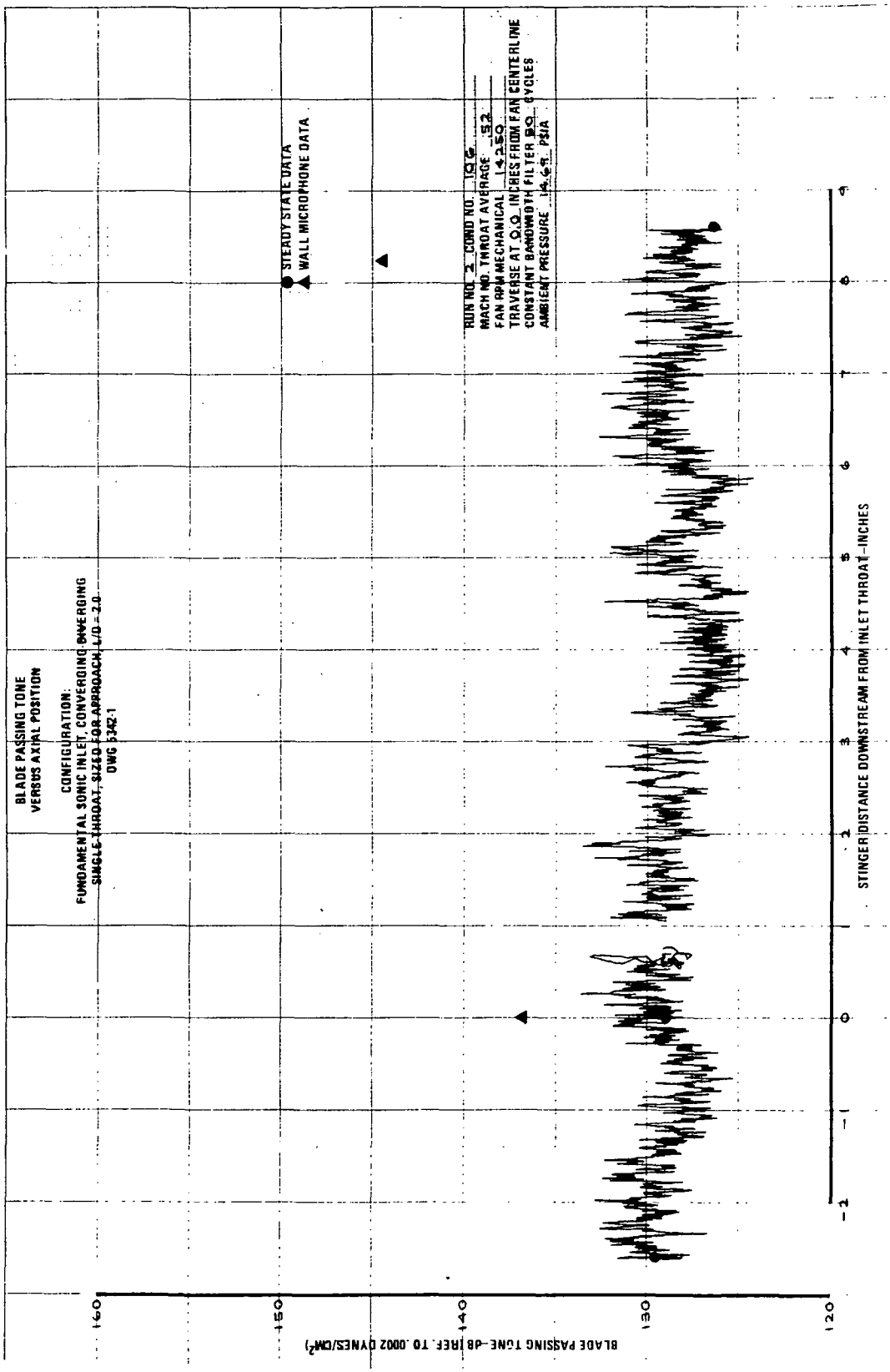

FIGURE B-5.—RUN 2-10G, BLADE PASSING TONE VS AXIAL POSITION AT 0.0 IN. FROM INLET CENTERLINE

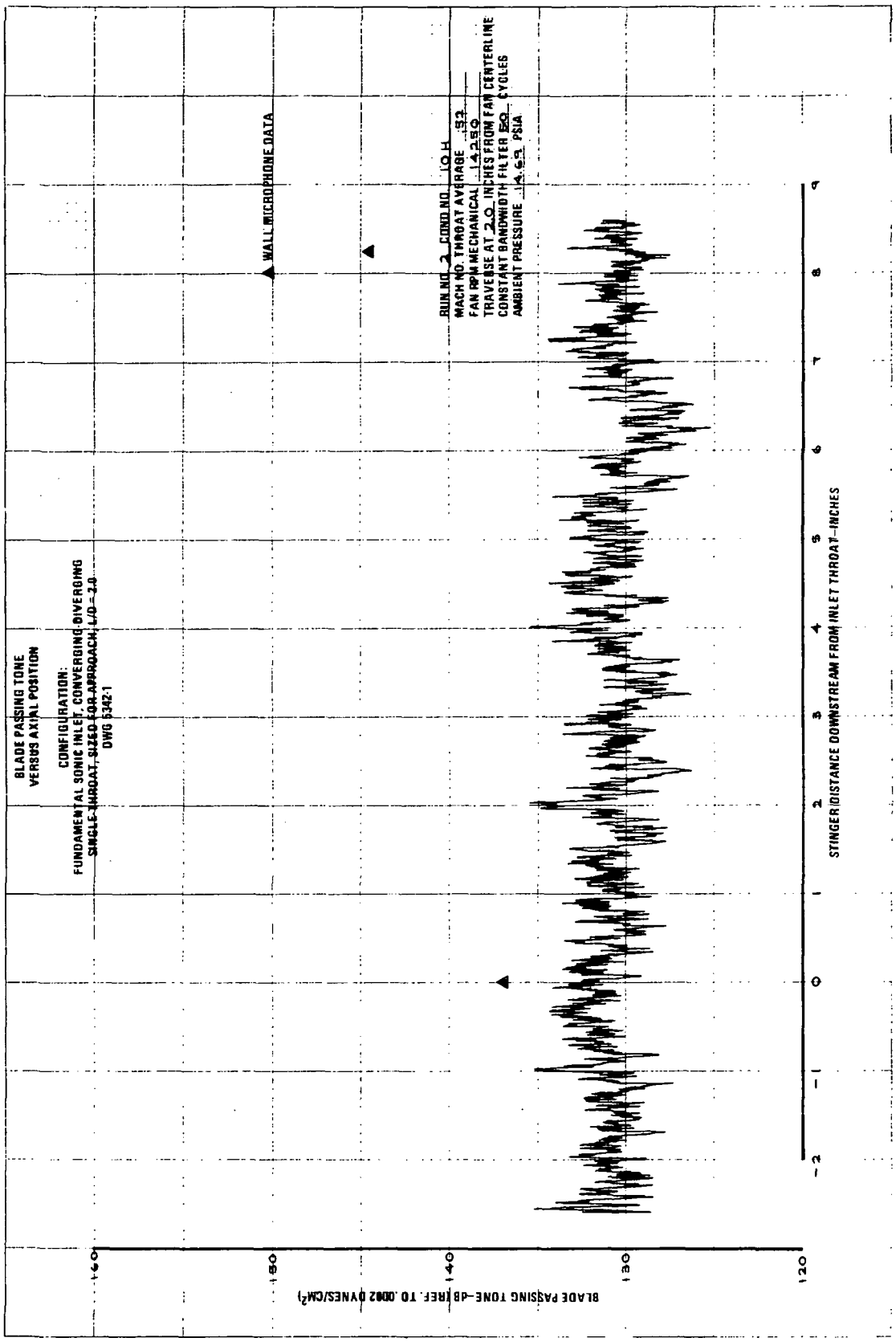

FIGURE B-6.—RUN 2-10H, BLADE PASSING TONE VS AXIAL POSITION AT 2.0 IN. FROM INLET CENTERLINE

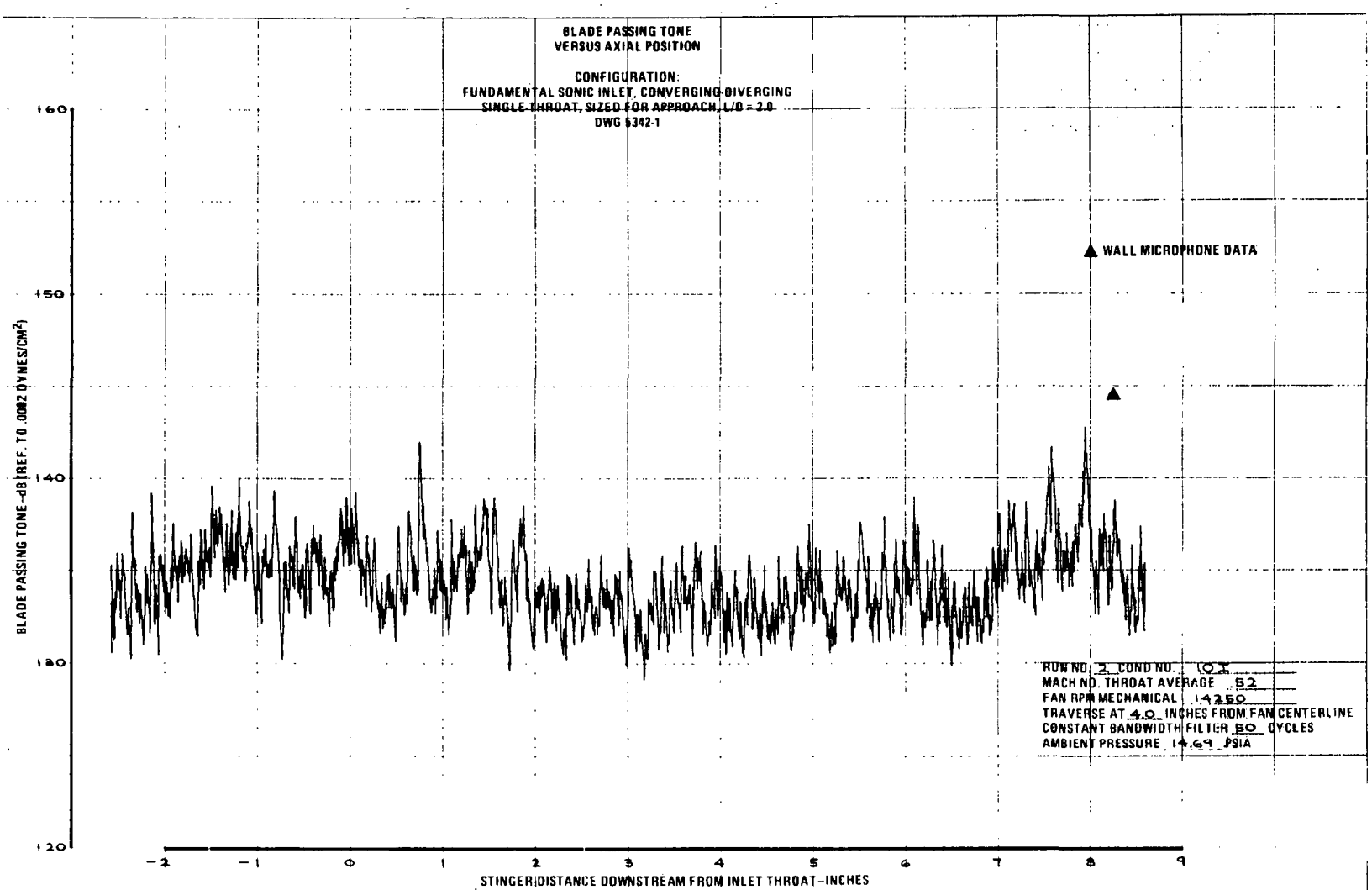

FIGURE B-7.—RUN 2-10I, BLADE PASSING TONE VS AXIAL POSITION AT 4.0 IN. FROM INLET CENTERLINE

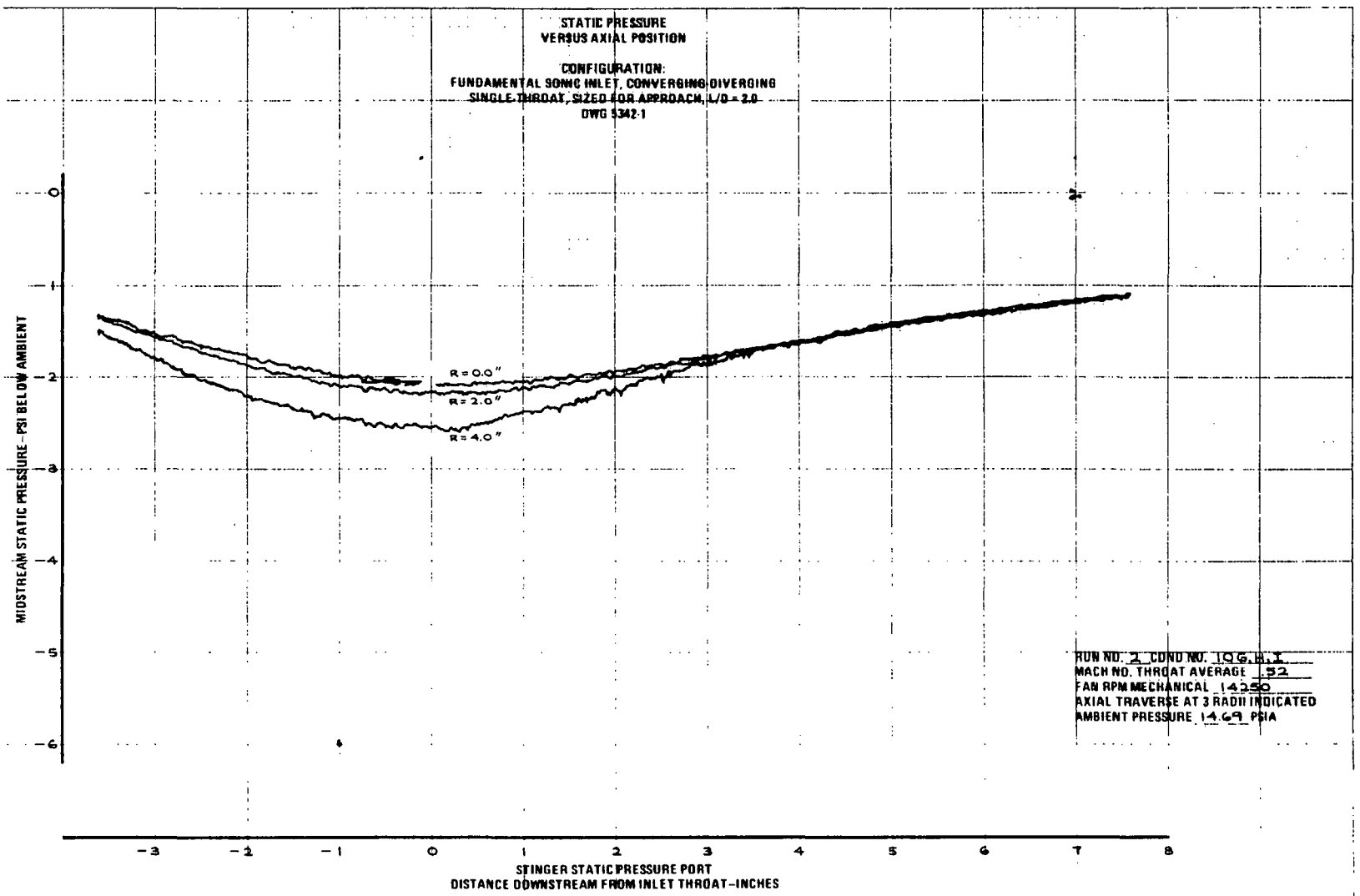

FIGURE B-8.—RUN 2-10 G,H,I, STATIC PRESSURE VS AXIAL POSITION AT R = 0.0, 2.0, AND 4.0 IN. FROM INLET CENTERLINE

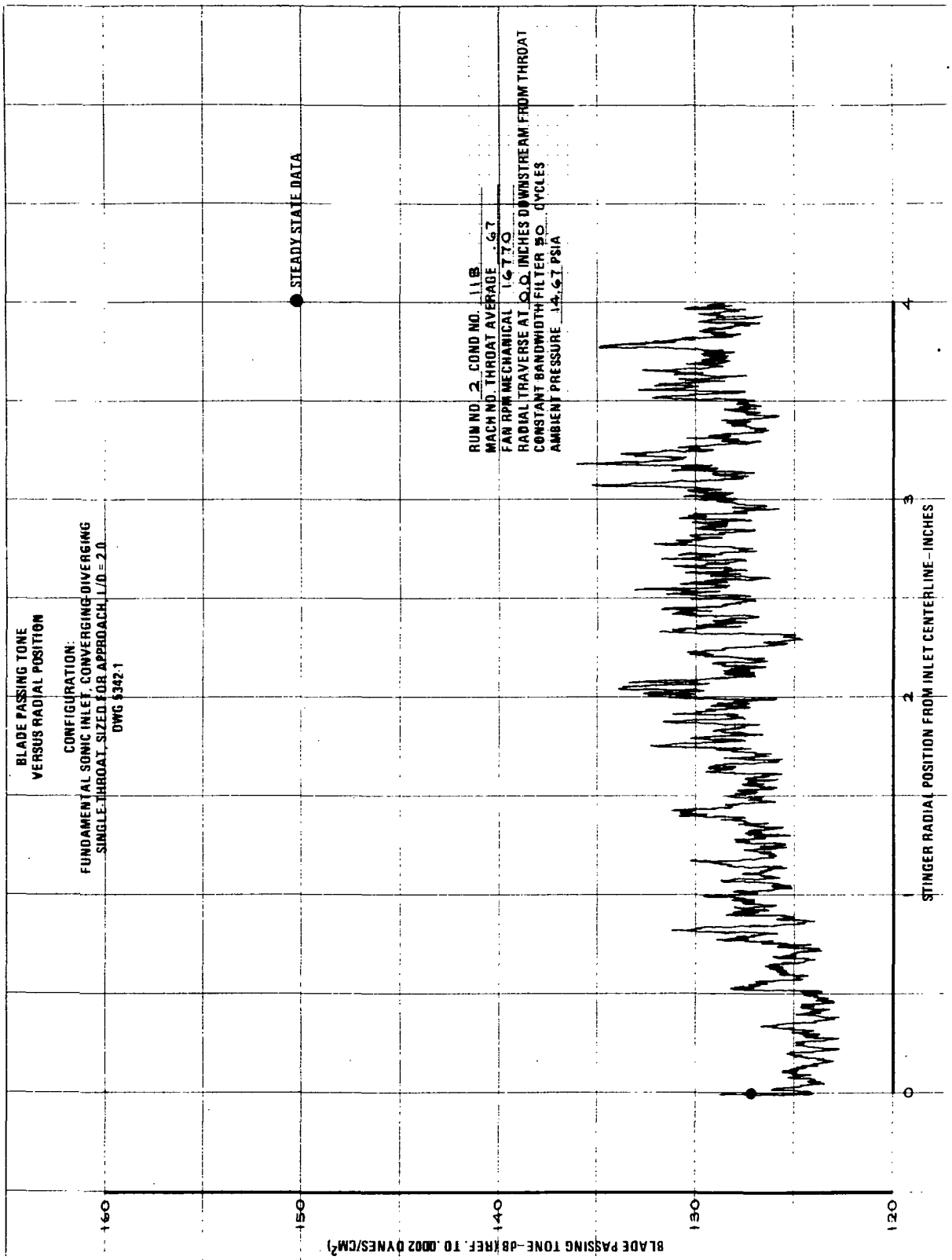

FIGURE B-9.—RUN 2-11B, BLADE PASSING TONE VS RADIAL POSITION IN A PLANE 0.0 IN. DOWNSTREAM FROM INLET THROAT

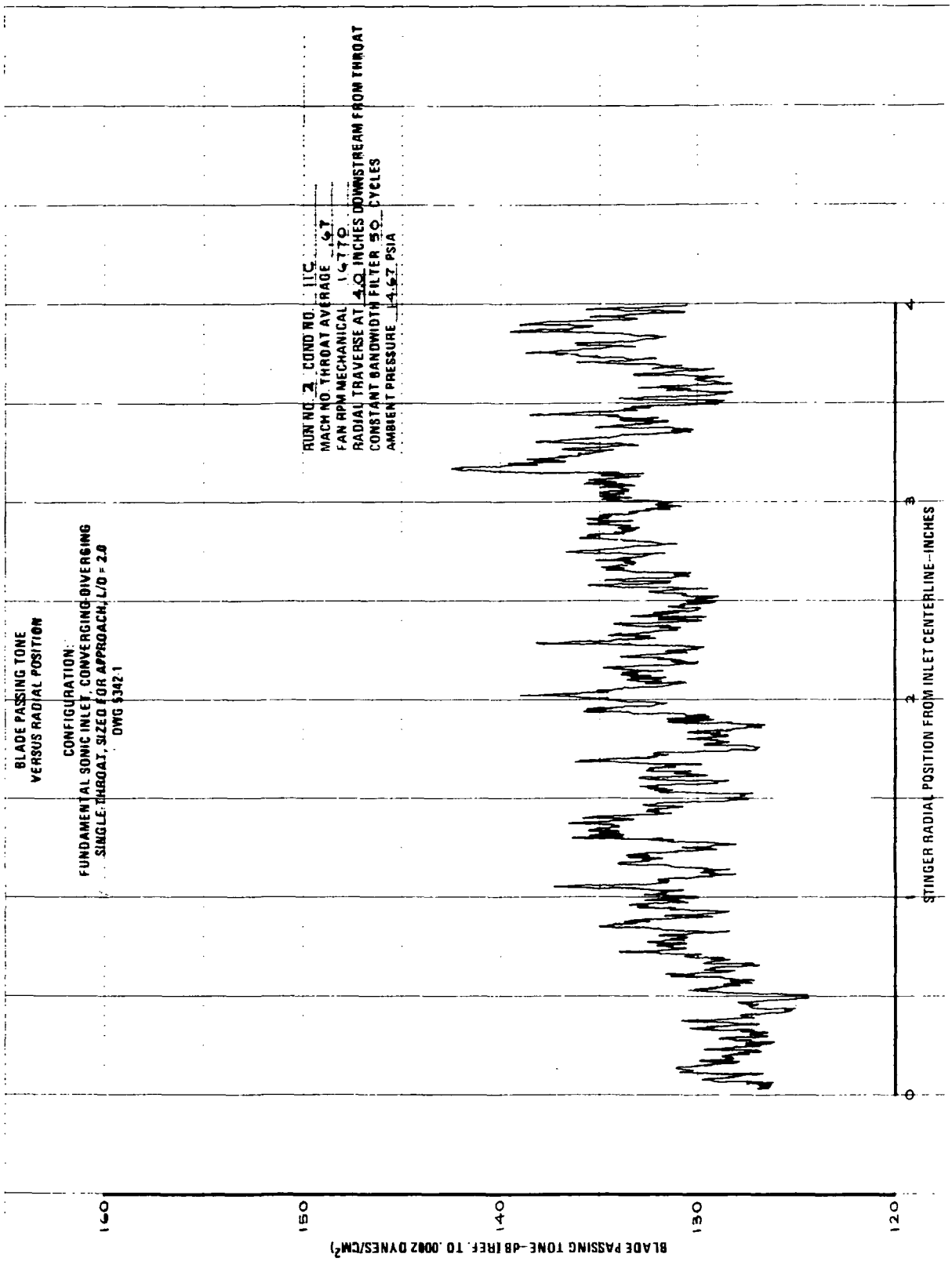

FIGURE B-10.—RUN 2-11C, BLADE PASSING TONE VS RADIAL POSITION IN A PLANE 4.0 IN. DOWNSTREAM FROM INLET THROAT

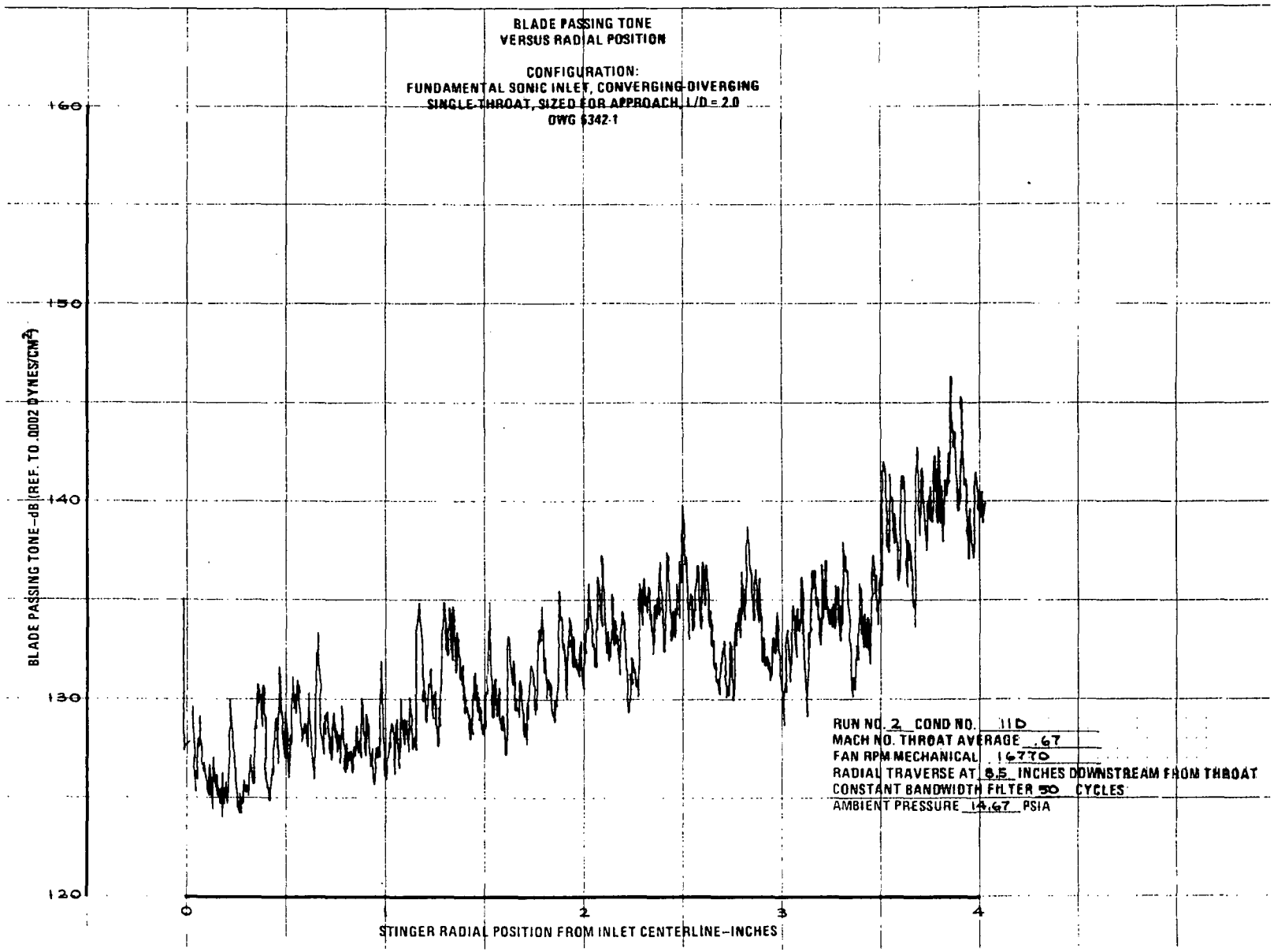

FIGURE B-11.—RUN 2-11D, BLADE PASSING TONE VS RADIAL POSITION IN A PLANE 8.5 IN. DOWNSTREAM FROM INLET THROAT

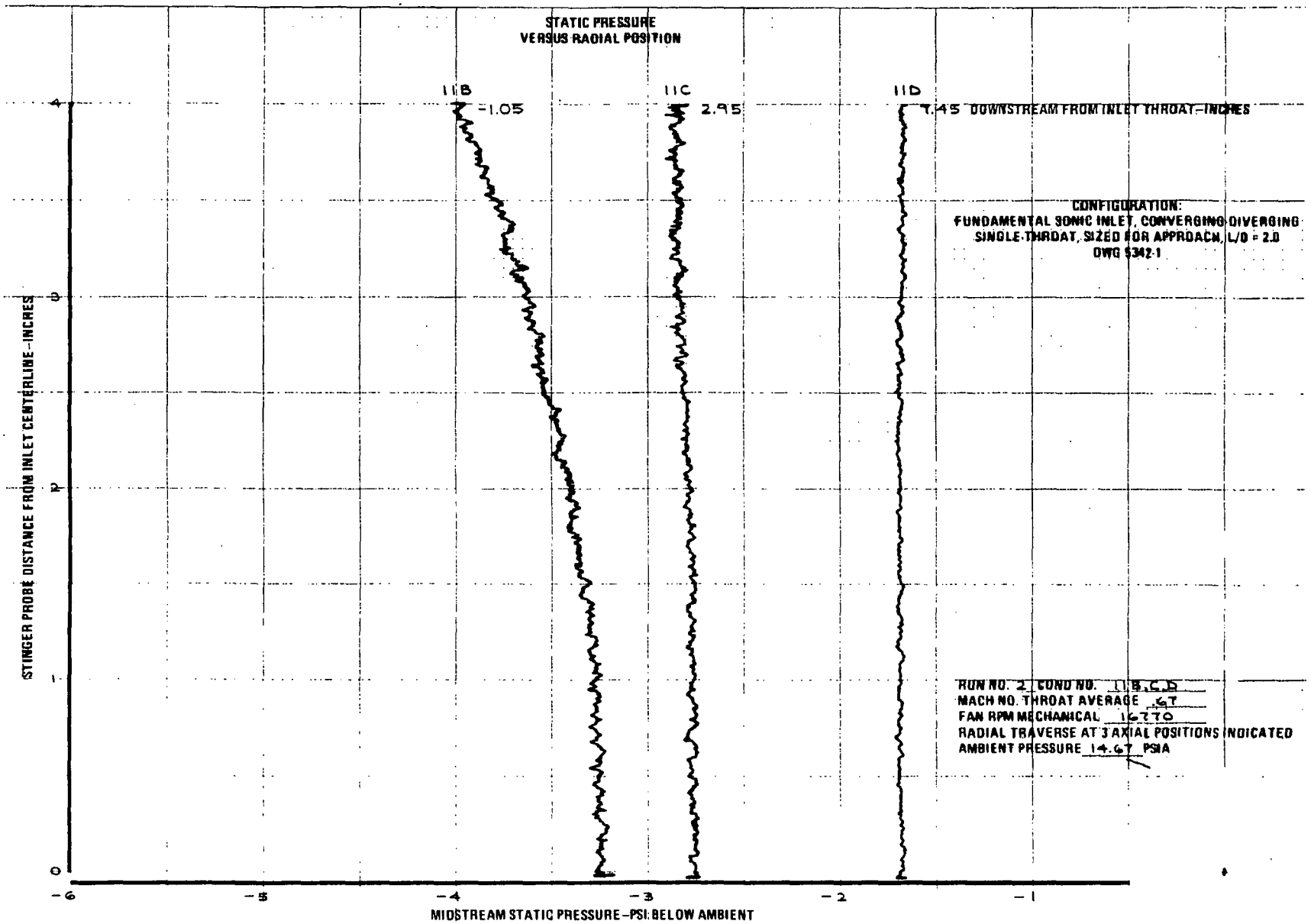

FIGURE B-12.—RUN 2-11 B,C,D, STATIC PRESSURE VS RADIAL POSITION IN PLANES AT -1.05, 2.95, AND 7.45 IN. DOWNSTREAM FROM INLET THROAT

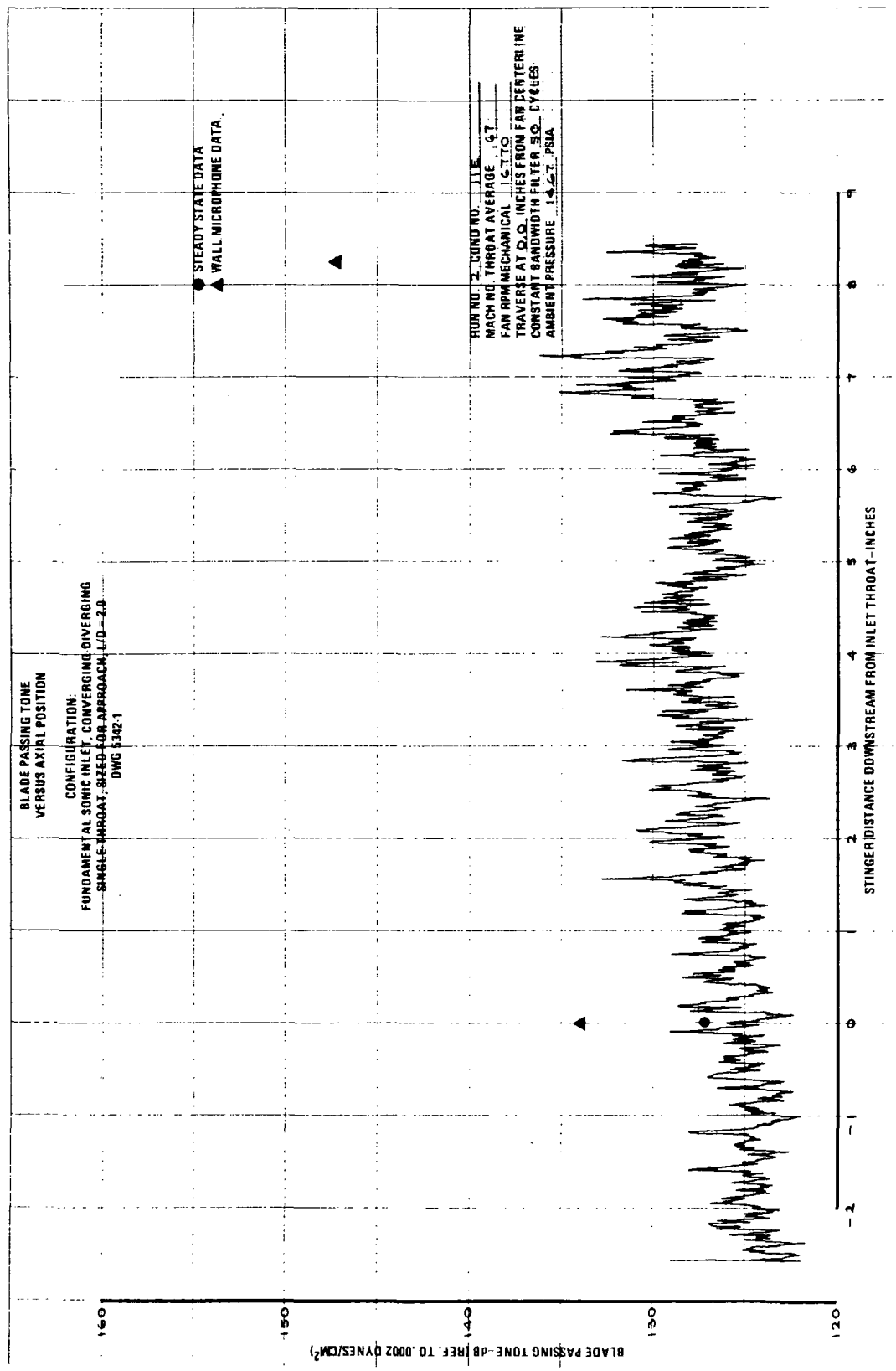

FIGURE B-13.—RUN 2-11E, BLADE PASSING TONE VS AXIAL POSITION AT 0.0 IN. FROM INLET CENTERLINE

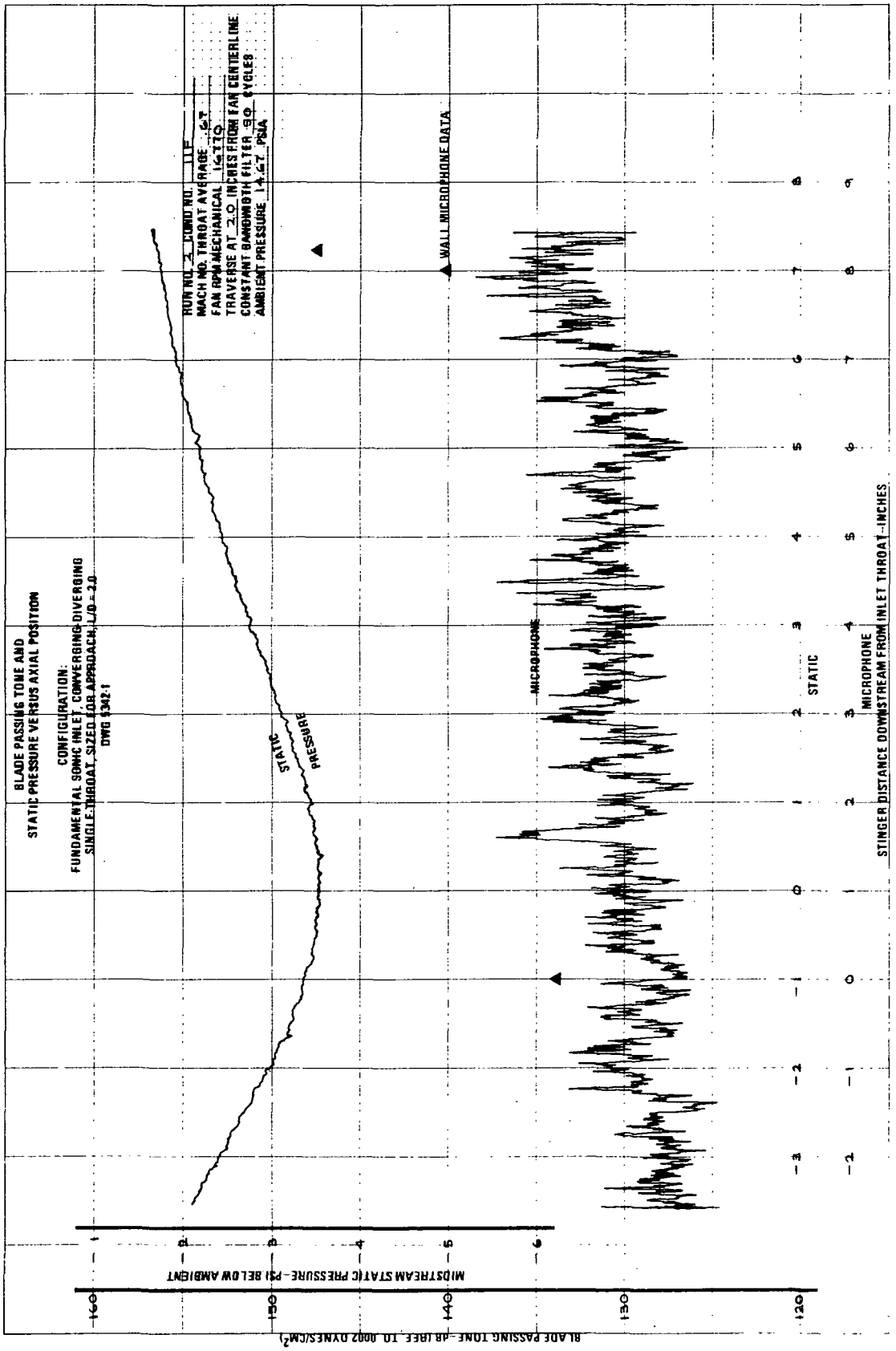

FIGURE B-14.–RUN 2-11F, BLADE PASSING TONE VS AXIAL POSITION AT 2.0 IN. FROM INLET CENTERLINE

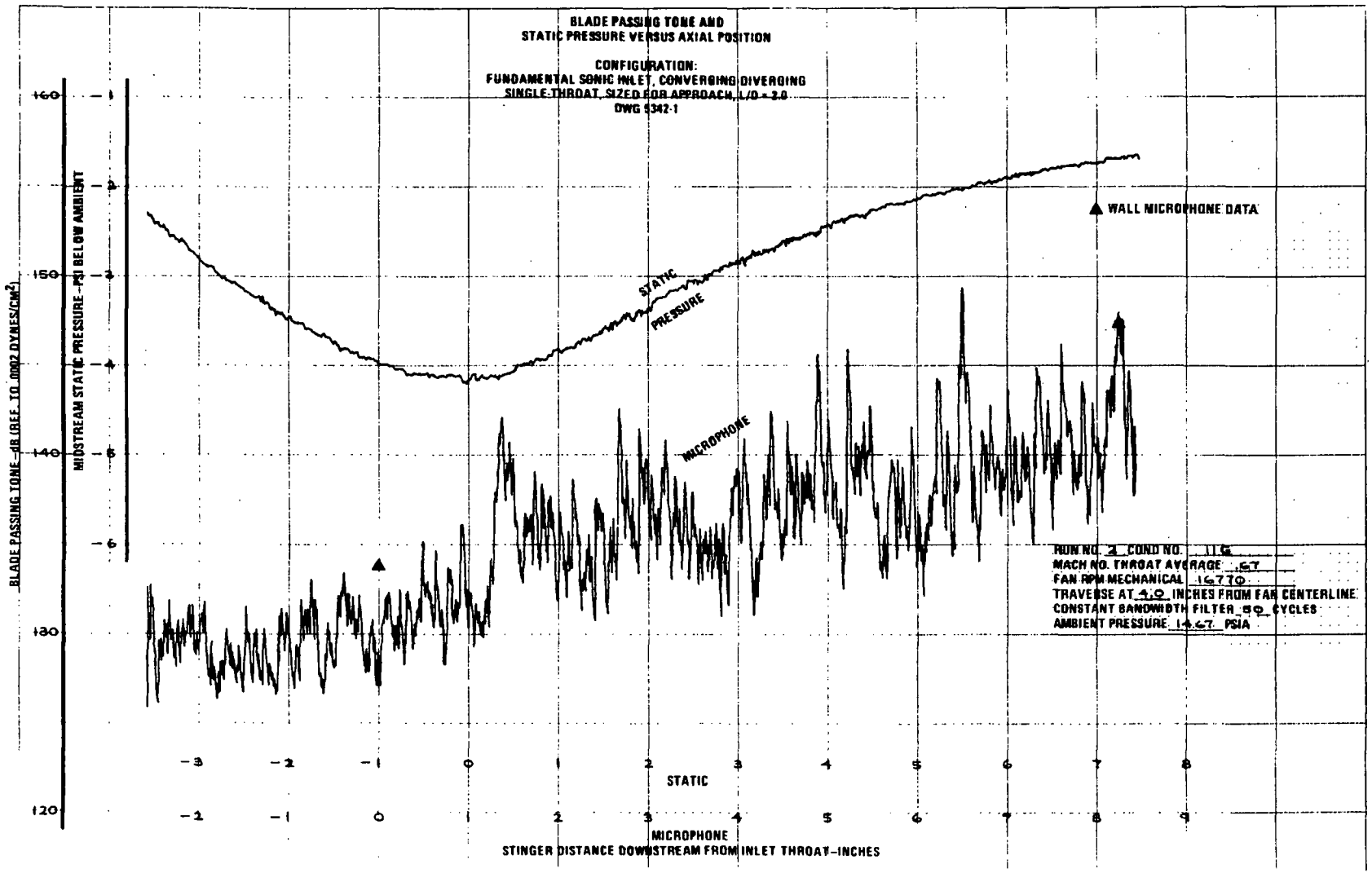

FIGURE B-15.—RUN 2-11G, BLADE PASSING TONE VS AXIAL POSITION AT 4.0 IN. FROM INLET CENTERLINE

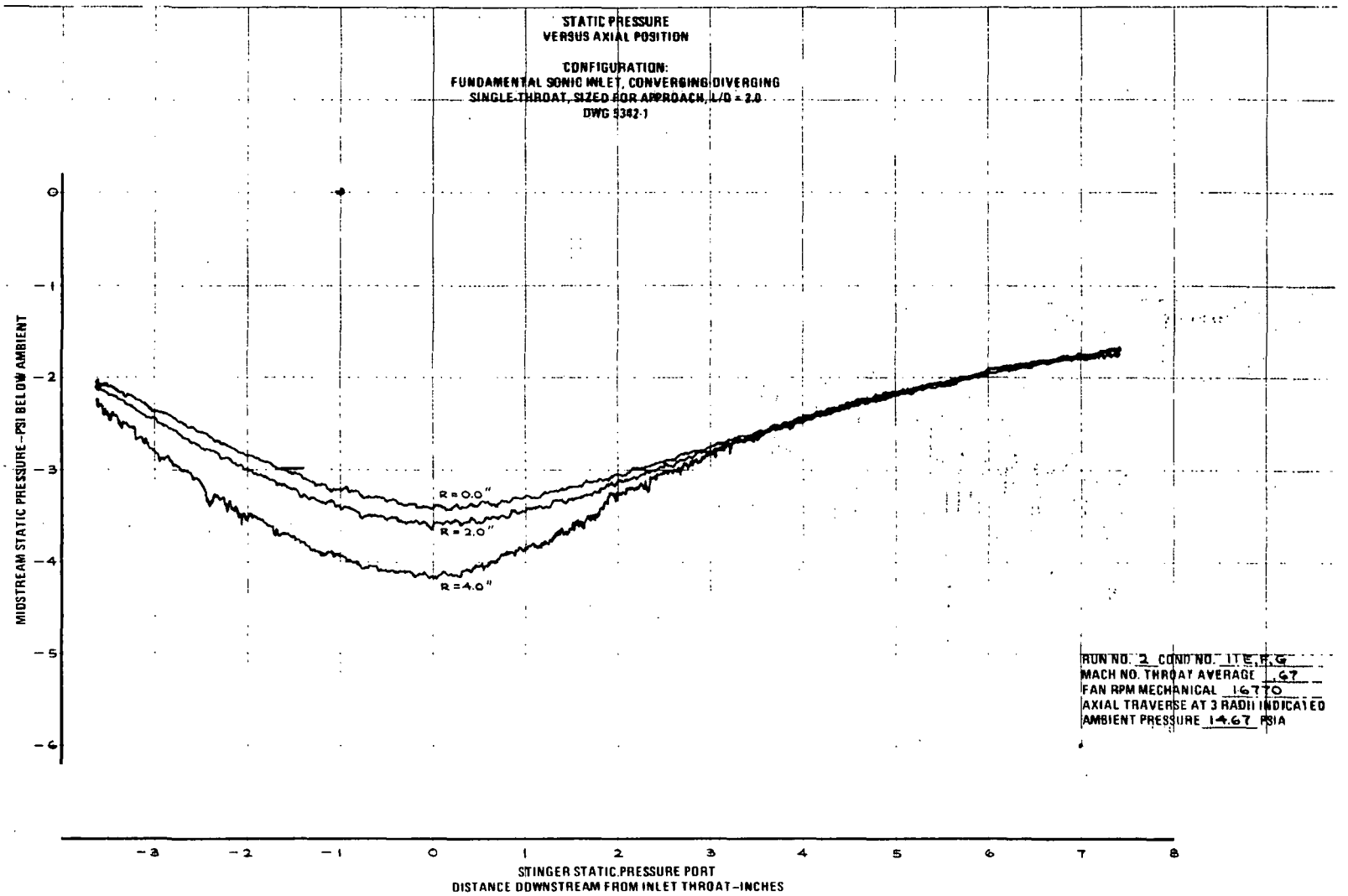

FIGURE B-16.—RUN 2-11 E, F,G, STATIC PRESSURE VS AXIAL POSITION AT 0.0, 2.0, AND 4.0 IN. FROM INLET CENTERLINE

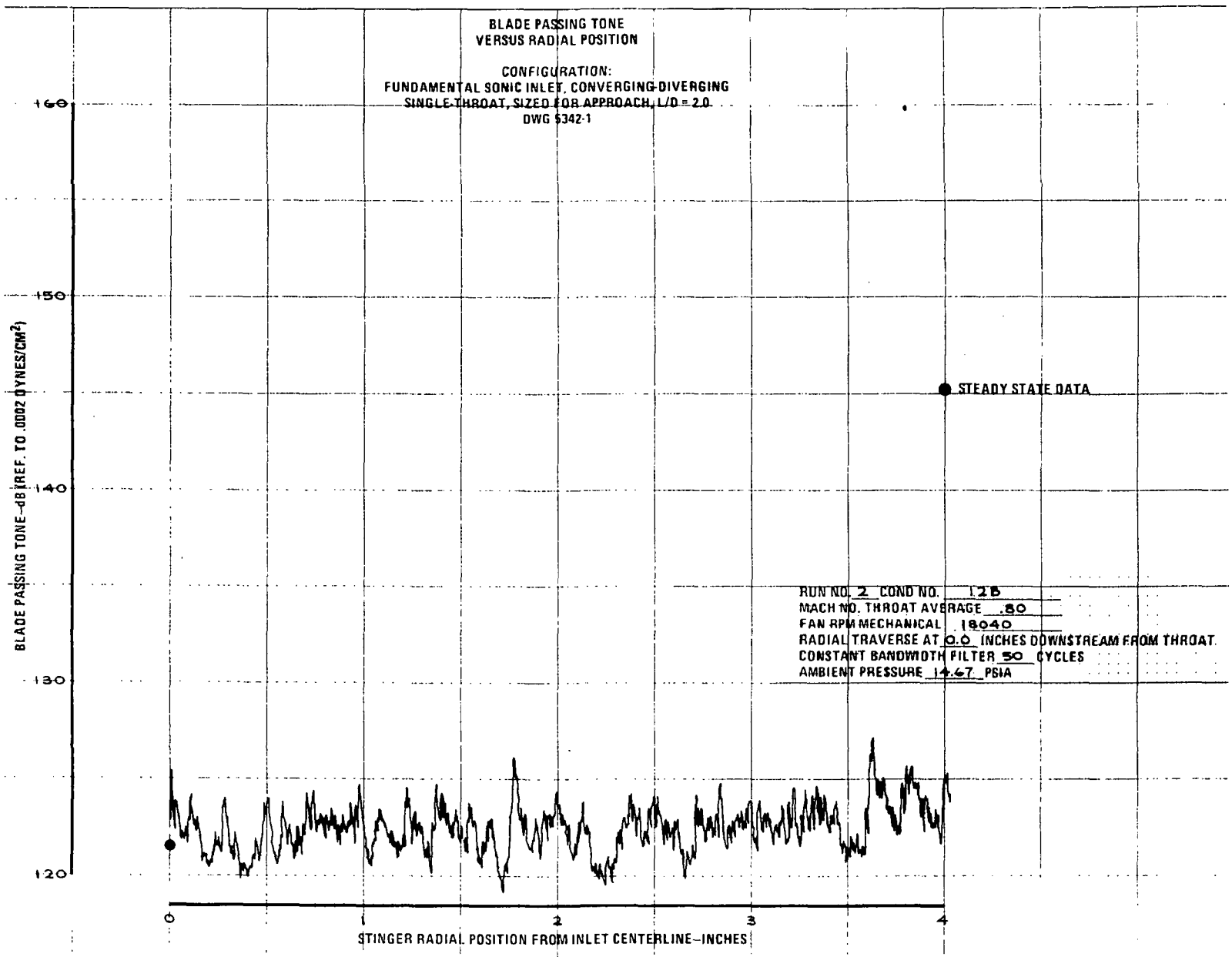

FIGURE B-17.–RUN 2-12B, BLADE PASSING TONE VS RADIAL POSITION IN A PLANE 0.0 IN. DOWNSTREAM FROM INLET THROAT

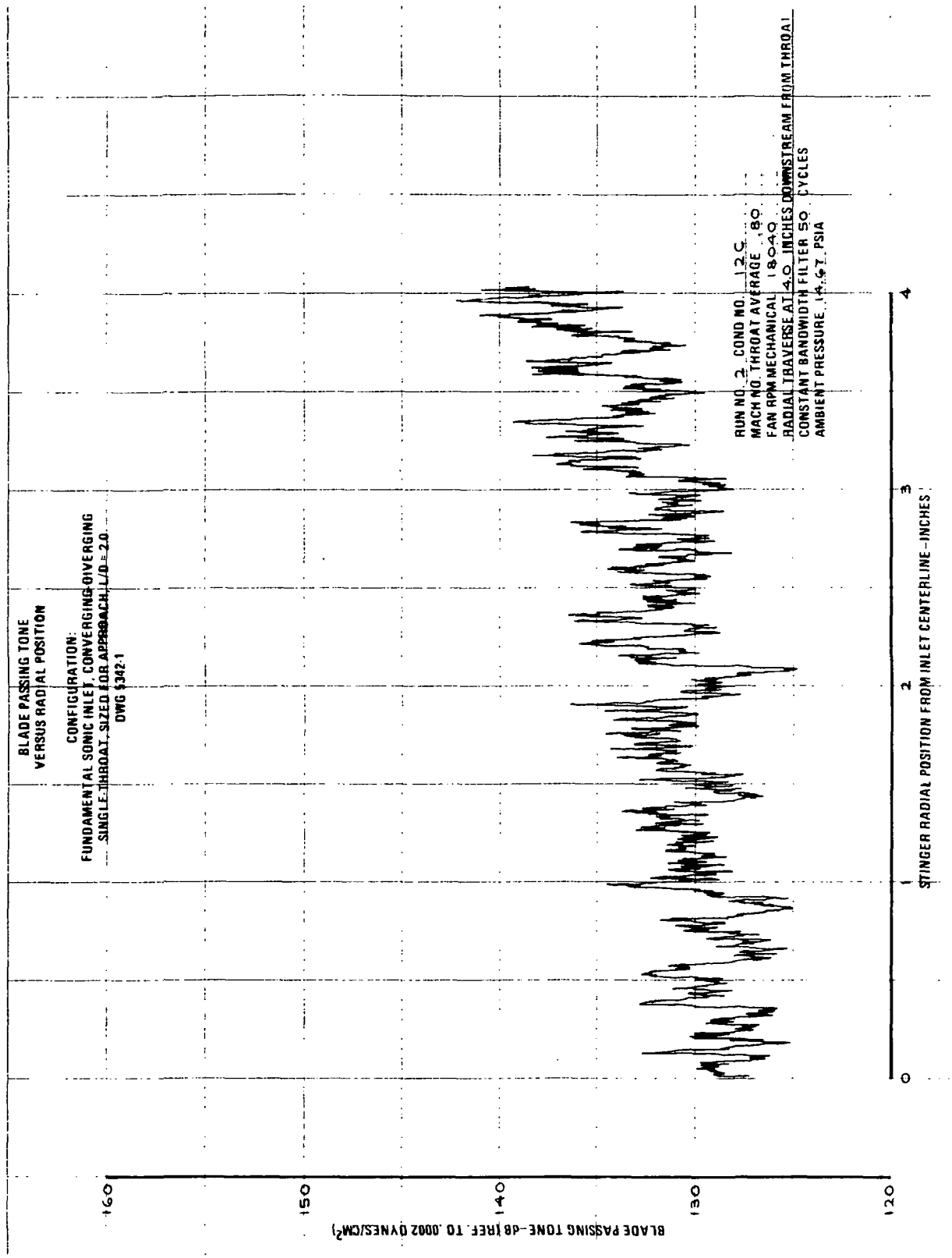

FIGURE B-18.—RUN 2-12C, BLADE PASSING TONE VS RADIAL POSITION IN A PLANE 4.0 IN. DOWNSTREAM FROM INLET THROAT

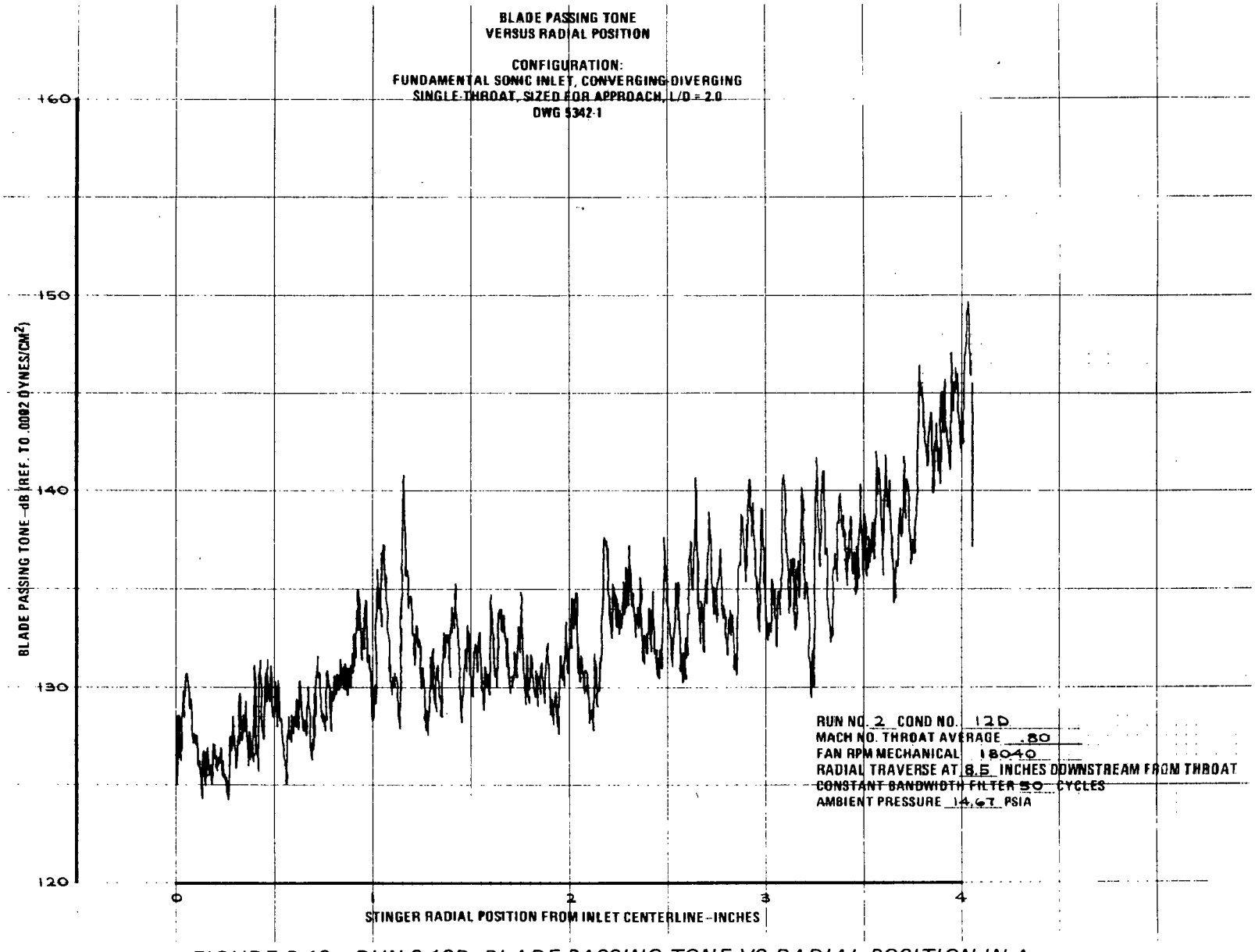

FIGURE B-19.—RUN 2-12D, BLADE PASSING TONE VS RADIAL POSITION IN A PLANE 8.5 IN. DOWNSTREAM FROM INLET THROAT

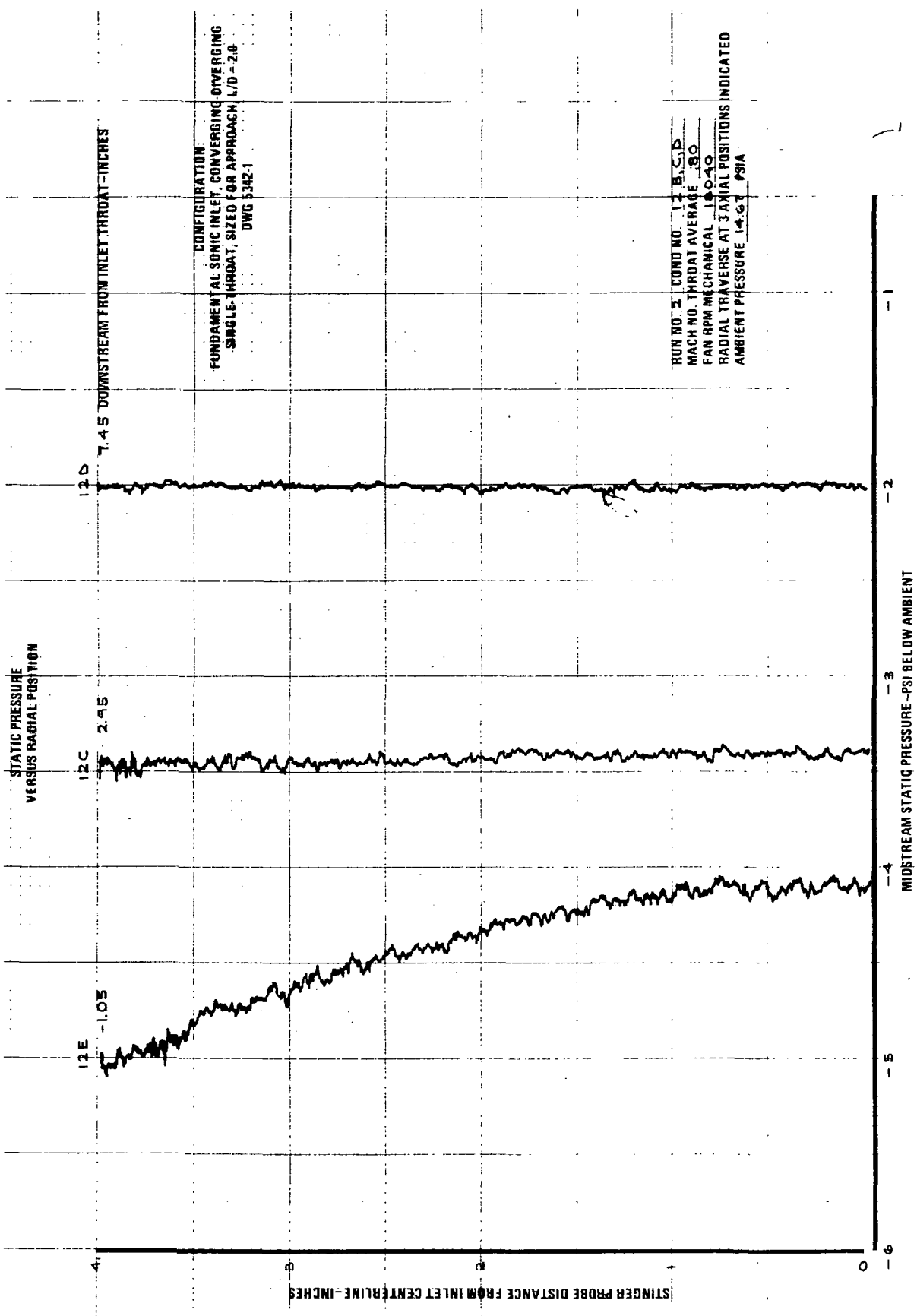

FIGURE B-20.—RUN 2-12 B,C,D, STATIC PRESSURE VS RADIAL POSITION IN PLANES AT -1.05, 2.95, AND 7.45 IN. DOWNSTREAM FROM INLET THROAT

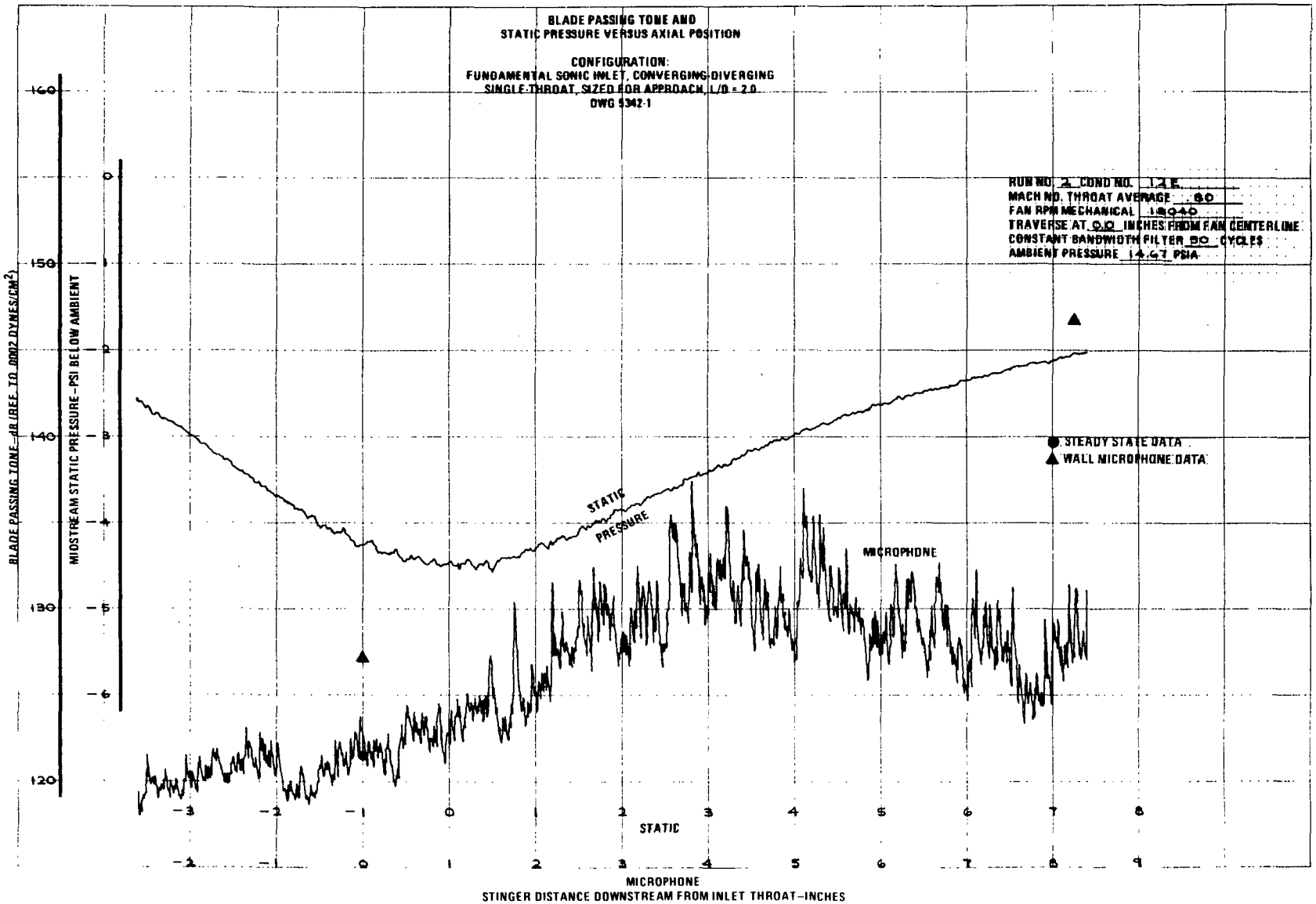

FIGURE B-21.—RUN 2-12E, BLADE PASSING TONE VS AXIAL POSITION AT 0.0 IN. FROM INLET CENTERLINE

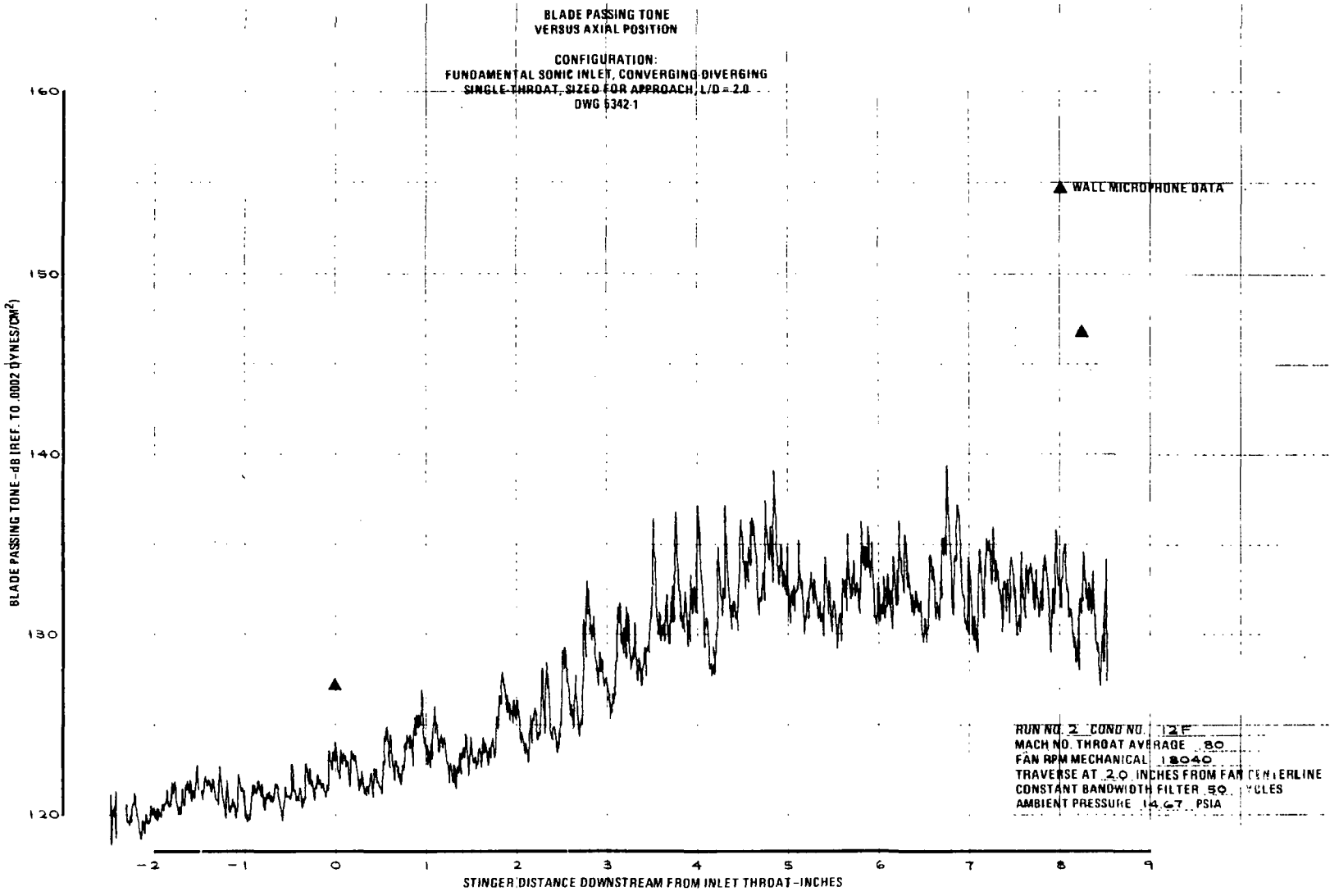

FIGURE B-22.—RUN 2-12F, BLADE PASSING TONE VS AXIAL POSITION AT 2.0 IN. FROM INLET CENTERLINE

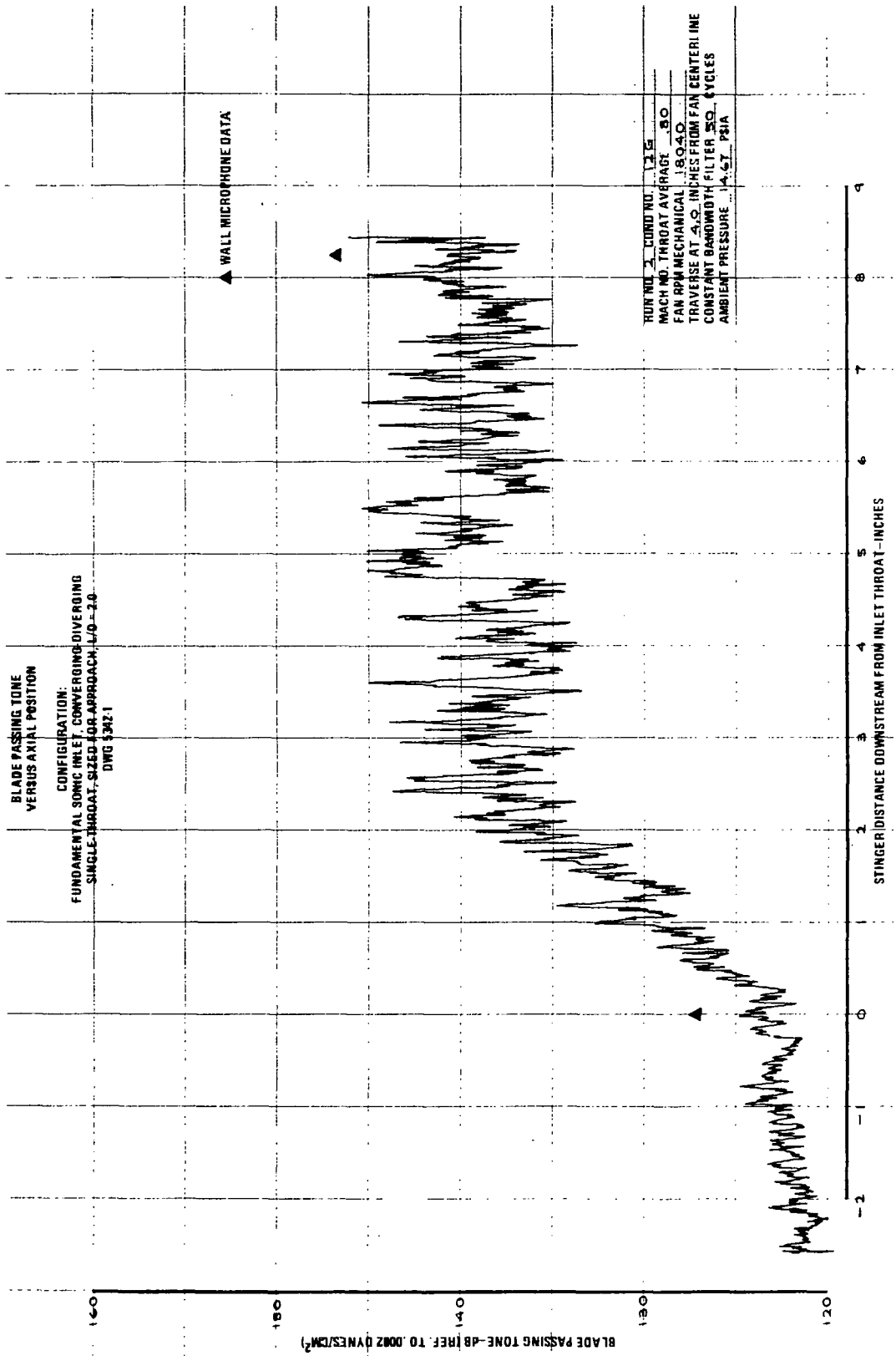

FIGURE B-23.—RUN 2-12G, BLADE PASSING TONE VS AXIAL POSITION AT 4.0 IN. FROM INLET CENTERLINE

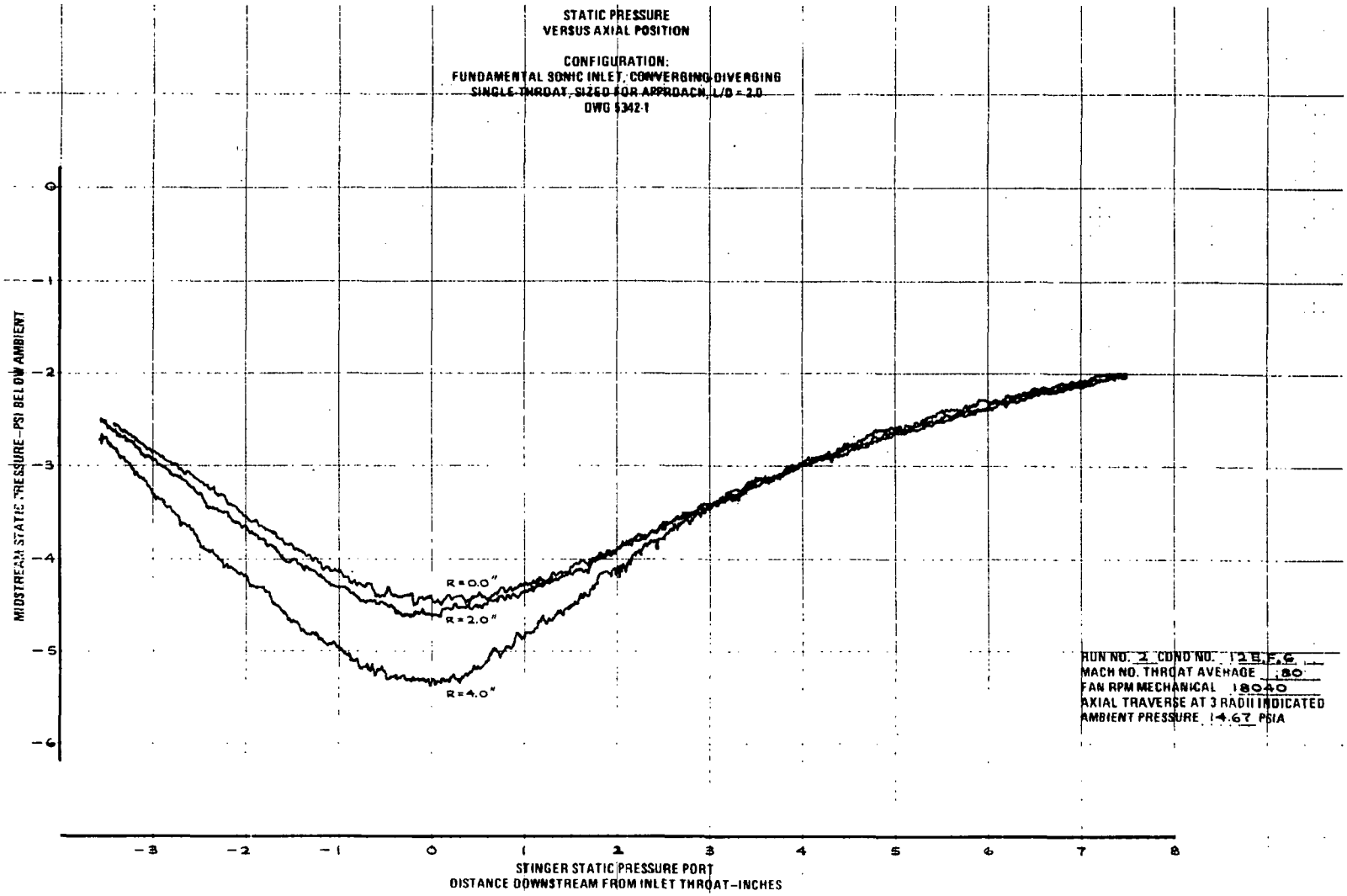

FIGURE B-24.—RUN 2-12 E,F,G, STATIC PRESSURE VS AXIAL POSITION AT 0.0, 2.0, AND 4.0 IN. FROM INLET CENTERLINE

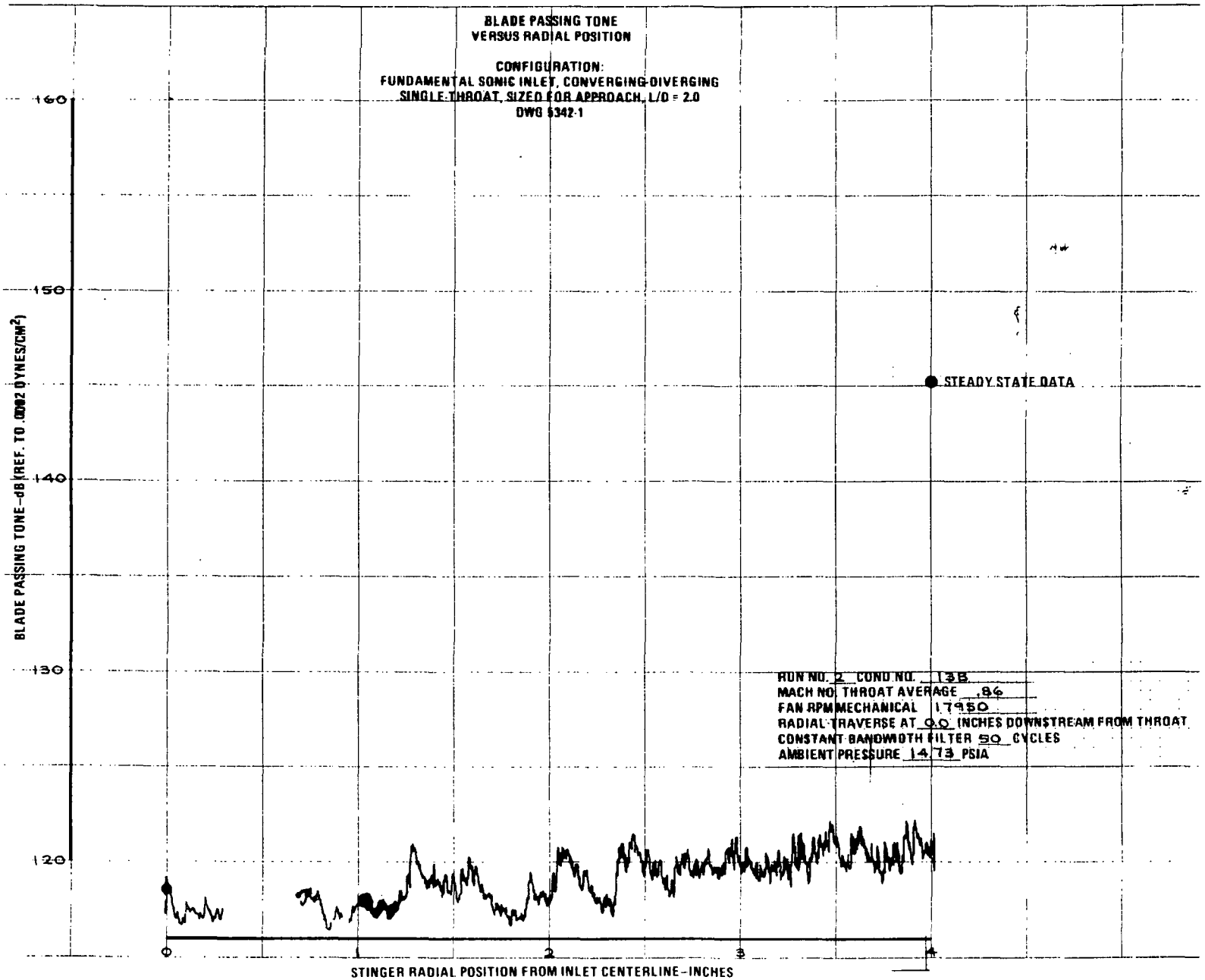

FIGURE B-25.—RUN 2-13B, BLADE PASSING TONE VS RADIAL POSITION IN A PLANE 0.0 IN. DOWNSTREAM FROM INLET THROAT

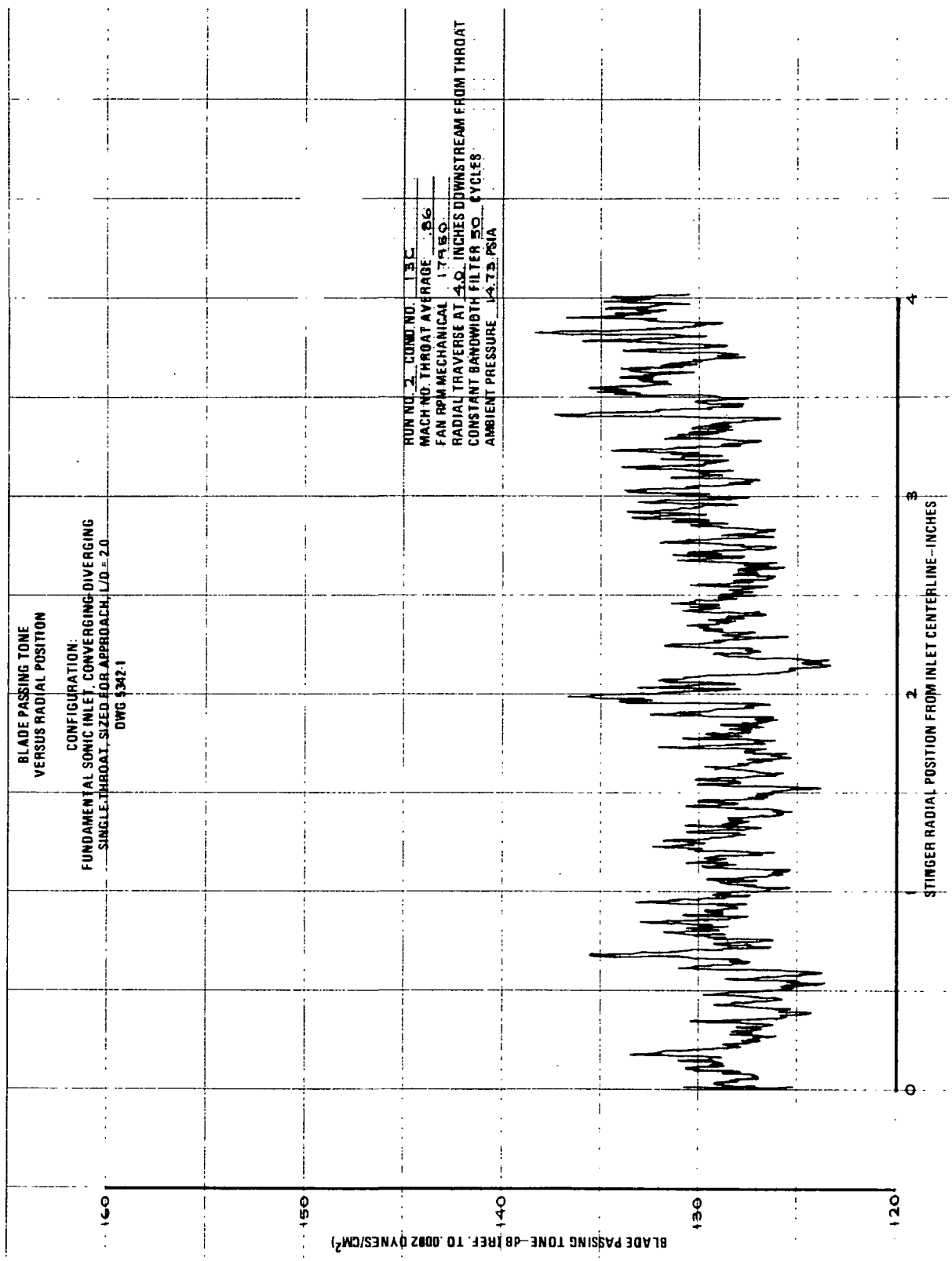

FIGURE B-26.—RUN 2-13C, BLADE PASSING TONE VS RADIAL POSITION IN A PLANE 4.0 IN. DOWNSTREAM FROM INLET THROAT

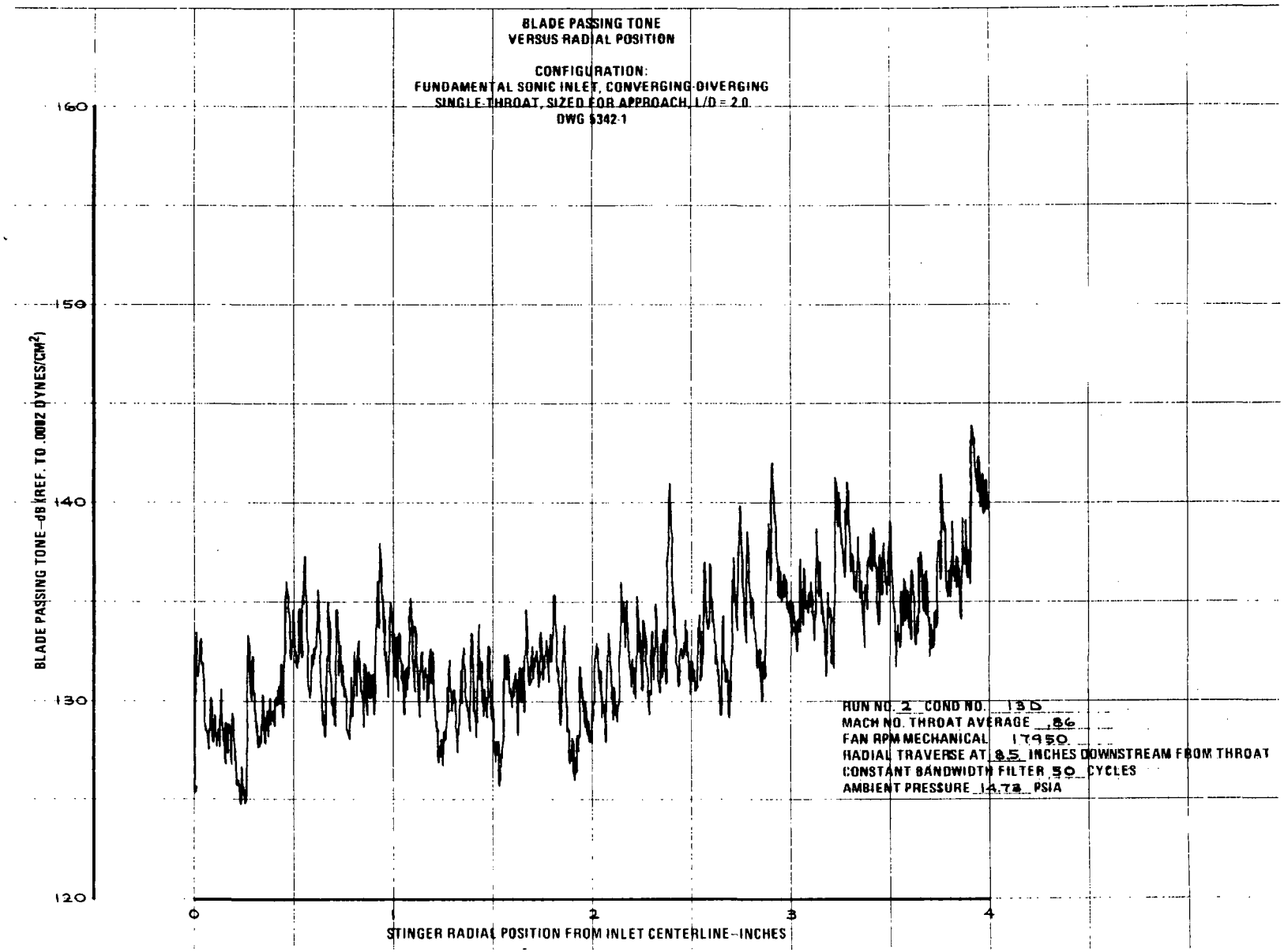

FIGURE B-27.—RUN 2-13D, BLADE PASSING TONE VS RADIAL POSITION IN A PLANE 8.5 IN. DOWNSTREAM FROM INLET THROAT

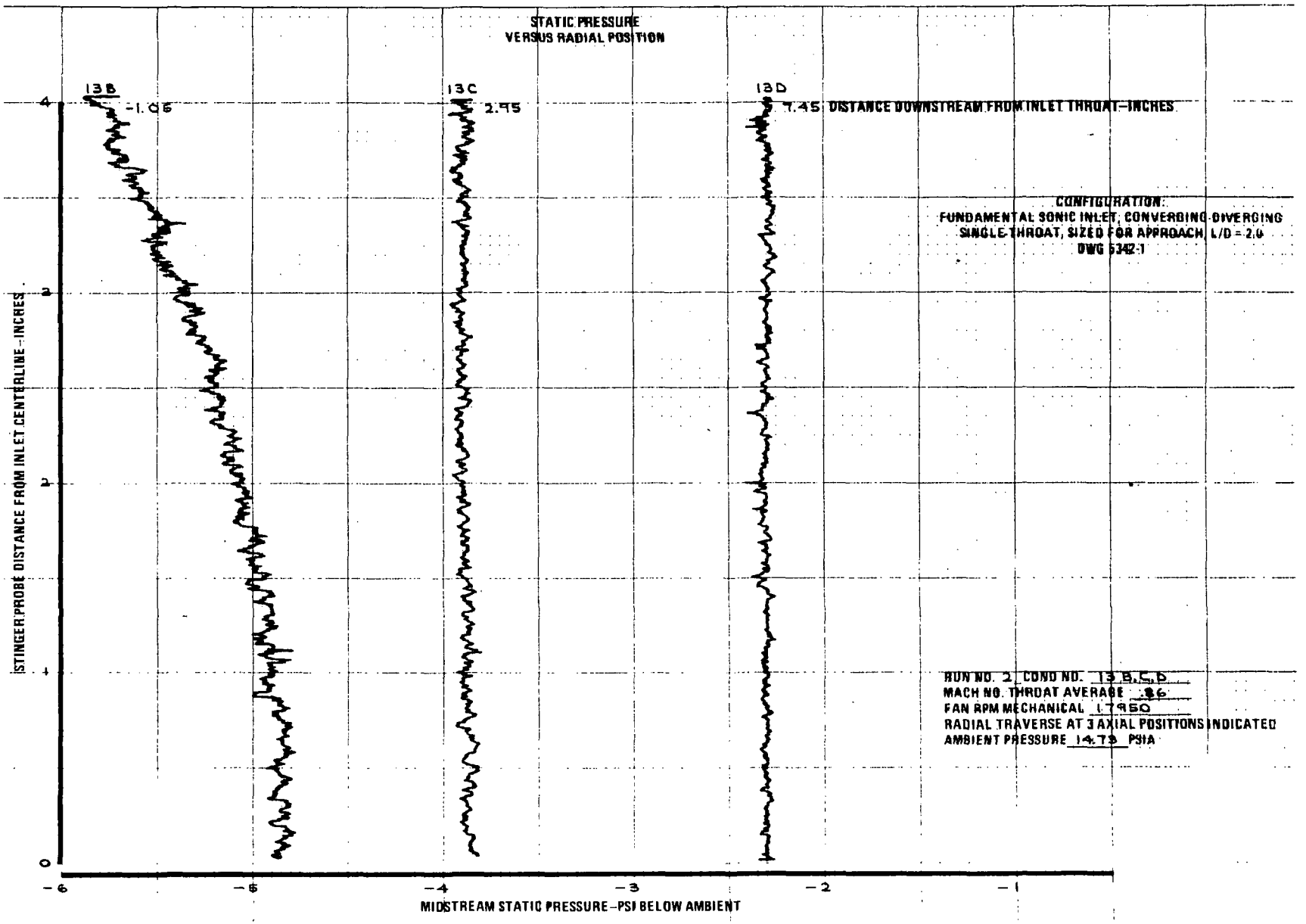

FIGURE B-28.–RUN 2-13 B,C,D, STATIC PRESSURE VS RADIAL POSITION IN PLANES AT -1.05, 2.95, AND 7.45 IN. DOWNSTREAM FROM INLET THROAT

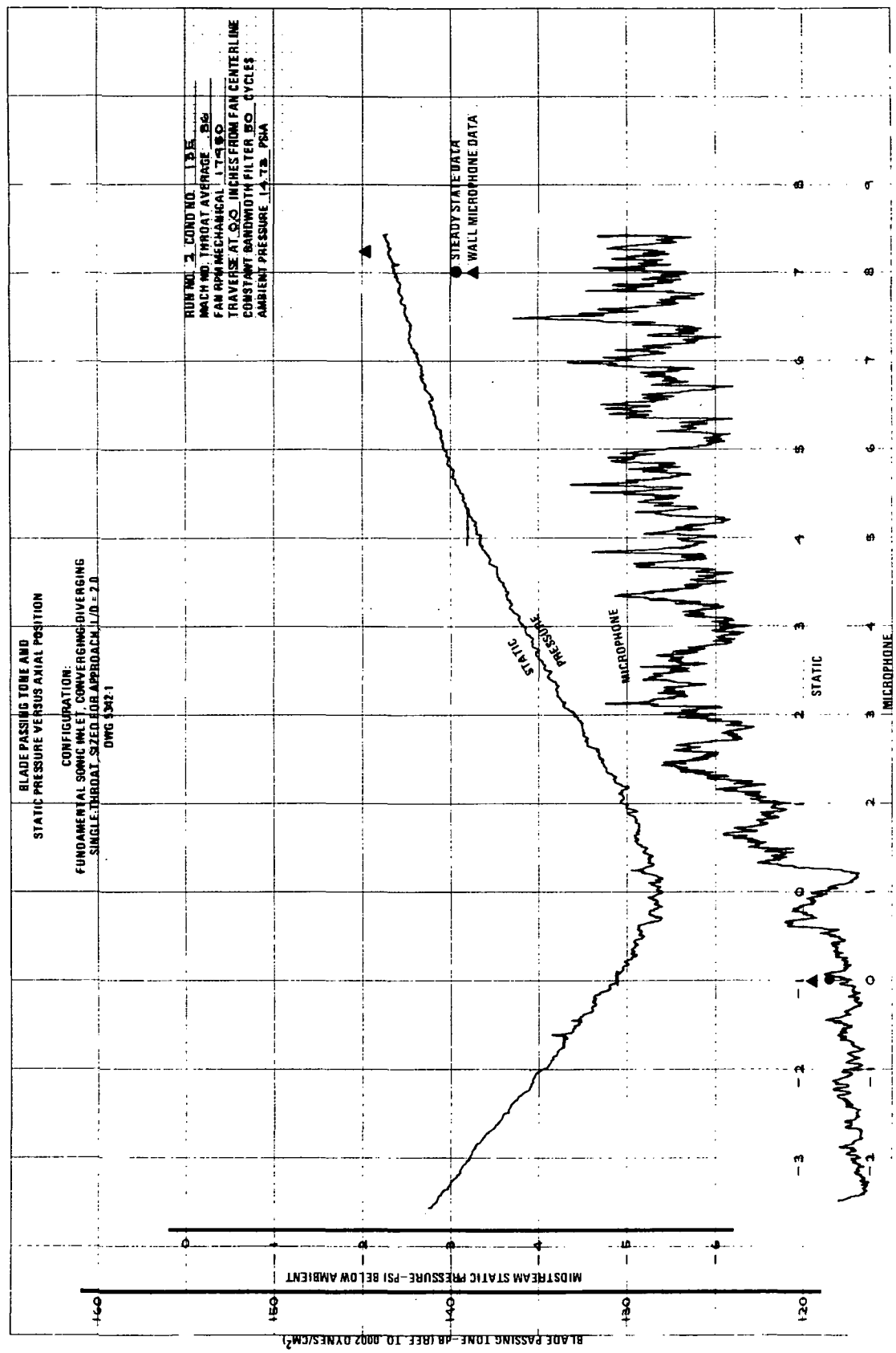

FIGURE B-29.—RUN 2-13E, BLADE PASSING TONE VS AXIAL POSITION AT 0.0 IN. FROM INLET CENTERLINE

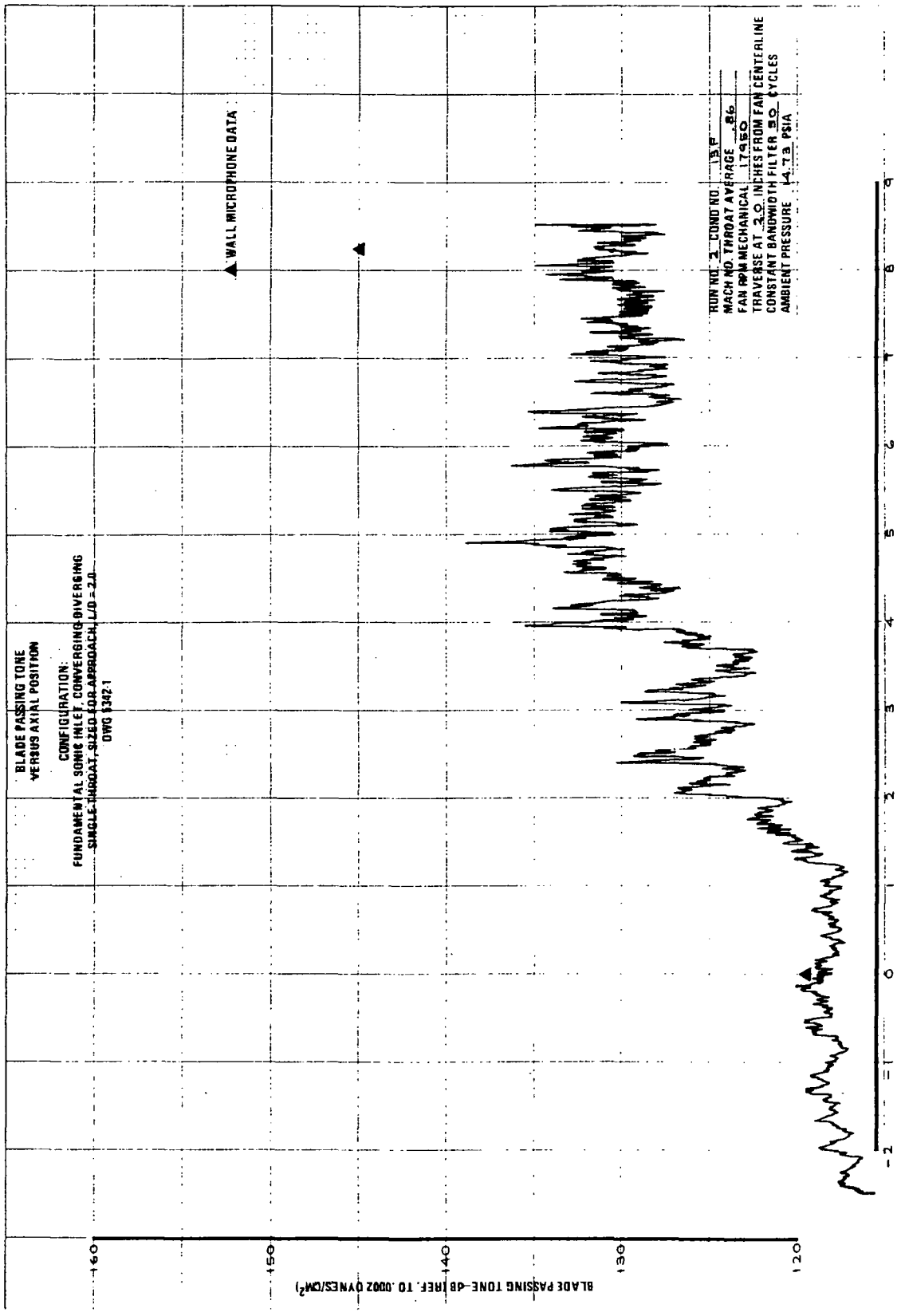

FIGURE B-30.–RUN 2-13F, BLADE PASSING TONE VS AXIAL POSITION AT 2.0 IN. FROM INLET CENTERLINE

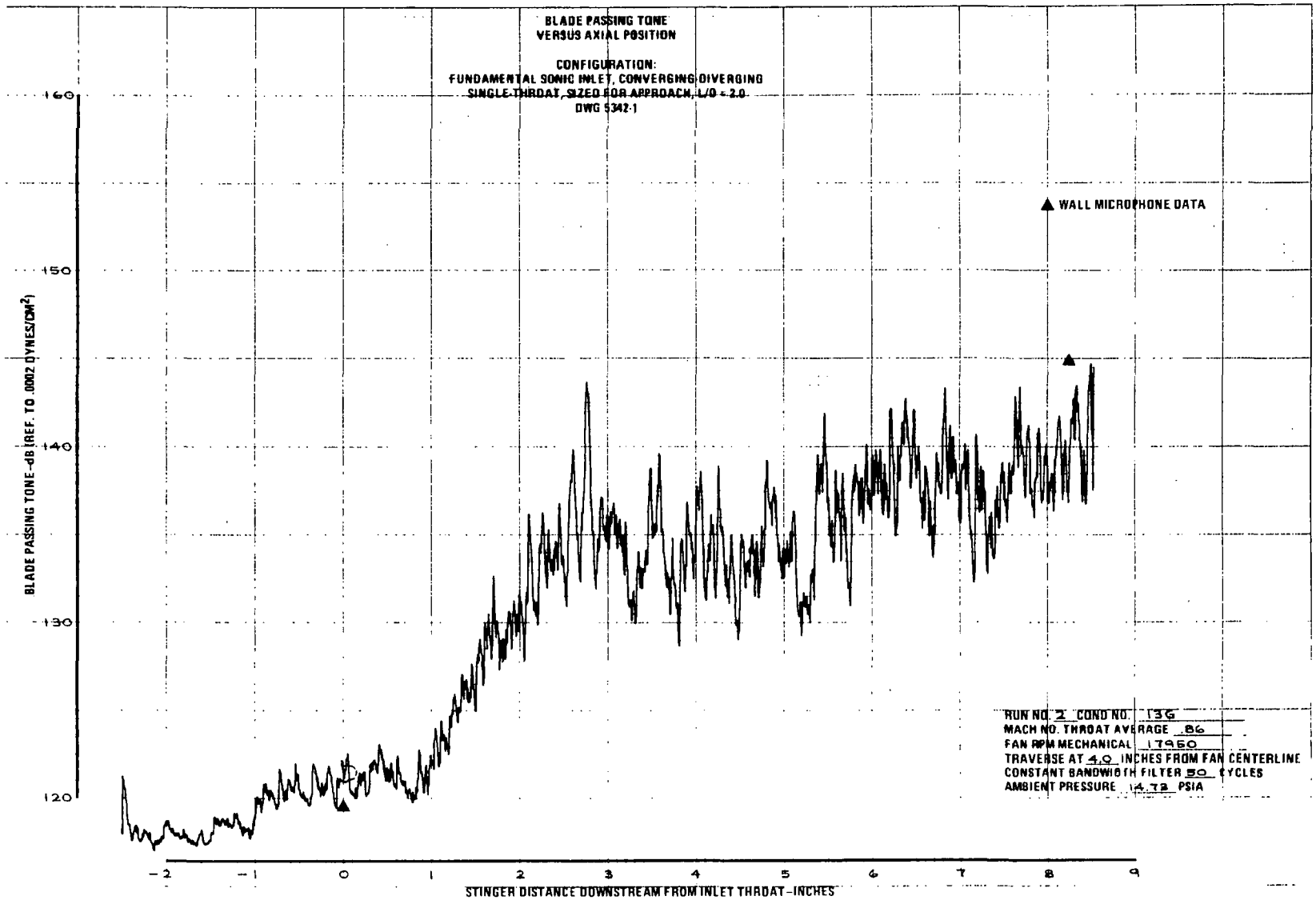

FIGURE B-31.—RUN 2-13G, BLADE PASSING TONE VS AXIAL POSITION AT 4.0 IN. FROM INLET CENTERLINE

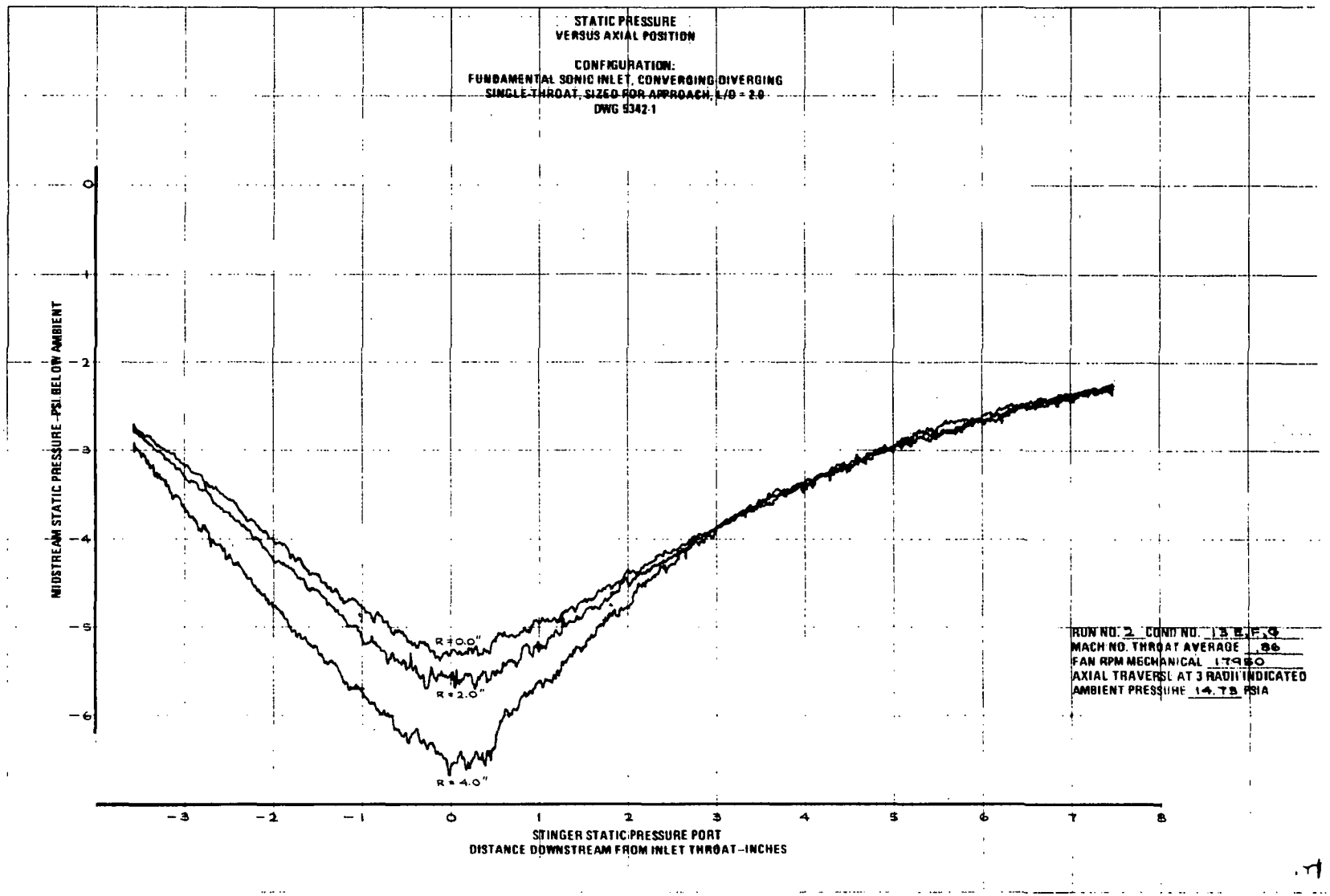

FIGURE B-32.—RUN 2-13 E,F,G, STATIC PRESSURE VS AXIAL POSITION AT 0.0, 2.0, AND 4.0 IN. FROM INLET CENTERLINE

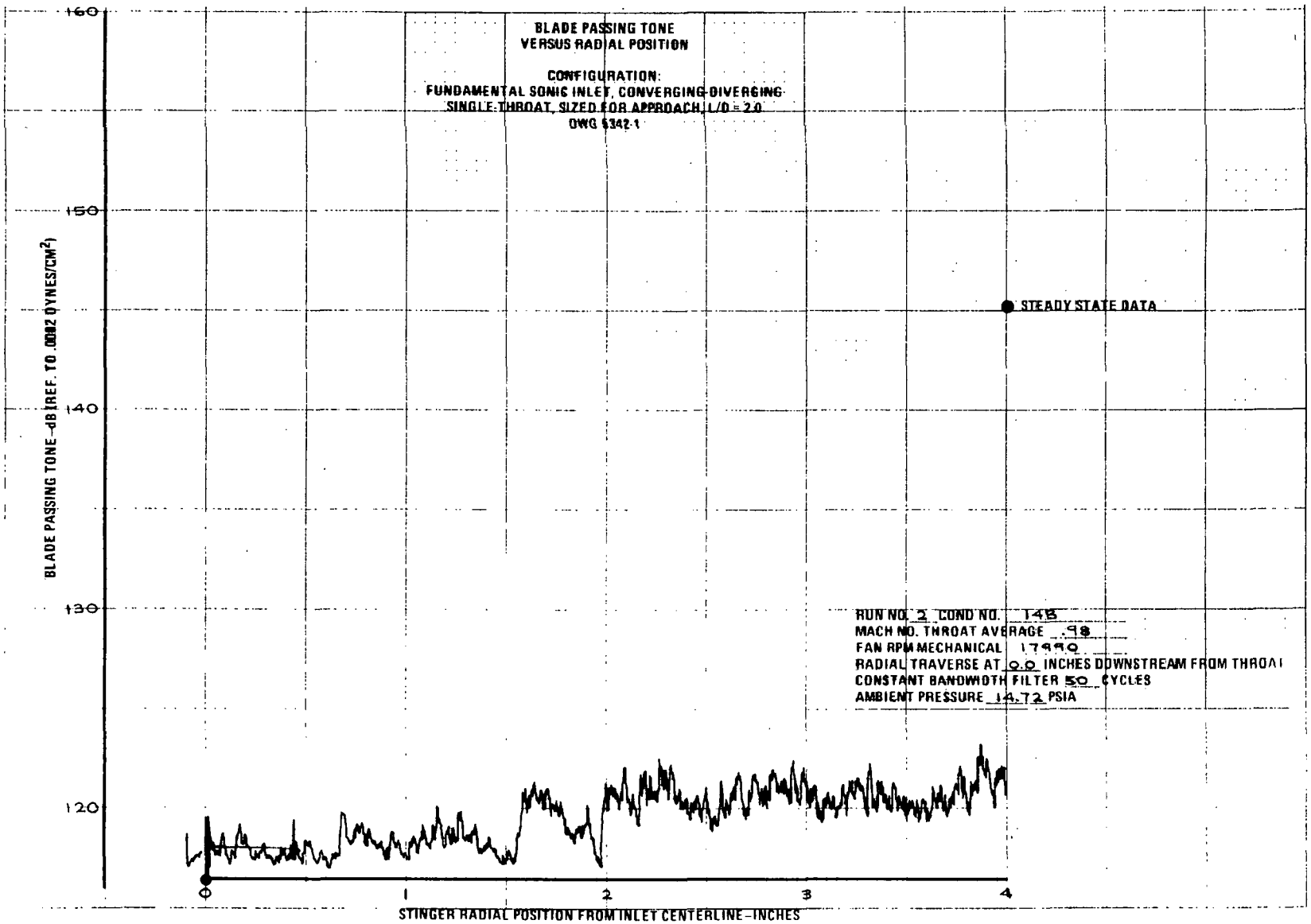

FIGURE B-33.—RUN 2-14B, BLADE PASSING TONE VS RADIAL POSITION IN A PLANE 0.0 IN. DOWNSTREAM FROM INLET THROAT

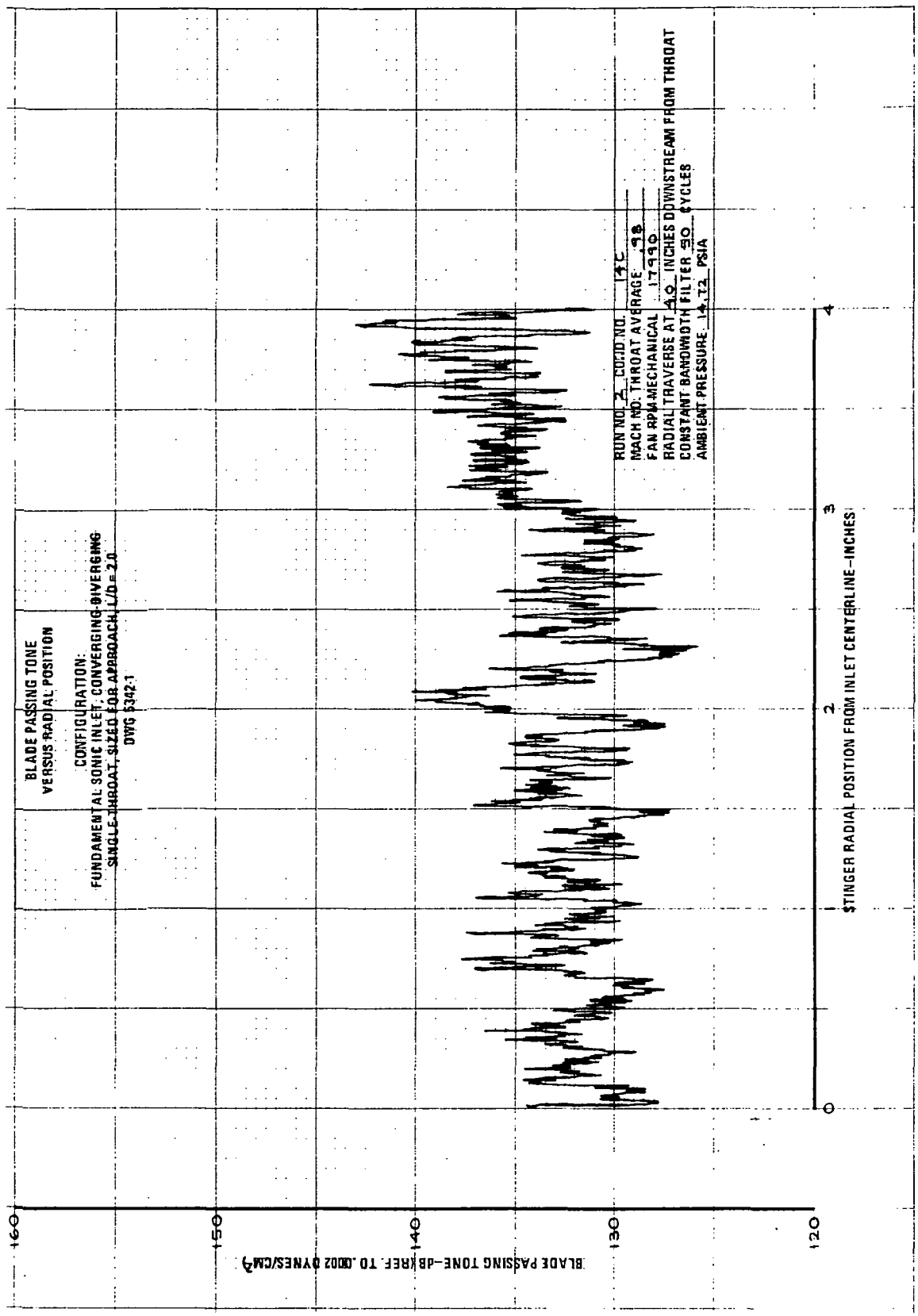

FIGURE B-34.—RUN 2-14C, BLADE PASSING TONE VS RADIAL POSITION IN A PLANE 4.0 IN. DOWNSTREAM FROM INLET THROAT

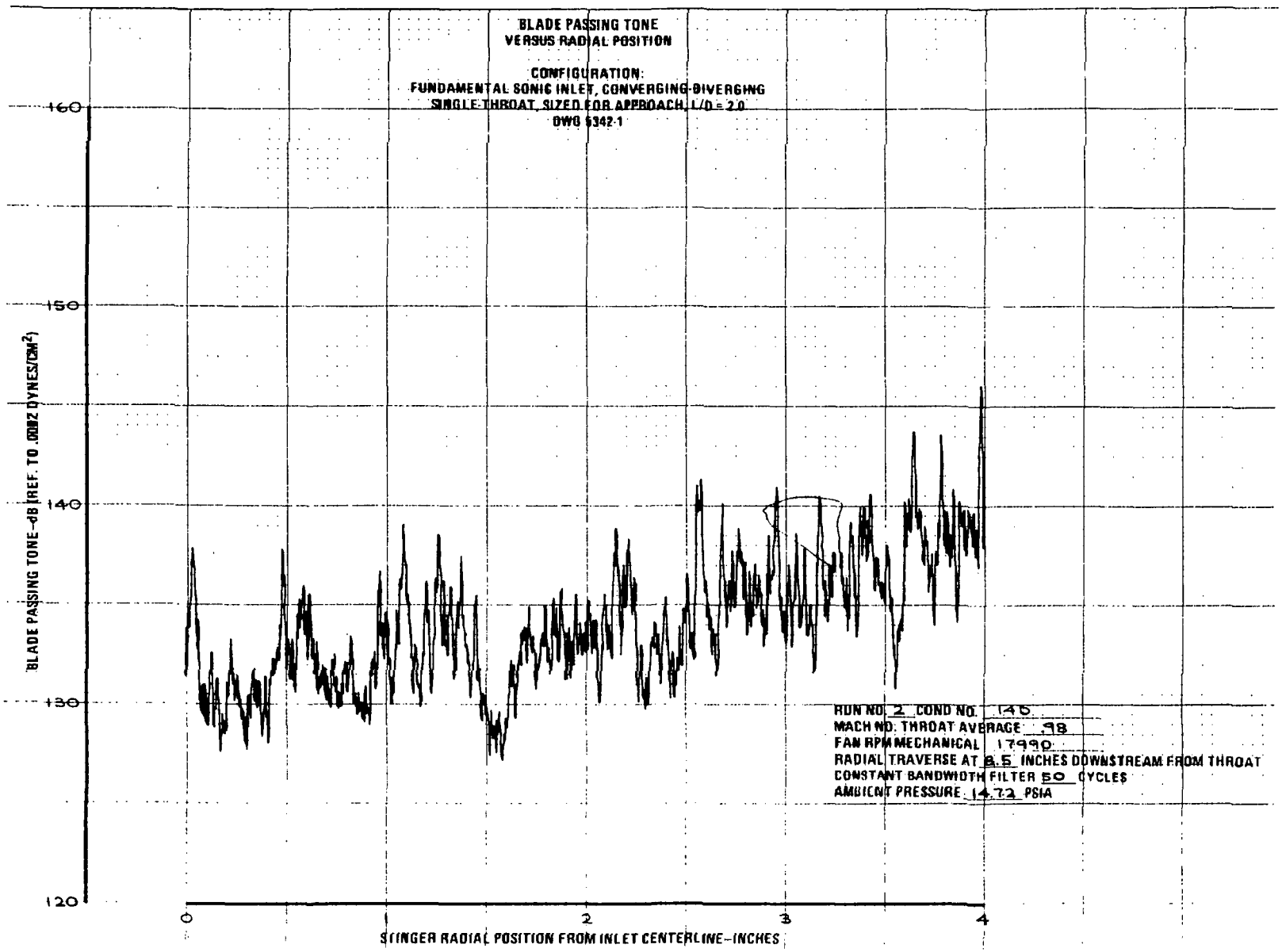

FIGURE B-35.—RUN 2-14D, BLADE PASSING TONE VS RADIAL POSITION IN A PLANE 8.5 IN. DOWNSTREAM FROM INLET THROAT

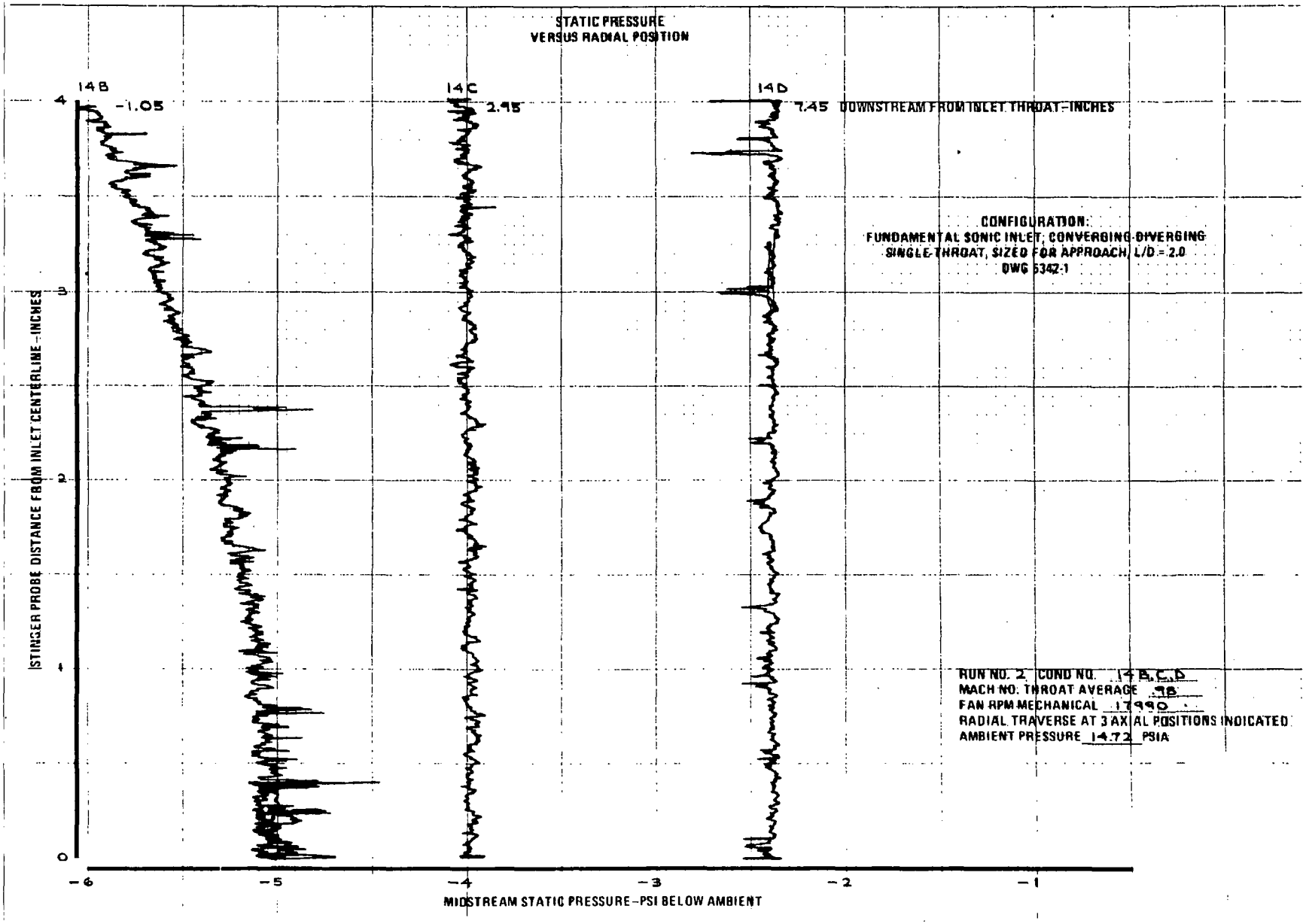

FIGURE B-36.—RUN 2-14 B,C,D, STATIC PRESSURE VS RADIAL POSITION IN PLANES AT -1.05, 2.95, AND 7.45 IN. DOWNSTREAM FROM INLET THROAT

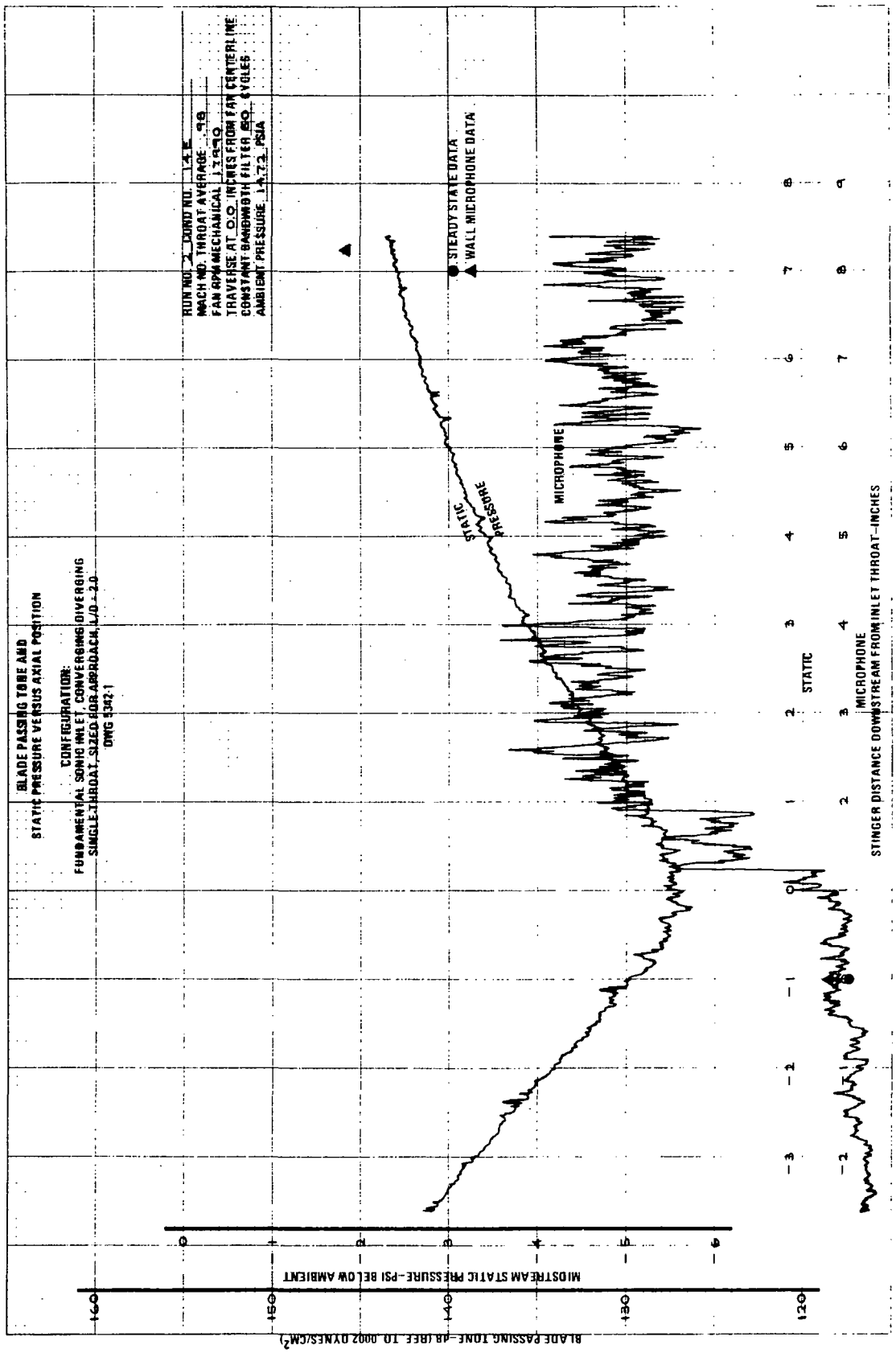

FIGURE B-37.–RUN 2-14E, BLADE PASSING TONE VS AXIAL POSITION AT 0.0 IN. FROM INLET CENTERLINE

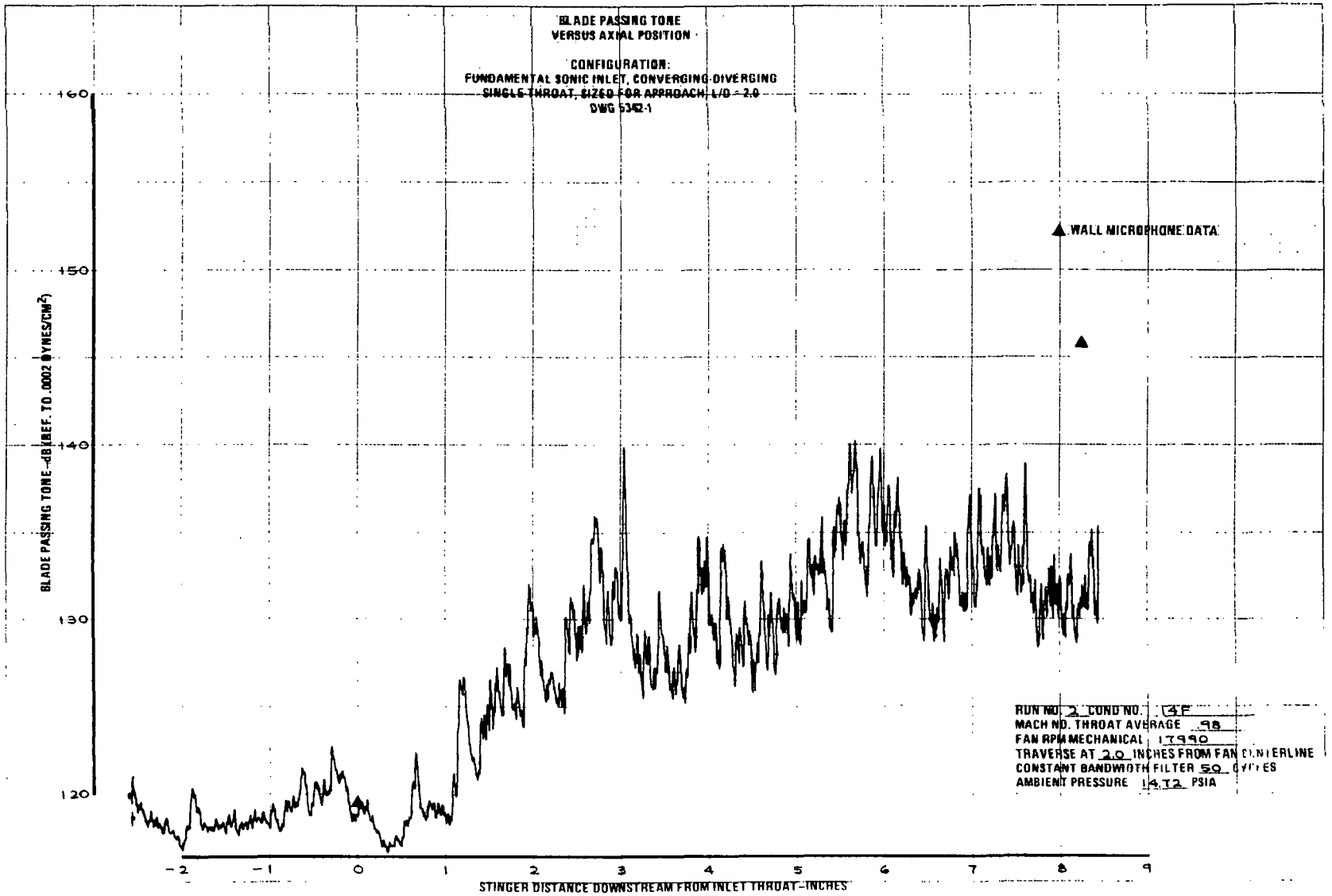

FIGURE B-38.—RUN 2-14F, BLADE PASSING TONE VS AXIAL POSITION AT 2.0 IN. FROM INLET CENTERLINE

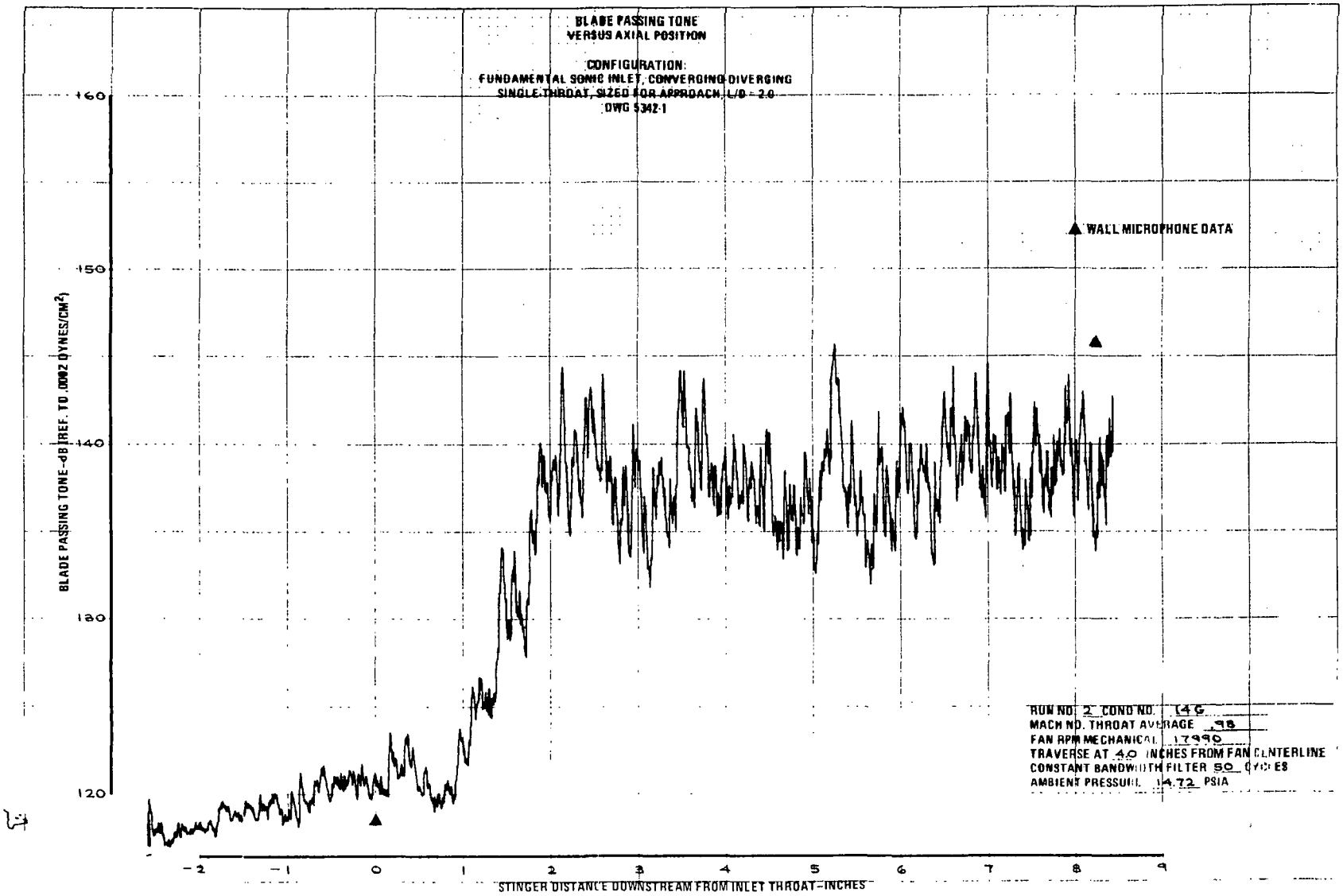

FIGURE B-39.—RUN 2-14G, BLADE PASSING TONE VS AXIAL POSITION AT 4.0 IN. FROM INLET CENTERLINE

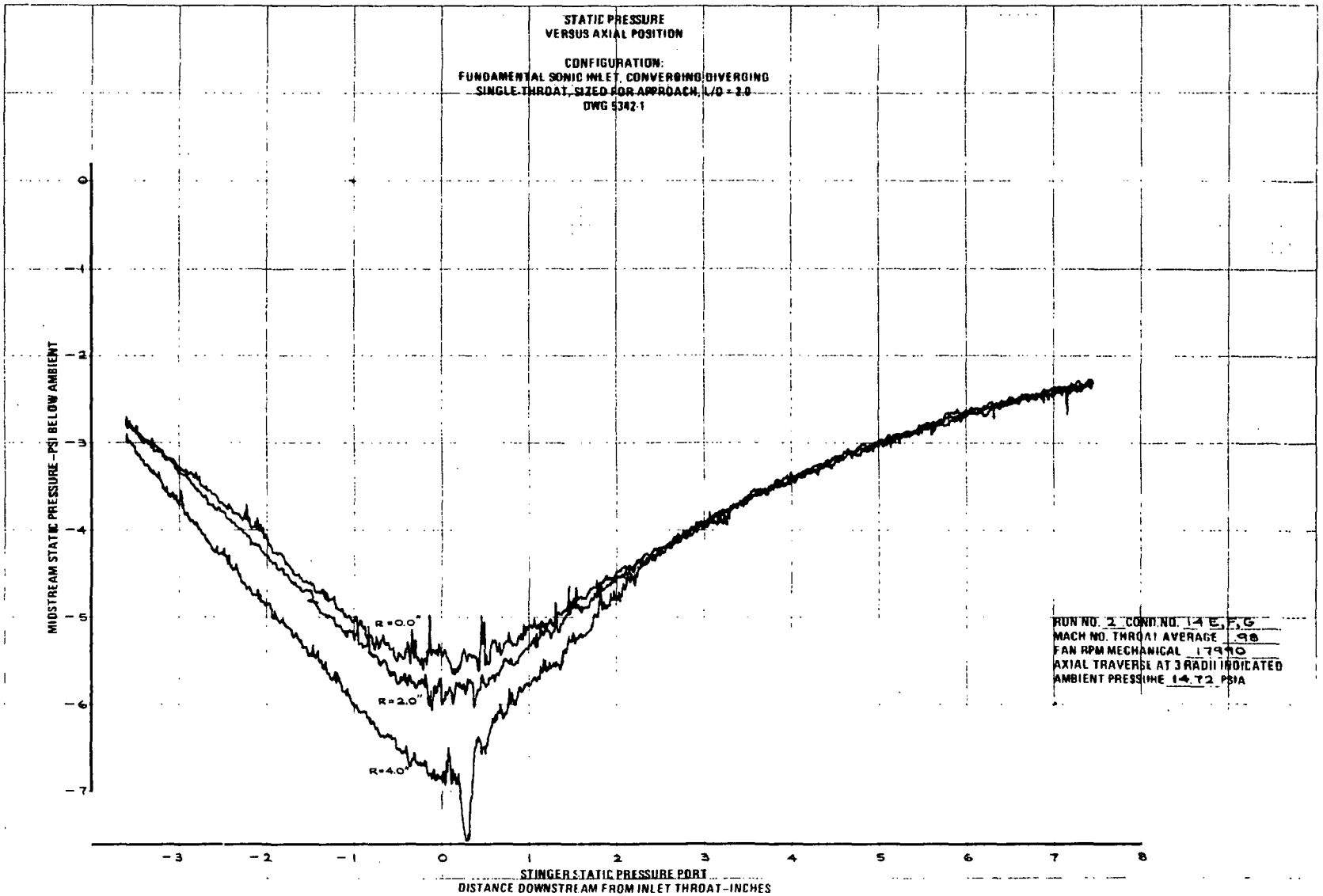

FIGURE B-40.—RUN 2-14 E,F,G, STATIC PRESSURE VS AXIAL POSITION AT 0.0, 2.0, AND 4.0 IN. FROM INLET CENTERLINE

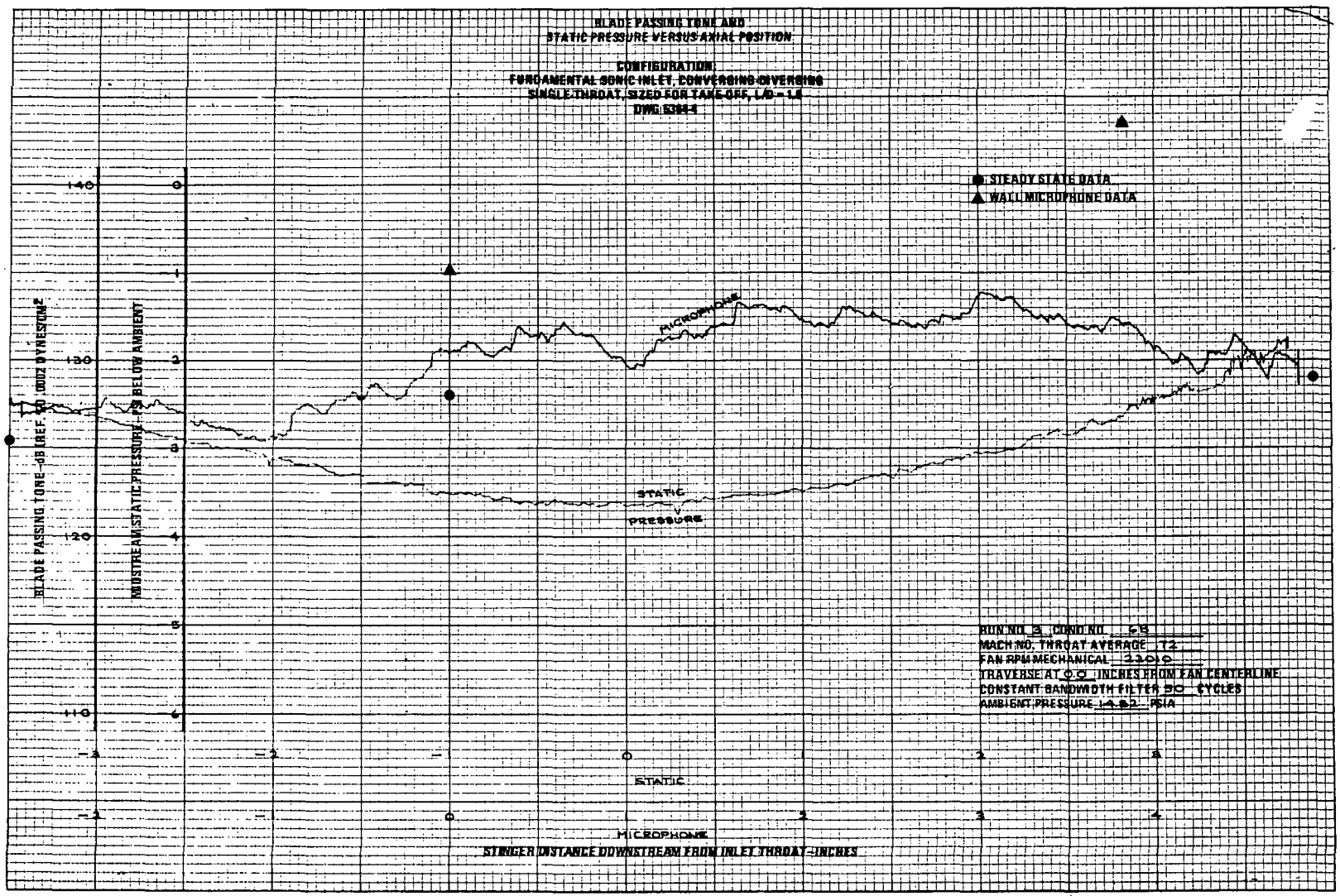

FIGURE B-41.—RUN 3-6B, BLADE PASSING TONE AND STATIC PRESSURE VS AXIAL DISTANCE AT 0.0 IN. FROM INLET CENTERLINE

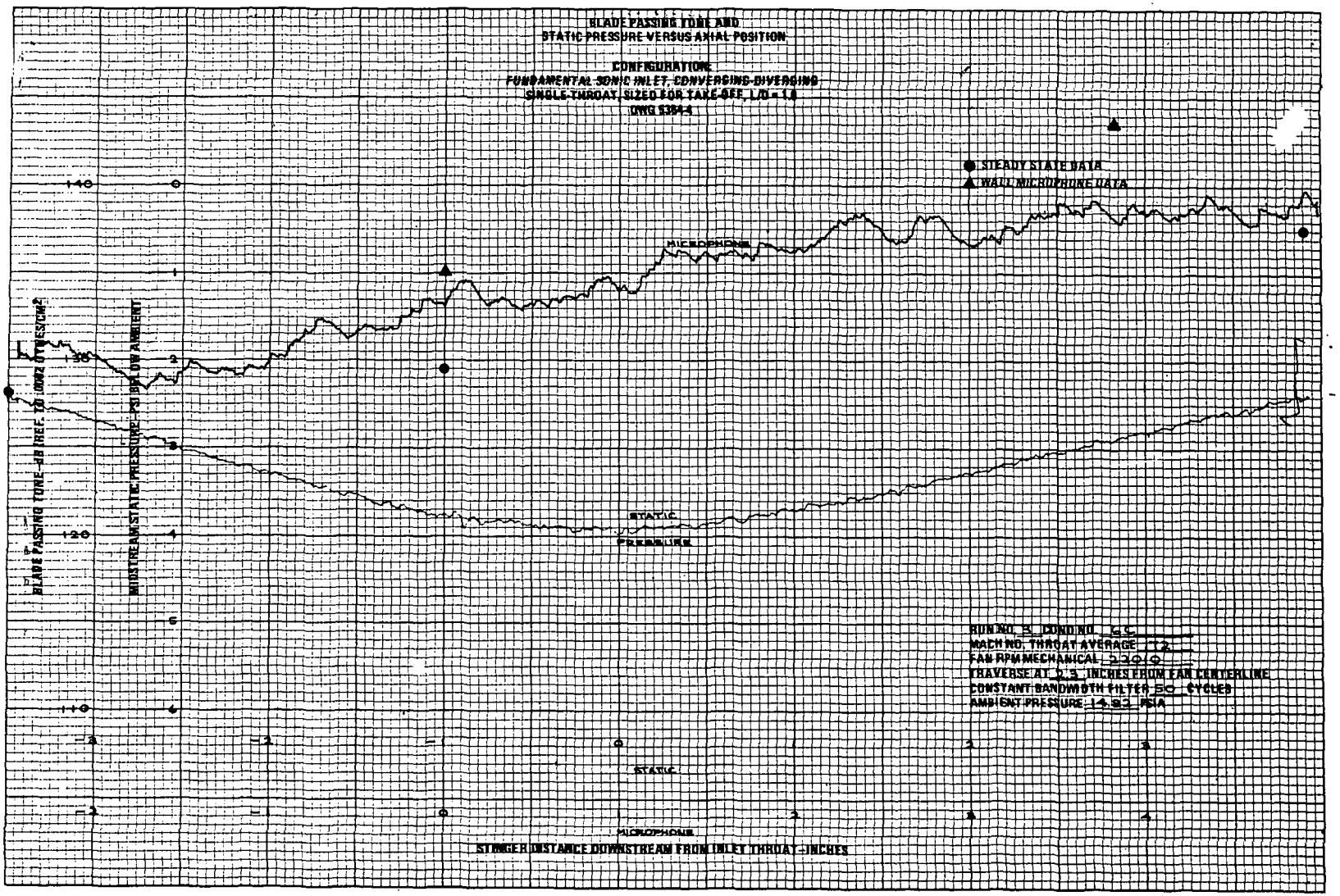

FIGURE B-42.—RUN 3-6C, BLADE PASSING TONE AND STATIC PRESSURE VS AXIAL DISTANCE AT 2.3 IN. FROM INLET CENTERLINE

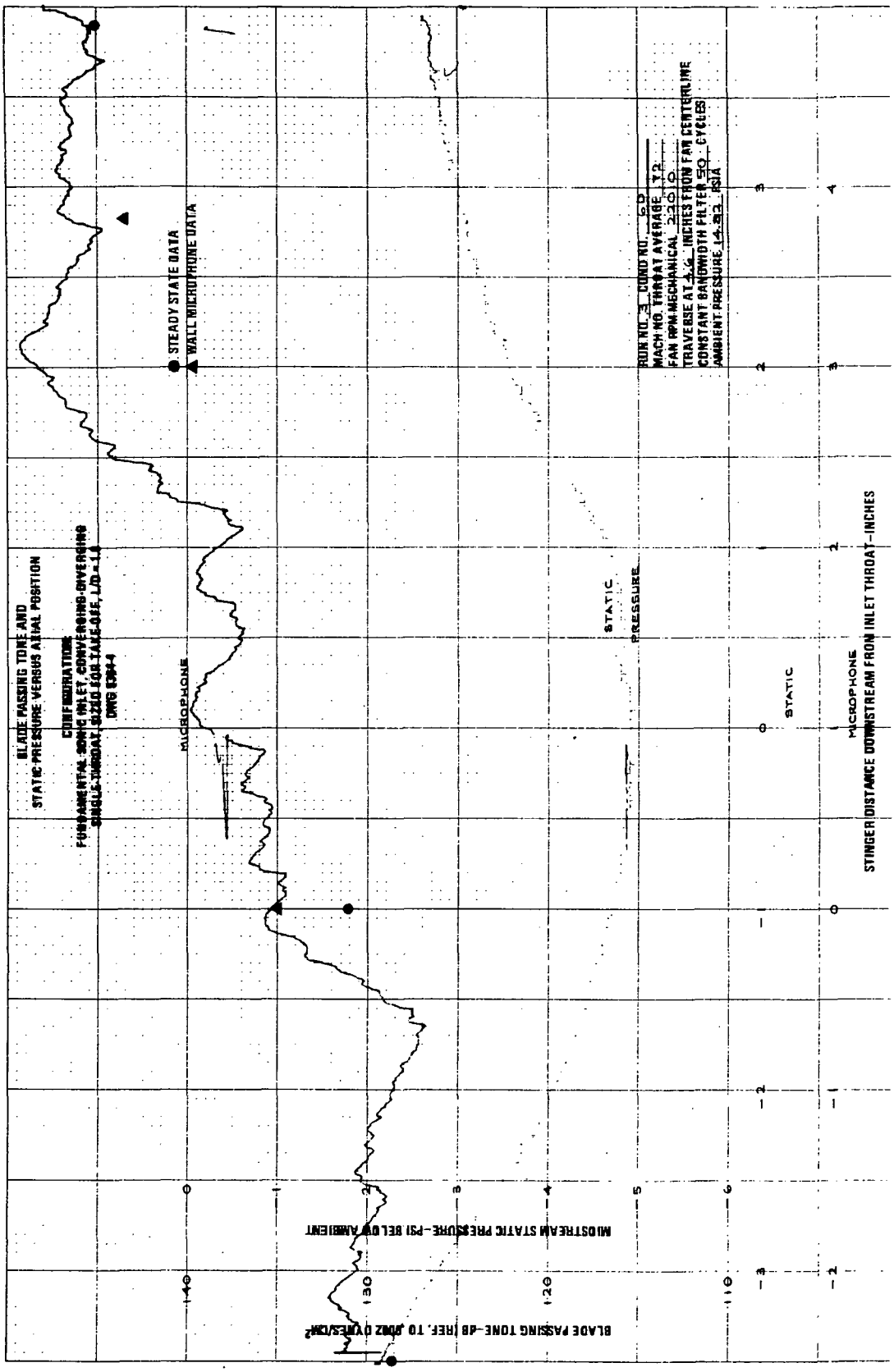

FIGURE B-43.—RUN 3-6D, BLADE PASSING TONE AND STATIC PRESSURE VS AXIAL DISTANCE AT 4.6 IN. FROM INLET CENTERLINE

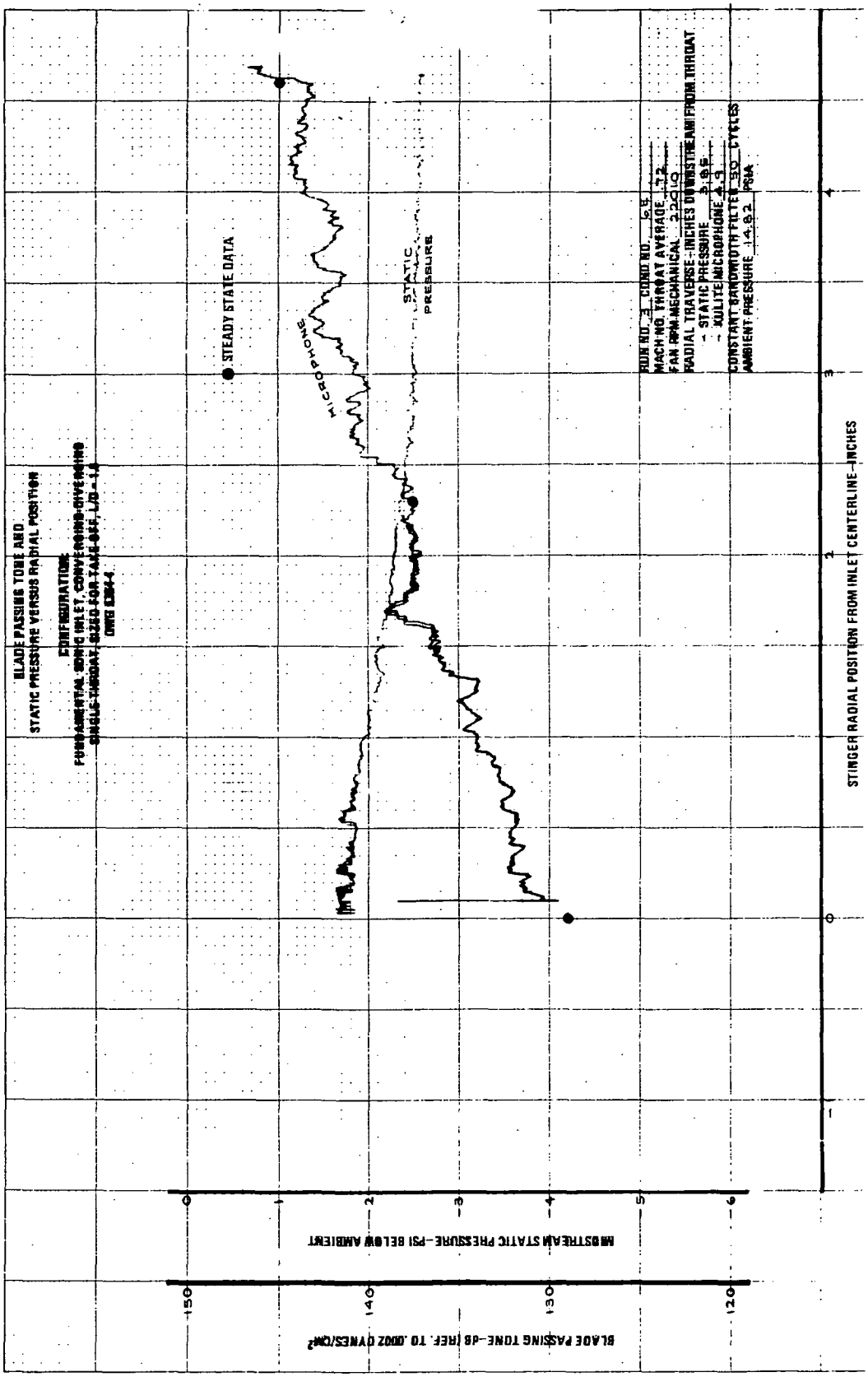

FIGURE B-44.—RUN 3-6E, BLADE PASSING TONE AND STATIC PRESSURE VS RADIAL POSITION AT 4.9 IN. DOWNSTREAM FROM INLET THROAT

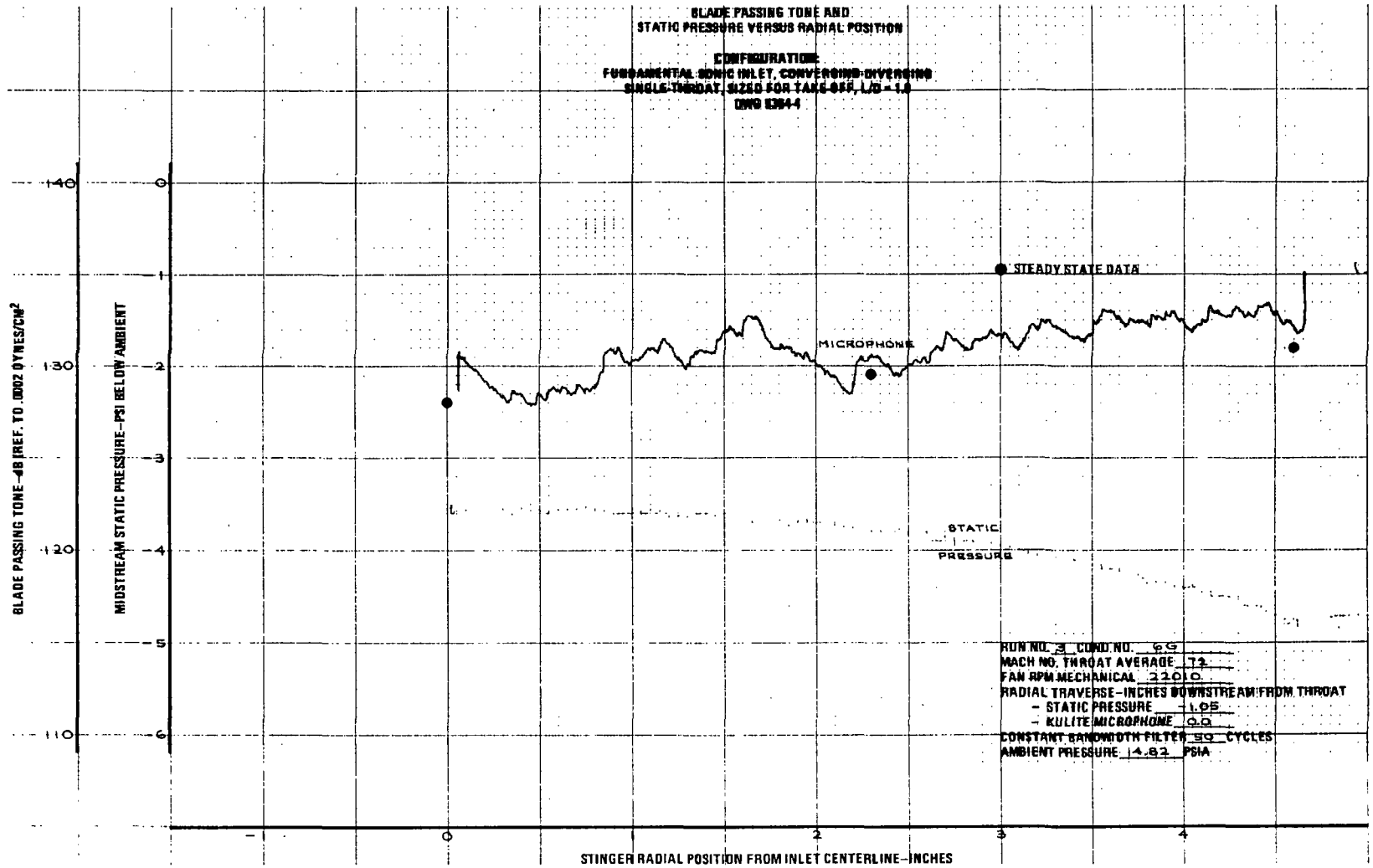

FIGURE B-45.—RUN 3-6G, BLADE PASSING TONE AND STATIC PRESSURE VS RADIAL POSITION AT 0.0 IN. DOWNSTREAM FROM INLET THROAT

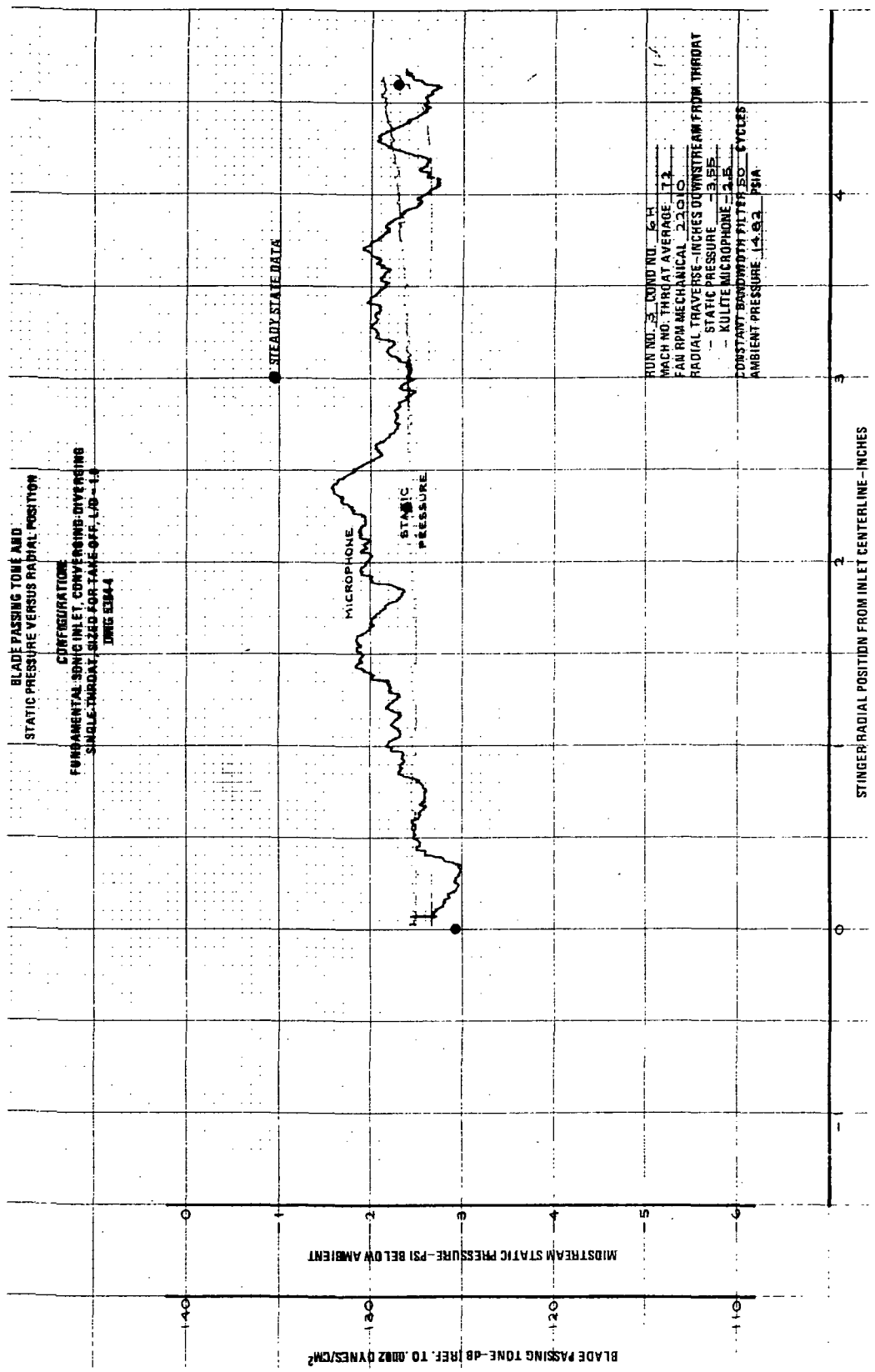

FIGURE B-46.—RUN 3-6H, BLADE PASSING TONE AND STATIC PRESSURE VS RADIAL POSITION AT -2.5 IN. DOWNSTREAM FROM INLET THROAT

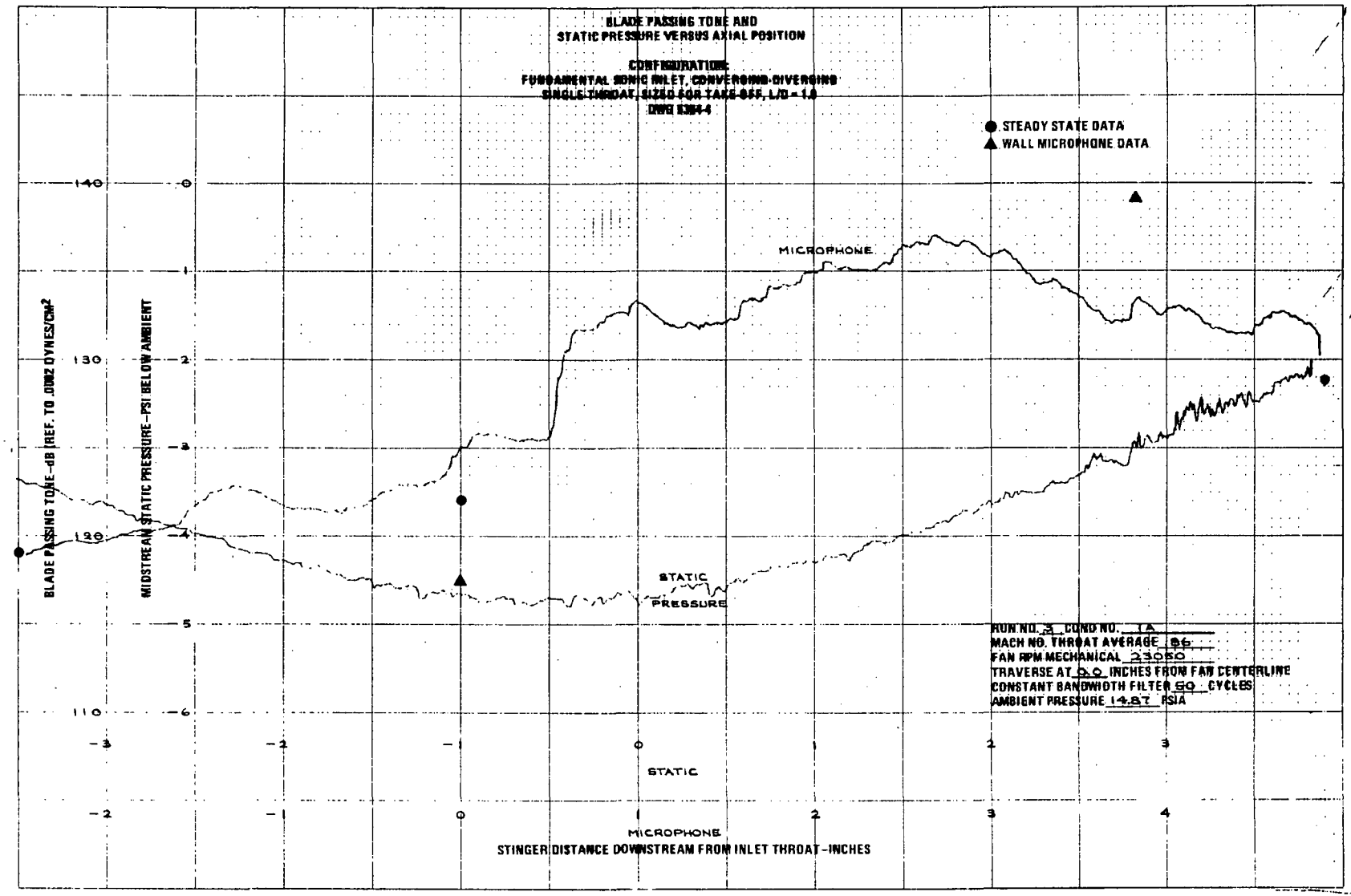

FIGURE B-47.—RUN 3-7A, BLADE PASSING TONE AND STATIC PRESSURE VS AXIAL POSITION AT 0.0 IN. FROM INLET CENTERLINE

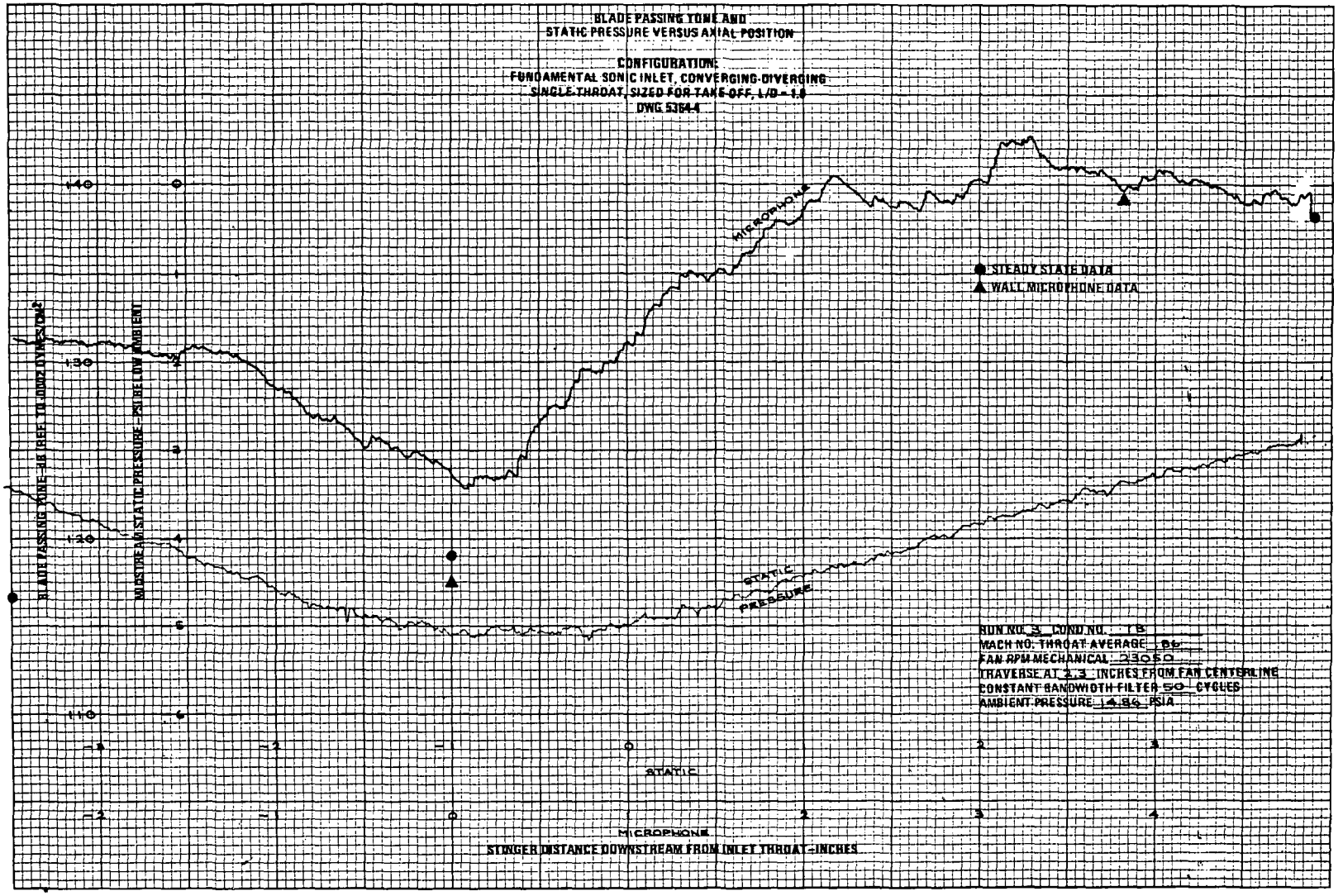

FIGURE B48.—RUN 3-7B, BLADE PASSING TONE AND STATIC PRESSURE VERSUS AXIAL POSITION AT 2.3 INCHES FROM INLET CENTERLINE

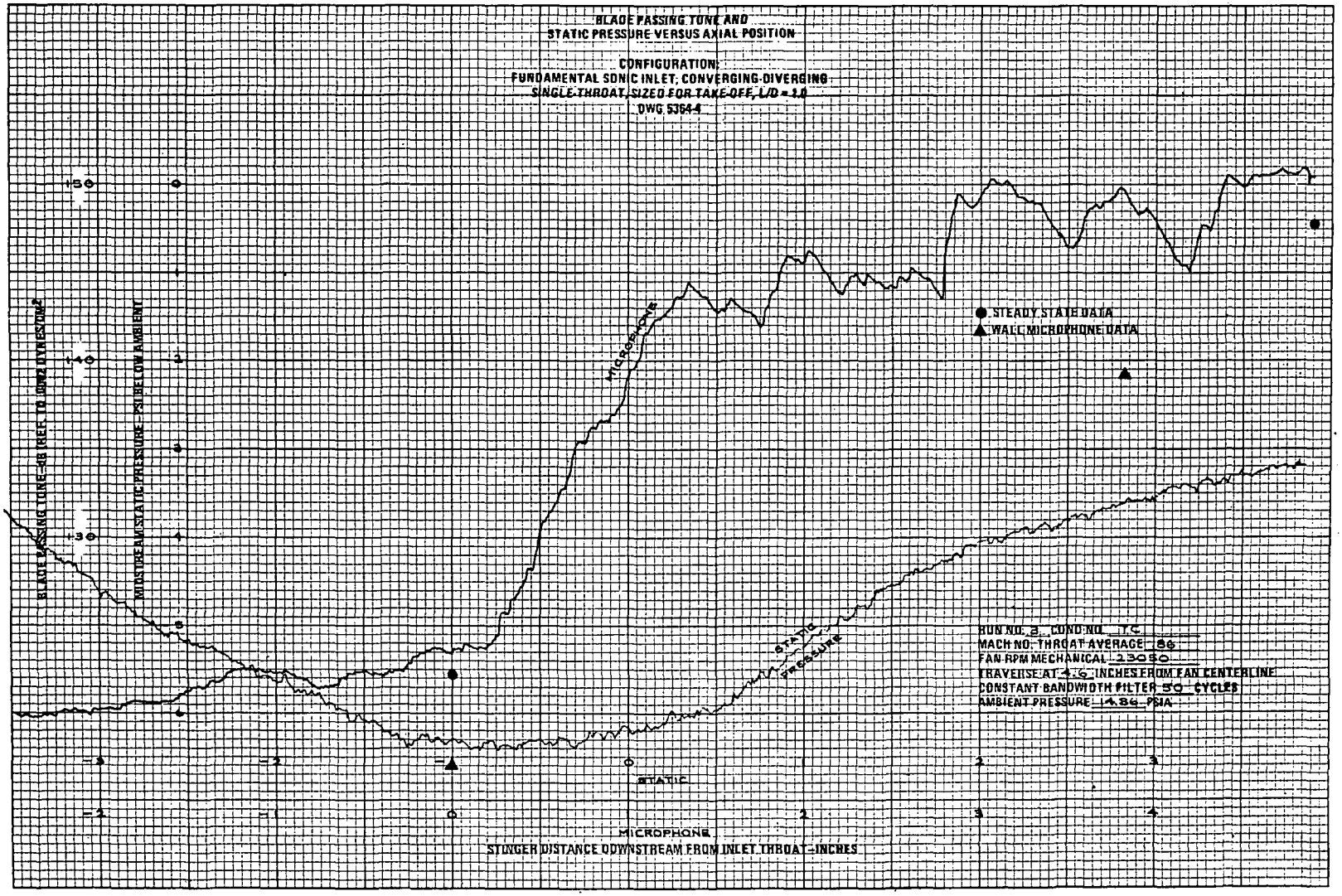

FIGURE B-49.—RUN 3-7C, BLADE PASSING TONE AND STATIC PRESSURE VS AXIAL POSITION AT 4.6 IN. FROM INLET CENTERLINE

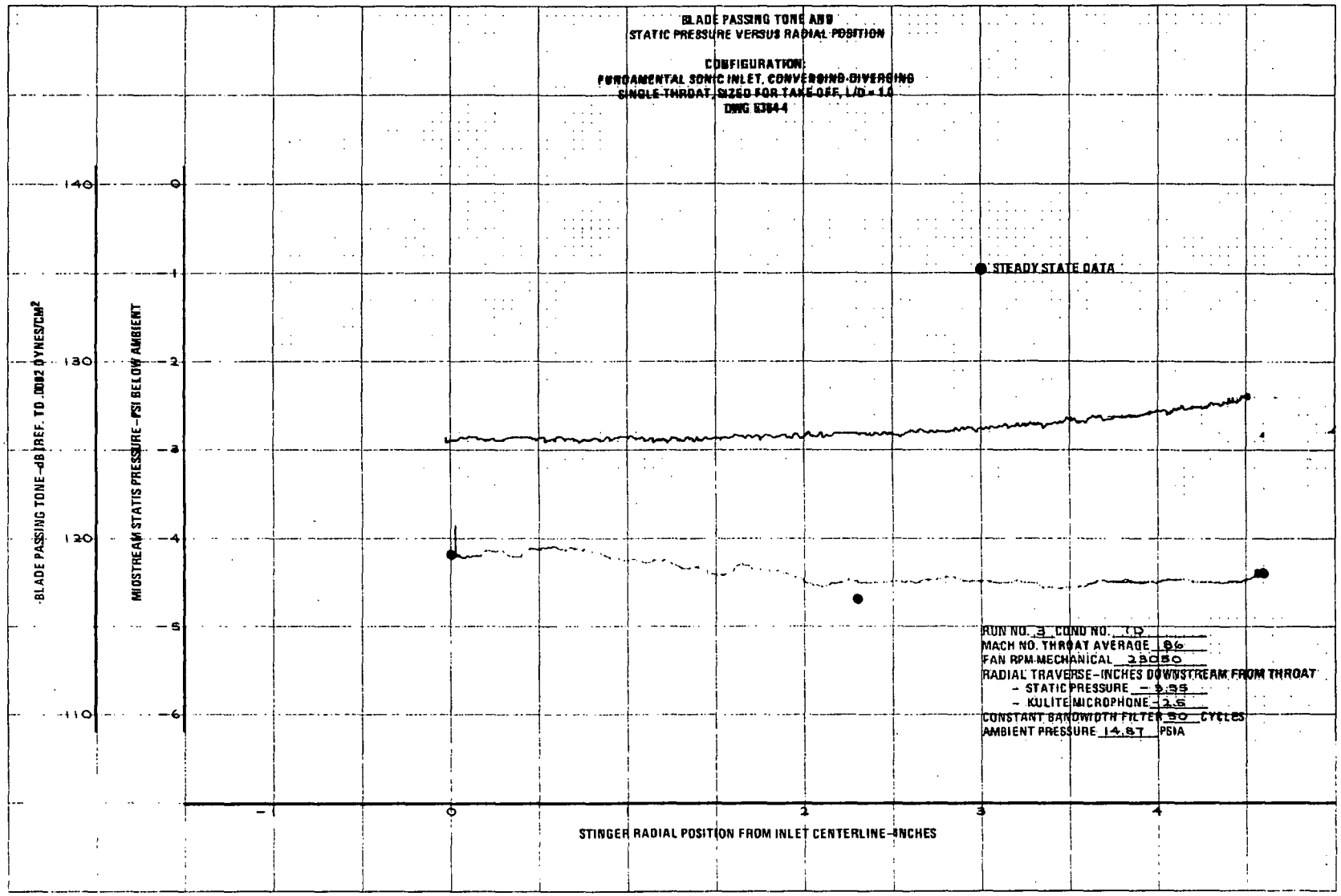

FIGURE B-50.—RUN 3-7D, BLADE PASSING TONE AND STATIC PRESSURE VS RADIAL POSITION AT -2.5 IN. DOWNSTREAM FROM INLET THROAT

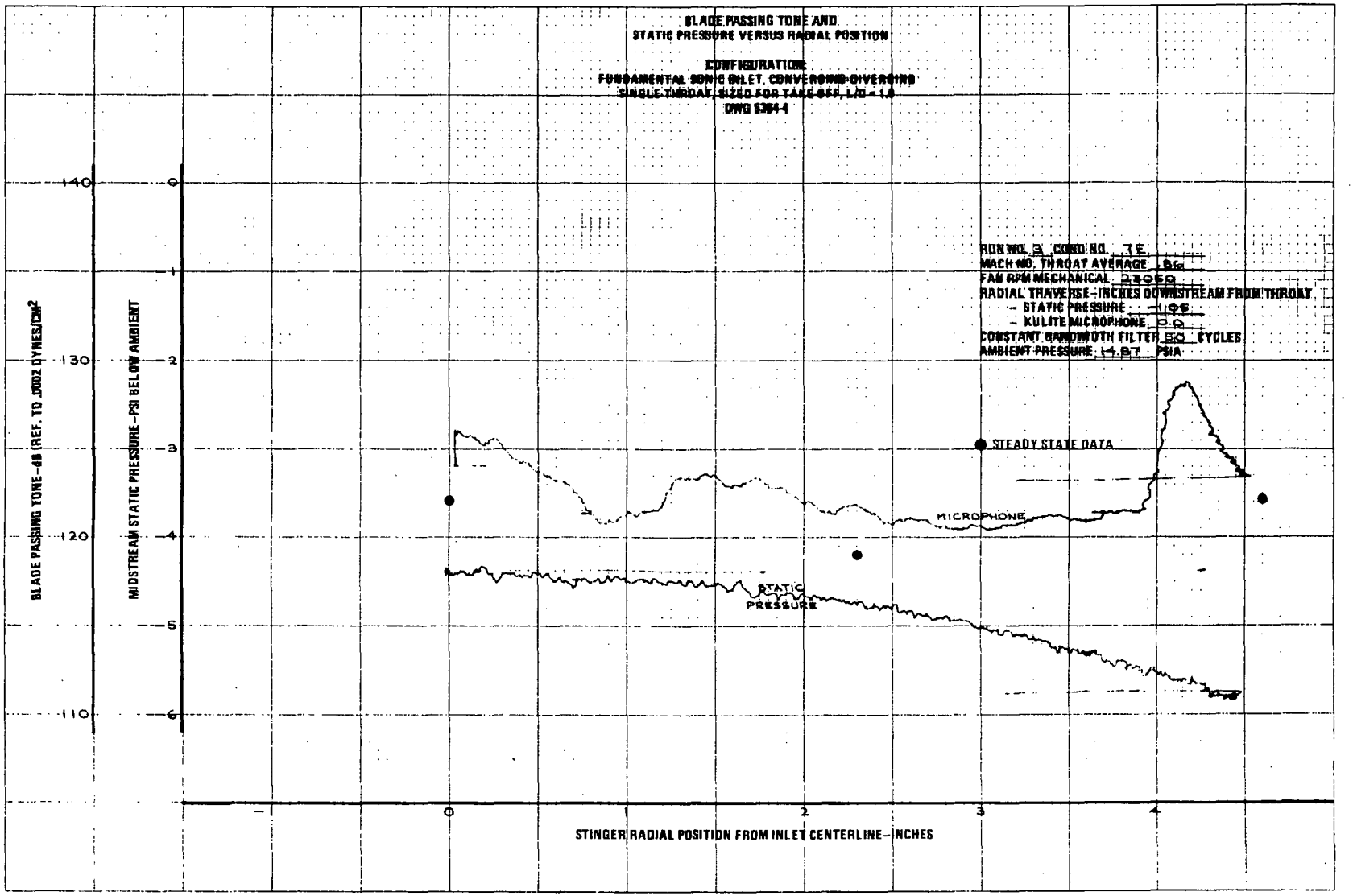

FIGURE B-51.—RUN 3-7E, BLADE PASSING TONE AND STATIC PRESSURE VS RADIAL POSITION AT 0.0 IN. DOWNSTREAM FROM INLET THROAT

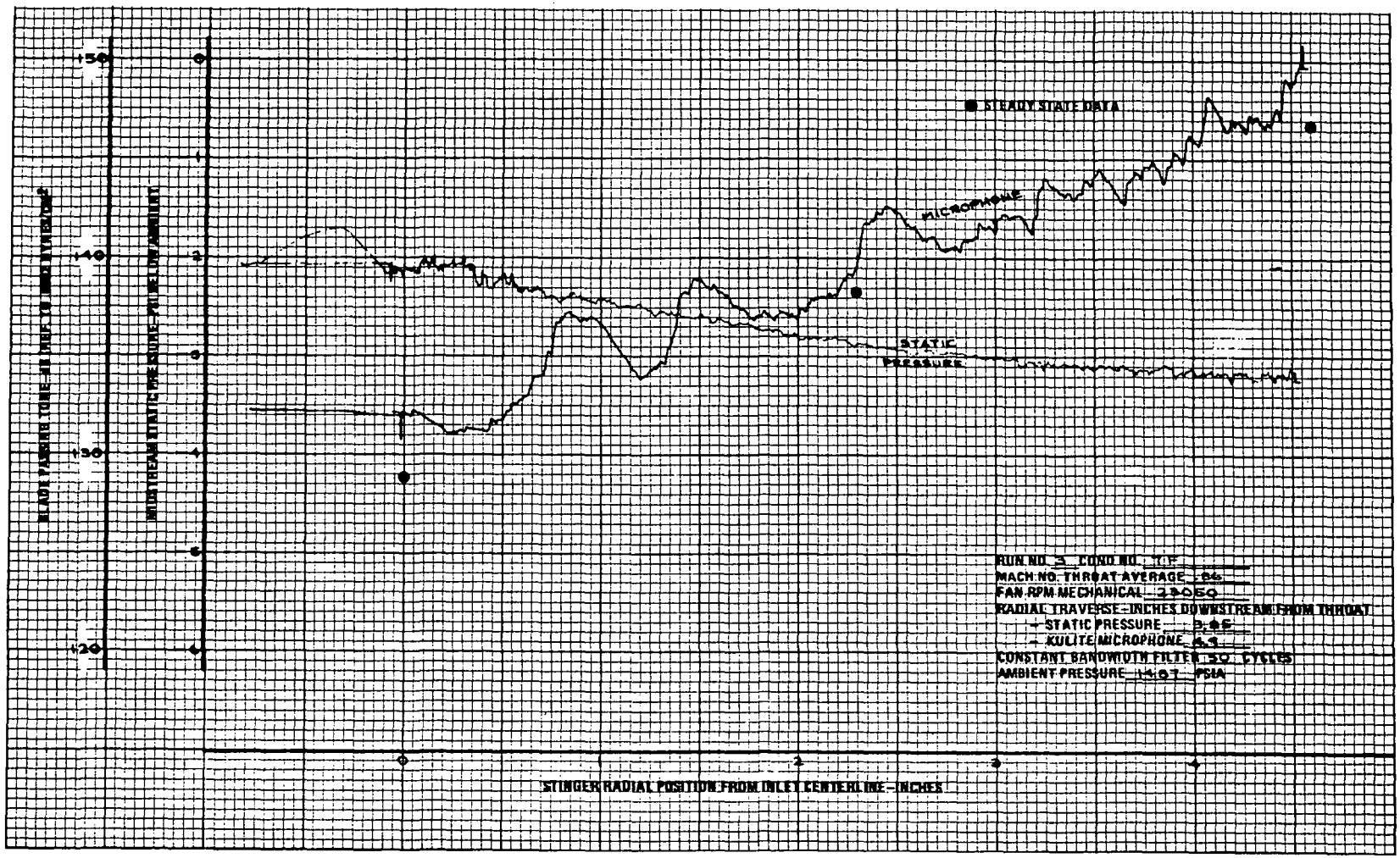

FIGURE B-52.—RUN 3-7F, BLADE PASSING TONE AND STATIC PRESSURE VS RADIAL POSITION AT 4.9 IN. DOWNSTREAM FROM INLET THROAT

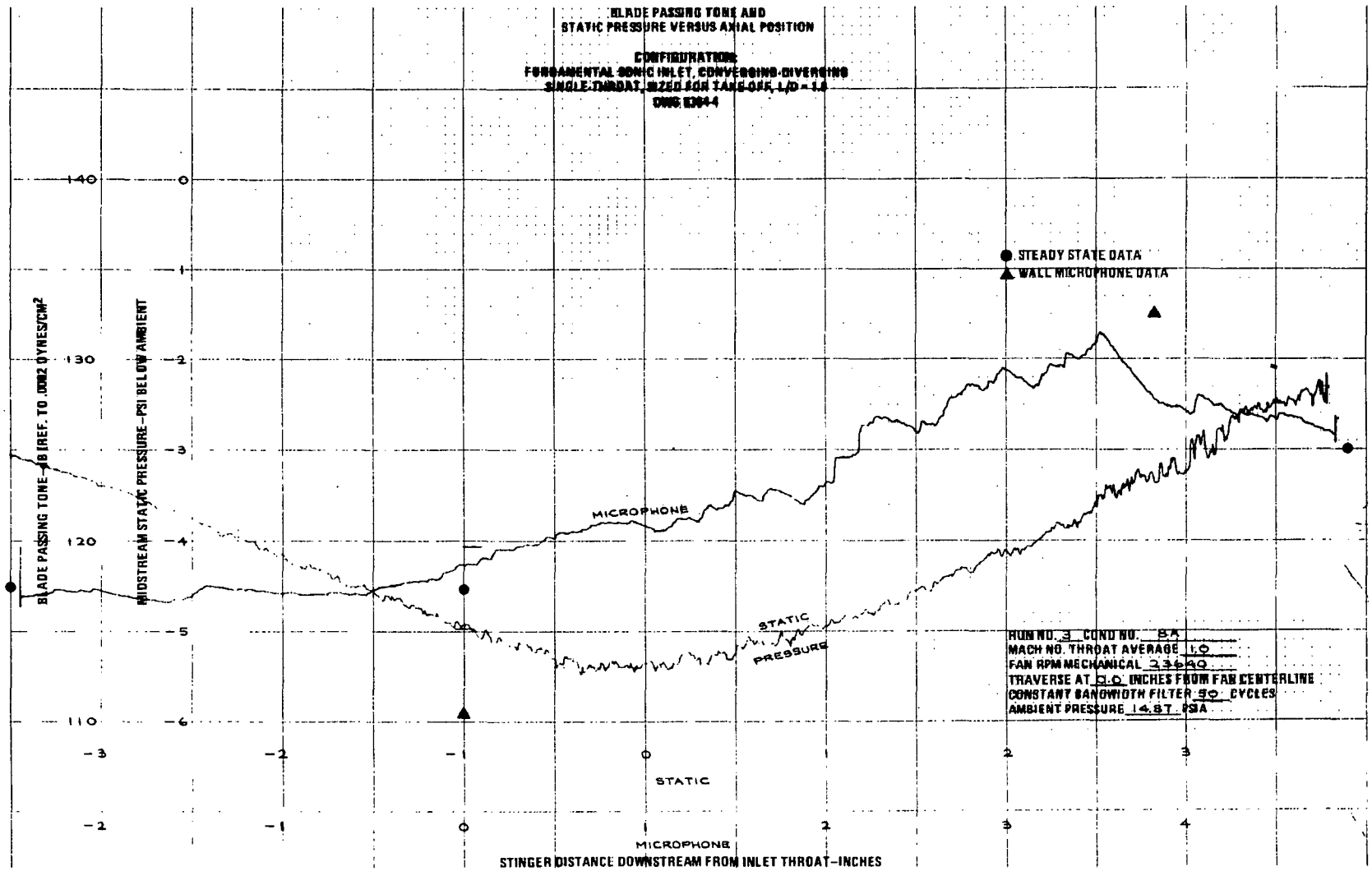

FIGURE B-53.—RUN 3-8A, BLADE PASSING TONE AND STATIC PRESSURE VS AXIAL DISTANCE AT 0.0 IN. FROM INLET CENTERLINE

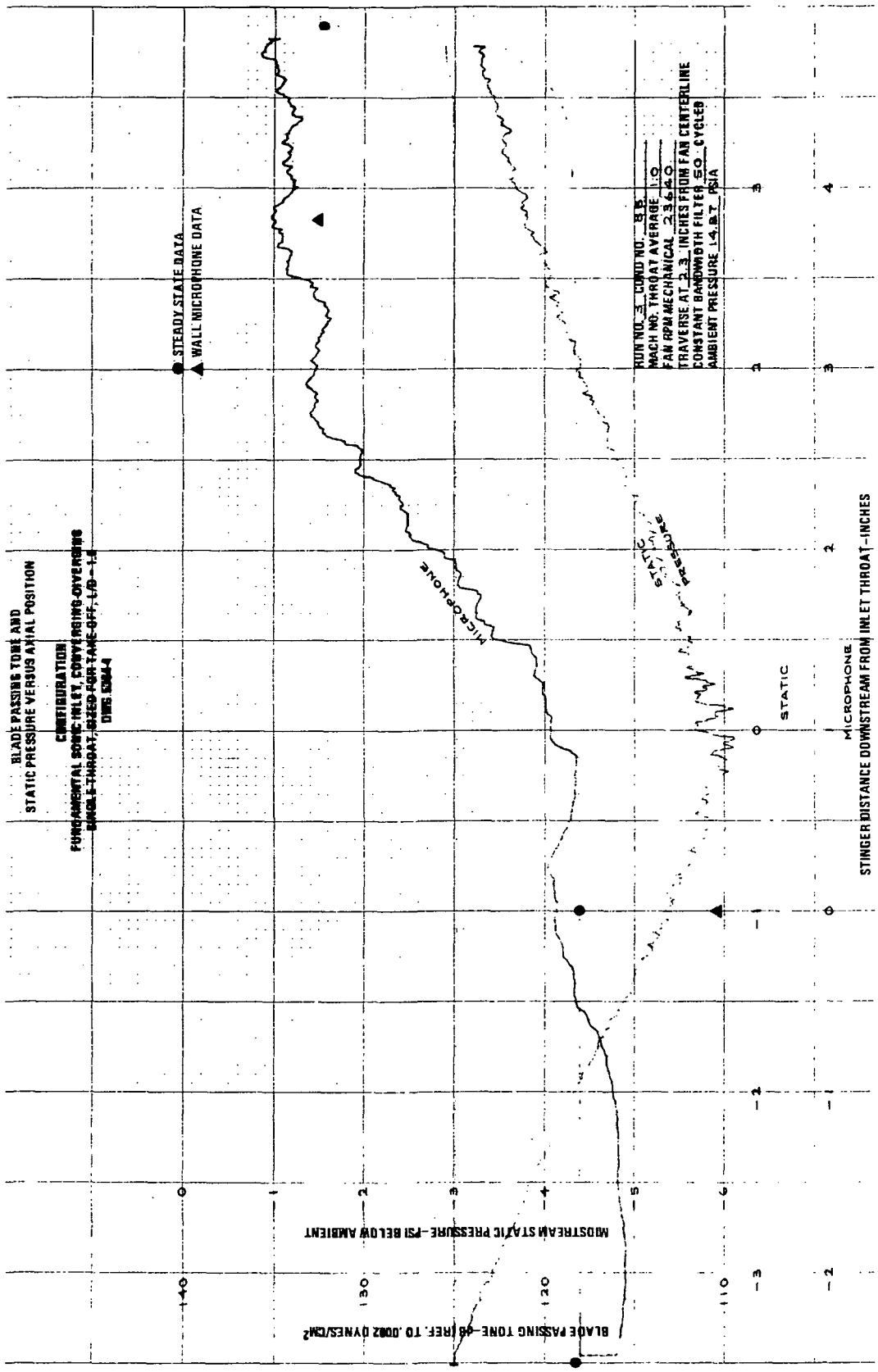

FIGURE B-54.–RUN 3-8B, BLADE PASSING TONE AND STATIC PRESSURE VS AXIAL DISTANCE AT 2.3 IN. FROM INLET CENTERLINE

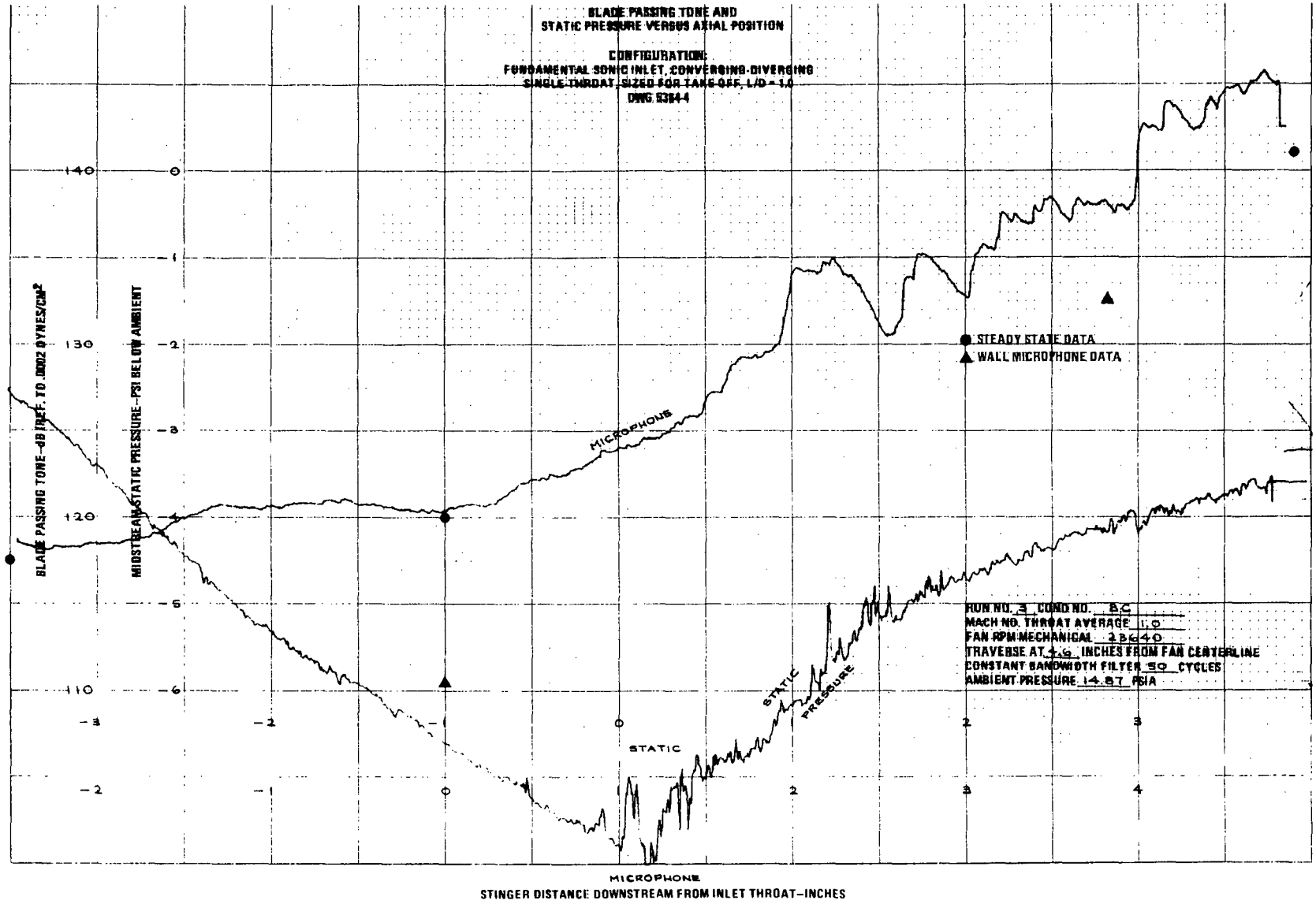

FIGURE B-55.—RUN 3-8C, BLADE PASSING TONE AND STATIC PRESSURE VS AXIAL DISTANCE AT 4.6 IN. FROM INLET CENTERLINE

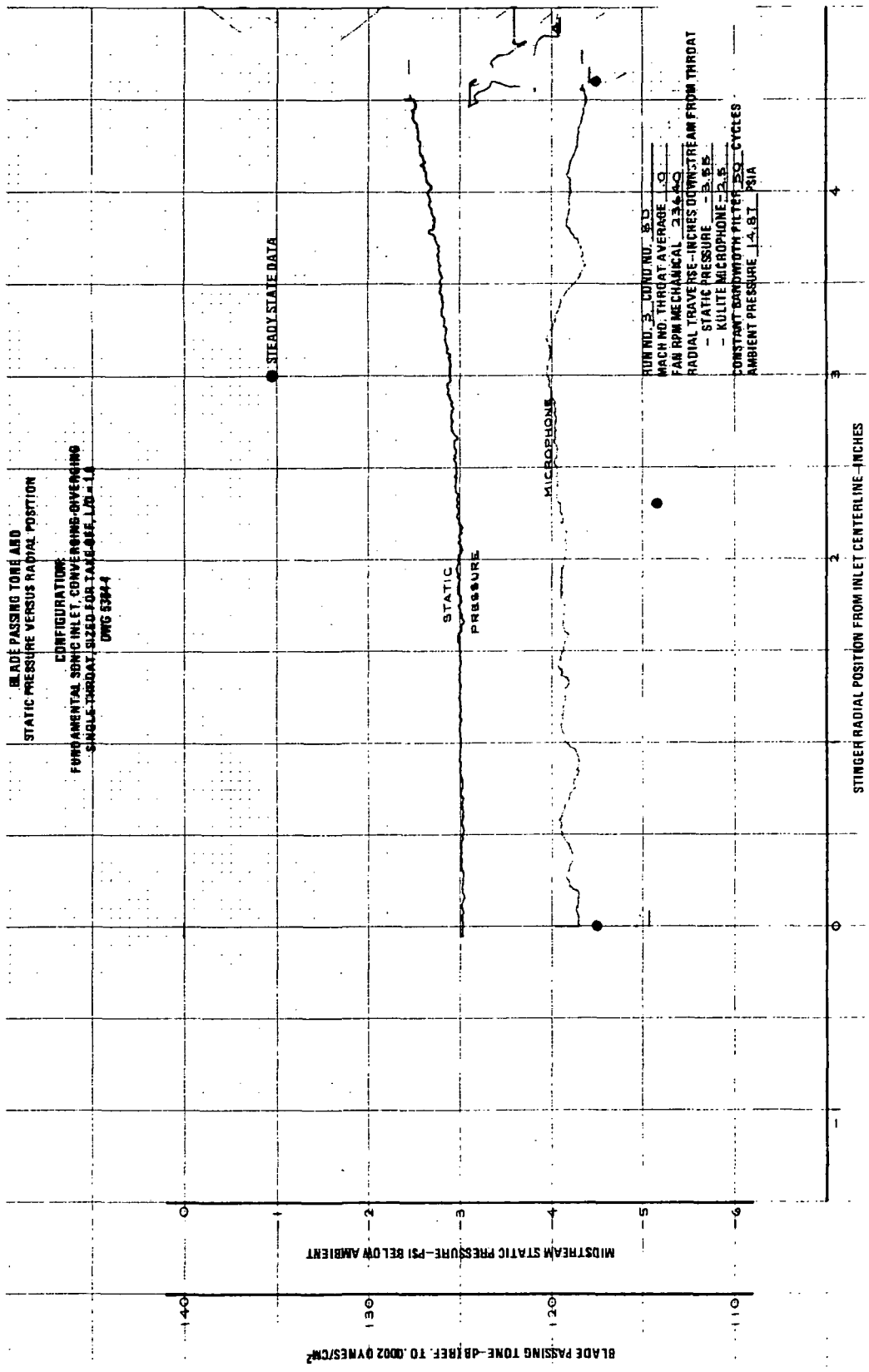

FIGURE B-56.—RUN 3-8D, BLADE PASSING TONE AND STATIC PRESSURE VS RADIAL POSITION AT -2.5 IN. DOWNSTREAM FROM INLET CENTERLINE

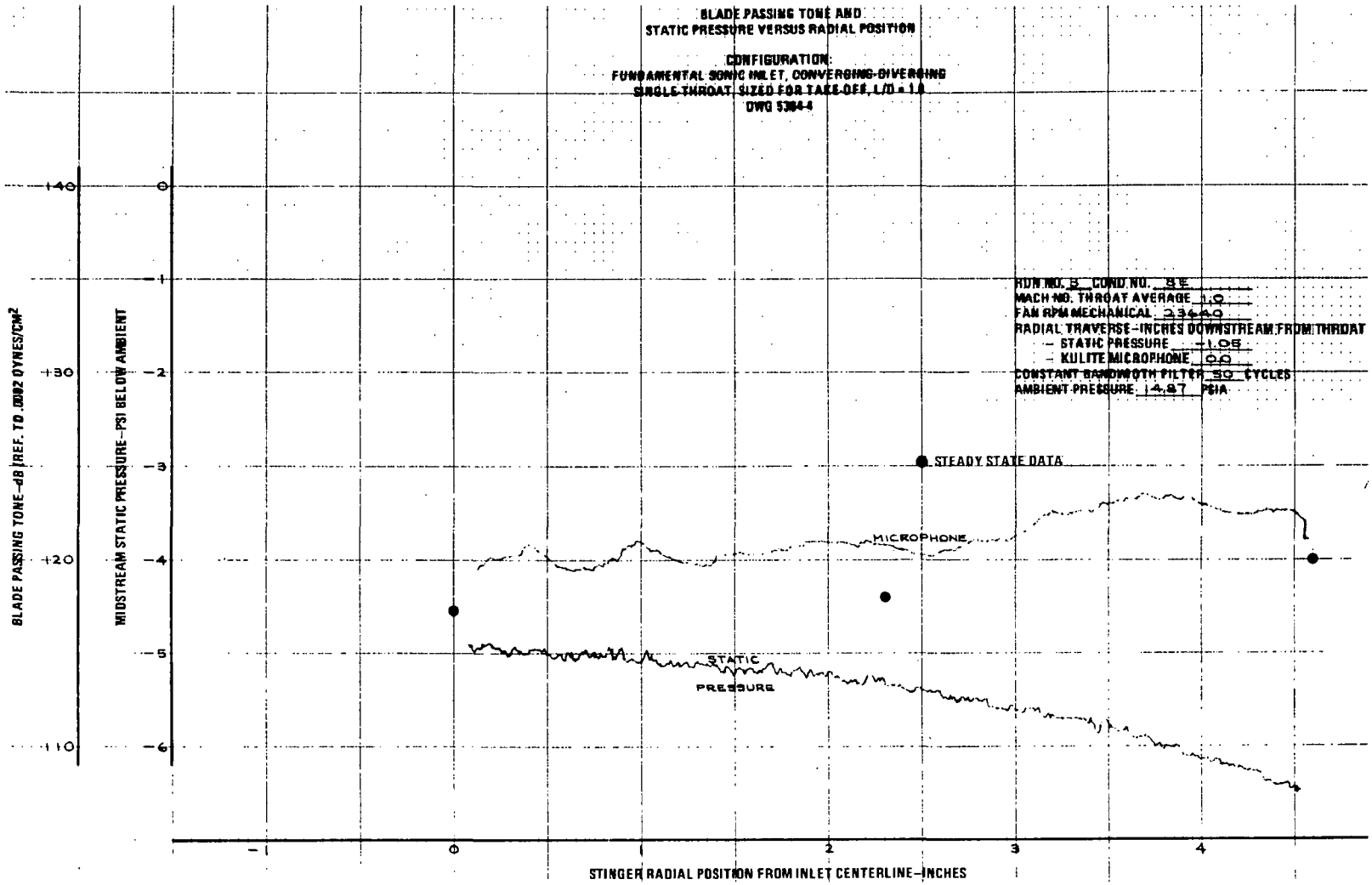

FIGURE B-57.—RUN 3-8E, BLADE PASSING TONE AND STATIC PRESSURE VS RADIAL POSITION AT 0.0 IN. DOWNSTREAM FROM INLET THROAT

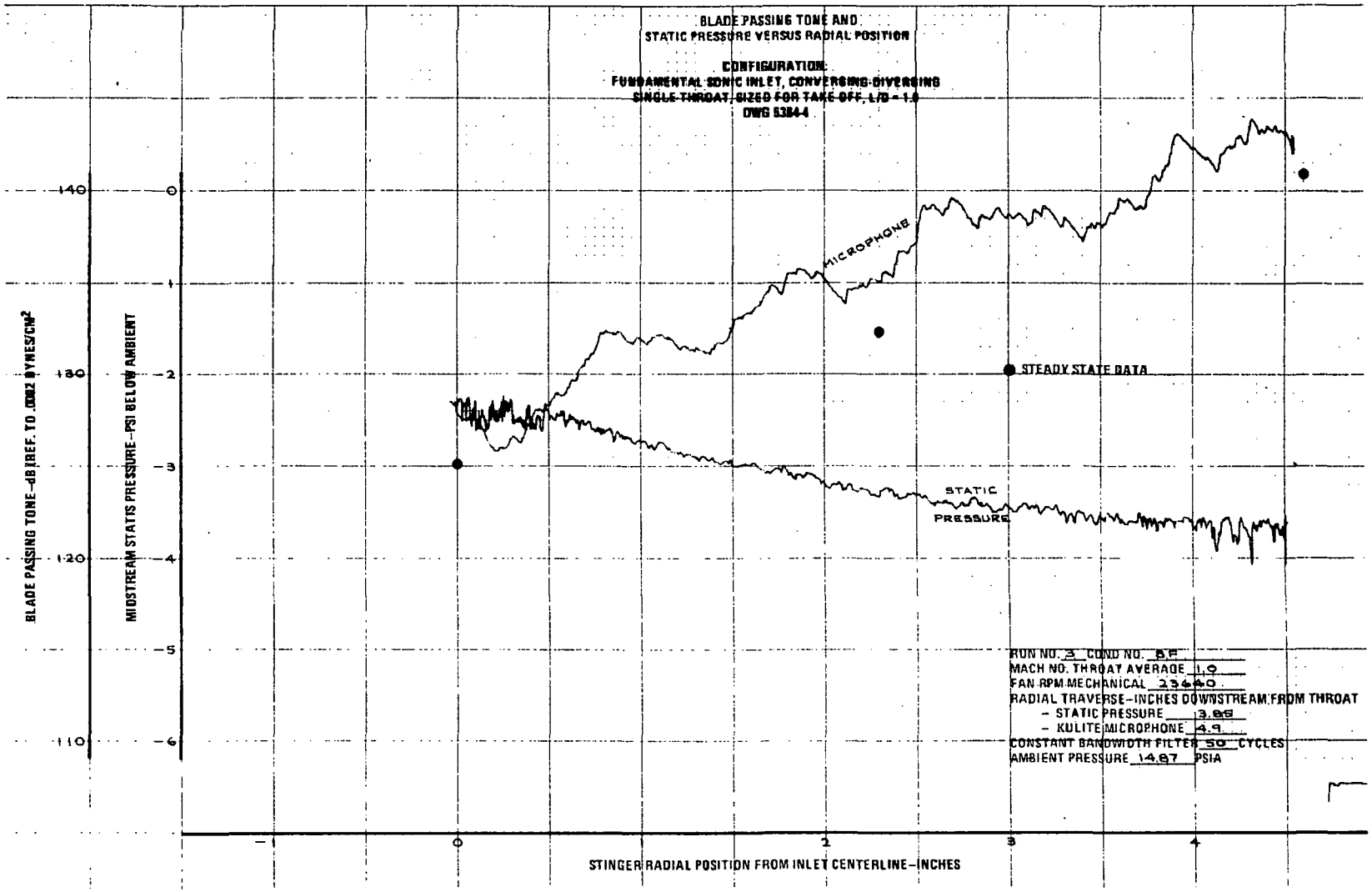

FIGURE B-58.—RUN 3-8F, BLADE PASSING TONE AND STATIC PRESSURE VS RADIAL POSITION AT 4.9 IN. DOWNSTREAM FROM INLET THROAT

APPENDIX C

FREESTREAM STATIC PRESSURE TIME HISTORIES AT DIFFERENT POSITIONS IN THE TWO SONIC INLETS

This appendix contains all steady-state, freestream static pressure data taken with the stinger probe in the two sonic inlets.

The freestream static pressure data are presented versus time.

For easy reference, the data are presented according to run number, as listed below.

Figure	Run	Title
C-1	2-10 A, B	Freestream Static Pressure Time History at -3.65 and -1.05 In. Downstream From Inlet Throat on the Centerline
C-2	2-13A	Freestream Static Pressure Time History at -1.05 In. Downstream From Inlet Throat on the Centerline
C-3	2-14A	Freestream Static Pressure Time History at -1.05 In. Downstream From Inlet Throat on the Centerline
C-4	2-15 A, F, G, L	Freestream Static Pressure Time History at -3.65, -1.05, 2.95, and 7.45 In. Downstream From Inlet Throat on the Centerline
C-5	2-15 B, E, H, K	Freestream Static Pressure Time History at -3.65, -1.05, 2.95 and 7.45 In. Downstream From Inlet Throat and 2.0 In. From Inlet Centerline
C-6	2-15 C, D, I, J	Freestream Static Pressure Time History at -3.65, -1.05, 2.95, and 7.45 In. Downstream From Inlet Throat and 4.0 In. From Inlet Centerline
C-7	3-6 I, J, K	Freestream Static Pressure Time History at -3.55 In. Downstream From Inlet Throat and 0.0, 2.3, and 4.6 In. From Inlet Centerline
C-8	3-6 L, M, N	Freestream Static Pressure Time History at -1.05 In. Downstream From Inlet Throat and 0.0, 2.3, and 4.6 In. From Inlet Centerline
C-9	3-6 O, P, Q	Freestream Static Pressure Time History at 3.85 In. Downstream From Inlet Throat and 0.0, 2.3, and 4.6 In. From Inlet Centerline
C-10	3-7 G, H, I	Freestream Static Pressure Time History at 3.85 In. Downstream From Inlet Throat and 0.0, 2.3, and 4.6 In. From Inlet Centerline
C-11	3-7 J, K, L	Freestream Static Pressure Time History at -1.05 In. Downstream From Inlet Throat and at 0.0, 2.3, and 4.6 In. From Inlet Centerline

Figure	Run	Title
C-12	3-7 M, N, O	Freestream Static Pressure Time History at -3.55 In. Downstream From Inlet Throat and 0.0, 2.3, and 4.6 In. From Inlet Centerline
C-13	3-8 G, H, I	Freestream Static Pressure Time History at 3.85 In. Downstream From Inlet Throat and 0.0, 2.3, and 4.6 In. From Inlet Centerline
C-14	3-8 J, K, L	Freestream Static Pressure Time History at -1.05 In. Downstream From Inlet Throat and 0.0, 2.3, and 4.6 In. From Inlet Centerline
C-15	3-8 M, N, O	Freestream Static Pressure Time History at -3.55 In. Downstream From Inlet Throat and 0.0, 2.3, and 4.6 In. From Inlet Centerline

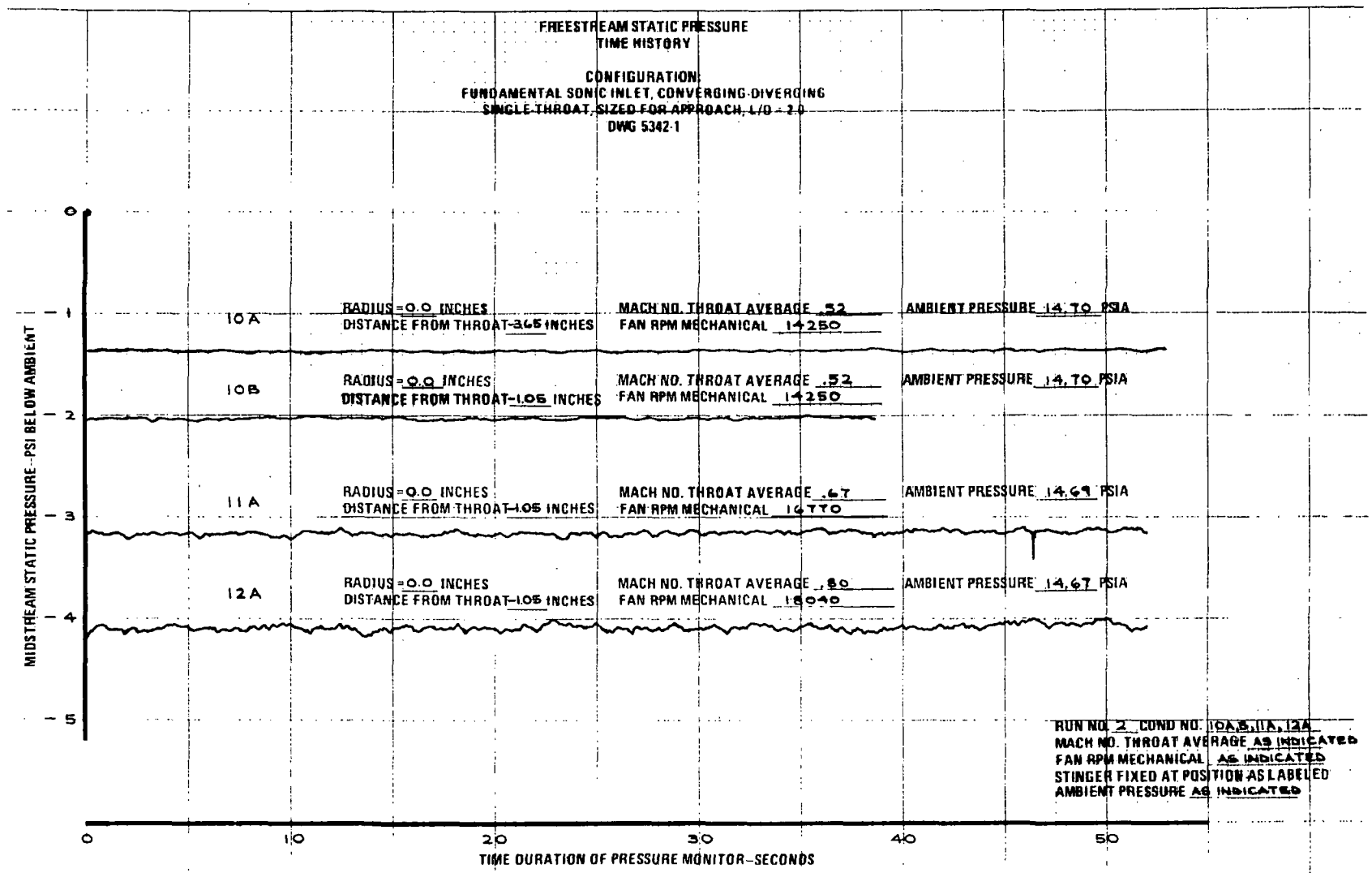

FIGURE C-1.—RUN 2-10 A,B, FREESTREAM STATIC PRESSURE TIME HISTORY AT -3.65 AND -1.05 IN. DOWNSTREAM FROM INLET THROAT ON THE CENTERLINE

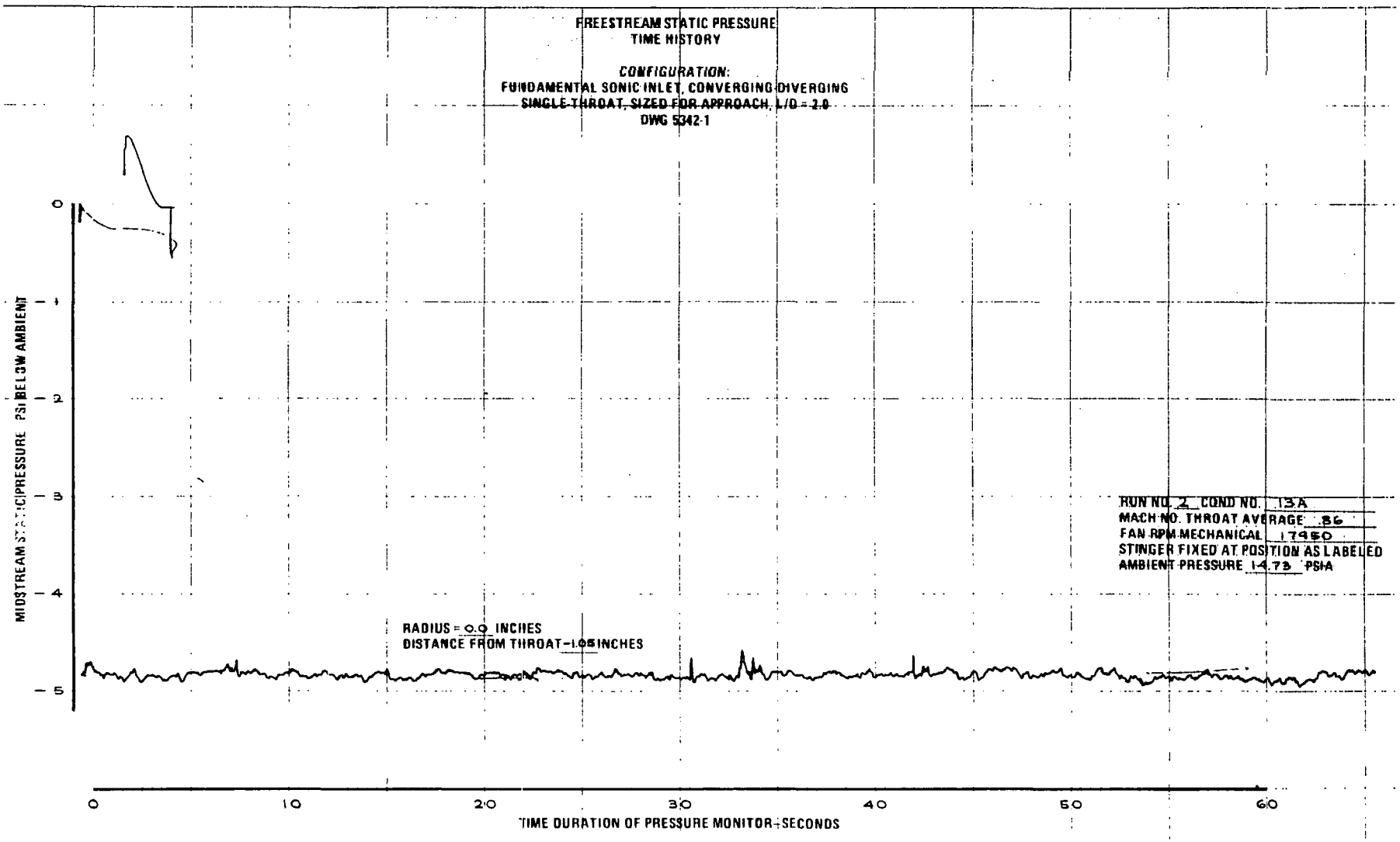

FIGURE C-2.—RUN 2-13A, FREESTREAM STATIC PRESSURE TIME HISTORY AT -1.05 IN. DOWNSTREAM FROM INLET THROAT ON THE CENTERLINE

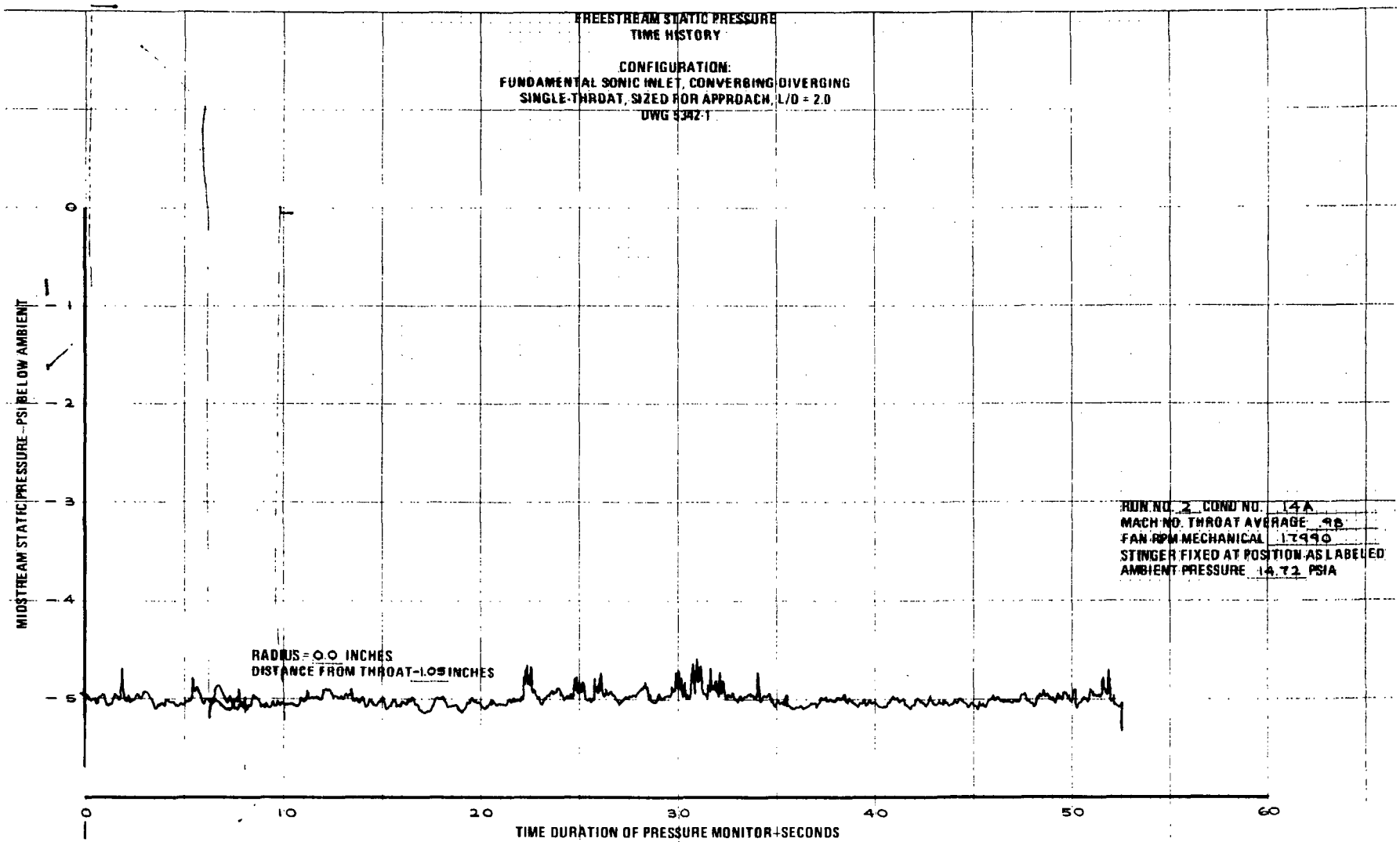

FIGURE C-3.—RUN 2-14A, FREESTREAM STATIC PRESSURE TIME HISTORY AT -1.05 IN. DOWNSTREAM FROM INLET THROAT ON THE CENTERLINE

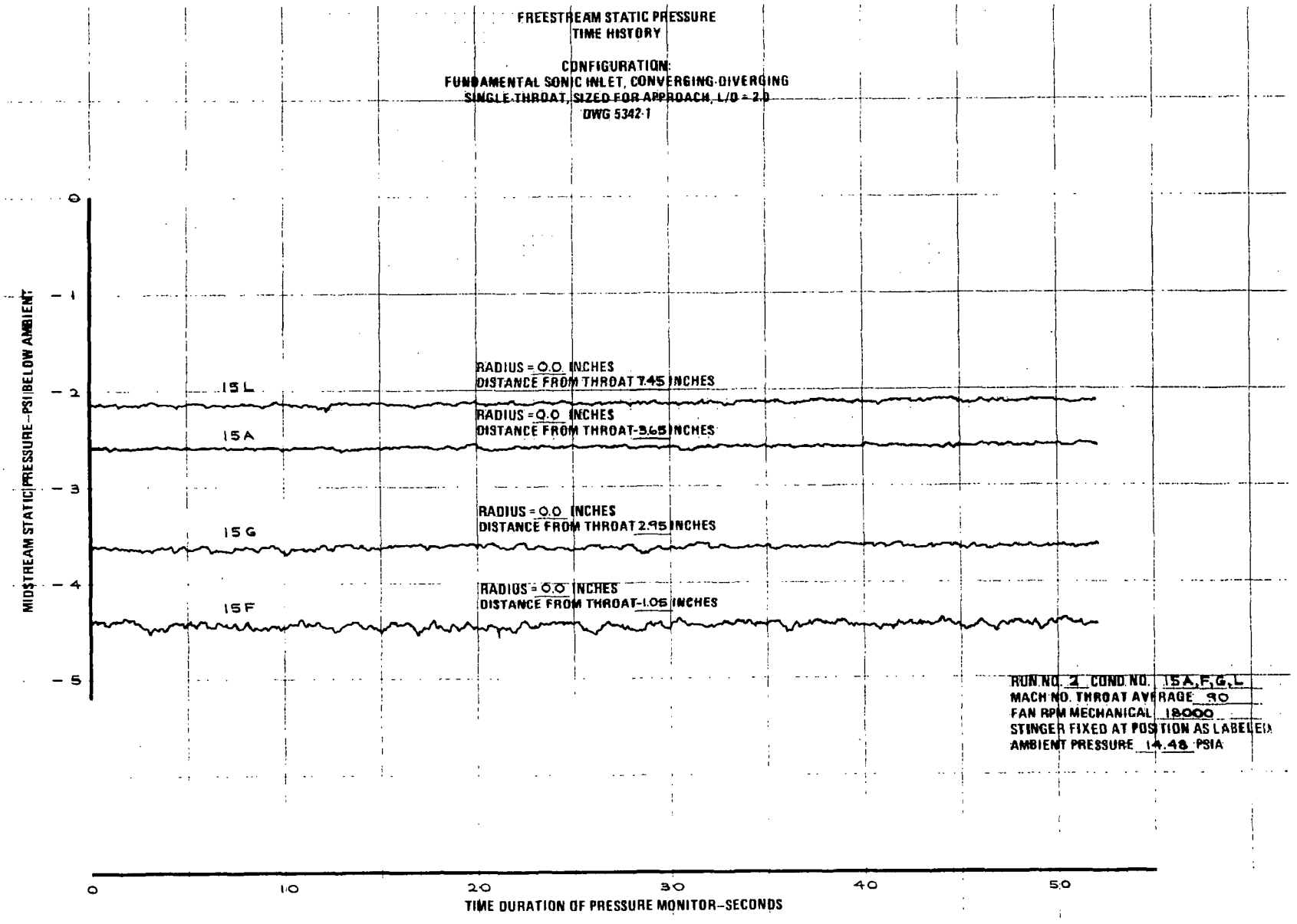

FIGURE C-4.—RUN 2-15 A,F,G,L, FREESTREAM STATIC PRESSURE TIME HISTORY AT -3.65, -1.05, 2.95, AND 7.45 IN. DOWNSTREAM FROM INLET THROAT ON THE CENTERLINE

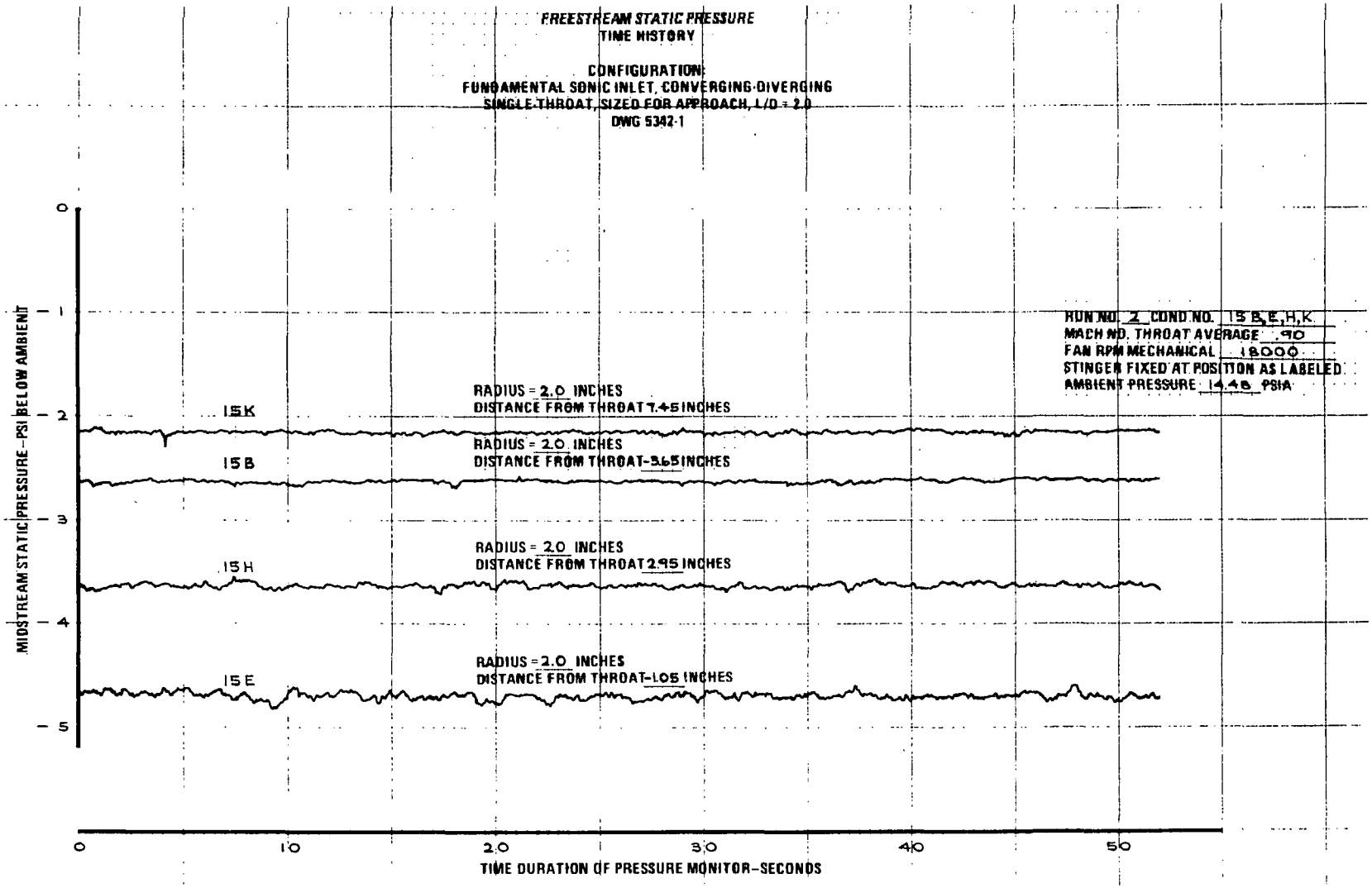

FIGURE C-5.—RUN 2-15 B,E,H,K, FREESTREAM STATIC PRESSURE TIME HISTORY AT -3.65, -1.05, 2.95, AND 7.45 IN. DOWNSTREAM FROM INLET THROAT AND 2.0 IN. FROM INLET CENTERLINE

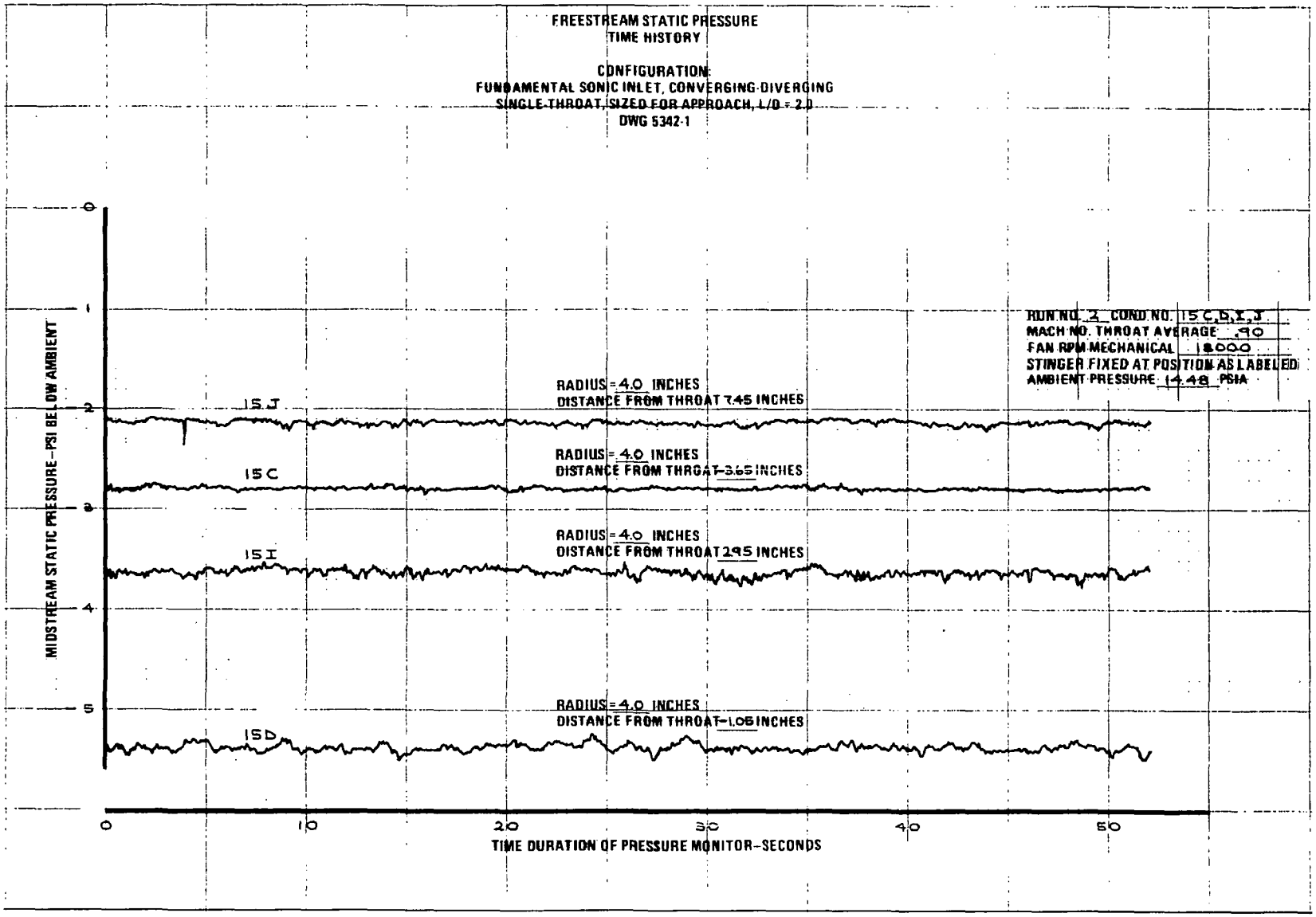

FIGURE C-6.—RUN 2-15 C,D,I,J, FREESTREAM STATIC PRESSURE TIME HISTORY AT -3.65, -1.05, 2.95, AND 7.45 IN. DOWNSTREAM FROM INLET THROAT AND 4.0 IN. FROM INLET CENTERLINE

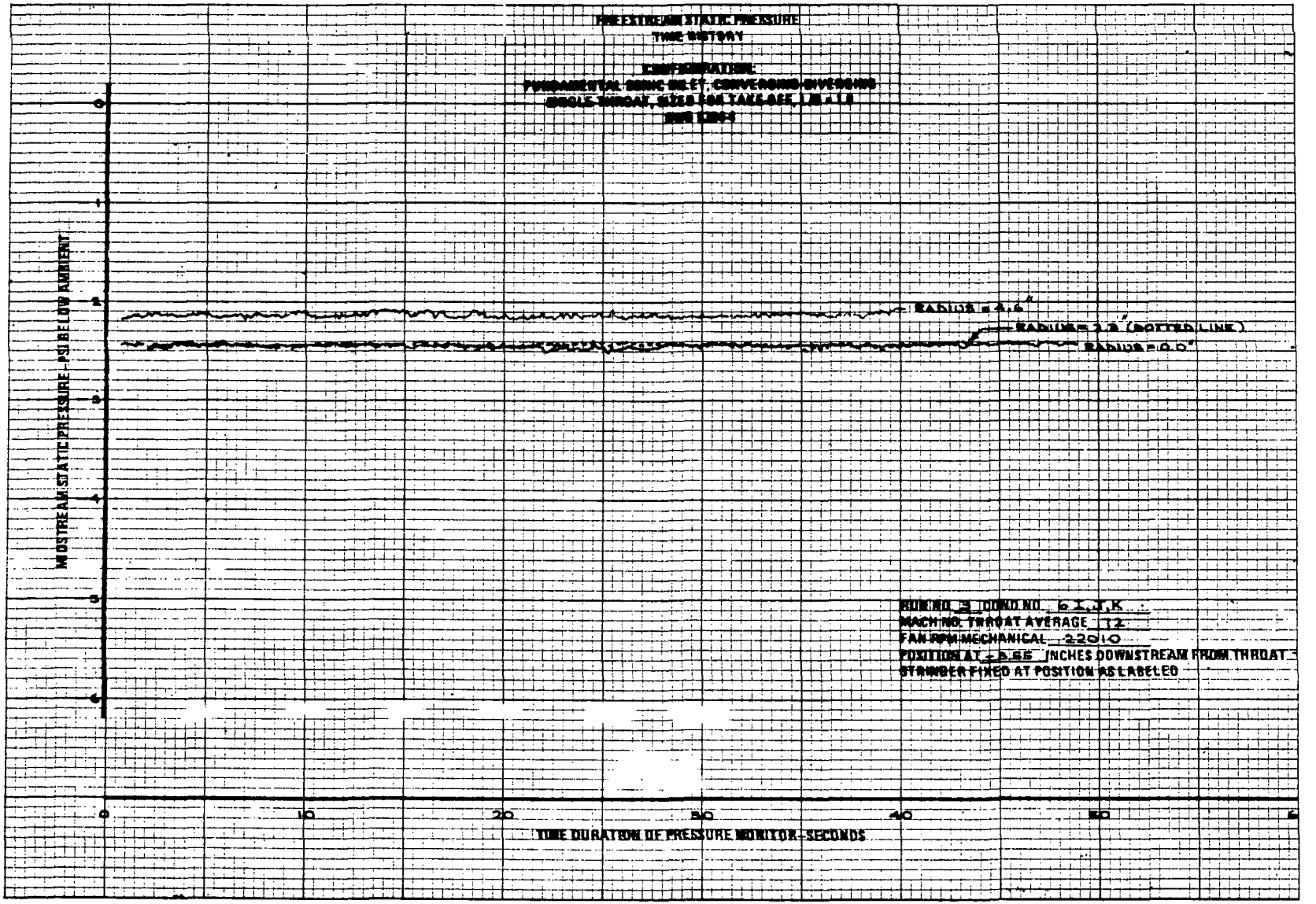

FIGURE C-7.–RUN 3-6 I,J,K, FREESTREAM STATIC PRESSURE TIME HISTORY AT -3.55 IN. DOWNSTREAM FROM INLET THROAT AND AT 0.0, 2.3, AND 4.6 IN. FROM INLET CENTERLINE

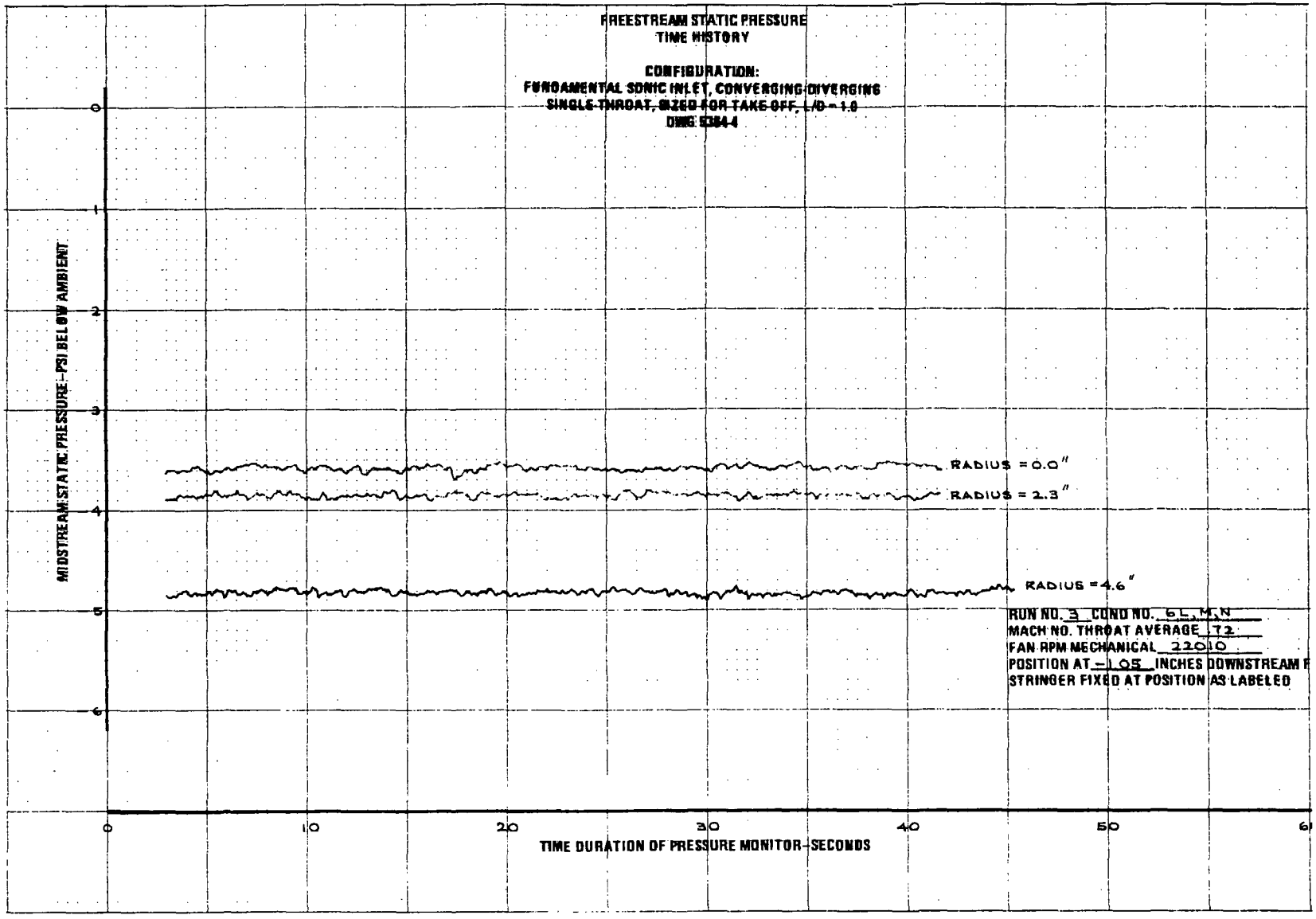

FIGURE C-8.—RUN 3-6 L,M,N, FREESTREAM STATIC PRESSURE TIME HISTORY AT -1.05 IN. DOWNSTREAM FROM INLET THROAT AND AT 0.0, 2.3, AND 4.6 IN. FROM INLET CENTERLINE

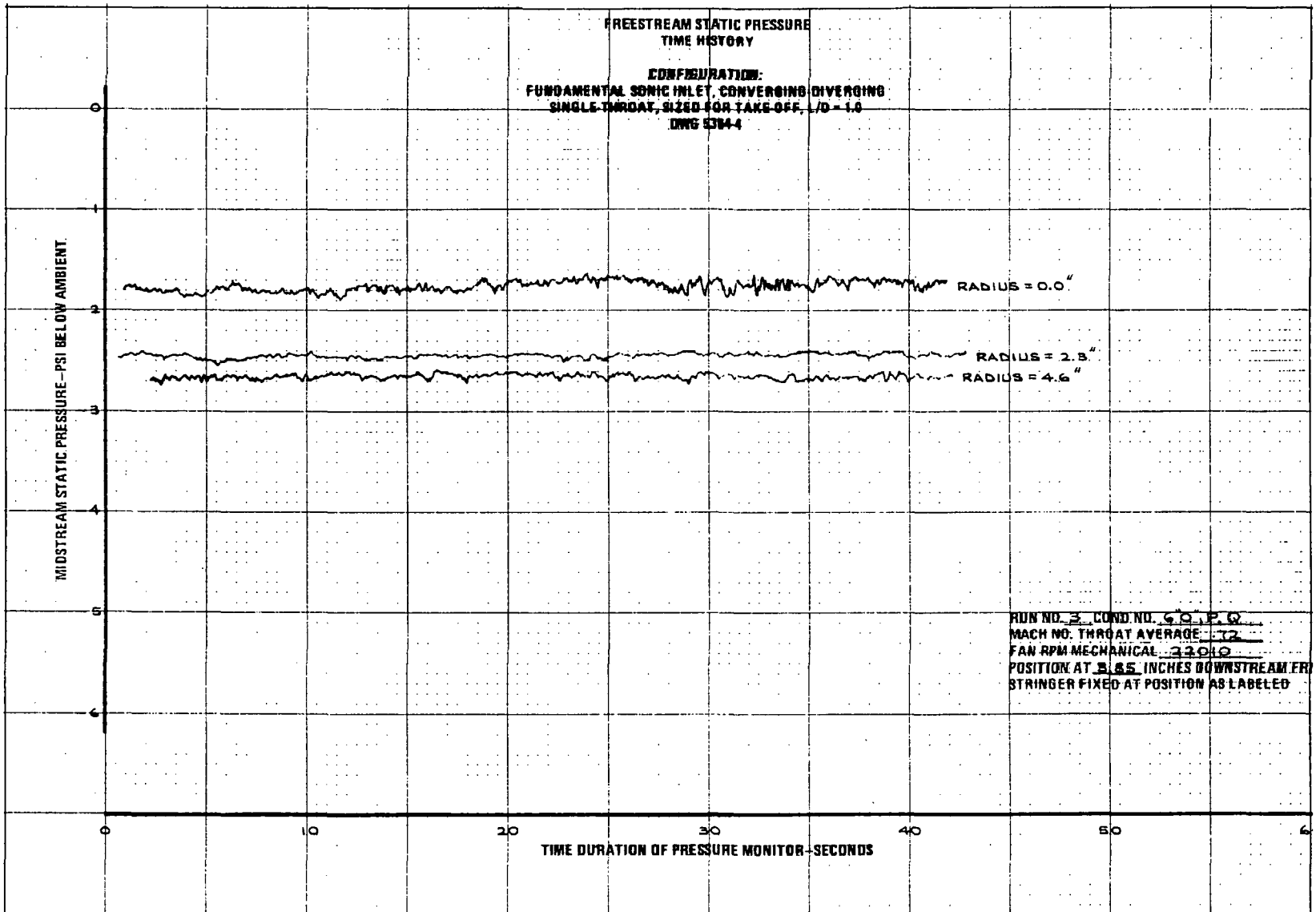

FIGURE C-9.—RUN 3-6 O,P,Q, FREESTREAM STATIC PRESSURE TIME HISTORY AT 3.85 IN. DOWNSTREAM FROM INLET THROAT AND AT 0.0, 2.3, AND 4.6 IN. FROM INLET CENTERLINE

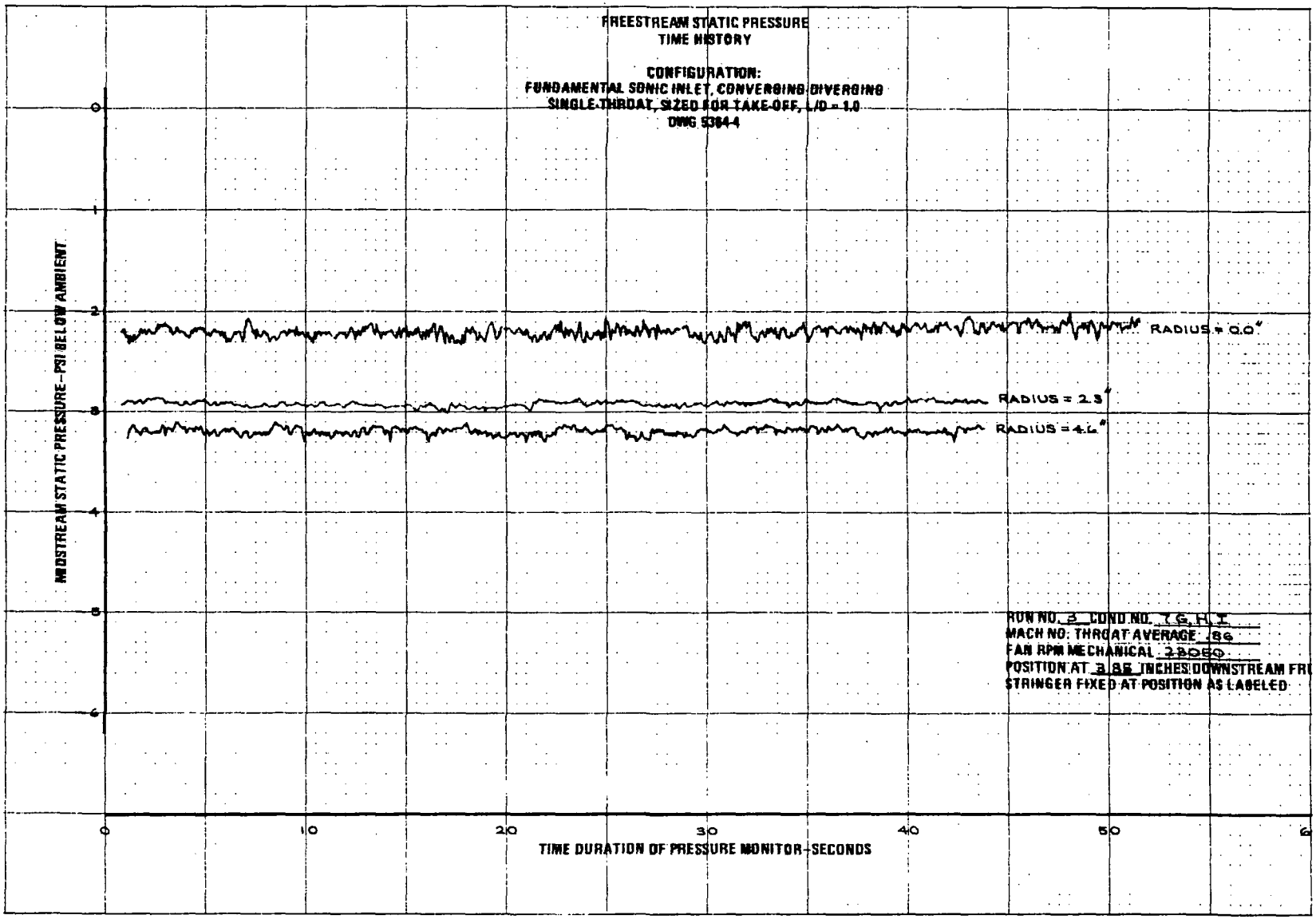

FIGURE C-10.—RUN 3-7 G,H,I, FREESTREAM STATIC PRESSURE TIME HISTORY AT 3.85 IN. DOWNSTREAM FROM INLET THROAT AND AT 0.0, 2.3, AND 4.6 IN. FROM INLET CENTERLINE

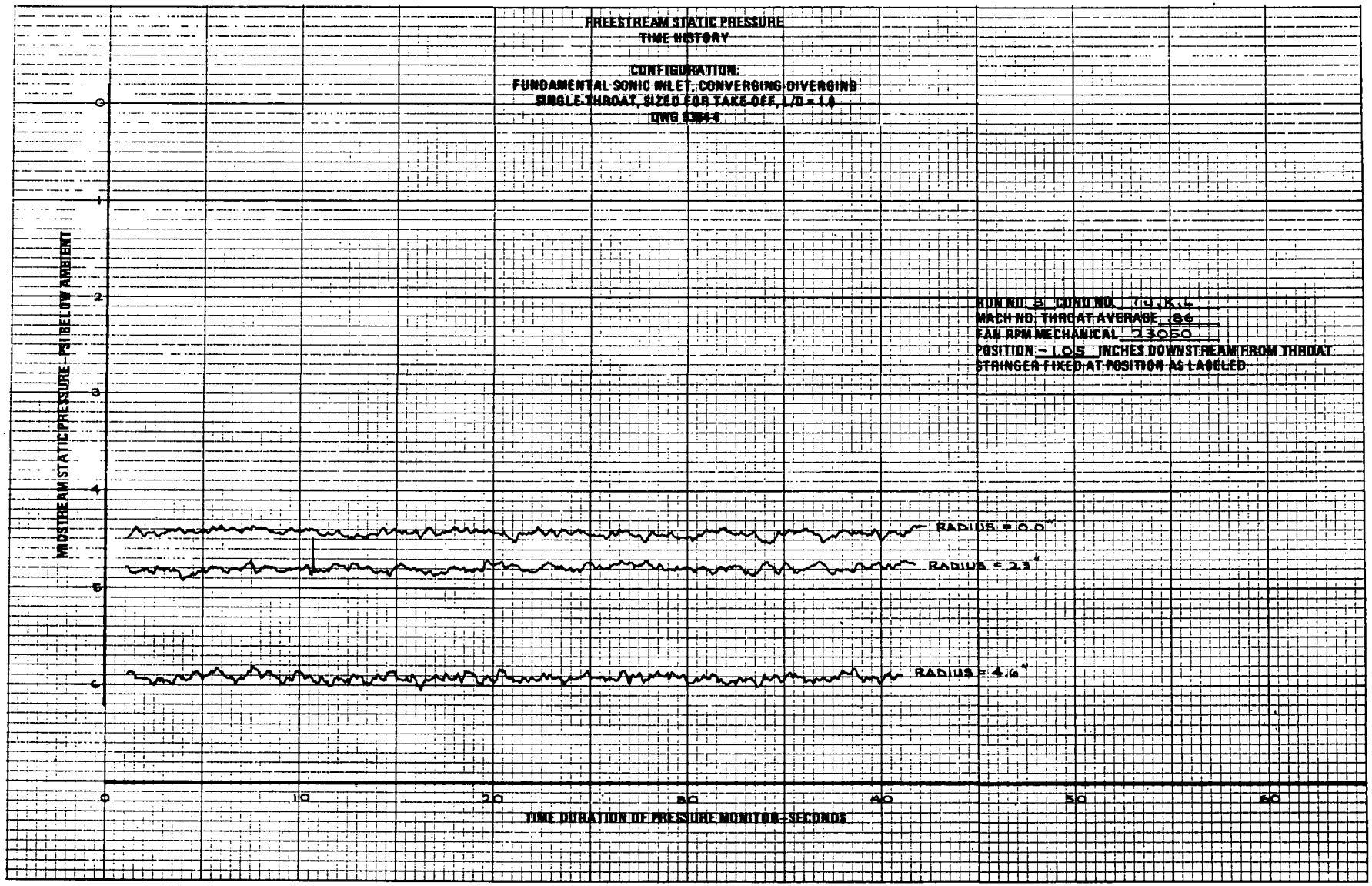

FIGURE C-11.—RUN 3-7 J,K,L, FREESTREAM STATIC PRESSURE TIME HISTORY AT -1.05 IN. DOWNSTREAM FROM INLET THROAT AND AT 0.0, 2.3, AND 4.6 IN. FROM INLET CENTERLINE

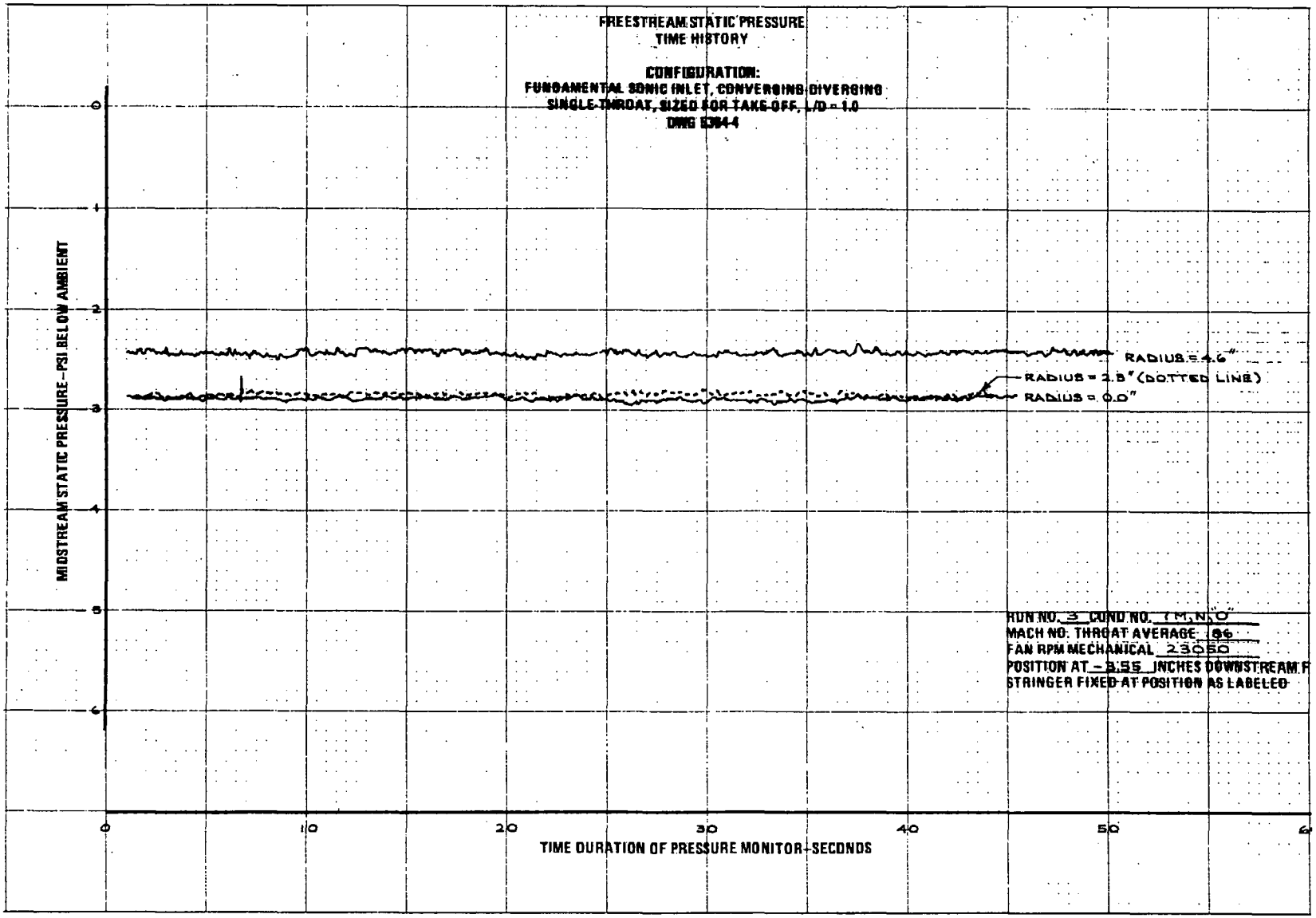

FIGURE C-12.—RUN 3-7 M,N,O, FREESTREAM STATIC PRESSURE TIME HISTORY AT -3.55 IN. DOWNSTREAM FROM INLET THROAT AND AT 0.0, 2.3, AND 4.6 IN. FROM INLET CENTERLINE

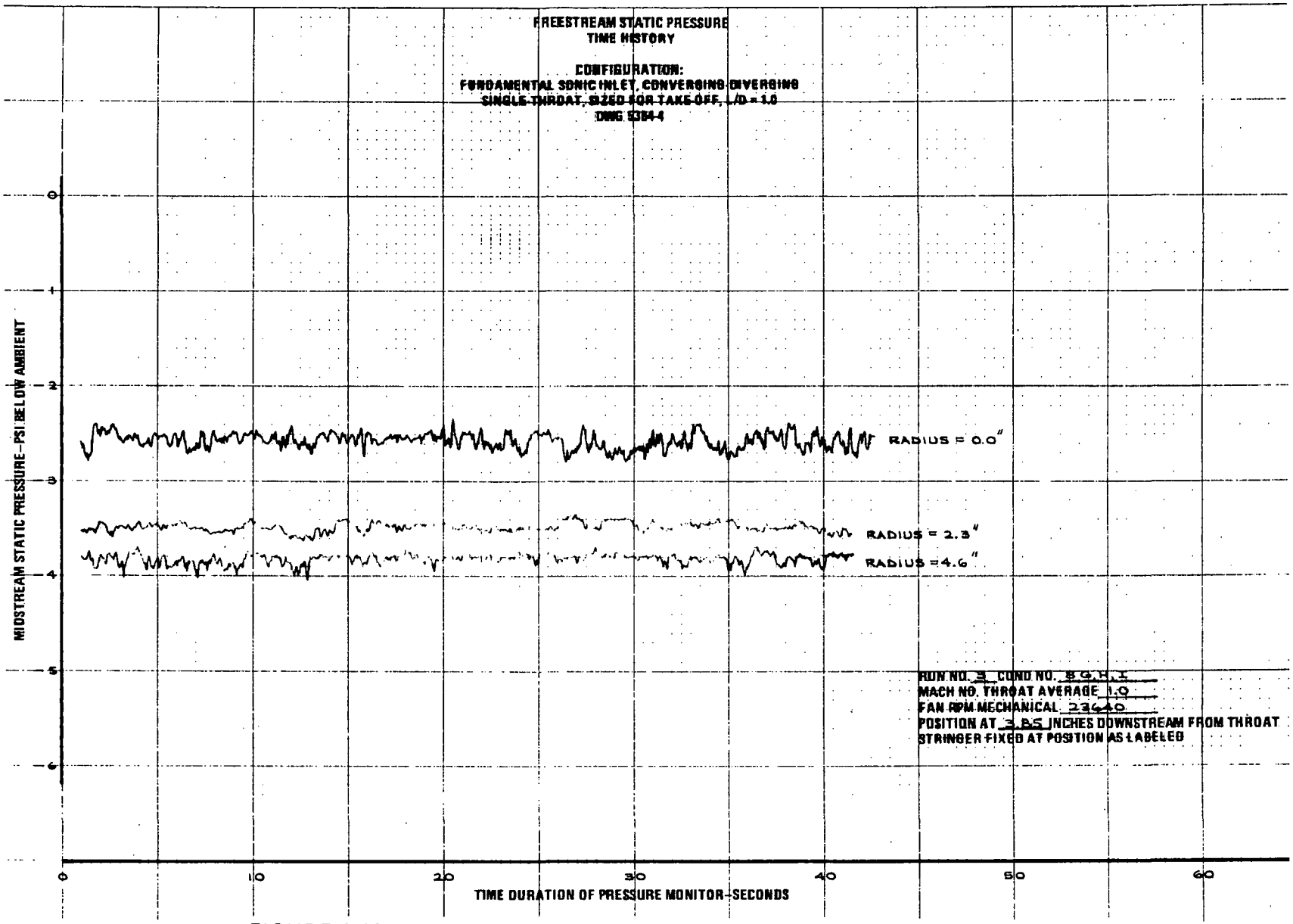

FIGURE C-13.—RUN 3-8 G,H,I, FREESTREAM STATIC PRESSURE TIME HISTORY AT 3.85 IN. DOWNSTREAM FROM INLET THROAT AT AND AT 0.0, 2.3, AND 4.6 IN. FROM INLET CENTERLINE

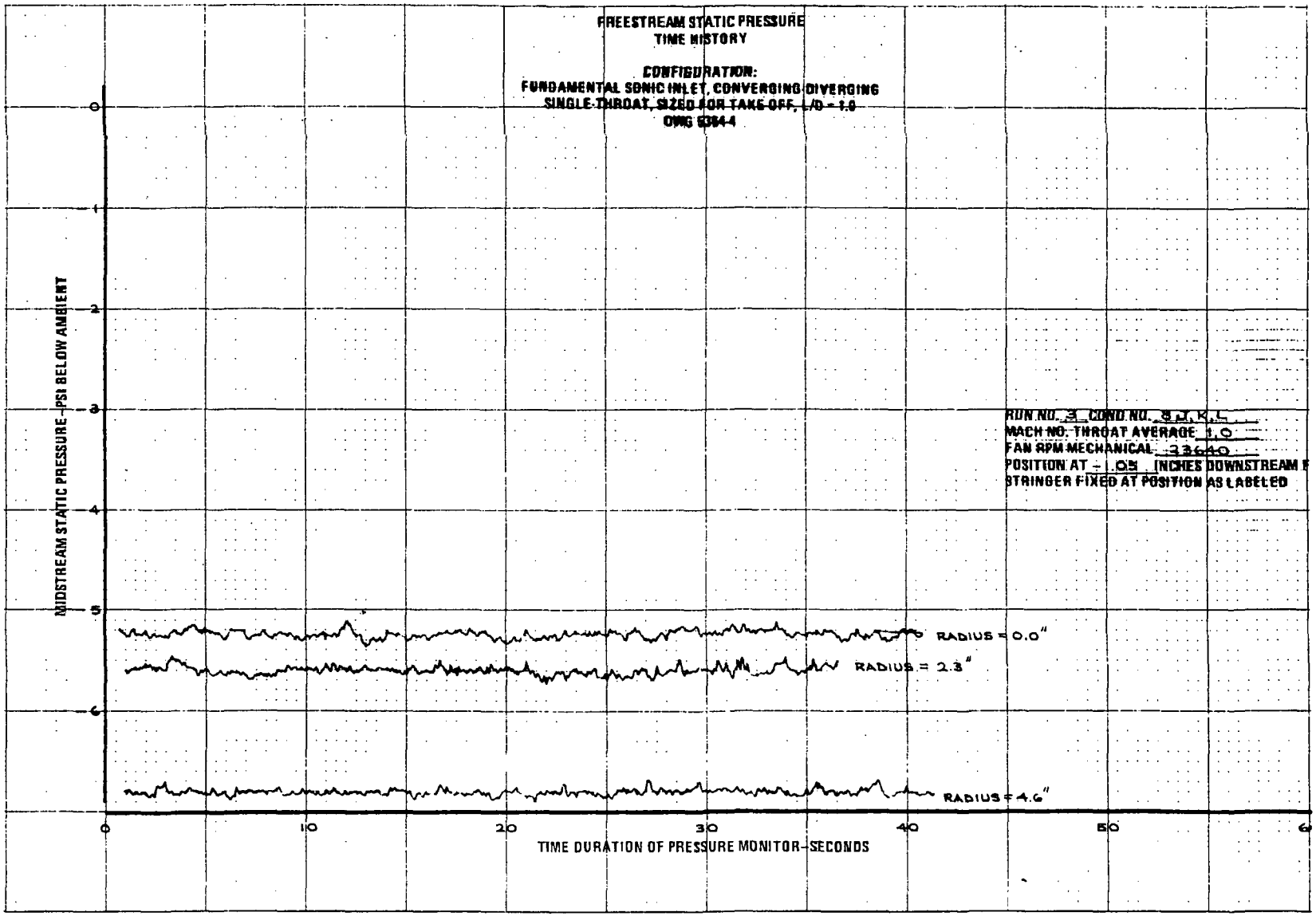

FIGURE C-14.—RUN 3-8 J,K,L, FREESTREAM STATIC PRESSURE TIME HISTORY AT -1.05 IN. DOWNSTREAM FROM INLET THROAT AND AT 0.0, 2.3, AND 4.6 IN. FROM INLET CENTERLINE

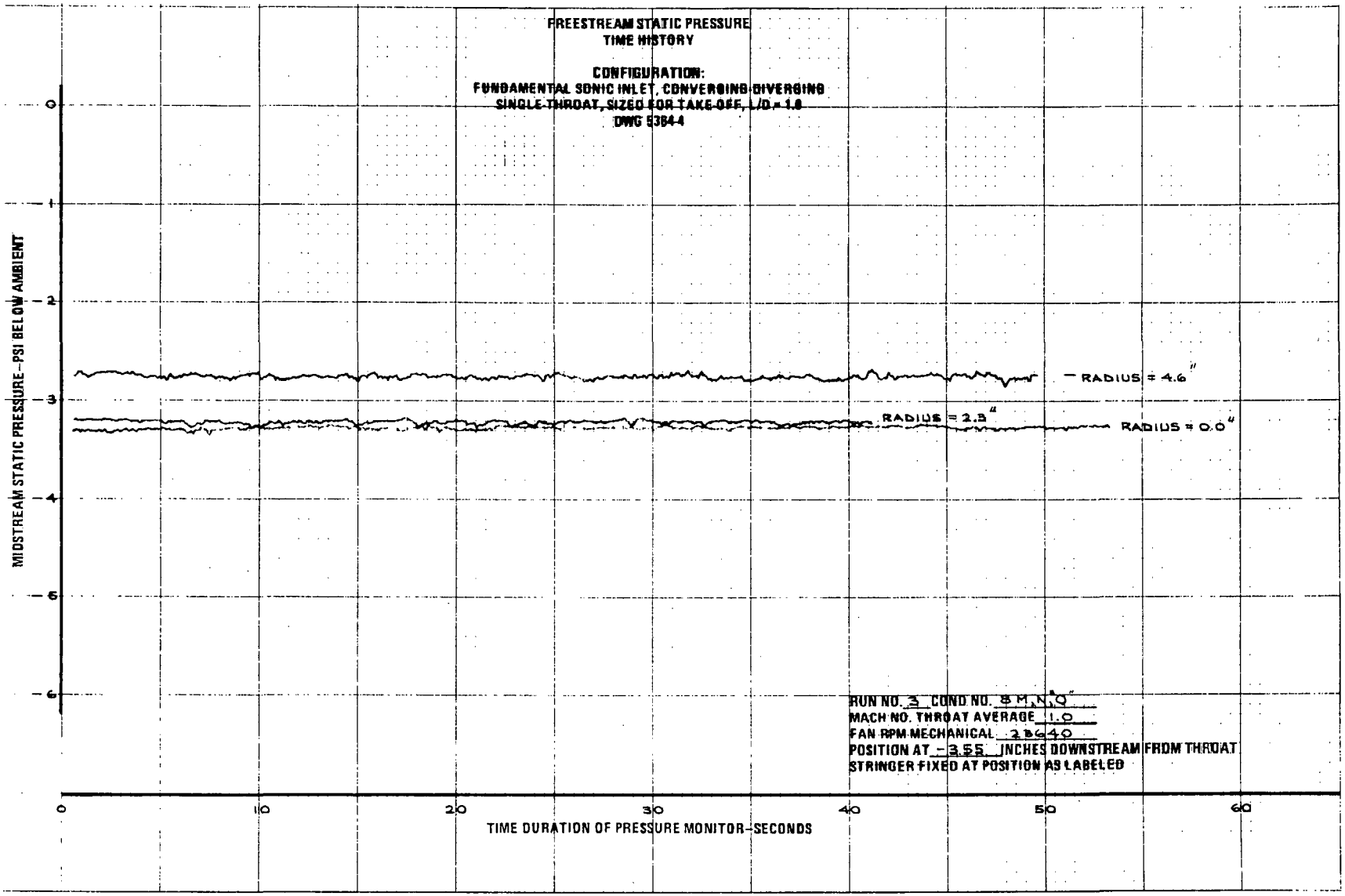

FIGURE C-15.—RUN 3-8 M,N,O, FREESTREAM STATIC PRESSURE TIME HISTORY AT -3.55 IN. DOWNSTREAM FROM INLET THROAT AND AT 0.0, 2.3, AND 4.6 IN. FROM INLET CENTERLINE

Page Intentionally Left Blank

APPENDIX D

FREQUENCY RESPONSE CALIBRATION OF NEAR-FIELD KULITE PROBES

Prior to the test with the stinger probe, the Kulite microphone was calibrated. The results of that calibration are presented in this appendix. A short discussion of the calibration procedure follows.

A block diagram of the microphone calibrator is shown in figure D-1.

Prior to the test, a certified* B&K condenser microphone was inserted into the non-resonant acoustic chamber and the output was compared with the reference microphone. The comparison showed that the deviation between the two calibrations curves was within ±0.1 dB at a level of 140 dB.

The certified B&K condenser microphone was removed and the stinger probe Kulite microphone inserted. The output recorded is shown in figure D-2.

During the test, prior to every run, the level of the Kulite microphone was checked by placing a calibrator with a level of 160 dB at 1000 Hz over the microphone. During the entire test, the output of the RMS voltmeter was found to be within the accuracy limits of the microphone calibration curve.

Note: The calibrator was being checked by the Boeing Primary Standards Group.

*By Boeing Primary Standards

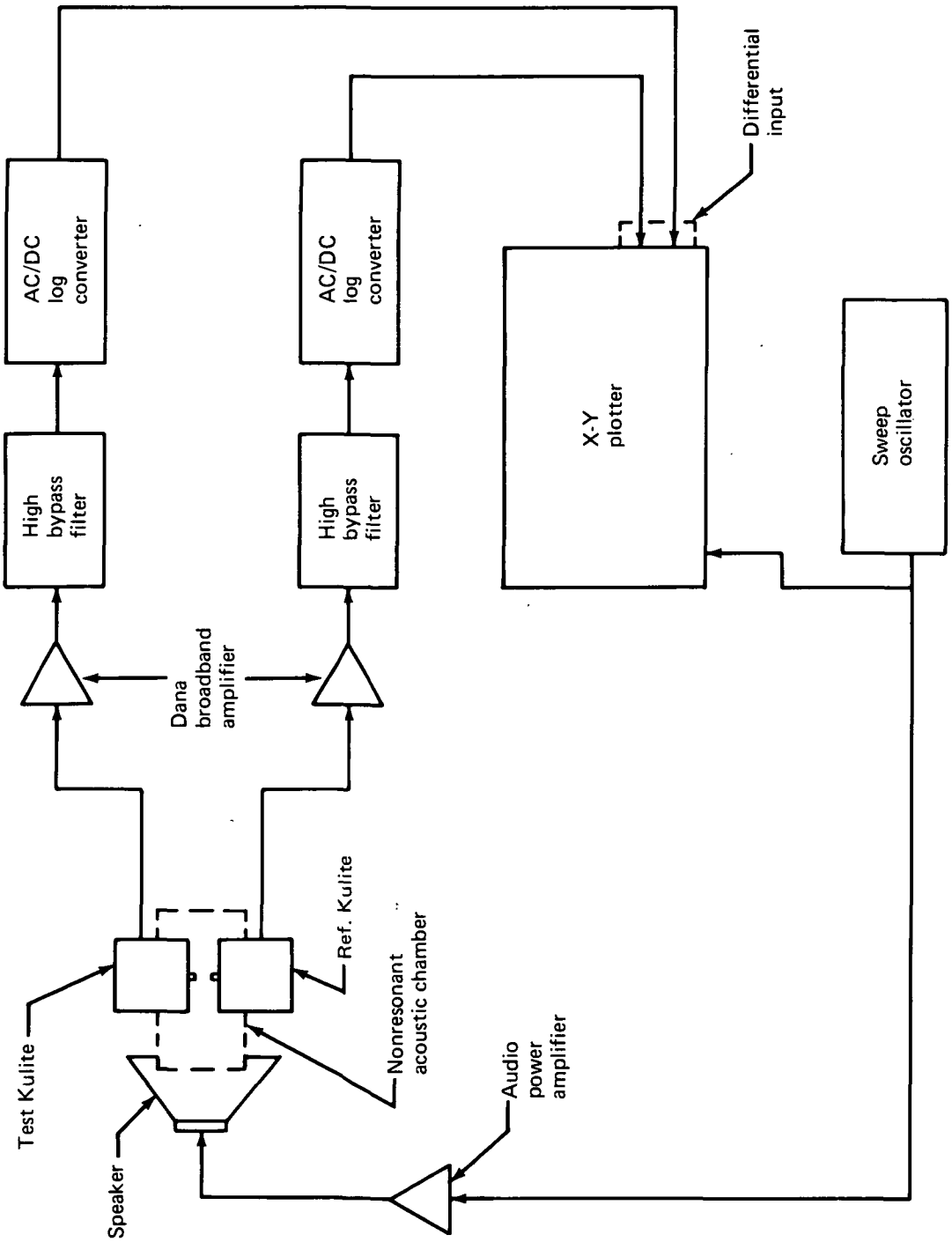

FIGURE D-1.—BLOCK DIAGRAM OF FREQUENCY CALIBRATOR

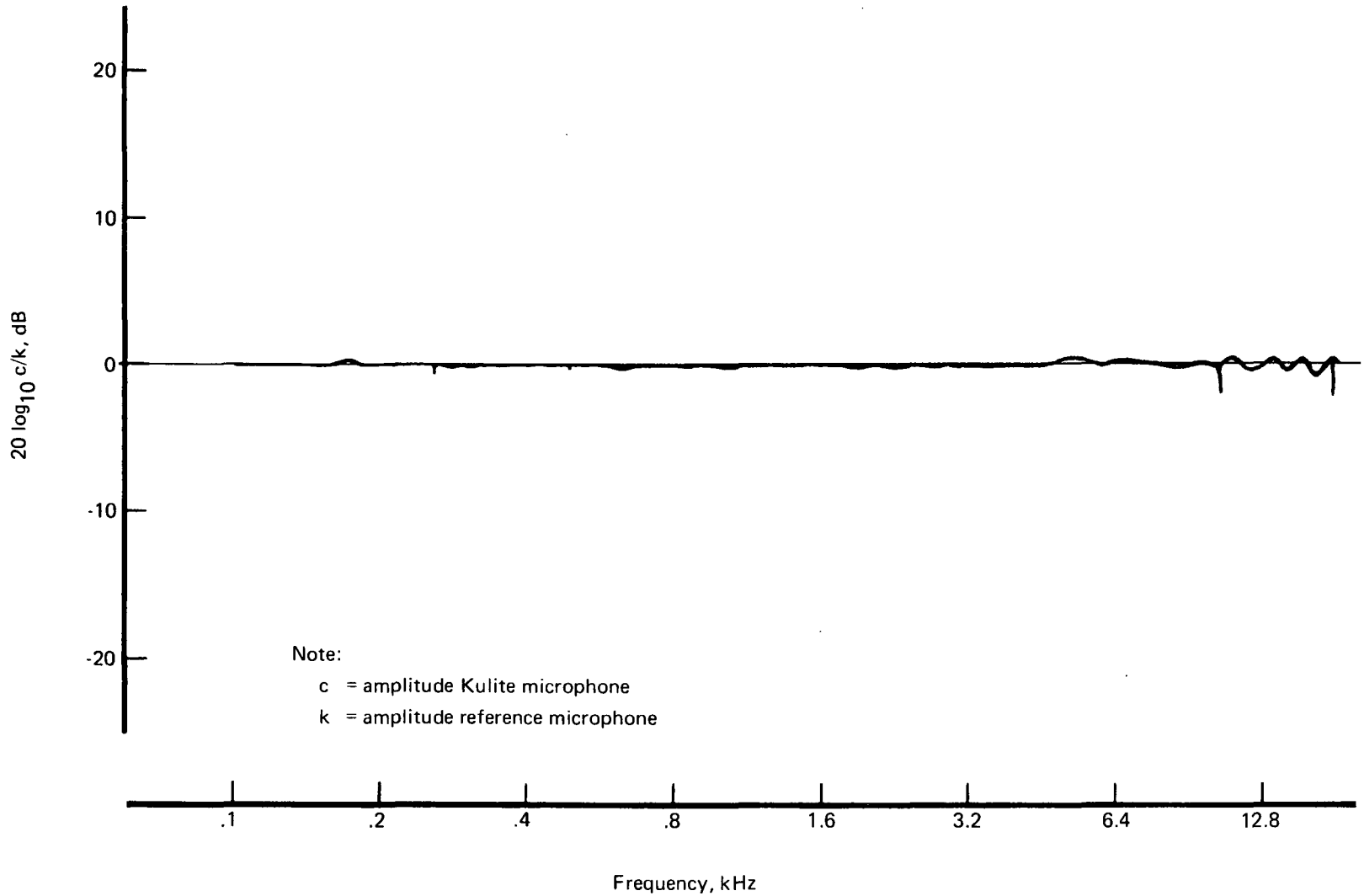

FIGURE D-2.—FREQUENCY RESPONSE CURVE OF KULITE MICROPHONE

Page Intentionally Left Blank

APPENDIX E

SYMBOLS

Symbol	Description	Dimension
A	area	L^2
A*	critical flow area	L^2
A_t	geometrical area in the inlet throat	L^2
B	number of blades of the compressor rotor	
D	diameter of compressor rotor	L
fo	blade passing frequency	T^{-1}
L	length of inlet measured from inlet highlight to fan face	L
M	Mach number	
$\bar{M}_t$	normalized throat average Mach number (defined in section 2.4)	
N_1	mechanical rpm of fan	RPM
PWL	sound power level (ref. to: 10^{-13} watts)	
R	radius of compressor rotor	L
SPL	sound pressure level (ref. to 2×10^{-5} Newton/m^2)	
X	distance measured downstream from inlet plane	L

Page Intentionally Left Blank

REFERENCES

1. Klujber, F.: Investigation of Noise Suppression by Sonic Inlets for Turbofan Engines–Technical Proposal. Boeing document D6-40195-1, September 1971.

2. Klujber, F.: Investigation of Noise Suppression by Sonic Inlets for Turbofan Engines–Volume I: Program Summary. Boeing document D6-40855, April 1973.